

Topics in Current Chemistry Collections

Margherita Venturi  
Mila D'Angelantonio *Editors*

# Applications of Radiation Chemistry in the Fields of Industry, Biotechnology and Environment

 Springer

# Topics in Current Chemistry Collections

## Journal Editors

Massimo Olivucci, Siena, Italy and Bowling Green, USA

Wai-Yeung Wong, Hong Kong

## Series Editors

Hagan Bayley, Oxford, UK

Kendall N. Houk, Los Angeles, USA

Greg Hughes, Codexis Inc, USA

Christopher A. Hunter, Cambridge, UK

Seong-Ju Hwang, Seoul, South Korea

Kazuaki Ishihara, Nagoya, Japan

Barbara Kirchner, Bonn, Germany

Michael J. Krische, Austin, Texas

Delmar Larsen, Davis, USA

Jean-Marie Lehn, Strasbourg, France

Rafael Luque, Córdoba, Spain

Jay S. Siegel, Tianjin, China

Joachim Thiem, Hamburg, Germany

Margherita Venturi, Bologna, Italy

Chi-Huey Wong, Taipei, Taiwan

Henry N.C. Wong, Hong Kong

Vivian Wing-Wah Yam, Hong Kong

Chunhua Yan, Beijing, China

Shu-Li You, Shanghai, China

## Aims and Scope

The series *Topics in Current Chemistry Collections* presents critical reviews from the journal *Topics in Current Chemistry* organized in topical volumes. The scope of coverage is all areas of chemical science including the interfaces with related disciplines such as biology, medicine and materials science.

The goal of each thematic volume is to give the non-specialist reader, whether in academia or industry, a comprehensive insight into an area where new research is emerging which is of interest to a larger scientific audience.

Each review within the volume critically surveys one aspect of that topic and places it within the context of the volume as a whole. The most significant developments of the last 5 to 10 years are presented using selected examples to illustrate the principles discussed. The coverage is not intended to be an exhaustive summary of the field or include large quantities of data, but should rather be conceptual, concentrating on the methodological thinking that will allow the non-specialist reader to understand the information presented.

Contributions also offer an outlook on potential future developments in the field.

More information about this series at <http://www.springer.com/series/14181>

Margherita Venturi • Mila D'Angelantonio  
Editors

# Applications of Radiation Chemistry in the Fields of Industry, Biotechnology and Environment

*With contributions from*

Krzysztof Bobrowski • Emilio Bucio • Ana Maria del Carmen Calvo  
Luigi Campajola • Maria Helena Casimiro • Andrzej G. Chmielewski  
Mila D'Angelantonio • Francesco Di Capua • C. Dispenza  
Andrea Docters • Luís M. Ferreira • Susana R. Gomes  
Bumsoo Han • M. Jonsson • Joana J. H. Lancastre  
Jesús E. López-Barriguete • Felipe López-Saucedo  
María Virginia Miranda • Suresh D. Pillai • Víctor H. Pino-Ramos  
Alejandro Ramos-Ballesteros • Alexandra P. Rodrigues  
Gabriela Rodrigues • Mario Carlos Nazareno Saparrat  
Shima Shayanfar • Konrad Skotnicki • G. Spadaro • Tomasz Szreder  
Erzsébet Takács • Gustavo H. C. Varca • Margherita Venturi  
László Wojnárovits • Raissa F. Zaikina • Yuriy A. Zaikin

 Springer



*Editors*

Margherita Venturi  
University of Bologna  
Bologna, Italy

Mila D'Angelantonio  
ISOF-CNR  
Bologna, Italy

Originally published in *Top Curr Chem (Z)* Volume 374 (2016),  
© Springer International Publishing Switzerland 2017

ISSN 2367-4067                      ISSN 2367-4075 (electronic)  
Topics in Current Chemistry Collections  
ISBN 978-3-319-54144-0              ISBN 978-3-319-54145-7 (eBook)  
DOI 10.1007/978-3-319-54145-7

Library of Congress Control Number: 2017933484

© Springer International Publishing AG 2017

This work is subject to copyright. All rights are reserved by the Publisher, whether the whole or part of the material is concerned, specifically the rights of translation, reprinting, reuse of illustrations, recitation, broadcasting, reproduction on microfilms or in any other physical way, and transmission or information storage and retrieval, electronic adaptation, computer software, or by similar or dissimilar methodology now known or hereafter developed.

The use of general descriptive names, registered names, trademarks, service marks, etc. in this publication does not imply, even in the absence of a specific statement, that such names are exempt from the relevant protective laws and regulations and therefore free for general use.

The publisher, the authors and the editors are safe to assume that the advice and information in this book are believed to be true and accurate at the date of publication. Neither the publisher nor the authors or the editors give a warranty, express or implied, with respect to the material contained herein or for any errors or omissions that may have been made. The publisher remains neutral with regard to jurisdictional claims in published maps and institutional affiliations.

Printed on acid-free paper

This Springer imprint is published by Springer Nature  
The registered company is Springer International Publishing AG  
The registered company address is: Gewerbestrasse 11, 6330 Cham, Switzerland

## Contents

<b>Editorial</b> .....	vii
Margherita Venturi, Mila D'Angelantonio	
<b>Radiation Induced Degradation of Organic Pollutants in Waters and Wastewaters</b> .....	1
László Wojnárovits, Erzsébet Takács	
<b>Electron Beam Technology for Environmental Pollution Control</b> .....	37
Andrzej G. Chmielewski, Bumsoo Han	
<b>Radiation Grafting for the Functionalization and Development of Smart Polymeric Materials</b> .....	67
Víctor H. Pino-Ramos, Alejandro Ramos-Ballesteros, Felipe López-Saucedo, Jesús E. López-Barriguete, Gustavo H. C. Varca, Emilio Bucio	
<b>Radiation Engineering of Multifunctional Nanogels</b> .....	95
C. Dispenza, G. Spadaro, M. Jonsson	
<b>Chitosan-Based Matrices Prepared by Gamma Irradiation for Tissue Regeneration: Structural Properties vs. Preparation Method</b> .....	121
Maria Helena Casimiro, Joana J. H. Lancastre, Alexandra P. Rodrigues, Susana R. Gomes, Gabriela Rodrigues, Luís M. Ferreira	
<b>Application of Radiation Chemistry to Some Selected Technological Issues Related to the Development of Nuclear Energy</b> .....	147
Krzysztof Bobrowski, Konrad Skotnicki, Tomasz Szreder	
<b>Upgrading and Refining of Crude Oils and Petroleum Products by Ionizing Irradiation</b> .....	195
Yuriy A. Zaikin, Raissa F. Zaikina	
<b>The Use of Gamma Radiation for the Treatment of Cultural Heritage in the Argentine National Atomic Energy Commission: Past, Present, and Future</b> .....	227
Ana Maria del Carmen Calvo, Andrea Docters, María Virginia Miranda, Mario Carlos Nazareno Saparrat	

---

<b>Electron Beam Technology and Other Irradiation Technology Applications in the Food Industry</b> .....	249
Suresh D. Pillai, Shima Shayanfar	
<b>Applications of Accelerators and Radiation Sources in the Field of Space Research and Industry</b> .....	269
Luigi Campajola, Francesco Di Capua	
<b>Erratum to: Radiation Engineering of Multifunctional Nanogels</b> .....	E1
C. Dispenza, G. Spadaro, M. Jonsson	
<b>Erratum to: Application of Radiation Chemistry to Some Selected Technological Issues Related to the Development of Nuclear Energy</b> .....	E3
Krzysztof Bobrowski, Konrad Skotnicki, Tomasz Szreder	

## Editorial

Margherita Venturi<sup>1</sup> · Mila D'Angelantonio<sup>2</sup>

© Springer International Publishing Switzerland 2017

The chemical effects of high-energy radiations, such as those emitted by radioactive substances, generated by high-energy machines and nuclear reactors, concern a branch of chemistry called radiation chemistry. This term was proposed by Milton Burton in 1942 for the needs of the Manhattan Project, the secret atomic energy research program carried out in the United States during the Second World War. It is interesting to notice, however, that the first radiation-chemical change was observed as early as 1895 by Röntgen when he established the existence of a penetrating, invisible radiation—X-rays—able to fog a photographic plate. Indeed, as Burton wrote (C&EN, 1969, Feb. 10, 86): In May 1942, the title radiation chemistry did not exist ... I sought an appropriate name for an area that we quickly realized has existed for 47 years without any name at all. The name radiation chemistry came out of the hopper; I didn't like it; I asked Robert Mulliken advice. He couldn't think of anything better and, with that negative endorsement, the old field received its present name.

Since that time, radiation chemistry has developed at an incredible rate. For at least 30 years the interest focused on basic research, exploiting steady-state and time-resolved techniques, in the field not only of chemistry, but also physics and biology. These studies, reported in a large number of papers and books, endeavored to understand the mechanisms of a wide variety of radiolytically induced reactions, and to collect kinetic data and absorption spectra of the unstable species formed by the interaction of high-energy radiations with very different systems, as far as chemical

---

This article is part of the Topical Collection “Applications of Radiation Chemistry”; edited by Margherita Venturi, Mila D'Angelantonio.

---

✉ Margherita Venturi  
[margherita.venturi@unibo.it](mailto:margherita.venturi@unibo.it)

<sup>1</sup> University of Bologna, Bologna, Italy

<sup>2</sup> ISOF-CNR, Bologna, Italy

composition and aggregation state are concerned. These radiations were soon found to induce useful chemical changes in various substrates resulting in their use for diverse applications. The first applications were in medicine for diagnostic and therapeutic purposes, but a variety of interesting industrial applications rapidly emerged, such as sterilization of different materials and polymer preparation, modification, and degradation. The applicative aspect of radiation chemistry strongly expanded, taking advantage of the great amount of results provided by basic studies, so that today high-energy radiations are employed with various aims in several other fields like environment, biotechnology, cultural heritage, and food treatment.

These spectacular advances are illustrated in the present topical collection of *Topics in Current Chemistry* that showcases contributions from the most prominent expert groups. It indeed reports the outstanding developments in the industrial, biotechnological, and environmental fields including several recent and interesting topics. These are (a) radiation-induced degradation of organic pollutants in waters and wastewaters, (b) advantages of radiation technology for upgrading and refining high-viscous oils and petroleum products, (c) use of gamma radiations for treating cultural heritage, (d) application of radiation chemistry to solve some technological issues related to nuclear energy, (e) radiation-induced grafting for the functionalization and development of smart polymeric materials, (f) radiation engineering of multifunctional nanogels, (g) chitosan-based matrices prepared by gamma irradiation for tissue regeneration, (h) electron beam technology for environmental pollution control, (i) radiation technology applications in the food industry, and (j) application of radiation sources and accelerators in the field of space research and industry.

We believe that this topical collection represents a good opportunity not only to highlight the research activities carried out by exploiting the peculiar features of the high-energy radiation with non-experts, but also to stimulate the interest of a wide range of readers for this relatively new field. Finally, we would like to express our gratitude to the colleagues who committed to deliver high-quality contributions, and to the editorial staff at Springer for their support throughout the development of this topical collection.



Margherita Venturi



Mila D'Angelantonio

# Radiation Induced Degradation of Organic Pollutants in Waters and Wastewaters

László Wojnárovits<sup>1</sup> · Erzsébet Takács<sup>1</sup>

Received: 18 March 2016 / Accepted: 28 June 2016 / Published online: 25 July 2016  
© Springer International Publishing Switzerland 2016

**Abstract** In water treatment by ionizing radiation, and also in other advanced oxidation processes, the main goal is to destroy, or at least to deactivate harmful water contaminants: pharmaceutical compounds, pesticides, surfactants, health-care products, etc. The chemical transformations are mainly initiated by hydroxyl radicals, and the reactions of the formed carbon centered radicals with dissolved oxygen basically determine the rate of oxidation. The concentration of the target compounds is generally very low as compared to the concentration of such natural ‘impurities’ as chloride and carbonate/bicarbonate ions or the dissolved humic substances (generally referred to as dissolved organic carbon), which consume the majority of the hydroxyl radicals. The different constituents compete for reacting with radicals initiating the degradation. This manuscript discusses the radiation chemistry of this complex system. It includes the reactions of the primary water radiolysis intermediates (hydroxyl radical, hydrated electron/hydrogen atom), the reactions of radicals that form in radical transfer reactions (dichloride-, carbonate- and sulfate radical anions) and also the contribution to the degradation of organic compounds of such additives as hydrogen peroxide, ozone or persulfate.

**Keywords** Water treatment · Advanced oxidation processes · Degradation · Radiolysis · Radical

---

This article is part of the Topical Collection “Applications of Radiation Chemistry”; edited by “Margherita Venturi, Mila D’Angelantonio.

✉ Erzsébet Takács  
[erzsebet.takacs@energia.mta.hu](mailto:erzsebet.takacs@energia.mta.hu)

<sup>1</sup> Institute for Energy Security and Environmental Safety, Centre for Energy Research, Hungarian Academy of Sciences, Konkoly-Thege M. út. 29-33, H-1121 Budapest, Hungary

## 1 Introduction

In water treatment by ionizing radiation, the reactive intermediates of water radiolysis and the radicals that form in radical transfer reactions induce the degradation of the target harmful organic pollutants, pharmaceuticals, pesticides, health care products, etc. [1, 2]. In real wastewater, there is always a competition between the reactions of different constituents of the aqueous solutions for the reactive water intermediates. The relative rates of reactions are determined by the product of the rate constant ( $k_x$ ) and the concentration of a given component ( $S_x$ ) in the water:  $k_x[S_x]$ . This product is called scavenging capacity. The weight of a reaction of a reactive intermediate with compound x ( $w_x$ ) may be calculated using the relation:

$$w_x = \frac{k_x[S_x]}{\sum k_x[S_x]} \quad (1)$$

where the summation should go on for all solutes.  $\sum k_x[S_x]$  represents the total scavenging capacity of the system [3]. The water that undergoes treatment beside dissolved  $O_2$  molecules ( $2.8 \times 10^{-4}$  mol  $dm^{-3}$ , at 20 °C) practically always contains chloride ions, carbonate and hydrogen carbonate (bicarbonate) ions, and a large number of different organic molecules. The organic content of drinking water, and the water of lakes and rivers, is referred to as dissolved organic carbon (DOC, defined as the fraction of organic substances that passes through a 0.45  $\mu m$  filter). DOC has diverse origin and composition within aquatic systems. Occasionally, high concentrations of organic carbon indicate anthropogenic influences, but DOC is mostly of natural origin. Organic carbon compounds usually form in decomposition processes of plants or organisms living in water. DOC in natural waters is composed of a heterogeneous mixture of organic compounds with molecular masses ranging from less than 100 to 300,000 Daltons. Humic substances (fulvic and humic acids) are the dominant DOC fractions in freshwater and coastal seawater [4]. Due to the undefined composition of DOC, scientific investigations with reactions of dissolved organic matter are often carried out with standard samples from the Suwannee River, purchased from the International Humic Substances Society (e.g., [5]).

The primary radicals that form during water irradiation react with the target harmful organic molecules and also with DOC, chloride and bicarbonate/carbonate ions, etc., forming secondary radicals. The properties and reactions of these secondary radicals and their participation in the degradation reactions are also detailed here, together with the reactions of primary water radiolysis intermediates. Some additives, like ozone, hydrogen peroxide or persulfate, are known to increase the oxidation efficiency of organic pollutants by transforming reductive intermediates to oxidizing species during irradiation. These reactions are also discussed. This paper concentrates on the radical reactions and mechanisms that are important from the point of view of water treatment. Practical implementation of the technique is discussed in another paper in this issue.

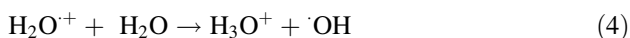


## 2 Reactions of Primary Radicals of Water Radiolysis with Organic Molecules

### 2.1 Radiolysis of Liquid Water

An important characteristic of ionizing radiation is that its energy is absorbed non-selectively so that molecules are ionized or excited according to their relative abundance in the medium of interest [6]. In dilute solutions, the energy is overwhelmingly absorbed by the solvent and the chemical reactions of the solute molecules occur through reactions of the reactive intermediates formed due to energy deposition in the solvent molecules. In radiation chemistry, there is a high probability that during the energy deposition and in the subsequent fast reactions, two or more reactive species are created close enough to each other that they can mutually influence each other's further reaction possibilities. This isolated space is called spur. There is a competition between the reaction of intermediates in the spur and their diffusing out of the spur (spur expansion). The intermediates that escape the spur in the bulk become homogeneously distributed with respect to solute molecules.

In the radiolysis of liquid water, the intermediates mainly form as a consequence of ionization of water molecules. Excited-state water molecules may play a much less significant role in radiolysis [6–10]:



The radical cation,  $\text{H}_2\text{O}^{*+}$  formed in reaction (2) may migrate over a distance of a few water molecules by resonance electron transfer, but since  $\text{H}_2\text{O}^{*+}$  is a strong acid within  $10^{-14}$  s it gives a proton to one of the surrounding water molecules according to (4), and the process gives a hydroxonium ion and hydroxyl radical ( $\cdot\text{OH}$ ). The electron released in reaction (2) (dry electron) loses its kinetic energy in collisions with surrounding water molecules and in less than  $10^{-12}$  s is localized in a potential energy well as a result of molecular dipoles rotating under the influence of the negative charge. Thus, in reaction (5), the smallest anion,  $\text{e}_{\text{aq}}^-$ , a solvated (hydrated) electron forms. The hydrated electron is also called aqueous electron. The excited water molecules,  $\text{H}_2\text{O}^*$ , formed in reaction (3), decompose to  $\cdot\text{OH}$  and  $\text{H}$  in reaction (6).

The yields (the so called *G*-values) of  $\cdot\text{OH}$ ,  $\text{e}_{\text{aq}}^-$  and  $\text{H}$  after the spur processes are 0.28, 0.28 and 0.06  $\mu\text{mol J}^{-1}$ , respectively. The intermediates with these yields

react with solute molecules present at a concentration level  $\leq 10^{-3}$  mol dm $^{-3}$ . It is estimated that about 40 % of the initially produced intermediates are consumed by spur processes [6]. In the spur processes, H $_2$  (0.047  $\mu$ mol J $^{-1}$ ) and H $_2$ O $_2$  (0.073  $\mu$ mol J $^{-1}$ ) form and there is also some reformation of water molecules (OH + H  $\rightarrow$  H $_2$ O).

## 2.2 The Diffusion Controlled Rate Constant

The rate constants of reactions of several inorganic radicals (e.g.,  $\cdot$ OH, Cl $^\cdot$  or SO $_4^{\cdot-}$ ) with organic molecules (mainly aromatics) approach the theoretical maximum, the so-called diffusion controlled value,  $k_{\text{diff}}$ . There are several equations in the literature for the estimation of the diffusion controlled limit; however, in practice, the Smoluchowski relation is the one that is most often used for this purpose [11, 12]:

$$k_{\text{diff}} = 4\pi(D_{\text{P}} + D_{\text{R}})(r_{\text{P}} + r_{\text{R}})N \times 10^3 (\text{mol}^{-1} \text{dm}^3 \text{s}^{-1}) \quad (7)$$

In the equation,  $D_{\text{P}}$  and  $D_{\text{R}}$  are the diffusion coefficients of the attacked molecule and the attacking radical, respectively, in m $^2$  s $^{-1}$  units.  $r_{\text{P}}$  and  $r_{\text{R}}$  are the reaction radii of the corresponding species in m.  $N$  is Avogadro's number. When the diffusion coefficients and the reaction radii are used in these units,  $k_{\text{diff}}$  is obtained in mol $^{-1}$  dm $^3$  s $^{-1}$ . For a typical aromatic molecule,  $D_{\text{P}}$  and  $r_{\text{P}}$  are around  $0.5 \times 10^{-9}$  m $^2$  s $^{-1}$  and  $3.2 \times 10^{-10}$  m, respectively [13]. In a study [12] on the temperature dependence of the  $\cdot$ OH + aromatic molecule reactions,  $2.2 \times 10^{-10}$  m and  $2.3 \times 10^{-9}$  m $^2$  s $^{-1}$  were used for  $r_{\text{OH}}$  and  $D_{\text{OH}}$ , respectively (Table 1). For the numerical values of  $D_{\text{SO}_4^{\cdot-}}$  and  $r_{\text{SO}_4^{\cdot-}}$ , Rickman and Mezyk [14] suggested  $1.1 \times 10^{-9}$  m $^2$  s $^{-1}$  and  $2.2 \times 10^{-10}$  m, respectively. For the diffusion coefficient and the reaction radius of the hydrogen atom,  $r_{\text{H}} = 1.9 \times 10^{-10}$  m and  $D_{\text{H}} = 7 \times 10^{-9}$  m $^2$  s $^{-1}$  were used in several papers (e.g., [15]). In the paper of the latter authors,  $r_{\text{Cl}_2^{\cdot-}} = 1.85 \times 10^{-10}$  m and  $D_{\text{Cl}_2^{\cdot-}} = 1.41 \times 10^{-9}$  m $^2$  s $^{-1}$  were used in the calculation of the diffusion controlled rate constant of Cl $_2^{\cdot-}$ . We assumed the same reaction radius and diffusion coefficient values for Cl $_2^{\cdot-}$  and CO $_3^{\cdot-}$ . The values for  $e_{\text{aq}}^-$  were taken from the book of Swallow [7].

The diffusion controlled rate constants for a given radical should vary with size and structure of the reacting organic molecule. However, these variations are probably small and the expected values do not change more than 10–20 %. In the following, when interpreting the rate constants, we use the same  $k_{\text{diff}}$  for a radical, independent of the reaction partner organic molecule [13].  $k_{\text{diff}}$  is the highest for  $e_{\text{aq}}^-$  and H $^\cdot$  reactions, due to the fast diffusion of these species in the matrix. It is the lowest for the heaviest, SO $_4^{\cdot-}$ . The  $k_{\text{diff}}$  values in the table are in reasonably good agreement, with the highest reliable rate constants measured for  $\cdot$ OH, H $^\cdot$ , Cl $_2^{\cdot-}$  and CO $_3^{\cdot-}$  reactions, respectively. The  $k_{\text{diff}}$  values for  $e_{\text{aq}}^-$  and SO $_4^{\cdot-}$  reactions seem to be slightly underestimated. The charges of the reactants and ionic strength effects also influence the reaction rates.

When the two reactants, the attacking radical and the organic molecule, approach each other by diffusion, the rate of the chemical step is basically determined by the

**Table 1** Diffusion coefficients and reaction radii for several inorganic radicals, and the estimated diffusion limited rate constants for reactions with simple aromatic molecules

Radical	OH	$c_{\text{aq}}^-$	H	$\text{Cl}_2^-$	$\text{CO}_3^-$	$\text{SO}_4^-$
$D_{\text{R}}, \text{m}^2 \text{s}^{-1}$	$2.3 \times 10^{-9,\text{a}}$	$4 \times 10^{-9,\text{d}}$	$7 \times 10^{-9,\text{b}}$	$1.41 \times 10^{-9,\text{b}}$	$1.41 \times 10^{-9,\text{e}}$	$1.1 \times 10^{-9,\text{e}}$
$r_{\text{R}}, \text{m}$	$2.2 \times 10^{-10,\text{a}}$	$3 \times 10^{-10,\text{d}}$	$1.9 \times 10^{-10,\text{b}}$	$1.85 \times 10^{-10,\text{b}}$	$1.85 \times 10^{-10,\text{e}}$	$2.2 \times 10^{-10,\text{e}}$
$k_{\text{diff}}, \text{mol}^{-1} \text{dm}^3 \text{s}^{-1}$	$1.1 \times 10^{10}$	$2.5 \times 10^{10}$	$2.9 \times 10^{10}$	$7.3 \times 10^9$	$7.3 \times 10^9$	$6.5 \times 10^9$

<sup>a</sup> [12]

<sup>b</sup> [15]

<sup>c</sup> [14]

<sup>d</sup> [7]

<sup>e</sup> We assumed the same values as for  $\text{Cl}_2^-$

chemical properties of the organic molecule. The rate constant of the chemical reaction ( $k_{\text{chem}}$ ) can be estimated by the Noyes relation [16]:

$$1/k_{\text{obsd}} = 1/k_{\text{diff}} + 1/k_{\text{chem}} \quad (8)$$

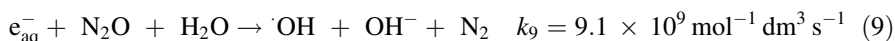
In the equation,  $k_{\text{obsd}}$  and  $k_{\text{diff}}$  stand for the observed and the diffusion controlled rate constant. The rate constant of the chemically activated reaction,  $k_{\text{chem}}$ , is the rate constant that would be measured if diffusion of the species was not rate influencing [11]. Due to the diffusion limitation,  $k_{\text{chem}}$  often shows much wider structural variation than  $k_{\text{obsd}}$ . This is especially true for radicals that can react with  $k_{\text{obsd}}$  close to the diffusion limitation [16].

The rate constants of hydrated electrons, hydrogen atoms and hydroxyl radicals, published until 1988, are collected in the work of Buxton et al. [17]; an updated version is available on the internet. The data for inorganic radicals other than  $\cdot\text{OH}$ ,  $e_{\text{aq}}^-$  and  $\text{H}\cdot$  have been compiled by Neta et al. [18].

### 2.3 Reactions of the Hydroxyl Radical

During water treatment by ionizing radiation, and in practically all of the other Advanced Oxidation Processes (AOP), hydroxyl radical is suggested to be the main reactive intermediate that induces the degradation of organic molecules. Due to its central role in different AOPs, the kinetics and mechanism of  $\cdot\text{OH}$  reactions with a large variety of organic pollutants have been detailed in a large number of publications. Here we give only a short overview.

In laboratory experiments, the primary processes of  $\cdot\text{OH}$  reactions are mostly studied in  $\text{N}_2\text{O}$  purged solutions (in the absence of dissolved  $\text{O}_2$ ) in order to convert the hydrated electron into hydroxyl radical in Reaction (9).  $\text{H}\cdot$  reacts slowly with  $\text{N}_2\text{O}$  [6].



In biochemical type investigations, when the presence of dissolved  $\text{O}_2$  is needed, the experiments are often carried out in  $\text{N}_2\text{O}:\text{O}_2$  mixtures with 4:1 ratio. Under these conditions, the hydrated electrons are converted to  $\cdot\text{OH}$ , but the aqueous solutions have dissolved  $\text{O}_2$  concentrations, just like under normal aerated conditions.

In reaction with dissolved organic molecules,  $\cdot\text{OH}$  may react in three different ways: direct electron transfer, abstraction of H-atoms from C–H bonds, and addition to the double bonds. Although the standard reduction potential of  $\cdot\text{OH}$  is high ( $E^0(\cdot\text{OH}/\text{OH}^-) = 1.9 \text{ V vs. NHE}$ , Table 2), direct electron transfer is rarely observed, and when it is observed, intermediate complexes are likely to be involved [21]. Electron transfer may take place in  $\cdot\text{OH}$  reaction with phenolates, although the electron transfer is also in competition with radical addition to the ring. These reactions are shown in the example of phenoxide in (10) and (11). The rate constant of the  $\text{C}_6\text{H}_5\text{O}^- + \cdot\text{OH}$  reaction is  $(k_{10} + k_{11}) = 9.6 \times 10^9 \text{ mol}^{-1} \text{ dm}^3 \text{ s}^{-1}$  [13].

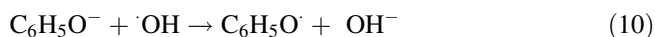
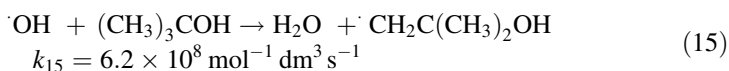
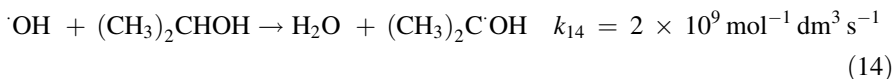


**Table 2** One-electron reduction potentials vs. normal hydrogen electrode (NHE) of some radicals used in radiation chemical studies [19, 20]

Pair	$E^\circ$ , V
aq/e <sub>aq</sub> <sup>-</sup>	-2.9
H <sub>aq</sub> <sup>+</sup> /H	-2.42
(CH <sub>3</sub> ) <sub>2</sub> CO, H <sup>+</sup> /(CH <sub>3</sub> ) <sub>2</sub> COH	-1.39
CH <sub>3</sub> CHO, H <sup>+</sup> /CH <sub>3</sub> CHOH	-1.25
CH <sub>2</sub> O, H <sup>+</sup> /CH <sub>2</sub> OH	-1.18
O <sub>2</sub> /O <sub>2</sub> <sup>-</sup>	-0.33
HO <sub>2</sub> , H <sup>+</sup> /H <sub>2</sub> O <sub>2</sub> , pH 0	1.48
CO <sub>3</sub> <sup>-</sup> , H <sup>+</sup> /HCO <sub>3</sub> <sup>-</sup> , pH 7	1.78
·OH/OH <sup>-</sup>	1.9
Cl <sub>2</sub> <sup>-</sup> /2 Cl <sup>-</sup>	2.1
SO <sub>4</sub> <sup>-</sup> /SO <sub>4</sub> <sup>2-</sup>	2.43
Cl <sup>·</sup> /Cl <sup>-</sup>	2.6



The rate constants of H-atom abstraction reactions are generally in the  $1 \times 10^7$ – $1 \times 10^9 \text{ mol}^{-1} \text{ dm}^3 \text{ s}^{-1}$  range. The reactions take place with a considerable selectivity: the rates increase in the order primary < secondary < tertiary H-atom. Here, we show the reactions with methanol, ethanol, isopropanol and *tert*-butanol [22]. In methanol and *tert*-butanol, three or nine primary H-atoms, respectively, are available for H-abstraction (bond dissociation energies  $402 \text{ kJ mol}^{-1}$  and  $418 \text{ kJ mol}^{-1}$  [23]), and in ethanol and isopropanol there are two secondary and one tertiary C–H bonds ( $389$  and  $384 \text{ kJ mol}^{-1}$ ), respectively, as preferred sites of H-abstraction. H-abstraction from the alcoholic OH also takes place, albeit with low weight [21].



The  $\alpha$ -hydroxymethyl,  $\alpha$ -hydroxyethyl and  $\alpha$ -hydroxyisopropyl radicals that form in H-abstraction from methanol, ethanol and isopropanol, respectively, [Reactions (12–14)] exhibit reducing character (Table 2). The radical formed in reaction with *tert*-butanol (15) is a non-reducing radical. In the presence of dissolved O<sub>2</sub>, the alkyl radicals transform to peroxides and the degradation may take place by Russel/Bennett mechanism [24].

**Table 3** Rate constants of selected ·OH reactions in mol<sup>-1</sup> dm<sup>3</sup> s<sup>-1</sup> units

Compound	Rate constant	References
Benzene	$7.8 \times 10^9$	Selected [13]
Phenol	$8.4 \times 10^9$	Selected [13]
<i>p</i> -Cresol	$9.2 \times 10^9$	Selected [13]
Aniline	$8.6 \times 10^9$	Selected [13]
Chlorobenzene	$5.6 \times 10^9$	[12]
Nitrobenzene	$3.5 \times 10^9$	Average [13]
Benzoic acid	$1.9 \times 10^9$	[12]
Benzoate ion	$5.9 \times 10^9$	Recommended [17]
17β-estradiol	$5.3 \times 10^9$	[25]
<i>p</i> -Nonylphenol	$1.1 \times 10^{10}$	[26]
Bisphenol	$6.9 \times 10^9$	[27]
Dimethyl-phthalate	$3.4 \times 10^9$	[28]
2,4-Dichlorophenol	$6.0 \times 10^9$	Average [29]
2,4-Dichlorophenoxyacetic acid	$5.5 \times 10^9$	Recommended [29]
Atrazine	$2.4 \times 10^9$	Recommended [29]
Simazine	$2.6 \times 10^9$	Average [29]
Prometon	$2.8 \times 10^9$	Average [29]
Fenuron	$8.3 \times 10^9$	Recommended [29]
Monuron	$7.3 \times 10^9$	[29]
Diuron	$6.0 \times 10^9$	Average [29]
Chloramphenicol	$2.5 \times 10^9$	[30]
Sulfacetamide	$5.3 \times 10^9$	[31]
Sulfamethoxazole	$8.5 \times 10^9$	[32]
Sulfamethazine	$8.3 \times 10^9$	[32]
Penicillin G	$8.1 \times 10^9$	Average [33–35]
Amoxicillin	$7 \times 10^9$	Average [14, 35, 36]
Ampicillin	$7.5 \times 10^9$	Average [33, 36]
Cloxacillin	$7.1 \times 10^9$	Average [33, 36]
Salicylic acid	$1.07 \times 10^{10}$	[37]
Paracetamol	$5.6 \times 10^9$	[38]
Diclofenac	$8.12 \times 10^9$	[39]
Ketoprofen	$4.6 \times 10^9$	[39]
Ibuprofen	$6.1 \times 10^9$	[39]
Acid Red 265	$9.3 \times 10^9$	[40]
Acid Blue 62	$1 \times 10^{10}$	[41]

Due to its electrophilic nature, ·OH reacts readily with C=C and C=N double bonds, but not with C=O double bonds, which are electron-deficient at the carbon atom, where the hydroxyl radical prefer to add. The rate constants of reactions with aromatics (Table 3) are in a narrow range, between  $2 \times 10^9$  mol<sup>-1</sup> dm<sup>3</sup> s<sup>-1</sup> and  $1 \times 10^{10}$  mol<sup>-1</sup> dm<sup>3</sup> s<sup>-1</sup> [13]. These  $k_{\text{OH}}$ s are close to the diffusion controlled limit of  $k_{\text{diff, ·OH}} = 1.1 \times 10^{10}$  mol<sup>-1</sup> dm<sup>3</sup> s<sup>-1</sup> (Table 1). The  $k_{\text{OH}}$ s show some regular

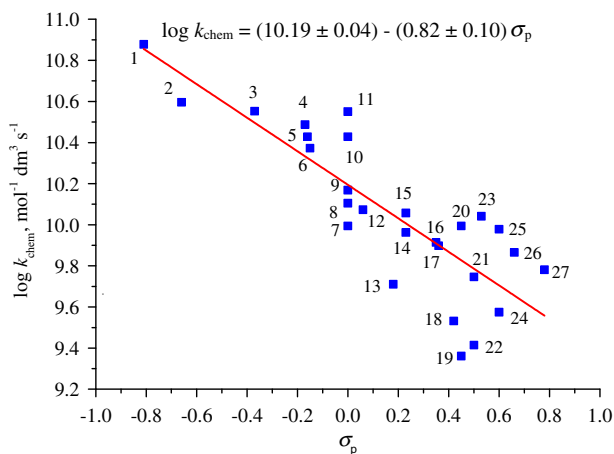
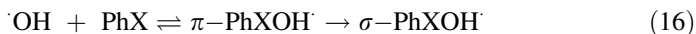


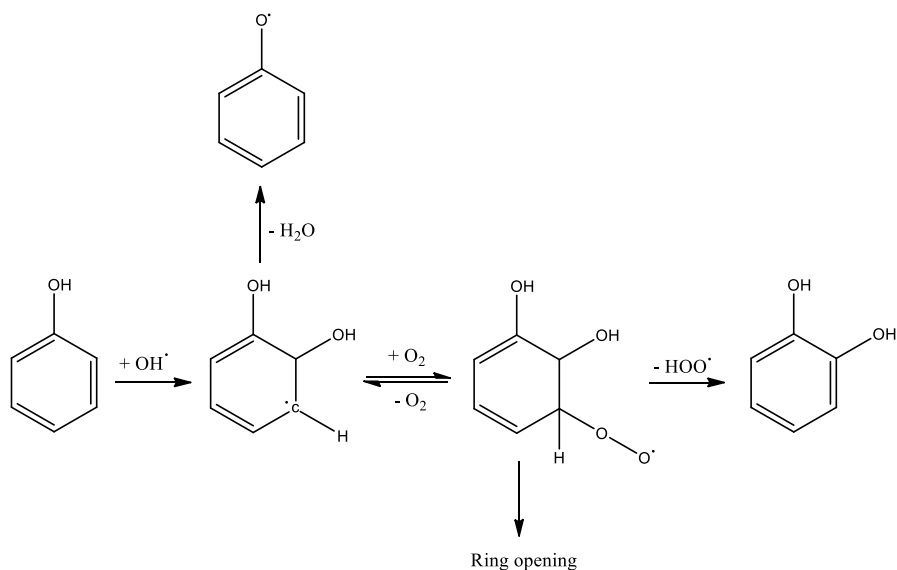
**Fig. 1** Correlation between the  $\log k_{\text{OH}, \text{chem}}$ -values and the  $\sigma_p$  Hammett substituent constants for monosubstituted benzenes {data from Table 3 [corrected for diffusion, (Eq. 8)] and Ref. [13]}: 1. phenoxide, 2. aniline, 3. phenol, 4. toluene, 5. phenylacetate ion, 6. ethylbenzene, isopropylbenzene, 7. acetanilide, 8. benzoic acid ion, 9. phenethylalcohol, 10. benzene, 11. benzyl alcohol, 12. fluorobenzene, 13. iodobenzene, 14. bromobenzene, 15. chlorobenzene, 16. benzenesulfonate ion, 17. benzamide, 18. benzaldehyde, 19. benzoic acid, 20.  $\alpha$ -methylbenzyl-ammonium ion, 21. acetophenone, 22. benzenesulfonic acid, 23. benzylammonium ion, 24. benzenesulfonamide, 25. anilinium ion, 26. benzonitrile, 27. nitrobenzene

trend with the Hammett substituent constants, but the logarithms of the rate constants do not give straight lines as a function of the substituent constants, because the  $k_{\text{OHS}}$  are controlled by both the chemical reactivity and the diffusion. The logarithms of rate constants corrected for diffusion (Eq. 8), however, show linear correlation with  $\sigma_p$  for monosubstituted benzenes (Fig. 1) and *para*-substituted phenols [13]. The negative slope in Fig. 1,  $\rho = -0.82$ , shows electrophilic reaction. The absolute value of  $\rho$  is smaller than that found in  $\text{Cl}_2^-$  ( $-1.5$  [42]) and  $\text{Br}_2^-$  ( $-1.1$  [43]) reaction with aromatic molecules or in  $\text{NH}_2$  ( $-3.3$  [44]) reaction with phenoxide ions. The smaller negative  $\rho$  is due to the low selectivity and high reactivity of  $\text{OH}$ .

As the first step, the reaction between the hydroxyl radical and the aromatic molecule (PhX) leads to the formation of a loosely bound  $\pi$ -complex in a reversible reaction [12]. The complex may dissociate, or transform to a  $\sigma$ -complex (hydroxycyclohexadienyl radical).



In aromatic compounds, electron-donating substituent directs  $\cdot\text{OH}$  into the *ortho*- and *para*-positions; in the case of the electron withdrawing substituents, *meta*-addition is preferred [45, 46]. The regioselectivity of hydroxyl radical addition reaction may occur in the transition from the  $\pi$ -complex to the  $\sigma$ -complex [21]. Addition to the *ipso*-position, presumably due to steric reasons generally has low weight [47]. In the case of phenol, *ipso*-, *ortho*-, *meta*- and *para*-additions take place with probabilities of 0.08, 0.50, 0.08 and 0.34, respectively.



**Scheme 1** Perhydroxyl radical elimination from the peroxy radical in phenol oxidation

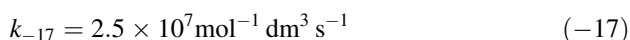
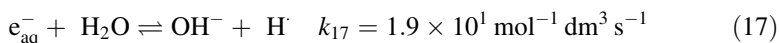
In  $\cdot\text{OH}$  addition to the aromatic ring, a carbon centered hydroxycyclohexadienyl type radical forms; the fate of this radical is determined by the substituents on the ring, on the pH of the solution and also on the dissolved  $\text{O}_2$  concentration. In neutral  $\text{O}_2$ -free solutions, these radicals mainly terminate in slow radical–radical reactions. When the starting molecule is a phenol type compound (Scheme 1), in acid/base catalyzed reactions, water elimination and phenoxyl radical formation is the preferred reaction, especially at low and high pH values [48–50]. Cyclohexadienyl type radicals readily react with dissolved  $\text{O}_2$ , and the rate constants are in the  $1 \times 10^8$ – $1 \times 10^9 \text{ mol}^{-1} \text{ dm}^3 \text{ s}^{-1}$  range [51]. The  $\text{O}_2$  addition is fast and the adduct is relatively stable when there is an electron donating substituent on the ring; the opposite is true for electron withdrawing substituent. It is generally assumed that the ring-opening takes place from a peroxy radical structure [52–54]. Scheme 1 shows *ortho*-addition to phenol and the reaction of the carbon centered hydroxycyclohexadienyl radical with dissolved  $\text{O}_2$ . The  $\text{HO}_2$  elimination from the peroxy radical is in competition with the ring-opening degradation.

The dissolved organic carbon (DOC) uses up a large fraction of available  $\cdot\text{OH}$  in AOP; therefore, several measurements are published for the  $\cdot\text{OH} + \text{DOC}$  reaction. Although the characteristics (average molecular mass, composition, etc.) of DOC of different origin may differ considerably, the rate constants determined fall in a narrow range:  $1.1 \times 10^4$ – $3 \times 10^4 \text{ mgC}^{-1} \text{ dm}^3 \text{ s}^{-1}$ . Westerhoff et al. [5] determined  $k_{\cdot\text{OH}, \text{DOC}}$  of  $1.3 \times 10^4 \text{ mgC}^{-1} \text{ dm}^3 \text{ s}^{-1}$  for the standard fulvic acid from the Suwannee River. Lutze [55] gives a  $k_{\cdot\text{OH}, \text{DOC}}$  of  $1.14 \times 10^4 \text{ mgC}^{-1} \text{ dm}^3 \text{ s}^{-1}$ . The DOC intermediates in pulse radiolysis were formed on the microsecond timescale and decayed on the millisecond timescale [5].



## 2.4 Reactions of the Hydrated Electron and Hydrogen Atom

Hydrogen atom ( $\text{H}^\cdot$ ) and hydrated electron ( $\text{e}_{\text{aq}}^-$ ) compose an acid/base pair with a  $\text{p}K_{\text{a}}$  of 9.1 [6]. Both the forward and the backward reactions (17) and (-17) are relatively slow, and due to the short lifetime of  $\text{e}_{\text{aq}}^-$ , these reactions do not have much importance in pulse radiolysis investigations [56]. In steady-state experiments, however, the  $\text{H}^\cdot \rightarrow \text{e}_{\text{aq}}^-$  conversion may have some effect on the product yields in alkaline solutions:



$\text{e}_{\text{aq}}^-$  is characterized by a strong light absorption band centered at 720 nm and a maximum molar absorption coefficient of  $\sim 20,000 \text{ mol}^{-1} \text{ dm}^3 \text{ cm}^{-1}$ . The majority of the oscillator strength is derived from the optical transitions from the equilibrated s state to a p-like excited state. This very strong transient absorption band is used for the determination of  $\text{e}_{\text{aq}}^-$  reaction rate constants by pulse radiolysis [21].

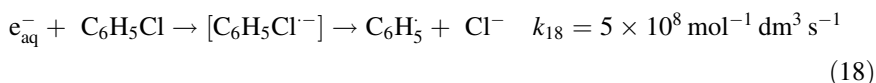
$\text{e}_{\text{aq}}^-$  reactions are generally investigated in the 3.5–9 pH range with an additive that removes  $\cdot\text{OH}$ . For this purpose, mostly 0.1–1  $\text{mol dm}^{-3}$  *tert*-butanol is applied: in such solutions, in reaction (15)  $\cdot\text{OH}$  is converted to  $\cdot\text{CH}_2\text{C}(\text{CH}_3)_2\text{OH}$ , and the latter radical has low reactivity with most of the solutes [57]. This technique is often very useful for pulse radiolysis experiments. It should be emphasized, however, that the *tert*-butanol-derived radicals are not always unreactive with certain substrates on the timescale of  $^{60}\text{Co}$   $\gamma$ -radiolysis experiments, where the lifetime of radicals is several orders of magnitude longer than under pulse radiolysis [58]. Therefore, the disadvantage of *tert*-butanol is that  $\cdot\text{CH}_2\text{C}(\text{CH}_3)_2\text{OH}$  may react with the other radical intermediates present.

In reactions with organic molecules,  $\text{e}_{\text{aq}}^-$  reacts as a nucleophile (standard one-electron reduction potential  $E^0(\text{aq}/\text{e}_{\text{aq}}^-) = 2.9 \text{ V}$ , Table 2). It reacts preferentially with low-lying vacant molecular orbital structures, such as aromatic hydrocarbons, conjugated olefins, carboxyl compounds, and halogenated hydrocarbons [6–10, 57–59]. Its reactivity is greatly enhanced by an electron withdrawing substituent adjacent to the double bonds or attached to the aromatic rings.

$\text{e}_{\text{aq}}^-$  reacts with many compounds that are capable of releasing an anion by dissociative electron capture; these reactions can occur only when single bonds are involved in the process [21]. In a number of reactions that are written as dissociative electron attachment, however, short-lived radical anions are the intermediates. Typically, these reactions take place with halogenated compounds, where the electron ‘scavenging’ at the halogen site is followed by the elimination of the halide ion. The reaction with chlorobenzene is assumed to be a two-step process via an intermediate radical anion [Reaction (18)]. The first step is electron addition to the vacant orbital, bond breakage occurs rapidly and the overall reaction essentially appears as a dissociative electron capture process with elimination of the halide ion  $\text{Cl}^-$  [6, 60]:

**Table 4** Rate constants of hydrated electron reactions in mol<sup>-1</sup> dm<sup>3</sup> s<sup>-1</sup> units

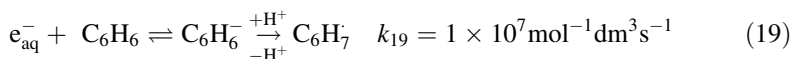
Compound	Rate constant	References
Benzene	1 × 10 <sup>7</sup>	[17]
Phenol	2 × 10 <sup>7</sup>	[17]
Aniline	3 × 10 <sup>7</sup>	[59]
Chlorobenzene	5 × 10 <sup>8</sup>	[60]
Nitrobenzene	3.7 × 10 <sup>10</sup>	[17]
Benzoic acid	7.1 × 10 <sup>9</sup>	[17]
Benzoate ion	3.2 × 10 <sup>9</sup>	[17]
Dimethyl-phthalate	1.6 × 10 <sup>10</sup>	[28]
2,4-Dichlorophenol	5 × 10 <sup>8</sup>	[61]
2,4-Dichlorophenoxyacetic acid	2.5 × 10 <sup>9</sup>	[62]
Atrazine	4.8 × 10 <sup>9</sup>	[63]
Fenuron	~ 1 × 10 <sup>9</sup>	[64]
Diuron	1 × 10 <sup>10</sup>	[65]
Monuron	2.1 × 10 <sup>9</sup>	[66]
Chloramphenicol	2.3 × 10 <sup>10</sup>	[30]
Sulfamethoxazole	1 × 10 <sup>10</sup>	[32]
Sulfamethazine	2.4 × 10 <sup>10</sup>	[32]
Penicillin G	2.7 × 10 <sup>9</sup>	[67]
Amoxicillin	5.2 × 10 <sup>9</sup>	[68]
Ampicillin	5.7 × 10 <sup>9</sup>	[67]
Cloxacillin	7.5 × 10 <sup>9</sup>	[67]
Salicylic acid	9 × 10 <sup>9</sup>	[37]
Paracetamol	5 × 10 <sup>8</sup>	[38]
Diclofenac	1.7 × 10 <sup>9</sup>	[39]
Ketoprofen	2.6 × 10 <sup>10</sup>	[39]
Ibuprofen	8.9 × 10 <sup>9</sup>	[39]
Acid Blue 62	3 × 10 <sup>10</sup>	[41]
Isobutylnaphthalene sulfonate	2.5 × 10 <sup>10</sup>	[69]



Compounds with high electron affinity (e.g., nitro- and cyano-derivatives) react with  $e_{\text{aq}}^-$  with diffusion-controlled rate constants of  $\sim 2.5 \times 10^{10} \text{ mol}^{-1} \text{ dm}^3 \text{ s}^{-1}$  (Tables 1, 4) with formation of the corresponding radical anions. The rate constants with aldehydes and ketones are  $\sim 4 \times 10^9 \text{ mol}^{-1} \text{ dm}^3 \text{ s}^{-1}$ . The electron is accommodated on the carbonyl carbon. The  $e_{\text{aq}}^-$  rate constants for the reactions with carboxylic acids, esters, and amides are in the order of  $\sim 10^7 \text{ mol}^{-1} \text{ dm}^3 \text{ s}^{-1}$  [17]. Simple olefins do not react with  $e_{\text{aq}}^-$  at appreciable rates, but compounds with extended  $\pi$ -electron delocalization react rapidly with the hydrated electron. The  $k_{\text{eaq-}}$  values of maleates and fumarates, which contain conjugated double bonds (e.g.,  $\text{O}=\text{C}(\text{OH})-\text{HC}=\text{CH}-\text{C}(\text{OH})=\text{O}$ ), are in the range of diffusion controlled-limit

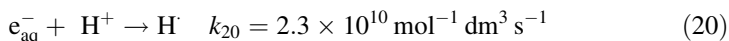
[70, 71]. The radical anion formed protonates instantaneously (Grotthuss mechanism). The protonation reaction results in a carbon-centered radical at the carbonyl.

In reactions with aromatic molecules,  $e_{\text{aq}}^-$  adds to the ring with formation of a radical anion. The rate constant is small ( $\sim 10^7 \text{ mol}^{-1} \text{ dm}^3 \text{ s}^{-1}$ ) in the case of benzene and alkylbenzenes, and the process is reversible;  $e_{\text{aq}}^-$  addition may be followed by a thermally activated dissociation [21]. This dissociation is in competition with the anion protonation, in which cyclohexadienyl radical ( $\text{C}_6\text{H}_7$ ) is produced [Reaction (19)].



$k_{\text{eaq}^-}$  is higher ( $10^8$ – $10^{10} \text{ mol}^{-1} \text{ dm}^3 \text{ s}^{-1}$ ), when an electron withdrawing substituent, such as  $-\text{COOH}$ ,  $-\text{Cl}$ , or  $-\text{NO}_2$  group, is attached to the ring (Table 4). The rate constants of  $e_{\text{aq}}^-$  reaction with benzoic acid, chlorobenzene (electron addition followed by  $\text{Cl}^-$  elimination reaction), and nitrobenzene are  $7.1 \times 10^9$ ,  $5 \times 10^8$  and  $3.7 \times 10^{10} \text{ mol}^{-1} \text{ dm}^3 \text{ s}^{-1}$ , respectively [15, 61].

The H-atom yield in neutral or alkaline solutions is low,  $G = 0.06 \mu\text{mol J}^{-1}$ . In acidic solutions due to the  $e_{\text{aq}}^- \rightarrow \text{H}$  conversion in (20), the yield is high,  $G = 0.34 \mu\text{mol J}^{-1}$ .



Under radiolysis conditions, the reactions of hydrogen atoms are usually investigated in acidic solutions, below pH 3, in order to convert  $e_{\text{aq}}^-$  to H in (20). The  $\cdot\text{OH}$  reactions are eliminated by using *tert*-butanol [Reaction (15)] [57]. The reactivity of H with *tert*-butanol is low ( $1 \times 10^6 \text{ mol}^{-1} \text{ dm}^3 \text{ s}^{-1}$  [72]) and this reaction leaves H largely untouched. When the rate constant with the compound of interest (S) is higher than  $1 \times 10^8 \text{ mol}^{-1} \text{ dm}^3 \text{ s}^{-1}$ , and its concentration is above  $1 \times 10^{-3} \text{ mol dm}^{-3}$ , the presence of *tert*-butanol practically does not influence the H + S reaction.

Alam et al. [73] in their pulse radiolysis experiments investigated the H reactions with several alcohols in  $\text{N}_2\text{O}$  saturated solutions.  $\cdot\text{OH}$  formed in such system with  $0.56 \mu\text{mol J}^{-1}$  yield reacted with the alcohols with rate constants an order of magnitude higher than H. This high difference in rate constants allowed differentiating  $\cdot\text{OH}$  and H reactions. Using this technique in rate constant determination, one is not restricted to work in the acidic pH range.

H and  $\cdot\text{OH}$  do not absorb the light in the usual wavelength range (200–800 nm) of pulse radiolysis studies. In transient measurements, the products of H or  $\cdot\text{OH}$  reaction or competitive techniques are used to determine the rate constants.

H is a slightly less powerful reducing agent than  $e_{\text{aq}}^-$  ( $E^0(\text{H}_{\text{aq}}^+/\text{H}) = 2.4 \text{ V}$  and  $E^0(\text{aq}/e_{\text{aq}}^-) = 2.9 \text{ V}$ ). It reduces metal ions with lower reduction potentials, e.g., transforms  $\text{Cu}^{2+}$  to  $\text{Cu}^+$ . There are two main types of H reactions with most organic molecules: H-atom abstraction (from saturated molecules) and H-atom addition (to the double bonds of unsaturated molecules). If there is a competition between addition and abstraction, addition is preferred [21]. For H reactions, very few rate constants are published compared to  $\cdot\text{OH}$  reactions, and the values are less reliable.

**Table 5** Rate constants of hydrogen atom reactions in mol<sup>-1</sup> dm<sup>3</sup> s<sup>-1</sup> units

Compound	Rate constant	References
Methanol	$1.1 \times 10^6$	[73]
Ethanol	$1.7 \times 10^7$	[73]
<i>tert</i> -Butanol	$1 \times 10^6$	[72]
Benzene	$9.1 \times 10^8$	[17]
Toluene	$2.6 \times 10^9$	[17]
Phenol	$1.7 \times 10^9$	[74]
Benzyl alcohol	$1.1 \times 10^9$	[17]
Aniline	$2.4 \times 10^9$	[17]
Acetanilide	$1 \times 10^9$	[17]
Benzoate ion	$1.1 \times 10^9$	[17]
Benzenesulfonate ion	$7.3 \times 10^8$	[17]
Benzoic acid	$9.2 \times 10^8$	[17]
2,4-dichlorophoxyacetic acid	$1.4 \times 10^9$	[62]
Chloramphenicol	$1 \times 10^9$	[30]
Salicylic acid	$2.3 \times 10^9$	[74]
Ibuprofen	$4 \times 10^9$	[76]

$k_{\text{H}}$ s determined in different laboratories (and eventually by different techniques) may differ by more than a factor of two [17, 74]. In Table 5, the tabulated  $k_{\text{H}}$ -values are mostly averages of several determinations.

The rate constants of H-atom abstraction reactions of H<sup>•</sup> are generally one to three orders of magnitude smaller than those of <sup>•</sup>OH; these abstraction reactions strongly depend on the bond strength in both cases. In the addition reactions, H<sup>•</sup> behaves similarly to <sup>•</sup>OH, i.e., as electrophiles [21, 75]. The rate constants for H<sup>•</sup> addition reactions are also similar to <sup>•</sup>OH reactions, although here <sup>•</sup>OH is also more reactive than H<sup>•</sup>. For aromatics, the  $k_{\text{H}}$ s vary in a narrow range, between  $7 \times 10^8$  and  $3 \times 10^9$  mol<sup>-1</sup> dm<sup>3</sup> s<sup>-1</sup> [17, 74]. The rate constant of H<sup>•</sup> reaction with benzene is  $9.1 \times 10^8$  mol<sup>-1</sup> dm<sup>3</sup> s<sup>-1</sup>. When electron-releasing -OH (in phenol), or -NH<sub>2</sub> (in aniline) group is attached to the benzene ring,  $k_{\text{H}}$  increases to  $1.7 \times 10^9$  and  $2.4 \times 10^9$  mol<sup>-1</sup> dm<sup>3</sup> s<sup>-1</sup>, respectively. However, due to the small number of the published values and the large uncertainty in the data, a clear log  $k_{\text{H}}$ -Hammett substituent constant relation cannot be established. This is in sharp contrast to the <sup>•</sup>OH reactions. In the absence of the necessary data, we do not know anything about the directing effect of the substituent, so we cannot decide whether *ortho-para* (like in electrophiles) or *meta* (nucleophiles) direction takes place in the H<sup>•</sup> + substituted aromatic molecule reactions. In a study of H<sup>•</sup> and <sup>•</sup>OH addition reactions to a large number of acrylate type olefins, a strong correlation was found between the H<sup>•</sup> and <sup>•</sup>OH addition rate constants [75].

H<sup>•</sup> reactions may contribute to pollutant degradation in the acidic pH range. Since in the H<sup>•</sup> + organic molecule reactions and also after protonation in the e<sub>aq</sub><sup>-</sup> + organic molecule reactions [see e.g., Reaction (19)], mainly carbon centered radicals form, which readily react with dissolved O<sub>2</sub>, these reductive radicals also

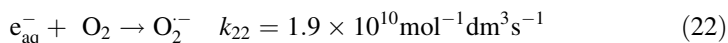
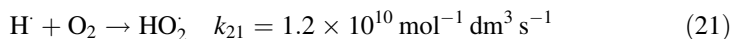
contribute to the oxidation of the organic molecules through the formed organic peroxides [77].

### 3 Reactions of Radicals Formed in Radical Transfer Reactions

Water radiolysis is originally a ‘hybrid’ process: in the primary processes, equal amounts of oxidizing and reducing species form. Due to the ‘natural’ impurities ( $\text{O}_2$ ,  $\text{Cl}^-$ ,  $\text{HCO}_3^-/\text{CO}_3^{2-}$ , etc.), the balance between oxidizing and reducing intermediates changes quickly, mostly in favor of the oxidizing species. In order to enhance the oxidizing capacity, the effects of some additives, like ozone, hydrogen peroxide or persulfate, were also tested in the laboratory or in pilot-plant experiments.

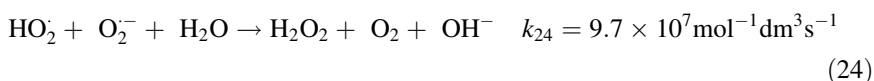
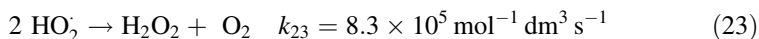
#### 3.1 Reactions in the Presence of Dissolved Oxygen

When irradiation is used for water treatment,  $\text{H}^\cdot$  and  $\text{e}_{\text{aq}}^-$  mostly disappear in reaction with the dissolved  $\text{O}_2$ , with rate constants of  $1.2 \times 10^{10}$  and  $1.9 \times 10^{10} \text{ mol}^{-1} \text{ dm}^3 \text{ s}^{-1}$ , respectively [17]:



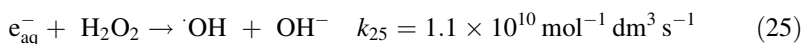
$\text{HO}_2^\cdot$  and  $\text{O}_2^{\cdot-}$  interconvert with a  $\text{p}K_{\text{a}}$  of 4.8 [78]. Due to the high rate constants, the  $\text{H}^\cdot$  and  $\text{e}_{\text{aq}}^-$  scavenging capacities ( $k[\text{S}]$ , where  $[\text{S}]$  represents  $\text{O}_2$  concentration,  $2.8 \times 10^{-4} \text{ mol dm}^{-3}$  at  $20^\circ\text{C}$ ), are high at  $3.4 \times 10^6$  and  $5.3 \times 10^6 \text{ s}^{-1}$ , respectively. Any solute can compete with the  $\text{H}^\cdot + \text{O}_2$  and  $\text{e}_{\text{aq}}^- + \text{O}_2$  reactions if the scavenging capacity calculated for the dissolved compound is in this range. With a diffusion controlled rate constant of  $\sim 10^{10} \text{ mol}^{-1} \text{ dm}^3 \text{ s}^{-1}$ , it requires a solute concentration of  $\sim 10^{-4} \text{ mol dm}^{-3}$ . Since this is a high concentration for environmental water samples,  $\text{H}^\cdot$  and  $\text{e}_{\text{aq}}^-$  reactions rarely play a determining role in micropollutant degradation. However, at relatively high solute concentrations, and at very high dose rates (electron beam irradiation) when considerable  $\text{O}_2$  depletion occurs, the  $\text{H}^\cdot$  and  $\text{e}_{\text{aq}}^-$  reactions may not be negligible.

$\text{O}_2^{\cdot-}$  is a weak reductant, while  $\text{HO}_2^\cdot$  is a moderate oxidant (Table 2). Unlike  $\cdot\text{OH}$ ,  $\text{O}_2^{\cdot-}$  and  $\text{HO}_2^\cdot$  may not directly contribute to the degradation of organic pollutants [78]. In the absence of suitable reaction partners,  $\text{O}_2^{\cdot-}$  and  $\text{HO}_2^\cdot$  disappear from the solution in slow radical–radical reactions giving  $\text{H}_2\text{O}_2$ ; in neutral solutions, the cross-reaction (24) dominates:



### 3.2 Reactions in the Presence of Hydrogen Peroxide

In aerated solutions, hydrogen peroxide is produced in the reactions of  $O_2^-/HO_2^-$  pair with relatively large yield. Under certain conditions,  $H_2O_2$  can be involved in reactions with the reactive intermediates generating species that can considerably influence the degradation of chemical pollutants. However, its effect on the degradation mechanism is usually neglected, and only a few publications mention the possible role of  $H_2O_2$  in the degradation [79, 80]. In gamma radiolysis experiments conducted in the presence of dissolved  $O_2$  in purified water,  $H_2O_2$  forms with a yield of  $0.3 \mu\text{mol J}^{-1}$ . At doses  $> 1 \text{ kGy}$ , the  $H_2O_2$  concentration-dose curve reaches a plateau due to the competition between formation and decomposition.  $H_2O_2$  in (25) transforms the reductive  $e_{\text{aq}}^-$  to the oxidizing  $\cdot\text{OH}$ .



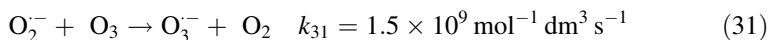
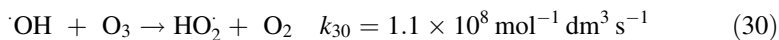
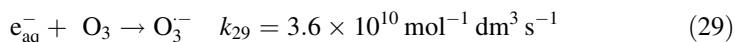
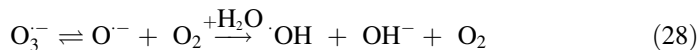
In real water treatment scenarios, in the presence of traces of transition metal ions,  $H_2O_2$  is expected to disappear in Fenton-like reactions. In experiments when a few times  $10^{-3} \text{ mol dm}^{-3}$   $H_2O_2$  was introduced into the solution to be irradiated, considerable increases in the degradation rates were found [80].

### 3.3 Reactions in the Presence of Ozone

Ozonization is a commonly employed method for the treatment of waters and wastewaters (e.g., to improve quality of drinking water or as a pre-treatment step to biodegradation).  $O_3$  reacts with dissolved organic molecules with two basically different reaction mechanisms: it may react directly with the solute molecules or through its decomposition products. In direct reaction, addition to double bonds, insertion into  $\sigma$  bonds, oxygen atom transfer, charge transfer, or hydrogen atom abstraction can take place. The latter reaction is characteristic to molecules in which the electron withdrawing groups decrease the C-H bond strength (aldehydes, acids, amines). The rate constants of the  $O_3 +$  organic molecule reactions vary between many orders of magnitude ( $10^{-2}$ – $10^8 \text{ mol}^{-1} \text{ dm}^3 \text{ s}^{-1}$ ). In the case of aromatic molecules, electron donating substituent increases, and electron withdrawing substituent decreases the rate constant [81].

In the presence of ozone/oxygen, the primary water radiolysis intermediates,  $H\cdot$  and  $e_{\text{aq}}^-$ , react quickly with  $O_3$  with rate constants in the  $10^{10} \text{ mol}^{-1} \text{ dm}^3 \text{ s}^{-1}$  range. The rate constant of the  $\cdot\text{OH} + O_3$  reaction is  $1.1 \times 10^8 \text{ mol}^{-1} \text{ dm}^3 \text{ s}^{-1}$  [17]. The reactions involving dissolved  $O_3$  result in reactive intermediates, among which is the highly oxidizing  $\cdot\text{OH}$  [82–84]. The injection of  $O_3$  before or during irradiation converts the reducing species of water radiolysis into the key intermediate, i.e., the ozonide radical anion ( $O_3^-$ ), responsible for enhancing the  $\cdot\text{OH}$  yield in this system. Here a simplified reaction mechanism is shown [85, 86]:



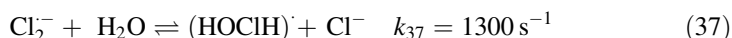
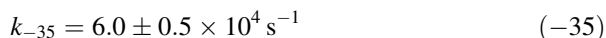
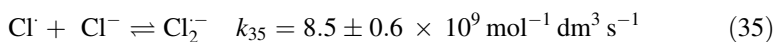
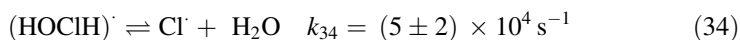
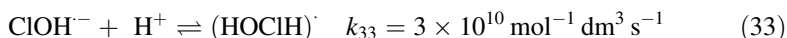
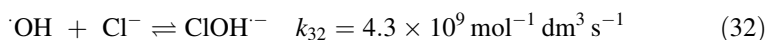


As a consequence of these reactions, almost all of the radiation energy is now used for  $\cdot\text{OH}$  generation, resulting in great enhancement of the degradation rate, as was demonstrated in laboratory and pilot plant experiments [83, 87].

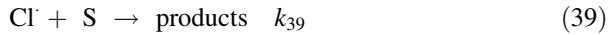
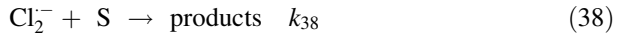
### 3.4 Reactions of the Chloride Atom and Dichloride Radical Anion

$\cdot\text{OH}$  reacts in fast reaction with  $\text{Cl}^-$  ions forming  $\text{ClOH}^{\cdot-}$  complex (Reaction 32), with an equilibrium constant of  $0.70 \pm 0.13 \text{ mol}^{-1} \text{ dm}^3$ . In acidic media (below pH 5–6),  $\text{ClOH}^{\cdot-}$  may transform to  $\text{Cl}^{\cdot}$  [Reaction (34)].  $\text{Cl}^{\cdot}$  is a strong oxidant that can react directly with dissolved organic material ( $E^0(\text{Cl}^{\cdot}/\text{Cl}^-) = 2.6 \text{ V}$ ). However, in rapid complexation (35) with  $\text{Cl}^-$ ,  $\text{Cl}^{\cdot}$  may transform to the dichloride radical anion ( $\text{Cl}_2^{\cdot-}$ ).  $\text{Cl}_2^{\cdot-}$  is also a strong oxidant with standard one-electron reduction potential of  $E^0(\text{Cl}_2^{\cdot-}/2 \text{ Cl}^-) = 2.1 \text{ V}$  [42].

The reactions of  $\text{Cl}_2^{\cdot-}$  are often investigated in  $\text{N}_2\text{O}$ -saturated solutions at high  $\text{Cl}^-$  concentration relative to the compound of interest (S), where most of  $\cdot\text{OH}$  are scavenged by  $\text{Cl}^-$ , forming  $\text{Cl}_2^{\cdot-}$ . The pH of the solution is adjusted to the acidic range (pH 2–4) to ensure the efficient formation of  $\text{Cl}_2^{\cdot-}$ . Manifold reactions proceed in such a system [17, 88].



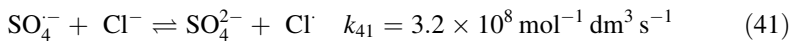
$$k_{-37} = (8 \pm 2) \times 10^9 \text{ mol}^{-1} \text{ dm}^3 \text{ s}^{-1} \quad (-37)$$



$\text{Cl}_2^-$  has an absorption maximum at 340 nm with  $\varepsilon_{340} = 9600 \text{ mol}^{-1} \text{ dm}^3 \text{ cm}^{-1}$ , the absorbance of  $\text{Cl}^\cdot$  is negligible at this wavelength (albeit  $\varepsilon_{340 \text{ nm}}$  is relatively high,  $3800 \text{ mol}^{-1} \text{ dm}^3 \text{ cm}^{-1}$ , the  $\text{Cl}^\cdot$  concentration in equilibrium is very low). When a compound of interest is present in the system (S), the decay of the 340-nm band obeys first-order kinetics. In laboratory experiments, at the usual  $\text{Cl}^-$  concentration ( $0.1\text{--}1 \text{ mol dm}^{-3}$ ), equilibrium (35) is assumed to be attained. If so,  $k_{\text{obs}}$  (the decay rate constant of the 340-nm band) can be expressed as (40) when  $k_{35}[\text{Cl}^-] + k_{35} \gg (k_{38} + k_{39})[\text{S}] + k_{37} + k_{-34}$  and  $K[\text{Cl}^-] \gg 1$  (for obtaining the exact rate law and derivation of (40), we refer to Buxton et al. [89]):

$$k_{\text{obs}} = k_{37} + k_{-34}/(K[\text{Cl}^-]) + \{(k_{39}/(K[\text{Cl}^-])) + k_{38}\}[\text{S}] \quad (40)$$

In the  $\cdot\text{OH} + \text{Cl}^-$  system, at sufficiently high  $\text{Cl}^-$  concentration in the acidic pH range the  $\text{Cl}_2^-$  species dominates, and in the neutral or alkaline pH range the  $\cdot\text{OH}$  dominates [90, 91]. In laboratory radiolysis experiments, in the neutral or alkaline pH ranges, the  $\text{Cl}^\cdot/\text{Cl}_2^-$  species can also be produced in reactions with sulfate radical anions:



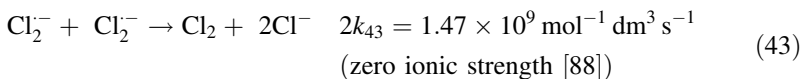
$$k_{-41} = 2.5 \times 10^8 \text{ mol}^{-1} \text{ dm}^3 \text{ s}^{-1} \quad (-41)$$

When  $\text{Cl}_2^-$  is produced in the  $\text{SO}_4^{\cdot-} + \text{Cl}^-$  reaction, the absorbance of  $\text{SO}_4^{\cdot-}$  slightly disturbs the observation of the  $\text{Cl}_2^-$  intermediate in pulse radiolysis, and  $\text{SO}_4^{\cdot-}$  has also a wide absorption band with  $\lambda_{\text{max}} = 450 \text{ nm}$  and  $\varepsilon_{450 \text{ nm}} = 1630 \pm 180 \text{ mol}^{-1} \text{ dm}^3 \text{ cm}^{-1}$  [91].

Under the usual experimental conditions in aqueous solutions, it is rather complicated to study the  $\text{Cl}^\cdot$  reactions [90, 92] due to the rapid complexation reaction (35). For this purpose, photolysis of  $\text{Cl}_2$  is recommended in  $\text{Cl}^-$  free systems.

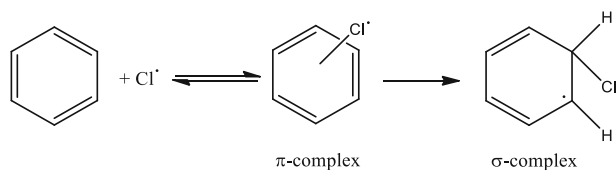


In purified water, in the absence of suitable reactants,  $\text{Cl}_2^-$  may disappear from the solution in disproportionation reaction:



The reaction of  $\text{Cl}^\cdot$  with benzene takes place with a rate constant of  $\sim 1 \times 10^{10} \text{ mol}^{-1} \text{ dm}^3 \text{ s}^{-1}$  [92]. It is assumed in the first step to produce  $\pi$ -complex that may transform to  $\sigma$ -complex (chlorocyclohexadienyl radical). This reaction and the transformation of the  $\pi$ -complex to the  $\sigma$ -complex was investigated several times in



**Scheme 2**  $\text{Cl}^\cdot$  reaction with benzene**Table 6** Rate constants of  $\text{Cl}_2^-$  reactions with organic molecules in  $\text{mol}^{-1} \text{dm}^3 \text{s}^{-1}$  units

Compound	Rate constant	References
Methanol	$3.5 \times 10^3$	[42]
Ethanol	$4.5 \times 10^4$	[42]
2-Propanol	$1.2 \times 10^5$	[42]
Acetic acid	$<10^4$	[42]
Fumaric acid	$1.2 \times 10^5$	[93]
Fumaric acid, monoanion	$2.0 \times 10^6$	[93]
Fumaric acid, dianion	$4.5 \times 10^6$	[93]
Maleic acid	$1.7 \times 10^6$	[93]
Maleic acid, monoion	$1.25 \times 10^6$	[93]
Maleic acid, dianion	$3.4 \times 10^6$	[93]
Benzene	$<10^5$	[92]
Benzenesulfonic acid	$<10^5$	[23]
Benzonitrile	$<10^5$	[42]
Benzoic acid	$2 \times 10^6$	[42]
Phenol	$2.8 \times 10^8$	[42]
Aniline	$1.2 \times 10^7$	[42]
Acetanilide	$\sim 2 \times 10^7$	[42]
Salicylic acid	$1.1 \times 10^8$	[42]
Pinene	$1.7 \times 10^8$	[94]

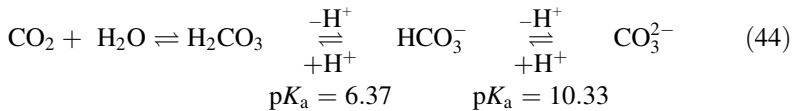
organic phases. In aqueous system, the transformation is too fast to observe the  $\pi$ -complex directly by the usual experimental techniques (Scheme 2).

The rate constants of  $\text{Cl}_2^-$  reactions with organic molecules are much smaller than the diffusion controlled limit of c.a.  $7.3 \times 10^9 \text{ mol}^{-1} \text{dm}^3 \text{s}^{-1}$  (Table 1).  $\text{Cl}_2^-$  can abstract an H-atom from aliphatic compounds (see methanol, ethanol, 2-propanol in Table 6) with rate constants between  $10^3$  and  $10^5 \text{ mol}^{-1} \text{dm}^3 \text{s}^{-1}$  [18]. Olefinic compounds react with  $\text{Cl}_2^-$  by three orders of magnitude more rapidly than the saturated analogues [42]. The reaction with olefins occurs with Cl-addition and the  $k_{\text{Cl}_2^-}$ s are in the  $10^5$ – $10^8 \text{ mol}^{-1} \text{dm}^3 \text{s}^{-1}$  range. Addition to the aromatic ring may also take place with  $k_{\text{Cl}_2^-}$  of  $\leq 10^7 \text{ mol}^{-1} \text{dm}^3 \text{s}^{-1}$ , but the direct oxidation of the aromatic ring by electron transfer seems to be the predominant pathway, and electron-donating functional groups such as  $-\text{OH}$ ,  $-\text{OCH}_3$  or  $-\text{NH}_2$  on the aromatic ring enhance the rate of oxidation.

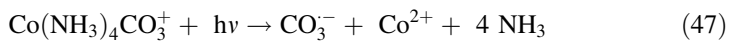
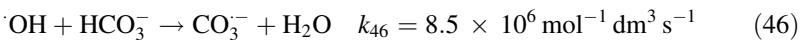
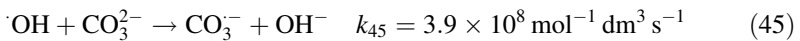
In the  $\text{Cl}_2^-$  + phenol reaction, chlorinated phenols were observed among the final products. The formation of these highly poisonous compounds underlines the importance of studying  $\text{Cl}_2^-$  reactions.

### 3.5 Reactions of the Carbonate Radical Anion

The  $\text{p}K_a$  of the bicarbonate/carbonate transition is at 10.33; in the neutral or slightly alkaline solution, the bicarbonate ion dominates.

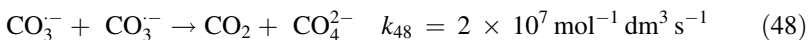


In  $\cdot\text{OH}$  reactions with  $\text{CO}_3^{2-}$  and  $\text{HCO}_3^-$ , carbonate radical anion forms ( $\text{CO}_3^{\cdot-}$ ) [95]. The reactions with these species (45, 46) generally strongly reduce the amount of  $\cdot\text{OH}$  reacting with the target organic molecules.

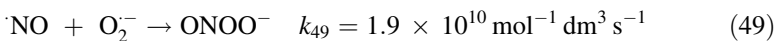


In laboratory experiments, the carbonate radical anion can also be produced according to Reaction (47), in 254 nm photolysis of cobalt(III)-tetraaminocarbonate ion ( $\text{Co}(\text{NH}_3)_4\text{CO}_3^+$ ) [96, 97]. Canonica et al. [98] suggested the reaction of photogenerated triplet aromatic ketones with carbonate ions to produce the carbonate radical anion. This photosensitization reaction may have a significant role in the production of  $\text{CO}_3^{\cdot-}$  in aquatic environment.

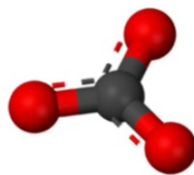
The carbonate radical anion is present in sunlit surface waters [3, 98].  $\text{CO}_3^{\cdot-}$  is a more selective oxidant than  $\cdot\text{OH}$  [99], and its self-termination reaction (48) is relatively slow [100], leading to one or two orders of magnitude higher steady-state concentrations compared to  $\cdot\text{OH}$ . The concentration of  $\text{CO}_3^{\cdot-}$  will be a function of hydroxyl radical production rates, and the relative proportion of scavenging by DOC or carbonate/bicarbonate. The rate constant of carbonate radical anion reaction with the dissolved organic matter is two orders of magnitude lower than that of the  $\cdot\text{OH}$  reaction ( $(280 \pm 80) \text{ mgC dm}^3 \text{ s}^{-1}$ , Svannee River fulvic acid [98]).



$\text{CO}_3^{\cdot-}$  has received much attention as a possible intracellular oxidant, because it is formed efficiently under physiological conditions, e.g., by reaction of peroxyxynitrite ( $\text{OONO}^-/\text{HOONO}$ ,  $\text{p}K_a = 6.6$ ) with carbon dioxide [3, 101, 102]:

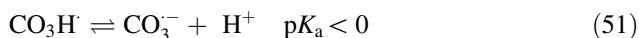


**Scheme 3** The suggested structure of  $\text{CO}_3^{\cdot-}$



The carbonate radical anion is also a strong one-electron oxidant: the relevant redox pair is the carbonate radical anion/bicarbonate anion (Table 2). The one-electron reduction potential of the pair is  $E^0(\text{CO}_3^{\cdot-}, \text{H}^+/\text{HCO}_3^-)$  1.78 V vs. NHE at pH 7.  $\text{CO}_3^{\cdot-}$  has a  $\text{C}_{2v}$  planar structure with the unpaired electron highly centered in the oxygen 2p orbital (Scheme 3) [101].

By analogy to the carbonate and bicarbonate anions,  $\text{CO}_3^{\cdot-}$  was believed to undergo protonation in the neutral pH range. Although the  $\text{p}K_a$  value of the carbonate radical anion has remained under discussion for many years, pulse radiolysis studies of Czapski et al. published in 1999 [100], have established that it is a very strong acid: the  $\text{p}K_a$  of the radical is suggested to be below zero. Therefore,  $\text{CO}_3^{\cdot-}$  is the only relevant carbonate radical species to be considered in most aquatic chemistry applications [98]:



The  $\text{CO}_3^{\cdot-}$  exhibits a broad transient absorption spectrum in the visible wavelength range with  $\lambda_{\text{max}}$  at 600 nm,  $\epsilon_{\text{max}} = 1860 \text{ mol}^{-1} \text{ dm}^3 \text{ cm}^{-1}$  [18]. In pulse radiolysis and photolysis,  $\text{CO}_3^{\cdot-}$  is produced in reactions (46) and (47), respectively, and the decay of the 600 nm band is used for rate constant determination. In competition kinetics system, Huang [3] employed three kinds of competition by *N,N*-dimethylaniline (DMA), *p*-chloroaniline (PCA) and *p*-nitroaniline (PNA), and their concentration was monitored by HPLC. The rate constants of  $\text{CO}_3^{\cdot-}$  to competitors are  $1.6 \times 10^9$ ,  $4.3 \times 10^8$ , and  $7.3 \times 10^7 \text{ mol}^{-1} \text{ dm}^3 \text{ s}^{-1}$  for DMA, PCA and PNA, respectively [17]. These competitors can be used to measure  $k_{\text{CO}_3^{\cdot-}}$  of probes to carbonate radical in the range of  $10^5$ – $10^{10} \text{ mol}^{-1} \text{ dm}^3 \text{ s}^{-1}$  [3].

$\text{CO}_3^{\cdot-}$  reacts more slowly with organic molecules than with  $\cdot\text{OH}$  [17, 18, 111]. The rate constants were found to be in the  $10^2$ – $10^9 \text{ mol}^{-1} \text{ dm}^3 \text{ s}^{-1}$  range (Table 7). The largest values are smaller by a factor of two to five than the diffusion limited rate constant ( $k_{\text{diff}} \approx 7.3 \times 10^9 \text{ mol}^{-1} \text{ dm}^3 \text{ s}^{-1}$ , Table 1). In some cases, the  $k_{\text{CO}_3^{\cdot-}}$ s determined in different laboratories for the same compound differ considerably, e.g., for benzene, values of  $3 \times 10^3$  and  $3.2 \times 10^5 \text{ mol}^{-1} \text{ dm}^3 \text{ s}^{-1}$  are published by Chen et al. [103] and Umschlag and Herrmann [104], respectively. At the same time, these authors gave similar values for toluene,  $4.3 \times 10^4$  and  $6.8 \times 10^4 \text{ mol}^{-1} \text{ dm}^3 \text{ s}^{-1}$ . All five values published for aniline are very close to each other, with an average of  $(6.5 \pm 0.7) \times 10^8 \text{ mol}^{-1} \text{ dm}^3 \text{ s}^{-1}$  [98, 103, 107, 109, 110]. In pH dependence studies, Chen et al. [103] observed an order of magnitude increase in  $k_{\text{CO}_3^{\cdot-}}$  when the pH passed through the  $\text{p}K_a$  of phenol (10.2).

Most  $\text{CO}_3^{\cdot-}$  reactions are oxidations by both electron transfer and hydrogen abstraction mechanisms that produce radicals from the targets [112]. Oxygen ( $\text{O}^-$ )

**Table 7** Rate constants of  $\text{CO}_3^{\cdot-}$  reactions with organic molecules in  $\text{mol}^{-1} \text{ dm}^3 \text{ s}^{-1}$  units

Compound	Rate constant	References
Methanol	$5.0 \times 10^3$	[99]
Ethanol	$2.0 \times 10^4$	[99]
Isopropanol	$5.0 \times 10^4$	[99]
Benzene	$3.0 \times 10^3$ ; $3.2 \times 10^5$	[103, 104]
Toluene	$5.6 \times 10^4$	Average [103, 104]
Chlorobenzene	$(2.7 \pm 0.6) \times 10^5$	[104]
Phenol	$5.9 \times 10^6$ ; $1.2 \times 10^8$ (pH 9)	[103, 3]
Phenoxide	$5.0 \times 10^7$ ; $2.7 \times 10^6$ ; $4.7 \times 10^8$ ; $3.3 \times 10^8$ ; $2.4 \times 10^8$	[103, 105, 106, 107], [108]
Aniline	$(6.5 \pm 0.7) \times 10^8$	Average [98, 103, 107, 109, 110]
<i>N,N</i> - Dimethylaniline	$1.6 \times 10^9$	Average [103, 107]
Nitrobenzene	$1.4 \times 10^4$	[104]
Benzonitrile	$<1.3 \times 10^2$	[104]
Methionine	$1.2 \times 10^8$	[105]
Fenuron	$5.4 \times 10^6$	[98]
Monuron	$1.5 \times 10^7$	[98]
Diuron	$8.3 \times 10^6$	[98]
Atrazine	$3.8 \times 10^6$	Average [98, 110]

transfer reaction is reported to occur when  $\text{CO}_3^{\cdot-}$  reacts with itself [Reaction (48)] or with another radical. The rate constants for H-abstraction are generally low (alcohols, primary amines, thiols), e.g., for ethanol  $k_{\text{CO}_3^{\cdot-}} = 2.0 \times 10^4 \text{ mol}^{-1} \text{ dm}^3 \text{ s}^{-1}$ . They decrease with C-H bond strength, and increase as the number of reactive bonds increases [99].

The rates of reactions with aromatic compounds show a correlation with the Hammett substituent constants with a negative  $\rho$  value [103, 108, 113]. Based on this observation, using the analogy of  $\cdot\text{OH}$  reactions,  $\text{CO}_3^{\cdot-}$  addition to the aromatic ring was suggested as the rate determining step in the overall reaction [101]. The addition complexes, however, are very unstable and decay too fast to be observed [108, 112].

Carbonate radical as a selective oxidant readily reacts with electron rich aromatic phenols and anilines [114]. According to the suggestion of Huie et al. [105], phenol oxidations generally take place thorough the abstraction of the phenolic H-atom, and the phenolates react via intermediate adduct formation. In the case of anilines, the rate-determining step is the removal of an electron by  $\text{CO}_3^{\cdot-}$ , that electron most likely being one of those associated with the basic nitrogen atom, to produce the nitrogen centered radical cation and CO [109, 114]. The formed radical can be stabilized through conjugation. During flash photolysis, a transient absorption observed was attributed to anilino radical [109].  $\text{CO}_3^{\cdot-}$  was also found to be capable of the one-electron oxidation of several amino acids and proteins [115].

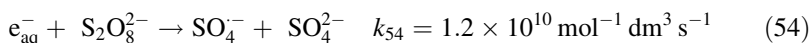
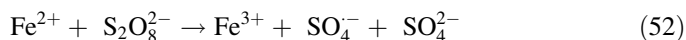
Although the second order rate constants are low for simple aliphatic molecules ( $k < 10^5 \text{ mol}^{-1} \text{ dm}^3 \text{ s}^{-1}$ ), they are higher ( $k = 10^6\text{--}10^7 \text{ mol}^{-1} \text{ dm}^3 \text{ s}^{-1}$ ) for sulfur compounds such as methionine [105, 113]. The proposed mechanism involves abstraction of an electron on sulfur to form a radical cation, which is then oxidized by dissolved  $\text{O}_2$  to sulfoxide ( $\text{R}_1\text{-S(O)-R}_2$ ) [3]. The other possibility is  $\text{CO}_3^{\cdot-}$  addition to the sulfur, producing the corresponding perthyl radical and then the thyl radical cation.

In surface waters, carbonate radical reactions may be a significant means of transformation of pollutants whose rate constants with  $\text{CO}_3^{\cdot-}$  are above  $5 \times 10^6\text{--}1 \times 10^7 \text{ mol}^{-1} \text{ dm}^3 \text{ s}^{-1}$  [98].  $\text{CO}_3^{\cdot-}$  is assumed to play an important role by limiting the persistence of sulfur-containing compounds, reactive pesticides, pharmaceuticals, etc., given the higher steady-state concentration.

### 3.6 Reactions of the Sulfate Radical Anion

In a number of publications,  $\text{SO}_4^{\cdot-}$ , the sulfate radical anion ( $E^\circ(\text{SO}_4^{\cdot-}/\text{SO}_4^{2-}) = 2.43 \text{ V vs. NHE}$ ) is considered as a strong oxidant in water treatment [55, 116–119].  $\text{SO}_4^{\cdot-}$  has some unique features, such as being a very strong electron acceptor enabling the degradation of recalcitrant compounds that are refractory to  $\cdot\text{OH}$ . One example is perfluorinated carboxylic acids, which can slowly be degraded by  $\text{SO}_4^{\cdot-}$ , but persist in other AOPs. This indicates that  $\text{SO}_4^{\cdot-}$ -based oxidation may complement more common ( $\cdot\text{OH}$ -based) AOPs.

$\text{SO}_4^{\cdot-}$  may be produced in thermal, chemical, photochemical or radiation chemical reactions of persulfate. In the chemical generation, transition metal ions are used for the transformation of persulfate to sulfate radical anion; the reaction with  $\text{Fe}^{2+}$  is shown in (52).



The photochemical generation [Reaction (53)] is based on the 254 nm line of the low-pressure mercury lamp. For thermal generation, elevated temperature at about  $60 \text{ }^\circ\text{C}$  is needed. In radiation chemistry (54), the  $e_{\text{aq}}^-$  of water radiolysis is used for persulfate activation [18].

The persulfate concentrations in scientific investigations are generally in the  $10^{-3} \text{ mol dm}^{-3}$  range. In radiolysis studies, when the aim is to clarify the details of sulfate radical reactions, mostly *tert*-butanol is used to eliminate the  $\cdot\text{OH}$  reactions. ( $\text{SO}_4^{\cdot-}$  reacts with *tert*-butanol with a rate constant of  $4.0\text{--}8.4 \times 10^5 \text{ mol}^{-1} \text{ dm}^3 \text{ s}^{-1}$  [18]). In pulse radiolysis [14] and pulse photolysis [120, 121] the decay of the unstructured  $\text{SO}_4^{\cdot-}$  band ( $\lambda_{\text{max}} = 450 \text{ nm}$  and  $\varepsilon_{\text{max}} = 1630 \text{ mol}^{-1} \text{ dm}^3 \text{ cm}^{-1}$ ) is utilized in the determination of rate constants of reactions with dissolved compounds. In competitive experiments, the relative value is converted to absolute

**Table 8** Rate constants of  $\text{SO}_4^{\cdot-}$  reactions with organic molecules in  $\text{mol}^{-1} \text{dm}^3 \text{s}^{-1}$  units

Compound	Rate constant	References
Benzene	$2.4 \times 10^9$	[122]
Toluene	$3.1 \times 10^9$	[123]
Phenol	$6.2 \times 10^9$	[124]
o-Cresol	$3.4 \times 10^9$ ; $6.8 \times 10^9$	[125]; [124]
m-Cresol	$3.8 \times 10^9$ ; $7.0 \times 10^9$	[125]; [124]
p-Cresol	$6.1 \times 10^9$ ; $5.8 \times 10^9$	[125]; [124]
Benzaldehyde	$7.1 \times 10^8$	[126]
Acetophenone	$1.8 \times 10^9$	[126]
Anisole	$4.9 \times 10^9$	[127]
Benzoic acid	$1.2 \times 10^9$	[128]
Fluorobenzene	$9.8 \times 10^8$	[123]
Chlorobenzene	$1.5 \times 10^9$	[129]
Bromobenzene	$1.8 \times 10^9$	[129]
Iodobenzene	$9 \times 10^7$	[130]
Acetanilide	$3.6 \times 10^9$	[128]
Benzamide	$1.9 \times 10^8$	[128]
Benzonitrile	$1.2 \times 10^8$	[128]
Nitrobenzene	$\leq 10^6$	[128]
Gallic acid	$6.3 \times 10^8$	[119]
Gallate ion	$2.9 \times 10^9$	[119]
$\alpha$ -Pinene	$1.2 \times 10^9$	[122]

one by using the  $k_{\text{SO}_4^{\cdot-}}$  of competitor, e.g., benzene, established in direct measurement [122].

For  $\text{SO}_4^{\cdot-}$  reactions, fewer rate constants are published in the literature compared to for  $\cdot\text{OH}$  reactions. In Table 8, there are only a few compounds for which several groups published  $k_{\text{SO}_4^{\cdot-}}$ . Therefore, it is difficult to judge the reliability of the determined values.

The kinetics of most  $\cdot\text{OH}$  addition reactions are close to diffusion controlled, whereas in H-abstraction, the rate constants are lower and the kinetics depend on the bond dissociation energy of the corresponding H-bond.  $\text{SO}_4^{\cdot-}$ , compared to  $\cdot\text{OH}$ , reacts more selectively in all of its reactions [18]. H-abstraction of  $\text{SO}_4^{\cdot-}$  is mostly slower compared to reactions with  $\cdot\text{OH}$ , and the dependency on the bond dissociation energy is much more pronounced [55]. The  $\text{SO}_4^{\cdot-}$  reaction rate constants of H-abstraction (e.g., reaction with saturated organic acids or alcohols) are typically in the  $10^7$ – $10^8 \text{ mol}^{-1} \text{dm}^3 \text{s}^{-1}$  range [18].

The rate constants of  $\cdot\text{OH}$  reactions with aromatic molecules are in a relatively narrow range, between  $2 \times 10^9$  and  $1 \times 10^{10} \text{ mol}^{-1} \text{dm}^3 \text{s}^{-1}$  [13, 29]. The range for  $\text{SO}_4^{\cdot-}$  reactions is much wider; most of the rate constants in Table 8 are between  $10^8$  and  $10^9 \text{ mol}^{-1} \text{dm}^3 \text{s}^{-1}$ . Only a few values are below this range. The lack of larger number of low values may also be due to technical reasons: by pulse radiolysis technique, it is rather difficult to measure values below  $10^7 \text{ mol}^{-1} \text{dm}^3 \text{s}^{-1}$ . Because

the rate constants for the compound of interest and for the competitor should be in the same order of magnitude, it is also difficult to measure low rate constants using competitive techniques.

The rate constant of the  $\text{SO}_4^{\cdot-}$  + benzene reaction is published as  $2.4 \times 10^9$  and  $3.0 \times 10^9 \text{ mol}^{-1} \text{ dm}^3 \text{ s}^{-1}$  based on competitive [122] and pulse radiolysis measurements [128], respectively. When there is an electron releasing substituent on the ring, the rate constant is expected to be higher. For toluene, Merga et al. [123] published  $3.1 \times 10^9 \text{ mol}^{-1} \text{ dm}^3 \text{ s}^{-1}$ . In the case of phenol,  $k_{\text{SO}_4^{\cdot-}}$  is definitively higher,  $6.2 \times 10^9 \text{ mol}^{-1} \text{ dm}^3 \text{ s}^{-1}$  [124], than for benzene. For cresols, the rate constants are in the  $3.4 \times 10^9$ – $7.0 \times 10^9 \text{ mol}^{-1} \text{ dm}^3 \text{ s}^{-1}$  range [124, 125]. The  $k_{\text{SO}_4^{\cdot-}}$  of anisole also shows an increase to  $4.9 \times 10^9 \text{ mol}^{-1} \text{ dm}^3 \text{ s}^{-1}$  [127], as compared to the rate constant for benzene.

Contrary to an electron donating substituent, an electron withdrawing substituent decreases the rate constant as compared to that of benzene: for benzaldehyde and acetophenone, Sharma et al. [126] determined values of  $7.1 \times 10^8$  and  $1.8 \times 10^9 \text{ mol}^{-1} \text{ dm}^3 \text{ s}^{-1}$ , respectively. For benzoic acid, benzamide and benzonitrile, Neta et al. [128] measured values of  $1.2 \times 10^9$ ,  $1.9 \times 10^8$  and  $1.2 \times 10^8 \text{ mol}^{-1} \text{ dm}^3 \text{ s}^{-1}$ , respectively. Nitrobenzene reacts with  $\text{SO}_4^{\cdot-}$  with a rate constant of  $\leq 10^6 \text{ mol}^{-1} \text{ dm}^3 \text{ s}^{-1}$  [128]. The electrophilic character of  $\text{SO}_4^{\cdot-}$  can be exemplified by its reaction with gallic acid and gallate ion; with the increase of electron density on the ring (deprotonation), the rate constant increases from  $6.3 \times 10^8$  to  $2.9 \times 10^9 \text{ mol}^{-1} \text{ dm}^3 \text{ s}^{-1}$  [119].

The highest values in Table 8 are around  $6 \times 10^9$ – $8 \times 10^9 \text{ mol}^{-1} \text{ dm}^3 \text{ s}^{-1}$ , and may represent the diffusion controlled limit. In Fig. 2, the logarithms of rate constants for monosubstituted benzenes are shown as a function of the Hammett  $\sigma_p^+$

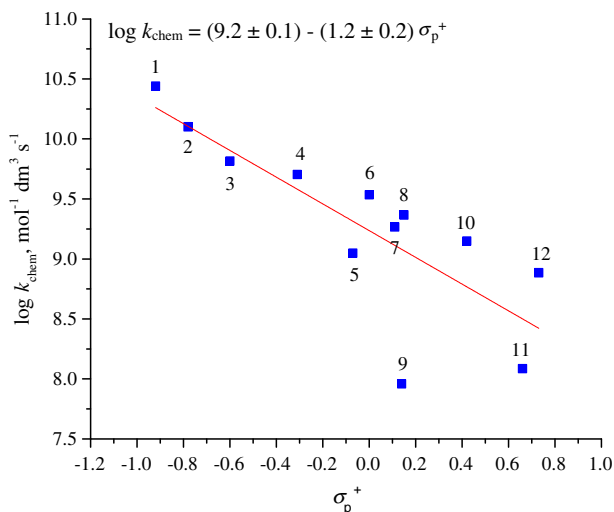
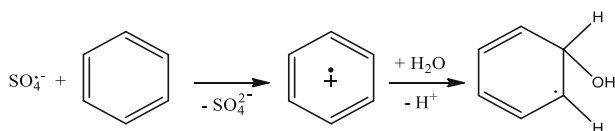
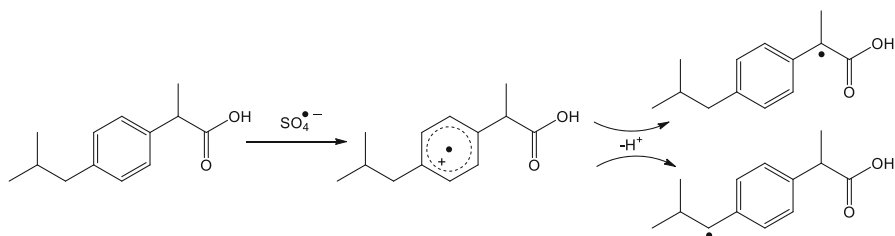


**Fig. 2** Rate constants of the chemical reactions of  $\text{SO}_4^{\cdot-}$  with monosubstituted benzenes as a function of the  $\sigma_p^+$  Hammett parameters. Data were taken from Table 8 (corrected for the diffusion controlled limit): 1. phenol, 2. anisole, 3. acetanilide, 4. toluene, 5. fluorobenzene, 6. benzene, 7. chlorobenzene, 8. bromobenzene, 9. iodobenzene, 10. benzoic acid, 11. nitrobenzene, 12. benzaldehyde



**Scheme 4** Reaction of benzene radical cation



**Scheme 5**  $\text{SO}_4^{\bullet-}$  reaction with ibuprofen

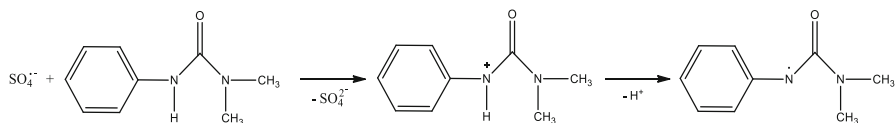
parameters. The values were corrected for the diffusion controlled limit (Eq. 8) by using  $k_{\text{diff}} = 8 \times 10^9 \text{ mol}^{-1} \text{ dm}^3 \text{ s}^{-1}$ . The latter  $k_{\text{diff}}$  was selected, higher than given in Table 1. The  $\log k_{\text{chem, SO}_4^{\bullet-}}$  vs.  $\sigma_{\text{p}}^+$  plot shows linear correlation similar to the  $k_{\text{chem, } \bullet\text{OH}}$  vs.  $\sigma_{\text{p}}$  plot (Fig. 1). The slopes, designated as  $\rho$ , are negative in both cases, indicating that the reactive species are electrophiles. This dependency is more distinctive in  $\text{SO}_4^{\bullet-}$  reactions ( $\rho = -1.2$ ) compared with  $\bullet\text{OH}$  ( $\rho = -0.82$  [13]). Aromatic compounds with strongly deactivating substituent (e.g., 4-nitrobenzoic acid) are nearly inert towards  $\text{SO}_4^{\bullet-}$ , but still react fast with  $\bullet\text{OH}$ .

The wider rate constant range for  $\text{SO}_4^{\bullet-}$  reactions than for  $\bullet\text{OH}$  reactions reflects not only higher selectivity, but may also indicate different reaction mechanisms. Although the reduction potentials of  $\bullet\text{OH}$  and  $\text{SO}_4^{\bullet-}$  do not differ much (Table 2), their reactions with double bonded compounds differ considerably.  $\bullet\text{OH}$  reacts with aromatic molecules preferentially by addition to the ring, and the probability of direct oxidation (electron transfer) is low. In  $\text{SO}_4^{\bullet-}$  reactions, however, in most cases the electron transfer dominates. Seemingly, the reactions are driven by kinetics rather than by thermodynamics [55]. In  $\text{SO}_4^{\bullet-}$  reaction with electron-rich aromatic compounds such as methoxybenzenes, the corresponding radical cations are generated by electron transfer as primary short-lived intermediates [131]. With benzene lacking electron-donating group, hydroxycyclohexadienyl radical has been observed (Scheme 4) [128]. A rapid reaction of water with primarily formed radical cation may account for this.

The reactions taking place from the radical cation may depend on the substituent of the aromatic ring. In contrast to the expectations, Merga et al. [123] suggest cyclohexadienyl radical formation from the radical cations of both toluene (electron donating substituent) and chlorobenzene (electron withdrawing substituent). In the case of ibuprofen, radical cation  $\text{H}^+$  elimination from the alkyl chains and benzyl radical formation is suggested (Scheme 5) [116].

In aminobenzenesulfonates, the radical cation is in equilibrium with the nitrogen centered anilino radical [132]. In phenylurea (fenuron (Scheme 6), monuron,





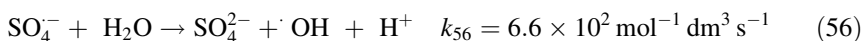
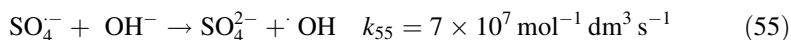
**Scheme 6**  $\text{SO}_4^{\cdot-}$  reaction with fenuron

diuron) and triazine (atrazine, propazine) type herbicide molecules formation of radical cations with positive charge on nitrogen atom attached to the aromatic ring is suggested; deprotonation yields the anilino type radical [120, 121].

In the reactions of the radical cation formed in triazines, dealkylation along with formation of carbonyl compounds and free amines take place [55]. O'Neil et al. [127] suggested dimerization of the radical cations of the methoxylated benzenes.

With regard to water treatment, it can be concluded from the previous discussion that  $\text{SO}_4^{\cdot-}$  tends to react at a similar rate or slower with most pollutants compared with  $\cdot\text{OH}$ .  $\text{SO}_4^{\cdot-}$  reacts more readily by electron transfer than  $\cdot\text{OH}$ , but slower by H-abstraction and addition. When persulfate is added to the solution with dissolved  $\text{O}_2$  present, the  $e_{\text{aq}}^-$  reaction with  $\text{O}_2$  (22) is replaced by the persulfate +  $e_{\text{aq}}^-$  reaction (54):  $\text{O}_2^-$  is replaced by  $\text{SO}_4^{\cdot-}$  [55, 118]. Many studies demonstrated that persulfate enhanced the degradation rate of organic compounds, e.g., carboxylic acids or aromatic molecules during irradiation treatment [115, 116, 133, 134].

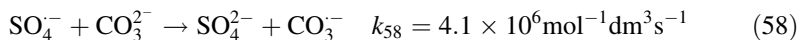
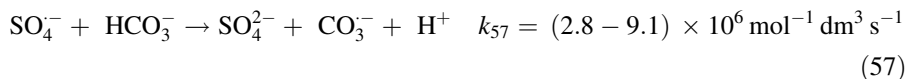
The main 'impurity' constituents of waters, i.e.,  $\text{Cl}^-$ ,  $\text{HCO}_3^-/\text{CO}_3^{2-}$  and DOC, largely affect the efficiency of  $\text{SO}_4^{\cdot-}$  based water treatment. Although the rate constant of the  $\text{SO}_4^{\cdot-} + \text{Cl}^-$  reaction (41) is an order of magnitude smaller than that of the  $\cdot\text{OH} + \text{Cl}^-$  reaction (32); the  $\text{Cl}^-$  concentration limits the applicability of persulfate-based techniques to waters with low  $\text{Cl}^-$  content [117].  $\text{Cl}^-$  formed in both reactions may react with  $\text{Cl}^-$  and form  $\text{Cl}_2^-$  in the acidic pH range [Reaction (35)], or in the alkaline range through complex equilibria transform to  $\cdot\text{OH}$  in (-32). The  $\text{SO}_4^{\cdot-} \rightarrow \cdot\text{OH}$  conversion may also take place in the slow (55) and (56) reactions [115].



When  $\cdot\text{OH}$  forms in the first reaction, strong pH dependence is expected. This pH dependence was not observed using nitrobenzene as probe molecule in the pH 2 to 7.4 range [135]. Nitrobenzene readily reacts with  $\cdot\text{OH}$  ( $3.5 \times 10^9 \text{ mol}^{-1} \text{ dm}^3 \text{ s}^{-1}$ ), while it is practically unreactive in reaction with  $\text{SO}_4^{\cdot-}$  ( $\leq 1 \times 10^6 \text{ mol}^{-1} \text{ dm}^3 \text{ s}^{-1}$ ). In the presence of large excess of methanol or *tert*-butanol  $\cdot\text{OH}$  scavengers, the nitrobenzene degradation was strongly diminished, showing the presence of  $\cdot\text{OH}$  and also suggesting the second alternative.

$\text{SO}_4^{\cdot-}$  oxidizes bicarbonate ( $\text{HCO}_3^-$ ) to carbonate radical ( $\text{CO}_3^{\cdot-}$ ) according to (57), with reported rate constants between  $k = 2.8 \times 10^6$  and  $9.1 \times 10^6 \text{ mol}^{-1} \text{ dm}^3 \text{ s}^{-1}$  [17]. The equivalent reaction for carbonate ( $\text{CO}_3^{2-}$ ) also proceeds fairly rapidly,

with a rate constant of  $4.1 \times 10^6 \text{ mol}^{-1} \text{ dm}^3 \text{ s}^{-1}$  [Reaction (58)]. In the natural pH range, the carbonate is present practically entirely in the  $\text{HCO}_3^-$  form.



These reactions are of concern because high (bi)carbonate concentrations could also result in suppressed concentrations of  $\text{SO}_4^-$ , and therefore slower degradation of the target pollutants are experienced. The alkalinity affects  $\text{SO}_4^-$  (57, 58) and  $\cdot\text{OH}$  reactions (45, 46) more or less to a similar extent.  $\text{SO}_4^-$  reacts more slowly with the dissolved organic matter than  $\cdot\text{OH}$  (by a factor of two to five), resulting in a weaker scavenging, which is an advantage of the techniques using  $\text{SO}_4^-$ . Lutze [55] gives  $k_{\text{SO}_4^-, \text{DOC}} = 6.6 \times 10^3 \text{ mg}^{-1} \text{ dm}^3 \text{ s}^{-1}$ .

## 4 Concluding Remarks

In dilute aqueous solutions, the radiation energy is mainly absorbed by the solvent, and the reactive intermediates formed in water radiolysis (hydroxyl radical, hydrated electron, hydrogen atom) induce the chemical changes of the solutes. The direct effect is negligible. The yield of the reducing intermediates ( $e_{\text{aq}}^- + \text{H}$ ) is nearly equal to the yield of the oxidizing intermediates [ $\cdot\text{OH} + \text{H}_2\text{O}_2$  (minor product)] in pure deoxygenated water.

In wastewater there is always a competition between the reactions of different solutes and the reactive water radiolysis intermediates. When the water is saturated with air, the  $e_{\text{aq}}^-$  and  $\text{H}$  species are mainly converted to the rather unreactive  $\text{O}_2^-/\text{HO}_2$  pair in reaction with dissolved  $\text{O}_2$ . The concentration of chloride ions is usually in the  $1 \times 10^{-3} \text{ mol dm}^{-3}$  range ( $k_{\cdot\text{OH}, \text{Cl}^-} = 4.3 \times 10^9 \text{ mol}^{-1} \text{ dm}^3 \text{ s}^{-1}$ ), and that of the bicarbonate ions may be higher, around  $8 \times 10^{-3} \text{ mol dm}^{-3}$  ( $k_{\cdot\text{OH}, \text{HCO}_3^-} = 8.5 \times 10^6 \text{ mol}^{-1} \text{ dm}^3 \text{ s}^{-1}$ ). The amount of dissolved organic matter changes greatly with the source of water; for the following calculation we take  $40 \text{ mgC dm}^{-3}$  ( $k_{\cdot\text{OH}, \text{DOC}} = 2 \times 10^4 \text{ mgC}^{-1} \text{ dm}^3 \text{ s}^{-1}$ ) while we assume that the concentration of the harmful (aromatic, P) molecules is  $1 \times 10^{-6} \text{ mol dm}^{-3}$  ( $k_{\cdot\text{OH}, \text{P}} = 5 \times 10^9 \text{ mol}^{-1} \text{ dm}^3 \text{ s}^{-1}$ ). Using the concentrations and rate constants mentioned before, one can calculate that in the acidic pH range ( $\text{pH} < 5$ ), the  $\text{Cl}^-$  ions consume most of  $\cdot\text{OH}$  (over 80 %) and about 0.1 % of  $\cdot\text{OH}$  reacts with the compounds of interest. In the neutral pH range,  $\cdot\text{OH}$  mostly disappears in reactions with  $\text{HCO}_3^-$  and DOC in nearly equal percentages, and the percentage of the  $\cdot\text{OH} + \text{P}$  reaction increases to  $\sim 0.6$  %. Although the percentage of  $\cdot\text{OH}$  reacting with the target compounds is low, at 1–3 kGy dose, practically all of the target molecules have a chance to react with  $\cdot\text{OH}$ .  $\text{Cl}_2^-$  (in the acidic pH range) and  $\text{CO}_3^-$  can also contribute to pollutants' degradation.

In irradiation experiments, persulfate enhances the degradation rate of organic compounds: with dissolved  $\text{O}_2$  present, the  $e_{\text{aq}}^- + \text{O}_2$  reaction is replaced by the

$e_{aq}^- + S_2O_8^{2-}$  reaction:  $O_2^-$  is replaced by  $SO_4^-$ .  $SO_4^-$  reacts more selectively than  $\cdot OH$ . For instance, its reactivity with aromatic molecules containing strong electron withdrawing substituent (e.g.,  $NO_2$ ) is very low. Sulfate radical reactions are strongly affected by the constituents of the solutions.  $SO_4^-$  may transform to  $\cdot OH$  in reactions with  $Cl^-$ ,  $OH^-$  or  $H_2O$ . Due to the high rate constant of the  $SO_4^- + Cl^-$  reaction, in solution with high  $Cl^-$  concentration in the acidic pH range,  $SO_4^-$  transforms to  $Cl_2^-$ ; above pH 5, the transformation takes place to  $\cdot OH$ .  $\cdot OH$  and  $SO_4^-$  react with  $HCO_3^-$  with similar rate constants forming  $CO_3^-$ . The rate constant of  $SO_4^-$  reaction with the dissolved organic matter is about two to five times smaller than the analogous reaction of  $\cdot OH$ .

Due to the complexity of the reaction systems, a careful optimization of the reaction conditions is needed, including dose, eventually adjusting the pH, and additives.

**Acknowledgments** The authors thank Hungarian Science Foundation (OTKA, NK 105802) and International Atomic Energy Agency (Contract No. 16485) for support.

## References

1. Spinks JWT, Woods RJ (1990) An introduction to radiation chemistry, 3rd edn. Wiley, New York
2. Woods RJ, Pikaev AK (1994) Applied radiation chemistry: radiation processing. Wiley, New York
3. Huang J (2000) Carbonate radical in natural waters, PhD thesis, University of Toronto, <https://tspace.library.utoronto.ca/bitstream/1807/14631/1/NQ50045.pdf>. Accessed 13 Febr 2016
4. Mostofa KMG, Liu C-Q, Mottaleb MA, Wan G, Ogawa H, Vione D, Yoshioka T, Wu F (2013) Dissolved organic matter in natural waters. In: Mostofa KMG, Yoshioka T, Mottaleb MA, Vione D (eds) Photobiogeochemistry of organic matter, environmental science and engineering. Springer, Berlin, pp 1–137
5. Westerhoff P, Mezyk SP, Cooper WJ, Minakata D (2007) Electron pulse radiolysis determination of hydroxyl radical rate constants with Suwannee River fulvic acid and other dissolved organic matter isolates. *Environ Sci Technol* 41:4640–4646
6. Buxton GV (2008) An overview of the radiation chemistry of liquids. In: Spothem-Maurizot M, Mostafavi M, Douki T, Belloni J (eds) Radiation chemistry: from basics to applications in material and life sciences. EDP Sciences, France, pp 3–16
7. Swallow AJ (1973) Radiation chemistry: an introduction. Longman, London
8. Buxton GV (1982) Basic radiation chemistry of liquid water. In: Baxendale JH, Busi F (eds) The study of fast processes and transient species by electron pulse radiolysis, NATO Advanced Study Institutes Series, D. Reidel Publishing Company, Dordrecht, pp 241–266
9. Buxton GV (1987) Radiation chemistry of the liquid state: (1) water and homogeneous aqueous solutions. In: Rodgers MAJ, Farhataziz (eds) Radiation chemistry, principles and applications. VHC Publishers, New York, pp 321–349
10. Buxton GV (2001) High temperature water radiolysis. In: Jonah CD, Rao BSM (eds) Radiation chemistry: present status and future trends, studies in physical and theoretical chemistry 87. Elsevier, Amsterdam, pp 145–162
11. Elliot AJ, McCracken DR, Buxton GV, Wood ND (1990) Estimation of rate constants for near-diffusion-controlled reactions in water at high temperatures. *J Chem Soc Faraday T* 86:1539–1547
12. Ashton L, Buxton GV, Stuart CR (1995) Temperature dependence of the rate of reaction of OH with some aromatic compounds in aqueous solution. Evidence for the formation of a  $\pi$ -complex intermediate? *J Chem Soc Faraday T* 91:1631–1633
13. Wojnárovits L, Takács E (2013) Structure dependence of the rate coefficients of hydroxyl radical + aromatic molecule reaction. *Radiat Phys Chem* 87:82–87
14. Rickman KA, Mezyk SP (2010) Kinetics and mechanism of sulfate radical oxidation of  $\beta$ -lactam antibiotics in water. *Chemosphere* 81:359–365

15. Kazmierczak L, Szala-Bilnik J, Wolszczak M, Swiatla-Wojcik D (2015) Temperature dependence of rate constants for hydrogen atom reaction with  $\text{Cl}_2^-$  in water by pulse radiolysis of aqueous HCl solution. *Radiat Phys Chem* 117:7–11
16. Noyes RM (1961) In: Porter G. (ed) *Progress in reaction kinetics*, Pergamon, London, Vol. 1
17. Buxton G, Greenstock CL, Helman, WP, Ross AB (1988) Critical review of rate constants for reactions of hydrated electrons, hydrogen atoms and hydroxyl radicals ( $\text{OH}/\text{O}^-$ ) in aqueous solution. *J Phys Chem Ref Data* 17:513–886. An extended database is available on the internet: <http://kinetics.nist.gov/solution/> Accessed 15 Febr 2016
18. Neta P, Hiue RE, Ross AB (1988) Rate constants of inorganic radicals in aqueous solution. *J Phys Chem Ref Data* 17:1027–1284
19. Armstrong DA, Huie RE, Lyman S, Koppenol WH, Merényi G, Neta P, Stanbury DM, Steenken S, Wardman P (2013) Standard electrode potentials involving radicals in aqueous solution: inorganic radicals. *BioInorg React Mech* 9:59–61
20. Wardman P (1989) Reduction potentials of one-electron couples involving free radicals in aqueous solution. *J Phys Chem Ref Data* 18:1637–1755
21. von Sonntag C (2006) *Free-radical-induced DNA damage and its repair. A chemical perspective*. Springer, Heidelberg
22. Alam MS, Rao BSM, Janata E (2003) -OH reactions with aliphatic alcohols: evaluation of kinetics by direct optical absorption measurement. A pulse radiolysis study. *Radiat Phys Chem* 67:723–728
23. Luo Y-Q (2002) *Handbook of bond dissociation energies in organic compounds*. CRC Press, Boca Raton
24. Cooper WJ, Cramer CJ, Martin NH, Mezyk SP, O'Shea KE, von Sonntag C (2009) Free radical mechanism for the treatment of methyl tert-butyl ether (MTBE) via advanced oxidation/reductive processes in aqueous solutions. *Chem Rev* 109:1302–1345
25. Kosaka K, Yamada H, Tsuno H, Shimizu Y, Matsui S (2003) Reaction rate constants of di-n-butyl phthalate and 17  $\beta$ -estradiol with ozone and hydroxyl radical. *J Jpn Soc Water Environ* 26:215–221
26. Ning B, Graham NJD, Zhang Y (2007) Degradation of octylphenol and nonylphenol by ozone – Part II: indirect reaction. *Chemosphere* 68:1173–1179
27. Peller JR, Mezyk SP, Cooper WJ (2009) Bisphenol A reactions with hydroxyl radicals: diverse pathways determined between deionized water and tertiary treated wastewater solutions. *Res Chem Intermediat* 35:21–34
28. Wu M-H, Liu N, Xu G, Ma J, Tang L, Wang L, Fu H-Y (2011) Kinetics and mechanisms studies on dimethyl phthalate degradation in aqueous solutions by pulse radiolysis and electron beam radiolysis. *Radiat Phys Chem* 80:420–425
29. Wojnárovits L, Takács E (2014) Rate coefficients of hydroxyl radical reactions with pesticide molecules and related compounds: a review. *Radiat Phys Chem* 96:120–134
30. Kapoor S, Varshney L (1997) Redox reactions of chloramphenicol and some aryl peroxy radicals in aqueous solutions: a pulse radiolytic study. *J Phys Chem A* 101:7778–7782
31. Sági Gy, Csay T, Szabó L, Pátzay Gy, Csonka E, Takács E, Wojnárovits L (2015) Analytical approaches to the OH radical induced degradation of sulfonamide antibiotics in dilute aqueous solutions. *J Pharm Biomed Anal* 106:52–60
32. Mezyk SP, Neubauer TJ, Cooper WJ, Peller JR (2007) Free-radical-induced oxidative and reductive degradation of sulfa drugs in water: absolute kinetics and efficiencies of hydroxyl radical and hydrated electron reactions. *J Phys Chem A* 111:9019–9024
33. Dail MK, Mezyk SP (2010) Hydroxyl-radical-induced degradative oxidation of  $\beta$ -lactam antibiotics in water: absolute rate constant measurement. *J Phys Chem A* 114:8391–8395
34. Dodd M, Buffle M-O, von Gunten U (2006) Oxidation of antibacterial molecules by aqueous ozone: moiety-specific reaction kinetics and application to ozone-based wastewater treatment. *Environ Sci Technol* 40:1969–1977
35. Song W, Chen W, Cooper WJ, Greaves J, Miller GE (2008) Free-radical destruction of  $\beta$ -lactam antibiotics in aqueous solution. *J Phys Chem A* 112:7411–7417
36. Szabó L, Tóth T, Takács E, Wojnárovits L (2016) One-electron oxidation of molecules with aromatic and thioether functions:  $\text{Cl}_2^-/\text{Br}_2^-$  and  $\text{OH}^-$  induced oxidation of penicillins studied by pulse radiolysis. *J Photochem Photobiol Chem* 326:50–59
37. Ayatollahi S, Kalnina D, Song W, Turks M, Cooper WJ (2013) Radiation chemistry of salicylic and methyl substituted salicylic acids: models for the radiation chemistry of pharmaceutical compounds. *Radiat Phys Chem* 92:93–98

38. Szabó L, Tóth T, Homlok R, Takács E, Wojnárovits L (2012) Radiolysis of paracetamol in dilute aqueous solution. *Radiat Phys Chem* 81:1503–1507
39. Jones KG (2007) Applications of radiation chemistry to understand the fate and transport of emerging pollutants of concern in coastal waters. PhD, North Carolina State University, Raleigh, North Carolina, USA. <http://repository.lib.ncsu.edu/ir/bitstream/1840.16/4346/1/etd.pdf>. Accessed 14 Febr 2016
40. Wojnárovits L, Takács E (2008) Irradiation treatment of azo dye containing wastewater: an overview. *Radiat Phys Chem* 77:225–244
41. Perkowski J, Gebicki JL, Lubis R, Mayer J (1989) Pulse radiolysis of anthraquinone dye aqueous solution. *Radiat Phys Chem* 33:103–108
42. Hasegawa K, Neta P (1978) Rate constants and mechanisms of reaction of  $\text{Cl}_2^-$ . *J Phys Chem* 82:854–857
43. Kemsley K, Moore JS, Phillips GO, Sosnowski A (1974) Reaction of radical probes with substituted phenols as models for the investigation of tyrosine in aldolase and chemically modified aldolase. *Acta Vitaminol Enzymol* 28:263–267
44. Neta P, Maruthamuthu P, Carton PM, Fessenden RW (1978) Formation and reactivity of the amino radical. *J Phys Chem* 82:1875–1878
45. Albarran G, Schuler RH (2007) Hydroxyl radical as a probe of the charge distribution in aromatics: phenol. *J Phys Chem A* 111:2507–2510
46. Albarran G, Mendoza E, Schuler RH (2016) Concerted effects of substituents in the reaction of  $\cdot\text{OH}$  radicals with aromatics: the hydroxybenzaldehydes. *Radiat Phys Chem* 124:46–51
47. Schuler RH, Albarran G, Zajicek J, George MV, Fessenden RW, Carmichael I (2002) On the addition of  $\cdot\text{OH}$  radicals to the ipso positions of alkyl-substituted aromatics: production of 4-hydroxy-4-methyl-2,5-cyclohexadien-1-one in the radiolytic oxidation of *p*-cresol. *J Phys Chem A* 106:12178–12183
48. Land EJ, Ebert M (1967) Pulse radiolysis studies of aqueous phenol. Water elimination from dihydroxycyclohexadienyl radicals to form phenoxyl. *T Faraday Soc* 63:1181–1190
49. Steenken S (1987) Addition-elimination paths in electron-transfer reactions between radicals and molecules. Oxidation of organic molecules by OH radical. *J Chem Soc Faraday T* 1 83:113–124
50. Wojnárovits L, Földiák G, D'Angelantonio M, Emmi SS (2002) Mechanism of OH radical-induced oxidation of *p*-cresol to *p*-methylphenoxyl radical. *Res Chem Intermediat* 28:373–386
51. Fang X, Pan X, Rahmann A, Schuchmann H-P, von Sonntag C (1995) Reversibility in the reaction of cyclohexadienyl radicals with oxygen in aqueous solution. *Chem-Eur J* 1:423–429
52. Getoff N (1997) Peroxyl radicals in the treatment of waste solutions. In: Alfassi ZB (ed) *Peroxyl radicals*. Wiley, New York, pp 483–506
53. von Sonntag C, Schuchmann H-P (1997) Peroxyl radicals in aqueous solution. In: Alfassi ZB (ed) *Peroxyl radicals*. Wiley, New York, pp 173–274
54. von Sonntag C, Schuchmann H-P (2001) The chemistry behind the application of ionizing radiation in water-pollution abatement. In: Jonah CD, Rao BSM (eds) *Radiation chemistry: present status and future trends, studies in physical and theoretical chemistry* 87. Elsevier, Amsterdam, pp 657–670
55. Lutze H (2013) Sulfate radical based oxidation in water treatment. Dissertation Dr. rer. nat. Duisburg-Essen. [https://duepublico.uni-duisburg-essen.de/servlets/DocumentServlet/135021/Lutze\\_Diss.pdf](https://duepublico.uni-duisburg-essen.de/servlets/DocumentServlet/135021/Lutze_Diss.pdf). Accessed 13 Febr 2016
56. Pálfi T, Wojnárovits L, Takács E (2010) Calculated and measured transient product yields in pulse radiolysis of aqueous solutions: concentration dependence. *Radiat Phys Chem* 79:1154–1158
57. Swallow AJ (1982) Application of pulse radiolysis to study of aqueous organic systems. In: Baxendale JH, Busi F (eds) *The study of fast processes and transient species by electron pulse radiolysis*. NATO Advanced Study Institutes Series, D. Reidel Publishing Company, Dordrecht, pp 289–315
58. von Sonntag C (1987) *The chemical basis of radiation biology*. Taylor and Francis, London
59. Solar S, Solar W, Getoff N (1986) Resolved multisite OH-attack on aqueous aniline studied by pulse radiolysis. *Radiat Phys Chem* 28:229–234
60. Lichtscheidl J, Getoff N (1979) Pulsradiolytische Untersuchungen der Reaktion des  $e_{aq}^-$  mit halogenierten aromatischen Verbindungen (Pulse radiolysis investigations on the reaction of  $e_{aq}^-$  with halogenated aromatic compounds). *Monatsh Chem* 110:1357–1375
61. Hoy AR, Bolton JR (1994) Determination of rate constants for reactive intermediates in the aqueous photodegradation of pollutants using a spin-trap/EPR method. In: Helz GR, Zepp RG, Crosby DG (eds) *Aquatic and surface photochemistry*. CRC Press, Boca Raton, pp 491–498

62. Zona R, Solar S, Sehested K, Holcman J, Mezyk SP (2002) OH-Radical induced oxidation of phenoxyacetic acid and 2,4-dichlorophenoxyacetic acid. Primary radical steps and products. *J Phys Chem A* 106:6743–6749
63. Varghese R, Mohan H, Manoj P, Manoj VM, Aravind UK, Vandana K, Aravindakumar CT (2006) Reactions of hydrated electrons with triazine derivatives in aqueous medium. *J Agr Food Chem* 54:8171–8176
64. Kovács K, Mile V, Csay T, Takács E, Wojnárovits L (2014) Hydroxyl radical-induced degradation of fenuron in pulse and gamma radiolysis: kinetics and product analysis. *Environ Sci Pollut R* 21:12693–12700
65. Kovács K, He S, Mile V, Csay T, Takács E, Wojnárovits L (2015) Ionizing radiation induced degradation of diuron in dilute aqueous solution. *Chem Central J* 9:21. doi:10.1186/s13065-015-0097-0
66. Kovács K, He S, Mile V, Földes T, Pápai I, Takács E, Wojnárovits L (2016) Ionizing radiation induced degradation of monuron in dilute aqueous solution. *Radiat Phys Chem* 124:191–197
67. Philips GO, Power DM, Robinson C, Davies JV (1973) Interactions of bovine serum albumin with penicillins and cephalosporins studied by pulse radiolysis. *Biochem Bioph Acta* 295:8–17
68. Szabó L, Tóth T, Rácz G, Takács E, Wojnárovits L (2016)  $\cdot\text{OH}$  and  $e_{\text{aq}}^-$  are yet good candidates for demolishing the  $\beta$ -lactam system of a penicillin eliminating the antimicrobial activity. *Radiat Phys Chem* 124:84–90
69. Pikaev AK (2001) Application of pulse radiolysis and computer simulation for the study of the mechanism of radiation purification of polluted water. *Res Chem Intermediat* 27:775–786
70. Takács E, Dajka K, Wojnárovits L, Emmi SS (2000) Protonation kinetics of acrylate radical anions. *Phys Chem Chem Phys* 2:1431–1433
71. Wojnárovits L, Takács E, Dajka K, Emmi SS (2001) On the reversible protonation of acrylic-type compounds. *Res Chem Intermediat* 27:847–854
72. Wojnárovits L, Takács E, Dajka K, Emmi SS, Russo M, D'Angelantonio M (2004) Re-evaluation of the rate coefficient for the H atom reaction with *tert*-butanol in aqueous solution. *Radiat Phys Chem* 69:217–219
73. Alam MS, Rao BSM, Janata E (2001) A pulse radiolysis study of H atom reactions with aliphatic alcohols: evaluation of kinetics by direct optical absorption measurements. *Phys Chem Chem Phys* 3:2622–2624
74. Madden KP, Mezyk SP (2011) Critical review of aqueous solution reaction rate constants for hydrogen atoms. *J Phys Chem Ref Data* 40:1–43
75. Wojnárovits L, Takács E, Dajka K, Emmi SS, Russo M, D'Angelantonio M (2003) Rate coefficient for the H atom reaction with acrylate monomers in aqueous solution. *Tetrahedron* 59:8353–8358
76. Illés E, Takács E, Dombi A, Gajda-Schranz K, Rácz G, Gonter K, Wojnárovits L (2013) Hydroxyl radical induced degradation of ibuprofen. *Sci Total Environ* 447:286–292
77. Homlok R, Takács E, Wojnárovits L (2013) Degradation of organic molecules in advanced oxidation processes: relation between chemical structure and degradability. *Chemosphere* 91:383–389
78. Bielski BHJ, Cabelli DE, Arudi RL, Ross AB (1985) Reactivity of  $\text{HO}_2/\text{O}_2^-$  radicals in aqueous solution. *J Phys Chem Ref Data* 14:1041–1100
79. Szabó L, Tóth T, Homlok R, Rácz G, Takács E, Wojnárovits L (2014) Hydroxyl radical induced degradation of salicylates in aerated aqueous solution. *Radiat Phys Chem* 97:239–245
80. Liu Y, Hu J, Wang J (2014)  $\text{Fe}^{2+}$  enhancing sulfamethazine degradation in aqueous solution by gamma irradiation. *Radiat Phys Chem* 96:81–8783
81. Staehelin J, Hoigne J (1982) Decomposition of ozone in water: rate of initiation by hydroxide ions and hydrogen peroxide. *Environ Sci Technol* 16:676–681
82. von Gunten U (2003) Ozonation of drinking water: part 1. Oxidation kinetics and product formation. *Water Res* 37:1443–1467
83. Drzewicz P, Trojanowicz M, Zona R, Solar S, Gehringer P (2004) Decomposition of 2,4-dichlorophenoxyacetic acid by ozonation, ionizing radiation as well as ozonation combined with ionizing radiation. *Radiat Phys Chem* 69:281–287
84. Gehringer P, Eschweiler H, Weiss S, Reemtsma T (2008) Effluent polishing by means of advanced oxidation. IAEA-TECDOC-1598, irradiation treatment of polluted water and wastewater. International Atomic Energy Agency, Vienna, pp 15–26
85. Merényi G, Lind J, Naumov S, von Sonntag C (2010) Reaction of ozone with hydrogen peroxide (peroxone process): a revision of current mechanistic concepts based on thermokinetic and quantum-chemical considerations. *Environ Sci Technol* 44:3505–3507



86. Fischbacher A, von Sonntag J, von Sonntag C, Schmidt TC (2013) The ·OH radical yield in the  $\text{H}_2\text{O}_2 + \text{O}_3$  (peroxone) reaction. *Environ Sci Technol* 47:9959–9964
87. Cooper WJ, Gehringer P, Pikaev AK, Kurucz CN, Mincher BJ (2004) Radiation processes. In: Parsons S (ed) *Advanced oxidation processes for water and wastewater treatment*. IWA Publishing, London, pp 209–245
88. Szala-Bilnik J, Pierscieniewska P, Wolszczak M, Swiatla-Wojcik D (2014) Temperature dependence of the rate constant for the bimolecular recombination of  $\text{Cl}_2^-$  in water—a pulse radiolysis study. *Radiat Phys Chem* 97:184–187
89. Buxton GV, Bydder M, Salmon GA (1988) Reactivity of chlorine atoms in aqueous solution Part 1. The equilibrium  $\text{Cl}^\cdot + \text{Cl}^- \rightleftharpoons \text{Cl}_2^-$ . *J Chem Soc Faraday T* 94:653–657
90. Yu X-Y, Bao Z-C, Barker JR (2004) Free radical reactions involving  $\text{Cl}$ ,  $\text{Cl}_2^-$ , and  $\text{SO}_4^{\cdot-}$  in the 248 nm photolysis of aqueous solutions containing  $\text{S}_2\text{O}_8^{2-}$  and  $\text{Cl}^-$ . *J Phys Chem A* 108:295–308
91. Yu X-Y, Barker JR (2003) Hydrogen peroxide photolysis in acidic aqueous solution containing chloride ions. I. Chemical mechanism. *J Phys Chem A* 107:1313–1324
92. Alegre ML, Geronés M, Rosso JA, Bertolotti SG, Braun AM, Mártire DO, Gonzalez MC (2000) Kinetic study of the reactions of chlorine atoms and  $\text{Cl}_2^-$  radical anions in aqueous solutions. 1. Reaction with benzene. *J Phys Chem A* 104:3117–3125
93. Wojnárovits L, Takács E, Emmi SS (2008) Nucleophilic and electrophilic radical attack on maleic and fumaric acids in aqueous solution. *Chem Phys Lett* 460:451–456
94. Kluge T, Pankonin D, Brede O (1998) Oxidation of  $\alpha$ -pinene by OH·, Cl· and  $\text{Cl}_2^-$  radicals. *J Radioanal Nucl Ch* 232:103–105
95. Armstrong DA, Waltz WL, Rauk A (2006) Carbonate radical anion—Thermochemistry. *84:1614–1619*
96. Cope VW, Chen S-N, Hoffman MZ (1973) Intermediates in the photochemistry of carbonato-amine complexes of cobalt(III). *J Am Chem Soc* 95:3116–3121
97. Mazellier P, Busset C, Delmont A, De Laat J (2007) A comparison of fenuron degradation by hydroxyl and carbonate radicals in aqueous solution. *Water Res* 41:4585–4594
98. Canonica S, Kohn T, Mac M, Real FJ, Wirz J, von Gunten U (2005) Photosensitizer method to determine rate constants for the reaction of carbonate radical with organic compounds. *Environ Sci Technol* 39:9182–9188
99. Clifton CL, Huie RE (1993) Rate constants for some hydrogen abstraction reactions of the carbonate radical. *Int J Chem Kinet* 25:199–203
100. Czapski G, Lyman SV, Schwartz HA (1999) Acidity of the carbonate radical. *J Phys Chem* 103:3447–3450
101. Augusto O, Bonini MG, Amanso AM, Linares E, Santos CCX, De Menezes SL (2002) Nitrogen dioxide and carbonate radical anion: two emerging radicals in biology. *Free Radical Biol Med* 32:841–859
102. Medinas DB, Cerchiaro G, Trindade DF, Augusto O (2007) The carbonate radical and related oxidants derived from bicarbonate buffer. *IUBMB Life* 59:255–262
103. Chen S-N, Hoffman M, Parsons GH Jr (1975) Reactivity of the carbonate radical toward aromatic compounds in aqueous solution. *J Phys Chem* 79:1911–1912
104. Umschlag Th, Herrmann H (1999) The carbonate radical ( $\text{HCO}_3^\cdot/\text{CO}_3^{\cdot-}$ ) as a reactive intermediate in water chemistry: kinetics and modelling. *Acta Hydroch Hydrob* 27:214–222
105. Huie RE, Shoute LCT, Neta P (1991) Temperature dependence of the rate constants for reactions of the carbonate radical with organic and inorganic reductants. *Int J Chem Kinet* 23:541–552
106. Simic MG, Hunter EPL (1984) The reactivities of organic oxygen (oxy) radicals. In: Bors W, Saran M, Tait D (eds) *Oxygen radicals chemistry and biology*, de Gruyter, Berlin. Fed. Rep., Germany, pp 109–121
107. Lilie J, Henglein A, Hanrahan RJ (1978) Reactions of the carbonate radical anion with organic and inorganic solutes in aqueous solution. Unpublished paper, data accessible: <http://kinetics.nist.gov/solution/> Accessed 16 Febr 2016
108. Moore JS, Phillips GO, Sosnowski A (1977) Reaction of the carbonate radical anion with substituted phenols. *Int J Radiat Biol Re* 31:603–605
109. Elango TP, Ramakrishnan V, Vancheesan S, Kuriacose JC (1984) Reaction of the carbonate radical with substituted anilines. *Proc Indian Acad Sci (Chem Sci)* 93:47–52
110. Huang J, Mabury SA (2000) A new method for measuring carbonate radical reactivity toward pesticides. *Environ Toxicol Chem* 19:1501–1507

111. Wu C, Linden KG (2010) Phototransformation of selected organophosphorus pesticides: roles of hydroxyl and carbonate radicals. *Water Res* 44:3585–3594
112. Augusto O, Miyamoto S (2011) Oxygen radicals and related species. Chapter II. In: Pantopoulos K, Schipper HM (eds) *Principles of free radical biomedicine*. Volume 1 ISBN: 978-1-61209-773-2, Nova Science Publishers, Inc. pp. 1-23
113. Chen SN, Hoffman MZ (1973) Rate constants for the reaction of the carbonate radical with compounds of biochemical interest in neutral aqueous solution. *Radiat Res* 56:40–47
114. Larson RA, Zepp RG (1988) Reactivity of the carbonate radical with aniline derivatives. *Environ Toxicol Chem* 7:265–274
115. Adams GE, Aldrich JE, Bisby RH, Cundall RB, Redpath JL, Willson RL (1972) Selective free radical reactions with proteins and enzymes: reactions of inorganic radical anions with amino acids. *Radiat Res* 49:278–289
116. Paul (Guin) J, Naik DB, Bhardwaj YK, Varshney L (2014) Studies on oxidative radiolysis of ibuprofen in presence of potassium persulfate. *Radiat Phys Chem* 100:38–44
117. Lutze H, Kerlin N, Schmidt TC (2015) Sulfate radical-based water treatment in presence of chloride: formation of chlorate, inter-conversion of sulfate radicals into hydroxyl radicals and influence of bicarbonate. *Water Res* 72:349–602
118. Criquet J, Karpel Vel Leitner N (2015) Reaction pathway of the degradation of the *p*-hydroxybenzoic acid by sulfate radical generated by ionizing radiations. *Radiat Phys Chem* 106:307–314
119. Caregnato P, Gara PMD, Bosio GN, Gonzalez MC, Russo N, Michelini MDC, Mártire DO (2008) Theoretical and experimental investigation on the oxidation of gallic acid by sulfate radical anions. *J Phys Chem A* 112:1188–1194
120. Canle Lopez M, Rodríguez S, Rodríguez Vazques LF, Santaballa JA, Steenken S (2001) First stages of photodegradation of the urea herbicides fenuron, monuron and diuron. *J Mol Struct* 565–566:133–139
121. Canle Lopez M, Fernandez MI, Rodríguez S, Santaballa JA, Steenken S, Vulliet E (2005) Mechanisms of direct and TiO<sub>2</sub>-photocatalysed UV degradation of phenylurea herbicides. *Chem Phys Phys Chem* 6:2064–2074
122. Ziajka J, Pasiuk-Bronikowska W (2005) Rate constants for atmospheric trace organics scavenging SO<sub>4</sub><sup>•-</sup> in the Fe-catalysed autoxidation of S(IV). *Atmos Environ* 39:1431–1438
123. Merga G, Aravindakumar CT, Rao BSM, Mohan H, Mittal JP (1994) Pulse radiolysis study of the reactions of SO<sub>4</sub><sup>•-</sup> with some substituted benzenes in aqueous solution. *J Chem Soc Faraday T* 90:597–604
124. Roder M, Földiák G, Wojnárovits L (1999) Electron transfer from cresols to N<sub>3</sub><sup>•</sup>, Br O<sub>2</sub><sup>•</sup>, ClO<sub>2</sub><sup>•</sup>, NO<sub>2</sub><sup>•</sup> and SO<sub>4</sub><sup>•-</sup> radicals: correlation between rate constants and one-electron reduction potentials. *Radiat Phys Chem* 55:515–519
125. Choure SC, Bamatraf MMM, Rao BSM, Das R, Mohan H, Mittal JP (1997) Hydroxylation of chlorotoluenes and cresols: a pulse radiolysis, laser flash photolysis, and product analysis study. *J Phys Chem A* 101:9837–9845
126. Sharma SB, Mudaliar M, Rao BSM, Mohan H, Mittal JP (1997) Radiation chemical oxidation of benzaldehyde, acetophenone and benzophenone. *J Phys Chem A* 101:8402–8408
127. O'Neil P, Steenken S, Schulte-Frohlinde P (1975) Formation of radical cations of methoxylated benzenes by reaction with OH radicals, Ti<sup>2+</sup>, Ag<sup>2+</sup> and SO<sub>4</sub><sup>•-</sup> in aqueous solution. An optical and conductometric pulse radiolysis and in situ radiolysis electron spin resonance study. *J Phys Chem* 79:2773–2779
128. Neta P, Madhavan V, Zemel H, Fessenden RW (1977) Rate constants and mechanism of reaction of SO<sub>4</sub><sup>•-</sup> with aromatic compounds. *J Am Chem Soc* 99:163–164
129. Mohan H, Mittal JP (1995) Direct evidence for H<sup>+</sup>-catalysed dehydration of fluorohydroxycyclohexadienyl radical: a pulse radiolysis study. *J Chem Soc Faraday T* 91:2121–2126
130. Mohan H (1997) Pulse radiolysis studies on ·OH radical induced reactions with substituted iodobenzenes in aqueous solutions. *Radiat Phys Chem* 49:15–19
131. Steenken S, O'Neill P, Schulte-Frohlinde D (1977) Formation of radical zwitterions from methoxylated benzoic acids. 1. One electron oxidation by Ti<sup>2+</sup>, Ag<sup>2+</sup>, and SO<sub>4</sub><sup>•-</sup>. *J Phys Chem* 81:26–30
132. Behar D, Behar B (1991) Pulse radiolysis studies of aminobenzenesulfonates: formation of cation radicals. *J Phys Chem* 95:7552–7556
133. Criquet J, Karpel Vel Leitner N (2011) Electron beam irradiation of aqueous solution of persulfate ions. *Chem Eng J* 169:258–262



134. Criquet J, Karpel Vel Leitner N (2012) Electron beam irradiation of citric acid aqueous solutions containing persulfate. *Sep Purif Technol* 88:168–173
135. He X, Mezyk SP, Michael I, Fatta-Cassinos D, Dionysiou DD (2014) Degradation kinetics and mechanism of  $\beta$ -lactam antibiotics by the activation of  $H_2O_2$  and  $Na_2S_2O_8$  under UV-254 nm irradiation. *J Hazard Mater* 279:375–383

# Electron Beam Technology for Environmental Pollution Control

Andrzej G. Chmielewski<sup>1</sup> · Bumsoo Han<sup>2</sup>

Received: 13 May 2016 / Accepted: 24 August 2016 / Published online: 12 September 2016  
© Springer International Publishing Switzerland 2016

**Abstract** Worldwide, there are over 1700 electron beam (EB) units in commercial use, providing an estimated added value to numerous products, amounting to 100 billion USD or more. High-current electron accelerators are used in diverse industries to enhance the physical and chemical properties of materials and to reduce undesirable contaminants such as pathogens, toxic byproducts, or emissions. Over the past few decades, EB technologies have been developed aimed at ensuring the safety of gaseous and liquid effluents discharged to the environment. It has been demonstrated that EB technologies for flue gas treatment (SO<sub>x</sub> and NO<sub>x</sub> removal), wastewater purification, and sludge hygienization can be effectively deployed to mitigate environmental degradation. Recently, extensive work has been carried out on the use of EB for environmental remediation, which also includes the removal of emerging contaminants such as VOCs, endocrine disrupting chemicals (EDCs), and potential EDCs.

**Keywords** Electron beam (EB) · Electron accelerator · Flue gas · Wastewater treatment · Sludge treatment · Radical reaction · Radiolysis product · Radiation Processing · Pollution control · Environmental pollution

---

This article is part of the Topical Collection “Applications of Radiation Chemistry”; edited by Margherita Venturi, Mila D’Angelantonio.

---

✉ Bumsoo Han  
[bshan@eb-tech.com](mailto:bshan@eb-tech.com)

<sup>1</sup> Institute of Nuclear Chemistry and Technology, Warsaw, Poland

<sup>2</sup> EB TECH Co., Ltd., Daejeon, Republic of Korea

## 1 Introduction

Electron accelerators are reliable and durable electrically sourced equipment that can produce ionizing radiation when it is needed for a particular commercial use. There are a large number of electron accelerators being used worldwide in industrial applications, most of which involve polymer processing [1]. The observed emission of pollutants and environmental degradation are reasons why the most developed countries have introduced emission limits; mostly such action started at the end of the twentieth century. Fossil fuel combustion leads to acidic pollutants such as  $\text{SO}_2$ ,  $\text{NO}_x$ ,  $\text{HCl}$  emission. Different control technologies are proposed; however, the most popular method is a combination of wet FGD (flue gas desulfurization) and SCR (selective catalytic reduction). First, using lime or limestone slurry leads to  $\text{SO}_2$  capture and gypsum as a product. In the second process, ammonia is used as a reagent, and nitrogen oxides are reduced over a catalyst surface to gaseous nitrogen, which removes  $\text{NO}_x$ . A new advanced method uses EB for simultaneous  $\text{SO}_2$  and  $\text{NO}_x$  removal. Early possibilities for EB applications in pollution control have been reported. The pioneering works in these applications were from Takasaki, Japan [2]. The special input for the technology application was the development of the new high power electron accelerators, which can be used for the processing on line of the huge flow streams of liquid or gaseous pollutants. The accelerators were applied for off-gases, wastewater treatment, and biological sludge from a wastewater treatment plant. In the case of the latter application EB treatment have higher throughput in comparison with gamma ray source. A variety of industrial electron accelerators can now provide electron energies from 0.3 MeV to more than 10 MeV with average beam power capabilities up to 700 kW.

EB processing of wastewater is non-chemical and uses fast formation of short-lived reactive radicals that can interact with a wide range of pollutants. Such reactive radicals are strong oxidizing or reducing agents that can transform the pollutants in the liquids wastes. The first studies on the radiation treatment of wastes were carried out in the 1950s principally for disinfection. In the 1960s, these studies were extended to the purification of water and wastewater. After some laboratory research on industrial wastewaters and polluted groundwater in the 1970s and 1980s, several pilot plants were built for extended research in the 1990s. The first full-scale application was reported for the purification of wastewater at the Voronezh synthetic rubber plant in Russia. Two electron accelerators (1.5 MeV 50 kW each) were used to convert the non-biodegradable emulsifier, "nekal", present in the wastewater to a biodegradable form [3]. The installation treats up to 2000 m<sup>3</sup> of effluent per day. An industrial plant for treating 10,000 m<sup>3</sup>/day of textile-dyeing wastewater has been constructed in Daegu, Korea with 1 MeV, 400 kW electron accelerator [4].

Sewage sludge, also known as biosolid, is the solid waste yield after completion of the secondary stage of biological wastewater treatment. The annual production of sewage sludge has been increasing around the world as stricter clean water regulations have begun to take effect. It is a rich source of both many micronutrients and fixed nitrogen, making it a valuable fertilizer. High energy ionizing radiation

has the ability to inactivate pathogens with a very high degree of reliability and in a clean and efficient manner. Ionizing radiation interacts with matter both directly and indirectly. Direct interaction takes place with critical molecules such as DNA and proteins present in microorganisms, thus causing cell death. During indirect interaction, radiolysis products of water result in the formation of highly reactive intermediates that then react with the target biomolecules, culminating in cell death. A plant for liquid sludge hygienization using gamma radiation has been in operation in Vadodara, India, since 1992 [5]. The plant is designed to treat 110 m<sup>3</sup> of sludge from a conventional treatment plant per day. The plant's operational experience has shown that the process is simple, effective, and easy to integrate into an existing sewage treatment plant, and the radiation hygienized sludge can be used as a fertilizer in agriculture. Similarly, an electron accelerator can also be used to treat dewatered sludge.

## 2 Industrial Off-Gas Treatment

Pollutants are emitted to the atmosphere with off-gassing from industry, power stations, residential heating systems, and municipal waste incinerators. Fossil fuels, which include coal, natural gas, petroleum, shale oil, and bitumen are the main source of heat and electrical energy. Recently, the main fuel used for renewable energy production in heat boilers is biomass as well. All these fuels contain, besides major constituents (carbon, hydrogen, oxygen), metal, sulfur, and nitrogen compounds.

During the combustion process different pollutants as fly ash, sulfur oxides (SO<sub>2</sub> and SO<sub>3</sub>), nitrogen oxides (NO<sub>x</sub> = NO<sub>2</sub> + NO), hydrochloride (HCl), and volatile organic compounds, including chlorinated species, are emitted. Ninety-five percent of emitted NO<sub>x</sub> is NO, an insoluble and non-reactive compound, which is difficult to remove. Fly ash contains different trace elements (heavy metals). Mercury is emitted as aerosolized, surface adsorbed, or free forms.

Gross emission of pollutants is tremendous in most countries all over the world. These pollutants are present in the atmosphere in such conditions that they can affect humans and their environment. Air pollution caused by particulate matter and other pollutants acts directly on the environment and also contaminates water and soil, leading to their degradation. Wet and dry deposition of inorganic pollutants leads to acidification of the environment. These phenomena affect health of the people, increase corrosion, destroy forest and plants.

Different air pollution control technologies are searched for. Conventional technologies, most often used for air pollution control, are: wet FGD (flue gas desulphurization), based on SO<sub>2</sub> absorption in lime or limestone slurry, and SCR (selective catalytic reduction), based on NO<sub>x</sub> reduction over a catalyst to atmospheric nitrogen with ammonia as a reductor. However, the technologies that treat different pollutants in one step are of special interest. The electron beam flue gas treatment (EBFGT) technology is such a process.

## 2.1 Interaction of Electrons with Flue Gas Components

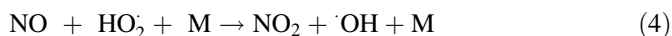
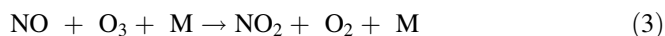
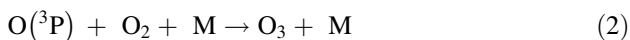
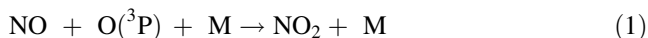
After irradiation of pollutant gas, fast electrons interact with the gas creating various ions and radicals; the primary species formed include  $e^-$ ,  $N_2^+$ ,  $N^+$ ,  $O_2^+$ ,  $O^+$ ,  $H_2O^+$ ,  $OH^+$ ,  $H^+$ ,  $CO_2^+$ ,  $CO^+$ ,  $N_2^*$ ,  $O_2^*$ ,  $N$ ,  $O$ ,  $H$ ,  $OH$ , and  $CO$ . In the case of a high water vapor concentration, the oxidizing radicals  $\cdot OH$  and  $HO_2$ , and excited ions such as  $O(^3P)$ , are the most important radiolysis products. The  $SO_2$ ,  $NO$ ,  $NO_2$ , and  $NH_3$  present cannot compete with the reactions because of very low concentrations, but react with  $N$ ,  $O$ ,  $OH$ , and  $HO_2$  radicals. Ammonia, mentioned above, is added to the gas to neutralize acids that are formed in reaction; aerosolized ammonium sulfate and nitrate are the final product of the reaction. The interaction of electrons with gas forms visible cold plasma (Fig. 1).

## 2.2 $SO_x$ and $NO_x$ Removal from Fossil Fuel Combustion Flue Gases

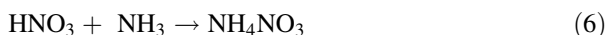
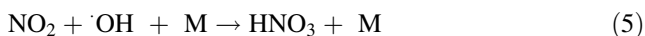
The method for sulfur and nitrogen oxides removal is based on the oxidation of both pollutants and their reaction with water to form acids [6]. Electrons from the accelerator and secondarily formed in gas pass energy to the gas components forming plasma in the process vessel (Fig. 1). The acids are neutralized with gaseous ammonia to form the solid aerosol: a mixture of ammonium nitrate and sulfate, which is the popular nitrogen bearing component of NPK (nitrogen, phosphor, potassium) fertilizer. There are several pathways of  $NO$  oxidation known. In the case of EBFGT the most common are as follows:



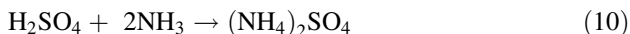
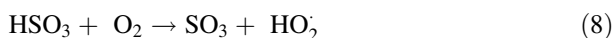
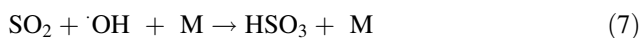
**Fig. 1** Visible light glow indicates that the cold plasma is formed inside the process vessel in which gas is irradiated (pilot plant at EPS Kaweczyn, Poland)



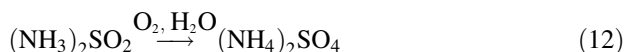
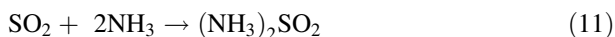
After the oxidation  $\text{NO}_2$  is converted to nitric acid in the reaction with  $\cdot\text{OH}$  and  $\text{HNO}_3$ , the aerosol reacts with  $\text{NH}_3$  giving ammonium nitrate. M is an inert component absorbing excess of energy. NO is partly reduced to atmospheric nitrogen.



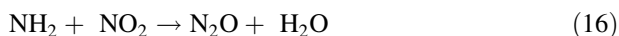
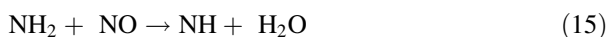
There can be also several pathways of  $\text{SO}_2$  oxidation depending on the conditions. In the EBFGT process the most important are radio-thermal and thermal reactions. Radio-thermal reactions proceed through radical oxidation of  $\text{SO}_2$  and  $\text{HSO}_3$  creates ammonium sulphate in the following steps [7].



The thermal reaction is based on the following process:



In the presence of ammonia some part of NO is reduced to nitrogen; therefore, the concentration of ammonium nitrate in the product is lower than expected from the reaction (6), the mechanism of reduction is shown below:





The total yield of  $\text{SO}_2$  removal consists of the yield of thermal and radio-thermal reactions that can be written as follows [8].

$$\eta_{\text{SO}_2} = \eta_1(\phi, T) + \eta_2(D, \alpha_{\text{NH}_3}, T) \quad (20)$$

where  $\eta$ ,  $\phi$ ,  $T$ ,  $D$ , and  $\alpha_{\text{NH}_3}$  are process efficiency, gas humidity, gas temperature, dose deposited (amount of energy transferred to gas by means of irradiation), and ammonia stoichiometry ( $\text{NH}_3$  concentration in relation to stoichiometric value), respectively. The yield of the thermal reaction ( $\eta_1$ ) depends on the temperature and humidity and decreases with the temperature increase. The yield of the radio-thermal reaction ( $\eta_2$ ) depends on the dose, temperature, and ammonia stoichiometry. The main parameter in  $\text{NO}_x$  removal is the dose. The rest of parameters play minor role in the process. The high dose is required for high concentrations of  $\text{NO}_x$  removal, while  $\text{SO}_x$  is removed at proper conditions, at low energy consumption. The  $\text{SO}_x$  removal efficiency equal to 95 % is easily achieved, while the nitrogen oxide concentrations observed at coal or oil fired boilers, a removal efficiency of 70–80 % is observed. This level of pollutant removal is requested by power plant operators, due to the existing standards of air pollution control. The scheme of flue gas treatment process is presented below (Fig. 2).

Recent tests have illustrated the possibility of process applications to treat the polycyclic aromatic hydrocarbon (PAH) and volatile organic compounds (VOC),

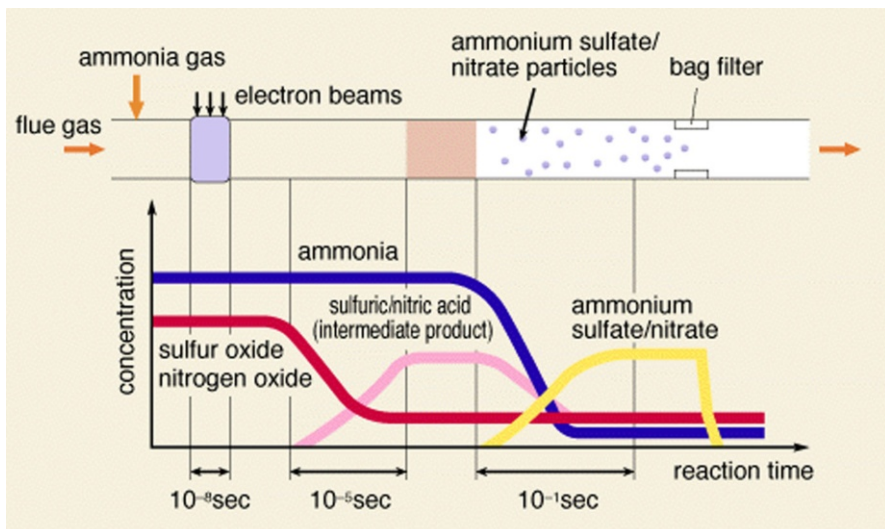


**Fig. 2** The scheme presenting sequences of the physicochemical reactions, which leads to acidic pollutants removal and solid fertilizer particles formation

including chlorinated VOCs, present in off-gases in trace concentrations [9], and the process has some features that may allow applying it to mercury control as well [10]. The process has been tested for boilers using high sulfur oil as a fuel [11, 12]. Parametric study was conducted for purification of exhaust gases from the burning of heavy fuel oil (HFO) mazut with sulfur content approximately 3 wt% to determine  $\text{SO}_2$ ,  $\text{NO}_x$ , and PAH removal efficiency as a function of temperature and humidity of irradiated gases, absorbed dose, and ammonia stoichiometry process parameters [13]. In the test performed under optimal conditions with a dose of 12.4 kGy, simultaneous removal efficiencies of approximately 98 % for  $\text{SO}_2$  and 80 % for  $\text{NO}_x$  were recorded. The simultaneous decrease of PAH and one-ringed aromatic hydrocarbon [benzene, toluene, and xylene (BTX)] concentrations were observed in irradiated flue gas. Overall removal efficiencies of approximately 42 % for PAHs and 86 % for BTXs were achieved with an absorbed dose of 5.3 kGy. The decomposition ratio of these compounds increased with an increase of absorbed dose. The decrease of PAH and BTX concentrations was followed by an increase of oxygen-containing aromatic hydrocarbon concentrations. The PAH and BTX decomposition process was initialized through the reaction with hydroxyl radicals that formed in the EB irradiated flue gas. Their decomposition process is based on similar principles as the primary reaction concerning  $\text{SO}_2$  and  $\text{NO}_x$  removal; that is, free radicals attack organic compound chains or rings, causing VOC decomposition. Thus, the EBFGT technology ensures simultaneous removal of acid ( $\text{SO}_2$  and  $\text{NO}_x$ ) and organic (PAH and BTX) pollutants from flue gas emitted from burning HFO. This technology is a multi-pollutant emission control technology that can be applied for treatment of flue gas emitted from coal-, lignite-, and HFO-fired boilers. Other thermal processes such as metallurgy and municipal waste incinerators are potential candidates for application of this technology. In the case of VOCs, decomposition process is based on the similar principles as primary reactions concerning  $\text{SO}_2$  and  $\text{NO}_x$  removal, i.e. free radicals attack on organic compounds chains or rings causing VOCs decomposition. For chlorinated aliphatic hydrocarbons decomposition (e.g. chloroethylene),  $\text{Cl}^-$  dissociated secondary electron attachment and  $\text{Cl}$ ,  $\text{OH}$  radicals reaction with VOCs play very important roles [14–18]. Application of scavengers such as alcohol may improve simultaneous  $\text{NO}_x$  removal efficiency [15]. The most important development concerns application for the reduction of polychlorinated dibenzodioxins (PCDDs, so-called dioxins) and polychlorinated dibenzofurans (PCDFs) emission from municipal solid waste incinerators [19]. Degradation of different organic pollutants in the gas phase was tested, including toluene [20], styrene [21], naphthalene, and acenaphthene [22]. Different factors affecting the process were studied [23–26]. The hybrid process based on EB generated plasma and catalyst enhancing reaction was studied to increase VOC removal efficiency and reduce energy consumption [27–29], combined use of EB, microwaves, and catalysts was investigated as well [30].

### 2.3 Industrial Application of the Process

The above mechanism of the process, studied in laboratory conditions, was the basis for technical implementation of the technology. However in real, industrial



conditions, dose distribution and gas flow patterns are important from a technological point of view. These parameters influence the electron energy, mass, and heat transfer, prior, after, and in the process vessel. After humidification and lowering of the temperature, flue gases are guided to the reaction chamber, where irradiation by EB takes place. The electrons are introduced to the process vessel via thin 50  $\mu\text{m}$  titanium foil.  $\text{NH}_3$  is injected upstream of the irradiation chamber. Ammonia is used to neutralize sulphuric and nitric acids and to form the aerosolized solid particles. The size of aerosol particles is about 1  $\mu\text{m}$ , and the byproduct is sticky; therefore, high efficiency dust collectors have to be applied downstream of the chemical reactor. The electrostatic precipitators (ESPs) are equipped in the screw conveyors installed at the heated bottom and hammering systems at the electrodes and other filter components. The insulators are protected by air jets. The solid byproduct is a high class fertilizer.

Japanese scientists demonstrated in 1970–1971 the removal of  $\text{SO}_2$  using an EB from a linear accelerator (2–12 MeV, 1.2 kW). A dose of 50 kGy at 100 °C led to the conversion of  $\text{SO}_2$  to an aerosol of sulfuric acid droplets, which were easily removed. Ebara Co. used an electron accelerator (0.75 MeV, 45 kW) to convert  $\text{SO}_2$  and  $\text{NO}_x$  into a dry product containing  $(\text{NH}_4)_2\text{SO}_4$  and  $\text{NH}_4\text{NO}_3$ , which could be used as a fertilizer. Using the Ebara process, two larger scale pilot plants were constructed in Indianapolis, IN, USA and Karlsruhe, Germany. The Indianapolis plant was equipped with two electron accelerators (0.8 MeV, 160 kW) and had a capacity of  $1.6\text{--}3.2 \times 10^4 \text{ m}^3/\text{h}$  with gas containing 1000 ppm  $\text{SO}_2$  and 400 ppm  $\text{NO}_x$ . In Karlsruhe, two electron accelerators (0.3 MeV, total power 180 kW) were used to treat  $1\text{--}2 \times 10^4 \text{ m}^3/\text{h}$  flue gas containing 50–500 ppm  $\text{SO}_2$  and 300–500 ppm  $\text{NO}_x$ .

However, the final engineering design technology for industrial applications was achieved at the pilot plants being operated in Nagoya, Japan [31] and Kaweczyn, Poland [32]. In the latter case, new engineering solutions were applied: double—longitudinal gas irradiation, air curtain separating secondary window from corrosive flue gases and modifications of the humidification/ammonia system (high enthalpy water or steam injection, ammonia water injection), and others. The obtained results have confirmed the physico-chemistry of the process discussed earlier. In Fig. 3 a sketch of the pilot plant and applied process vessel is presented. A double window

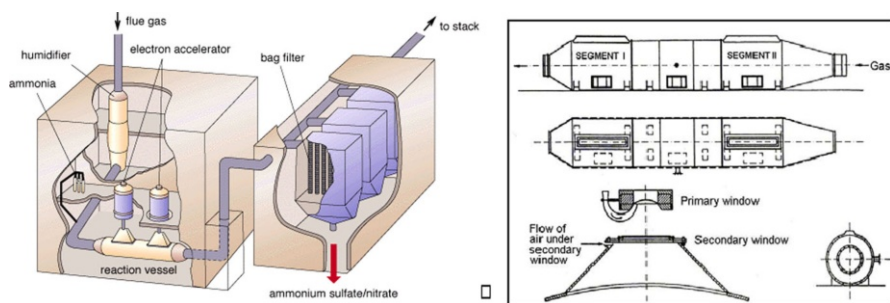


**Fig. 3** Scheme of the flue gas pilot plant and irradiation vessel applied at EPS Kaweczyn, Poland

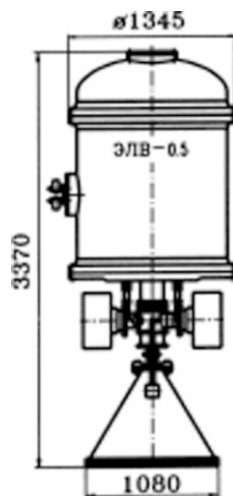
was applied to protect the window of the accelerator from corrosive flue gas atmosphere, and an air curtain protects a secondary window from such effects as well [33]. **Figure 4** is a scheme of the accelerator used in this pilot plant.

These new solutions led to the economical and technical feasibility improvement and final industrial scale plant construction. Ebara Co. constructed a full scale plant in Chengdu, China, mostly for  $\text{SO}_x$  removal; therefore, the power of accelerators applied is 320 kW for treatment of  $270,000 \text{ Nm}^3/\text{h}$  of the flue gas. Reported efficiency is 80 % for  $\text{SO}_x$  and 20 % for  $\text{NO}_x$  [34].

The flue gas treatment industrial installation is located in EPS Pomorzany in Szczecin in the north of Poland (**Fig. 5**) [35]. The installation purifies flue gases from two Benson boilers of  $65 \text{ MW}_e$  and  $100 \text{ MW}_{th}$  each. The maximum flow rate of the gases is  $270,000 \text{ Nm}^3/\text{h}$  and the total beam power exceeds 1 MW. Upstream of the EBFGT installation fly ash is removed from flue gas to a content equal to less than  $25 \text{ mg}/\text{Nm}^3$  to avoid contamination of the byproduct, since it is a component of fertilizer. Then the flue gases are cooled and humidified in a spray cooler, a tower with rubber lining, and gaseous ammonia is injected to the gas stream. The concentration of ammonia is regulated at a concentration equal to 0.9 stoichiometric ratio calculated to both acidic pollutants, which allows keeping the ammonia slip lower than 5 ppm. After such treatment flue gases inflow into plasma reactors where plasma is generated by electrons emitted by electron accelerators. There are two reaction vessels with nominal flow gas rate of  $135,000 \text{ Nm}^3/\text{h}$ . Gases in each vessel are irradiated by two accelerators (700 keV, 260 kW) installed in series. The applied dose is in the range of 7–12 kGy. The removal of  $\text{SO}_2$  approaches 80–90 % in this dose range and that of  $\text{NO}_x$  is 50–60 % (**Fig. 6**). The byproduct is collected by the ESP and is shipped to the fertilizer plant. Pilot and industrial scale electron EBFGT plants are listed in **Table 1**.

Recently a pilot scale EBFGT was tested at Saudi Aramco's Refinery in Jeddah, Saudi Arabia [36]. The plant was designed to treat  $2000 \text{ Nm}^3/\text{h}$  of flue gas emitted from a heavy fuel oil fired boiler. A unique mobile electron accelerator unit

**Fig. 4** An example of accelerators used for EBFGT. ELV –3a accelerator has been applied at the EPS Kaweczyn pilot plant



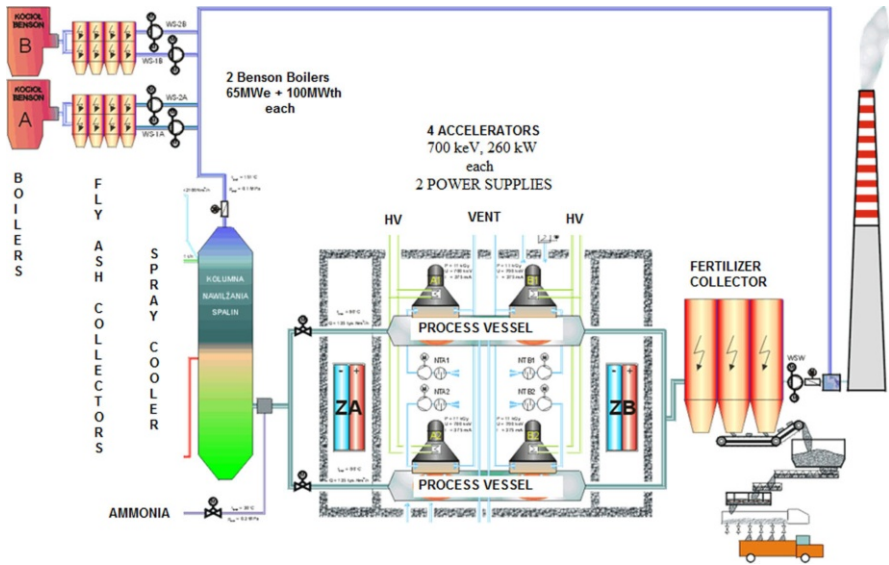


**Fig. 5** Scheme of industrial plant for EBFGT, EPS Pomorzany, Szczecin, Poland

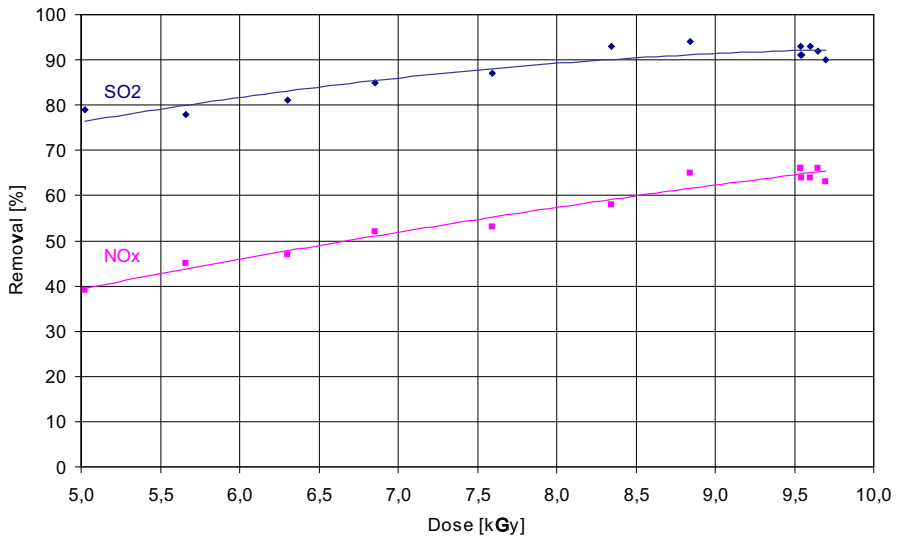


**Fig. 6** Removal efficiency of SO<sub>2</sub> and NO<sub>x</sub> as a function of energy absorbed in gas

(600 keV, 20 kW) made by EB TECH Co., Ltd., Korea was used as a beam source. The general view of the pilot plant is presented in Fig. 7.

The pilot plant operation proved the high potential of the technology for simultaneous control of sulfur dioxide (SO<sub>2</sub>) and nitrogen oxides (NO<sub>x</sub>) emissions. The obtained removal efficiencies reached 98.5 % for SO<sub>2</sub> and 83.1 % for NO<sub>x</sub> (Fig. 8).

**Table 1** Pilot and industrial scale EBFGT plants

Plant	Flow rate (Nm <sup>3</sup> /h)	Accelerator	Dose (kGy)	SO <sub>2</sub> /NO <sub>x</sub> (ppm)
Indianapolis, USA (1984)	24,000	800 keV × 2, 160 kW	30	1000/400
Badenwerk, Germany (1985)	20,000	300 keV, 180 kW	–	500/500
Kawęczyn, Poland (1992)	20,000	700 keV × 2, 100 kW	18.8	600/250
Nagoya, Japan (1992)	12,000	800 keV × 3, 108 kW	10.5	1000/300
EB-TECH, Korea (1995)	10,000	1000 keV, 50 kW	8	600/400
Chengdu, China (1997)	300,000	800 keV × 2, 400 mA, 640 kW	3	1800/400
Pomorzany, Poland (1999)	270,000	700 keV × 4, 375 mA, 1050 kW	10	1630/540
Hangzhou, China (2002)	305,400	800 keV × 2, 400 mA 640 kW	3	1800/400
Mariza East, Bulgaria (2004)	10,000	800 keV × 3, 108 kW	4	1000/300
Beijing, China (2006)	640,000	1000 keV × 2, 500 mA, 1000 keV, 300 mA, 2850 kW	3	1900/400
Shandong, China (2007)	279,000	800 keV, 200 mA × 2, 1600 kW	3	1900/400
Jeddah, Saudi Arabia (2014)	2000	600 keV, 20 kW (mobile)	8	1400/130



**Fig. 7** General view of the pilot plant at Jeddah Refinery. 1 stack of F 1001 boiler, 2 boiler F 1001, 3 flue gas duct, 4 control room of pilot plant, 5 gas conditioning column, 6 pilot plant stack, 7 cartridge bag filter, 8 thermal insulated duct, 9 cyclone, 10 ammonia dosing unit, 11 mobile accelerator unit

Two types of byproduct collection devices—cartridge bag filter and electrostatic precipitator—were tested. The obtained byproduct was a high-quality fertilizer that can be used directly or as a substrate for NPK blends manufacturing. The soluble part of the byproduct was almost pure ammonium sulfate (98–99 %) with some amount of ammonium nitrate. The content of heavy metals in the byproduct was very low, two orders of magnitude lower than the allowed standards.

The tests performed at industrial conditions have proven that the technology can be applied for flue gas treatment for coal (hard and lignite) and oil fired boilers and the byproducts is a high class fertilizer.

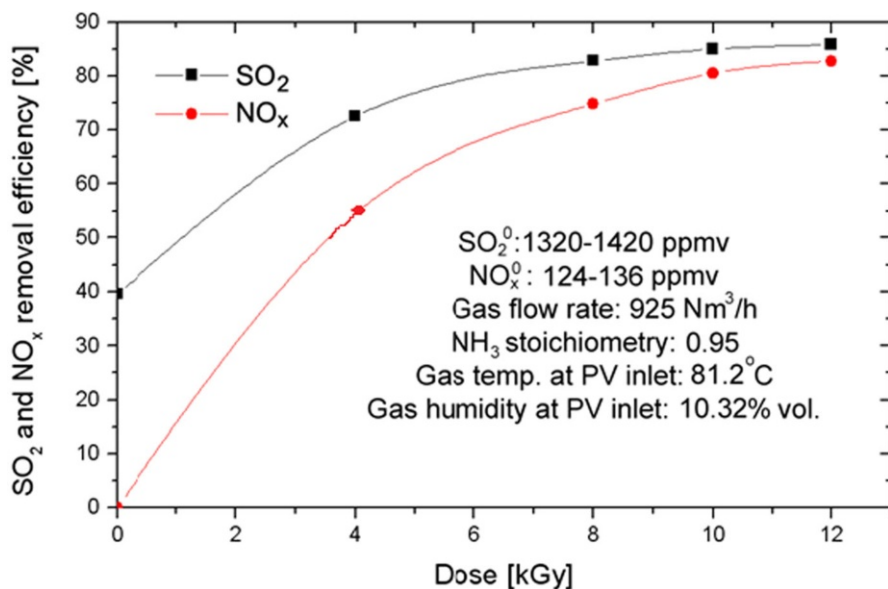


**Fig. 8** SO<sub>2</sub> and NO<sub>x</sub> removal efficiency as a function of absorbed dose

Coal and natural gas are the most often used fossil fuels for electricity and heat generation. However, the prices of fossil fuels will follow again increasing trend and the reserves of clean fuel like gas will become depleted in the future, taking into account that methane is one of the main chemical industry substrates. Heavy fuel oil is essentially industrial fuel used in industrial boilers containing up to 4.0 % of sulfur. This oil is used in diesel engines as well. The combustion of this fuel results in high emission of sulfur and nitrogen oxides. Computer simulations for high concentrations of NO<sub>x</sub> removal from oil-fired waste off-gases under EB irradiation were carried out by using the computer code “Kinetic” and GEAR method. Two hundred and ninety-three reactions involving 64 species were used for the modeling calculations. The composition of simulated oil-fired off-gas was the same as the experimental conditions. Calculation results qualitatively agree with the experimental results. Furthermore the influence of temperature, SO<sub>2</sub> concentration and ammonia addition were studied [37]. The results have shown that in the case of high NO<sub>x</sub> concentrations the hybrid methods have to be applied. Development of the technology and reducing of energy consumption may lead to the most challenging applications such as treatment of huge diesel engine exhaust gases, a problem that has not been solved up to now [38]. One of the solutions proposed was based on increasing electron energy from 0.7 to 1–2 MeV when it is possible to reduce the energy losses in the windows and in the air gap between them (transformer accelerators can be applied as well as in the process). In order to use these mid-energy accelerators it is necessary to reduce their penetration depth through gas and this can be achieved by increasing the density of the reaction medium by means of dispersing a sufficient amount of fine water droplets (FWD). The presence of FWD

has a favorable effect on the overall process by increasing the level of liquid phase reactions. A special reactor was designed and built to test the effect of FWD on the treatment of flue gases with high concentrations of SO<sub>2</sub> and NO<sub>x</sub> using high energy. By determining the energy efficiency of the process the favorable effect of using FWD and high energy EB was demonstrated [39].

### 3 Wastewater Treatment

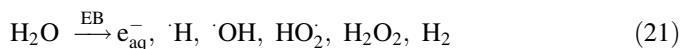
EB processing of water/wastewater is non-chemical and uses fast formation of short-lived reactive radicals that can interact with a wide range of pollutants. Such reactive radicals are strong oxidizing or reducing agents that can transform the pollutants in the liquid wastes from industry and different origins.

EB treatment of wastewater leads to purification by the decomposition of pollutants as a result of their reactions with highly reactive species formed from water radiolysis: hydrated electrons, OH free radicals, and H atoms [40, 41]. Sometimes such reactions are accompanied by other processes, and the synergistic effect upon the use of combined methods such as electron beams with biological treatment, adsorption, and others improves the effect of EB treatment of the wastewater purification. In the process of EB treatment of wastewater, chemical transformation of pollutants induced by ionizing radiation are used. At sufficiently high absorbed doses these transformations can result in complete decomposition (removal) of the substance. Under real conditions, at a rather high content of pollutants in wastewater and economically acceptable doses, partial decomposition of pollutants takes place, as well as transformation of pollutant molecules that results in improving subsequent purification stages, efficiency of the process, which is notably influenced by irradiation conditions and wastewater composition [42].

#### 3.1 Interaction of Electrons with Water Molecules in Aqueous Media

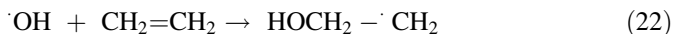
Radiation technologists have been investigating the use of high-energy radiation for treatment of wastewater. The major advantage of radiation technology is that the reactive species are generated in situ during the radiolysis process without addition of any chemicals. The results of practical applications have confirmed that radiation technology can be easily and effectively used for treating large quantities of wastewater [3, 43, 44].

High-energy irradiation produces instantaneous radiolytical transformations by energy transfer from accelerated electrons to orbital electrons of water molecules. Absorbed energy disturbs the electron system of the molecule and results in breakage of inter-atomic bonds [42]. Hydrated electrons e<sub>aq</sub><sup>-</sup>, H atoms, ·OH and HO<sub>2</sub>· radicals, hydrogen peroxide (H<sub>2</sub>O<sub>2</sub>), and H<sub>2</sub> are the most important intermediates and products of the primary interactions (radiolysis products).



with yields ( $G$  value,  $\mu\text{mol/J}$ ) of 0.28 ( $e_{\text{aq}}^-$ ), 0.062 (H), 0.28 (OH), 0.072 ( $\text{H}_2\text{O}_2$ ).

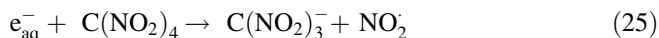
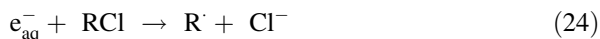
High reactivity is characteristic of water radiolysis products. The typical time of their reactions with impurities in water is less than 1  $\mu\text{s}$ .  $\text{H}_2\text{O}_2$  and  $\cdot\text{OH}$  and  $\text{HO}_2\cdot$  radicals are oxidizing species, while H atoms and  $e_{\text{aq}}^-$  are reducing [41]. Simultaneous existence of strong oxidants and strong reductants within wastewater under treatment is remarkable and important characteristics of radiation processing. In reactions with unsaturated hydrocarbons,  $\cdot\text{OH}$  adds onto the double bond



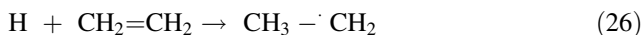
and, upon reaction with alkyl-compound, the  $\cdot\text{OH}$  captures H-atom to produce



Hydrated electrons  $e_{\text{aq}}^-$  and H atoms are strong reductants. In reactions involving cations of metals,  $e_{\text{aq}}^-$  is able to produce neutral atoms and ions with anomalous valency. Typical reactions of  $e_{\text{aq}}^-$  consist of  $e^-$ -addition to reagents,



In its reactions with organic compounds,  $\cdot\text{H}$  shows higher reactivity than  $e_{\text{aq}}^-$ . Reactions with unsaturated hydrocarbon consist of  $\cdot\text{H}$  addition to double bond:



With alkyl-compounds,  $\cdot\text{H}$  produces a hydrogen molecule and an alkyl-radical

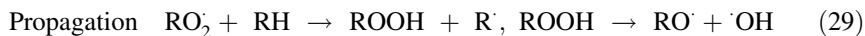


EB treatment aims at the degradation of pollutants at a faster rate than the generally slow rates of conventional processes. EB treatment of wastewater generally has maximum efficiency at pollutant concentrations of  $10^{-3}$  mol/L ( $\sim 100$  ppm) or less. The treatment of such wastewater is simple, requires a low dose ( $\sim 1$  kGy or less) and provides almost complete elimination of odour, colour, taste, and turbidity. The EB treatment of polluted water containing specific contaminants may require the creation of special conditions to achieve the predominant type of transformation—reduction, oxidation, addition or removal of functional groups, aggregation, disintegration, etc. However, in general, pollutant transformation involves the following pathways: chain oxidation, formation of insoluble compounds, coagulation of colloids, and enhancement of pollutant biodegradability.

Chain oxidation constitutes one of the most efficient processes realized in radiation processing of wastewater. Radiolytic oxidation at moderate dose leads to the formation of carbonyl, carboxyl, hydroxyl, and/or peroxide groups in organic molecules [3]. The conditions of irradiation can be specifically chosen to achieve



chain oxidation of various pollutants. The general mechanism of chain oxidation consists of the following stages:



The products of radiolytic oxidation differ from the initial pollutants in terms of their physicochemical properties and increased ability to biodegradation. Biodegradation of wastewater depends on oxidation level and structure of pollutants, and preliminary oxidation and fragmentation of biologically resistant molecules contribute to improvement in their biodegradability. Radiolytic oxidation shows possibility for the required transformation of various pollutants. Research and industrial treatments testify to significant improvement of pollutant biodegradability after radiation-oxidation of aerated wastewater [43–45]. Usually, a dose of about 1–2 kGy is necessary for complete transformation of pollutants from a biologically resistant to a biodegradable state. Several pilot scale and a number of industrial scale plants based on radiation technology are in operation and under construction. A simplified technological scheme of e-beam wastewater treatment plant is shown in Fig. 9.

### 3.2 Electron Beam Treatment of Wastewater

The increasing levels of pollution and complexity of effluents from municipalities and industry demand effective technologies to reduce pollutants to the desired levels, and the use of current wastewater treatment technologies for such reclamation often is not successful. Advanced wastewater treatment technologies are essential for the treatment of municipal wastewater to protect public health and

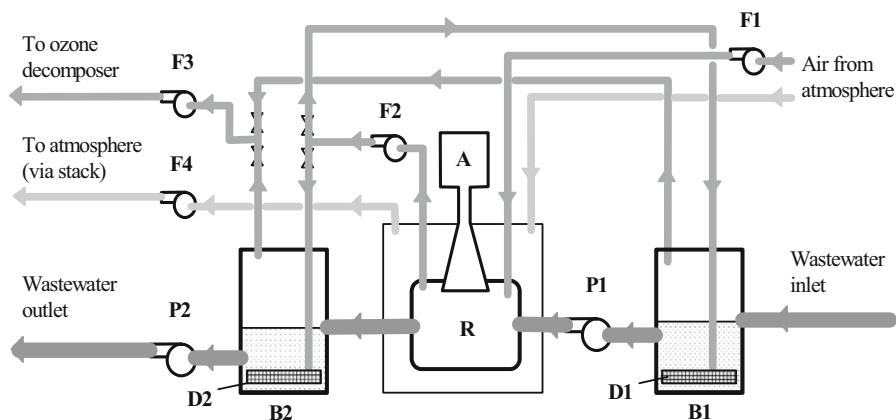


**Fig. 9** Simplified technological scheme of industrial e-beam wastewater treatment plant; *F1–F4* air fans, *P1–P2* water pumps, *D1–D2* diffusers, *A* accelerator, *R* reactor, *B1* and *B2* primary and secondary basins



to meet water quality criteria for the aquatic environment and for water recycling and reuse. Among the possible water treatment alternatives, radiation processing is a very effective option, as it can simultaneously degrade both the toxic organic compounds and the biological contaminants that are present. Radiation disinfection of effluent from municipal wastewater treatment plants for reuse has been successfully demonstrated by a number of researchers. It has been demonstrated that inactivation of faecal coliforms in secondary effluents from municipal wastewater plants can be achieved with absorbed doses of less than 1 kGy. While the efficiency of conventional disinfectants is adversely affected by the water matrix, radiation processing for bacteria inactivation is generally unaffected by it. Therefore, radiation processing has a clear advantage over existing methods for municipal wastewater disinfection. Radiation processing is technically much easier than conventional processes for wastewater disinfection (Fig. 10). A cost assessment based on a dose of 1 kGy has indicated that for a plant capacity of about 1150 m<sup>3</sup>/h, the cost of treating secondary effluent is about USD 0.1/m<sup>3</sup>, which is acceptable, considering the advantages that the radiation induced disinfection provides compared with conventional technologies [46].

Radiation treatment of textile dyeing wastewater and several dyes has also been actively studied in Brazil [47], Hungary [48], and Turkey [49]. A pilot scale wastewater treatment plant was set up at the Institute of Energy and Nuclear Research (IPEN) in Brazil to study the efficiency of removal and degradation of toxic and refractory pollutants present in industrial wastewater. Combined biological and radiation treatment of domestic sewage and sludge was carried out to investigate disinfection. Radiation processing of many other industrial wastewater samples collected at the public wastewater treatment plant in Sao Paulo State were also tested. For industrial wastewater from chemical industries, a dose of 20 kGy was necessary to degrade about 99 % of the organic compounds [47].

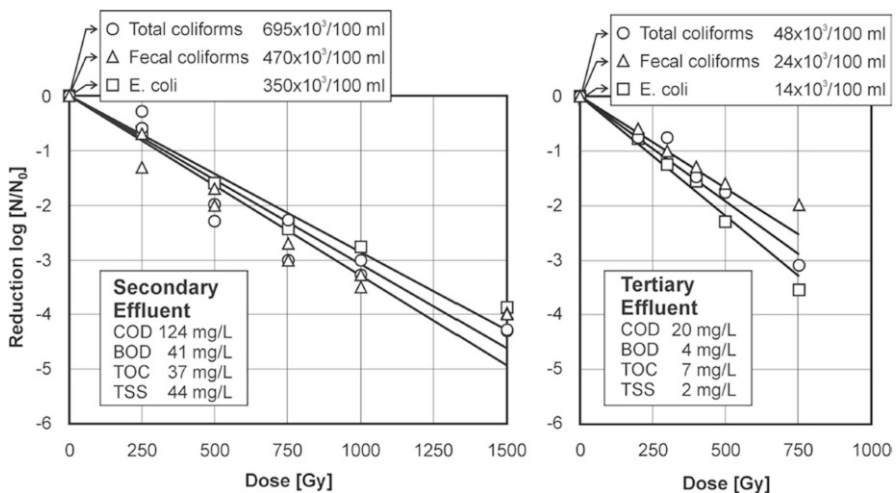


**Fig. 10** Radiation induced inactivation of some coliforms in different effluents by means of EB irradiation [46]

Purification of the complex wastewater from textile dyeing companies has demonstrated in Daegu Dyeing Industrial Complex (DDIC) as an industrial scale. DDIC includes about a hundred factories with high consumption of water (90,000 m<sup>3</sup>/day), steam, and electric power, characterized by a large amount of highly coloured industrial wastewater (80,000 m<sup>3</sup>/day), and extracting thereby up to 500 m<sup>3</sup>/d of sludge. Rather high cost of purification results from high contamination of water with various dyes and ultra-dispersed solids. Chemical composition of wastewater consists of organic dyes, surfactants, and other organic compounds. In organic compounds, terephthalic acid (TPA) and ethylene glycol (EG) are the major components of pollutants. Organic dyes and surfactants, even at comparatively low concentration, determine such objectionable properties of the wastewater as colour and foaming, so concentration of these compounds should be substantially reduced.

After a successful operation of pilot scale (1000 m<sup>3</sup>/day of wastewater) EB plant [43], an industrial plant with an electron accelerator of 1 MeV, 400 kW for treating 10,000 m<sup>3</sup>/day of textile dyeing wastewater from DDIC has been constructed and operated from 2005 (Fig. 11). This plant is combined with biological treatment system and it shows the reduction of chemical reagent consumption, and also the reduction in retention time with the increase in removal efficiencies of COD<sub>Cr</sub> and BOD<sub>5</sub> up to 30–40 % (Fig. 12) [50]. Increase in biodegradability after EB treatment of aqueous-organic systems is due to radiolytical conversions of non-biodegradable compounds. The total construction cost for this plant was about USD 4 M and the operation cost has been obtained approximately USD 0.5 M per year. Even with including the depreciation and interest, it is not more than USD 1 M per year and it is about USD 0.3 per each cubic meter of wastewater [50].

### 3.3 Removal of Emerging Contaminants

Endocrine disrupting chemicals (EDCs) and pharmaceutical compounds are mostly man-made, found in various materials such as pesticides, polymer additives, and personal care products. EDCs and pharmaceutical residues have been suspected to be associated with altered reproductive function in males and females, increased

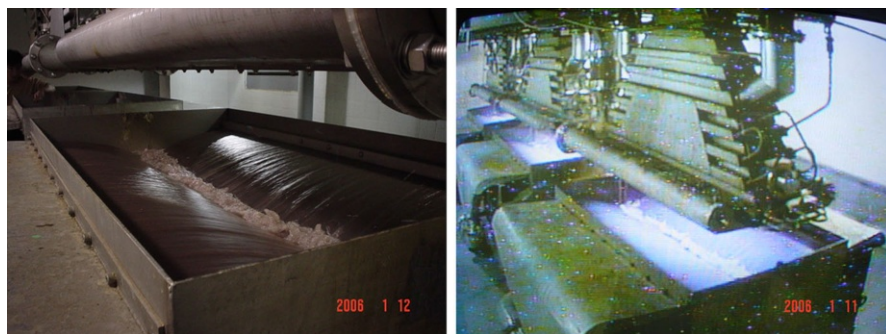


**Fig. 11** Industrial EB plant (10,000 m<sup>3</sup>/day) for textile dyeing wastewater in Daegu, Korea

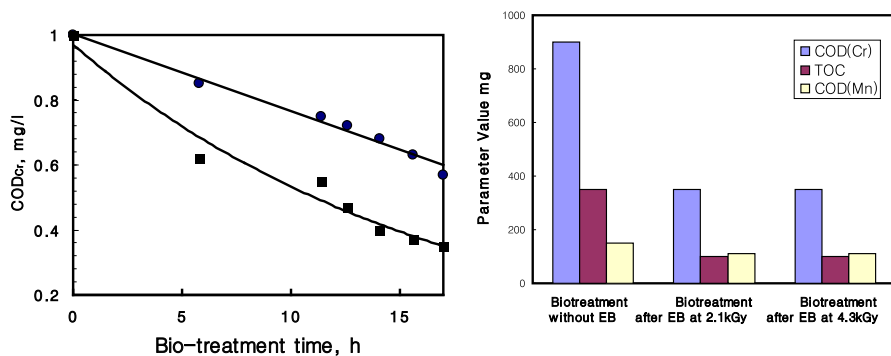


**Fig. 12** Effect of electron-beam treatment on biological treatment of dyeing wastewater: **a** kinetics of biotreatment of irradiated (*filled square*) and unirradiated (*filled circle*) wastewater; **b** absorbed dose effect on combined electron-beam/biological treatment

incidence of breast cancer, abnormal growth patterns, and neuro-developmental delays in children, as well as changes in immune function [51–53]. A number of processes were investigated regarding their removal potential of endocrine disrupters. Those processes are ferric chloride coagulation, powdered activated carbon, magnetic ion exchange combined with microfiltration or ultrafiltration, as well as nanofiltration and reverse osmosis. While they show a certain limitation in removal of EDCs in aqueous solution, the EB has the ability to remove the EDCs and pharmaceutical residues with a very high degree of reliability and in a clean and efficient manner. The EB interacts with them according to the mechanism described above [54, 55]. Radiolysis products of water result in the formation of highly reactive intermediates which then react with the target molecules, culminating in structural changes.

#### 4 Sludge Treatment

The sludge resulting from municipal or industrial wastewater treatment is usually in the form of a liquid or semisolid liquid that typically contains 0.25–12 % solids by weight, depending on the operations and processes used. Of the components removed in wastewater treatment, sludge is by far the greatest in volume, and the problems associated with its processing and disposal are complex because:

- It is composed of the substances responsible for the offensive character of untreated wastewater;
- The portion of sludge produced from biological treatment and requiring disposal is composed of the organic matter contained in the wastewater, but in a form that can decompose and become offensive;
- Only a small portion of the sludge is solid matter.

The sludge can be used as a soil conditioner and as an additive to animal fodder. However, it contains bacteria, viruses, and parasites (and possibly toxic compounds) and should be disinfected prior to any such use. Guidelines by the US

Environmental Protection Agency (EPA) recommend that in sewage sludge to be applied in agricultural practice, the number of *E. coli* bacteria (used as an indicator of the presence of pathogens) not exceed 1000 per gram of dry sludge [56]. In addition to this, industrial sludge contains EDCs, and they may have a broad range of health effects. When absorbed in the body, an endocrine disruptor can decrease or increase normal hormone levels, mimic the body's natural hormones, or alter the natural production of hormones.

#### 4.1 Inactivation of Microorganisms

The high energy ionizing radiation from radioactive sources such as  $^{60}\text{Co}$  or an electron accelerator has the ability to inactivate pathogens with a very high degree of reliability and in a clean and efficient manner. Ionizing radiation interacts with matter both directly and indirectly. Direct interaction takes place with critical molecules like DNA and the proteins present in microorganisms, thus causing cell death. During indirect interaction, as is described in Eq. (20), radiolysis products ( $e_{\text{aq}}^-$ ,  $\cdot\text{H}$ ,  $\cdot\text{OH}$ ,  $\text{HO}_2$ ,  $\text{H}_2\text{O}_2$ ,  $\text{H}_2$ ) of water result in the formation of highly reactive intermediates that then react with the target biomolecules, culminating in cell death.

The presence of oxygen is important in the process, as it is a known radiosensitizer that helps fix the radiation damage done to cells, thereby inhibiting their self-repair mechanism and resulting in the inactivation of microorganisms.

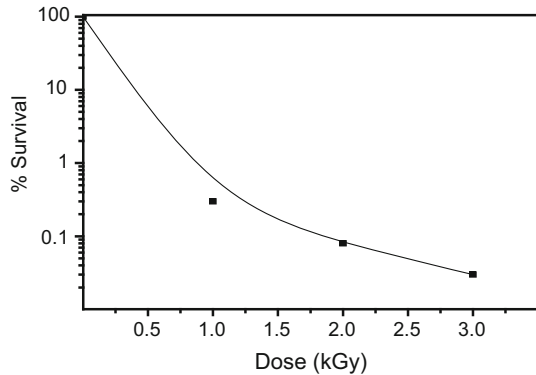
The absorbed dose required to inactivate the pathogenic bacteria is generally defined in terms of the  $D_{10}$  value, which is the dose required to reduce (through inactivation or cell death) the microbial concentration by a factor of ten or by one log cycle. In fact, this principle was the basis for producing radiation sterilized, single use medical products and is now well established in industry worldwide [3]. Based on the same principle, the pathogens present in sewage sludge can also be effectively removed by exposure to high energy radiation. The radiation treatment of sewage sludge offers an efficient, simple and reliable method for producing pathogen free sludge that can be further upgraded to produce a value added biofertilizer and allow waste recycling. Therefore, in recent years, irradiation of sewage sludge as a tertiary treatment process has been investigated [57–60].

It has been shown [61] that a dose of 2–3 kGy destroys more than 99.9 % of the bacteria present in sewage sludge and leads to the almost complete removal of helminth eggs and to the inactivation of the agents that cause disease in animals (Fig. 13).

Doses of this magnitude are employed for the radiation treatment of sewage sludge at an industrial plant in Geiselbullach, Germany [62], and slightly higher doses (4 kGy) are used at a pilot plant near Boston, MA, USA [63]. Higher doses (up to 10 kGy) are required to inactivate more radiation resistant organisms. Doses of 10 kGy were used at a sewage treatment plant in Albuquerque, NM, USA [64, 65], and at an installation in Ukraine [66].

In addition to disinfection, irradiation has a beneficial effect on physicochemical properties of sewage sludge such as the specific resistance to filtration, water separation and sedimentation. An increase of the sedimentation rate is observed

**Fig. 13** Survival of coliform microbial population as a function of absorbed dose [61]



when sludge are irradiated [67]. The changes are due to a decrease in the stability of colloidal particles in the irradiated sludge accompanying radiation induced changes in the charge on the particles. The changes in the physical properties of sludge do not affect their quality as fertilizers or fodder additives [66].

#### 4.2 Pilot and Industrial Scale Operation of Sludge Hygienization

The previous works, listed in Table 2, are mainly to disinfect the microorganisms since the sludge generated by a sewage plant contains a high concentration of pathogens, which limits the reuse of this waste—a rich source of plant nutrients, the disposal of sewage sludge in its original form is an economic loss to society. However, the industrial sludge is used to send to incineration plant or sanitary landfilling area, but to cause the secondary problems by the release of EDCS to environment. Thus, it is necessary to enhance the treatment process to ensure the removal of the EDCs with a high degree of reliability.

A typical EB sludge treatment plant consists of sludge feeding system, electron accelerator with shield structure (Fig. 14). Dewatered sludge is spread through a flat wide nozzle onto a stainless steel conveyor belt and fed past the EB in an 8–40 mm thick layer at a rate that provides an absorbed dose of 5–10 kGy; the maximum feed rate is 3 ton/h [68]. The thickness of sludge depends on the energy of EB. After irradiation, the sludge is moved to a conveyor belt where it is composted under conditions of controlled aeration and frequent mixing. The irradiated sludge, being pathogen free, can be beneficially used as manure in agricultural fields, as it is rich in required soil nutrients.

Applying the EB approach for sludge hygienization has also been studied in Israel [69]. Digested sludge from municipal wastewater treatment plants have long been used directly in agriculture in Israel. However, owing to infection by pathogenic microorganisms, the sludge must be processed to reduce the number of pathogens. An industrial scale plant with the capacity to treat 600 m<sup>3</sup> of dewatered sludge per day (18 % solid contents) with 10 kGy has been planned. This plant will be equipped with two electron accelerators (50 kW each) and handling facilities, and is expected to be more economical than other sludge disposal processes, such as incineration or lime stabilization.

**Table 2** Sludge treatment plant by radiation (Gamma ray or EB)

Facilities	Irradiation Source	Irradiated material	Operation	Remarks
Munich, Germany (1973–1984)	Gamma-ray ( $^{60}\text{Co}$ ) 0.57 MCi	Liquid sewage sludge, 145 m <sup>3</sup> /day	2–3 kGy	Commercial
New Mexico, USA (1978)	Gamma-ray ( $^{137}\text{Cs}$ ) 0.9 MCi	Sewage sludge cake, 22–90 t/day	10 kGy	Pilot plant
Vadodara, India (1989)	Gamma-ray ( $^{60}\text{Co}$ ) 0.5 MCi	Liquid sewage, 110 m <sup>3</sup> /day (4 % SS)	3–5 kGy	Commercial
Tucuman, Argentina (1998)	Gamma-ray ( $^{60}\text{Co}$ ) 0.7 MCi	Liquid sewage sludge 180 m <sup>3</sup> /day (8–10 % SS)	3 kGy	
Weldel, Germany (1980)	EB 50 kW (1.0 MeV, 50 mA)	Liquid sewage sludge, 500 m <sup>3</sup> /day	4 kGy	
Verginia Key, USA (1984)	EB (ICT type) (75 kW/ 1.5 MeV/50 mA)	Liquid sewage sludge, 645 m <sup>3</sup> /h, 4 % SS	4 kGy 10 mm	Pilot plant
Takasaki, Japan (1991)	EB (Cockcroft-Walton) (15 kW/2 MeV/ 15 kW)	Sewage sludge cake, 300 kg/h	5 kGy 1–10 mm	Pilot scale
Sao paulo, Brazil (1993)	EB 25 kW (1.5 MeV, 25 mA)	Liquid sewage sludge, 3 m <sup>3</sup> /h	3 kGy	Pilot plant
Warsaw, Poland (1994)	EB (LAE13/9) (10 MeV, 15 kW)	Sewage sludge cake, 70 t/day	5–7 kGy 2–3 cm	Design
Daejeon, Korea (2005)	EB 40 kW (1.0 MeV, 40 mA)	Dewatered sludge	1–3 kGy 6 mm thick	Pilot scale

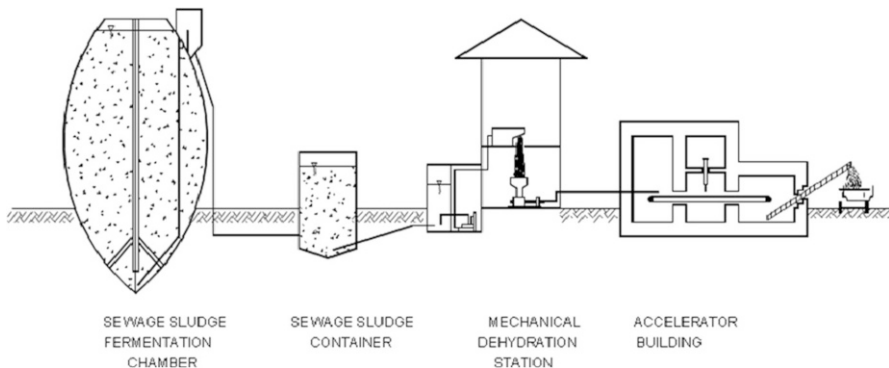


**Fig. 14** Industrial scale sludge treatment plant with EB (70 ton/day) [68]

### 4.3 Enhanced Composting of Radiation Disinfected Sewage Sludge

Problems concerning the land application of sewage sludge include the need to improve handling through reduced water content and to remove odours and pathogens. Regulations put into place by the US EPA require that sludge applied to

land surfaces or incorporated into the soil be treated using a process that significantly reduces pathogens (e.g. anaerobic digestion, aerobic digestion, air drying, composting, lime stabilization). In addition, public access to the site must be controlled for at least 12 months, and grazing by animals used as foodstuff for humans must be prevented for at least 1 month [70]. To address these problems, treatment to stabilize the sludge—for example, composting—is recommended.

Composting of irradiated sludge may have two advantages:

- The composting period may be shortened by seeding of controlled bacterial flora in sludge;
- Contamination by pathogens or their growth can be prevented by inoculating the sludge with innocuous composting bacteria.

Studies on composting of radiation disinfected sewage sludge have been carried out by many researchers [71–73]. For isothermal composting, the optimal temperature and pH are approximately 50 °C and pH 7–8, respectively. The repeated use of the product as seed increased the rate of CO<sub>2</sub> evolution. The rate reached a maximum within 10 h and then decreased rapidly, and the conversion of organic carbon to CO<sub>2</sub> was approximately 40 % [71]. By composting irradiated sludge, the process can be carried out under optimum conditions; moreover, the composting period is expected to be shorter, because it is not necessary to maintain the fermentation temperature at a high level long enough to reduce the number of pathogens in the sludge. The growth of inoculated microorganisms is greatly affected by the bacterial flora in the medium in which it is growing. *Salmonella* grew rapidly in irradiated compost, but this growth was able to be inhibited by saturation of coliform bacteria after irradiation [72].

#### 4.4 Removal of EDCs from Soil and Industrial Sludge

EDCs and potential EDCs are also found in contaminated soil and sludge. Sewage disposal into water sources may be a major exposure pathway for EDCs and potential EDCs to humans and wildlife, directly and via the food chain. This concerns disposal of treated effluents and applications of recycled water. Some environmental endocrine disrupting chemicals, such as the pesticide DDT, dioxins, and polychlorinated biphenyls (PCBs) used in electrical equipment, are highly persistent and slow to degrade in the environment, making them potentially hazardous over an extended period of time [74]. Similar processes that have been applied to aqueous solution were applied to sludge, but do not show good removal efficiency when EDCs are in sludge [75].

During water radiolysis, highly reactive intermediates form that then react with the target molecules, culminating in structural changes. To confirm the radiation reduction of EDCs in industrial sludge, pilot scale experiments up to 50 kGy of EB were conducted with samples from the textile dyeing industries. The experimental result showed over 90 % of reduction of nonylphenol and di-ethylhexyl phthalate (DEHP) at around 10 kGy of absorbed doses [76]. The initial concentration nonylphenol in raw sludge was 1.5 mg/kg. The experimental result of nonylphenol



is shown Fig. 15. The concentration of nonylphenol decrease with absorbed doses, and showed 83 % removal at 10 kGy and 95 % removal at 20 kGy.

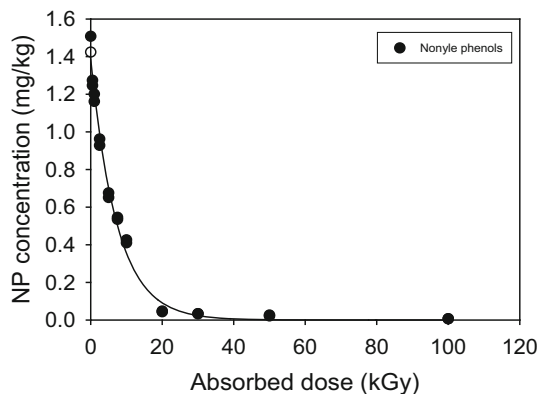
Studies have demonstrated that 2,3,7,8-tetrachlorodibenzo-p-dioxin (TCDD) in soil can be converted to products of negligible toxicity by radiation. Destruction of more than 98 % of the contaminants was achieved with a dose of 800 kGy in a soil containing 100 ppb of TCDD. The addition of contaminants such as dichlorobenzene and hexachlorobenzene did not affect the result. The addition of 25 % water and 2.5 % nonionic surfactant was beneficial to the soil studied [77, 79].

## 5 Electron Accelerator for Environmental Pollution Control

The most important factor determining the economic feasibility of the use of EB technology in environmental pollution control is the proper selection of the electron accelerator. Accelerator manufacturers produce many types of electron accelerators with energies ranging from 0.5 to 10 MeV and beam powers ranging from 50 to 700 kW. For flue gas treatment, electron energies of approximately 0.7–1.0 MeV are adequate, but EBs with energies above 1.0 MeV are useful for wastewater and sludge treatment. Such energy levels provide the necessary penetration of accelerated electrons into wastewater and sludge when applied to admissible hydrodynamic flow regimes. Accelerators with beam energy greater than 5 MeV are being manufactured at low beam power (less than 50 kW). Low beam power is adequate for experimental and pilot plants, but not for large scale treatment in industrial applications. Therefore, medium energy accelerators achieve maximum practical use for flue gas, wastewater and sludge treatment. The beam power of such accelerators reaches 700 kW, and there are several applications that call for the manufacture of accelerators with a beam power of up to 1 MW. The basic criteria for accelerators for environmental application are:

- High beam power to increase productivity and reduce unit operating costs;
- High electrical efficiency to reduce demand and unit operating costs;
- High beam utilization to increase productivity and reduce unit operating costs.

**Fig. 15** Decrease of nonylphenol in sludge cake from a textile dyeing complex [76]





## 5.1 Accelerators for Environmental Application

Because of the electrons energy requirements (up to 5 MeV), transformer accelerators, like the one presented in the Fig. 4, are the most popular. Direct current (DC) voltage power supplies that are used as high voltage sources are usually based on the use of oil or gas filled transformers with a rectifier circuit. They are relatively simple and are the most reliable accelerator component. High voltage cable is frequently used to connect the power supply and accelerating head when the voltage level is less than or equal to 0.7 MV. A voltage level above 0.7 MV in a conventional transformer is impractical because of technical problems with the insulation and dimensions of such a device. Medium energy (0.5–5 MeV) can be obtained by a high voltage generator. A different type of inductance or capacitance coupling makes it possible to multiply alternating current (AC) primary voltage and obtain up to 5 MV of DC output voltage. The main parameters of selected transformer accelerators are shown in Table 3. Many different configurations have been built by major accelerator producers such as NHV Corporation of Japan; Energy Science Inc., USA; BINP, Russia; NIIIEFA, Russia; Radiation Dynamics, Inc., USA; and others [79].

The lessons learned from pilot and industrial installations have shown that the technology itself is superior and very competitive with more conventional technology for environmental pollution [80]. However the problems reported at the industrial EBFGT plants in China were connected to failure of accelerators; a similar problem occurred at an installation in Poland as well. The technology requires application of accelerators of very high power. Therefore, the accelerators applied in the mentioned installations were of power higher than 250 kW, and power to two of them was supplied from single high power supply. This was a breakthrough in the technology, since the required availability of the system is equal to 92 % of boiler operation time (7000–8000 h/year). The problems related to the accelerators can be avoided by proper system design, manufacturing and quality control. One reason for some of the quality issues may be the fact that the equipment manufacturers themselves have not performed sufficient research in the development of very high power accelerators. However, for the industrial wastewater plant in Korea adopted a 1 MeV, 400 kW with three solid connected irradiation heads showed a reliable operation of over 8000 h/year [4, 50]. Reliable and moderately priced accelerators are a key factor for progress in the field.

## 5.2 Mobile Electron Beam for Pilot Test

Even the advantages of radiation technology on environmental pollution control, there are very few commercial scale plants in operation since the cost for proving this technology by pilot scale test on site. Therefore, the needs for economical methods applying pilot scale are getting more and more the issues in the field.

A low energy electron accelerator in container was used for FGT in FZK, Germany [81]. The accelerator with the energy and power of 0.2 MeV, 150 mA was installed in the shielded container for this experiments. A larger mobile equipment to treat the wastewater was developed [82]. This system mounted on trailer

**Table 3** Parameters of selected accelerators

Accelerator type Parameter	EPS-800-375	Dynamitron	ELV-12
Nominal energy	800 keV	1–5 MeV	0.6–1.0 MeV
Energy stability	–	±2 %	±1 %
Nominal beam current	375 mA	50 mA	500 mA
Beam current stability	–	±2 %	±2 %
Beam power	300 kW × 2	250 kW	400 kW (3 heads)
Scan width	225 cm	200 cm	200 cm
Dose uniformity	±5 %	<±5 %	<±5 %
Mode of operation	Continuous	Continuous	Continuous
No. of scanner	2 heads	One head	3 heads
Total beam power	600 kW	250 kW	400 kW
Power consumption	682 kW	350 kW	500 kW
Electrical efficiency	88 %	71 %	80 %
Producer	NHV, Japan	IBA (RDI), USA	BINP, EB TECH

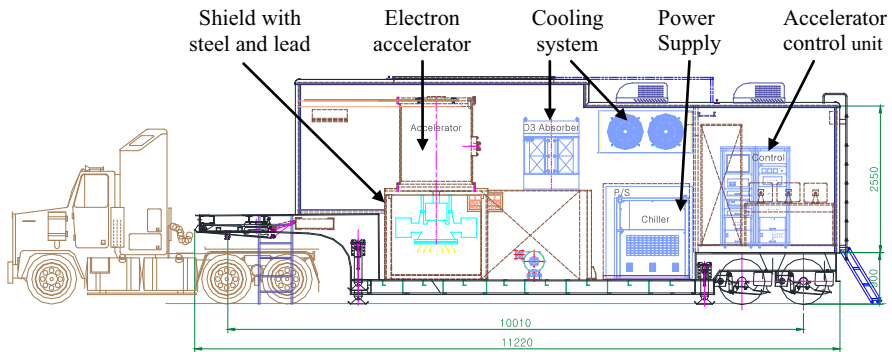


**Fig. 16** Mobile EB plant (0.7 MeV, 20 kW), mounted on a trailer

consisting of pump room, process room, and control room. In the process room, a transformer type accelerator of 0.5 MeV, 20 kW is installed. This system was designed to treat up to 200 m<sup>3</sup>/day of water/slurry, however, due to the penetration limit of EB, it was difficult to treat larger amount of wastewater with uniform doses.

Because of the necessity of a pilot scale test facility for continuous treatment of a certain amount of wastewater and gases on the spot, a mobile EB irradiation system with sufficient beam energy and power was required. Therefore, a mobile EB irradiation system mounted on a trailer has been developed (Fig. 16). This mobile EB irradiation system is designed for the individual field application with self-shielded structure of steel plate and lead block which will satisfy the required safety figures of International Commission on Radiological Protection (ICRP) [83]. Shielding of a mobile electron accelerator of 0.7 MeV, 30 mA has been designed

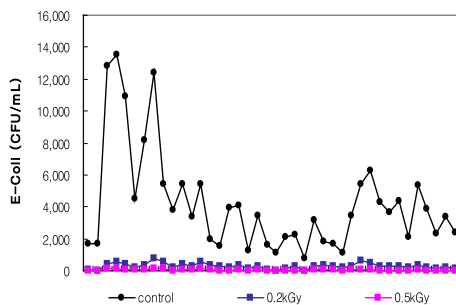


**Fig. 17** Mobile EB plant on a pilot scale test of municipal wastewater in Korea

and examined by Monte Carlo technique. Based on a 3D model of electron accelerator shielding which is designed with steel and lead shield, radiation leakage was examined using the MCNP code. Calculations of MCNP showed agreements within statistical uncertainties, and the highest leakage expected is  $0.55061 (\pm 0.0454) \mu\text{Sv/h}$ , which is far below the tolerable radiation dose limit of  $1 \text{ mSv/week}$  [84]. This mobile unit could treat up to  $500 \text{ m}^3/\text{day}$  of liquid waste or  $2000 \text{ Nm}^3/\text{h}$  of gases. This unit has been used to demonstrate an on-site pilot facility for stack gases in Saudi Arabia and for municipal wastewater in Korea (Figs. 7, 17).

The wastewater treatment experiments with mobile EB plant were for the disinfection of effluent from the municipal wastewater treatment plant in Daejeon, Republic of Korea. The continuous treatment of effluent showed 95 % removal of coli-forms at the dose of  $0.2 \text{ kGy}$  and 99 % removal at  $0.5 \text{ kGy}$ . The mobile EB plant has also used for the pilot scale experiments of flue gas treatment from the oil refinery plant in Jeddah, Saudi Arabia. The experiments were done under the continuous flow of stack gases bypassed from the chimney. The flow rate was  $2000 \text{ Nm}^3/\text{h}$  and the obtained removal efficiencies showed good removal of  $\text{SO}_2$  and  $\text{NO}_x$  as described in Sect. 2.3.

## 6 Conclusion

Rapid population growth combined with industrialization, urbanization, and energy-intensive lifestyles has resulted in severe problems in environment, especially in large cities. In many countries where industry is concentrated in urban areas, severe air and water pollution problems have arisen in most of the large cities. Therefore, the pollution control has become an important subject in the field of environmental engineering. EB processing of off-gas, wastewater, and sludge is a non-chemical and additive free process that uses the short-lived reactive species formed during the radiolysis of EB process for efficient decomposition of the pollutants. Such reactive radicals are strong oxidizing or reducing agents that can transform the pollutants in the wastes from the industries and different origins.

Thousands of electron accelerators based on different principles have been constructed and used in the field of radiation chemistry and radiation processing.

The progress in the accelerator technology means not only a growing number of units, but also lower cost, higher dose rate, more compact size suitable to the production line, beam shaped adequately to the process, reliability, and other parameters that are important in radiation processing application.

At present, EB technology for environmental pollution control has not found wide application, and it is used much less often than conventional methods. However, in recent years pilot plants and industrial scale studies have shown that EB treatment could occupy an important place in the future. Currently, EB treatment in combination with conventional methods has been shown to provide noticeable reductions in the amount of time, area, and power needed for environmental pollution control. Continuous emphasis on ecological standards will be an additional motivation for the elaboration and industrial application of EB treatment. Propagation of EB treatment can improve environmental protection and provide essential support in industrial development.

**Acknowledgments** Polish coauthor acknowledgments Ministry of Science and Higher Education, Poland, and International Irradiation Association for support under co-financed project W68/IIA/2015 “Fostering of scientific and R&D collaboration in the field of radiation technologies”.

## References

1. Chmielewski AG et al (2014) Recent developments in the application of electron accelerators for polymer processing. *Rad Phys Chem* 94:147–150
2. Machi S (2011) Trends for electron beam accelerator applications in industry. *Rev Accel Sci Technol* 4:1–10
3. Woods RJ, Pikaev AK (1994) Applied radiation chemistry: radiation processing. Wiley, New York
4. Han B, Kim JK, Kim Y, Choi JS, Jeong KY (2012) Operation of industrial-scale electron beam wastewater treatment plant. *Rad Phys Chem* 81:1475–1478
5. Gautam S, Shah MR, Sabharwal S, Sharma A (2005) Radiation hygienization and value addition to municipal sewage sludge. *Water Environ Res* 77:472–479
6. Tokunaga O, Suzuki N (1984) Radiation chemical reactions in  $\text{NO}_x$  and  $\text{SO}_2$  removals from flue gas. *Rad Phys Chem* 24(1):145–165
7. Maetzing H, Namba H, Tokunaga O (1993) Kinetics of  $\text{SO}_2$  removal from flue gas by electron beam technique. *Rad Phys Chem* 42(4–6):673–677
8. Chmielewski AG (1995) Technological development of eb flue gas treatment based on physics and chemistry of the process. *Rad Phys Chem* 46(4–6):1057–1062
9. Chmielewski AG et al (2007) Review on gaseous chlorinated organic pollutants electron beam treatment. *Rad Phys Chem* 76(11–12):1795–1801
10. Kim J et al (2010) Electron beam irradiation for mercury oxidation and mercury emissions control. *J Environ Eng* 136(5):554–559
11. Basfar AA et al (2008) Electron beam flue gas treatment (EBFGT) technology for simultaneous removal of  $\text{SO}_2$  and  $\text{NO}_x$  from combustion of liquid fuels. *Fuel* 87(8–9):1446–1452
12. Tan E et al (2015) New “wet type” electron beam flue gas treatment pilot plant. *Rad Phys Chem* 119:109–115
13. Chmielewski AG, Ostapczuk A, Licki J (2010) Electron beam technology for multipollutant emissions control from heavy fuel oil-fired boiler. *J Air Waste Manage Assoc* 60:932–938
14. Chang JS, Kaufman F (1977) Kinetics of the reactions of hydroxyl radicals with some halocarbons:  $\text{CHFCl}_2$ ,  $\text{CHF}_2\text{Cl}$ ,  $\text{CH}_3\text{CCl}_3$ ,  $\text{C}_2\text{HCl}_3$ , and  $\text{C}_2\text{Cl}_4$ . *J Chem Phys* 66(11):4989–4994
15. Chmielewski AG et al (2003)  $\text{NO}_x$  and PAHs removal from industrial flue gas by using electron beam technology with alcohol addition. *Rad Phys Chem* 67(3–4):555–560

16. Nichipor H et al (2003) The kinetics of 1,1-dichloroethene ( $\text{CCl}_2=\text{CH}_2$ ) and trichloroethene ( $\text{HCIC}=\text{CCl}_2$ ) decomposition in dry and humid air under the influence of electron Beam. *Nukleonika* 48(1):45–50
17. Nichipor H et al (2008) Theoretical study of dose and dose rate effect on trichloroethylene ( $\text{HCIC}=\text{CCl}_2$ ) decomposition in dry and humid air under electron beam irradiation. *Nukleonika* 53(1):11–16
18. Sun Y et al (2009) Simulation calculations of tetrachloroethylene decomposition in air mixtures under electron beam irradiation. *Nukleonika* 54(2):65–70
19. Hirota K et al (2003) Application of electron beam for the reduction of PCDD/F emission from municipal solid waste incinerators. *Env Sci Technol*. 37(14):3164–3170
20. Sun Y, Chmielewski AG, Bułka S, Zimek Z (2009) Decomposition of toluene in air mixtures under electron beam irradiation. *Nukleonika* 54(2):65–70
21. Ostapczuk A et al (1999) Preliminary test in decomposition of styrene by electron beam treatment. *Rad Phys Chem* 56(4):369–371
22. Ostapczuk A, Hakoda T, Shimada A, Kojima T (2008) Naphthalene and ace-naphthene decomposition by electron beam generated plasma application. *Plasma Chem Plasma Process* 28(4):483–494
23. Kim JC (2002) Factors affecting aromatic VOC removal by electron beam treatment. *Rad Phys Chem* 65(4–5):429–435
24. Han DH et al (2003) Oxidative decomposition of aromatic hydrocarbons by electron beam irradiation. *Rad Phys Chem* 67(1):51–60
25. Ostapczuk A, Licki J, Chmielewski A (2008) Polycyclic aromatic hydrocarbons in coal combustion flue gas under electron beam irradiation. *Rad Phys Chem* 77(4):490–496
26. Hirota H, Sakai H, Washio M, Takuji K (2004) Application of electron beams for the treatment of VOC streams. *Ind Eng Chem Res* 43(5):1185–1191
27. Jeon EC et al (2008) Novel hybrid technology for VOC control using an electron beam and catalyst. *Res Chem Intermed* 34(8–9):863–870
28. Kim J et al (2004) Removal of VOCs by hybrid electron beam reactor with catalyst bed. *Rad Phys Chem* 71(1–2):427–430
29. Kim KJ et al (2005) Development of hybrid technology using E-beam and catalyst for aromatic VOCs control. *Rad Phys Chem* 73(2):85–90
30. Ighigeanu D, Calinescu I, Martin D, Matei C (2008) A new hybrid technique for the volatile organic compounds removal by combined use of electron beams, microwaves and catalysts. *NIMB B* 266(10):2524–2528
31. Namba H et al (1995) Pilot-scale tests for electron beam purification of flue gas from coal-combustion boiler. *Rad Phys Chem*. 46(6):1103–1106
32. Chmielewski AG et al (1995) Pilot plant for flue gas treatment—continuous operation tests. *Rad Phys Chem* 46:1067–1070
33. Chmielewski AG, Zimek Z, Panta P, Drabik W (1995) The double window for electron beam injection into the flue gas process vessel. *Rad Phys Chem* 45(6):1029–1033
34. Doi Y, Nakanishi I, Konno Y (2000) Operational experience of a commercial scale plant of electron beam purification of flue gas. *Rad Phys Chem* 57(3–6):495–499
35. Chmielewski AG et al (2004) Operational experience of the industrial plant for electron beam flue gas treatment. *Radiat Phys Chem* 71:439–442
36. Pawelec A et al (2016) Pilot plant for electron beam treatment of flue gases from heavy fuel oil fired boiler. *Fuel Proc Technol* 145:123–129
37. Zwolinska E et al (2015) Modelling study of  $\text{NO}_x$  removal in oil-fired waste off-gases under electron beam irradiation. *Rad Phys Chem* 113:20–23
38. Chmielewski AG et al (2012) Treatment of off-gases containing  $\text{NO}_x$  by electron beam. *Catal Today* 191:159–164
39. Calinescu I et al (2013) E-Beam  $\text{SO}_2$  and  $\text{NO}_x$  removal from flue gases in the presence of fine water droplets. *Rad Phys Chem* 85:130–138
40. Pikaev AK (1986) Modern radiation chemistry, radiolysis of gases and liquids. Nauka, Moscow, p 440 (in Russian)
41. Buxton GV, Greenstock CL, Helman WP, Ross AB (1988) Critical review of rate constants for reactions of hydrated electrons, hydrogen atoms and hydroxyl radicals ( $\text{OH}/\text{O}^-$ ) in aqueous solutions. *J Phys Chem Ref Data* 17:513–886

42. Makarov IE, Ponomarev AV, Han B (2003). Demonstration plant for electron beam treatment of Daegu Dye Industrial Complex wastewater. In: Report from a technical meeting on emerging applications of radiation processing for 21st century, IAEA
43. Han B, Ko J, Kim JK, Kim Y, Chung W, Makarov IE, Ponomarev AV, Pikaev AK (2002) Combined electron-beam and biological treatment of dyeing complex wastewater. Pilot plant experiments. *Rad Phys Chem* 64:53–59
44. Han B, Kim DK, Boo JY, Kim JK, Kim Y, Chung W, Choi JS, Kang HJ, Pikaev AK (2000) Irradiation Treatment of Water, Wastewater and Sludge. In: Report from a technical meeting on recycling of wastes by radiation processing, IAEA
45. Wang T, Waite TD, Kurucz C, Cooper WJ (1994) Oxidant reduction and biodegradability improvement of paper mill effluent by radiation. *Wat Res* 28:237–241
46. Gehringer P, Eschweiler H, Han B (2004) High energy electrons for reclamation of effluents from municipal wastewater treatment plants. In: Proc. 5th IWA Congress, Marrakech
47. Sampa MHO et al (1995) The use of electron beam accelerator for the treatment of drinking water and wastewater in Brazil. *Rad Phys Chem* 46(4–6):1143–1146
48. Homlok R, Takács E, Wojnárovits L (2013) Degradation of organic molecules in advanced oxidation processes: relation between chemical structure and degradability. *Chemosphere* 91:383–389
49. Solpan D, Gueven O (2002) Decolouration and degradation of some textile dyes by gamma irradiation. *Rad Phys Chem* 64:549–558
50. Han B, Kim JK, Kim Y, Choi JS, Makarov IE, Ponomarev AV (2005) Electron beam treatment of textile dyeing wastewater : operation of Pilot plant and Industrial plant construction. *Water Sci Technol* 52(10–11):317–324
51. Colborn T, Vom Saal FS, Soto AM (1993) Developmental effects of endocrine-disrupting chemicals in wildlife and humans. *Environ Health Perspect* 101(5):378–384
52. Farré M, Barceló D (2003) Toxicity testing of wastewater and sewage sludge by biosensors, bioassays and chemical analysis. *Trends Anal Chem* 22(5):299–310
53. Lucia HM, Santos LM, Araujo AN, Fachini A, Pena A, Delerue-Matos C (2010) Montenegro MCBSM. *J Hazard Mater* 175:45–95
54. Al-Ahmad A, Dashner FD, Kummerer K (1999) Biodegradability of cefotiam, ciprofloxacin, meropenem, penicillin G and sulfamethoxazole and inhibition of waste bacteria. *Archiv Environ Contam Toxicol* 37:158–163
55. Lafitte-Trouque S, Forster CF (2002) The use of ultrasound and gamma-irradiation as pre-treatment for the anaerobic digestion of waste activated sludge at mesophilic and thermophilic temperatures. *Bioresour Technol* 84:113–118
56. United States Environmental Protection Agency (1993) Standards for the use and disposal of sewage sludge. US EPA, Washington DC
57. Lowe HN, Lacy WG, Surkiewicz BF, Yaeger R (1956) Destruction of micro-organisms in water, sewage and sewage sludge by ionizing radiation. *J Am Water Works Assoc* 48:1363–1372
58. Suess A (1975) Radiation for a clean environment. In: Proc. Symp., Munich, IAEA, Vienna
59. Trump JG (1975) Radiation physics and chemistry. In: Paper presented at Int. Sem. on the Use of Isotopes and Ionizing Radiation in Environmental Engineering, Sao Paulo
60. Jung J, Yoon JH, Chung H, Lee MJ (2002) Radiation treatment of secondary effluent from a sewage treatment plant. *Rad Phys Chem* 65:533–537
61. Sabharwal S, Shah MR, Kumar N, Patel JB (2004) Technical and economical aspects of radiation hygienization of municipal sewage sludge using gamma irradiator. In: Report from a Consultants Meeting on Radiation Processing of Gaseous and Liquid Effluents, IAEA
62. Lessel T, Suess A (1984) Ten years experience in operation of sewage treatment plant using gamma irradiation. *Rad Phys Chem* 24:3–16
63. Trump JG, Merrill EW, Wright KA (1984) Disinfection of sewage waste water and sludge by electron treatment. *Radiat Phys Chem* 24:55–66
64. Sivinski JS (1983) Environmental applications of cesium-137 irradiation technology: sludge and foods. *Rad Phys Chem* 22:99–118
65. Sivinski JS, Ahlstrom S (1984) Summary of cesium-137 sludge irradiation activities in the United States. *Rad Phys Chem* 24:19–27
66. Vysotskaya NA (1983) Radiation treatment of sewage sludge in role of chemistry in environmental conservation. *Naukova Dumka, Kiev*, p 205 (in Russian)
67. Sawai T, Yamazaki M, Shimokawa T, Sekiguchi M (1990) Improvement of sedimentation and dewatering of municipal sludge by radiation. *Rad Phys Chem* 35:465–468

68. Chmielewski AG et al (1995) Disinfection of municipal sewage sludges in installation equipped with electron accelerator. *Rad Phys Chem* 46(4–6):1071–1074
69. Han B, Kim JK, Kim Y (2005) Sludge Hygienization with Electron Beam, public hearing on sludge treatment methods. Institute of Soil, Water and Environmental Sciences, Volcani Center, Tel Aviv
70. United States Environmental Protection Agency (1992) Environmental regulations and technology: control of pathogens and vector attraction in sewage sludge (including domestic septage) under 40 CFR part 503. The Office, Washington, DC, pp 27–30
71. Kawakami W, Hashimoto S (1984) Enhanced composting of radiation disinfected sewage sludge. *Rad Phys Chem* 24:29–40
72. Morris ME, Sivinsky JS, Brandon JR, Neuhauser KS (1978) Irradiation of sewage sludge using cesium-137: a comparative analysis. In: Proc. 3rd International Conference of Working Group on “Waste Irradiation”
73. Kawakami W et al (1981) Composting of gamma radiation disinfected sludge. *Rad Phys Chem* 18(3–4):771–777
74. Melnick R et al (2002) Summary of the national toxicology program’s report of the endocrine disruptors low-dose peer review. *Environ Health Perspect* 110(4):427–431
75. Chaoman H (2003) Removal of endocrine disruptors by tertiary treatments and constructed wetlands in subtropical Australia *Water Sci Technol.* 47(9):151–156
76. Han B et al (2015) Removal of nonylphenol from industrial sludge by electron beam. *J Korean Indus Rad Assoc* 102:583–587
77. Hilarides RJ, Gray KA, Guzzetta J, Cortellucci N, Sommer C (1994) Radiolytic degradation of 2,3,7,8-TCDD in artificially contaminated soils. *Environ Sci Technol* 28:2249–2258
78. Cooper WJ, Curry RD, O’shea KE (1998) Environmental applications of ionizing radiation. John Wiley & Sons Inc, New York, pp 537–556
79. Zimek Z (1995) High power electron accelerators for flue gas treatment. *Rad Phys Chem* 45(6):1013–1015
80. Chmielewski AG (2005) Application of ionizing radiation to environment protection. *Nukleonika* 50(S3):17–24
81. Fuch P, Roth B, Schwing U, Angele H, Gottstein J (1988) Removal of NO<sub>x</sub> and SO<sub>2</sub> by the electron beam Process. *Rad Phys Chem* 31:45–56
82. Cooper WJ, Curry RD, O’shea KE (1998) Environmental applications of ionizing radiation. John Wiley & Sons Inc, New York, pp 451–466
83. ICRP (2003) Relative biological effectiveness (RBE), quality factor (Q), and radiation weighting factor (w<sub>R</sub>): ICRP Publication 92. *Ann ICRP* 33(4):1–121
84. Han B et al (2016) Development of mobile electron beam plant for environmental applications. *Rad Phys Chem* 124:174–178



# Radiation Grafting for the Functionalization and Development of Smart Polymeric Materials

Víctor H. Pino-Ramos<sup>1</sup> · Alejandro Ramos-Ballesteros<sup>1</sup> ·  
Felipe López-Saucedo<sup>1</sup> · Jesús E. López-Barriguete<sup>1</sup> ·  
Gustavo H. C. Varca<sup>2</sup> · Emilio Bucio<sup>1</sup>

Received: 19 April 2016 / Accepted: 3 August 2016 / Published online: 22 August 2016  
© Springer International Publishing Switzerland 2016

**Abstract** Gamma radiation has been shown particularly useful for the functionalization of surfaces with stimuli-responsive polymers. This method involves the formation of active sites (free radicals) onto the polymeric backbone as a result of the high-energy radiation exposition over the polymeric material. Thus, a microenvironment suitable for the reaction among monomer and/or polymer and the active sites is formed and then leading to propagation to form side-chain grafts. The modification of polymers using high-energy irradiation can be performed by the following methods: direct or simultaneous, pre-irradiation oxidative, and pre-irradiation. The most frequently used ones correspond to the pre-irradiation oxidative method as well as the direct one. Radiation-grafting has many advantages over other conventional methods because it does not require the use of catalyst nor additives to initiate the reaction and usually no changes on the mechanical properties with respect to the pristine polymeric matrix are observed. This chapter is focused on the synthesis of smart polymers and coatings obtained by the use of gamma radiation. In addition, the diverse applications of these materials in the biomedical area are also reported, with focus in drug delivery, sutures, and biosensors.

---

This article is part of the Topical Collection “Applications of Radiation Chemistry”; edited by Margherita Venturi, Mila D’Angelantonio.

✉ Alejandro Ramos-Ballesteros  
[alejandro.ramos@correo.nucleares.unam.mx](mailto:alejandro.ramos@correo.nucleares.unam.mx)

✉ Emilio Bucio  
[ebucio@nucleares.unam.mx](mailto:ebucio@nucleares.unam.mx)

<sup>1</sup> Departamento de Química de Radiaciones y Radioquímica, Instituto de Ciencias Nucleares, Universidad Nacional Autónoma de México, Circuito Exterior, Ciudad Universitaria, 04510 México, DF, Mexico

<sup>2</sup> Instituto de Pesquisas Energéticas e Nucleares (IPEN/CNEN-SP), Av. Prof. Lineu Prestes, 2242, Cidade Universitária, São Paulo, SP 05508-000, Brazil



**Keywords** Radiation-grafting · Smart polymers · Sutures · Drug delivery · Biosensors · Polymer functionalization

## 1 Introduction

Since the synthesis of PVC obtained by Henri Victor Regnault in 1838, a large number of polymeric synthetic materials with chemical–mechanical–thermal properties of the most diverse have been developed [1]. There are a high number of degrees of freedom for the synthesis conditions; and consequently, the properties of the resulting material can be as varied. Polymer chemistry has advanced to the point where it is often possible to tailor-make a variety of different types of polymers with specified molecular weights and structures [2]. However, sometimes a small change in the synthesis conditions or concentrations of reagents generates undesirable changes in the final properties of the material. Surface modification of polymeric materials has come to represent an interesting and useful alternative for generation of polymers with specific physical–chemical properties, coupled with the properties conferred by surface modifications.

There are several means to modify polymers properties, viz. blending, grafting, and curing. ‘Blending’ is the physical mixture of two (or more) polymers to obtain the requisite properties. ‘Grafting’ is a method wherein monomers are covalently bonded (modified) onto the polymer chain, whereas in curing, the polymerization of an oligomer mixture forms a coating which adheres to the substrate by physical forces [3].

Among the methods for polymer modification, “grafting” is a promising technique for the introduction of special functional groups in order to modify their original properties and broad its applications [4].

## 2 Grafting Techniques

A graft copolymer is a polymer that is composed of two or more chemically different polymeric parts [5]. Generally, graft copolymers are polymers composed of a main polymer chain (backbone) to which one or more side chains (branches) are chemically connected through covalent bonds [6]. On a random, statistical, or alternate copolymerization processes, the different monomers compete with each other to add to propagating centers (radical or ionic), unlike grafting processes wherein synthesis is carried out not simultaneously; instead, a sequence of separate noncompetitive polymerizations is used to incorporate the different monomers into one polymer chain [7].

Graft copolymers have very different properties to raw materials and that has gained great interest in recent years because it is possible to obtain new materials from already available ones. The main purposes of a surface modification are improving the wettability, biocompatibility, and mechanical properties, etc., of a surface polymer. Grafting copolymers can be obtained mainly by two mechanisms known as grafting from and grafting to [8]. There are several parameters that control

the brush properties, such as grafting density, chain length, and chemical composition of the chains [9].

The processes of “grafting to” and “grafting from” are two different ways to change the chemical and physical properties of a polymeric surface (Fig. 1). “Grafting to” allows a preformed polymer to adhere to either polymeric surface through covalent bonds. Due to the larger volume of the coiled polymer to graft and the steric hindrance this causes, the grafting density obtained by this technique is low [10]. On the other hand, the “grafting from” process requires the activation of a backbone polymer previously, which can be carried out by chemical (chemical initiators) or physics methods (ionizing radiations), initiating the polymerization process with monomer units around it. With the “grafting from” mechanism, it is possible to obtain high grafting densities, since there is more access to the chain ends [11].

Grafting a polymer can be achieved by several techniques, such as chemical, radiation, photochemical, plasma-induced, and enzymatic means. The different types of initiators give their name to each grafting technique. Chemical grafting involves free-radical or ionic initiators; radiation induces graft copolymerization that uses high-energy radiation (generally gamma, UV, and electrons); photochemical techniques include photo-sensitive reagents as initiators [12] and plasma-induced grafting implies electron-induced excitation, ionization, and dissociation attained by slow discharge conditions. Then the accelerated electrons from the plasma have sufficient energy to induce cleavage of the chemical bonds in the polymeric structure to form macromolecule radicals, which subsequently initiate graft copolymerization [3].

Among the grafting techniques, radiation processing is presented as an alternative with interesting features over other conventional synthesis and

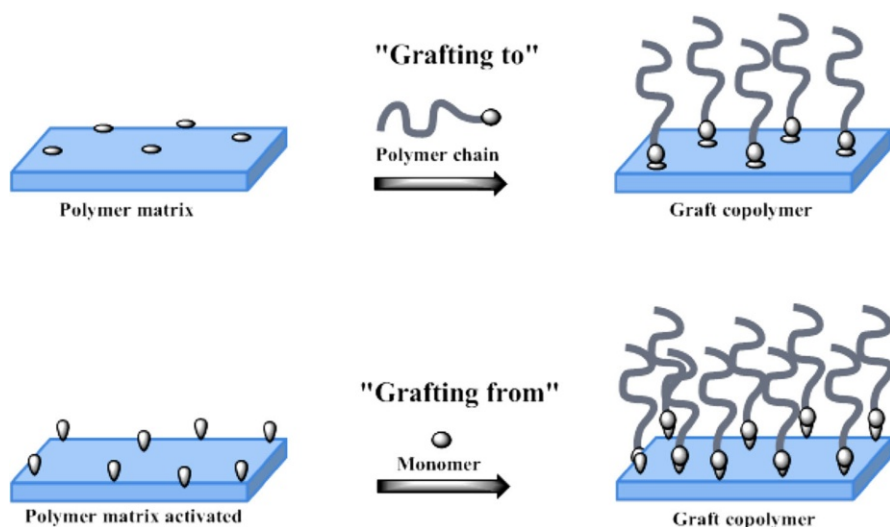


**Fig. 1** Synthesis of polymer brushes using “grafting to” and “grafting from” approaches

modification of polymer matrices methods. The lack of catalysts or additives in order to initiate the reaction as well as its simplicity are issues to consider [13]. Polymer modification by radiation grafting techniques has been extensively applied to prepare novel materials (including adsorbents for environmental and industrial applications) and it is of particular interest to achieve specific chemical properties as well as excellent mechanical properties [14].

### 3 Radiation-Induced Grafting

The process of radiation-induced grafting is based on the deposition of energy from the radiation in the material to be modified. From this energy, highly reactive free radicals, which give rise to secondary reactions with molecules present in the medium, will be generated. These radicals easily react with appropriate functional monomers to form covalent bonds and, as a consequence, growth of macromolecular chains [15], and all of this without the use of chemical initiators.

Each type of ionizing radiation produces the same effect by interacting with matter (ionization and excitation) [16], but according to their specific nature (charge, penetrating power (range), linear energy transfer (LET) and stopping power of the material), highly concentrated free radical areas or homogeneous radical production along the material can be produced. In the case of electrons, ions, and protons; due to its high LET, charge and particle size; each particle delivers its entire energy in a few millimeters and almost without path deviations). For gamma radiation, an homogeneous delivery of energy will occur, both surface and bulk due to the high penetration of gamma rays [17]. In some cases, the types of radiation are combined to generate uniform changes in the material [18], so the type and energy of ionizing radiation used will determine the changes in structure of the resulting material.

Due to the inclusion of “new” molecules in the material, the polymer properties change. Graft copolymerization has been commonly used to modify properties in polymer structures like poly(ethylene terephthalate) (PET), cellulose, polypropylene (PP), and polyethylene (PE), with a wide variety of monomers [19].

Another advantage presented by radiation-induced graft copolymerization is that it enables imparting tailored modifications ranging from surface to bulk of backbone polymers unlike photo- and plasma initiation, which impart surface modification only [20].

The degree of grafting in the copolymer may be adjusted by selection of irradiation and reaction parameters to develop specially designed selective copolymers for specific applications. Radiation-induced graft copolymerization may also be initiated over a wide range of temperatures, including sub-ambient temperatures for monomers available in bulk, solution, or emulsion [20].

There are two basic methods for radiation-induced grafting; including the pre-irradiation, as well as the mutual or the simultaneous method; with an energy source being either gamma ray, UV, or electrons [21–23].

### 3.1 Methods of Synthesis

Since graft copolymers result from the chemical combination of two macromolecules of different chemical nature, and since radiation is known to create “active sites” in polymeric matrix, it is logical to think that various chemical routes can be followed for the combination of these macromolecules. Among the various methods that can be envisaged for this purpose, four have received special attention; these include direct radiation grafting and grafting on radiation-peroxidized polymers. When polymers are exposed to ionizing radiation under aerated conditions, trapped radicals and peroxides (or hydroperoxides) are formed and remain ready to initiate grafting copolymerization reactions [24].

#### 3.1.1 Direct Radiation Grafting Method

In the direct or simultaneous method (Fig. 2), the simple radiation-chemical method for producing graft copolymers is directly derived from the study of radiation polymerizations. Most radiation-initiated polymerizations proceed via free-radical mechanisms, initiated by the free radicals produced from the radiolysis of the monomer. Nevertheless, since the action of ionizing radiation on matter is unselective, any substance that is added to the monomer also undergoes radiolysis and consequently contributes to the initiation of polymerization [5].

In this method, the polymer substrate is immersed in a monomer-solvent mixture, which may be liquid or vapor and may contain additives. Irradiation produces active sites in the polymer matrix, mainly macroradicals, which can initiate the graft polymerization but also the interaction of radiation with monomer can generate homopolymerization. The latter is an untoward side reaction. As polymer degradation requires higher absorbed doses than the grafting process, it is possible to perform direct grafting under controlled conditions without significant damage to the substrate [21].

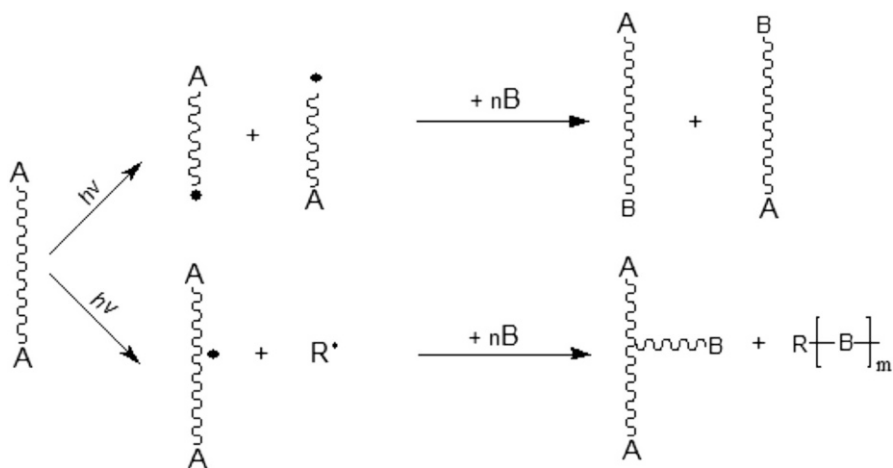


**Fig. 2** Grafting by  $\gamma$ -irradiation applying a direct method

### 3.1.2 Pre-Irradiation Grafting Method

The polymer matrix is irradiated in the absence of air (in vacuo or under an inert atmosphere). Grafting is initiated by macroradicals trapped in the irradiated polymer and homopolymerization is avoided. A disadvantage of this method is the possible degradation of the polymer matrix due to the need of higher doses than the direct method. Besides, there's a significant dependence on the reaction temperature and crystallinity of the polymer because the concentration of trapped macroradicals is higher in a crystalline than in an amorphous polymer, and a comparatively low degree of grafting is obtained [5, 21].

### 3.1.3 Pre-Irradiation Oxidative Grafting Method

This method involves pre-irradiation of the polymer, but in the presence of air or oxygen. In this way, the macroradicals formed are converted to peroxides and/or hydroperoxides, and when the irradiated polymer is heated in the presence of monomer (in the absence of air), the peroxides decompose to give the macroradicals, which are the active sites for graft polymerization (Fig. 3).

An advantage of the peroxide method is the possibility of storing the irradiated polymer some time before grafting. Some disadvantages are that the hydroxyl radical ( $\text{OH}\cdot$ ) produced by the homolytic cleavage of the hydroperoxide group

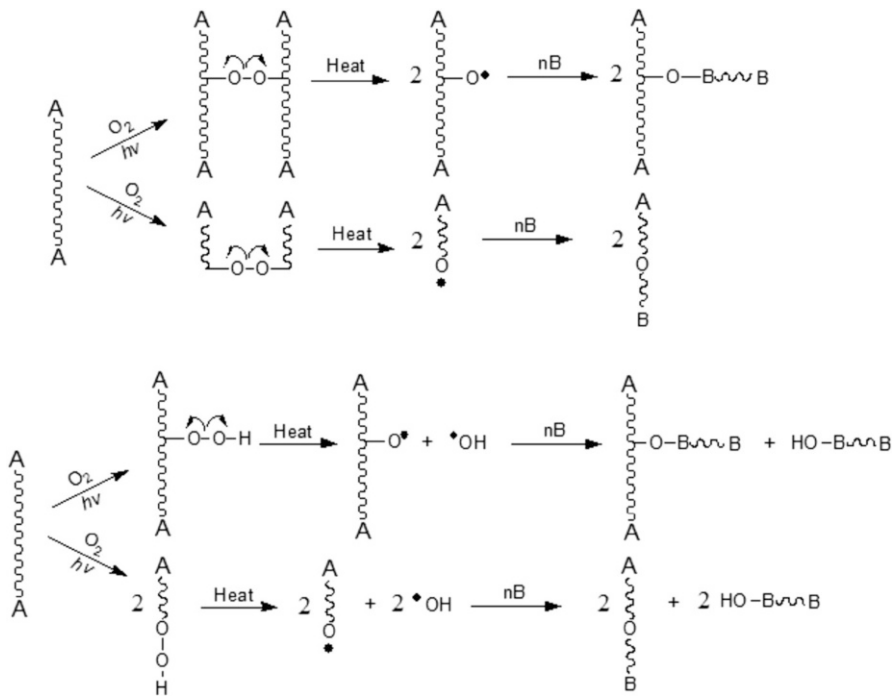


**Fig. 3** Grafting by  $\gamma$ -irradiation applying a pre-irradiation method

induces homopolymerization and the pre-irradiation method requires a higher dose of radiation than the direct method [5, 21].

The pre-irradiation technique is a clean and effective method for modification of PP, PE, poly(tetrafluoroethylene) (PTFE), etc. Some reports on grafting polar monomers onto pre-irradiated films have been published [25].

### 3.2 Modifying Properties by Grafting

Irradiation produces active sites in the polymer matrix, mainly macroradicals, which can initiate the graft polymerization and homopolymerization of the monomer. If the polymer has the tendency to crosslinking [e.g., PP, PE, polystyrene (PS), poly(vinyl chloride) (PVC), etc.] a grafted copolymer is formed. On the other hand, when a polymer has the tendency to chain cleavage [e.g., PTFE, poly(isobutylene), cellulose, poly(methyl methacrylate) (PMMA), and polymers containing tetrasubstituted carbon atoms in the main chain] the process can result in a block copolymer formation. Because degradation of polymers requires higher absorbed doses than the grafting process, it is possible to perform grafting on these polymers [5, 26].

As mentioned before, the type of monomer grafted into the polymer matrix will determine the resulting properties, and of course, the properties of the monomers are dictated by the functional groups' content. Grafting hydrophilic or hydrophobic monomers can improve the hydrophilicity or hydrophobicity of the material respectively; with pH-sensitive monomers we can electrically charge the surface of a material, or modify its swelling properties at different pH's; grafting self-repairing materials can improve the mechanical resistance to scratches, etc. Thermosensitive polymers are a special category of polymers which have in their structure a hydrophobic and a hydrophilic functional groups [e.g., poly(*N*-isopropylacrylamide), PNIPAAm] [27]; pH-sensitive polymers has ionizable functional groups [e.g., poly(acrylic acid), PAAc]. Monomers with amines affect the swelling behavior of the polymer, because amine protonation results in swelling under acid conditions due to the formation of the ammonium polyelectrolyte, similarly carboxylic acid substituents form ionized salts at basic pH resulting in increased network swelling [28]. Polymers that form complexes may associate due to Van der Waals interactions, ionic bonds, hydrogen bonds, coordination interactions, or salt bridges formed by polyvalent metal ions [29].

### 3.3 Grafting Quantification and Characterization Techniques

Innumerable techniques are currently available for polymer characterization in terms of the assessment of polymer properties. Of those, thermal [30], mechanical [31], optical [32], and rheological [33] approaches might be determined and used for further comparison with the grafted material.

Characterization methods used to confirm or track down the grafting process include Fourier transform infrared spectroscopy (FTIR) [34], nuclear magnetic resonance (NMR) [35], and X-ray diffraction analysis (XRD) [36]. Considering that these analyses may detail with precision the grafting process as well as the novel chemical linkages, such techniques are currently in the spotlight.

In addition to the above-mentioned techniques, surface studies may also play a key role in the characterization of grafted copolymers due to their ability to reveal important information in terms of microstructure and overall morphology of the grafted polymer [32, 37]. For instance, scanning electron microscopy corresponds to a very usual technique of choice [38]. Other approaches may be used to evidence the graft copolymerization, including differential scanning calorimetry [30, 39] and water contact angle [40, 41], among other techniques.

On the other hand, regarding approaches to quantify grafting, the determination of grafting yields and grafting efficiency are perhaps the most representative ones. Both estimations can be performed based on weight of the samples, as represented in Eqs. (1) and (2) for grafting yields and grafting efficiency, respectively, whereas  $W_a$  stands as the initial weight of the sample,  $W_b$  corresponds to the dried weight of the grafted sample before the extraction, and  $W_c$  represents the dried weight of the grafted sample after extraction [42–44].

$$\text{Grafting yield (\%)} = \frac{W_c - W_a}{W_a} \times 100 \quad (1)$$

$$\text{Grafting efficiency (\%)} = \frac{W_c - W_a}{W_b - W_a} \times 100. \quad (2)$$

When it comes to functionalized materials aside from the careful and precise characterization to assure and provide experimental evidence of the functionalization itself, the tailored function or modification shall be assessed in order to demonstrate and detail the acquired properties, e.g., thermo-responsiveness is well demonstrated by LCST measurements [45, 46], while pH-responsivity is commonly evaluated by determining the pH critical point [47]. In practical means, the characterization and experimental evaluation of the functionality should be carefully designed and performed on a responsiveness or “functionality”-based approach.

## 4 Smart Polymers

Stimuli-responsive polymers are polymers that respond sharply to small changes in physical or chemical conditions with relatively large phase or property changes [48]. The stimuli in which smart polymers respond to are commonly classified into three categories: physical, chemical, or biological [49]. Temperature and pH stimuli-responsive macromolecular materials have attracted great attention due to their obvious applications in biomedicine and biotechnology [50].

### 4.1 Smart Polymeric Materials Obtained by Ionizing Radiation

Responsive behavior of polymeric materials could be formally considered as a combination or sequence of several events: (a) reception of an external signal (physical or chemical), (b) chemical change of the material and/or changes in the material properties, and finally (c) transduction of the changes into a macro/

microscopically significant event such as aggregation-deaggregation (commonly referred to as *response*). For example, microgel particles from a crosslinked weak polyelectrolyte (polybase) dispersed in water are sensitive to variations in pH of the medium. Changes (decreases) in pH cause changes in the ionization degree of the polyelectrolyte, and with the change in the ionization degree of the polyelectrolyte comes a molecular conformational modification [51, 52]. One of the smart polymers most studied is probably PNIPAAm, which exhibits a lower critical solution temperature (LCST) between 30 and 35 °C [53]. Acrylic acid (AAc) is one of the important monomers grafted on the matrix of different polymers, where their chains act as reaction sites to introduce various functions through carboxyl groups, and because of its pH-sensitive response [54].

#### 4.1.1 Temperature-Responsive Polymers

Temperature-sensitive polymers exhibit LCST behavior where phase separation is induced at a certain temperature threshold. Polymers of this type undergo thermally induced reversible phase transition. They are soluble in aqueous solutions at low temperatures but become insoluble as the temperature rises above the LCST. It is possible to increase the functionality of microgel particles by finding the right balance of hydrophobic and hydrophilic co-monomers or by tuning to a desired temperature range by copolymerization using more hydrophilic (which raises the LCST) or more hydrophobic (which lowers the LCST) co-monomers [55, 56].

Heskins and Gillet were the first to report an endotherm observed at the LCST upon heating an aqueous solution of PNIPAAm [57]. Grinberg [58] have studied the volume phase transition in responsive polymers using high-sensitivity differential scanning calorimetry (DSC) and as well as the swelling behavior of the polymers at different scanning rates. It was possible to measure the dependence of the transition parameters on the heating rate. The DSC measurements, by heating at different rates (from 1 to 10 °C/min), provided results nearly approximating equilibrium and LCST or UCST. The transition temperature, enthalpy, and entropy of this thermosensitive behavior as well as the transition LCST are parameters that may be estimated.

#### 4.1.2 pH-Responsive Polymers

pH-responsive polymers consist of ionizable pendants capable of accepting and donating protons in response to environmental changes in pH such as carboxylic acids and basic amino alkyl moieties [59]. The change in the charge of pendant groups causes an alteration of the hydrodynamic volume of the polymer chains [60]. Then, the transition from collapsed state to swollen state is caused by the osmotic pressure generated by mobile counterions which neutralize the charges [61]. The phase transition of pH-sensitive polymers is nominated critical pH. In the human body, pH variations are present along the gastrointestinal tract and in problematic sectors like tumor areas and surrounding tissues [62]. Drug delivery in these specific areas make relevant the need for the development of pH-sensitive systems with fast response to changes in environmental stimuli. A fast response of a polymer and a repetitive function of another polymer may be combined using different



functionalization techniques such as  $\gamma$ -irradiation. Most grafting reactions, which take place on the surface or in the bulk polymeric matrix, allow the design of clinically effective controlled drug-delivery systems, supported by the concept of achieving optimized combinations between monomer and the polymer itself.

## 5 Applications

Applications of functionalized materials by grafting abound in the literature, as such modifications brought to light novel applications and perspectives in terms of their usage, considering the possibility to tailor the materials as desired or required [63]. Examples of materials based on functionalized polymers include smart membranes for separation science [3], conducting polymers [63] for energy and wire technology, responsive materials, including pH- [4], thermo-responsive polymers [64], as well as light- [65] and magnetic-responsive polymers [66], for a wide variety of biomedical and technological applications.

In terms of biomedical applications, functionalized polymers are currently applied for tissue engineering and cell cultivation, biotechnology, biomedicine, and pharmaceutical technology, among others areas that may directly benefit from the advancement of material sciences. A highlighted application is related to cell and tissue cultivation as the grafting of biological substances or other bioactive ones onto polymer substrates has been proven effective towards controlling important parameters for cell growth and tissue development, which may somehow modulate cell affinity, and therefore provide control over the process. However, this work debates the biomedical applications of grafted functionalized polymers by means of sensors, drug delivery, and sutures specifically.

As reviewed earlier, grafting different functional groups in polymer matrices allows us to modify the original properties of the irradiated material, but if we graft molecules with stimuli-responsive properties, we can obtain materials with unique properties that change their behavior according to the environment in which they are. Researchers around the world have found various application fields of intelligent polymers grafted on polymeric surfaces in the areas of development of medical devices for drug delivery, biosensors, and implant development.

### 5.1 Surface Modification Polymers for Medical Purposes

Gamma-ray irradiation enables the grafting of medical devices with polymers containing functional groups capable of interacting with drug molecules. Depending on the chemical structure of the substrate and the monomers to be grafted, different levels of performance can be achieved [67].

The synthesis of new polymeric materials for biomedical applications are of great interest. However, they should pass exhaustive testing to demonstrate their non-toxicity, biocompatibility, and industrial feasibility; so a lot of time will pass before these kinds of materials have real application and then most of them will be discarded [68]. Instead of synthesis of new materials, biomaterial modifications seem to be the short-term solution for improvement of medical devices to some

extent, as biological safety will have to be determined as a brand new system. Applying surface modification on materials already approved for medical use, we could enhance their properties as biocompatibility, resistance to degradation, mechanical properties, and thermal stability providing perhaps a shorter way for novel alternatives for most.

Device-related infections are among the most serious complications in medical procedures. Its importance arises from the high occurrence and the consequences that it implies in terms of morbidity and mortality. As a result, the presence of these two factors increases hospital costs significantly. If scientists get to synthesize drug-coated biomaterials, it will be possible to reduce device-related infections contracted at surgery during the early post-insertion period, and most infections identified in patients that have been treated with polymeric implants should be delayed, even infections caused by microorganisms from the skin flora and nosocomial environment.

Surface modification of materials used on medical device manufacturing to obtain drug impregnated polymers takes relevance when we talk about microbial resistance to antibiotics. Research has recently been published that accounts for the existence of antimicrobial-resistant strains. Many of them indicate the existence of methicillin-resistant *Staphylococcus aureus* (MRSA), *Pseudomonas aeruginosa*, and *Escherichia coli* cells. The direct treatment of microbial infections with drug-impregnated medical devices suggests a simple method that releases the drug at a specific site, decreases costs [69], avoids or reduces invasive dosage forms, and minimizes the antimicrobial-resistance effect by not unnecessarily exposing other bacteria to antibiotics [70, 71]. Another area of opportunity for surface modification includes body-contacting materials [72]. Surgical devices and biomedical materials could incorporate drug-delivery systems through insertion of hydrophilic groups with hosting drugs capability through ionic interactions, van de Waals, and hydrogen bond.

The effort should focus mainly on three aspects. First of all, improving the treatment of the complication (treatment and administration routes); secondly, enhancing the hydrophilicity (obtaining lubricity) of biomedical devices, improving biocompatibility [73], and reducing protein adhesion [74]; and finally, increasing preventive measures. This latter point may be the most interesting of all because it focuses on prevention [68].

Medical devices used in vivo should satisfy requirements for performance, bio-interaction, and biocompatibility. The understanding of structure–properties relationships in polymers is advanced, so the desired mechanical properties, durability, and functionality can be achieved [75]. Bio-integration is the ideal outcome expected of an artificial implant. This implies that the phenomena that occur at the interface between the implant and host tissues do not induce any deleterious effects such as chronic inflammatory response or formation of unusual tissues [76].

The most interesting methods to modify a polymer for biomedical purposes are plasma and high energies, (Fig. 4) due to simultaneous sterilization of the material provided by the method [75] and no need of chemical initiators that could represent a biocompatibility problem. It is possible to change many properties with this kind of method (Table 1). Surface treatments can be broadly categorized as functionalization, derivatization, polymerization, and mechanical or surface architecture modification.

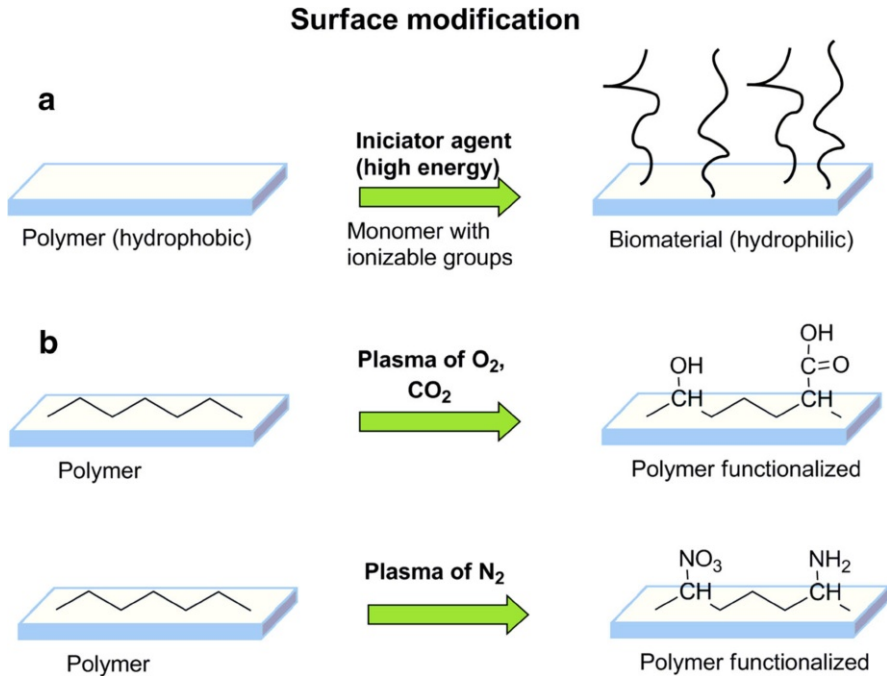


**Fig. 4** Surface modification of polymers using ionizing radiation: gamma rays, UV, and electrons (a). Functionalization using plasma with different agents (b)

**Table 1** Surface modification of polymer materials

Physically	Physical adsorption; Langmuir–Blodgett films
Chemically	Alkaline or acid-etching oxidation, e.g., through ozone; other chemical transformations
Physico-chemically	Photo activation (UV); corona treatment; treatment with electron or ion irradiation; laser treatment, gamma irradiation; plasma treatment

Dozens of review articles have been reported about surface-modified materials trying to provide a possible solution to biocompatibility and drug release [77]. Materials such as poly (acrylonitrile butadiene styrene) (ABS), silicone rubber (SR), PE [78], PP, and polyurethanes (PU) [79, 80] have been functionalized grafting organic compounds with ionizable groups [e.g., poly(carboxylic acids), poly(*N,N*-diakyl aminoethyl methacrylate) [81], chitosan, etc.] in order to host anti-inflammatory drugs or antimicrobials such as ibuprofen, sodium diclofenac (bacteriostatic), naproxen, vancomycin, or for biomolecule immobilization (enzymes) [82, 83]. Several reports mention that inclusion of poly(ethylene oxide) or poly(ethylene oxide)-acrylic acid mix on catheters surface [84] present a reduction in bacterial adhesion caused for negatively charged surface [85]. On the other hand, fabrication of surfaces with positive charge results in broad-spectrum antimicrobial

## Infections catheter-associated

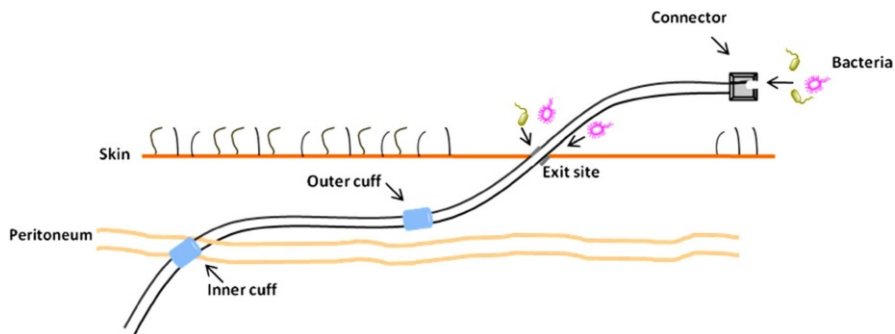


**Fig. 5** Infection sites in an implanted urinary catheter. Bacteria can gain access to the peritoneal cavity either by contaminating the connector and the catheter lumen, or by migration from the skin exit site down the catheter track through the tissue

activity [86, 87]. Although the mechanism of action is still subject of debate, the general consensus is that the positive charge disrupts the lipid membrane of microbes. Polysaccharides such as chitosan and poly(4-vinylpyridine) show this activity due to the high nitrogen content of the polymer creating a cationic surface.

### 5.1.1 Catheters

A polymeric implant is another type of application (probes, prosthetic valves, and catheters). The infection process starts in the implant site; there, the bacteria slowly grow and the antimicrobial hardly gets there, mainly when drugs are intravenously administered or by pills. The cell-adhesion profiles depend of surface architecture and roughness of implants [88]. There are studies that indicate the existence between cell adhesion and polymer surface; the bacteria adhesion occurs mainly when the polymer has a hydrophobic surface [89, 90]. Complications associated with catheters are very common around the world (450,000 cases per year in the USA alone) and the direct costs amount to over a billion dollars [91]. The main reason for the infection is due to adhesion of (Fig. 5) *Escherichia coli*, *Candida spp.*, *Enterococcus spp.*, *Pseudomonas aeruginosa*, *Enterobacter spp.*, *Staphylococcus epidermidis*, *Bacillus subtilis*, and *Staphylococcus aureus* [92, 93]. Avoiding and solving this problem when it occurs is very important in preventing complications that could cause a patient's death.

### 5.1.2 Coating with Shape-Memory Polymers

Temperature-sensitive polymers, and more specifically shape-memory polymers, have been used in the preparation of minimally invasive surgery medical devices. The unique properties of these materials allow the introduction of the medical device in a compressed form followed by expansion once it is located in the desired place by minimally invasive surgery procedures [68]. Materials such as guidewires,

stents, and others biomedical metallic materials have been surface-modified using an exterior coating method with poly(tetrafluoroethylene) (PTFE) or a hydrophilic polymer to reduce friction and simultaneously provide the necessary properties for a guidewire to negotiate a tortuous ureter path [94].

The chemical and physical characterization of biomaterials generally focus on the structure and properties of the polymer matrix, however, in the case of surface-modification polymers, the characterization techniques focuses mainly on surface functional groups, functional layer thickness, roughness, etc. Roughness is a very important factor to analyze in biomaterials because it is intrinsically related to bacterial adhesion [88].

The three most commonly used surface composition characterization techniques are ATR-FTIR, XPS, and SEM (Table 2); each with different penetration depths. Cell adhesion and toxicity tests with some cell (biocompatibility) are necessary to know if materials have toxic effects [95].

### 5.1.3 Graft Sutures

Suture is a fiber or fibrous structure attached to a metallic needle [96], mainly employed in surgery procedures as biomaterial device, used to ligate blood vessels and hold tissues together [97]. They can be classified according to the origin of the materials which they are made of (natural or synthetic), the permanence of the material in the body (absorbable or non-absorbable) and the construction process (braided, monofilament) [98, 99]. Suture materials should satisfy specific requirements: easy to handle, elicit minimal tissue reaction, do not support bacterial growth, possess high tensile strength, easy to sterilize, hypoallergenic properties, and do not induce carcinogenic action [97].

**Table 2** Biomedical-related surface properties with corresponding measuring methods

Surface characteristics	Methods
Geometry: roughness, topography, specific surface, layer thickness	Profilometry, field emission, REM, AFM, interface microscopy-adsorption isotherms, BET surface area, pore radius distribution
Surface energy: wettability (specially; hydrophilicity)	Contact angle geometry; for biomaterials, mainly the captive bubble method is used
Physical characteristics: adsorption, scratch resistance, other mechanical, electric and optical characteristics, adhesion	Adhesion test after cross-hatch cut, and/or thermo test, permeation measurements, elastic characteristics; for diagnostic purposes; refractive index and fluorescence background radiation
Chemical composition: surfaces and thin layer, chemical functionality of surfaces	FTIR-ATR, IR microscopy and spectroscopy, ESCA-imaging, AES/SAM, fluorescence spectrometry, MALDI-TOF-SIMS
Biological characteristics: biocompatibility, cell adhesion, specific/non-specific, protein adsorption	Growth and toxicity tests with various cells, protein adsorption with IR and fluorescence labeling

In general terms the most important requirements of sutures materials are physical and mechanical properties, biocompatibility and antimicrobial nature [96]; in this sense, some materials currently marketed may become fallible and, as a result, multiple side-infections related to suturing procedures occur in a certain percentage of the patients [100]. This raises the need to develop or modify the existing suture devices in order to make them able to acquire antimicrobial activity analogous to the drug design, either by coating [101] or grafting pristine sutures with antimicrobial polymers and/or containing functional groups capable to load or adhere antimicrobial drugs onto the surface of the modified suture (Fig. 6).

Most commonly, reports for grafting sutures employs  $^{60}\text{Co}$  as  $\gamma$ -radiation source (Fig. 7). Radiation grafting has proved to be a very effective technique to get desirable properties onto a polymeric material without any consideration of the shape of the material [102].

The irradiated materials may retain most of their original characteristics and also acquire additional properties of the grafted moiety; the structure, in some cases, changes during the modification process, depending on the nature and the amount of monomer grafted [103, 104]. It is true that the radiation-grafting technique may have limitations to generate biomedical devices because it produces changes not only in the biomaterial surface but throughout the polymer matrix, which can lead to undesirable changes in the structure and properties of the device [105]. In other cases, the use of ionizing radiation provides the energy required for activation of molecules in the material that under other conditions cannot be achieved by the lack of reactive groups.

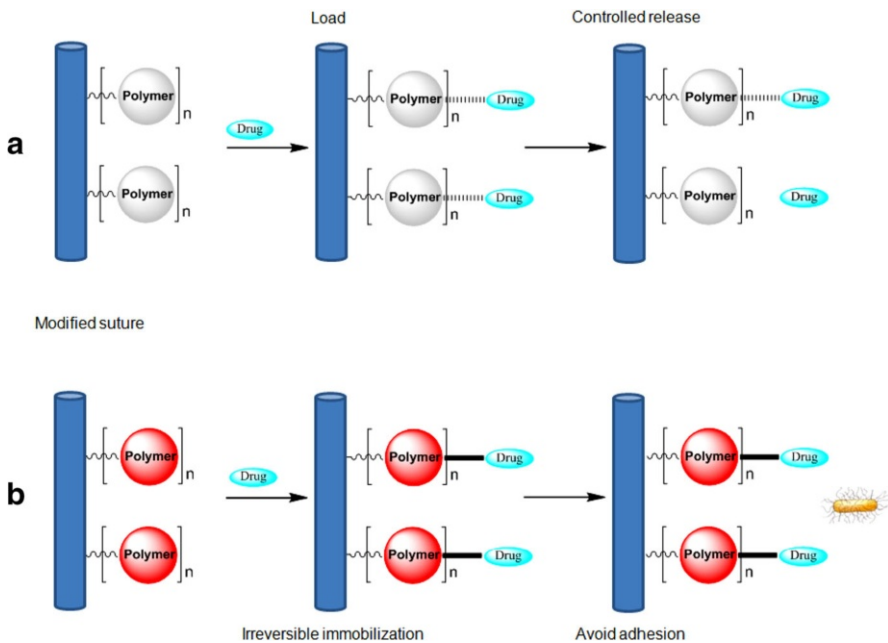


**Fig. 6** Electrostatic load-release (a) and covalent immobilization (b) of drugs on modified sutures

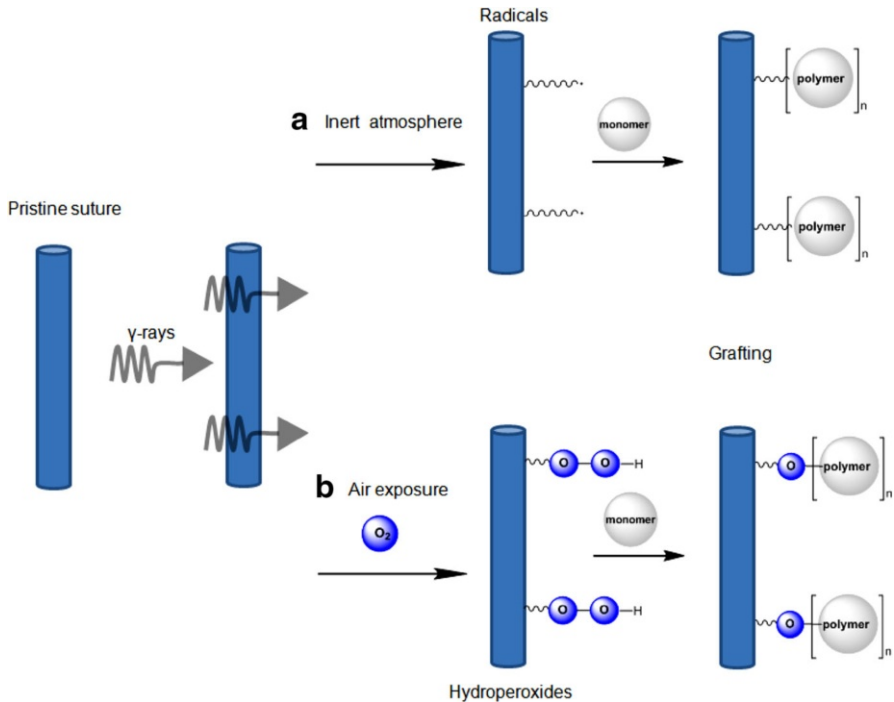


**Fig. 7** Suture  $\gamma$ -radiation grafting: **a** direct irradiation and **b** pre-irradiation grafting method

Some examples of PP grafting matrix are described below [102, 104, 106]:

PP-*g*-PAN and PP-*g*-PAAc: Acrylic acid is one of the most popular monomers that have been grafted onto different polymeric matrices and its polymer or copolymers with pH-sensitive response have the capability to undergo further chemical reaction to produce new functional groups [4]. The grafting percentage of AAc onto PP films by pre-irradiation method was increased as a function of reaction time and reaction temperature [14].

Due to the inherent reactivity of the acrylic acid, homopolymer formation is the main polymerization reaction when radiation-grafting technique is used. Efforts have been made to obtain carboxylic acids' high-content surfaces without compromising the sutures' physical properties.

The grafting polymerization using pre-irradiation technique of acrylonitrile (AN) onto PP monofilament leads to an increase in tenacity up to a graft level of 5 % [104]. Subsequent hydrolysis is an effective way to introduce carboxylic groups into the monofilament. The transformation of nitrile groups into carboxylic groups proceeds under sodium hydroxide conditions to achieve PP-*g*-AAc, as this reaction is necessary for loading the drug; the hydrolysis leads to a considerable loss of mechanical strength in the grafted suture. This approach produces a suture with carboxyl functionality PP-*g*-AAc of 62 % or about 0.25 mmol/g, which is enough for subsequent antimicrobial drug immobilization [102, 106].

PP-g-PVIm: Here, sutures were prepared by the simultaneous radiation grafting of 1-vinylimidazole (VIm) onto PP monofilament with results around 5–20 %. The tenacity slightly decreases, whereas the elongation augments with the increment in the degree of grafting.

The grafted suture has reasonably good water uptake. The PP-g-PVIm grafting was immobilized with an antimicrobial drug, ciprofloxacin. The modified suture releases the drug over a period of 4–5 days, the same period of time that the material showed antimicrobial activity in vitro against *Escherichia coli* [107].

PP-g-PAAc and PP-g-PGMA: Recently, our investigation group developed separately grafting AAc and glycidyl methacrylate, GMA onto PP sutures applying  $\gamma$ -ray pre-irradiation oxidative method under various experimental conditions, therefore a different range of grafting was obtained (GMA: 25–800 %, AAc: 9–454 %). Synthesis and antimicrobial activity from this study was: (a) with PP-g-AAc load and release of vancomycin drug, here only ionic interactions are involved and (b) the irreversible covalent immobilization of the drug onto PP-g-GMA via the opening ring of the epoxy groups, then, the alcohol oxidation to the aldehyde, which reacts with the amino groups of the vancomycin and finally to the reductive amination of the copolymer. In both cases, antimicrobial activity against *Staphylococcus aureus* was corroborated [103].

## 5.2 Biosensors

Sensors are transducers that detect changes or events in the environment to produce an outcome, i.e., have the feature to convert one sort of energy (signal) to another, generally into an electrical signal. The advantage of sensors against chemical analysis techniques results from the fact that they are specialized, small size, portable, and inexpensive devices that are suitable for in situ analysis and real-time monitoring of chemical and physical parameters [108].

Within the different types of sensors used today, biosensors have gained importance and interest in the scientific community due to their performance and application possibilities for knowledge and monitoring of biological processes. Biomedical sensors acquire signals thanks to a bioreceptor (biological recognition element), representing biomedical variables or phenomena and transform them into electrical signals. These kinds of sensors have an interface between a biologic part and an electronic system; thus both parts must function in such a way that do not change or affect adversely the systems. Table 3 shows different types of sensors according to its interface. In the last years, these sort of sensors have been defined as biosensors.

A variety of sensors can be applied for biomedical purposes; it is possible to classify them into two wide groups according to the transduction principles involved. Table 4 shows the two groups of sensors.

The sensors with physical structure can measure the changes in electrical and optical phenomena inside the human body, e.g., quantify pressure, blood flow, corporal temperature, muscular stretching, and bone growth [108]. On the other hand, although chemical sensors can be applied to measure these changes too, they are particularly useful for detecting, quantifying, and monitoring the presence of



**Table 3** Types of sensors (interface)

Non-contacting (non-invasive)
Skin surface (contacting)
Indwelling (minimally invasive)
Implantable (invasive)

**Table 4** General classification of sensors (biomedical application)

Physical structure	Chemical structure
Mechanical	Electrochemical
Electric	Photometric
Thermal	Bioanalytic
Optical	Gas
Geometric	Physical chemical methods
Hydraulic	

different elements or compounds in specific concentrations, as well as for determining the activity and interaction with other elements inside a determined biological process to generate a possible diagnosis and therapy [109].

The materials to design and develop biosensors have been changing over time. One of the main problems faced by the biosensor technology is the rejection of the device by biological systems [110]. Thus, efforts have been focused to provide different materials that permit the correct integration between systems (biocompatibility). Moreover, it is well known that sensor performance can be modified by the interaction with biological systems. The degradation due to the exposition to biological matter is related to the type of sensor. In the case of internal sensors (inside the body) degradation degree is faster and, as a consequence, the performance would be decreased and the structure-design will be compromised. Biomedical sensors should have a flexible base structure capable of deforming and adapting to body form. The latest research has been testing and developing biocompatible polymers with excellent mechanical properties. The principal biomedical applications are generating wound-relief membranes with drug delivery [111], adhesives for biological implants, sensor skin support [112], cartilage and artificial meniscus [113], and eye-drop lubricant and fibers [114].

Radiation-induced grafting is presented as an alternative method for functionalization of polymer surfaces to improve biocompatibility of biosensors. Not only can they improve biocompatibility, molecules or polymers sensitive to electrical, magnetic, or chemical changes can be grafted, meaning a higher sensitivity, resistance, and specificity to certain biological processes. Poly(vinyl alcohol) (PVA) is one of the polymers used for this purpose. It is both water-soluble and flexible, characteristics that increase biocompatibility and mechanical resistance, respectively. Another polymer is PS, which excellent biocompatibility, low permeability, non toxicity, has good adsorption, mechanical, and chemical resistance. All of these features make polystyrene a candidate for use as a base for immobilizing enzymes [115] and drug delivery [116]. PMMA is another biomedical material that is

resistant to inorganic solvents, has good optical capacity (92 % transparency), a high rate of refraction and biocompatibility. A common application is for intra-ocular lenses, dental prosthesis [114], thin films, electronic skin devices, and support [112].

Other materials with the possibility of being grafted for sensor applications are conductive polymers (CP). Unless the knowledge about the amorphous structure on polymers and classified like electrical isolators, the CP have conducting properties achieved by incorporation of small concentrations of conducting materials (doping) or by inclusion of conjugated  $\pi$  electrons systems [117]. In some cases, CP let a good flow of electrons closing to conductivity values of some metals ( $>10^3$  S/cm). Polymeric materials with conductive properties gather structural physical–chemical characteristics inherent to polymers with electrical conductivity of metals [118]. One of the most used conductive polymers is polypyrrole (PPy) due to its characteristics of high conductivity, biocompatibility, oxide-reduction activity, ductility, possibility of surface modification [119], capability to form thin films [120], and corrosion protection [121]. Grafting polypyrrole molecules onto different substrates generates materials with applications in organic electronic devices [121], rechargeable batteries, light emission diodes (LED) [118], electrochemical sensors [121], thin films [119], synthetic fibers, and protection shields on semiconductors [120]. Another CP is the polyaniline (PANI). Chemical and thermal stability, controllable conductivity, high conductivity in terms of frequency, electromagnetic shield interference and microwave absorption [122] are their common characteristics, and are usually used to fabricate low-cost photovoltaic panels, high-performance batteries [119], organic volatile compound detectors [123], and organic electronic circuits [124]. Another material is the polythiophene (PT), with properties like biocompatibility, possibility of chemical modification, high conductivity, and stability, being one of the early organic materials used in the electronic industry, like FET transistors [125] and semiconductor films [126]. All of these materials modify their conductive properties through increasing or decreasing the electrical resistance based upon reactions of oxide-reduction.

### 5.3 Grafting Polymer Matrixes for Cell and Tissue Cultivation

Another important application for radiation grafting technique is the modification of biomaterials to enhance or lighten-up interactions with living tissues. The surface of the biomaterial comes in contact with the living tissues, thus the initial response of the body towards a biomaterial depends on its characteristics. Hence, proper designing and/or modification of the surface is of considerable importance for enhanced compatibility of the biomaterial. In the tissue compatibility case, two types of reactions can occur: inflammation and immunogenicity, but in the blood compatibility the fastest reaction is often thrombogenicity. The inevitable inflammation in the tissue compatibility occurs around the implanted material and its function is to allow elimination of dead cell debris and further tissue repair. A material of optimal biocompatibility should not increase the intensity and duration to the basic response, nor prevent the tissue repair. The interactions between blood and a polymer surface depend on various parameters determined by the structure

(e.g., crystallinity, molecular conformation, roughness, rigidity, and degradation), composition (e.g., chemical group associated with the hydrophilic/hydrophobic balance, type of electrical charge, ionizable groups, and micro-domains), and dimensions (e.g., surface area and size) of the material. Grafting several molecules on the biomaterial surface allows us to modify these parameters and characteristics in order to promote tissue growth and, as a consequence, the acceptance of the polymeric material by living tissue and biocompatibility. These reactions are generally different for each material, but at the design and synthesis of a polymer for biomedical use, these parameters must be taken into account [127, 128].

Current approaches are giving considerable efforts in providing niche theories and solid bases considering a pore-size perspective ranging from nano to micrometer range, trying to establish a direct connection with cell growth. In this context, several works are being carried out considering the development of scaffolds with well-defined pore size and distribution [129, 130]. Apart from a size perspective, grafting of biomolecules of biomedical interest may also be directed towards functionalization of surfaces and polymers that were seek for site specific delivery, provide biological affinity, among other properties. From a developmental point of view, several modifications may be carried out on a surface or backbone level for improving biological affinity [131–133]. Within this perspective, several potential biomolecules may be grafted onto polymeric matrixes, also along polymer structure, including growth proteins [131–134], growth factors [135], among other biomolecules of interest.

A highlighted and renowned application for grafted polymer and grafted polymer matrices is related to cell and tissue cultivation, whereas grafting of biological substances or other bioactive compounds onto polymer substrates has been proven effective towards controlling important parameters for cell growth and tissue development, which may somehow modulate cell affinity and therefore provide control over the process. Thus, when it comes to tissue engineering or cell cultivation, lots of attention has been driven towards the development of smart matrices capable of promoting cell attachment and adhesion and cell growth [136–139].

Advanced systems comprise stimuli-responsive materials, e.g., thermoresponsive matrices [135], which may modulate cell affinity as a function of temperature. In practical terms, these systems allow cell cultivation with adequate adherence by providing a suitable microenvironment for cell and tissue growth, and when appropriate, changes in temperature lead to complete cell detachment, which is adequate for quick tissue removal, without requiring direct handling.

## 6 Conclusions and Remarks

In terms of relevance, the contribution of polymer grafting to the advancement of materials science is well established, as it unraveled novel applications for conventional materials as a result of the responsive or tunable properties added to the products through the grafting process. Within this context, this chapter detailed the state of the art of polymer grafting, by means of high-energy irradiation,

including fundamental aspects of synthesis and characterization, with focus on the functionalization of surfaces for biomedical applications.

Three techniques are currently available for the development of grafted polymers or functionalization of surfaces with stimuli-responsive polymers by the use of high-energy irradiation, known as the pre-irradiation method, pre-irradiation oxidative method, and the direct method. Such techniques lead to distinct grafting and homopolymer formation yields and require different experimental parameters or conditions to be applied. Thus, the selection of the method should rely on the characteristics of the monomer or functional group, and the polymer itself, as well as the desired properties to be achieved.

Radiation-grafting has advantages over conventional methods, including the lack of a needed catalyst or additives to initiate the reaction, and usually, no changes of the mechanical properties with respect to the pristine polymeric matrix are observed. In addition to these characteristics, irradiation may allow simultaneous sterilization of the systems, depending upon the irradiation dose.

Finally, some applications of grafted polymers and grafted polymer-based materials were described including the development of graft biomaterials for drug delivery, graft sutures, and for use as biosensors. The main advancement provided by the technique towards biomaterial development concerns the possibility to originate materials capable of responding to biological or microenvironmental changes, without the need for an external interference. In terms of drug delivery as an example, the benefits arise as low doses of medicines may be administered in longer periods of time with less toxicity as a consequence. On this account, future perspectives abound as novel possibilities and functionalized materials are created continuously in the search to solve issues regarding drawbacks of polymers or polymer-based materials.

**Acknowledgments** The authors thank M. L. Escamilla, A. A. Ramírez, M. Cruz, and B. Leal from ICN-UNAM for their technical assistance. This work was supported by DGAPA-UNAM Grant IN200714.

## References

1. Mulder K, Knot M (2001) A history of systems development and entrenchment. *Technol Soc* 23:265–286. doi:10.1016/S0160-791X(01)00013-6
2. Odian G (2004) *Principles of polymerization*, 4th edn. Wiley, New Jersey. ISBN 0-471-27400-3
3. Bhattacharya A, Misra BN (2004) Grafting: a versatile means to modify polymers: techniques, factors and applications. *Prog Polym Sci* 29:767–814. doi:10.1016/j.progpolymsci.2004.05.002
4. Bucio E, Burillo G (2009) Radiation-induced grafting of sensitive polymers. *J Radioanal Nucl Chem* 280:239–243. doi:10.1007/s10967-009-0505-9
5. Chapiro A (1962) *Radiation chemistry of polymeric systems*. Interscience Publishers, New York
6. Hadjichristidis N, Pispas S, Pitsikalis M, Iatrou H, Lohse DJ (2002) *Encyclopedia of polymer science and technology*. Graft Copolymers chapter. Wiley, New York. doi:10.1002/0471440264.pst150
7. Stevens M (1999) *Polymer chemistry. An Introduction*, 3rd edn. Oxford University Press, New York. ISBN 0-19-512444-8
8. Zdyrko B, Luzinov I (2011) Polymer brushes by the “grafting to” method. *Macromol Rapid Commun* 32:859–869. doi:10.1002/marc.201100162

9. Berger S, Synytska A, Ionov L, Eichhorn KJ, Stamm M (2008) Stimuli-responsive bicomponent polymer Janus particles by “grafting from”/“grafting to” approaches. *Macromolecules* 41:9669–9676. doi:10.1021/ma802089h
10. El-Sayed AH, Ishigaki I, Okamoto J (1981) Radiation grafting of acrylic acid onto fluorine-containing polymers. I. Kinetic study of preirradiation grafting onto poly(tetrafluoroethylene). *J Appl Polym Sci* 26:3117–3124. doi:10.1002/pol.1984.170220309
11. Fijiki K, Tsubokawa N, Sone Y (1990) Radical grafting from carbon black. Graft copolymerization of vinyl monomers initiated by azo groups introduced onto carbon black surface. *Polym J* 22:661–670. doi:10.1295/polymj.22.661
12. Kato K, Uchida E, Kang E-T, Uyama Y, Ikada Y (2003) Polymer surface with graft chains. *Prog Polym Sci* 28:209–259. doi:10.1016/S0079-6700(02)00032-1
13. Chapiro A (1964) Radiation chemistry of polymers, basic mechanisms in the radiation chemistry of aqueous media. *Radiat Res Suppl.* 4:179–191
14. Ramírez-Fuentes YS, Bucio E, Burillo G (2007) Radiation-induced grafting of *N*-isopropylacrylamide and acrylic acid onto polypropylene films by two step method. *Nucl Instrum Methods B* 265:183–186. doi:10.1016/j.nimb.2007.08.046
15. Hanh TT, Huy HT, Hien NQ (2015) Pre-irradiation grafting of acrylonitrile onto chitin for adsorption of arsenic in water. *Radiat Phys Chem* 106:235–241. doi:10.1016/j.radphyschem.2014.08.004
16. Tsoufanidis N (1995) Measurement and detection of radiation, 2nd edn. Taylor & Francis, Missouri. ISBN 1-56032-317-5
17. Leroy C, Rancoita P-G (2009) Principles of radiation interaction in matter and detection, 2nd edn. World Scientific Publishing, Massachusetts. ISBN 9789812818270
18. Kimura Y, Chen J, Asano M, Maekawa Y, Katakai R, Yoshida M (2007) *Nucl Instrum Methods B* 263:463–467. doi:10.1016/j.nimb.2007.07.010
19. Mandal DK, Bhunia H, Bajpai PK, Chaudharib CV, Dubeyb KA, Varshney L (2016) Radiation-induced grafting of acrylic acid onto polypropylene film and its biodegradability. *Radiat Phys Chem* 123:37–45. doi:10.1016/j.radphyschem.2016.02.011
20. Nasef MM, Güven O (2012) Radiation-grafted copolymers for separation and purification purposes: status, challenges and future directions. *Prog Polym Sci* 37:1597–1656. doi:10.1016/j.progpolymsci.2012.07.004
21. Alvarez-Lorenzo C, Bucio E, Burillo G, Concheiro A (2010) Medical devices modified at the surface by Gamma-ray grafting for drug loading and delivery. *Expert Opin Drug Deliv* 7:173–185. doi:10.1517/17425240903483174
22. Dennis GR, Garnett JL, Zilic E (2003) Cure grafting—a complementary technique to preirradiation and simultaneous processes? *Radiat Phys Chem* 67:391–395. doi:10.1016/S0969-806X(03)00073-2
23. Desmet G, Takács E, Wojnárovits L, Borsa J (2011) Cellulose functionalization via high-energy irradiation-initiated grafting of glycidyl methacrylate and cyclodextrin immobilization. *Radiat Phys Chem* 80:1358–1362. doi:10.1016/j.radphyschem.2011.07.009
24. Magaña H, Palomino K, Cornejo-Bravo JM, Alvarez-Lorenzo C, Concheiro A, Bucio E (2015) Radiation-grafting of acrylamide onto silicone rubber films for diclofenac delivery. *Radiat Phys Chem* 107:164–170. doi:10.1016/j.radphyschem.2014.10.011
25. Gupta B, Jain R, Anjum N, Singh H (2006) Preirradiation grafting of acrylonitrile onto polypropylene monofilament for biomedical applications: I. Influence of synthesis conditions. *Radiat Phys Chem* 75:161–167. doi:10.1016/j.radphyschem.2005.04.003
26. Meléndez-Ortiz HI, Varca GHC, Lugão AB, Bucio E (2015) Smart polymers and coatings obtained by ionizing radiation: synthesis and biomedical applications. *OJP Chem* 5:17–33. doi:10.4236/ojpchem.2015.53003
27. Hoffman AS, Stayton PS, Bulmus V, Chen G, Chen J, Cheung C (2000) Really smart bioconjugates of smart polymers and receptor proteins. *J Biomed Mater Res* 52:577–586. doi:10.1002/1097-4636(2000)1215
28. Klier J, Scranton AB, Peppas NA (1990) Self-associating networks of poly(methacrylic acid-glycol). *Macromolecules* 23:4944–4949. doi:10.1021/ma00225a011
29. Osada Y (1987) Conversion of chemical into mechanical energy by synthetic polymers (chemomechanical systems). *Adv Polym Sci* 82:1–46. doi:10.1007/BF0024041
30. Richardson MJ (1989) Thermal analysis. In: Allen G, Bevington JC (eds) *Comprehensive polymer science and supplements*. Pergamon, Amsterdam, pp 867–901. doi:10.1016/B978-0-08-096701-1.00036-7

31. Li Z, Tang M, Dai J, Wang T, Bai R (2016) Effect of multiwalled carbon nanotube-grafted polymer brushes on the mechanical and swelling properties of polyacrylamide composite hydrogels. *Polymer* 85:67–76. doi:10.1016/j.polymer.2016.01.025
32. Meléndez-Ortiz HI, Bucio E, Isoshima T, Hara M (2010) Surface characterization of binary graft copolymers (PP-g-DMAEMA)-g-NIPAAm and (PP-g-4VP)-g-NIPAAm by using SEM and AFM. *Smart Coat Book Ref Am Chem Soc Publ* 1050:107–120. doi:10.1021/bk-2010-1050.ch008
33. Wu F, Zhang S, Chen Z, Zhang B, Yang W, Liu Z, Yang M (2016) Interfacial relaxation mechanisms in polymer nanocomposites through the rheological study on polymer-grafted nanoparticles. *Polymer* 90:264–275. doi:10.1016/j.polymer.2016.03.034
34. Percot A, Zhu XX, Lafleur M (2000) A simple FTIR spectroscopic method for the determination of the lower critical solution temperature of *N*-isopropylacrylamide copolymers and related hydrogels. *J Polym Sci Part B: Polym Phys* 38:907–915. doi:10.1002/(SICI)1099-0488(20000401)38:7<907:AID-POLB1>3.0.CO;2-5
35. Kwan S, Marić M (2016) Thermoresponsive polymers with tunable cloud point temperatures grafted from chitosan via nitroxide mediated polymerization. *Polymer* 86:69–82. doi:10.1016/j.polymer.2016.01.039
36. Mutalik S, Suthar NA, Managuli RS, Shetty PK, Avadhani K, Kalthur G, Kulkarni RV, Thomas R (2016) Development and performance evaluation of novel nanoparticles of a grafted copolymer loaded with curcumin. *Int J Biol Macromol* 86:709–720. doi:10.1016/j.ijbiomac.2015.11.092
37. Wyart Y, Georges G, Deumié C, Amra C, Moulin P (2008) Membrane characterization by optical methods: ellipsometry of the scattered field. *J Membr Sci* 318:145–153. doi:10.1016/j.memsci.2008.02.039
38. Wu Q, Wu B (1995) Study of membrane morphology by image analysis of electron micrographs. *J Membr Sci* 105:113–120. doi:10.1016/0376-7388(95)00055-H
39. Rieger J (2001) The glass transition temperature  $T_g$  of polymers—comparison of the values from differential thermal analysis (DTA, DSC) and dynamic mechanical measurements (torsion pendulum). *Polym Test* 20:199–204. doi:10.1016/S0142-9418(00)00023-4
40. Gu H, Wang C, Gong S, Mei Y, Li H, Ma W (2016) Investigation on contact angle measurement methods and wettability transition of porous surfaces. *Surf Coat Technol* 292:72–77. doi:10.1016/j.surfcoat.2016.03.014
41. Letellier P, Mayaffre A, Turmine M (2007) Drop size effect on contact angle explained by nonextensive thermodynamics. Young's equation revisited. *J Colloid Interface Sci* 314:604–614. doi:10.1016/j.jcis.2007.05.085
42. Kalia S, Sabaa MW (2013) Polysaccharide based graft copolymers. Springer, Berlin, Heidelberg. doi:10.1007/978-3-642-36566-9\_2
43. Ferraz CC, Varca GHC, Ruiz JC, Lopes PS, MATHOR MB, Lugão AB, Bucio E (2014) Radiation-grafting of thermo- and pH-responsive poly(*N*-vinylcaprolactam-co-acrylic acid) onto silicone rubber and polypropylene films for biomedical purposes. *Radiat Phys Chem* 97:298–303. doi:10.1016/j.radphyschem.2013.12.027
44. Pathania D, Sharma R (2012) Synthesis and characterization of graft copolymers of methacrylic acid onto gelatinized potato starch using chromic acid initiator in presence of air. *Adv Mater Lett* 3:136–142. doi:10.5185/amlett.2011.829
45. Zhang J, Peppas NA (2000) Synthesis and characterization of pH- and temperature-sensitive poly(methacrylic acid)/poly(*N*-isopropylacrylamide) interpenetrating polymeric networks. *Macromolecules* 33:102–107. doi:10.1021/ma991398q
46. Tsukasa S, Kazutaka K, Takaki S, Tomoo S (1998) UCST and LCST behavior in polymer blends containing poly(methyl methacrylate-stat-styrene). *Polymer* 39:773–780. doi:10.1016/S0032-3861(97)00339-X
47. Bucio E, Burillo G (2007) Radiation grafting of pH and thermosensitive *N*-isopropylacrylamide and acrylic acid onto PTFE films by two-steps process. *Radiat Phys Chem* 76:1724–1727. doi:10.1016/j.radphyschem.2007.02.109
48. Hoffman AS (2013) Stimuli-responsive polymers: biomedical applications and challenges for clinical translation. *Adv Drug Deliv Rev* 65:10–16. doi:10.1016/j.addr.2012.11.004
49. Peppas NA, Hilt JZ, Khademhosseini A, Langer R (2006) Hydrogels in biology and medicine: from molecular principles to bionanotechnology. *Adv Mater* 18:1345–1360. doi:10.1002/adma.200501612
50. Zhou L, Yuan W, Yuan J, Hong X (2008) Preparation of double-responsive SiO<sub>2</sub>-g-DMAEMA nanoparticles via ATRP. *Mater Lett* 62:1372–1375. doi:10.1016/j.matlet.2007.08.057

51. Bignotti F, Penco M, Sartore L, Peroni I, Mendichi R, Casolaro M, D'Amore A (2000) Synthesis, characterization and solution behavior of thermo- and pH-responsive polymers bearing L-leucine residues in the side chains. *Polymer* 41:8247–8256. doi:10.1016/S0032-3861(00)00177-4
52. Burillo G, Bucio E, Arenas E, Lopez GP (2007) Temperature and pH sensitive swelling behavior of binary DMAEMA/4VP grafts on polypropylene films. *Macromol Mater Eng* 292:214–219. doi:10.1002/mame.200600394
53. Bucio E, Burillo G, Adem E, Coqueret X (2005) Temperature sensitive behavior of poly(*N*-isopropylacrylamide) grafted onto EB-irradiated polypropylene. *Macromol Mater Eng* 290:745–752. doi:10.1002/mame.200500074
54. Adem E, Avalos-Borja M, Bucio E, Burillo G, Castellon FF, Cota L (2005) Surface characterization of binary grafting of AAC/NIPAAm onto poly(tetrafluoroethylene) (PTFE). *Nucl Instrum Methods B* 234:471–476. doi:10.1016/j.nimb.2005.02.009
55. Yan L, Zhu Q, Kenkare PU (2000) Lower critical solution temperature of linear PNIPA obtained from a Yukawa potential of polymer chains. *J Appl Polym Sci* 78:1971–1976. doi:10.1002/1097-4628(20001209)78:11<1971:AID-APP170>3.0.CO;2-P
56. Feil H, Bae YH, Feijen J, Kim SW (1993) Effect of comonomer hydrophilicity and ionization on the lower critical solution temperature of *N*-isopropylacrylamide copolymers. *Macromolecules* 26:2496–2500. doi:10.1021/ma00062a016
57. Heskins M, Guillet JE (1969) Solution properties of poly(*N*-isopropylacrylamide). *J Macromol Sci Chem* 2:1441–1455. doi:10.1007/s00396-012-2694-y
58. Grinberg VY, Dubovik AS, Kuznetsov DV, Grinberg NV, Grosberg AY, Tanaka T (2000) Studies of the thermal volume transition of poly(*N*-isopropylacrylamide) hydrogels by high-sensitivity differential scanning microcalorimetry. 2. Thermodynamic functions. *Macromolecules* 33:8685–8692. doi:10.1021/ma000527w
59. Gil ES, Hudson SM (2004) Stimuli-responsive polymers and their bioconjugates. *Prog Polym Sci* 29:1173–1222. doi:10.1016/j.progpolymsci.2004.08.003
60. Siegel RA (1993) Hydrophobic weak polyelectrolyte gels: studies of swelling equilibria and kinetics. *Adv Polym Sci* 109:233–267. doi:10.1007/3-540-56791-7\_6
61. Tonge SR, Tighe BJ (2001) Responsive hydrophobically associating polymers: a review of structure and properties. *Adv Drug Deliv Rev* 53:109–122. doi:10.1016/S0169-409X(01)00223-X
62. Stubbs M, McSheehy PMJ, Griffiths JR (1999) Causes and consequences of acidic pH in tumors: a magnetic resonance study. *Adv Enzyme Regul* 39:13–30. doi:10.1016/S0065-2571(98)00018-1
63. Bhattacharya A (2000) Radiation and industrial polymers. *Prog Polym Sci* 25:371–401. doi:10.1016/S0079-6700(00)00009-5
64. Ward MA, Georgiou TK (2011) Thermoresponsive polymers for biomedical application. *Polymers* 3:1215–1242. doi:10.3390/polym3031215
65. Yager KG, Barrett CJ (2008) Azobenzene polymers for photonic applications. Wiley, Hoboken. doi:10.1002/9780470439098.ch1
66. Andrade A, Ferreira R, Fabris J, Domingues R (2011) Coating nanomagnetic particles for biomedical applications. In: Fazel-Rezai R (ed) *Biomedical engineering—frontiers and challenges*. InTech, Rijeka. doi:10.5772/19519
67. Contreras-García A, Alvarez-Lorenzo C, Taboada C, Concheiro A, Bucio E (2011) Stimuli-responsive networks grafted onto polypropylene for the sustained delivery of NSAIDs. *Acta Biomater* 7:996–1008. doi:10.1016/j.actbio.2010.10.001
68. Gagliardi M (2012) In vitro haematic proteins adsorption and cytocompatibility study on acrylic copolymer to realize coatings for drug-eluting stents. *Mater Sci Eng C* 32:2445–2451. doi:10.1016/j.msec.2012.07.020
69. Li X, Li P, Saravanan R, Basu A, Mishra B, Lim SH, Su X, Tambyah PA, Leong SS (2014) Antimicrobial functionalization of silicone surfaces with engineered short peptides having broad spectrum antimicrobial and salt-resistant properties. *Acta Biomater* 10:258–266. doi:10.1016/j.actbio.2013.09.009
70. Costa F, Carvalho IF, Montelaro RC, Gomes P, Martins MCL (2011) Covalent immobilization of antimicrobial peptides (AMPs) onto biomaterial surfaces. *Acta Biomater* 7:1431–1440. doi:10.1016/j.actbio.2010.11.005
71. Kho K, Cheow WS, Lie RH, Hadinoto K (2010) Aqueous re-dispersibility of spray-dried antibiotic-loaded polycaprolactone nanoparticle aggregates for inhaled antibiofilm therapy. *Powder Technol* 203:432–439. doi:10.1016/j.powtec.2010.06.003



72. Adal KA, Farr BM (1996) Central venous catheter-related infections: a review. *Nutrition* 12:208–213. doi:10.1016/S0899-9007(96)91126-0
73. Ma Z, Mao Z, Gao C (2007) Surface modification and property analysis of biomedical polymers used for tissue engineering. *Colloids Surf B* 60:137–157. doi:10.1016/j.colsurfb.2007.06.019
74. Takashima K, Shimomura R, Kitou T, Terada H, Yoshinaka K, Ikeuchi K (2007) Contact and friction between catheter and blood vessel. *Tribol Int* 40:319–328. doi:10.1016/j.colsurfb.2007.06.019
75. Oehr C (2003) Plasma surface modification of polymers for biomedical use. *Nucl Instrum Methods B* 208:40–47. doi:10.1016/S0168-583X(03)00650-5
76. Bilek MMM (2014) Biofunctionalization of surfaces by energetic ion implantation: review of progress on applications in implantable biomedical devices and antibody microarrays. *Appl Surf Sci* 310:3–10. doi:10.1016/j.apsusc.2014.03.097
77. Fadeeva E, Truong VK, Stiesch M, Chichkov BN, Crawford RJ, Wang J, Ivanova EP (2011) Bacterial retention on superhydrophobic titanium surfaces fabricated by femtosecond laser ablation. *Langmuir* 27:3012–3019. doi:10.1021/la104607g
78. Melendez-Ortiz HI, Díaz-Rodríguez P, Alvarez-Lorenzo C, Concheiro A, Bucio E (2014) Binary graft modification of polypropylene for anti-inflammatory drug-device combo products. *J Pharm Sci* 103:1269–1277. doi:10.1021/la104607g
79. Buddy D (1995) Polymers: chemical, biological and surface analytical challenges. *Biosens Bioelectron* 10:797–804. doi:10.1016/0956-5663(95)99218-A
80. Nowatzki PJ, Koepsel RR, Stoodley P, Min K, Harper A, Murata H, Donfack J, Hortelano ER, Ehrlich GD, Russell AJ (2012) Salicylic acid-releasing polyurethane acrylate polymers as anti-biofilm urological catheter coatings. *Acta Biomater* 8:1869–1880. doi:10.1016/j.actbio.2012.01.032
81. Aguilar MR, San Román J (2014) Introduction to smart polymers and their applications. *Smart Polym Appl*. doi:10.1533/9780857097026.1 (**chapter 1**)
82. Primo GA, Alvarez-Igarzabal CI, Pino GA, Ferrero JC, Rossa M (2016) Surface morphological modification of crosslinked hydrophilic co-polymers by nanosecond pulsed laser irradiation. *Appl Surf Sci* 369:422–429. doi:10.1016/j.apsusc.2016.02.047
83. Kingshott P, Wei J, Bagge-Ravn D, Gadegaard N, Gram L (2003) Covalent attachment of poly(ethylene glycol) to surfaces, critical for reducing bacterial adhesion. *Langmuir* 19:6912. doi:10.1021/la034032m
84. Desai NP, Hossainy SFA, Hubell JA (1992) Surface-immobilized polyethylene oxide for bacterial repellence. *Biomaterials* 13:417–420. doi:10.1016/0142-9612(92)90160-P
85. Kohnen W, Jansen B, Ruiten D, Steinhäuser H (1994) Novel antiinfective biomaterials by polymer modification. In: Gebelein CG, Carraher CE (eds) *Biotechnology and Bioactive Polymers*. Springer US, Boston, MA, pp 317–325. doi:10.1007/978-1-4757-9519-6\_31
86. Moore LE, Ledder RG, Gilbert P, McBain AJ (2008) In vitro study of the effect of cationic biocides on bacterial population dynamics and susceptibility. *Appl Environ Microbiol*. doi:10.1128/AEM.00573-08
87. Murata H, Koepsel RR, Matyjaszewski K, Russell AJ (2007) Permanent non-leaching antibacterial surfaces-2: how high density cationics surfaces kill bacterial cells. *Biomaterials* 28:4870–4879. doi:10.1016/j.biomaterials.2007.06.012
88. Crawford RJ, Webb HK, Truong VK, Hasan J, Ivanova EP (2012) Surface topographical factors influencing bacterial attachment. *Adv Colloid Interface Sci* 179–182:142–149. doi:10.1016/j.cis.2012.06.015
89. Ma Z, Mao Z, Gao C (2007) Surface modification and property analysis of biomedical polymers used for tissue engineering. *Colloids Surf B* 60:137–157. doi:10.1016/j.colsurfb.2007.06.019
90. Seedat N, Kalthapure RS, Mocktar C, Vepuri S, Jadhav M, Soliman M, Govender T (2016) Co-encapsulation of multi-lipids and polymers enhances the performance of vancomycin in lipid-polymer hybrid nanoparticles: in vitro and in silico studies. *Mater Sci Eng C* 61:616–630. doi:10.1016/j.msec.2015.12.053
91. Glinel K, Thebault P, Humblot V, Pradier CM, Jouenne T (2012) Antibacterial surfaces developed from bio-inspired approaches. *Acta Biomater* 8:1670–1684. doi:10.1016/j.actbio.2012.01.011
92. Maki DG, Tambyah PA (2001) Engineering out the risk of infection with urinary catheters. *Emerg Infect Dis* 7:342–347. doi:10.3201/eid0702.700342
93. Hasan J, Crawford RJ, Ivanova EP (2013) Antibacterial surfaces: the quest for a new generation of biomaterials. *Trends Biotechnol* 31:295–304. doi:10.1016/j.tibtech.2013.01.017



94. Patriciu A, Mazilu D, Bagga HS, Petrisor D, Kavoussi L, Stoianovici D (2007) An evaluation method for the mechanical performance of guide-wires and catheters in accessing the upper urinary tract. *Med Eng Phys* 29:918–922. doi:10.1016/j.medengphy.2006.09.002
95. Tanaka N, Bohnenberger S, Kunkelmann T, Munaro B, Ponti J, Poth A, Sabbioni E, Sakai A, Salovaara S, Sasaki K, Thomas BC, Umeda M (2012) Prevalidation study of the BALB/c 3T3 cell transformation assay for assessment of carcinogenic potential of chemicals. *Mutat Res/Genet Toxicol Environ Mutagen* 744:20–29. doi:10.1016/j.mrgentox.2011.12.008
96. Saxena S, Ray AR, Kapil A, Pavon-Djavid G, Letourneur D, Gupta B, Meddahi-Pelle A (2011) Development of a new polypropylene-based suture: plasma grafting, surface treatment, characterization, and biocompatibility studies. *Macromol Biosci* 11:373–382. doi:10.1002/mabi.201000298
97. Pillai KKS, Sharma CP (2010) Review paper: absorbable polymeric surgical sutures: chemistry, production, properties, biodegradability, and performance. *J Biomater Appl* 25:291–366. doi:10.1177/0885328210384890
98. Viju S, Thilagavathi G (2011) Effect of chitosan coating on the characteristics of silk-braided sutures. *J Ind Text* 42:256–268. doi:10.1177/1528083711435713
99. Chu CC, von Fraunhofer JA, Greisler HP (1996) Wound closure biomaterials and devices. CRC Press, Florida
100. National Institute for Health and Clinical Excellence (2008) Rozzelle and collection. <http://www.ncbi.nlm.nih.gov/books/NBK11822/>. Accessed April 2016
101. Li Y, Kumar KN, Dabkowski JM, Corrigan M, Scott RW, Nüsslein K, Tew GN (2012) New bactericidal surgical suture coating. *Langmuir* 28:12134–12139. doi:10.1021/la302732w
102. Gupta B, Jain R, Singh H (2008) Preparation of antimicrobial sutures by preirradiation grafting onto polypropylene monofilament. *Polym Adv Technol* 19:1698–1703. doi:10.1002/pat.1146
103. García-Vargas M, González-Chomón C, Magariños B, Concheiro A, Alvarez-Lorenzo C, Bucio E (2014) Acrylic polymer-grafted polypropylene sutures for covalent immobilization or reversible adsorption of vancomycin. *Int J Pharm* 461:286–295. doi:10.1016/j.ijpharm.2013.11.060
104. Jain R, Gupta B, Anjum N, Revagade N, Singh H (2004) Preparation of antimicrobial sutures by preirradiation grafting of acrylonitrile onto polypropylene monofilament. II. mechanical, physical, and thermal characteristics. *J Appl Polym Sci* 93:1224–1229. doi:10.1002/app.20543
105. Saxena S, Ray AR, Gupta B (2010) Graft polymerization of acrylic acid onto polypropylene monofilament by RF plasma. *J Appl Polym Sci* 116:2884–2892. doi:10.1002/app.31823
106. Gupta B, Jain R, Nishat Anjum N, Singh H (2004) Preparation of antimicrobial sutures by preirradiation grafting of acrylonitrile onto polypropylene monofilament. III. hydrolysis of the grafted suture. *J Appl Polym Sci* 94:2509–2516. doi:10.1002/app.21211
107. Gupta B, Anjum N, Gulrez SKH, Singh H (2007) Development of antimicrobial polypropylene sutures by graft copolymerization. II. Evaluation of physical properties, drug release, and antimicrobial activity. *J Appl Polym Sci* 103:3534–3538. doi:10.1002/app.24360
108. Bronzino J, Peterson D (2008) The biomedical engineering handbook. 3rd Edition. CRC Press Taylor & Francis Group, Boca Raton, Florida. ISBN 9781439825334
109. Turner APF, Karube I, Wilson GS (1987) Biosensors: fundamentals and applications. Oxford University Press, Oxford. ISBN 0-19-854724-2. doi:10.1016/S0003-2670(00)85361-1
110. Ponmzhi J, Torres-Marques CF, Frazão O (2012) Smart sensors/actuators for biomedical applications: review. *Measurement* 45:1675–1688. doi:10.1016/j.measurement.2012.02.006
111. Razzak M, Darwis D, Zainuddin Sukirno (2001) Irradiation of PVA and PVP blended hydrogel for wound dressing. *Radiat Phys Chem* 62:107–113. doi:10.1016/S0969-806X(01)00427-3
112. Webb RC, Bonifas AP, Behnaz A, Zhang Y, Yu KJ, Cheng H, Shi M, Bian Z, Liu Z, Kim YS, Yeo WH, Park JS, Song J, Li Y, Huang Y, Gorbach AM, Rogers JA (2013) Ultrathin conformal devices for precise and continuous thermal characterization of human skin. *Nat Mater* 12:938–944. doi:10.1038/nmat3755
113. Kobayashi M, Chang Y, Oka M (2005) In vivo study of PVA hydrogel artificial meniscus. *Biomaterials* 26(16):3243–3248. doi:10.1016/j.biomaterials.2004.08.028
114. Ottenbrite RM, Park K, Okano T (2010) Biomedical applications of hydrogels handbook. Springer, New York. ISBN 978-1-4419-5918-8. doi:10.1007/978-1-4419-5919-5
115. Carretta N, Tricoli V, Pichionni F (2000) Ionomeric membranes based on partially sulfonated PS: synthesis, proton conduction and methanol permeation. *J Membr Sci* 166:189–197. doi:10.1016/S0376-7388(99)00258-6

116. Ouyang J, Chu C, Chen F, Xu Q, Yang Y (2005) High conductivity poly(3,4-ethylenedioxythiophene): poly(styrene sulfonate) film and its application in polymer optoelectronic devices. *Adv Funct Mater* 15:203–208. doi:10.1002/adfm.200400016
117. Balint R, Cassidy NJ, Cartmell SH (2014) Conductive polymers: towards a smart biomaterial for tissue engineering. *Acta Biomater* 10:2341–2353. doi:10.1016/j.actbio.2014.02.015
118. Wang X, Uchiyama S (2013) Polymers for biosensors construction. In: Rinken T (eds) State of the art in biosensors – general aspects. InTech. doi:10.5772/54428 (**chapter 3**)
119. Guimard N, Gomez N, Schmidt C (2007) Conduction polymers in biomedical engineering. *Prog Polym Sci* 32:876–921. doi:10.1016/j.progpolymsci.2007.05.012
120. Ramanavicius A, Ramanaviciene A, Malinauskas A (2006) Electrochemical sensors based on conducting polymer-polypyrrole. *Electrochim Acta* 51:6025–6037. doi:10.1016/j.electacta.2005.11.052
121. Vernitskaya TV, Efimov ON (1997) Polypyrrole: a conducting polymer; its synthesis, properties and applications. *Russ Chem Rev* 66(5):443–457. doi:10.1070/RC1997v066n05ABEH000261
122. Sun Y, Gou G, Yang B, He M, Tian Y, Cheng J, Liu Y (2012) Simple synthesis of polyaniline microtubes for the application on silver microrods preparation. *J Mater Res* 27(2):457–462. doi:10.1557/jmr.2011.408
123. Weerakoon K, Shu J, Park M, Chin B (2012) Polyaniline sensors for Early detection of insect infestation. *J Solid State Sci Technol* 1:100–105. doi:10.1149/2.014205js
124. Loo Y, Yoo J, Cross J, Bucholz T, Lee K, Espe M (2007) Improving the electrical conductivity of polymer acid-doped polyaniline by controlling the template molecular weight. *J Mater Chem* 17:1268–1275. doi:10.1039/b618521e
125. Tsumura A, Koezuka H, Ando T (1986) Macromolecular electronic device: field-effect transistor with a polythiophene thin film. *Appl Phys Lett* 49:1210. doi:10.1063/1.97417
126. Clark J, Silva C, Friend R, Spano F (2007) Role of intermolecular coupling on the photophysics of disordered organic semiconductors: aggregate emission in regioregular polythiophene. *Phys Rev Lett* 98:206406. doi:10.1103/PhysRevLett.98.206406
127. Muñoz-Muñoz FD, Bucio E (2013) Surface modification and functionalization of polymer materials by gamma irradiation for biomedical applications. *Radiat Synth Mater Compd* 10:265-301. ISBN:9781466505223
128. Anderson JM, Rodriguez A, Chang DT (2008) Foreign body reaction to biomaterials. *Semin Immunol* 20:86–100. doi:10.1016/j.smim.2007.11.004
129. Fukano Y, Usul ML, Underwood RA, Isenhat S, Marshall AJ, Hauch KD, Ratner BD, Olerud JE, Fleckman P (2010) Epidermal and dermal integration into sphere-templated porous poly(2-hydroxyethyl methacrylate) implants in mice. *J Biomed Mater Res* 94:1172–1186. doi:10.1002/jbm.a.32798
130. Marshall AJ, Ratner BD (2005) Quantitative characterization of sphere-templated porous biomaterials. *AIChE* 51(4):1221–1232. doi:10.1002/aic.10390
131. Kasálková NS, Slepíčka P, Kolská Z, Hodačová P, Kučková S, Švorčík V (2014) Grafting of bovine serum albumin proteins on plasma-modified polymers for potential application in tissue engineering. *Nanoscale Res Lett* 9:161. doi:10.1186/1556-276X-9-161
132. Halstenberg V, Panitch A, Rizzi S, Hall H, Hubbell JA (2002) Biologically engineered protein-graft-poly(ethylene glycol) hydrogels: a cell adhesive and plasmin-degradable biosynthetic material for tissue repair. *Biomacromolecules* 3(4):710–723. doi:10.1021/bm015629o
133. Akiyama Y, Kikuchi A, Yamato M, Okano T (2004) Ultrathin poly(*N*-isopropylacrylamide) grafted layer on polystyrene surfaces for cell adhesion/detachment control. *Langmuir* 20(13):5506–5511. doi:10.1021/la036139f
134. Hobzova R, Pradny M, Zhunusbekova NM, Sirc J, Guryca V, Michalek J (2011) Bioactive support for cell cultivation and potential grafting. Part 1: surface modification of 2-hydroxyethyl methacrylate hydrogels for avidin immobilization. *E Polymers* 11(1):474–490. doi:10.1515/epoly.2011.11.1.474
135. von Recum H, Okano T, Wan Kim S (1998) Growth factor release from thermally reversible tissue culture substrates. *J Control Release* 55(2–3):121–130. doi:10.1016/s0168-3659(98)00042-x
136. Bhat RR, Chaney BN, Rowley J, Liebmann-Vinson A, Genzer J (2005) Tailoring cell adhesion using surface-grafted polymer gradient assemblies. *Adv Mater* 17(23):2802–2807
137. Ohya S, Nakayama Y, Matsuda T (2001) Material design for an artificial extracellular matrix: cell entrapment in poly (*N*-isopropylacrylamide) (PNIPAM)-grafted gelatin hydrogel. *J. Artif. Organs* 4(4):308–314. doi:10.1007/BF02480023

138. Ross AM, Nandivada H, Ryan AL, Lahann J (2012) Synthetic substrates for long-term stem cell culture. *Polymer* 53(13):2533–2539. doi:10.1016/j.polymer.2012.03.064
139. Fonseca KB, Bidarra SJ, Oliveira MJ, Granja PL, Barrias CC (2011) Molecularly designed alginate hydrogels susceptible to local proteolysis as three-dimensional cellular microenvironments. *Acta Biomater* 7:1674–1682. doi:10.1016/j.actbio.2010.12.029

## Radiation Engineering of Multifunctional Nanogels

C. Dispenza<sup>1,2</sup> · G. Spadaro<sup>1</sup> · M. Jonsson<sup>2</sup>

Received: 13 June 2016 / Accepted: 30 August 2016 / Published online: 19 September 2016  
© Springer International Publishing Switzerland 2016

**Abstract** Nanogels combine the favourable properties of hydrogels with those of colloids. They can be soft and conformable, stimuli-responsive and highly permeable, and can expose a large surface with functional groups for conjugation to small and large molecules, and even macromolecules. They are among the very few systems that can be generated and used as aqueous dispersions. Nanogels are emerging materials for targeted drug delivery and bio-imaging, but they have also shown potential for water purification and in catalysis. The possibility of manufacturing nanogels with a simple process and at relatively low cost is a key criterion for their continued development and successful application. This paper highlights the most important structural features of nanogels related to their distinctive properties, and briefly presents the most common manufacturing strategies. It then focuses on synthetic approaches that are based on the irradiation of dilute aqueous polymer solutions using high-energy photons or electron beams. The reactions constituting the basis for nanogel formation and the approaches for controlling particle size and functionality are discussed in the context of a qualitative analysis of the kinetics of the various reactions.

**Keywords** Nanogels · Synthesis of nanoparticles · Radiation processing · Crosslinking

---

This article is part of the Topical Collection “Applications of Radiation Chemistry”; edited by Margherita Venturi, Mila D’Angelantonio.

---

✉ C. Dispenza  
[clelia.dispenza@unipa.it](mailto:clelia.dispenza@unipa.it)

<sup>1</sup> Dipartimento di Ingegneria Chimica, Gestionale, Informatica, Meccanica, Università degli Studi di Palermo, Viale delle Scienze, Edificio 6, 90128 Palermo, Italy

<sup>2</sup> School of Chemical Science and Engineering, Royal Institute of Technology (KTH), 100 44 Stockholm, Sweden

## 1 Nanogels: Soft, Dynamic, Challenging Nanoparticles

Hydrogels are macroscopic, three-dimensional networks of hydrophilic polymer chains that can absorb a significant amount of water. The presence of chemical (i.e. covalent or ionic) crosslinks, physical crosslinks (e.g. van der Waals interactions, hydrogen bonds, crystalline domains, intermolecular complexes), or a combination of both, prevents or delays polymer dissolution when these materials are exposed to aqueous solutions. Nanogels are nanoscale polymeric networks. The IUPAC defines a nanogel as a gel particle of any shape with an equivalent diameter of 1–100 nm [1]. The definition has often been extended to sub-micron gel particles, thus overlapping with the size range of microgels, which spans 100 nm to 100  $\mu\text{m}$ .

Many different polymeric architectures have been classified as nanogels, including hydrophilic or hydrophobic crosslinked polymer nanoparticles, core-crosslinked or shell-crosslinked micelles of amphiphilic polymers, liposomes modified with crosslinkable polymers, and various composite inorganic/crosslinked polymer nanostructures [2]. Here, we will be mainly concerned with *hydrophilic* polymer networks that can be swollen by water or aqueous solutions.

Nanogels are characterised by an “equilibrium” swelling condition that is the result of the same force balance that governs the swelling of their macroscopic analogues [3]. Hydration and osmotic “*repulsive*” forces drive the polymer segments apart, favouring the ingress of solvent, while elastic “*attractive*” forces are attributed to chain stretching and bond deformation that tend to restore the unstrained chain conformation. When nonpolar chain segments, hydrogen bonding groups or complexing moieties are present in the network (as part of the backbone or as lateral grafts), further components of the attractive forces shall be considered; they can be classified as hydrophobic [4], hydrogen-bonding [5] and coordination bonding forces [6], respectively. If ionisable groups are present, repulsion between fixed electric charges in the network should also be taken into account, alongside the extra contribution to the osmotic pressure owing to the presence of counterions [7]. The swelling degree of nanogels, and thus their hydrodynamic size, is the result of their chemical structure, crosslinking degree and density, and the quality of the solvent (its chemical composition and temperature) in which they are dispersed.

Aside from intraparticle forces, inter-particle forces also affect the behaviour of nanogels. In general, nanogels are characterised by high colloidal stability in aqueous media, mainly due to the steric stabilisation exerted by the dangling chains stretching out in the solvent and the very small density mismatch with the solvent. When ionisable groups are present, electrostatic stabilisation can also contribute to the overall stability, provided that the ionic strength of the dispersing medium is not too high. As expected, there is a very strong interplay between intra- and inter-particle interactions, and the conditions that favour the collapse of the network can also affect the colloidal stability of the nanoparticles, leading to their association [8].

This highly dynamic internal structure of nanogels makes them flexible and adaptive in shape. When nanogels are used as drug carriers, their flexibility and shape-changing ability can facilitate the bypass of biological barriers, ensure protection of the payload, and enable the interaction of any attached ligand with its

receptors. For example, poly(*N*-vinylpyrrolidone)-based nanogels covalently conjugated to insulin can protect the hormone from enzymatic degradation by conforming around the protein. When they reach the cell membrane, the insulin becomes exposed to the receptors where the hormone activates its signalling cascade. The multiple weak interactions established between the polymeric segments of the nanogel and the protein when in the culture medium are reverted by the stronger interactions between the protein and its receptor when the nanocarriers approach the cell membrane [9].

Numerous techniques have been applied for measuring the particle size and size distribution of nanogels, most of which express the results in terms of equivalent spherical radius. In most cases, when the nanoparticles are non-spherical, different measurement techniques produce different size distributions. Therefore, a form factor should be preliminarily determined. All characterisations will be sensitive to heterogeneous impurities; therefore, particular care should be taken in sample preparation, storage and handling.

Some analytical techniques can strongly influence the size and shape of nanogels, especially when the preparation forces the nanogels to lose part or most of their hydration water and to interact with other materials and surfaces or, for example, with the substrates used for sample deposition such as in scanning electron microscopy (SEM), transmission electron microscopy (TEM) or atomic force microscopy (AFM). It must also be emphasised that these techniques require the analysis of numerous images to obtain statistically relevant morphological characterisations.

Laser light scattering is the most common methodology for characterising nanogel particle size as dispersions in a given medium. Particle size is determined as the radius of the impenetrable sphere that would scatter light at the same angle and intensities. In particular, dynamic light scattering (DLS) measurements are related to the Brownian motion of the dispersed particles in the medium [10]. This movement causes fluctuations in the total intensity of the scattered light, which in turn are related to the velocity of the particles moving with their hydration shell. Larger particles move less rapidly than smaller particles, and the intensity fluctuations yield information on particle size through the determination of an average diffusion coefficient and the use of the Stokes–Einstein equation, which relate the diffusion coefficient with the hydrodynamic radius,  $R_h$ , of the particle. The equation is valid for spherical, smooth, rigid non-interacting particles, and the method is rigorously applicable only to monodisperse systems. Light scattering should always characterise non-interacting objects (i.e. dilute systems). It is also advisable to perform the analysis at several scattering angles (multiangle DLS) in order to establish whether the unknown particle size and/or shape distribution is actually affecting the results, since at certain angles the scattering intensity of some particles may completely overwhelm the weak scattering signal of other particles, thus making them invisible.

Static light scattering (SLS), performed on dispersions of different concentrations, can be applied to determine the weight average molecular weight,  $M_w$ , from total intensity measurements; the root mean square radius of the nanoparticle or radius of gyration,  $R_g$ , and the second virial coefficient,  $B_2$ , which represents the interaction potential between two particles (negative values indicate attractive

forces, positive values denote repulsive forces), from the dependence of the total intensity on the angle [11]. Since solvent quality can affect the internal organisation of nanogels and their interaction with the dispersing/swelling medium, laser light scattering can depict the system only in a set of specific measurement conditions, which may or may not be close to the application conditions.

Nanogels, similar to their macroscopic analogues, can be designed to be stimuli-responsive, i.e. to change their swelling behaviour and permeability upon the application of a trigger [12].

For example, if the nanogel is made by a weak polyelectrolyte (a polyacid or a polybase), changes in the environmental pH (*stimulus*) can cause changes in the degree of ionisation of the polyelectrolyte. The related change in the osmotic pressure will result in nanogel swelling or shrinking, respectively. As a result, nanogels can modify their optical behaviour (refractive index) and take up or release molecules (*response*). Protonation/deprotonation processes can also change the surface charge density of the nanoparticles [13, 14].

If the nanogels are made by polymers with functional groups such as azobenzene, spirobenzopyran, triphenylmethane, or cinnamonyl, which undergo reversible structural changes under UV–vis light irradiation, hydrophilic to hydrophobic transitions can be induced by a specific wavelength [15].

Similarly, when the network is formed by homo- or copolymers that exhibit a lower critical solution temperature (LCST), hydrophilic to hydrophobic transitions can be induced by a temperature increase. Such is the case with nanogels based on poly(*N*-alkylacrylamides), poly(NIPAm) being the most investigated, as well as poly(*N*-vinylcaprolactam), poly(methyl vinyl ether), block copolymers of poly(ethylene oxide) and polypropylene oxide, and various derivatives of cellulose (e.g. hydroxypropyl methylcellulose, hydroxypropylcellulose and carboxymethylcellulose) often crosslinked with divinyl sulfone [16]. The quality of the solvent is worsened by the increase in temperature, and hydrophobic association of polymeric segments occurs (hydration water molecules are released, increasing the overall entropy of the system). The responsiveness manifests as volume collapse, and the specific transition temperature is referred to as the “volume phase transition temperature” (VPTT), generally similar to the LCST of the corresponding linear polymer.

Nanogels made of polypeptides and polysaccharides can undergo segmental helix–coil transition, generally at a temperature lower than their “upper critical solution temperature” (UCST). Gelatin nanogels containing triple helices have displayed significant volume transitions when heated above the helix–coil transition temperature [17].

A wide range of interactions have also been demonstrated between specific functional groups grafted onto nanogels with (bio)molecules present in their environments. Coupling of complementary portions of DNA or RNA semi-helices and interactions between an immobilised enzyme and its substrate, or an antibody or a fragment of the antibody with its antigen, are some examples. These interactions, characterised by high selectivity and often also by reversibility, can be exploited to provide specific functions. When nanogels are designed as drug delivery devices (DDD), ligand–receptor interactions can be exploited for preferential accumulation of the nanocarriers at a target site and/or for cellular internalisation [18].

The molecular imprinting approach has been used to synthesise nanogels capable of catalysing specific reactions or that exhibit protein-binding/release properties toward specific biomolecules, with potential application in areas such as bioseparation, biosensing and drug delivery [19–21].

Attempts to produce self-oscillating nanogels are also documented [22, 23]. For example, networks of *N*-isopropylacrylamide (NIPAM), a monomer carrying the ruthenium catalyst for the Belousov–Zhabotinsky (BZ) reaction, 2-acrylamido-2-methylpropane sulfonic acid (AMPS) and methacryloamido propyl trimethylammonium chloride (MATAC) as a capture site for an ionic oxidising agent (bromate ion) in the presence of malonic acid have been produced. Self-motility is the target function [23].

In conclusion, the combination of the typical properties of hydrogels, including soft and rubbery consistency, high solvent uptake, stimuli-responsiveness and biocompatibility, and those of nanocolloids, such as controlled size at the nanoscale, extremely large specific surface area, and enormous possibilities for surface functionalisation, render nanogels very fascinating nanoparticles. The main limitations are strictly connected to their manufacturing, as will be discussed below.

## 2 Nanogel Manufacturing

Nanogels have been designed and synthesised for application in a large number of technological areas, including medicine, mainly as drug nanocarriers [2, 4, 9, 12, 14, 15], in vivo imaging tracers and biological sensors [6, 24], for separation and water treatment [25, 26], in catalysis [27], and as nano-biomachines [22, 23]. They can also be used as building blocks for the self-assembly of well-organised 3D structures at a relatively high concentration by exploiting hydrophobic association or electrostatic interactions [28–31]. The supramolecular macrogels thus obtained have been proposed as smart gating membranes [32], for the fabrication of active photonic crystals and coatings with physical and chemical patterns [33, 34], and for generating bioactive scaffolds for regenerative medicine [35].

Although nanogel applications can be very diverse, some general manufacturing requirements can be identified. It is generally helpful to limit the size to between ten and a few hundred nanometres, with a narrow particle size distribution. In addition to controlling size and size distribution, control of the macromolecular architecture is often required. Core–shell structures, hollow nanoparticles, particles with a density gradient, or non-spherical or shape-changing nanoparticles may be desired. Further requirements can be related to industrialisation, such as ease of scale-up, limited use of toxic or expensive chemicals, and the achievement of high yields of the recovered (purified) product. The synthetic route should be chosen so as to avoid degradation of the precursor or any other component eventually present in the system (e.g. through hydrolysis). One other very important requirement, especially for biomedical applications, is the absence of residual organic solvents, catalysts, monomers or other potentially toxic compounds.

Many comprehensive and highly specialised reviews of different synthetic strategies have already been published [36–40]. In this review, the main features and



the commonly recognised advantages and disadvantages of conventional approaches will be briefly highlighted, with particular focus on processes that yield permanent nanogels, i.e. covalent networks. In the following sections we will focus on a specific synthetic approach that exploits the interaction of high-energy radiation with aqueous solutions of polymers.

The most common synthetic approaches for the preparation of nanogels are:

- (i) micro-/nanofabrication methodologies;
- (ii) synthesis from monomers with di- or multifunctional comonomers (crosslinkers) in homogeneous or heterogeneous phase;
- (iii) self-assembly processes that exploit ionic, hydrophobic or covalent interactions of pre-synthesised polymers.

## 2.1 Nanogel Micro-/Nanofabrication Methodologies

One of the most interesting approaches to micro-/nanofabrication of nanogels is based on the possibility of transferring a pattern generated onto a photomask into an elastomeric mould, which in turn is used to shape the particles [41]. The method of choice for fabricating masters with nanoscale features ( $\geq 10$  nm) and arbitrary geometries is electron beam lithography. This technology is not widely accessible, since it requires costly equipment and expert operators. Conventional photolithography is much less expensive and more widespread, but cannot generate features smaller than about 1  $\mu\text{m}$ , being limited by the wavelength of the UV–vis laser light used. It can be applied either to harden (negative photoresists) or to etch materials (positive photoresists) at the site of irradiation. More recently, multi-photon absorption (MPA) photolithography (also known as direct laser writing) offers the opportunity to produce sophisticated patterns in two or three dimensions, with features that are smaller than the wavelength of light (up to 100 nm), by combining shorter-wavelength laser light (near-infrared [NIR] femtosecond lasers) with focusing systems. MPA can induce photochemical reactions anywhere in the focal volume of a laser beam that is passed through the objective of a microscope. The photochemical reactions can take place only at the centre of the spot where the intensity is sufficiently high.

The lithographically produced masters are used to generate “soft” moulds, which replicate their nanoscale features into the nanoparticles, provided that they are wet and filled by the nanoparticle precursors. After polymerisation and crosslinking, the nanogels must be detached from their nano-moulds and harvested. These steps imply the use of suitable solvent baths and drying stages [42]. While this approach has the greatest flexibility in terms of shape and composition (which can be controlled independently), it still appears to be far from a possible application for large-scale nanogel production, since it requires several consecutive steps and integration of different technologies. It is worth mentioning that one-dimensional temperature-responsive nanogels with an aspect ratio as high as 130 have been produced by nano-moulding [43].

In the production of nanogels with microfluidic devices, the nanogel microstructure can be nicely controlled by adjusting the flow ratio and mixing time in the microchannels. In this case, productivity is low [44, 45]. In principle, the chemical reactions that transform monomers and/or polymers into covalently crosslinked networks can be any of those already applied to produce macrogels—e.g. polymerisation of methacrylate groups, reactions between complementary functional groups (isocyanates and alcohols), Michael-type addition, click chemistry—provided that the device materials are inert and compatible with the reactants and the reaction conditions.

## 2.2 Nanogels Prepared by Polymerisation in Dilute Solutions or Heterogeneous Systems

Polymerisation in dilute solutions or in heterogeneous systems is the oldest and most common route for the production of nanogels [46]. Since the early 1990s, colloidal gels, with dimensions ranging tens to hundreds of nanometres, have been prepared by free-radical polymerisation in dilute solutions or by heterophase polymerisation, such as (inverse) miniemulsion or (inverse) microemulsion, or by precipitation and dispersion polymerisation. As a result, permanent chemical linkages (covalent bonds) between polymeric segments are formed.

In the polymerisation of dilute monomer systems, crosslinking is achieved by the use of di/multi-functional monomers, and the formation of long-range networks is prevented by a relatively low concentration of monomers. Reducing the monomer concentration increases the distance between propagating chains and limits the probability of intermolecular crosslinking. The major limitation of this approach is the low reaction rate and low yield of recovered product, owing to the low concentration of reactants in the system. Another possibility is to start with a higher concentration of monomers and to stop the polymerisation at low conversions by adding a chain terminator or a monofunctional monomer. With this technique, product purification from the unreacted monomers is required.

A higher reaction rate can be achieved by a local increase in monomer concentration in self-assembled nanoreactors, such the nanodroplets of a mini- or microemulsion or the micro-/nanoparticles of a phase-separating polymer. In particular, several nanogel systems have been produced in the aqueous pods of inverse mini- or microemulsion, using from C6 to C10 linear or cyclic alkanes as a nonpolar continuous phase, water-soluble initiators and catalysts, and one or a mixture of surface-active agents (surfactants) [47–50].

In the case of miniemulsion polymerisation, the monomers are dispersed in the continuous phase with the aid of a surfactant, by providing significant amounts of (mechanical) energy for the generation of a large interfacial area, e.g. by ultrasonication or high-pressure homogenisation. The locus of polymerisation and simultaneous crosslinking is confined to the interior of the droplets, and the surfactants responsible for droplet stabilisation also prevent inter-particle crosslinking. Submicron-sized polymer nanogels (50–500 nm) have been obtained at high yields and with very good control of particle size distribution. An important consequence for the industry is that water-soluble compounds can be directly

incorporated/encapsulated into the polymer particles by dissolving/dispersing them in the monomer prior to polymerisation. Since these systems are only kinetically stable, they are strongly dependent on process parameters, i.e. on the shear rate. The produced nanoparticles generally have dimensions that are larger than a few hundred nanometres. Unlike miniemulsions, microemulsions are thermodynamically stable systems due to the presence of a large amount of surfactant. The final products are nanogel particles that can be much smaller (5–50 nm), coexisting with empty micelles. The chemical structure of the nanogels is controlled by the nature, concentration and relative ratio of the monomers and crosslinking agent, by their solubility and hence the partition coefficient between the dispersed and continuous phase, and by the concentration and distribution of the initiator in the system. The major drawback is the high amount of surfactant required. Removal of surfactants and residual monomers often necessitates repeated treatments with water and organic solvents and a final drying step. Re-dispersion from the dry form often causes irreversible aggregation.

In dispersion or precipitation polymerisation, the polymerisation starts in the continuous phase (the solvent), up to the point where the propagating polymer chain is no longer soluble, and phase separation from the solvent occurs, forming particles (nucleation). These nuclei may aggregate and precipitate, or they can be stabilised by the presence of low molecular weight or polymeric surfactants or by electrostatic stabilisation, e.g. when either the initiator or the monomers carry electric charges. Core–shell crosslinked structures can be produced by seeded polymerisation, where the core (nucleated seeds) and the shell are composed of two different crosslinked polymers that are not covalently connected. This approach has also been applied for the production of hollow nanogels using a sacrificial degradable core, or hairy nanogels by the sequential addition of a macromolecular comonomer [51].

Another strategy for producing nanogels relies on reversible-deactivation radical polymerisation (RDRP) techniques, such as atom-transfer radical polymerisation (ATRP), nitroxide-mediated polymerisation (NMP) or reversible addition-fragmentation chain transfer (RAFT) [52]. All these techniques are based on reversible deactivation of growing chains, most of which are in a dormant form. Given that interconversion of active and dormant forms is rapid compared to propagation, all chains are able to grow at the same rate. RDRP makes possible the synthesis of nanogel architecture by the sequential addition of different monomers. Moreover, if the initiating species are fully consumed prior to any appreciable chain growth, all chains grow at the same rate, and the molecular weight distribution of the polymer and particle size is much narrower than in conventional free-radical polymerisation. Synthesis can be carried out at much higher monomer and crosslinker concentrations (up to 20 % in weight) than in conventional methods. Electrically charged molecular or macromolecular initiators can be used as stabilisers. With this technique, hairy nanogels with covalently linked polymer chains have been produced. Reaction kinetics and mechanisms are affected by the specific nature of the monomers, crosslinkers and initiators used. Despite the enormous progress made, however, not all RDRP techniques known today are equally well suited for upscaling from small laboratory experiments to large-scale industrial processes. For example, the controlling agent must be cost effective and ecologically sound.

Furthermore, residual metals in ATRP or the chemical nature of the end groups (RAFT) may be an issue for some applications [53].

### 2.3 Nanogels Produced by Self-Assembly and Crosslinking of Preformed Polymers

This approach has led to a variety of nanoconstructs. Liquid–liquid phase separation of a polymer solution into a polymer-rich (coacervate phase) and a polymer-depleted phase is induced by a change in the quality of solvent (addition of a non-solvent, change in temperature, pH, etc.). The microscopic droplets of the coacervate phase are kept in suspension by stirring. The droplet size can be “transferred” into the nanogel particle size by securing the polymeric colloid through chemical crosslinking [54].

Electrostatic self-assembly of polyelectrolytes by complex coacervation is another example. This process is strongly driven by the release of counterions to increase the overall entropy of the system, and requires the presence of two oppositely charged polyelectrolytes in non-stoichiometric ratios to impart a non-balanced charge (electrostatic stabilisation of the nanoparticles). Colloids based on electrostatic chitosan–DNA [55, 56], chitosan–protein [57] and chitosan–polysaccharide [58] complexes are among the most studied. Because of the electrostatic nature of these complexes, they are intrinsically pH- and ionic strength-responsive.

Chelating ligands, iminodiacetic acid or malonic acid, have been conjugated to hyaluronic acid (HA) and used as a precursor polymer [59]. By mixing the ligand-conjugated HA with cisplatin (CDDP), crosslinking occurred via coordination of the ligands with the platinum in CDDP, resulting in the spontaneous formation of CDDP-loaded HA nanogels. The nanogels showed pH-responsive release of CDDP, because the stability of the ligand–platinum complex decreases in an acidic environment.

Suspension polymerisation of temperature-sensitive photo-crosslinkable polymers can be followed by UV-induced crosslinking at a temperature higher than polymer LCST [60]. Surfactant concentration for the polymerisation is kept below the critical micelle concentration (CMC) to prevent suppression of the temperature-driven coil-to-globule transition by the repulsive electrostatic forces between the ionic heads of the adsorbed surfactant molecules. Particle size decreases with increased sodium dodecyl sulfate (SDS) concentration (nucleation of a larger number of particles) and decreases with increased chromophores, and the nanogels also display significant temperature responsiveness.

## 3 Radiation-Engineered Nanogels

Radiation chemistry, i.e. the use of ionising radiation from radioisotopes and accelerators to induce chemical changes in materials, is a versatile tool for polymer synthesis and modification. The use of water as the primary medium for the absorption of ionising radiation and the effects of aqueous radiolysis products on dissolved monomers and polymers have formed the basis of a variety of applications

in polymer synthesis and modification, particularly in the formation of polymer nanoparticles, which are unique with respect to conventional free-radical polymerisation and crosslinking [61]. The advantages of using radiation chemistry for this purpose are many, and include low energy consumption, minimal use of potentially harmful chemicals, easier control of the exothermal heat of the reaction and simple production schemes. An additional advantage for medical applications is that the material can be sterile as manufactured.

Many macroscopic hydrogels have been prepared by irradiation of aqueous polymer solutions to absorbed radiation doses higher than a critical value, called gelation dose (Dg), when the polymer concentration is above a critical polymer concentration (Cpc) [62]. These parameters have generally been determined by sol-gel analysis based on the gravimetric determination of the sol and gel fractions after irradiation. The filter cut-off affects the separation of the gel fraction from its sol, and traditional paper filters may be unable to separate the gel nanoparticles from the soluble fraction. Therefore, the reported Dg and Cpc can define only the low dose and concentration thresholds for wall-to-wall hydrogels to form. For concentrations below Cpc, macroscopic gelation is not observed, and only micro-/nanogels are expected to form.

A more detailed explanation of how ionising radiation leads to the formation of micro-/nanogels from polymer aqueous solutions will now be provided.

Briefly, high-energy radiation induces the formation of radical sites on the polymer backbone and/or on side chains, which should then evolve mainly through combination to form the desired product. The prevalence of combination over other possible reactions depends primarily on the polymer chemical structure and on the radical concentration [63]. Typical polymers that mainly undergo crosslinking upon irradiation are poly(ethylene oxide) (PEO), poly(vinyl alcohol) (PVA), poly(*N*-vinyl pyrrolidone) (PVP), poly(vinyl methyl ether) (PVME), poly(*N*-isopropyl acrylamide) (PNIPAM) and poly(acrylic acid) (PAA). Temperature and the presence of co-solutes and dissolved gases also affect the chemistry of polymers irradiated in aqueous solution [64, 65]. A distinct advantage of using ionising irradiation of polymer aqueous solutions for the synthesis of micro-/nanogels is that the process requires no surfactants to control the locus of reaction, and chemically stable polymers can be used as a starting material. As a result, purification is simpler and products are non-toxic.

The first syntheses of micro-/nanogels via irradiation of dilute aqueous solution of polymers date back to the 1960s, although the formation of such micro-/nanos-structures was reported a few years earlier by Charlesby and Alexander [64]. Sakurada and Ikada [66] described the synthesis of PVA micro-/nanogels. Schnabel and Borwardt [67] reported the formation of PEO nanogels. In both cases gamma rays were used. For PVA, micro-/nanogel formation was generally associated with a reduction in intrinsic viscosity (after an initial increase) and simultaneous increase in the turbidity of the solutions. In particular, nanoparticles in the 10–60-nm range were detected by SEM, whereas particles with diameters of 80–240 nm resulted from turbidity experiments. This apparent discrepancy between the values derived by the two measurements was attributed to the fact that turbidity measures the overall microparticle, which results from both inter- and intramolecular

crosslinking, whereas SEM detects the primary nanoparticle, meaning the intramolecularly crosslinked, single chain. From both measurements, the smaller particles were obtained for the higher doses.

In the late 1990s, Rosiak and Ulanski proposed a closed-loop system, where aqueous solutions were continuously pumped to a quartz irradiation cell and subjected to intense (about 1 kGy) pulses of 6 MeV electrons. This laboratory, and many others in the world, began successfully applying pulsed e-beams to produce micro-/nanogels. [68] Most of the crosslinking type polymers, including PVP [68, 69], PVA [70], PAA [71, 72], PVME [73–75], PAAm [76] and polyNIPAM copolymers [77], have been used.

With pulsed e-beam irradiation, the reaction kinetics that lead to nanogel formation can be affected by several irradiation parameters in addition to the total absorbed dose. In particular, the “average” dose rate is governed by the combination of the three adjustable parameters: pulse length, pulse frequency and dose rate during the pulse (proportional to the current). The electron energy is generally a fixed parameter that depends on the design of accelerator, and mainly affects the depth of radiation penetration. It is also worth mentioning that changes in temperature may occur due to the high dose rate [78].

Nanogels have also been successfully synthesised using industrial accelerators and the typical set-ups and doses applied for sterilisation (20–40 kGy). One advantage is the ability to produce already sterile nanogels for biomedical applications [79–82].

## 4 Mechanism of Radiation Synthesis of Nanogels

When nanogels are produced upon irradiation of dilute aqueous polymer solutions, the ionising radiation is primarily absorbed by water, the most abundant component. Direct energy absorption by the polymer molecules is negligible. Hence, the starting point of nanogel formation is the radiolysis of water, which leads to the production of oxidising and reducing species. The primary oxidising species are  $\cdot\text{OH}$  and  $\text{H}_2\text{O}_2$ , while the primary reducing species are  $e_{\text{aq}}^-$ ,  $\text{H}^\cdot$  and  $\text{H}_2$ . The radiation chemical yields ( $G$  values) in gamma- and electron-irradiated aqueous solutions are 0.28, 0.073, 0.28, 0.062 and  $0.047 \mu\text{mol J}^{-1}$  for  $\cdot\text{OH}$ ,  $\text{H}_2\text{O}_2$ ,  $e_{\text{aq}}^-$ ,  $\text{H}^\cdot$  and  $\text{H}_2$ , respectively [83].

For most polymers, only the hydroxyl radical and the hydrogen atom are capable of producing a macroradical, mainly by hydrogen abstraction. As can be seen from the radiation chemical yields, the contribution from the hydrogen atom is less than 20 %. By saturating the aqueous solution with  $\text{N}_2\text{O}$  prior to irradiation, the yield ( $G$  value) of the hydroxyl radical can be doubled, since the solvated electron is scavenged by  $\text{N}_2\text{O}$  to produce hydroxyl radicals.

The desired reaction for gel formation is the combination of two carbon (C)-centred macroradicals—in other words, crosslinking. For nanogel formation, a prevalence of intramolecular crosslinking is a prerequisite. However, C-centered macroradicals can also undergo intermolecular crosslinking, and other reactions such as radical–radical disproportionation, reaction with molecular oxygen and, depending on the structure of the radical, unimolecular fragmentation. These

reactions do not contribute to the formation of the network but can still be important for the functionalisation of the nanogel. The relative importance of the disproportionation reaction in relation to the radical–radical combination reaction depends on the nature of the radicals and solvent properties, and can thus be seen as an inherent property of a given polymer in a given solvent. Hence, nothing can be done to favour the combination reaction relative to the disproportionation reaction for a given polymeric solution [84].

The reaction between the C-centred radical and molecular oxygen can result either in the formation of a peroxy radical or, if the radical is reducing, in oxidation of the radical and formation of a superoxide. The latter reaction is possible for C-centred radicals with –OR and –NR<sub>2</sub> substituents in the  $\alpha$ -position. Reducing C-centred radicals can also be oxidised by H<sub>2</sub>O<sub>2</sub>. The reaction with molecular oxygen can be efficiently suppressed, at least initially, by purging the solution with N<sub>2</sub>O or an inert gas prior to irradiation.

Intermolecular crosslinking can also compete with intramolecular crosslinking and lead to the formation of larger particles.

The possible reactions of the polymer macroradical are depicted in Scheme 1.

When nanogels are produced by pulsed electron beams, irradiation is not continuous, and every short pulse of electrons is followed by a relatively long interval without irradiation. Radical reactions are induced during the electron pulse, but they may not be entirely completed before the next electron pulse is absorbed by the sample. Follow-up chemical reactions will also occur between and during pulses. These factors make the kinetic analysis of the reaction system more complex than that for a system exposed to continuous irradiation.

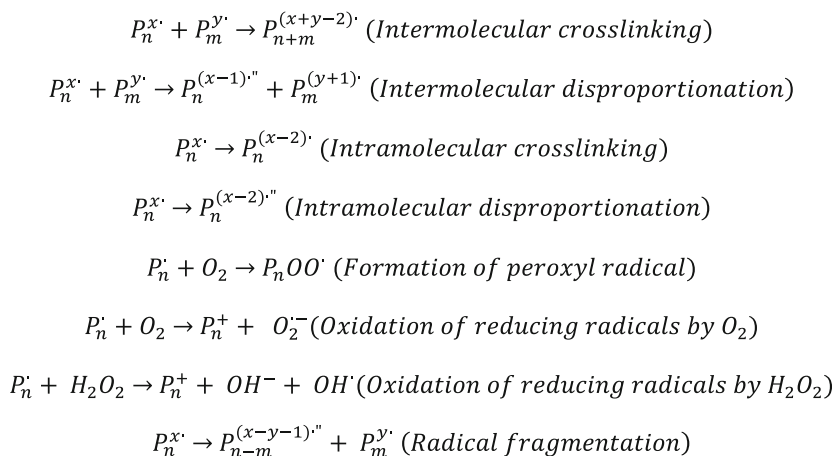
Ideally, we can divide the overall process into two steps:

- (i) Polymer radical formation by interaction of water–radiolysis product with the polymer or nanogel embryos.
- (ii) Polymer radical follow-up reactions.

#### 4.1 Polymer Radical Formation

With regard to the first step, a simplification that can be made when analysing data from pulsed e-beam irradiation of aqueous polymer solutions is that all hydroxyl radicals produced upon radiolysis of water are scavenged by the polymeric solute to form carbon-centered macroradicals. The average number of macroradical centers formed in a pulse would then be determined simply from the radiation chemical yield of hydroxyl radicals and the dose per pulse. This may be true at higher polymer concentrations but not necessarily at lower concentrations, where other reactions involving the hydroxyl radical, such as hydroxyl radical recombination, could efficiently compete with the reaction of hydroxyl radicals with the polymer. Even though the concentration can be fairly high in terms of repeating units, the actual polymer molar concentration is low, and therefore the average distance between polymer chains is large. This distance increases with polymer molecular





**Scheme 1** Possible reactions of polymer macroradical. Disproportionation and fragmentation result in the formation of double bonds (denoted with the apex“)

weight at a given weight fraction of polymer in solution (i.e. with decreasing polymer molar concentration).

At a high dose rate (as in most cases of pulsed e-beam irradiation), radical-radical combination reactions are favoured, and a higher molar concentration of the polymer is required to scavenge all the hydroxyl radicals formed. If the polymer concentration is not high enough, the hydroxyl radical combination will yield hydrogen peroxide, and conversion of initially formed hydroxyl radicals to polymer radicals will not be quantitative. This was recently demonstrated for PVP nanogel formation, where it was experimentally shown that the formation of hydrogen peroxide as a function of dose increases with decreasing polymer concentration [85]. These experimental findings were further supported by numerical simulations of the kinetics of the reaction system (aqueous polymer solution exposed to e-beam pulses at a given frequency) [85]. The fact that  $H_2O_2$  build-up is possible under certain conditions also means that the chemical environment in the irradiated polymer solution will be different at low and high polymer concentrations, as the production of  $H_2O_2$  will be higher in the more dilute polymer solutions. At low polymer concentration, only a fraction of the produced hydroxyl radicals are scavenged by the polymer chains. This will have an impact on the overall process.  $H_2O_2$  is an oxidant but also a precursor for  $O_2$ , which will strongly influence the chemistry of C-centred polymer radicals.

To achieve full hydroxyl radical scavenging capacity, the distance between hydroxyl radicals and scavengers must be short enough to prevent the occurrence of all other possible reactions for the hydroxyl radical. For polymer solutions, since the repeating units are clustered in chains, the scavenging capacity is unevenly distributed in the solution. Hence, for a fraction of the radiolytically formed and homogeneously distributed hydroxyl radicals, the polymer is out of reach. The competing reactions involved in the overall process can be accounted for by normal competition kinetics on the basis of the Smoluchowski model, and have been



illustrated here by introducing the concept of an “active scavenging volume”, within which there is a significant probability for reaction between hydroxyl radicals and the polymer chain. This distance is the average diffusion distance given by the hydroxyl radical lifetime in a specific system. At a low dose rate, the lifetime—taking only hydroxyl radical recombination into account—is long and the average diffusion distance is also long. At a high dose rate, the hydroxyl radical lifetime—and thus also the average diffusion distance—is short. Hydroxyl radicals produced farther away than the average diffusion distance, i.e. outside the active scavenging volume, will not be able to react with the polymer, since this reaction is outcompeted by the radical–radical combination of hydroxyl radicals, and the hydroxyl radical will therefore not exist long enough to reach the polymer. This situation is illustrated in Fig. 1a. The number of radicals per polymer chain will depend on the number of hydroxyl radicals that are within reach of the polymer chain (i.e. within the active scavenging volume) (see Fig. 1a’). For a given dose rate, this number will be independent of the polymer concentration up to the polymer concentration at which the hydroxyl radical could theoretically reach more than one polymer chain. At this point, the active scavenging volumes can be regarded as overlapping. From this polymer concentration upwards, the number of radicals per polymer chain will begin to decrease with increasing polymer concentration (i.e. with increasing overlap of the active scavenging volumes). The concentration effect is illustrated in Fig. 1a, a’, b, b’. The dose rate affects the concentration at which the active scavenging volume overlap occurs, as well as the number of radicals per macromolecule formed at lower concentrations. At a higher dose rate, the hydroxyl radical concentration during the electron pulse is higher, which means that the number of hydroxyl radicals available for each polymer chain is higher. However, the distance between hydroxyl radicals and polymer chains within which there is a significant probability for reaction is shorter than at the lower dose rate, due to the increased probability of radical–radical reactions at the higher hydroxyl radical concentration. This implies that the active scavenging volume of the polymer chain is smaller at a higher dose rate. Nevertheless, the radical concentration per macromolecule will increase with increasing dose rate, although the increase is not proportional to the dose rate. A direct consequence of the decreased active scavenging volume at higher dose rates is that a higher polymer concentration is required to achieve active scavenging volume overlap, i.e. full scavenging capacity. The dose rate effect is illustrated in Fig. 1a, a’, c, c’.

## 4.2 Polymer Radical Follow-up Reactions

The radical follow-up reactions are also affected by polymer concentration and dose rate. The polymer radicals formed are not identical, as there are numerous possible radical sites. Furthermore, under conditions where it is possible to induce more than one radical site per macromolecule, neither the number of radical sites nor the distance between radical sites will be uniform. For these reasons, the reactive species in these systems will display varying reactivity depending on the type of reaction and the nature of the reactive species. In studying the disappearance of radical functionality in such a system, the kinetics cannot be described by simple

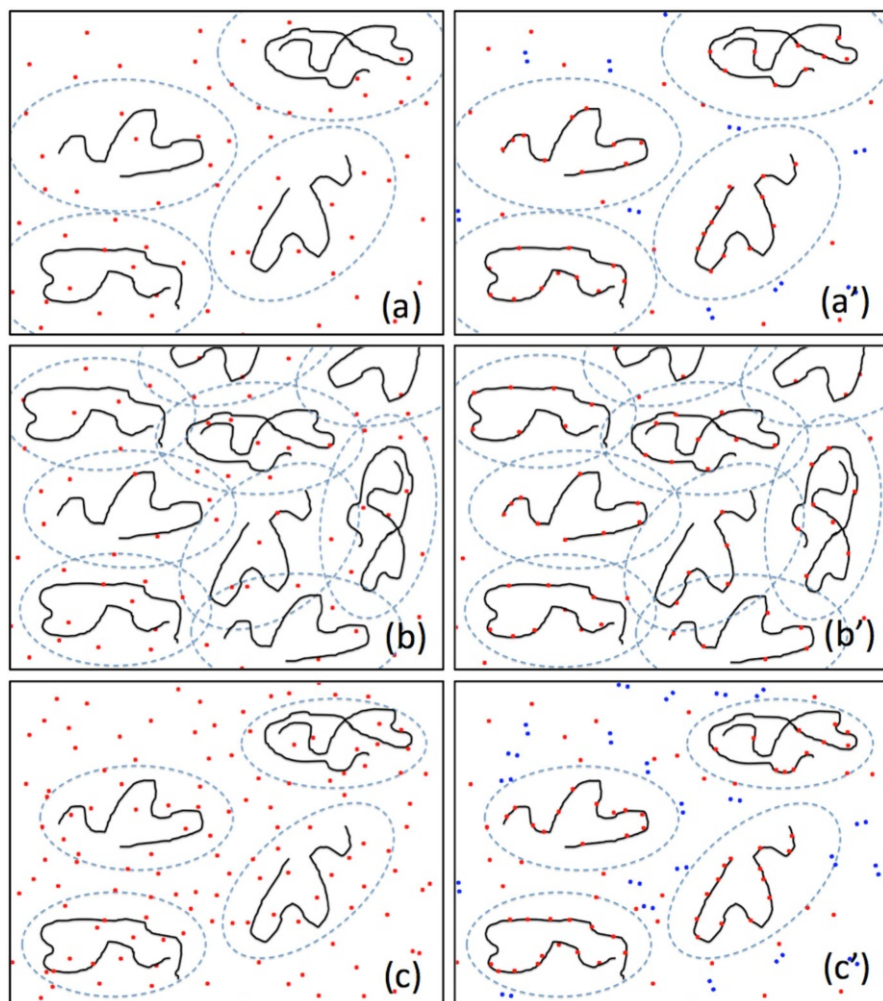


**Fig. 1** Schematic representation of radiolytic radical formation. *Solid black line* polymer chain; *dotted line* contours of the “active scavenging volume”; *red dots* hydroxyl radicals formed in water (*left panels*) and transferred to the polymer (*right panels*), completely or only partially; pairs of *blue dots* hydrogen peroxide formed from combination of hydroxyl radicals. Three possible situations are depicted: **a–a'** low polymer concentration, relatively low dose rate; **b–b'** higher polymer concentration, relatively low dose rate; **c–c'** low polymer concentration, higher dose rate

first- or second-order rate expressions, as the reaction order changes during the course of the reaction. This has led to the development of so-called dispersive kinetics for analysing experimental results [86].

Under conditions where the average number of radicals per chain is constant, i.e. below a certain polymer molar concentration, the kinetics of follow-up reactions can be treated in a slightly simplified manner. It is important to note that we are

discussing rates of intra- and intermolecular crosslink formation here rather than disappearance of radical functionality. Furthermore, we focus on initial events of the polymer radical follow-up reactions (i.e. formation of the first intra- or intermolecular crosslink). The rate constant (or distribution of rate constants, to be more exact, since there will be a distribution of radical species and positions of sites) for intramolecular combination (i.e. formation of intramolecular bonds) will depend on the average number of radicals per chain, and will therefore be constant in the polymer concentration range up to full scavenging capacity (at a given dose rate). Also, the rate constant (or distribution of rate constants) for intermolecular combination will depend on the average number of radicals per chain, and will thus be independent of polymer concentration below the polymer concentration corresponding to full hydroxyl radical scavenging capacity. Hence, the competition between intra- and intermolecular combination in this concentration region is given by the following expression:

$$\frac{k_1[\text{P}]}{k_1[\text{P}] + k_{11}[\text{P}]^2} = \frac{k_1}{k_1 + k_{11}[\text{P}]},$$

where  $[\text{P}]$  is the molar concentration of radical-bearing polymer chains (equal to the total concentration of polymer chains under the present conditions),  $k_1$  is the rate constant for intramolecular combination, and  $k_{11}$  is the rate constant for intermolecular combination. Here,  $k_1$  and  $k_{11}$  can be represented by the average rate constants based on the distribution of reactive radical species. From this expression it is also obvious that intramolecular combination is favoured by low polymer concentration, and that the ratio between intra- and intermolecular combination can simply be controlled by the polymer concentration under the present conditions. The rate constants for both intra- and intermolecular combination will depend on the dose rate. A higher dose rate gives a higher number of radicals per polymer chain, thereby increasing the likelihood of both types of crosslinking reactions.

The influence of various parameters on intramolecular combination was investigated by Jeszka et al. [87] using Monte Carlo simulations. The dynamics of intramolecular radical–radical combination in oxygen-free aqueous solutions of PEO was studied, taking into account the number of radicals per chain, distance between radical sites, polymer chain length, formation of loops and radical transfer. This study clearly shows that the radical half-life due to intramolecular radical–radical combination reactions is strongly dependent on the number of radicals per polymer chain. The predicted first half-life of the radical is typically in the range of  $10^{-5}$  to  $10^{-3}$  s. For multiple radical-bearing polymer chains, the half-life following the first intramolecular combination can be considerably longer. Consequently, the dose rate and the dose per pulse will have a strong impact on the reaction kinetics of the system.

It is interesting to note that the products from pulsed e-beam radiation-induced synthesis of PVP aqueous solutions at four different concentrations, exposed to the same total dose (40 kGy) at two different average dose rates, display very different particle size and molecular weight [79, 80]. The data are shown in Fig. 2. The average dose rate in this context is calculated as the dose delivered in the unit time

that corresponds to the dose per pulse (ca. 0.74 and 13 Gy, for the low and high average dose rates, respectively), multiplied by the pulse frequency (37.5 and 300 Hz, respectively). The higher dose rate yields smaller particles with lower average molecular weight compared to the lower dose rate. This demonstrates that the number of radicals per polymer chain has a major influence not only on the kinetics of intramolecular crosslinking, but also on the competition between inter- and intramolecular crosslinking.

The concentration dependence is well in line with the discussion above. It is clear that particle size increases with polymer concentration at both dose rates; however, the concentration dependence is more pronounced at the lower dose rate. This implies that the two effects are not entirely independent of each other.

A similar trend was observed for PVP by An et al. [88]. These authors also studied the kinetics of PVP radical consumption using pulse radiolysis. The approximate half-life of the radical in this study is  $5 \times 10^{-6}$  s, which is in fairly good agreement with the shortest half-life (for the highest radical concentration) presented by Jeszka et al. [87].

At polymer concentrations above the limit for full hydroxyl radical scavenging capacity, the number of radicals per polymer chain will decrease with increasing polymer concentration. Eventually, the average radical density per chain will reach one and below. At the point where the average radical density per chain is one, the concentration of radical-bearing chains has reached its maximum. Once the average radical density drops below one, the concentration of radical-bearing chains is dictated by the dose rate, and becomes independent of polymer molecule concentration (when increasing the concentration). The only process that can occur

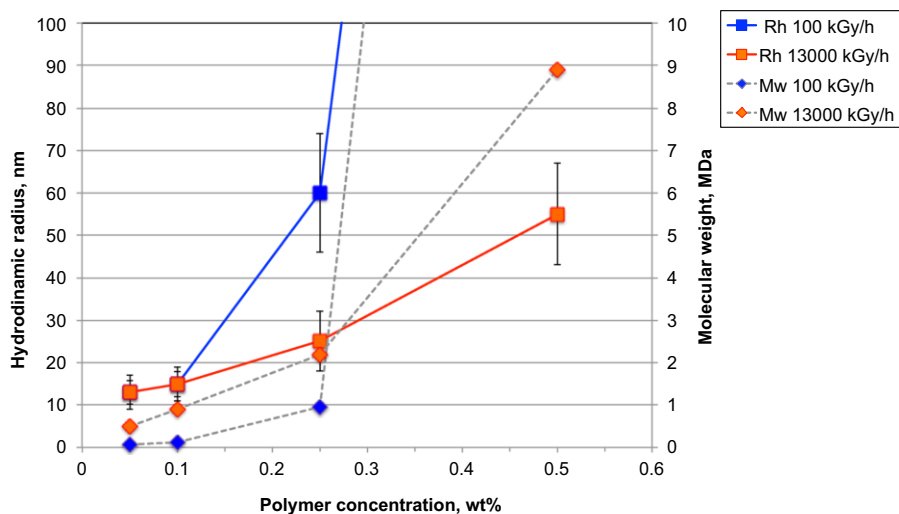


**Fig. 2** Hydrodynamic radius (Rh) from DLS and weight average molecular weight (Mw) from Zimm plot analysis of SLS measurements as a function of the polymer concentration for two different dose rates. Error bars for Rh represent the width of the size distributions. Batch-to-batch variability is lower than 5 %. Hydrodynamic radius and molecular weight of the non-irradiated polymer is  $20 \pm 10$  nm and 0.41 MDa, respectively (Adapted from refs. [79, 80])

after a single pulse under these conditions is intermolecular combination. However, it should be kept in mind that the rate constant for intermolecular combination is also dependent on the number of radicals per chain, and reaches its minimum at one radical per chain. At high pulse repetition frequency, multiple radical sites per chain may still be formed, and the intramolecular crosslinking can also occur.

The polymer concentration dependence of the number of radical-bearing chains and average number of radicals per chain described above is illustrated in Fig. 3.

The trends discussed here are further confirmed by numerous other studies carried out with various polymers, irradiation set-ups and dose ranges. Schmitz and co-workers investigated the influence of the irradiation dose (0–7.5 kGy) by gamma irradiation on PVA aqueous solutions by measuring  $R_h$  and  $R_g$  of the polymer using DLS and SLS, respectively [89]. They also applied a Monte Carlo simulation to the dynamics of polymer chains, assuming that all the “contacts” between polymer segments resulted in a strong bond. The model was developed to support the interpretation of light scattering data. The starting system is formed by relatively short polymer chains in chain-extended conformation. As the chains are joined together in the intermolecular crosslinking process, the resulting structures increasingly resemble hairy cylinders with branches and looped regions. The predominant intermolecular crosslinking is well in line with the description above, given the relatively high molar polymer concentration and the low dose rate. It also explains the initial rapid increase of  $M_w$ ,  $R_g$  and  $R_h$  with dose experimentally observed. Since intermolecular crosslinking progressively reduces the molar concentration of polymer and its diffusion coefficient, intramolecular crosslinking at some point becomes a competitive process. With time (dose), the hairy cylinders transform into soft spheres with a clearly identifiable surface. This explains why  $M_w$  continues to increase but much less steeply,  $R_h$  levels off, and  $R_g$  decreases.

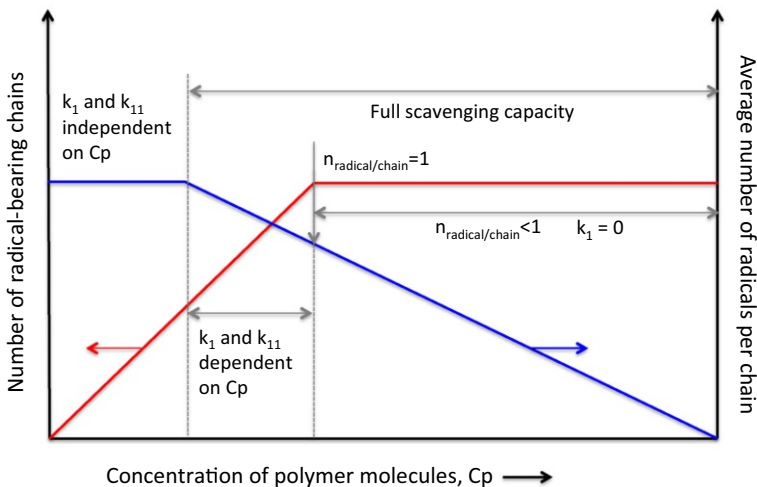


**Fig. 3** Schematic illustration of the number of radical-bearing chains and average number of radicals per chain as a function of polymer concentration

This model is actually similar to the one proposed by Brash and Burchard for the chemical crosslinking of PVA microgels [90].

A similar shift from inter- to intramolecular crosslinking with increasing dose was recently observed for e-beam-irradiated aqueous PVP solutions [91]. For semi-dilute polymer solutions, the particle size increases to a point where the molar concentration becomes low enough to favour intramolecular crosslinking. At higher doses, no further particle growth is observed.

One limitation of irradiating dilute systems with highly energetic pulses lies in the difficulty of controlling particle size and molecular weight of nanogels in an independent way. Intramolecularly crosslinked, single polymer chains may result in nanoparticles that are too small, especially if the molecular weight of the starting polymer is relatively low (below a few hundred kiloDaltons). This problem has been circumvented by performing a first irradiation step at a higher polymer concentration, low dose rate, e.g. with gamma photons, and with a total dose lower than the gelation dose for the polymer. As shown above, these conditions favour intermolecular crosslinking, and thereby an increase in polymer molecular weight by chain extension and branching. The irradiation was then continued at a high “average” dose rate, with e-beams, after dilution of the system [83]. These conditions favour intramolecular crosslinking and the close up of polymer chains to yield particles. While this combination of irradiations yield the desired product, the need for two types of irradiation facilities makes the industrial scale-up of the process more complicated.

Polyelectrolytes in general, and PAA homopolymer and copolymers in particular, require a proper control of pH of the irradiated solutions to yield nanogels. It is fairly intuitive, but also confirmed by kinetic studies, that the bimolecular rate constant for radical combination and competition between inter and intra molecular crosslinking, should depend on the content of ionised base units,  $x_i$ , in the polymer [92]. When  $x_i$  is very small, the polyelectrolyte behaves like a nonionic polymer (pH <2 for PAA). In addition, hydrogen bonding can favour intramolecular association. With increased pH, intermolecular radical–radical combination becomes favoured, since ionisation induces expansion of the coils by intramolecular Coulomb repulsion. At high degrees of ionisation, the polymer conformation is chain-extended (rod-like and stiff), and intermolecular electrostatic repulsion slows recombination by several orders of magnitude. Chain scission then becomes a competitive process (pH >9 for PAA).

Changes in the chemical composition of nanogels are documented only for PVP-based systems irradiated at substantial doses. Sabatino et al. [79] showed that succinimide, carboxyl groups, ether-links and non-carboxylic hydroxyl groups were formed upon irradiation, and it was clear that the chemical change was most significant in systems of low polymer concentration. However, this is not surprising given the fact that the functionalisation process is radiation-driven and depends mainly on the absorbed dose, while the methods used to detect the chemical change are sensitive to the relative chemical change of the system rather than to the absolute change (that is why the chemical modification effects are most evident at low polymer concentration). The systems studied by Sabatino et al. [79] were saturated with  $N_2O$  prior to irradiation, and therefore the only expected oxidising species



would be the hydroxyl radical. As shown above, in systems containing low polymer concentrations, hydrogen peroxide can also be formed. At the very high doses applied (40 kGy),  $N_2O$  will be completely consumed, and the chemical conditions during irradiation will become different from the starting conditions. Hence, several species may form that have the potential to influence the chemical functionality of the product. As shown for PVP, functionalisation appears to be a consequence of oxidative conditions.

Another experimental study on PVP functionalisation was conducted more recently [85]. In this work, Fourier transform infrared spectroscopy (FTIR) analysis also provides useful insights. The formation of succinimide rings and COOH groups is confirmed and shown to increase with dose. Primary amino groups were also detected and their concentration also increases with dose. The corresponding radiation chemical yields for their formation are in the range of  $nmol J^{-1}$ . It is obvious that  $NH_2$ -groups can only be formed as a consequence of double N–C bond scission of the pyrrolidone ring and that COOH groups can only be formed upon oxidative scission of the polymer backbone or the pyrrolidone rings. It has been speculated that the C–N bond scission required for  $NH_2$  formation is facilitated by the presence of  $H_2O_2$  or the subsequently formed  $O_2$ . The most probable macroradical reactant for this reaction is an  $\alpha$ -amino alkyl radical capable of reducing both  $H_2O_2$  and  $O_2$ .

Moreover, nanogels with specific functional groups, such as reactive moieties useful for bioconjugation of drugs or ligands or for providing stimuli-responsive-ness, have been obtained by irradiating the polymer in the presence of unsaturated monomers [93] or through co-crosslinking of mutually complexing polymers [94, 95]. In the first case, a small amount of acrylic acid (AA) added to PVP competes with intermolecular crosslinking, and smaller nanogel particles than those of corresponding PVP systems irradiated without AA are obtained [93]. The AA grafted on PVP provides accessible carboxyl groups for the covalent attachment of peptides [96], proteins [9] and oligonucleotides [97]. In the second approach, where much lower dose rates and higher amounts of AA were used, the monomer polymerises first, then interacts with PVP by multiple hydrogen bonds. PVP act as a soft template for the forming PAA and binds it by the radiation-induced radical–radical combination process. The nanogels thus obtained showed pH responsiveness and were used to encapsulate and release an ophthalmic drug [98]. Similarly, aminopropyl methacrylamide (APMAM), a primary amino group carrying an acrylic monomer, has been simultaneously irradiated with aqueous PVP nanogels and grafted onto the nanogels. The nanoparticles were then decorated with fluorescent molecules and antibodies through a peptide linkage, showing active targeting functions [81, 82].

It is also worth mentioning that temperature- and pH-responsive nanogels have been produced starting from amphiphilic block copolymers organised in micellar aggregates, and inducing crosslinking by means of electron beam irradiation. Temperature responsiveness was provided by the polyNIPAAm block, while pH responsiveness was obtained by 5-methacryloyloxy pentanoic acid (5MPA) or 4-methacryloyloxy benzoic acid (4MBA) units [99]. Other researchers have produced nanogels by irradiating micellar systems or microemulsions [100, 101].

## 5 Concluding Remarks

Nanogels are fascinating polymer nanoparticles that, because of their tuneable chemical structure and highly permeable interiors to solvent molecules, can change shape and/or volume, electric charge and hydrophilic–lipophilic balance. As a result, nanogels can be stable colloids in aqueous media but can also assemble into supramolecular structures under a proper trigger.

These soft and dynamic nanoparticles are under intense development in cancer imaging, molecular diagnosis and targeted therapy. The basic rationale is that they can offer large and conformable cavities to incorporate bulky active ingredients such as therapeutic proteins, as well as hydrophobic pockets (in the proximity of crosslinking points) within which to host barely polar molecules, which is the case of many medical drugs. They can display several reactive groups, either directly linked to the network or at the terminus of dangling chains that stretch out in the solvent. When conjugated with targeting ligands such as monoclonal antibodies, peptides, oligonucleotides or small molecules, these nanoparticles can be used to target malignant tumor cells and the tumor microenvironment with high specificity and affinity.

The possibility of producing nanogels as aqueous dispersions, without necessarily going through a drying step for purification, is the best guarantee for controlled size, and hence functionality, at the nanoscale. Solvent removal that is required when organic solvents and toxic chemicals are used in manufacturing can cause irreversible aggregation and loss of performance.

The radiation chemistry of aqueous polymer solutions provides very interesting opportunities for the synthesis of nanomaterials in aqueous media. No initiators or catalysts are required to generate polymer radicals, and no soft (surfactants) or hard templates (moulds) are necessary to control the size of the nanoparticles. This possibility has been demonstrated with a variety of polymers, irradiation sources and processing conditions. The nanogels produced have generally shown average hydrodynamic diameter in a range of 20 to 200 nm and relatively narrow particle size distribution (polydispersity index [PDI] < 0.3). This is actually the target size range for intravenously administered soft drug nanocarriers so that they are able to evade the reticuloendothelial system (RES) (provided that the surface is hydrophilic and not strongly charged) and to display extravasation capability from the newly formed blood vessels at the tumor site.

Irradiation conditions that favour intramolecular crosslinking at some point in the process shall be chosen in order to transform the starting polymer into a crosslinked nanoparticle. The most important parameter to control appears to be the polymer molar concentration. Low molar concentrations favour intramolecular crosslinking over intermolecular crosslinking. There are some implications for excessive reduction of polymer concentration: the throughput in terms of valuable material becomes too low for the process to be attractive; nanogels size and crosslinking density become somewhat fixed; the radicals produced in water may not be completely scavenged by the polymer, yielding to other reactive molecules, which may provide reaction routes for the macroradicals different from their mutual



combination. This last condition may or may be not desired. Dose and dose rate, in conjunction with polymer concentration, are two other important tuneable parameters for the process. Irradiation at lower dose rates with relatively high polymer concentrations can be pursued when chain extension or branching is desired in the early phase of the process, in order to increase the molecular weight, and thus the size, of the nanogel ultimately formed. Despite what has already been demonstrated and rationalised with kinetic studies, molecular simulations and product analysis, looking into the future, we feel that there are a number of research directions that are particularly promising but require a concerted effort for success. These include:

1. Strengthening the foundations of radiation chemistry of aqueous polymer systems. A better understanding of the role of the various irradiation parameters and their inter-relationships is of paramount importance in controlling nanogel size and functionality and in establishing process design guidelines.
2. Enlarging the library of polymers used as starting materials. The use of water-soluble or water-dispersible natural polymers and their derivatives can open up further application opportunities, especially when bioadsorption or biodegradability is required.
3. Standardisation and manufacturability. Especially for future use in biomedical applications, radiation-engineered nanogels—as well as other nanoparticles—must be standardised in terms of structural, physicochemical, morphological and biological properties; characterisations and manufacturing protocols should be defined to ensure the quality and safety of the products in collaboration with the relevant regulatory agencies.

## References

1. IUPAC (1997) Compendium of Chemical Terminology, 2nd ed. (the “Gold Book”). Compiled by A. D. McNaught and A. Wilkinson. Blackwell Scientific Publications, Oxford. XML on-line corrected version: <http://goldbook.iupac.org> (2006) created by M. Nic, J. Jirat, B. Kosata; updates compiled by A. Jenkins
2. Motornov M, Roiter Y, Tokarev I, Minko S (2010) Stimuli-responsive nanoparticles, nanogels and capsules for integrated multifunctional intelligent systems. *Prog Polym Sci* 35:174–211
3. Ricka J, Tanaka T (1984) Swelling of ionic gels: quantitative performance of the Donnan theory. *Macromolecules* 17:2916–2921
4. Akiyoshi K, Kobayashi S, Shichibe S, Mix D, Baudys M, Kim SW, Sunamoto J (1998) Self-assembled hydrogel nanoparticle of cholesterol-bearing pullulan as a carrier of protein drugs: complexation and stabilization of insulin. *J Control Release* 54(3):313–320
5. Chen Y, Ballard N, Bon SAF (2013) Waterborne polymer nanogels non-covalently crosslinked by multiple hydrogen bond arrays. *Polym Chem* 4:387–392
6. Lim C-K, Singh A, Heo J, Kim D, Lee KE, Jeon H, Koh J, Kwon I-C, Kim S (2013) Gadolinium-coordinated elastic nanogels for in vivo tumor targeting and imaging. *Biomaterials* 34:6846–6852
7. López-León T, Carvalho ELS, Seijo B, Ortega-Vinuesa JL, Bastos-González D (2005) Physicochemical characterization of chitosan nanoparticles: electrokinetic and stability behaviour. *J Colloid Interf Sci* 283:344–351
8. Israelachvili JN (2011) Intermolecular and surface forces, 3rd edn. Academic Press, San Diego


9. Picone P, Ditta LA, Sabatino MA, Militello V, San Biagio PL, Di Giacinto ML, Cristaldi L, Nuzzo D, Dispenza C, Giacomazza D, Di Carlo M (2016) Ionizing radiation-engineered nanogels as insulin nanocarriers for the development of a new strategy for the treatment of Alzheimer's disease. *Biomaterials* 80:179–194
10. Brown W, Nicolai T (1993) *Dynamic light scattering: the method and some applications*. Ed. Clarendon Press, Oxford
11. Wyatt PJ (1993) Light scattering and the absolute characterization of macromolecules. *Anal Chim Acta* 272:1–40
12. Maya S, Sarmiento B, Nair A, Rejinold NS, Nair SV, Jayakumar R (2013) Smart stimuli sensitive nanogels in cancer drug delivery and imaging: a review. *Curr Pharm Des* 19(41):7203–7218
13. Shen X, Zhang L, Jiang X, Hu Y, Guo J (2007) Reversible surface switching of nanogel triggered by external stimuli. *Angew Chem Int Ed* 46:7104–7107
14. Du J-Z, Sun T-M, Song W-J, Wu J, Wang JA (2010) Tumor-acidity-activated charge-conversional nanogel as an intelligent vehicle for promoted tumoral-cell uptake and drug delivery. *Angew Chem Int Ed* 49:3621–3626
15. Zha L, Banik B, Alexis F (2011) Stimulus responsive nanogels for drug delivery. *Soft Matter* 7:5908–5916
16. Bromberg LE, Ron ES (1998) Temperature-responsive gels and thermogelling polymer matrices for protein and peptide delivery. *Adv Drug Deliv Rev* 31:197–221
17. Gandhi SS, Yan H, Kim C (2014) Thermoresponsive gelatin nanogels. *ACS Macro Lett* 3:1210–1214
18. Xu S, Olenyuk BZ, Okamoto CT, Hamm-Alvarez SF (2013) Targeting receptor-mediated endocytotic pathways with nanoparticles: rationale and advances. *Adv Drug Deliv Rev* 65(1):121–138
19. Lei Ye (ed) (2013) *Molecular imprinting: principles and applications of micro- and nanostructured polymers*. CRC Press
20. Carboni D, Flavin K, Servant A, Gouverneur V, Resmini M (2008) The first example of molecularly imprinted nanogels with aldolase type I activity. *Chemistry* 14(23):7059–7065
21. Pan G, Guo Q, Cao C, Yang H, Li B (2013) Thermo-responsive molecularly imprinted nanogels for specific recognition and controlled release of proteins. *Soft Matter* 9:3840–3850
22. Varga I, Szalai I, Mészáros R, Gilányi T (2006) Pulsating pH-responsive nanogels. *J Phys Chem B* 110(41):20297–20301
23. Sakai T, Yoshida R (2004) Self-oscillating nanogel particles. *Langmuir* 20(4):1036–1038
24. Wu W, Zhou S (2010) Hybrid micro-/nanogels for optical sensing and intracellular imaging. *Nano Rev* 1:5730
25. Kondo K, Kaji N, Toita S, Okamoto Y, Tokeshi M, Akiyoshi K, Baba Y (2010) DNA separation by cholesterol-bearing pullulan nanogels. *Biomicrofluidics* 4(3):32210–32218
26. Akl MA, Sarhan AA, Shoueir KR, Atta AM (2013) Application of crosslinked ionic poly(vinyl alcohol)nanogel as adsorbents for water treatment. *J Dispers Sci Technol* 34(10):1399–1408
27. Resmini M, Flavin K, Carboni D (2012) Microgels and nanogels with catalytic activity. *Top Curr Chem* 325:307–342
28. Kuroda K, Fujimoto K, Sunamoto J, Akiyoshi K (2002) Hierarchical self-assembly of hydrophobically modified pullulan in water: gelation by networks of nanoparticles. *Langmuir* 18(10):3780–3786
29. Nakai T, Hirakura T, Sakurai Y, Shimoboji T, Ishigai M, Akiyoshi K (2012) Injectable hydrogel for sustained protein release by salt-induced association of hyaluronic acid nanogel. *Macromol Biosci* 12(4):475–483
30. Li Y, Ye Z, Shen L, Xu Y, Zhu A, Wu P, An Z (2016) Formation of multidomain hydrogels via thermally induced assembly of pisa-generated triblock terpolymer nanogels. *Macromolecules* 49(8):3038–3048
31. Xia L-W, Xie R, Ju X-J, Wang W, Chen Q, Chu L-Y (2013) Nano-structured smart hydrogels with rapid response and high elasticity. *Nat Commun* 4:2226–2236
32. Luo F, Xie R, Liu Z, Ju X-J, Wang W, Lin S, Chu L-Y (2015) Smart gating membranes with in situ self-assembled responsive nanogels as functional gates. *Sci Rep* 5:14708–14721
33. Reese CE, Mikhonin AV, Kamenjicki M, Tikhonov A, Asher SA (2004) Nanogel nanosecond photonic crystal optical switching. *J Am Chem Soc* 126(5):1493–1496
34. Tian L, Liu K-K, Fei M, Tadepalli S, Cao S, Geldmeier JA, Tsukruk VV, Singamaneni S (2016) Plasmonic nanogels for unclonable optical tagging. *ACS Appl Mater Interfaces* 8(6):4031–4041

35. Saez-Martinez V, Olalde B, Juan MJ, Jurado MJ, Garagorri N, Obieta I (2010) Novel bioactive scaffolds incorporating nanogels as potential drug eluting devices. *J Nanosci Nanotechnol* 10(4):2826–2832
36. Oh JK, Drumright R, Siegwart DJ, Matyjaszewski K (2008) The development of microgel/nanogels for drug delivery applications. *Prog Polym Sci* 33(4):448–477
37. Kabanov AV, Vinogradov SV (2009) Nanogels as pharmaceutical carriers: finite networks of infinite capabilities. *Angew Chem Int Ed Engl* 48(30):5418–5429
38. Sanson N, Rieger J (2010) Synthesis of nanogels/microgels by conventional and controlled radical crosslinking copolymerization. *Polym Chem* 1:965–977
39. Zhang X, Malhotra S, Molina M, Haag R (2015) Micro- and nanogels with labile crosslinks—from synthesis to biomedical applications. *Chem Soc Rev* 44:1948–1973
40. Ulański P, Rosiak JM (2004) Polymeric Nano/Microgels. In: Nalwa HS (ed) *Encyclopedia of nanoscience and Nanotechnology*, vol VIII, pp 845–871, ISBN 1-58883-001-2. American Scientific Publishers, Stevenson Ranch
41. Lipomi DJ, Martinez RV, Cademartiri L, Whitesides GM (2012) Soft lithographic approaches to nanofabrication, chapter 7.11. In: Matyjaszewski K and Möller M (eds) *Polymer science: a comprehensive reference*, 1st edn. Elsevier, Amsterdam, pp 211–231
42. Rolland JP, Maynor BW, Euliss LE, Exner AE, Denison GM, DeSimone JM (2005) Direct fabrication and harvesting of monodisperse, shape-specific nanobiomaterials. *J Am Chem Soc* 127(28):10096–10100
43. Omichi M, Marui H, Takano K, Tsukuda S, Sugimoto M, Kuwabata S, Seki S (2012) Temperature-responsive one-dimensional nanogels formed by the cross-linker-aided single particle nanofabrication technique. *ACS Appl Mater Interfaces* 4(10):5492–5497
44. Zhang H, Tumarkin E, Sullan RMA, Walker GC, Kumacheva E (2007) Exploring microfluidic routes to microgels of biological polymers. *Macromol Rapid Commun* 28(5):527–538
45. Bazban-Shotorbani S, Dashtimoghdam E, Karkhaneh A, Hasani-Sadrabadi MM, Jacob KI (2016) Microfluidic directed synthesis of alginate nanogels with tunable pore size for efficient protein delivery. *Langmuir* 32(19):4996–5003
46. Nesvadba P (2012) Radical polymerization in industry. In: Chatgililoglu C, Studer A (eds) *Encyclopedia of radicals in chemistry, biology and materials*. John Wiley & Sons, Inc, New York
47. Oh JK, Bencherif SA, Matyjaszewski K (2009) Polymer atom transfer radical polymerization in inverse miniemulsion: a versatile route toward preparation and functionalization of microgels/nanogels for targeted drug delivery applications. *Polymer* 50(19):4407–4423
48. Medeiros SF, Santos AM, Fessi H, Elaissari A (2010) Synthesis of biocompatible and thermally sensitive poly(*N*-vinylcaprolactam) nanogels via inverse miniemulsion polymerization: effect of the surfactant concentration. *J Polym Sci A Polym Chem* 48:3932–3941
49. Klinger D, Aschenbrenner EM, Weiss KC, Landfester K (2012) Enzymatically degradable nanogels by inverse miniemulsion copolymerization of acrylamide with dextran methacrylates as crosslinkers. *Polym Chem* 3:204–216
50. Sarika PR, James NR (2015) Preparation and characterisation of gelatin–gum arabic aldehyde nanogels via inverse miniemulsion technique. *Int J Biol Macromol* 76:181–187
51. Blackburn WH, Lyon LA (2008) Size controlled synthesis of monodispersed, core/shell nanogels. *Colloid Polym Sci* 286(5):563–569
52. Muller AHE, Matyjaszewski K (eds) (2010) *Controlled and living polymerizations from mechanisms to applications*. Wiley-VCH Verlag GmbH, Weinheim
53. Destarac M (2010) Controlled Radical Polymerization: industrial stakes, obstacles and achievements. *Macromol React Eng* 4(3–4):165–179
54. Lupitskyya R, Minko S (2010) Robust synthesis of nanogel particles by an aggregation-crosslinking method. *Soft Matter* 6:4396–4402
55. Li Y, Maciel D, Rodrigues J, Shi X, Tomás H (2015) Biodegradable polymer nanogels for drug/nucleic acid delivery. *Chem Rev* 115(16):8564–8608
56. Lee JI, Kim HS, Yoo HS (2009) DNA nanogels composed of chitosan and Pluronic with thermosensitive and photo-crosslinking properties. *Int J Pharma* 373(1–2):93–99
57. Zubareva A, Ilyina A, Prokhorov A, Kurek D, Efremov M, Varlamov V, Senel S, Ignatyev P, Svirshchevskaya E (2013) Characterization of protein and peptide binding to nanogels formed by differently charged chitosan derivatives. *Molecules* 18(7):7848–7864
58. Siqueira Franco Picone C, Lopes Cunha R (2013) Chitosan–gellan electrostatic complexes: influence of preparation conditions and surfactant presence. *Carbohydr Polym* 94(1):695–703

59. Hiramoto S, Amano Y, Sato M, Suzuki Y, Shinohara M, Emoto S, Yamaguchi H, Ishigami H, Sakai Y, Kitayama J, Ito T (2016) Production of cisplatin-incorporating hyaluronan nanogels via chelating ligand-metal coordination. *Bioconjug Chem* 27(3):504–508
60. Vo CD, Kuckling D, Adler H-JP, Schonhoff M (2002) Preparation of thermosensitive nanogels by photo-cross-linking. *Colloid Polym Sci* 280:400–409
61. Dispenza C, Grimaldi N, Sabatino MA, Soroka IL, Jonsson M (2015) Radiation-engineered functional nanoparticles in aqueous system. *J Nanosci Nanotech* 15(5):3445–3467
62. Rosiak JM (1994) Radiation formation of hydrogels for drug delivery. *J Control Release* 31(1):9–19
63. Charlesby A (1960) Atomic radiation and polymers. Pergamon Press, Oxford
64. Charlesby A, Alexander P (1955) Reticulation of polymers in aqueous solution by  $\gamma$ -rays. *J Chim Phys PCB* 52:699–709
65. Charlesby A, Alexander P (1957) Effect of X-rays and  $\gamma$ -rays on synthetic polymers in aqueous solution. *J Polym Sci* 23:355–375
66. Sakurada I, Ikada Y (1996) Effects of Gamma Radiation on Polymer in Solution (IX): a turbidimetric study on solution of poly(vinyl alcohol) irradiated below critical concentration for gel-formation (Special Issue on Physical, Chemical and Biological Effects of Gamma Radiation, VII). *Bull Inst Chem Res Kyoto Univ* 44(1):66–73
67. Schnabel W, Borgwardt U (1969) Über die vernetzung von polyäthylenoxid in lösung unter der einwirkung von  $^{60}\text{CO}$ - $\gamma$ -strahlen. *Makromol Chem* 123:73–79
68. Ulanski P, Rosiak JM (1999) The use of radiation technique in the synthesis of polymeric nanogels. *Nucl Instrum Methods Phys Res B* 151(1–4):356–360
69. Kadlubowski S (2014) Radiation-induced synthesis of nanogels based on poly(*N*-vinyl-2-pyrrolidone)—a review. *Radiat Phys Chem* 102:29–39 and references herein
70. Ulanski P, Janik I, Rosiak JM (1998) Radiation formation of polymeric nanogels. *Radiat Phys Chem* 52:289–294
71. Ulanski P, Kadlubowski S, Rosiak JM (2002) Synthesis of poly (acrylic acid) nanogels by preparative pulse radiolysis. *Radiat Phys Chem* 63(3–6):533–537
72. Kadlubowski S, Grobelny J, Olejniczak W, Cichomski M, Ulanski P (2003) Pulses of fast electrons as a tool to synthesize poly (acrylic acid) nanogels. Intramolecular cross-linking of linear polymer chains in additive-free aqueous solution. *Macromolecules* 36(7):2484–2492
73. Arndt K-F, Schmidt T, Reichelt R (2001) Thermo-sensitive poly(methyl vinyl ether) micro-gel formed by high energy radiation. *Polymer* 42:6785–6791
74. Querner C, Schmidt T, Arndt K-F (2004) Characterization of structural changes of poly(vinyl methyl ether) gamma-irradiated in diluted aqueous solutions. *Langmuir* 20(7):2883–2889
75. Schmidt T, Janik I, Kadlubowski S, Ulanski P, Rosiak JM, Reichelt R, Arndt K-F (2005) Pulsed electron beam irradiation of dilute aqueous poly (vinyl methyl ether) solutions. *Polymer* 46(23):9908–9918
76. El-Rehim HAA (2005) Swelling of radiation crosslinked acrylamide-based microgels and their potential applications. *Radiat Phys Chem* 74(2):111–117
77. Picos-Corrales LA, Licea-Claverie A, Arndt K-F (2012) Stimuli-responsive nanogels by e-beam irradiation of dilute aqueous micellar solutions: Nanogels with pH controlled LCST. Chapter 7: Polymer Nanotechnology. In: Nanotechnology 2012: advanced materials, CNTs, particles, films and composites, vol 1. NSTI publication
78. Chmielewski AG, Haji-Saeid M, Shamshad Ahmed S (2005) Progress in radiation processing of polymers. *Nucl Instrum Methods Phys Res Sect B* 236(1):44–54
79. Sabatino MA, Bulone D, Veres M, Spinella A, Spadaro G, Dispenza C (2013) Structure of e-beam sculptured poly(*N*-vinylpyrrolidone) networks across different length-scales, from macro to nano. *Polymer* 54(1):54–64
80. Dispenza C, Sabatino MA, Grimaldi N, Spadaro G, Bulone D, Bondi ML, Adamo G, Rigogliuso S (2012) Large-scale radiation manufacturing of hierarchically assembled nanogels. *Chem Eng Trans* 27:229C–234C
81. Dispenza C, Sabatino MA, Grimaldi N, Bulone D, Bondi ML, Casaletto MP, Rigogliuso S, Adamo G, Ghersi G (2012) Minimalism in radiation synthesis of biomedical functional nanogels. *Biomacromolecules* 13:1805–1817
82. Adamo G, Grimaldi N, Sabatino MA, Walo M, Dispenza C, Ghersi G (2016) E-beam crosslinked nanogels conjugated with monoclonal antibodies in targeting strategies. *Biol Chem*. doi:10.1515/hsz-2016-0255

83. Spinks JWT, Woods RJ (1990) An introduction to radiation chemistry. Wiley-Interscience, Wiley, New York
84. Alfassi ZB (1999) General aspects of the chemistry of radicals. Wiley, New York
85. Dispenza C, Sabatino M, Grimaldi N, Mangione M, Walo M, Murugan E, Jonsson M (2016) On the origin of functionalisation in one-pot radiation synthesis of nanogels from aqueous polymer solutions. *RSC Adv* 6(4):2582–2591
86. Plonka A (1991) Developments in dispersive kinetics. *Prog React Kinet* 16:157–333
87. Jeszka JK, Kadlubowski S, Ulanski P (2006) Monte Carlo simulations of nanogels formation by intramolecular recombination of radicals on polymer chain. Dispersive kinetics controlled by chain dynamics. *Macromolecules* 39:857–870
88. An JC, Weaver A, Kim B, Barkatt A, Poster D, Vreeland WN, Silverman J, Al-Sheikhly M (2011) Radiation-induced synthesis of poly(vinylpyrrolidone) nanogel. *Polymer* 52:5746–5755
89. Schmitz KS, Wang B, Kokufuta E (2001) Mechanism of microgel formation via cross-linking of polymers in their dilute solutions: mathematical explanation with computer simulations. *Macromolecules* 34:8370–8377
90. Brasch U, Burchard W (1996) Preparation and solution properties of microhydrogels from poly(vinyl alcohol). *Macromol Chem Phys* 197:223–235
91. Kadlubowski S, Ulanski P, Rosiak JM (2012) Synthesis of tailored nanogels by means of two-stage irradiation. *Polymer* 53:1985–1991
92. Gorlich W, Schnabel W (1973) Untersuchungen über die Eiffler der Ladungsdichte auf die gegenseitige Desaktivierung von Polyon-Mackroradikalen. *Die Macromolekulare Chemie* 164:225–235
93. Grimaldi N, Sabatino MA, Przybytniak G, Kaluska I, Bondi ML, Bulone D, Alessi S, Spadaro G, Dispenza C (2014) High-energy radiation processing, a smart approach to obtain PVP-graft-AA nanogels. *Radiat Phys Chem* 94:76–79
94. Henke A, Kadlubowski S, Ulański P, Arndt K-F, Rosiak JM (2005) Radiation-induced cross-linking of polyvinylpyrrolidone-poly(acrylic acid) complexes. *Nucl Instr Meth Phys Res B* 236:391–398
95. El-Rehim HAA, Hegazy ESA, Hamed AA, Swilem AE (2013) Controlling the size and swellability of stimuli-responsive polyvinylpyrrolidone-poly(acrylic acid) nanogels synthesized by gamma radiation-induced template polymerization. *Eur Polym J* 49(3):601–612
96. Adamo G, Grimaldi N, Campora S, Sabatino MA, Dispenza C, Ghersi G (2014) Glutathione-sensitive nanogels for drug release. *Chem Eng Trans* 38:457–462
97. Dispenza C, Adamo G, Sabatino MA, Grimaldi N, Bulone D, Bondi ML, Rigogliuso S, Ghersi G (2014) Oligonucleotides-decorated-poly(*N*-vinyl pyrrolidone) nanogels for gene delivery. *J Appl Polym Sci* 131(2):239774–239780
98. El-Rehim HAA, Swilem AE, Klingner A, Hegazy ESA, Hamed AA (2013) Developing the potential ophthalmic applications of pilocarpine entrapped into polyvinylpyrrolidone-poly(acrylic acid) nanogel dispersions prepared by  $\gamma$  radiation 2013. *Biomacromolecules* 14(3):688–698
99. Lorenzo A, Picos-Corrales LA, Angel Licea-Claverie A, Arndt K-F (2014) *React Funct Polym* 75:31–40
100. Meléndez-Orti HI, Peralta RD, Bucio E, Zerrweck-Maldonado L (2014) Preparation of stimuli-responsive nanogels of poly [2-(dimethylamino) ethyl methacrylate] by heterophase and microemulsion polymerization using gamma radiation *Polym. Eng Sci* 54:1625–1631
101. Yusof H, Naurah MI, Liyana MAN (2014) Polyethylene glycol diacrylate microgels from irradiated micelles. *Adv Mater Res* 1024:316–319

# Chitosan-Based Matrices Prepared by Gamma Irradiation for Tissue Regeneration: Structural Properties vs. Preparation Method

Maria Helena Casimiro<sup>1</sup>  · Joana J. H. Lancastre<sup>1</sup> ·  
Alexandra P. Rodrigues<sup>1</sup> · Susana R. Gomes<sup>2</sup> ·  
Gabriela Rodrigues<sup>2</sup> · Luís M. Ferreira<sup>1</sup>

Received: 15 July 2016 / Accepted: 27 November 2016  
© Springer International Publishing Switzerland 2016

**Abstract** In the last decade, new generations of biopolymer-based materials have attracted attention, aiming its application as scaffolds for tissue engineering. These engineered three-dimensional scaffolds are designed to improve or replace damaged, missing, or otherwise compromised tissues or organs. Despite the number of promising methods that can be used to generate 3D cell-instructive matrices, the innovative nature of the present work relies on the application of ionizing radiation technology to form and modify surfaces and matrices with advantage over more conventional technologies (room temperature reaction, absence of harmful initiators or solvents, high penetration through the bulk materials, etc.), and the possibility of preparation and sterilization in one single step. The current chapter summarizes the work done by the authors in the gamma radiation processing of biocompatible and biodegradable chitosan-based matrices for skin regeneration. Particular attention is given to the correlation between the different preparation conditions and the final polymeric matrices' properties. We therefore expect to demonstrate that instructive matrices produced and improved by radiation technology bring to the field of skin regenerative medicine a supplemental advantage over more conservative techniques.

---

This article is part of the Topical Collection “Applications of Radiation Chemistry”; edited by Margherita Venturi, Mila D’Angelantonio.

✉ Maria Helena Casimiro  
[casimiro@ctn.tecnico.ulisboa.pt](mailto:casimiro@ctn.tecnico.ulisboa.pt)

✉ Luís M. Ferreira  
[ferreira@ctn.tecnico.ulisboa.pt](mailto:ferreira@ctn.tecnico.ulisboa.pt)

<sup>1</sup> Centro de Ciências e Tecnologias Nucleares (C2TN), Instituto Superior Técnico, Universidade de Lisboa, E.N. ao km 139.7, Bobadela, 2695-066 Loures, Portugal

<sup>2</sup> Departamento de Biologia Animal, Faculdade de Ciências, Centro de Ecologia, Evolução e Alterações Ambientais (cE3c), Universidade de Lisboa, Campo Grande, 1749-016 Lisbon, Portugal

**Keywords** Chitosan · Gamma irradiation · Porous scaffolds · Skin substitute · Tissue engineering

## 1 Introduction

Scaffolds are three-dimensional supports that are used as a template at the body site injury to help in guiding cell growth, regeneration, and secretion of their own extracellular matrix (ECM), thereby assisting the body in growing new, functional tissue. Scaffolds work in two ways; they either help direct cell growth or simply provide a shape for the final tissue. To be used as a scaffold in tissue engineering, a material must satisfy a number of requirements: it should not elicit severe inflammatory responses and it should degrade into non-toxic compounds within the time frame required for new tissue formation. Alongside the scaffolds should be suitable porosity for cell in-growth, a surface that balances hydrophilicity and hydrophobicity for cellular attachment, and mechanical properties that are compatible with those of the tissue as well as maintaining mechanical strength during most part of the tissue regenerating process.

Engineered scaffolds are thus designed to augment or completely replace damaged, missing, or otherwise compromised tissue or organs. These scaffolds may be permanently integrated into or bioresorbed by the body and must not only be capable of mimicking the structure and biological functions of ECM but should also provide a good environment for the cells so that they can easily attach, proliferate, and differentiate. The ECM defines the three-dimensional architecture of an organ and is engaged in a complex relationship with the cellular elements of the surrounding environment. Consequently, communication between the cell and ECM molecules influences various cellular processes, such as adhesion, proliferation, differentiation, migration, and apoptosis, as well as growth factor and cytokine modulation. Moreover, the timing of these events critically affects tissue formation and remodeling, processes that are crucial for the integration of a tissue-engineered scaffold into the surrounding environment [1]. In the case of skin, a double-layered organ whose deep-partial and full-thickness wounds pose serious threats to preserving its integrity and normal functions, it is well established that severe damaged skin requires a protective barrier for proper healing [1, 2]. Thus, the ideal skin scaffold should have high liquid absorbing capacity and be a biodegradable, biomimetic, and multilayered 3-D structure comprising dermal and epidermal equivalents. However, regardless of tissue type, a number of key considerations are important when designing or determining the suitability of a scaffold for use in tissue engineering; besides the biocompatibility, biodegradability, and mechanical properties already referred to, scaffold architecture and manufacturing technology are also determinant factors [2]. Considering this, it is not difficult to realize that the design of an ideal tissue-engineering scaffold is one of the most important challenges in regenerative medicine.

New generations of synthetic biomaterials are being developed at a rapid pace. Particularly biopolymer-based hydrogels [3], nano-scale-size fibers composed of natural and/or synthetic materials [4–6], and ceramics [7] have attracted



attention in the last decade aiming its application as scaffolds for tissue engineering. A number of methods can be used to generate instructive matrices to be employed in tissue engineering (casting [8], electrospinning [9, 10], plasma [11], etc.). However, despite the potential use of radiation technology to facilitate the development of tissue engineering, only a few studies have been reported in the preparation of instructive scaffolds and their sterilization using this technology [12–15]. The application of radiation technology for formation and functionalization of surfaces and matrices has remarkable advantages such as: room temperature reaction, absence of harmful initiators or solvents, and high penetration through the bulk materials. Additionally, radiation-synthesized scaffolds and surfaces might be simultaneously functionalized and sterilized.

Chemical formulations under study combine the use of natural and synthetic polymers in an attempt to take advantage of the biological activity of the natural materials and the hydrophilicity and mechanical strengthness of the synthetic ones. Natural materials, owing to their bioactive properties, display better interactions with the cells, and in that way enhance the cells' performance in biological systems. A good example is the frequent use of polysaccharides and proteins (like chitosan and collagen) due to their biocompatibility, biodegradability, and similarity to macromolecules recognized by the human body, which partly mimic the ECM of tissues. Inducing and stimulating the wound-healing process, these natural polymers are involved in the repair of damaged tissues and consequently in skin regeneration. Simultaneously, synthetic polymers are highly useful in the biomedical field since their properties (e.g., porosity, degradation time, and mechanical characteristics) can be tailored through gamma irradiation for specific applications. Some synthetic polymers like poly( $\epsilon$ -caprolactone), which is a biodegradable polyester in physiological conditions, poly(vinyl alcohol), a hydrophilic biocompatible polymer and others also exhibit wound-healing properties and enhance re-epithelialization [14–17]. Compounds with plasticizer, humectant, and/or crosslinking properties, with good human body tolerance (e.g., glycerol), have also being studied as additives to polymeric matrix formulations.

Thus, blends/copolymers with natural and synthetic materials are believed to be an effective way to develop a tissue-engineered material.

We have been working on the consolidation of the ionizing radiation techniques for the preparation of new materials for biomedical applications in C<sup>2</sup>TN/IST aiming to establish a strong synergy between materials and biomedical studies, consolidating thus in a unique research laboratory a real bridge between these two complementary areas. In this framework, authors have been carrying out a systematic study in order to simultaneously prepare/optimize and sterilize three-dimensional biocompatible and biodegradable skin scaffolds by  $\gamma$ -irradiation. The main components used in the present study were chitosan, poly(vinyl alcohol) and glycerol. A brief description of the materials used in the preparation of the scaffolds discussed in this chapter is outlined next.



## 1.1 Chitosan

Chitosan (Chit) is a linear polysaccharide composed of poly- $\beta$ (1-4)-D-glucosamine and poly- $\beta$ (1-4)-D-acetylglucosamine as shown in Fig. 1a. It is a cationic polysaccharide of natural origin that is obtained by alkaline deacetylation of chitin, the main exoskeleton component in crustaceans, and one of the most abundant natural polymers. Due to an unusual combination of properties such as non-toxicity, biocompatibility, biodegradability, bioactivity, acceleration of wound healing, fat-binding capacity, etc., chitosan and its chemically modified structures have been subject of many studies for use in biomedical and pharmaceutical applications [16–22]. Chitosan bears two types of reactive groups: the C-2 amino groups on deacetylated units and the hydroxyl groups on C-3 and C-6 carbons on acetylated or deacetylated units [23]. In an acidic medium or without a catalyst, the reaction takes place at the amino group [24]. Furthermore, chitosan, being a polysaccharide, is known as a degradative-type polymer when  $\gamma$ -irradiated [25, 26]. One of the strategies to overcome this is the introduction of a crosslink-type polymer to the reactional system (e.g., 2-hydroxyethyl methacrylate, HEMA), which may result in a new matrix prepared/functionalized by gamma irradiation that combines the useful properties of both polymers [27]. Additionally, in order to obtain a sponge-type porous structure, blends were irradiated in a dry state.

## 1.2 Poly(vinyl alcohol)

Poly(vinyl alcohol), PVA (vd. Fig. 1b) is a water-soluble, white (colorless), and odorless synthetic polymer. It has a crystalline nature associated with good

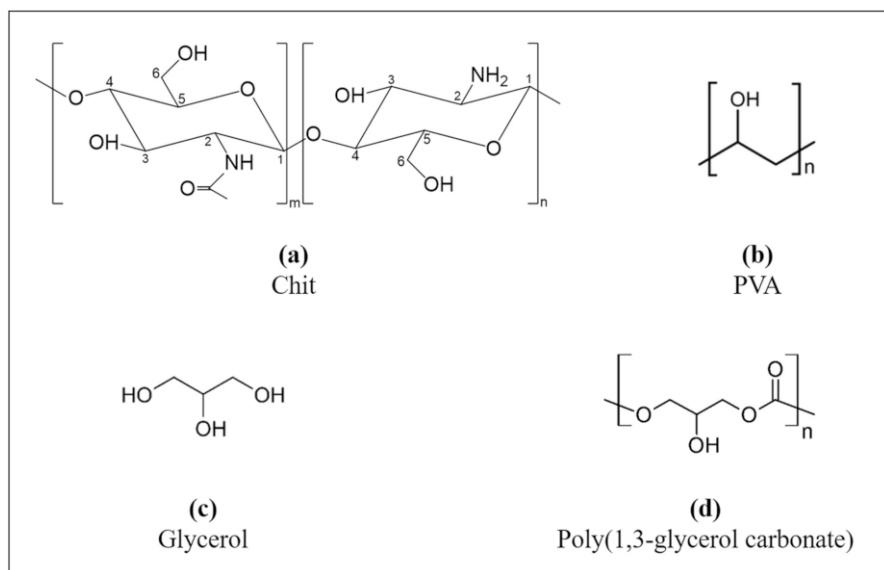


**Fig. 1** Chemical structures: **a** chitosan; **b** poly(vinyl alcohol); **c** glycerol; **d** poly(1,3-glycerol carbonate)

mechanical (high tensile strength and flexibility) and barrier properties, excellent film-forming, emulsifying, and adhesive properties as well as good thermal stability. It also shows good resistance to organic solvents. However, these properties are dependent on the hydration level, since water, acting as a plasticizer agent, reduces its tensile strength, accelerating its degradation [28]. Due to its biocompatibility, nontoxicity, and the ability to easily form physically cross-linked hydrogels, the use of PVA and PVA blends has been reported successfully in several biomedical and pharmaceutical applications and still continues to be a very promising material [29]. PVA has multiple pendant alcohol groups that can work as attachment sites for biological molecules and/or cells as well as its elasticity can induce cell orientation or matrix synthesis by enhancing the transmission of mechanical stimuli to seeded cells [30].

PVA is known to be a truly biodegradable synthetic polymer since the early 1930s [31]. However, its biodegradability very much depends on the degree of polymerization, degree of hydrolysis, distribution of hydroxyl groups, stereoregularity and crystallinity. As so, the degradation rate of PVA could be controlled through these parameters. For instance, the creation of crystalline regions in PVA through physical crosslinking improves its mechanical integrity and reduces the respective water absorption capacity [32], which consequently reduces the PVA degradation rate by hydrolytic mechanisms once in contact with body tissues [33]. This behavior can be used in PVA blends with natural fast degradative polymers (e.g., chitosan) to overcome the weak physical integrity of these. It is therefore obvious that the evaluation of the biodegradability of PVA should be made in function of its polymer structure framed in the application and intended performance. In our study, the crosslinking promoted on PVA during polymeric blend irradiation for scaffold preparation results in an added mechanical stability and consequently, in a decrease in its degradation rate. This effect is desired in order to compensate the higher degradation rate of chitosan. By this way, the skin scaffold will maintain for an extended period of time their barrier and cell growth matrix properties.

### 1.3 Glycerol

Glycerol (vd. Fig. 1c) is a water-soluble, non-toxic, colorless, viscous sweet-tasting polyol, commonly used in the pharmaceutical, personal care, and food industries. It presents a high hydrophilicity associated with a high humectant capacity. Regarding pharmaceutical applications it is being widely used in various products such as capsules syrups, topical creams, suppositories, eye-strain reducers, etc.

In recent years, increased attention has been given to glycerol-based polymers for biomedical applications due to the multiplicity of possible formulations/compositions and molecular architectures. The presence of multiple hydroxyl groups, which can either form new hydrogen bonds with the polymer chains and/or be synthetically converted into various other functional groups, allows to improve their potential biomedical applications. Special areas of interest, involving new market opportunities, includes carriers for drug-delivery systems, sealants or coatings for tissue repair, and anti-bacterial activity agents/barriers [34].

For a better understanding, Fig. 1 presents the chemical structures of the polymers used as well as the glycerol and an example of a glycerol-based polymer [poly(1,3-glycerol carbonate)].

This chapter presents and discusses the results obtained with matrices of composition chitosan/PVA prepared by gamma irradiation by two different methods and in vitro tested as potential skin scaffolds. Results regarding matrices with other compositions are still under validation.

## 2 Strategy

This study aims to clarify the correlation between the different preparation conditions and the final polymeric matrices properties given their intended use as scaffolds for skin tissue engineering. With this purpose, a detailed comparative study of the properties shown by the different samples' groups was performed and divided in three main tasks:

1. Optimization of the polymeric matrices preparation (methodology, composition, polymer concentration, range of absorbed dose).
2. Evaluation of structural and functional properties of the obtained matrices.
3. In vitro biocompatibility evaluation where the cellular viability and proliferation of Human Caucasian Foetal Foreskin Fibroblast cell line was analyzed as a measure of chitosan-based matrices biocompatibility and ability to assist skin regeneration.

## 3 Experimental

### 3.1 Materials

Chitosan, Chit (medium molecular weight 190–375 kDa, 75–85% deacetylated chitin), poly(vinyl alcohol), PVA (Mw 89,000–98,000, 99%+ hydrolyzed) and glycerol (puriss p.a. ACS reagent, anhydrous, dist.) were purchased from Sigma-Aldrich and used as raw materials. All other reagents were of analytical grade and used as received.

### 3.2 Preparation Methodologies

In this study, chitosan-based matrices were prepared by two methods using casting and  $\gamma$ -irradiation procedures. The chitosan solution (2% W/V) was prepared by dissolution of the appropriate amount of chitosan in acetic acid (1% V/V) with stirring at room temperature (RT) for 24 h. A PVA solution (10% W/V) was prepared by dissolution of PVA in bi-distilled water at 80 °C until the solution was clear. Both solutions were filtered and kept at room temperature for 24 h to remove air bubbles. To the chitosan matrix-specific volumes of the PVA solution were

added under continuous stirring to get a homogeneous mixture. Chit–PVA blends with different PVA content (1, 3, 5 or 8% W/V of the final solution) were obtained. The addition of glycerol was also tested as a humectant/plasticizer agent (0.25% V/V). Depending on composition, the matrices will be ahead referred to as C2/ $x$ PVA or C2/ $x$ PVA/0.25Gly, where  $x$  represents the PVA content (% W/V).

The main steps of the matrices' preparation methods are depicted in Fig. 2. The first approach, Method 1, included solvent evaporation at RT of the polymeric-blend solutions in polystyrene Petri dishes until film formation (casting). Afterwards, samples were neutralized with 0.5% sodium hydroxide and washed with distilled water, followed by freeze-drying and irradiation procedures. The second method, Method 2, involved the freeze-drying of the copolymeric solutions and subsequent irradiation. Furthermore, in order to improve porosity and thus create 3D polymeric matrices with adequate features to promote cellular growth, in Method 2, immediately after the homogenization step, an additional procedure was introduced where solutions were bubbled with nitrogen before the freeze-drying process (these procedures will be mentioned ahead as Freeze (F) and Bubble freeze (BF)

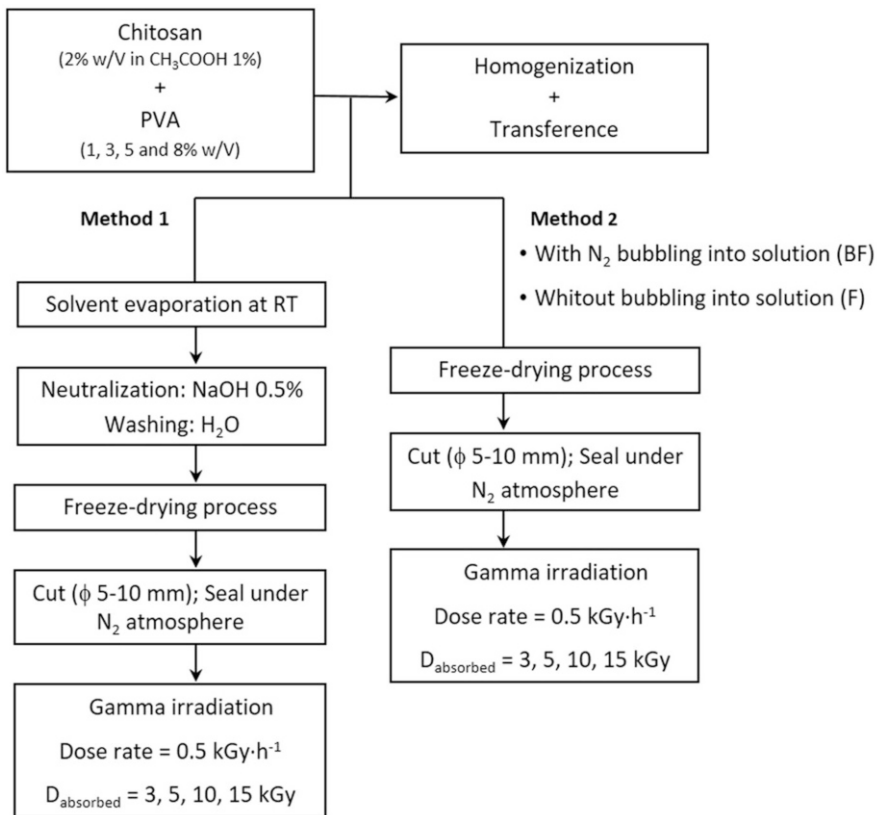


**Fig. 2** Schematic representation of the experimental procedure for the preparation of chitosan-based matrices

procedures). In both tested methods, the freeze-drying step comprised the membrane freeze at  $-80\text{ }^{\circ}\text{C}$  for 3 h and lyophilization for 48 h. Afterwards, small circular samples, from 5 to 10 mm in diameter, were cut with cutting hole punches, sealed under nitrogen, and irradiated. The  $\gamma$ -irradiation was performed in the experimental Co-60 chamber (Precisa 22) at the Ionizing Radiation Facility of Nuclear and Technological Campus of Instituto Superior Técnico (Lisbon University). A dose rate of  $0.5\text{ kGy h}^{-1}$  was used for the purpose to achieve final doses of 3, 5, 10 and 15 kGy.

In order to give confidence and reproducibility to the irradiation processes, the validation of irradiation geometries and respective dose distribution was previously accessed by Fricke dosimetry and ionizing chamber method. Amber Perspex dosimeters (Harwell) were used to monitor the samples' absorbed dose.

### 3.3 Evaluation of Structural Properties

In order to clarify the correlation between the different preparation conditions (including methodology, composition, and absorbed dose) and the final polymeric matrices properties, the samples obtained by the different experimental approaches were characterized in terms of their structural properties, thermal behavior, degradation, and in vitro cells assays.

#### 3.3.1 Structural Characterization

Structural characterization of the irradiated samples was carried out by means of attenuated total reflectance Fourier transform infrared (ATR-FTIR) using a micro-FTIR Thermo Scientific (Nicolet) i50 spectrometer equipped with an ATR slide-on diamond tip. The spectra were recorded in the  $400\text{--}4000\text{ cm}^{-1}$  region at room temperature and with a resolution of  $4\text{ cm}^{-1}$  (64 scans).

The microstructural characterization of previously Au-coated samples that were studied before and after degradation tests was performed by scanning electron microscopy (SEM) using a SEM instrument FEG-SEM JEOL 7001F.

#### 3.3.2 Thermal Analysis

Thermal behavior of the samples was assessed by thermo-gravimetric analysis (TGA) using a TA instrument TGA 951. The assays were carried out under a nitrogen atmosphere from 25 to  $500\text{ }^{\circ}\text{C}$ , using a  $10\text{ }^{\circ}\text{C min}^{-1}$  heating rate.

#### 3.3.3 Water Absorption Capacity

The water absorption capacity of the prepared samples was calculated through the following procedure: matrices' dried specimens ( $\phi$  8 mm) were weighted dried ( $W_{\text{dry}}$ ) and immersed in distilled water at  $37\text{ }^{\circ}\text{C}$ . After having reached equilibrium ( $\approx 1\text{ h}$ ), the swollen samples were carefully removed from the water, the excess wiped off with filter paper, and weighted ( $W_{\text{swollen}}$ ). The water absorption capacity of the samples was found through Eq. (1):

$$\text{Water absorption}(\%) = \frac{W_{\text{swollen}} - W_{\text{dry}}}{W_{\text{dry}}} \times 100. \quad (1)$$

All measurements were performed in triplicate and the result was expressed as mean value  $\pm$  standard deviation (SD).

### 3.3.4 *In Vitro Stability*

*In vitro* stability of the scaffolds was performed in phosphate-buffered solution (PBS 1X, pH 7.4) at 37 °C based on the extent of the matrices' mass loss. Samples were dried under vacuum, weighted ( $W_0$ ), and immersed in PBS solution. After 24 h of immersion, the matrices were taken out of the solution, wiped of excess fluid with filter paper, dried under vacuum, and weighted ( $W_{\text{deg}}$ ). Matrices' mass loss was calculated as the percentage of weight loss before and after PBS treatment according to Eq. (2):

$$\text{Mass loss}(\%) = \frac{W_0 - W_{\text{deg}}}{W_0} \times 100. \quad (2)$$

All measurements were performed in triplicate and the result was expressed as mean value  $\pm$  SD.

## 3.4 *In Vitro Cellular Viability*

The scaffolds used in this study were  $\gamma$ -irradiated in sealed bags at 3, 5, 10 and 15 kGy. According to previous sterilization results on similar chitosan/pHEMA matrices [22], it is possible to assure that the exposure to 4–5 kGy allows obtaining matrices microbiologically safe (i.e., the probability of obtaining a contaminated item will be much less than 1 in  $10^6$  items). Consequently, even if it is necessary to apply specific microbiological methodology to validate the sterilization procedure, one can say that preparation and sterilization procedures of the prepared samples occurred in one simultaneous step. Thus, no previous sterilization procedure was needed before cellular seeding.

### 3.4.1 *Cell Culture*

A Human Caucasian Foetal Foreskin Fibroblast cell line (HFFF2) was selected for the biological assays (*in vitro* study) in order to evaluate the effect of chitosan-based matrices on cell adhesion and viability. The HFFF2 commercial cell line was obtained from European Collection of Cell Cultures (ECACC, UK). The cells were cultured in Dulbecco's modified Eagle's medium (DMEM, Glutamax), supplemented with heat-inactivated fetal bovine serum (FBS) 10% (V/V) and streptomycin and penicillin 100 U/ml (all from Gibco), and incubated at 37 °C in a humidified atmosphere with 5% of CO<sub>2</sub>. The culture medium was changed every 2 days. After reaching 80% confluence, the cells were trypsinized and resuspended in culture medium at a concentration of  $2 \times 10^4$  cell/ml medium.

### 3.4.2 Cell Viability Assay (alamarBlue<sup>®</sup>)

Chitosan-based matrices ( $\phi$  10 mm) were placed in a 48-well tissue culture plate and pre-wetted with 200  $\mu$ l of culture medium to promote their expansion so that the matrices contact the walls of the well in the bottom of the chamber, avoiding floating. The fact that the matrices are soaked with culture medium enables the eventual migration of the cells inside its porous structure. After 10 min, the samples were seeded with 500  $\mu$ l of the HFFF2 suspension (20,000 cells) and cultured for 1, 4, and 7 days at 37 °C. Control samples were established by culturing cells directly over the polystyrene surface of the wells.

The cellular viability was monitored with the alamarBlue<sup>®</sup> cell viability assay (Life Technologies). At days 1, 4 and 7, the supernatant of each well was replaced by 300  $\mu$ l of fresh culture medium and 30  $\mu$ l of alamarBlue<sup>®</sup> reagent and incubated for 2 h at 37 °C in a 5% CO<sub>2</sub> atmosphere. After the incubation period, the media with alamarBlue<sup>®</sup> were transferred to a 96-well plate and the optical density (OD) was read in a microplate reader (Tecan Spectra) at 570 nm with a reference wavelength of 600 nm. The measurements were made in triplicate for each treatment and time point (1, 4 and 7 days). Data were expressed as mean  $\pm$  SD.

### 3.4.3 Cytochemistry

At 7 days of culture, the chitosan-based matrices and cytochemistry control samples (glass coverslips containing cells cultured in 24-well chambers) were fixed with paraformaldehyde, PFA 4% (in PBS), permeabilized in 0.2% TritonX-100 (Sigma-Aldrich), and stained with ToPro3 (1:500 in PBS) and Alexa488 conjugated Phalloidin (1:400 in PBS) (both from Molecular Probes), to observe cell's nuclei and actin cytoskeleton, respectively. The samples were mounted on fresh PBS on a glass slide and imaged on a Leica SPE confocal system using either a 10  $\times$  0.3 NA or a 20  $\times$  0.7 NA lens. Confocal images were acquired in 2–5 different fields chosen randomly at the center of scaffolds.

## 4 Results and Discussion

### 4.1 Method 1 (Casting/Freeze-Dry/Irradiation)

#### 4.1.1 Thermal Analysis

The thermal behavior of  $\gamma$ -irradiated and non-irradiated chitosan-based matrices with and without PVA (prepared by Method 1) at a constant heating rate of 10 °C min<sup>-1</sup> is displayed in Fig. 3. A noticeable change is observed in the relative degradation pattern of chitosan matrices when those are  $\gamma$ -irradiated at 5 kGy. The weight loss at 25–100 °C is generally attributed to the loss of bind/adsorbed water, however, in  $\gamma$ -irradiated chitosan matrices it cannot be assigned only to that. The chitosan degradation can also be responsible for this first step. When chitosan is exposed to ionizing radiation, it preferably undergoes chain scission by cleavage of

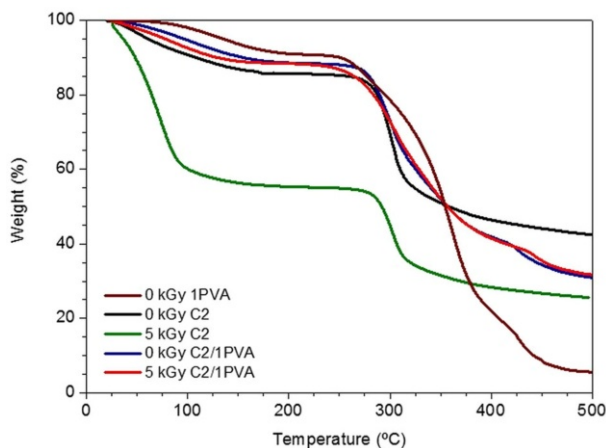


**Fig. 3** Thermogravimetric curves of non-irradiated (0 kGy) and  $\gamma$ -irradiated at 5 kGy chitosan (C2) and chitosan-based C2/1PVA matrices

$\beta$ -glucosidic linkages [35]. Moreover, as this process may include the dehydration of the saccharide ring [36], it would explain the sharpest decrease in the weight observed for the  $\gamma$ -irradiated chitosan matrices. The second weight loss, with an onset temperature near 255 °C for both irradiated and non-irradiated chitosan matrices, can be due to an exhaustive degradation of the saccharide structure of the molecule, including decomposition of deacetylated (and acetylated) units of chitosan. In the case of Chit/PVA matrices, Fig. 3 shows that the introduction of PVA promoted changes in the mentioned weight-loss trend of chitosan matrices. It is clear that  $\gamma$ -irradiated Chit/PVA matrices are more thermally stable than the chitosan-irradiated ones. This higher stability may be assigned to a Chit/PVA denser and crosslinked structure, meaning that PVA confers a stabilizing effect in the structure of irradiated chitosan matrices.

#### 4.1.2 ATR-FTIR Characterization

ATR-FTIR spectroscopy was used to assess the polymer chemical groups and investigate the formation of crosslinked networks in chitosan-based matrices upon irradiation. Results suggest that chitosan and PVA are bonded together in the obtained matrices and that peak intensity evolution is in accordance with the expected changes promoted in the structure due to  $\gamma$ -irradiation. Figure 4 shows the FTIR spectra of  $\gamma$ -irradiated and non-irradiated chitosan-based matrices with and without PVA. It can be observed that depending on composition, spectra exhibit the major peaks related to the typical chitosan and PVA patterns. The broad peak around 3350  $\text{cm}^{-1}$  is assigned to N–H and O–H stretching from the intermolecular and intramolecular hydrogen bonds. The characteristic absorption peaks appear at about 1648 (amide I band), 1570 (amide II, N–H deformation mode), and 1322  $\text{cm}^{-1}$  (amide III band). The absorption peaks at 1151 (anti-symmetric stretching of the C–O–C bridge), 1058 and 1028  $\text{cm}^{-1}$  (skeletal vibrations involving



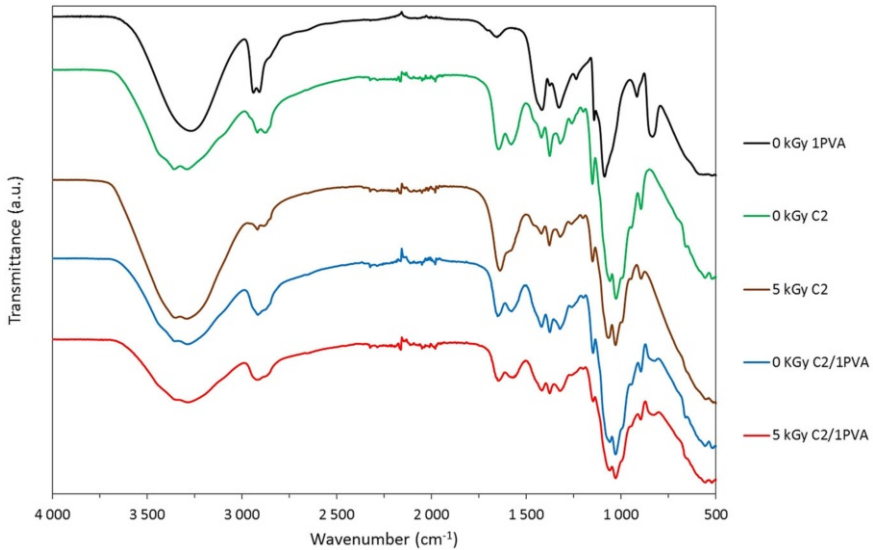


**Fig. 4** FTIR spectra of non-irradiated (0 kGy) and  $\gamma$ -irradiated at 5 kGy chitosan (C2) and chitosan-based C2/1PVA matrices

the C–O stretching) are characteristics of saccharide structure of chitosan. The small absorption peak at  $895\text{ cm}^{-1}$  can be used to identify the presence of the C–O–C bridge as well as  $\beta$ -glucosidic linkages between the sugar units in chitosan [37]. Concerning  $\gamma$ -irradiated chitosan matrices, it should be noted that they exhibit much similarity in the IR peaks as those of non-irradiated ones. However, a peaks' intensity decrease at  $895$  and  $1151\text{ cm}^{-1}$ , which correspond to the saccharide structure, suggests some degradation by cleavage of  $\beta$ -glucosidic linkages due to  $\gamma$ -radiation exposure, which is in accordance with results obtained by TGA analysis. An intensity reduction at amine region ( $1570\text{ cm}^{-1}$ ) also supports the chitosan's degradation occurrence. Regarding the spectra of Chit/PVA matrices, all major absorption peaks related to PVA are also presented, for instance, the slightly board peak at  $2880\text{ cm}^{-1}$  refers to the C–H stretching from alkyl groups and  $1415\text{ cm}^{-1}$  to the –C–O group. Moreover, the increase in the intensity peaks at  $1415$  and  $1570\text{ cm}^{-1}$  at the FTIR Chit/PVA matrices suggests chemical crosslinking between chitosan and PVA molecules. Additionally, the boarder band at  $3350\text{ cm}^{-1}$ , when compared with the other spectra, also seems to corroborate this.

#### 4.1.3 Water Absorption Capacity

Due to the secretion of body fluid during skin wound healing, in the process of constructing skin engineered scaffolds it is necessary to evaluate its water absorption capacity.

According to thermogravimetric and ATR-FTIR results, the introduction of PVA into chitosan-based matrices' confers an additional structural stability to those matrices. Moreover, as  $\gamma$ -irradiation seems to promote some level of crosslinking

between chitosan and PVA chains and/or intermolecular bonds, it is expected that matrices' structures become more closed and stable. Water absorption capability results seem to confirm this since the percentage of absorbed water of Chit/PVA  $\gamma$ -irradiated matrices decreases when compared to the non-irradiated ones. Figure 5 displays the water absorption capacity of non-irradiated and  $\gamma$ -irradiated at 5 kGy Chit 2%/PVA 1% (W/V) matrix (referred as C2/IPVA). The images of the dry (150  $\mu\text{m}$  thickness) and swollen irradiated matrices can also be observed.

#### 4.1.4 Morphological Analysis

The morphology of chitosan-based matrices was studied through SEM. Despite showing some structural network and good surface homogeneity, the matrices prepared by Method 1 do not evidence porosity as depicted in Fig. 6 where representative matrices' images are shown.

Considering the required porous characteristics for the intended skin scaffolds application, it is clear that the chitosan-based matrices prepared by Method 1 (casting of the solutions followed by freeze-drying and irradiation) do not possess the three-dimensional interconnected porous architecture where cells could easily attach and proliferate. Consequently, aiming the improvement of cell adhesion and growth properties onto those matrices no further characterization was performed on them. Instead, a different preparation methodology was tested (Method 2).

## 4.2 Method 2 (Freeze-Dry/Irradiation)

### 4.2.1 Thermal Analysis

The thermal behavior of the  $\gamma$ -irradiated chitosan-based matrices obtained through Method 2, i.e., obtained through irradiation of freeze-dried polymeric blend solutions, was similar to the one observed for matrices prepared by Method 1 and

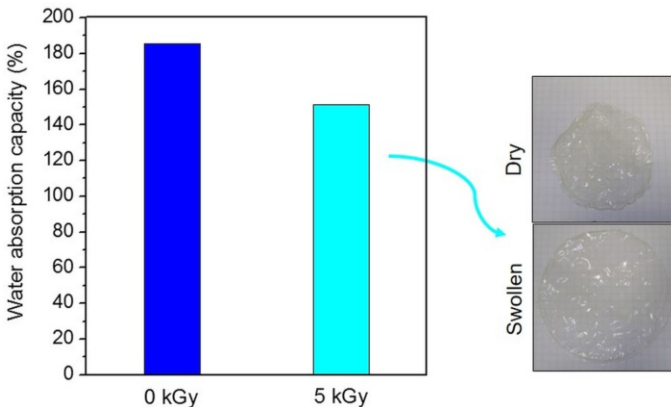


**Fig. 5** Water absorption capacity (37 °C) of non-irradiated and  $\gamma$ -irradiated at 5 kGy C2/IPVA matrices; images of dry and swollen C2/IPVA irradiated matrix

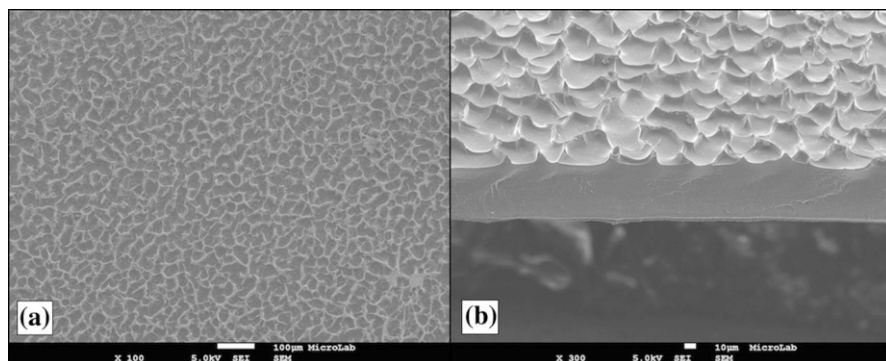


**Fig. 6** SEM micrographs of C2/1PVA matrix  $\gamma$ -irradiated at 5 kGy: **a** surface (scale bar 100  $\mu$ m); **b** surface and cross-section (scale bar 10  $\mu$ m)

already reported. **Figure 7a**, where the thermal profile of non-irradiated and 5 kGy-irradiated C2/1PVA matrices are shown, reinforces the argument that introduction of PVA in matrices' composition can provide a shield to the chitosan backbone against radiation-induced degradation. This kind of behavior has already been reported in the literature [38]. It is also observed that the irradiation of matrices with different content in PVA promotes the same effect (**Fig. 7b**): the introduction of increasing amounts of PVA promotes lower initial weight losses. Thus, we may conclude that PVA confers a stabilizing effect in the matrices' molecular structure.

Comparing the dose effect on structural properties of the matrix it is possible to understand the changes in the structure (vd. **Fig. 8**). Up to an irradiation dose of 5 kGy the structure stability of the matrices slightly decreases while for higher irradiation doses it is possible to observe some recovery of the structural stability of the materials.

In fact, comparing the TGA curves of samples prepared through Method 1 and Method 2 with and without  $N_2$  bubbling (vd. **Fig. 9**), although showing a similar thermal profile, Method 2 (freeze-drying of the solutions) leads to matrices with lower structural stability. This is understandable since the referred methodology introduces more porosity in the final matrices.

#### 4.2.2 ATR-FTIR Characterization

The ATR-FTIR spectra of samples C2/3PVA and C2/3PVA0.25Gly irradiated at a total dose of 10 kGy depicted in **Fig. 10** show the typical peaks related to chitosan, PVA, and glycerol previously mentioned. To a better understanding that information is also summarized in the figure. A better peak definition and higher intensity can be observed in the spectrum of the matrix obtained through the freeze procedure, suggesting a more organized and stable structure when compared with the one of bubble-freeze procedure. This is in accordance with TGA data.

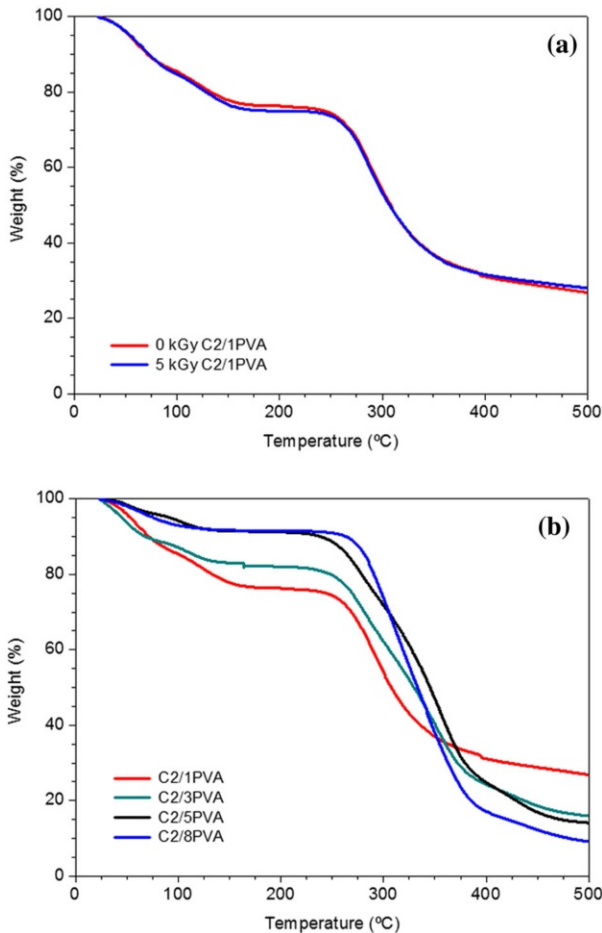


**Fig. 7** Thermogravimetric curves of Chit/PVA matrices  $N_2$  bubbled: **a** non-irradiated and  $\gamma$ -irradiated at 5 kGy C2/1PVA; **b** effect of PVA concentration on matrices  $\gamma$ -irradiated at 5 kGy

#### 4.2.3 Water Absorption Capacity

It is well known that the water absorption and swelling capacity is one of the important issues in skin scaffold development. In fact, when the scaffolds are capable of swelling, they allow their pore size to increase, which facilitates the cells to attach and penetrate inside the inter-polymeric network. Figure 11 shows the increase of surface area and volume of bubble freeze (BF) prepared matrices from dry to swollen state. In the present study, similarly to what occurs in Method 1, results suggest that the higher the PVA content or the higher the radiation dose is (within the studied concentration and radiation dose ranges), more crosslinking between chitosan and PVA chains and/or intermolecular bonds are introduced in matrices. This confers a stabilizing effect in the structure, which became more compact and with smaller pores (the pore structures of the matrices were further

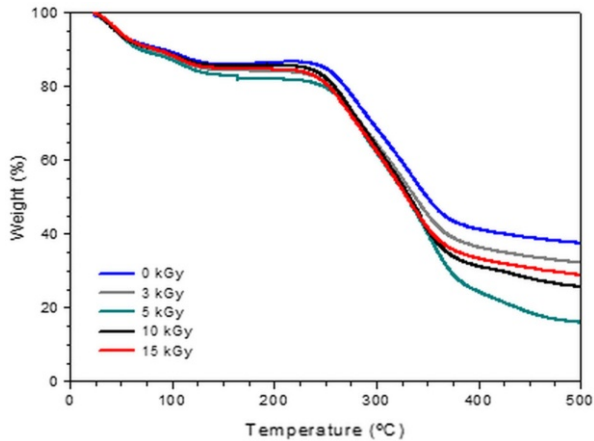


**Fig. 8** Thermogravimetric curves: effect of radiation dose on C2/3PVA matrices (prepared by bubbling N<sub>2</sub> into the solution)

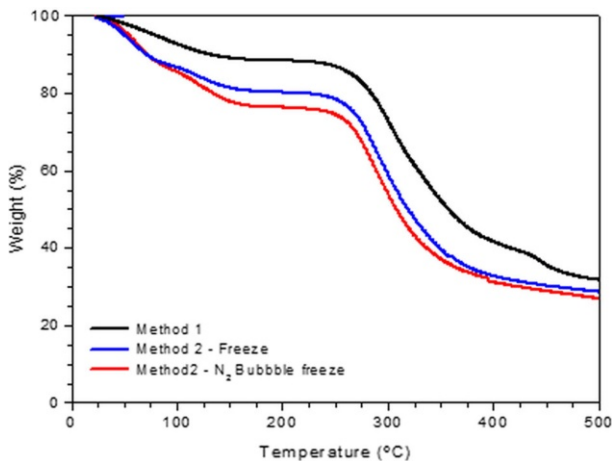


**Fig. 9** Thermogravimetric curves of C2/1PVA  $\gamma$ -irradiated at 5 kGy. Matrices prepared by the different methods in study

confirmed by SEM). Thus, the swelling capability of these bubble freeze matrices decreases. However, for PVA contents of 8%, the increase in hydrophilic functional groups (that overcome probably from the content increase of  $-OH$  groups due to PVA linkage to chitosan C-2 amino groups) overrides the dose effect and a slight increase in the swelling capability of these matrices is observed (vd. Fig. 12). In terms of the purposed biomedical application, considering the results of water absorption capacity, chitosan-based matrices with 5% of PVA was considered to be the most promising prepared samples to be used as skin scaffold.

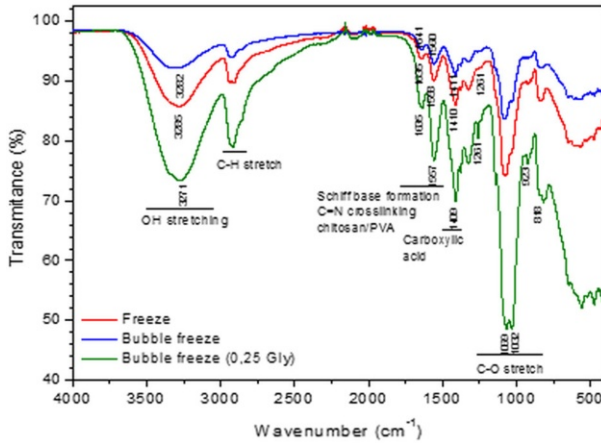


**Fig. 10** ATR-FTIR spectra of C2/3PVA and C2/3PVA0.25Gly matrices irradiated at a total dose of 10 kGy

Matrice	Dry	Swollen	Matrice	Dry	Swollen
C2/3PVA 5 kGy w/ Glycerol (0.25%)			-----	-----	-----
C2/5PVA 10 kGy			C2/8PVA 10 kGy		
C2/5PVA 15 kGy			C2/8PVA 15 kGy		

**Fig. 11** BF chitosan-based matrices  $\gamma$ -irradiated at different radiation doses in a dry and swollen state

#### 4.2.4 In Vitro Stability

The stability of a skin scaffold assumes an important role in the entire wound-healing process. Generally, it should have a steerable degradability and degradation rate to match the tissue regeneration. In the particular case of the obtained Chit/PVA matrices, preliminary studies of its in vitro stability were performed in phosphate-buffered solution (PBS 1X, pH 7.4) at 37 °C for 24 h. Overall results show that the higher the radiation dose, the lower the matrices' mass loss is, since more crosslinks

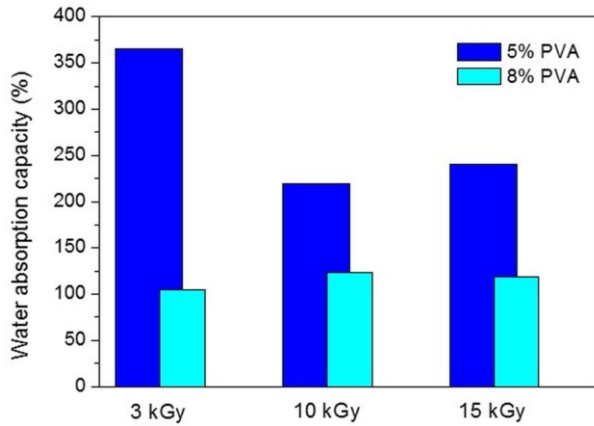


**Fig. 12** Water absorption capacity of bubble freeze C2/5PVA and C2/8PVA matrices  $\gamma$ -irradiated at 3, 10 and 15 kGy

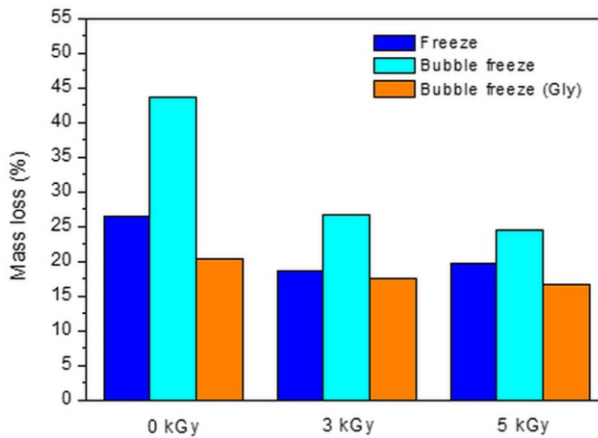


**Fig. 13** Mass loss (%) after 1 day of immersion in PBS solution at 37 °C of matrices C2/8PVA non-irradiated and  $\gamma$ -irradiated at 3 and 5 kGy

are introduced, conferring more stability to the structure of the material. Comparing both procedures (vd. Fig. 13), freeze (without bubbling  $N_2$ ) and bubble freeze (with bubbling  $N_2$ ), the latter one shows higher mass loss. This is observed in all PVA contents and doses studied and is understandable since in the bubble-freeze procedure, porosity was introduced in the matrices “weakening” its structure and helping to washing out eventually free polymer chains. When glycerol is introduced in these matrices, the presence of multiple hydroxyl groups and the manifoldness of its new bonds allows to keep the stability of the polymeric network, fulfilling its function as plasticizer agent in the blend.



#### 4.2.5 Morphological Analysis

The morphology of the “bubble freeze samples” was evaluated with SEM. [Figure 14](#) shows representative SEM micrographs of matrices’ surface morphology of chitosan-based matrices with different PVA content (without glycerol). It can be observed that matrices show a good surface homogeneity and an increase in PVA percentage leads to a decrease in porosity matrices’ surface. Once again, results suggest that a higher PVA content in Chit/PVA blends leads to a more crosslinked structure possibly due to more Chit-PVA bonds and OH intramolecular interactions as already mentioned. Even so, a comparison between [Figs. 6](#) and [14](#) (SEM micrographs of C2/1PVA 5 kGy matrix prepared by Method 1) evidences the three-dimensional porous structure that Method 2 can promote in this type of polymeric matrix. For the same sample composition, it can be seen that the morphology of matrices’ surface is also dependent on the radiation dose (vd. [Fig. 15](#)). Thus, radiation dose can be used too to tailor the morphology of the matrices. In the first irradiation stage, there seems to exist a widespread presence of crosslinking reactions that lead to a smoother surface due the increasing network density. However, for higher irradiation doses, some degradation of the terminal chains of PVA and chitosan ones can occur, promoting “surface erosion” exposing and

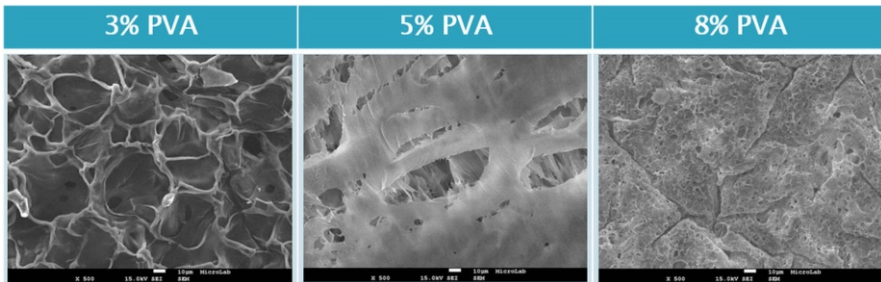


**Fig. 14** SEM micrographs of the surface of bubble freeze Chit/PVA matrices irradiated at 3 kGy (*scale bar 10 μm*)

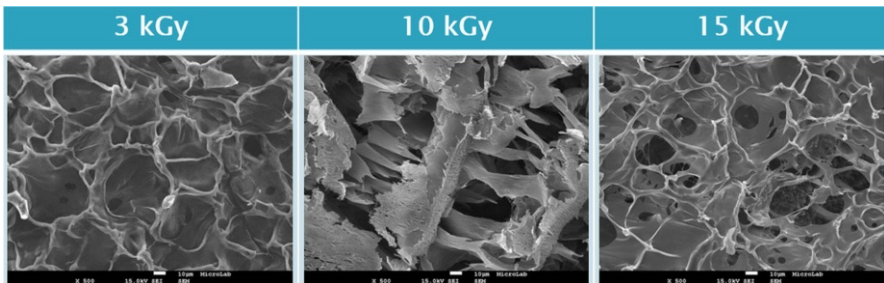


**Fig. 15** SEM micrographs of the surface of bubble freeze C2/3PVA matrices when irradiated at different doses (*scale bar 10 μm*)



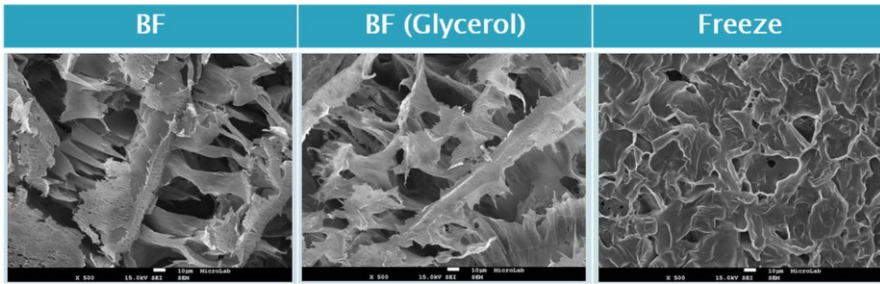


**Fig. 16** SEM micrographs of C2/3PVA 10 kGy matrices' surface using different procedures: with N<sub>2</sub> bubbling (bubble freeze) and without (freeze) (scale bar 10 μm)

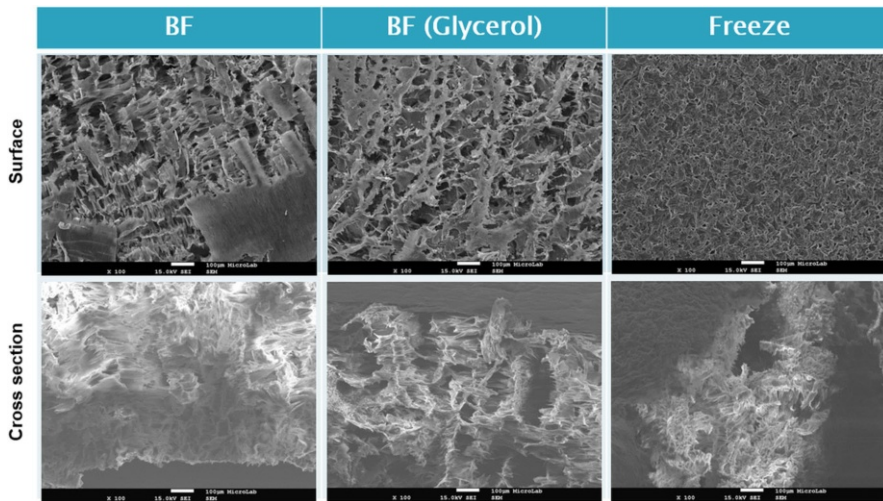


**Fig. 17** Surface and cross-section SEM micrographs of C2/3PVA 10 kGy (scale bar 100 μm)

accentuating a rougher surface [38]. Together, these results stress out the importance of this preparation method to achieve in trimming surface properties.

Figure 16 shows the SEM micrographs of the C2/3PVA matrices irradiated at 10 kGy and prepared using the different procedures of Method 2: with N<sub>2</sub> bubbling (bubble freeze) and without (freeze). It can be observed that there is no significant difference on the surface morphology in the matrices prepared with and without glycerol. On the other hand, the micrographs also reveal that bubbling of N<sub>2</sub> leads to more open structures, showing to be a good procedure to introduce more porosity in the matrices.

Additionally, as seen in Fig. 17, despite having some differences in the surface morphology, all the matrices present a sponge-type “inner structure”.

#### 4.2.6 In Vitro Cellular Viability

The cellular viability of the HFFF2 fibroblasts was assessed on Chit/PVA matrices as a means to evaluate their ability to promote cell adhesion and proliferation. Tested matrices were chosen according to the best structural results previously obtained. Preliminary cell viability results on Chit/3PVA matrices (bubble freeze, BF, freeze, F, and with glycerol, Gly) irradiated at different radiation doses (Fig. 18) show that HFFF2 cells adhere well to the matrices surface but proliferate slower than control (control = HFFF2 cell cultured under the same condition but without matrices).

Results point out that only matrices  $\gamma$ -irradiated at 10 kGy display cellular growth on day 1. This is in accordance with SEM analysis, which has revealed that chitosan-based matrices  $\gamma$ -irradiated at 3 and 15 kGy lead to matrices with small surface pores hindering cells to attach. However, despite showing a good porosity, the matrix with glycerol (irradiated at 10 kGy) does not show cell growth after the first day. It appears that cells were able to attach but unable to follow this attachment with spreading. This might be due to changes in ionic equilibrium (pH) introduced by glycerol that would be intolerable to cell viability. On the other hand, still within this group of matrices  $\gamma$ -irradiated at 10 kGy, results at day 4 revealed that only matrices N<sub>2</sub> bubbled presented an increase in cell proliferation.

Given the obtained results, only matrices with 3 and 5% of PVA prepared by bubble freeze and freeze procedure were further evaluated in terms of cell viability. To comprise all the information concerning irradiation dose ( $x$ ), PVA content ( $y$ ), and preparation procedure [bubble freeze (BF) and freeze (F)], matrices in the figures of this section are referred to as “ $x$ kGy  $y$  BF” or “ $x$ kGy  $y$  F”. The results of matrices irradiated at 5 and 10 kGy (Fig. 19) confirm the HFFF2 cell viability, i.e., cells adhesion and proliferation capability into the substrates in study. Once again, cells adhered to all matrices, which is indicative of the non-cytotoxic nature of the prepared matrices. However, cells proliferated slower than in controls with the “freeze procedure” matrices presenting a very low proliferation with the matrix C2/

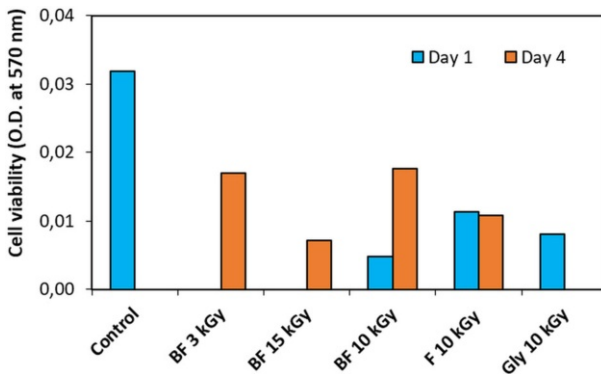


**Fig. 18** Cells growing on C2/3PVP and C2/3PVP0.25Gly matrices in culture days 1 and 4. Matrices prepared by bubble freeze (BF) and freeze (F) procedures, and  $\gamma$ -radiation doses of 3, 10 and 15 kGy

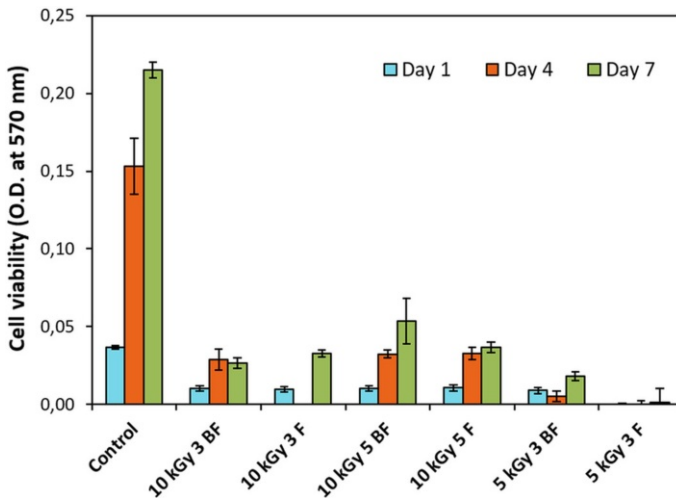


**Fig. 19** Cells growing on different Chit/PVA matrices (10 and 5 kGy irradiated; 3 and 5% PVA; bubble freeze (BF) and freeze (F) preparation procedure) in culture days 1, 4 and 7 ( $n = 3$ ; mean value  $\pm$  SD)

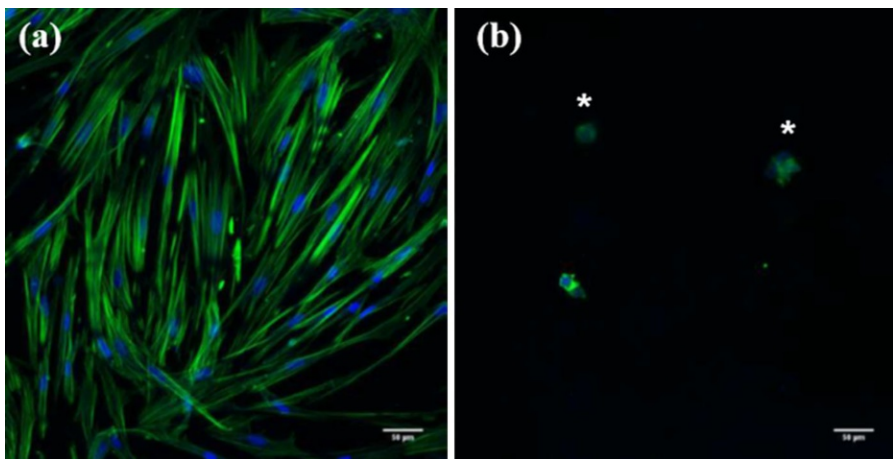


**Fig. 20** HFFF2 cells growing in culture for 7 days on: **a** control cells; **b** 10 kGy 5 BF matrices (out of focus cells asterisk; green actin; blue DNA; scale bar 50  $\mu$ m)

5PVA N<sub>2</sub> “bubble freeze” presenting the best results. Moreover, the cytochemical stainings performed showed that cell morphology at day 7 is different to glass coverslip-seeded fibroblasts (Fig. 20).

Confocal images of control samples at day 7 of culture showed HFFF2 cells with the expected morphology, a fusiform shape. In confocal images of the Chit2/5PVA BF 10 kGy  $\gamma$ -irradiated matrix (10 kGy 5 BF as referred on Fig. 19), we can only observe a few cells with round morphology and poor actin cytoskeletal organization as compared to control cells. This result may indicate that cells are not attaching to the substrate and growing in the best conditions but, even so, some cells were able

to invade the depth of the matrix, as can be seen by the out-of-focus cells in Fig. 20. This is consistent with the viability assay, which showed reduced cell number. Huang et al. [39] observed similar results having suggested that inhibition of cell proliferation on chitosan scaffolds is due to the loss of cell–matrix binding. This would prevent cells from recognizing and anchoring to new binding sites, and thus cells would lose some cytoskeleton integrity. Furthermore, the incorporation of proteins or peptides in the matrix that would allow the presence of multiple cell-binding ligands or the surface modification of matrix by plasma treatment that would change the electrostatic interactions may be tested in the future in order to improve cell affinity for the matrices and to achieve better morphology and behavior of the fibroblasts growing on these scaffolds.

## 5 Conclusions

Chitosan-based matrices for tissue regeneration were successfully prepared by gamma irradiation. Two preparation methods were tested in order to optimize the methodology. The first one involved the casting of copolymeric solutions and solvent evaporation at room temperature followed by freeze-drying and irradiation. The second approach involved the freeze-drying of copolymeric solutions followed by irradiation.

The matrices were evaluated in terms of methodology, composition, absorbed dose, structural and functional properties, and in vitro biocompatibility (cellular viability, morphology and cytochemistry). It was found that  $\gamma$ -irradiation and PVA content can be used to tailor the matrices' surface in terms of porosity/roughness with simultaneous sterilization. The bubbling of  $N_2$  before freeze-dry showed to be a good procedure for introducing more porosity in the matrices although it led to higher matrices' mass loss. The swelling capability of non-irradiated matrices increases with the number of hydrophilic groups, i.e., with the PVA content. Moreover, the swelling properties are also dependent on the density of network structure.

Concerning the evaluation of cell viability, it was shown that HFFF2 cells adhered to the surface of all matrices obtained by solutions freeze-drying method, but do not reveal favorable cellular growth if glycerol is present in the composition.

Bubbling the polymer solution during the homogenization step followed by freeze-drying and a  $\gamma$ -irradiation dose up to 10 kGy seems to be the most promising procedure. Further modifications to introduce multiple cell-binding ligands in the matrices should be applied in order to improve cell affinity for the matrices and to achieve a better morphology and behavior of the fibroblasts growing on these scaffolds. Nevertheless, the study herein described evidence the versatility of radiation technology to tailor polymeric materials for specific applications such as skin regenerative medicine.

**Acknowledgements** C<sup>2</sup>TN/IST authors gratefully acknowledge the Fundação para a Ciência e Tecnologia support through the UID/Multi/04349/2013 project. The authors also acknowledge the International Atomic Energy Agency under the Research Contract No. 18202 for financial support of this


work. The authors would also like to thank the Erasmus student Reda Paitian (University of Vilnius, Lithuania) for her collaboration in the preparation and characterization of chitosan-based matrices.

## References

1. Ayres CE, Jha BS, Sell SA, Bowlin GL, Simpson DG (2010) Nanotechnology in the design of soft tissue scaffolds: innovations in structure and function—advanced review. *WIREs Nanomed Nanobiotechnol* 2:20–34
2. O'Brien CE (2011) Biomaterials & scaffolds for tissue engineering. *Mater Today* 14:88–95
3. Van Vlierberghe S, Dubruel P, Schacht E (2011) Biopolymer-based hydrogels as scaffolds for tissue engineering applications: a review. *Biomacromolecules* 12:1387–1408
4. Hasirci V, Vrana E, Zorlutuna P, Ndreu A, Yilgor P, Basmanav FB, Aydin E (2006) Nanobiomaterials: a review of the existing science and technology, and new approaches. *J Biomater Sci Polym Ed* 17:1241–1268
5. Shalumona KT, Anulekhaa KH, Chennazhia KP, Tamurab H, Naira SV, Jayakumar R (2011) Fabrication of chitosan/poly(caprolactone) nanofibrous scaffold for bone and skin tissue engineering. *Int J Biol Macromol* 48:571–576
6. Gomes SR, Rodrigues G, Martins GG, Henriques CMR, Silva JC (2013) In vitro evaluation of crosslinked electrospun fish gelatin scaffolds. *Mater Sci Eng C* 33:1219–1227
7. Dorozhkin SV (2010) Bioceramics of calcium orthophosphates. *Biomaterials* 31:1465–1485
8. Liao S, Wang W, Uo M, Ohkawa S, Akasaka T, Tamura K, Cui F, Watari F (2005) A tree-layered nano-carbonated hydroxyapatite/collagen/PLGA composite membrane for guided tissue regeneration. *Biomaterials* 26:7564–7571
9. Frohbergh ME, Katsman A, Botta GP, Lazarovici P, Schauer CL, Wegst UGK, Lelkes PI (2012) Electrospun hydroxyapatite-containing chitosan nanofibers crosslinked with genipin for bone tissue engineering. *Biomaterials* 33:9167–9178
10. Martins A, Reis R, Neves N (2008) Electrospinning: processing technique for tissue engineering scaffolding. *Int Mater Rev* 53:257–274
11. Safinia L, Datan N, Hohse M, Mantalaris A, Bismarck A (2005) Towards a methodology for the effective surface modification of porous polymer scaffolds. *Biomaterials* 26:7537–7547
12. Rodas ACD, Ohnuki T, Mathor MB, Lugao AB (2005) Irradiated PVAI membrane swelled with chitosan solution as dermal equivalent. *Nucl Instrum Methods B* 236:536–539
13. Plikk P, Odelius K, Hakkarainen M, Albertsson AC (2006) Finalizing the properties of porous scaffolds of aliphatic polyesters through radiation sterilization. *Biomaterials* 27:5335–5347
14. Odelius K, Plikk P, Albertsson AC (2008) The influence of composition of porous copolyester scaffolds on reactions induced by irradiation sterilization. *Biomaterials* 29:129–140
15. Cottam E, Hukins DWL, Lee K, Hewitt C, Jenkins MJ (2009) Effect of sterilisation by gamma irradiation on the ability of polycaprolactone (PCL) to act as a scaffold material. *Med Eng Phys* 31:221–226
16. Luyen DV, Huang DM (1996) In: Salamone JC (ed) *Polymeric Materials Encyclopedia*, vol 2. CRC Press, New York
17. Risbud MV, Hardikar AA, Bhat SV, Bhonde RR (2000) pH-sensitive freeze-dried chitosan-polyvinyl pyrrolidone hydrogels as controlled release system for antibiotic delivery. *J Control Release* 68:23–30
18. Ishihara M, Nakanishi K, Ono K, Sato M, Kikuchi M, Saito Y, Yura H, Matsui T, Hattori H, Uenoyama M, Kurita A (2002) Photocrosslinkable chitosan as a dressing for wound occlusion and accelerator in healing process. *Biomaterials* 23:833–840
19. Jayakumar R, Prabaharan M, Reis RL, Mano JF (2005) Graft copolymerized chitosan-present status and applications. *Carbohydr Polym* 62:142–158
20. Casimiro MH, Leal JP, Gil MH (2005) Characterisation of gamma irradiated chitosan/pHEMA membranes for biomedical purposes. *Nucl Instrum Methods B* 236:482–487
21. Shi C, Zhu Y, Ran X, Wang M, Su Y, Cheng T (2006) Therapeutic potential of chitosan and its derivatives in regenerative medicine. *J Surg Res* 133:185–192
22. Casimiro MH, Gil MH, Leal JP (2010) Suitability of gamma irradiated chitosan based membranes as matrix in drug release system. *Int J Pharm* 395:142–146

23. Alves NM, Mano JF (2008) Chitosan derivatives obtained by chemical modifications for biomedical and environmental applications. *Int J Biol Macromol* 43:401–414
24. Luyen DV, Huong DM (1996) In: Salamone JC (ed) *Polymeric materials encyclopedia chitin and derivatives*. CRC, New York
25. Ulański P, Rosiak J (1992) Preliminary studies on radiation-induced changes in chitosan. *Radiat Phys Chem* 39:53–57
26. Lim LY, Khor E, Koo O (1998) Gamma irradiation of chitosan. *J Biomed Mater Res* 43:282–290
27. Casimiro MH, Leal JP, Gil MH (2005) Characterisation of gamma-irradiated chitosan/pHEMA membranes for biomedical purposes. *Nucl Instrum Methods B* 236:482–487
28. Wiley Billmeyer FW (1984) *Textbook of polymer science*, 3rd edn. Wiley, New York
29. Hassan CM, Peppas NA (2000) In: Dusek K (ed) *Structure and applications of poly(vinyl alcohol)*, vol 153. Springer, Berlin
30. Schmedlen RH, Masters KS, West JL (2002) Photocrosslinkable polyvinyl alcohol hydrogels that can be modified with cell adhesion peptides for use in tissue engineering. *Biomaterials* 23(22):4325–4332
31. Solaro R, Corti A, Chiellini E (2000) Biodegradation of poly(vinyl alcohol) with different molecular weights and degree of hydrolysis. *Polym Adv Technol* 11:873–878
32. Bolto B, Tran T, Hoang M, Xie Z (2009) Crosslinked poly(vinyl alcohol) membranes. *Prog Polym Sci* 34:969–981
33. Tamariz E, Rios-Ramírez A (2013) Biodegradation of medical purpose polymeric materials and their impact on biocompatibility. *INTECH*. doi:10.5772/56220
34. Zhang H, Grinstaff MW (2014) Recent advances in glycerol polymers: chemistry and biomedical applications. *Macromol Rapid Commun* 35:1906–1924
35. Lim L-Y, Khor E, Koo O (1998)  $\gamma$  irradiation of chitosan. *J Appl Polym Sci* 43:290–382
36. Paulino AT, Simionato JI, Garcia JC, Nozaki J (2006) Characterization of chitosan and chitin produced from silkworm chrysalides. *Carbohydr Polym* 64:98–103
37. Yue W (2014) Prevention of browning of depolymerized chitosan obtained by gamma irradiation. *Carbohydr Polym* 101:857–863
38. Ferreira LM, Leal JP, Casimiro MH, Cruz C, Lancastre JJH, Falcão NA (2014) Evidence of structural order recovery in LDPE based copolymers prepared by gamma irradiation. *Radiat Phys Chem* 94:31–35
39. Huang Y, Onyeri S, Siewe M, Moshfeghian A, Madihally SV (2005) In vitro characterization of chitosan-gelatin scaffolds for tissue engineering. *Biomaterials* 26:7616–7627

# Application of Radiation Chemistry to Some Selected Technological Issues Related to the Development of Nuclear Energy

Krzysztof Bobrowski<sup>1,2</sup>  · Konrad Skotnicki<sup>1</sup> · Tomasz Szreder<sup>1</sup>

Received: 28 April 2016 / Accepted: 22 July 2016 / Published online: 18 August 2016  
© Springer-Verlag Berlin Heidelberg (outside the USA) 2016

**Abstract** The most important contributions of radiation chemistry to some selected technological issues related to water-cooled reactors, reprocessing of spent nuclear fuel and high-level radioactive wastes, and fuel evolution during final radioactive waste disposal are highlighted. Chemical reactions occurring at the operating temperatures and pressures of reactors and involving primary transients and stable products from water radiolysis are presented and discussed in terms of the kinetic parameters and radiation chemical yields. The knowledge of these parameters is essential since they serve as input data to the models of water radiolysis in the primary loop of light water reactors and super critical water reactors. Selected features of water radiolysis in heterogeneous systems, such as aqueous nanoparticle suspensions and slurries, ceramic oxides surfaces, nanoporous, and cement-based materials, are discussed. They are of particular concern in the primary cooling loops in nuclear reactors and long-term storage of nuclear waste in geological repositories. This also includes radiation-induced processes related to corrosion of cladding materials and copper-coated iron canisters, dissolution of spent nuclear fuel, and changes of bentonite clays properties. Radiation-induced processes affecting stability of solvents and solvent extraction ligands as well oxidation states of actinide metal ions during recycling of the spent nuclear fuel are also briefly summarized.

---

This article is part of the Topical Collection “Applications of Radiation Chemistry”; edited by Margherita Venturi, Mila D’Angelantonio.

---

✉ Krzysztof Bobrowski  
[k.bobrowski@ichtj.waw.pl](mailto:k.bobrowski@ichtj.waw.pl)

<sup>1</sup> Centre of Radiation Research and Technology, Institute of Nuclear Chemistry and Technology, Dorodna 16, 03-195 Warsaw, Poland

<sup>2</sup> Radiation Laboratory, University of Notre Dame, Notre Dame, IN 46556, USA



**Keywords** High pressure and temperature water radiolysis · Water radiolysis in heterogeneous systems · Radiation-induced processes in nuclear fuel cycles · Radiation-induced processes in nuclear waste repositories

## 1 Introduction

The knowledge gained from studies in the field of radiation chemistry was found to be important and essential to a number of technological applications associated with various areas of nuclear technology [1, 2]. These areas are related to (1) water-cooled reactors where the radiolytic processes have to be carefully controlled in order either to avoid or at least to decrease deleterious effects of water radiolysis, (2) reprocessing of spent nuclear fuel and high-level radioactive wastes in order to develop advanced fuel cycles [3], and (3) fuel evolution during final radioactive waste disposal in order to assess the long-term safety of storage in final repositories [4].

Radiolysis of water and aqueous solutions in various and extreme environmental conditions (high temperatures and pressures, high LET of radiation) [5], and in heterogeneous systems (solid surfaces or near-surface layers) [6], was found to be of vital importance for mitigation of the unwanted effects [e.g. stress corrosion cracking (SCC)] by applying hydrogen water chemistry (HWC) technology in nuclear power plants running on light water reactors (LWR). These reactors are categorized into two types: boiling (BWR) and pressurized (PWR) water reactors. Moreover, the recent development of supercritical water-cooled reactors (SCWR) because, inter alia, of their higher thermal efficiency stimulated studies on the radiolysis of supercritical water. These reactors operate above the thermodynamic critical point of water [1].

Radiation-induced processes occurring during reprocessing of spent nuclear fuel can have unpredictable and profound effects on separation of radioisotopes. Current strategies involve dissolution of the spent nuclear fuel and the use of complex organic ligands designed for highly selective solvent extraction-based separation. A large number of complexing agents has been tested for application in these steps [7, 8]. Radiation chemistry is crucial to these processes since the design of successful separation systems for the nuclear fuel cycle relies on the use of reagents that are stable in an acidic and radioactive environment. Adverse effects of radiolysis on separation systems can be predicted ahead of time by elucidation of kinetics and mechanisms of reactions involving reactions of ligands and diluents with the transient and stable products derived from bulk diluent and  $\text{HNO}_3$  radiolysis [3, 9].

High-level radioactive waste disposal is one of the most challenging issues related to nuclear technology since it is directly connected to the long-term safety concern. A deep geological disposal is one of the most commonly discussed alternatives. At the present time, the majority of wastes are held in surface stores at nuclear facilities (e.g. nuclear power stations), and are kept safe and separated from the environment and people only by institutional controls. They could present a potential hazard and, therefore, a more permanent disposal site is required.

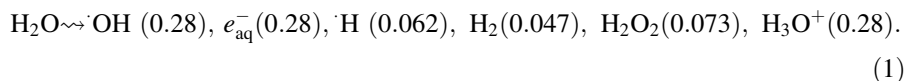


Geological disposals have been already considered in some countries (USA, Finland, Sweden, Belgium, UK) [10]. This concept is based on the system of engineered barriers (i.e. a waste form, a waste package, and a buffer material surrounding the package) and a natural barrier (geological environment). Radiation effects on these barriers should be considered in order to understand time evolution of the spent fuel, which might occur in the presence of ground water, air, H<sub>2</sub> coming from the insert corrosion and radiolysis, and possibly hyperalkaline fluids due to the presence of cement radiation effects [1].

This paper highlights the most important contributions of radiation chemistry to some selected technological issues related to the development of nuclear energy.

## 2 Radiation Chemistry of Water in Nuclear Reactors

The mechanisms of water radiolysis at ambient temperatures have been established for over many decades of the last century [11]. For low LET irradiation i.e.  $\sim 0.23 \text{ eV nm}^{-1}$  radiolysis of water can be summarized by Eq. (1) [12], where the numbers in parenthesis represent radiation chemical yields ( $G$  values) in units  $\mu\text{mol J}^{-1}$ .

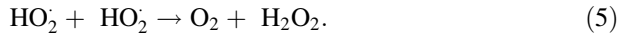
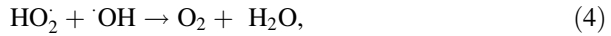
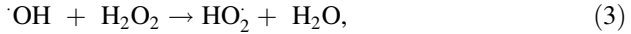


On the other hand, measurements related to water radiolysis under extreme conditions (including supercritical water) have been performed only within the last three decades. These studies were initiated in order to understand the key features of water radiolysis under these conditions, which might have crucial implications for the corrosion processes occurring in the primary cooling loop in nuclear LWR and SCWR when the temperature and pressure increase beyond the critical point.

It is well known that the tetrahedral-like water structure, existing at ambient temperatures, starts to decompose with increasing temperature to subcritical and supercritical regimes. These changes affect substantially water structure, which consists of small aggregates and even monomeric gas-like water structure, and also increase long-distance water–water interaction. This results in a dramatic decrease of the dielectric constant (from 78 at the room temperature to 2.6 at 400 °C/25 MPa).

The property changes mentioned above can have a tremendous influence on spectral properties, radiation–chemical yields ( $G$  values), and rate constants of primary and secondary transient species formed during water radiolysis. The spectral properties (i.e.  $\lambda_{\text{max}}$  and  $\epsilon_{\text{max}}$ ) are important for a proper evaluation of their concentrations that in turn are necessary for a proper evaluation of  $G$  values and rate constants of second-order reactions. These two last parameters are crucial and strongly required since they serve as input data to the model of water radiolysis in the primary loop of LWR and SCWR. These models enable calculations of the concentration of oxygen (O<sub>2</sub>), hydrogen (H<sub>2</sub>), hydrogen peroxide (H<sub>2</sub>O<sub>2</sub>), and various radicals [1, 13–18].

Molecular products  $\text{H}_2\text{O}_2$  and  $\text{O}_2$  promote corrosion and stress corrosion cracking (SCC) in the cooling system materials and pipe work. They are formed in the following secondary reactions involving  $\cdot\text{OH}$  radicals (Eqs. 2–5):



In order to predict feasibility of reactors cooled with supercritical water (SCWR), there is a strong need to model radiation-induced chemistry in the reactor heat transport piping since this can significantly improve economics of the power generation.

## 2.1 Spectral Properties of Primary Transients from Water Radiolysis and Some Selected Secondary Transient Species

Studies on spectral properties of primary transients as well as other radicals at high temperatures and pressures are very important since the changes of water properties may affect the position of absorption bands. In another words, they can induce the optical absorption spectral shift. This phenomenon is directly connected to the radical/radical ions-solvent interactions, which can be affected by the hydrogen bonding network, the dielectric constant, the electrostatic forces and polarity of solvent, and clustering effects of water molecules under supercritical conditions. More detailed information about the character and reasons for changes in spectral parameters can be found in the recent review chapter and original papers cited therein [5].

A general tendency observed in the spectral shift of  $e_{\text{aq}}^-$  was the following: a strong shift to longer wavelengths with increasing temperature going from 25 to 390 °C. In the range of supercritical temperatures, the spectra of  $e_{\text{aq}}^-$  also shift slightly to longer wavelengths as the density of water decreases [19–23].

As far as the  $\cdot\text{OH}$  spectrum is concerned, the temperature-dependent studies performed in the range up to 200 °C revealed that the position of the absorption maximum did not show significant changes with temperature [24, 25]. However, it was reported in the later studies that at 350 °C at the expense of the primary absorption band with  $\lambda_{\text{max}} = 230$  nm, a new weak absorption band with  $\lambda_{\text{max}} = 310$  nm appeared. These bands have been assigned to hydrogen-bonded and “free” OH radicals, respectively. Moreover, a monotonic decrease of the molar absorption coefficient of  $\cdot\text{OH}$  radicals at elevated temperatures was also observed [from  $\varepsilon_{250}(25\text{ °C}) = 535 \text{ day m}^3 \text{ mol}^{-1} \text{ s}^{-1}$  to  $\varepsilon_{250}(350\text{ °C}) = 224 \text{ day m}^3 \text{ mol}^{-1} \text{ s}^{-1}$ ] [26].

Generally, in going from the room temperature to the elevated temperatures, the radical ions showed a shift towards longer wavelengths (lower energies) [e.g.  $\text{Ph}_2\text{CO}^-$  [27],  $(\text{SCN})_2^-$  [28, 29],  $\text{Ag}_2^+$  [30],  $\text{CO}_2^-$  [31]] while the radicals derived

from aromatic compounds show a shift towards shorter wavelengths (higher energies) (e.g. Ph<sub>2</sub>-COH [27], 4,4'-BpyH) [32]. Interestingly, carbonate radical anions (CO<sub>3</sub><sup>-</sup>) [33], and methyl viologen (MV<sup>+</sup>) [34], showed no change in absorption maximum with increasing temperature.

## 2.2 Radiation Chemical Yields (*G* Values) of Primary Transients from Water Radiolysis

The measurements of *G* values of primary transients from water radiolysis can be performed either by pulse radiolysis technique or steady-state radiolysis coupled with product analysis [35]. Interestingly, the yields of primary transients in  $\gamma$ -irradiated supercritical water at 400 °C were already measured in 1981 [36], and further re-analyzed [35]. Suitable scavenging systems applied can be found in the literature [5, 32, 34]. A recent review summarized data available for *G* values from room temperature up to 350 °C using different and relatively large scavenger concentrations [13]. However, one has to keep in mind that the yields of primary transients escaping from “spurs” do not reflect their yields in pure water. Moreover, *G* values are actually a function of time following energy deposition and the rates of spur reactions involved in the inter-conversion of  $e_{aq}^-$  and H atoms increase with temperature [5, 37]. Recently, temperature-dependent measurements were performed at low scavenger concentrations and dose ranges that initial “spur chemistry” was not significantly perturbed, and the yield of the product (N<sub>2</sub>) nearly corresponds to the yields of reducing radicals that escape recombination in pure water. Moreover, it was shown that the yield of  $G_{esc}(\text{OH})$  was incorrect [38].

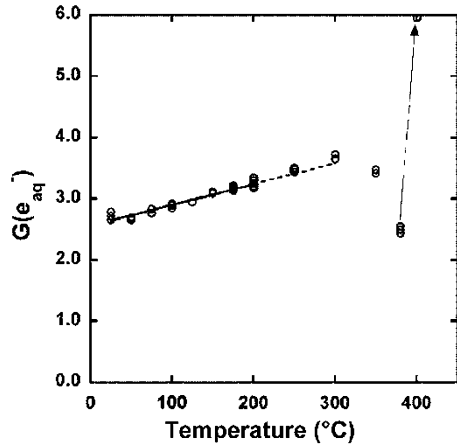
The first attempts to measure the  $G(e_{aq}^-)$  at elevated temperature up to 250 °C were performed using Cd<sup>2+</sup> and benzonitrile as electron scavengers. They showed that  $G(e_{aq}^-)$  values increase significantly with temperature to  $\sim 0.36$  and  $\sim 0.39 \mu\text{M J}^{-1}$  at 200 and 250 °C, respectively [39, 40].

Subsequent experiments over the temperature range 25–400 °C at constant pressure of 25 MPa, and using methyl viologen (MV<sup>2+</sup>) as an electron scavenger show a monotonic increase of *G* values from  $\sim 0.29 \mu\text{M J}^{-1}$  (at 25 °C) to  $\sim 0.39 \mu\text{M J}^{-1}$  (at 300 °C), then a decrease to a minimum  $\sim 0.25 \mu\text{M J}^{-1}$  near  $T_c$ , followed by a sharp increase to  $\sim 0.62 \mu\text{M J}^{-1}$  (at 400 °C) (Fig. 1) [34], and again a monotonic decrease to  $\sim 0.24 \mu\text{M J}^{-1}$  (at 450 °C), reaching *G* value slightly below  $0.21 \mu\text{M J}^{-1}$  (at 500 °C) [5].

These high *G* values obtained in supercritical water when the density decreases below  $0.5 \text{ kg day m}^{-3}$  were confronted with the *G* values measured based on N<sub>2</sub> product yield when N<sub>2</sub>O was used as a scavenger for  $e_{aq}^-$  and were found to be threefold larger [41].

The  $G(\text{OH})$  values in the  $\gamma$ -radiolysis of light and heavy water were measured as a function of temperature up to 300 °C at constant pressure 10.3 MPa. They showed a monotonic increase of *G* values from  $\sim 0.29 \mu\text{M J}^{-1}$  (at 25 °C) to  $\sim 0.50 \mu\text{M J}^{-1}$  (at 300 °C) in the full temperature range [42]. Later, the temperature range was expanded to 400 °C at constant pressure of 25 MPa, and the *G* value was found to reach slightly above  $0.62 \mu\text{M J}^{-1}$  (at 400 °C) [5].

**Fig. 1**  $G(e_{aq}^-)$  as a function of temperature at 25 MPa obtained by pulse radiolysis of a solution of 0.5 mM  $MV^{2+}$  and 0.2 M *tert*-butyl alcohol Reprinted with permission from Ref. [34]



The temperature-dependent  $G(H)$  values were not measured directly. They were extracted either by subtraction of  $G(H_2)$  from  $G(H + H_2)$  [42], by subtraction of  $G(e_{aq}^-)$  and  $G(\cdot OH)$  from  $G(e_{aq}^- + \cdot OH + H)$  [34], and by applying ethanol- $d_6$  as a scavenger for H atoms, giving HD as a stable product [41].

### 2.3 Kinetic Parameters of Reactions Involving Primary Transients from Water Radiolysis

In the subsequent subchapters, the kinetic parameters of the most important chemical reactions occurring at the operating temperatures of reactors and involving primary transients ( $e_{aq}^-$ ,  $\cdot OH$  and  $\cdot H$ ) and stable products ( $H_2$  and  $H_2O_2$ ) from water radiolysis are presented. This knowledge is necessary in order to make a reliable prediction of the concentrations of radiolytic species at various positions in water-cooled reactors.

#### 2.3.1 Hydrated Electrons ( $e_{aq}^-$ )

There are several critical reactions involving the hydrated electrons for which kinetic parameters are necessary to predict the effects of the radiation on the cooling water system. Therefore, many attempts have been made to study these reactions in the high-temperature range.

The first one represents recombination of two  $e_{aq}^-$  (Eq. 6):



In the 5–150 °C range, the rate constant ( $k_6$ ) showed a normal Arrhenius behavior, with a diffusion-controlled activation energy of 23 kJ mol<sup>-1</sup>. Surprisingly, between 150 and 250 °C, the rate constant ( $k_6$ ) rapidly decreased with

increasing temperature, and then remained constant up to 300 °C. Interestingly, the rate constant ( $k_6$ ) at 250 °C was found to be similar to that measured at room temperature. The explanation for the non-Arrhenius behavior involved a two-step mechanism (Eqs. 6a, 6b):



in which the rate constant of reverse reaction ( $k_{-6a}$ ) is low at RT, and the reaction itself has higher activation energy than the forward one and, therefore, can compete with reaction (6b) at higher temperatures [43]. The reaction depicted in Eq. (6) was re-investigated in the 100–325 °C range. The behavior of  $k_6$  was found to be similar to that previously reported, showing a maximum value of  $5.9 \times 10^{10} \text{ day m}^3 \text{ mol}^{-1} \text{ s}^{-1}$  at 150 °C with a diffusional activation energy of  $20 \text{ kJ mol}^{-1}$ , it then decreased, and above 250 °C was found to be too small to measure it reliably [44].

The rate constants of reaction with hydrogen atoms (Eq. 7):



were measured over the very wide range of temperatures (5–250 °C), and indicated Arrhenius behavior over the entire temperature range, with an activation energy of  $14.0 \text{ kJ mol}^{-1}$  [45].

The same reaction (Eq. 7) was re-investigated over the 100–325 °C temperature range showing reasonable agreement with the previous data up to 200 °C. However, the rate constant  $k_7$  showed a rapid increase with increasing temperature

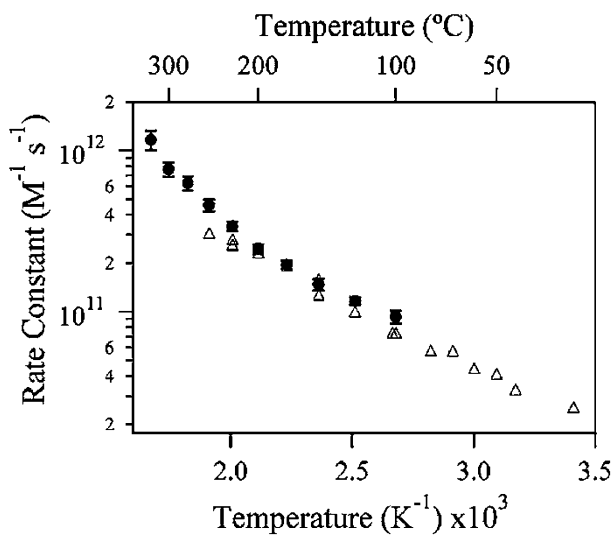


**Fig. 2** Arrhenius plot for reaction (7) showing the averages of the current data across all measured  $\text{OH}^-$  concentrations (circles) and previous data from ref 45 (triangles). Reprinted with permission from Ref. [44]

( $k_7 = 9.3 \times 10^{10} \text{ day m}^3 \text{ mol}^{-1} \text{ s}^{-1}$  at 100 °C and  $1.2 \times 10^{12} \text{ day m}^3 \text{ mol}^{-1} \text{ s}^{-1}$  at 325 °C) and an increase of the activation energy above 150 °C, and thus non-Arrhenius behavior over the entire studied temperature range (Fig. 2). This reaction was considered to be a long-range electron transfer (LRET) reaction [44].

The rate constants of reaction with  $\text{H}^+$  (Eq. 8):



were measured as a function of temperature between 25 and 250 °C and showed significant concave upward curvature in a region corresponding to temperature above 150 °C. Moreover, it was shown that the reaction depicted in Eq. (8) represents equilibrium, where  $pK_{\text{a}}$  decreases with temperature from  $9.59 \pm 0.03$  at 25 °C to  $6.24 \pm 0.09$  at 250 °C. In contrast, the rate constants of the back reaction (in Eq. 8) showed concave downward curvature in the same temperature region [46]. The same reaction (forward reaction in Eq. 8) was re-investigated over the temperature range 25–380 °C showing a very good agreement with the previous data up to 250 °C. The rate constant of  $e_{\text{aq}}^-$  with  $\text{H}^+$  started to increase more strongly at elevated temperatures, between 200 and 350 °C [47]. These observations were rationalized in terms of changes of the dielectric constant of water. Since the dielectric constant of water decreases substantially with increasing temperature, the forward reaction (Eq. 8) is accelerated more and more by a coulombic attraction between the two opposite charged species. Later, it turned out that the rate constants >275 °C were incorrect and were re-measured, showing slightly higher values in comparison to those previously measured [48]. However, these corrected values do not affect earlier conclusions. Interestingly, the rate constant of this reaction decreased sharply at supercritical temperatures (at 380 °C). This phenomenon was explained by ion-pairing (clustering) of reactants at supercritical temperatures, which decreases their effective concentration [47].

The decay of the hydrated electrons in supercritical conditions showed a fast component at a short time below 500 ps, which was assigned to the reaction of the hydrated electron with the hydronium cation formed by radiolysis. The dependence of the kinetics on the density of SCW was also examined [49].

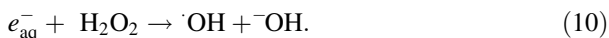
Interestingly, as the density of SCW is decreased, the decay of a hydrated electron at short time (<500 ps) becomes slower. This is because SCW becomes more inhomogeneous and, when the density is low, behaves like a gas. At such conditions, the cage effect is not so important, and solvated electrons can avoid spur reaction more easily.

The rate constants of reaction with hydroxyl radicals (Eq. 9):



were measured as a function of temperature between 5 and 225 °C and indicated Arrhenius behavior over the temperature range 5–175 °C with an activation energy of  $14.7 \text{ kJ mol}^{-1}$ . The reaction of  $\cdot\text{OH}$  radicals with silicate was suggested as a possible explanation for the observed deviation from the straight line Arrhenius plot above 175 °C [45].

The temperature-dependent rate constants for reaction of  $e_{\text{aq}}^-$  with  $\text{H}_2\text{O}_2$  (Eq. 10) have been measured at the temperature range between 5 and 200 °C, with activation energies ranging between 10.0 and 15.6 kJ mol<sup>-1</sup> [25, 45]. For example, the rate constants for reaction (Eq. 10) determined at 20 and 150 °C are equal to  $1.2 \times 10^{10} \text{ M}^{-1} \text{ s}^{-1}$  and  $8.5 \times 10^{10} \text{ M}^{-1} \text{ s}^{-1}$ , respectively [45]. The corresponding values measured by another group are equal to  $1.1 \times 10^{10} \text{ M}^{-1} \text{ s}^{-1}$  and  $5.6 \times 10^{10} \text{ M}^{-1} \text{ s}^{-1}$ , respectively [25].



The rate constants for scavenging of  $e_{\text{aq}}^-$  by  $\text{O}_2$  (Eq. 11) follow Arrhenius behavior with an activation energy 11.3 kJ mol<sup>-1</sup> [25]; however, at higher temperatures they become increasingly dependent on water density [50].



A strong decrease by a factor of 4 between 0.55 and 0.45 g cm<sup>-3</sup> and then increase at lower density at 0.1 g cm<sup>-3</sup> was observed for  $k_{11}$  in supercritical water at 380 °C. These observations were rationalized in terms of a potential of mean force separating the ion and hydrophobic species ( $\text{O}_2$ ), which is maximized at 0.45 g cm<sup>-3</sup> [50].

The temperature-dependent rate constants for reactions of  $e_{\text{aq}}^-$  with  $\text{NO}_2^-$  and  $\text{NO}_3^-$  ions have been measured at the temperature range between 25 and 350 °C [47]. These reactions can serve as models for the ionic reactions occurring at high temperatures and supercritical water. The rate constants of  $e_{\text{aq}}^-$  with  $\text{NO}_3^-$  were found to follow Arrhenius behavior only to 125 °C, reaching a maximum at ~175 °C, and then decreased up to 350 °C. Similarly for the reaction with  $\text{H}^+$  (Eq. 8), these observations were rationalized in terms of changes of the dielectric constant of water. Since the dielectric constant of water decreases substantially with increasing temperature, the reaction begins to be slowed at some point due to the repulsive forces between the two negatively charged species.

Reaction of  $e_{\text{aq}}^-$  with nitrobenzene was used as a probe for studying the density dependence on the ionic reaction rates in supercritical water. The studies were extended up to 400 °C showing that the rate constants display a similar density dependence observed previously for reaction with  $\text{O}_2$  (Eq. 11) [51].

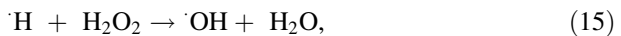
Reactions of transition metal ions with the primary water radiolysis products seem to be involved in the complex processes leading to crud deposits, which can promote local corrosion that with time can create a rupture in the cladding, so the fission products can be released into the coolant [52]. In order to interpret the chemistry effects on such crud deposition behavior, the kinetics information on all possible reactions at high temperature and pressure involving transition metal cations is required to complete simulation of these systems [53]. The rate constants for hydrated electron with aqueous transition metal cations that might be present in the cooling loops, were investigated up to 300 °C. The activation energies obtained from the Arrhenius plots are in the range 14.5–40.6 kJ mol<sup>-1</sup> [54].

### 2.3.2 Hydroxyl Radicals ( $\cdot\text{OH}$ )

Reaction of  $\cdot\text{OH}$  radicals with molecular hydrogen (Eq. 12) is one of the key reactions that must be taken into account in current models of water radiolysis in BWR reactors.



Occurrence of this reaction is a simple and effective measure to maintain reducing conditions in the cooling loop. The oxidizing  $\cdot\text{OH}$  radicals are converted to reducing  $\cdot\text{H}$  atoms, which can in turn reduce the corrosive  $\text{H}_2\text{O}_2$  and  $\text{O}_2$  that leads eventually to formation of water molecules (Eqs. 13–16):



These conditions can be achieved by addition of a sufficient quantity of excess  $\text{H}_2$  to the reactant coolant. Moreover, the rate constant of reaction (Eq. 12) is the most important parameter that allows prediction of the minimum concentration of  $\text{H}_2$  or critical hydrogen concentration (CHC), which is necessary to suppress the yield of oxidizing species [55].

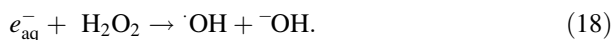
The first experiments to measure the rate constant  $k_{12}$  at elevated temperatures were performed in the temperature range 20–230 °C [56]. The rate constants determined at 20 and 230 °C were found to be  $(3.4 \pm 0.3) \times 10^7 \text{ day m}^3 \text{ mol}^{-1} \text{ s}^{-1}$  and  $(7.7 \pm 0.1) \times 10^8 \text{ day m}^3 \text{ mol}^{-1} \text{ s}^{-1}$ , respectively. The activation energy of the reaction was determined from the linear Arrhenius plot as 19 kJ mol<sup>-1</sup>.

Later studies in PWR reactor loops have shown that experimental CHC was larger than that predicted by using the rate constant ( $k_{12}$ ) measured at 230 °C, which is lower than the operational temperature (300 °C) in PWR reactors.

Therefore, the reaction depicted in Eq. (12) was studied up to 350 °C. At higher temperatures, the values of the rate constant are lower than those obtained from the extrapolation of Arrhenius plot [56]. For example, the rate constant measured at 350 °C ( $k_{12} = 3.5 \times 10^8 \text{ day m}^3 \text{ mol}^{-1} \text{ s}^{-1}$ ) is fivefold lower than that obtained from extrapolation [57]. This was due to the non-Arrhenius behavior of reaction depicted in Eq. (12). The rate constant measured at 350 °C was later reevaluated giving  $(6.0 \pm 0.5) \times 10^8 \text{ day m}^3 \text{ mol}^{-1} \text{ s}^{-1}$  [58].

In principle, all species formed depicted in Eq. (1), including  $\text{HO}_2\cdot/\text{O}_2^{\cdot-}$ , react with each other; however, reactions depicted in Eqs. (12), (15), (17), and (18) are more important since they represent chain reactions responsible for consumption of  $\text{H}_2\text{O}_2$ .





In water-cooled nuclear power plants  $\cdot\text{OH}$  radical recombination is a primary source of corrosive  $\text{H}_2\text{O}_2$  (vide supra Eq. 2) and  $\text{O}_2$  (vide supra Eqs. 3–5). The rate constants for the self-recombination of  $\cdot\text{OH}$  radicals were measured in the 150–350 °C range [26]. It was found that the values above 200 °C are smaller than previously predicted by extrapolation using activation energy of 3.7 kJ mol<sup>-1</sup> [25]. In principle, the rate constants are at the same level around  $1.2 \times 10^{10}$  - day m<sup>3</sup> mol<sup>-1</sup> s<sup>-1</sup>, showing no change in the 200–350 °C range [26].

The reaction between  $\cdot\text{OH}$  and  $\text{H}_2\text{O}_2$  (vide supra Eq. 3) was studied in the temperature range 14–160 °C, and an activation energy of 14 kJ mol<sup>-1</sup> was derived from the Arrhenius plot. The rate constant measured at 160 °C was found to be  $1.5 \times 10^8$  M<sup>-1</sup>s<sup>-1</sup> [59].

The reaction between  $\cdot\text{OH}$  and  $\cdot\text{H}$  (vide supra Eq. 16) was first studied in the temperature range 20–200 °C [60]. The rate constants ( $k_{19}$ ) of  $1.5 \times 10^{10}$  day m<sup>3</sup> - mol<sup>-1</sup> s<sup>-1</sup> and  $4.9 \times 10^{10}$  day m<sup>3</sup> mol<sup>-1</sup> s<sup>-1</sup> were found at 20 and 200 °C, respectively, with a non-linear Arrhenius plot. This reaction was later re-investigated in the temperature range 5–233 °C [61]. The corresponding rate constants measured at 20 and 200 °C were found to be  $9.3 \times 10^{10}$  day m<sup>3</sup> mol<sup>-1</sup> - s<sup>-1</sup> and  $3.3 \times 10^{10}$  day m<sup>3</sup> mol<sup>-1</sup> s<sup>-1</sup>, which were slightly lower than those previously measured. The activation energy was found to be  $8.2 \pm 0.4$  kJ mol<sup>-1</sup>, which is lower than that expected for a diffusion controlled reaction.

The reaction of  $\cdot\text{OH}$  radicals with  $\text{HO}_2$  radicals (vide supra Eq. 4) was studied in the temperature range 20–296 °C. The rate constant ( $k_4$ ) of  $7.0 \times 10^9$  day m<sup>3</sup> - mol<sup>-1</sup> s<sup>-1</sup> was measured at 20 °C. The activation energy was found to be 7.0 kJ mol<sup>-1</sup> which was obtained from the linear Arrhenius plot [62].

### 2.3.3 Hydrogen Atoms ( $\cdot\text{H}$ )

The reaction of  $\cdot\text{H}$  atoms with  $\text{}^-\text{OH}$  has been considered a “proton transfer”, in which the electron remains in the solvation cavity, originally occupied by the  $\cdot\text{H}$  atom (Eq. 19):



An immediate contact between  $\cdot\text{H}$  and  $\text{}^-\text{OH}$  is probably necessary to effect the proton transfer [63]. It was shown that extrapolation of the rate constants ( $k_{19}$ ) measured up to 95 °C was not possible since the rate constants measured above 100 °C fall below numbers extrapolated because Arrhenius activation energy becomes smaller above 100 °C [50].

The reaction of  $\cdot\text{H}$  atoms with water (Eq. 20) was suggested to contribute to the spur chemistry in radiolysis of water and to be responsible for the unexplained increase of the radiation chemical yield of molecular hydrogen ( $\text{H}_2$ ) at high temperatures and pressures [64].



There are no direct measurements of  $k_{20}$  at any temperature except some estimations which vary from  $3.6 \times 10^{-5} \text{ day m}^3 \text{ mol}^{-1} \text{ s}^{-1}$  [46], to  $10 \pm 2 \text{ day m}^3 \text{ mol}^{-1} \text{ s}^{-1}$  [65], at room temperature. Several attempts have been made to estimate the rate constant of the forward reaction in Eq. (20) at high temperatures [64, 66, 67]. A diffusion-kinetic modelling of spur processes in neutral water was used and the possible value  $(3.18 \pm 1.25) \times 10^4 \text{ day m}^3 \text{ mol}^{-1} \text{ s}^{-1}$  of  $k_{20}$  at 573 K was computed [64]; however, it was later corrected to  $1.75 \times 10^4 \text{ day m}^3 \text{ mol}^{-1} \text{ s}^{-1}$  [66].

The reaction of H atoms with  $\text{H}_2\text{O}_2$  (vide supra Eq. 15) was studied as a function of temperature by several groups in the temperature range between 10 and 120 °C [68–70]. The rate constant  $k_{15}$  measured at 25 °C ranged from  $3.6 \times 10^7 \text{ day m}^3 \text{ mol}^{-1} \text{ s}^{-1}$  [69], to  $5.1 \times 10^7 \text{ day m}^3 \text{ mol}^{-1} \text{ s}^{-1}$  [68]. Some discrepancies in the activation energy measured were observed:  $10.7 \pm 0.5 \text{ kJ mol}^{-1}$  [68],  $16 \text{ kJ mol}^{-1}$  [70], and  $21 \text{ kJ mol}^{-1}$  [69].

The reaction of H atoms with  $\text{HO}_2$  radicals (vide supra Eq. 14) was studied in the temperature range 5–149 °C. The rate constant ( $k_{14}$ ) of  $8.5 \times 10^9 \text{ day m}^3 \text{ mol}^{-1} \text{ s}^{-1}$  was measured at 20 °C. The activation energy was found to be  $17.5 \text{ kJ mol}^{-1}$ , which was obtained from the linear Arrhenius plot [62]. This reaction was later reinvestigated showing non-Arrhenius behavior above 200 °C. Moreover, it was suggested that reaction between H atoms with  $\text{HO}_2$  radicals can occur via a different reaction channel (Eq. 21):



which further can recreate H atoms via reaction depicted in Eq. (12) [58].

The bimolecular decay of H atoms (Eq. 22) was studied in the temperature range 20–250 °C [71].



The activation energy was found to be  $14.7 \text{ kJ mol}^{-1}$  which was obtained from the linear Arrhenius plot. Since there was some indication that molar absorption coefficient of H atoms increases with temperature, this value can be considered as a lower limit. It was confirmed later that this reaction follows Arrhenius behavior up to 350 °C [58].

The reaction of H with molecular oxygen ( $\text{O}_2$ ) is of great importance for oxidation processes occurring in water-cooled reactors (in SCWR, in particular) and connected to the HWC technology (Eq. 23):



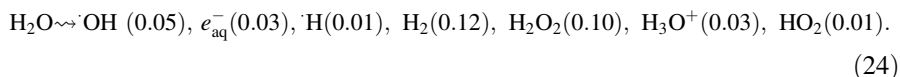
The reaction was studied at first in the temperature range 20–200 °C. The rate constant ( $k_{23}$ ) of  $3.2 \times 10^{10} \text{ day m}^3 \text{ mol}^{-1} \text{ s}^{-1}$  was measured at 25 °C. The activation energy was found to be  $6.2 \text{ kJ mol}^{-1}$ , which was obtained from the linear Arrhenius plot [25]. This reaction was later reinvestigated up to 350 °C, showing non-Arrhenius behavior above 200 °C. At 350 °C, the rate constant ( $k_{23}$ ) is 2.5-fold

lower [58], than the value extrapolated using the activation energy from the previous study [25].

## 2.4 Radiolysis of Water at Ambient Temperatures with High LET Irradiation

The first studies on radiolysis of water with high LET irradiation were performed just after the discovery of radiation; however, only with  $\alpha$  particles, which were available at that time. Later, the development of ion accelerators and ion beams enabled studies with ions (e.g.  $H^+$ ,  $D^+$ ,  $He^{2+}$ ) and heavier ions with higher energies (e.g. C–Kr, H–Au, H–U, and Ne–Au) [72]. Knowledge about radiolysis of water with high LET irradiation is important for evaluation of radiation-induced processes during recycling management and geological disposal of spent nuclear fuel, which are exposed to  $\alpha$ -irradiation generated by the actinide decay and other fission products.

For high LET irradiation, i.e.  $\sim 156 \text{ eV nm}^{-1}$  radiolysis of water (an environment in extraction systems during recycling management, vide infra) can be summarized by Eq. (24) [1, 3, 73], where the numbers in parenthesis represent radiation chemical yields ( $G$  values) in units  $\mu\text{mol J}^{-1}$ .



The most intensively studied products of water radiolysis were hydrated electrons ( $e_{aq}^-$ ), hydroxyl radicals ( $\cdot OH$ ), and hydrogen peroxide ( $H_2O_2$ ). Many of the results were obtained by the scavenging method; however, some were from the heavy-ion pulse radiolysis [72]. The two most important findings as far as the  $G$  values of primary species are concerned are as follows: the primary yields of  $e_{aq}^-$  and  $\cdot OH$  radicals decrease with increasing LET; on the other hand, the primary yield of  $H_2O_2$  increases with increasing LET (Table 1).

Information about the intra-track dynamics can be extracted by increasing scavenger concentration. With increasing scavenger concentration, the scavenging reactions begin to occur more efficiently, and thus they can compete more significantly with intra-track reactions and diffusions. However, with increasing LET, scavenging reactions become less efficient due to increased radical density in the track and in a consequence increased efficiency of intra-track reactions. These

**Table 1** Primary radiation chemical yields ( $\mu\text{M J}^{-1}$ ) of  $e_{aq}^-$ ,  $\cdot OH$  radicals, and  $H_2O_2$  as a function of LET

Species/ions	He <sup>a</sup>	C <sup>b</sup>	Ne <sup>c</sup>	Si <sup>d</sup>	Ar <sup>e</sup>	Fe <sup>f</sup>
$e_{aq}^-$	0.25	0.20	0.17	0.12	0.11	0.082
$\cdot OH$	0.27	0.20	0.17	0.13	0.11	0.100
$H_2O_2$	0.072	0.082	0.082	0.077	0.093	0.11

<sup>a</sup>  $\sim 2 \text{ eV nm}^{-1}$ ; <sup>b</sup>  $\sim 15 \text{ eV nm}^{-1}$ ; <sup>c</sup>  $\sim 30 \text{ eV nm}^{-1}$ ; <sup>d</sup>  $\sim 60 \text{ eV nm}^{-1}$ ; <sup>e</sup>  $\sim 150 \text{ eV nm}^{-1}$ ; <sup>f</sup>  $\sim 600 \text{ eV nm}^{-1}$

trends have been confirmed using irradiation with He, C, Ne, Si, Ar, and Fe ions, and successfully reproduced by the Monte Carlo simulations using the IONLYS-IRT code [74].

Comprehensive reviews addressing all aspects of radiolysis of water with high LET irradiation have been recently published [72, 74, 75]. The reader is referred to those studies for details, which cannot be covered in depth here.

### 3 Radiation Chemistry of Water at Solid–Liquid Interfaces

Radiation chemistry of water at solid–liquid interfaces is directly associated with various aspects of nuclear technology. The presence of a solid–liquid interface can drastically change the radiation-induced decomposition of water molecules, which are adsorbed on surfaces as compared to water molecules present in the form of a homogeneous liquid. Studies on radiolysis of water in heterogeneous systems are necessary to predict the aging of the existing reactors, information that is crucial for evaluation of their safe operation. Cladding of fuel rods ( $\text{ZrO}_2$ ), control elements ( $\text{BeO}$ ), and cooling coils ( $\text{Al}_2\text{O}_3$ ,  $\text{Fe}_2\text{O}_3$ ) (which are parts of nuclear reactors) are in constant contact with water. In addition to the interface, water is also present within the construction materials of reactors as well in the clays that are used to contain the spent nuclear fuel. An understanding of the radiolytic processes in confined water is important for the safe long-term storage of nuclear waste. They can lead to high quantities of gases not only from direct radiolysis of water, but from the radiation energy absorbed by the solid material (vide 5.1 and 5.3).

#### 3.1 Radiolysis of Aqueous Nanoparticle Suspensions and Slurries

An enhanced generation of molecular hydrogen during radiolysis of aqueous nanoparticle suspensions is a very important issue of a very practical concern in nuclear technologies. In extreme cases, i.e. severe meltdown, core debris will be in inevitable contact with water, which can lead to production of water suspensions (e.g. zircalloy oxidation products such as  $\text{ZrO}_2$  in water). Radiation chemistry of water in nanoparticle suspensions has been extensively described [76]. Since then, suspensions were not so often investigated because a modern approach to interfacial radiation chemistry was focused on water molecules adsorbed on powders or confined in nanoscopic dimensions. Moreover, the energy/charge transfer mechanism were not prominent enough when a liquid phase greatly outweighs solid phase. However, an interesting issue has been recently considered with respect to application of  $\gamma$  rays energy from nuclear reactors or high level waste to produce hydrogen ( $\text{H}_2$ ). A suspension or turbidities of metals or their oxides can be used to enhance production of hydrogen for commercial use [77, 78].

Slurries have attracted more attention since they have direct impact on nuclear industry, especially for waste storage. Hydrogen ( $\text{H}_2$ ) generation at the silicon carbide ( $\text{SiC}$ )–water interfaces was investigated in slurries instead of powders since the latter does not adsorb enough water [79]. Hydrogen yields were found to be higher than expected “using a simple mixture rule”. An increase in hydrogen

generation has been observed with decreasing amount of water. This observation clearly indicates energy transfer from the solid to liquid phase. Sensitizing effect of SiC on the adsorbed water was given as another possible explanation. The yields of hydrogen increased from  $0.048 \mu\text{M J}^{-1}$  for pure water to about  $0.09 \mu\text{M J}^{-1}$  at 60 % water content on SiC and remained unchanged until the content of water reached 10 %. Then, with further decrease of water content, a large increase in hydrogen generation was observed.

Hydrogen production induced either by gamma or heavy ions ( $\text{He}^{2+}$ ) irradiation in aqueous slurries of various iron oxides ( $\text{FeO}$ ,  $\text{Fe}_2\text{O}_3$  and  $\text{Fe}_3\text{O}_4$ ) was investigated as a function of water content (5–90 % as a function of mass) [80]. The yields of  $\text{H}_2$  depend on the oxide type, content of water and the type of irradiation. Hydrogen yields in  $\text{Fe}_2\text{O}_3$  and  $\text{Fe}_3\text{O}_4$  slurries were found to be around  $0.062\text{--}0.078 \mu\text{M J}^{-1}$  (related to a dose deposited in the water) when water loading ranged from 10 to 90 %. There is a minor increase in  $\text{H}_2$  production when water loading is 5 % for  $\text{Fe}_2\text{O}_3$  (to  $0.078 \mu\text{M J}^{-1}$ ) and more pronounced for  $\text{Fe}_3\text{O}_4$  (to  $0.13 \mu\text{M J}^{-1}$ ). On the other hand,  $\text{FeO}$  showed a linear decrease in  $\text{H}_2$  yield in the range of 20–100 % of water content (from about  $2.59 \mu\text{M J}^{-1}$  to the values in pure water. Below 20 % there is a dramatic increase up to  $41.44 \mu\text{M J}^{-1}$  when water loading is 5 %. Comparison of  $\text{H}_2$  yields obtained during  $\alpha$  and heavy ions radiolysis did not show major differences in  $\text{Fe}_2\text{O}_3$  and  $\text{Fe}_3\text{O}_4$ . On the other hand, a large difference was observed for  $\text{FeO}$ .  $\text{He}^{2+}$  irradiation resulted in a significant decrease of  $\text{H}_2$  yields to  $0.19 \mu\text{M J}^{-1}$ . These observations can be rationalized by a higher number of defects in the  $\text{FeO}$  bulk lattice, which can act as traps for the migration of energy to the surface.

The same research approach was applied to elucidate hydrogen production from copper (I) ( $\text{Cu}_2\text{O}$ ) and copper (II) ( $\text{CuO}$ ) oxides [81]. The amount of  $\text{H}_2$  produced for both copper oxides slightly increased as the amount of water present on the surface decreased: for  $\text{Cu}_2\text{O}$  from  $0.062 \mu\text{M J}^{-1}$  at 90 % content of water to  $0.083 \mu\text{M J}^{-1}$  molecules at 5 % water content, and for  $\text{CuO}$  from  $0.078$  to  $0.096 \mu\text{M J}^{-1}$ , respectively. Irradiation with  $\text{He}^{2+}$  ions doubled the hydrogen yield at 5 % content of water as compared to  $\gamma$ -rays.

Hydrogen generation during radiolysis has been explored in turbid solutions containing titanium and water suspensions of zirconium oxide nanoparticles during radiolysis [77, 82]. The enhanced formation of  $\text{H}_2$  was rationalized in terms of reaction of  $\cdot\text{OH}$  radicals with  $\text{Ti}^{3+}$  ions (present in the Ti turbidity), which prevents consumption of  $\text{H}_2$  by  $\cdot\text{OH}$  radicals (vide Eq. 12) or by a positive surface charge on  $\text{ZrO}_2$  particles, respectively.

Suspensions of gold nanoparticles (hundreds of nanometers size) in water were  $\gamma$ -irradiated in order to elucidate their influence on molecular hydrogen production [83]. Hydrogen yields were not much affected by the presence of gold nanoparticles, which led to the conclusion that no reducing species escape from solid metal to contribute to  $\text{H}_2$  yield. Nevertheless, this escape could be diminished by relatively large particle size, so it cannot be excluded for smaller metallic particles.

Hydrogen production during water radiolysis was measured in suspensions of  $\text{ZrO}_2$  and Zircalloy-4 oxidation products [84]. Zircalloy is a typical cladding material used in PWRs which under normal operation and as well as during nuclear

accidents is oxidized to  $\text{ZrO}_2$ . Pure and also seawater was studied since the last one was used for cooling the melted core after Fukushima accident. There was nearly no enhancement in  $\text{H}_2$  production in seawater in the presence of  $\text{ZrO}_2$  and Zircalloy-4 oxidation products.

The electron transfer from various oxides ( $\text{SiO}_2$ ,  $\text{ZnO}$ ,  $\text{Al}_2\text{O}_3$ ,  $\text{Nd}_2\text{O}_3$ ,  $\text{Sm}_2\text{O}_3$ , and  $\text{Er}_2\text{O}_3$ ) into water was studied in nanoparticle suspensions [85]. It was found that irrespective of the bandgap and the electron affinity of the oxide, the “hot” electrons are able to cross the semiconductor–liquid interface.

As one can conclude from this section, suspension and slurries of ceramic oxides (or in a broader sense, any material) in water exposed to radiation is a complicated and nontrivial system. The most important issues that have to be taken into consideration during interpretation of the results are the following: (1) the solid to liquid phase volume ratio, (2) the amount of radiation energy deposited in each phase, (3) the efficiency of energy/charge transfer between phases, (4) the reactions on interfacial surfaces, and (5) the non-radiation reactions on solid surface.

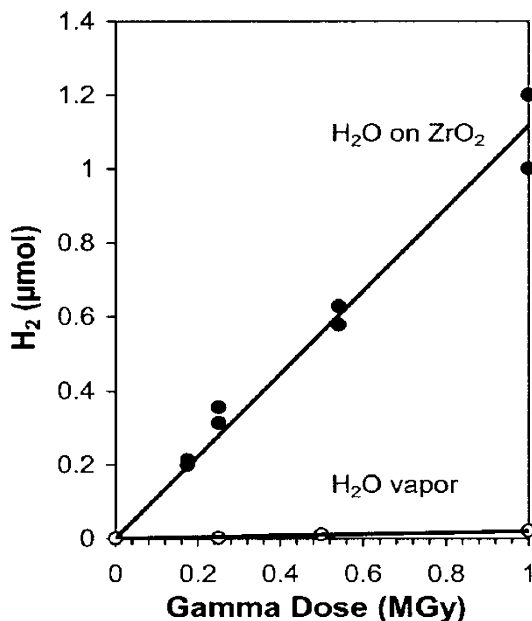
### 3.2 Radiolysis of Water on Ceramic Oxides Surfaces

Radiolysis of water in contact with ceramic oxides has gained a lot of attention since this issue is important in various branches of nuclear industry, including nuclear power plants, waste reprocessing facilities, and storage of nuclear waste (vide 5.1). In recent years, several important original papers [86–91] and comprehensive reviews, [4, 6, 92, 93] addressing radiolysis of water on ceramic oxides surfaces were published. The reader is referred to them for details that cannot be covered in depth here.

This section highlights only the very recently obtained results concerning radiolysis of water on various ceramic iron and copper oxides [80, 81]. This topic is directly connected to radiation-induced corrosion in stainless steel containers and oxidation of copper containers, which have been currently proposed for long-term radioactive waste storage (vide 5.1). Three different types of iron oxides, namely iron (II) oxide ( $\text{FeO}$ ), iron (III) oxide ( $\text{Fe}_2\text{O}_3$ ), and iron (II, III) oxide ( $\text{Fe}_3\text{O}_4$ ) with the adsorbed water were irradiated with  $\gamma$ -rays and  $^4\text{He}$  ions. Formation of  $\text{H}_2$  was observed only in the system containing  $\text{Fe}_2\text{O}_3$ . Its yield determined with respect to the energy deposited in water layers was found as  $15.54 \pm 6.22 \mu\text{M J}^{-1}$ , which is considerably higher than in bulk water ( $0.047 \mu\text{M J}^{-1}$ ). Similar results were obtained with other ceramic oxides for which these high yields were rationalized in terms of energy transfer from the oxide into adsorbed water [87, 88]. A definitive character of this energy transfer is not resolved, but presumably involves an exciton migration to the oxide–water interface (Fig. 3) [86].

Interestingly,  $\text{H}_2$  production in the systems containing two different copper oxides, namely copper (I) oxide ( $\text{Cu}_2\text{O}$ ) and copper (II) oxide ( $\text{CuO}$ ), was much lower, respectively,  $0.130 \pm 0.021$  and  $0.055 \pm 0.007 \mu\text{M J}^{-1}$  with respect to energy deposited in water layers [81]. These values are slightly higher than in the bulk water (vide supra) suggesting that copper oxides are inefficient in energy transfer from the bulk solid oxide to adsorbed water.

**Fig. 3** Amount of the produced hydrogen vs. absorbed gamma dose for radiolysis of 20  $\mu\text{mol}$  of water in vapor phase and 20  $\mu\text{mol}$  of water adsorbed on the  $\text{ZrO}_2$  surface with coverage of  $\sim 10 \text{ mol nm}^{-2}$ . Reprinted with permission from ref [86]



### 3.3 Radiolysis of Confined Water in Nanoporous Materials

Reactions occurring during radiolysis of confined water can be significantly modified for several reasons: (1) homogeneous kinetics can be disrupted or even prevented due to the confined space, which does not allow a homogeneous distribution of species after physicochemical stage of water radiolysis, (2) reactions between species from different cavities can be hindered or even precluded depending on the diameter of the cavity and/or the size of the openings to the cavity, (3) water confined in small cavities is in continuous contact with solid interface, creating a favorable environment for heterogeneous reactions, and last but not least, (4) the physical properties of water are altered. An attempt was made to elaborate theoretical models describing kinetics in nonhomogeneous systems. According to these models, a free diffusion of molecules within pores is assumed while the long-range transport of material is described as “pore hopping”, in which the activation energy is needed to penetrate pores or diffusion in an effective medium with a low diffusion coefficient [94]. Deformation of hydrogen bond network [95] and substantial reduction in mobility near surfaces has been observed [96]. In recent work, it was demonstrated that the confinement freezes the molecular motions and induce specific modifications of the hydrogen bond properties, not only near surfaces, but even in large pores [97]. By using molecular dynamics it was shown that depending on the type of silanol surface groups (fixed or movable) different patterns of interfacial hydrogen bonds can evolve, leading to different water behavior [98]. Solvation patterns of water depend on the pore size, with predominant cage-like structures in small cavities, and bulk-like structures in larger ones [99]. There are two types of confined water: (1) bound water strongly

interacting with confining material walls and (2) free water, located farther from a solid surface, with the bulk-like properties [100–102]. There is still a debate at what distance one can distinguish between the two types of water: 0.7 nm [103] or 0.4 nm [104]. All these differences on a microscale lead to differences in macroscopic properties of water, mostly in viscosity, which directly affects reaction kinetics. Viscosity of nanoconfined water can differ by a factor of two for small pores as compared to the bigger ones [105]. Furthermore, viscosity of confined water is not uniform across the pore, and simulations have shown that diffusion coefficient depends on the pore size.

Radiolysis of water in different porous materials such as zeolites, clays, porous silica, and mesoporous sieves has been performed by probing the yield of  $H_2$  [106–114]. These studies have shown that the radiolysis of water is different at and near solid interfaces than in the bulk water. In order to resolve the mechanisms of radiolytic decomposition, the better characterization of water molecules adsorbed or located near to solid surfaces is needed. The reader is referred for more details to the recent review chapter and references therein [6]. Recently, the radiolysis of water confined in montmorillonites was studied as a function of their composition, nature of the exchangeable cation, and the relative humidity aiming at elaboration of  $H_2$  production mechanisms [115]. It was found that the amount of water in the interlayer space is the key factor influencing the efficiency of  $H_2$ . The effect of the exchangeable cations was assigned to their hydration enthalpy. For a distance smaller than 1.3 nm, the radiation yield of  $H_2$  increases with the relative humidity, in another words, with the water amount. The cleavage of the O–H bond inside the clay layer leading to  $H$  atoms in interlayer space seems to account for the  $H_2$  production.

Recently, nanoporous metals have been used as specific surface materials to study radiolysis of confined water in the vicinity of metal surfaces [116, 117]. The behavior of radiolytic species forming during radiolysis in such “metallic nanosponges” may be relevant for explanation occurring in fissures during stress corrosion cracking. The radiation chemical yields of  $\cdot OH$  radicals formed in water confined in porous gold were compared to the radiation chemical yields in water confined in silica (with similar pore size) and in “bulk” water. The porous gold has a significant effect on the yield of  $\cdot OH$  radicals measured at short time scale, over sevenfold increase in comparison to the yield in the “bulk” water and confined in silica. Their yield on the longer time-scale is nearly suppressed, probably due to the reaction with the metal [116].

Similar observations were made for water confined in slits of stainless steel and nickel-base alloy [117]. For both materials, 2.5–3.5-fold increase of the yield of  $\cdot OH$  radicals at short time scale was measured, respectively. Interestingly, it was found that at the same scavenging time the yield of  $e_{aq}^-$  is significantly lower than the yield of  $\cdot OH$  radicals. This observation was tentatively rationalized by the scavenging of presolvated electrons by the lowest energy traps, which are the Fermi metal levels. As a consequence, this might shift the oxidative/reductive balance toward higher potential, which can have an impact on corrosion.

Direct probing of the time evolution of hydrated electrons formed in nanoconfined water in porous glasses with various pore diameters was performed by



nanosecond pulse radiolysis [118]. The following important conclusions can be derived from these experiments: (1) confinement enhances the encounter probability of reactive species what is reflected in higher reaction rates of the solvated electrons with decreasing pore size, going from  $6.8 \times 10^6 \text{ s}^{-1}$  in the bulk water to  $3.5 \times 10^7 \text{ s}^{-1}$  in a 1 nm pore, (2) electrons are likely hydrated in a part of pore with bulk-like properties, not on the surface what is supported by the similarity of the absorption spectrum recorded in a 1 nm pore to that in “bulk” water, (3) the yield of hydrated electrons is higher in confined water in comparison to “bulk” water, suggesting migrations of excitons to the surface where they dissociate injecting electrons in the confined water.

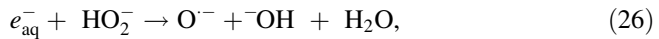
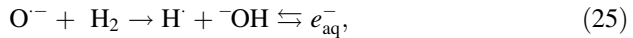
### 3.4 Radiolysis of Water in Cement-Based Materials

Radiolysis of water in cement-based materials is very poorly understood, though it has a huge impact on nuclear industry. In France, some nuclear wastes are stored in concrete canisters in which cement-based materials are constantly exposed to ionizing radiation, resulting in radiolysis of confined and residual water, and as a consequence to  $\text{H}_2$  production. These materials differ from those described previously. Portlandite, the naturally occurring form of calcium hydroxide, is a main product of Portland cement hydrolysis causing an increase of pH of adsorbed water up to 13. The structure of cement-based materials differs significantly due to different types of cement used and/or various manufacturing procedures. Nowadays, the most commonly used is Portland cement, which consists of  $>60\%$  CaO,  $>20\%$   $\text{SiO}_2$ ,  $7\%$   $\text{Al}_2\text{O}_3$ , and small amounts of other compounds ( $\text{MgO}$ ,  $\text{SO}_3$ ,  $\text{Fe}_2\text{O}_3$ ). A specific surface area varies significantly; however, it can be approximately estimated as  $400 \text{ m}^2/\text{kg}$  [119].

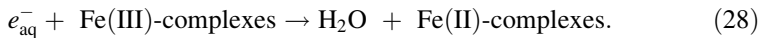
The cement-based materials undergo radiation damage, which depends on their structure and chemical composition. Different mineral additives change the cement paste phase composition by decreasing fraction of crystalline phases [e.g. portlandite (C–H)], increases that of the fraction of gel phases, e.g. tobermorite-like phases (C–S–H), and reduces the number of large pores [119–121]. Water, occupying pores in cement-based materials, is not pure since it contains a wide variety of mineral substances and exists in a constant equilibrium with the surrounding cement paste. The aforementioned solutions are strongly alkaline with pH values exceeding 13.

Combination of such extreme factors such as high pH, high irradiation dose rate, and confinement has a tremendous effect on radiolysis of water. There are not much experimental data addressing this issue, except for those in which influence of iron on formation of  $\text{H}_2$  was studied, and confronted with a model describing radiolytic processes in cement matrix [122–125]. An amount of  $\text{H}_2$  releasing during storage into the operational area is an important issue directly connected to the problem of safety. In order to identify the main “source” of  $\text{H}_2$ , a complete set of the reactions induced by radiolysis together with associated phenomena (e.g. precipitation, gaseous exchange) is necessary. This represents a serious challenge taking into account a composite and porous character of the cementitious materials where the pore water radiolysis is strongly affected by the gas and solid phases [122].

Reactions depicted in Eqs. (12) and (15) (*vide supra*) represent the chain reactions responsible for the consumption of  $H_2$  with the respective rate constants  $k_{12} = 4.2 \times 10^7 \text{ M}^{-1} \text{ s}^{-1}$  and  $k_{15} = 3.6 \times 10^7 \text{ M}^{-1} \text{ s}^{-1}$ . However, at high pH  $\approx 13$ , these reactions become faster since  $\cdot\text{OH}$  radicals and  $H_2O_2$  are replaced respectively by oxide radical anions  $O^{\cdot-}$  and peroxide anion  $HO_2^-$  (Eqs. 25, 26).



with the respective rate constants:  $k_{25} = 1.2 \times 10^8 \text{ M}^{-1} \text{ s}^{-1}$  and  $k_{26} = 3.5 \times 10^9 \text{ M}^{-1} \text{ s}^{-1}$ . A direct consequence of faster rates is a better efficiency in the consumption of  $H_2$  in this environment. This is beneficial since the quantity of  $H_2$  emitted within disposal sites for cemented radioactive wastes should be reduced. However, another aspect has to be taken into account, namely the presence of impurities. They can lower recycling capability of reactions depicted in Eqs. (25) and (26) and as a consequence reduce the rate of  $H_2$  and  $H_2O_2$  decomposition. One of the most frequently occurring impurities in cement-based materials are Fe(III) and Fe(II) complexes. They can be anticipated to interfere with  $O^{\cdot-}$  and  $e_{\text{aq}}^-$  reactions (Eqs. 25, 26) via reactions (Eqs. 27, 28):



Simulations of water radiolysis in cement-based materials containing Fe(III) and Fe(II) complexes using rate constants for  $k_{27} \approx 3.8 \times 10^9 \text{ M}^{-1} \text{ s}^{-1}$  and  $k_{28} \approx 6.0 \times 10^{10} \text{ M}^{-1} \text{ s}^{-1}$  confirmed this hypothesis [123]. Experimental data obtained in  $\gamma$ -irradiated hydrated tri-calcium silicate based cement containing amorphous iron oxy-hydroxide were successfully simulated [125], using CHEM-SIMUL application [122].

#### 4 Radiation-Induced Processes During Recycling of the Spent Nuclear Fuel

Worldwide production of nuclear wastes is estimated to be around 10,500 tons per year [1]. Therefore, management of spent nuclear fuel is a crucial issue of the modern nuclear industry. Fissionable elements produced in reactors as a result of neutron capture by uranium fuel can be re-used instead of being finally disposed in geological repositories. Recycling these elements reduces consumption of energy resources, costs of the uranium enrichment, simplifies and makes safer waste disposal, provides the potential for recovery of other useful elements from spent nuclear fuel, and significantly reduces a risk arising from long-term radiotoxicity and heat load of produced wastes [126]. Thus, it is necessary to separate highly radioactive isotopes from spent nuclear fuel and return them into a reactor for transmutation. Currently, two potential technologies are available for separation:

hydrometallurgy and pyrometallurgy [127]. This subchapter is focused on the former option. General hydrometallurgical separation can be achieved in four steps: (a) water pool storage of the spent nuclear fuel up to 5 years for cooling and removing of several undesired radioactive elements, (b) uranium and/or plutonium partitioning, (c) co-extraction of minor trivalent actinides and lanthanides, (d) selective extraction of trivalent actinides from trivalent lanthanides [7, 128]. Separation of plutonium and uranium from the spent nuclear fuel in various versions of plutonium uranium redox extraction (PUREX) has been used by the industry in several countries for many years [128, 129]. It significantly saves energy resources and reduces potential radiotoxicity hazard from wastes from approximately 250,000 (once-through cycle) to 10,000 years (twice-through cycle). Further reduction to about 300–400 years can be achieved by removing of minor actinides [126, 127, 130]. Currently the most promising systems for carrying out of this task are: European diamide extraction (DIAMEX) followed by regular selective actinide extraction (r-SANEX), innovative SANEX (i-SANEX), 1-cycle SANEX, grouped actinide extraction (GANEX), extraction of Americium (ExAm) [126, 127], as well as US variants transuranic extraction (TRUEX) followed by advanced trivalent actinide–lanthanide separation by phosphorous-reagent extraction from aqueous complexes (TALSPEAK) or actinide–lanthanide separation (ALSEP) systems [131].

All extraction systems mentioned above are subjected to the high energy radiation coming mostly from  $\alpha$ -emitters. Radiation chemistry of these systems may significantly affect separation processes in many ways. These include: decreasing of the extraction efficiency, loading capacity or separation factor due to ligand radiation degradation or accumulation of irradiation products, alteration of the oxidation state of extracting metal ions, changes of physical properties of the solvent (density, viscosity, third phase formation). This subchapter describes several aspects of radiation chemistry of extraction systems.

#### 4.1 Radiation Chemical Reactions Affecting Stability of Solvents Used in the Separation of Products of Fission

Absorption of the ionizing radiation takes place mainly in the constituent part of the extraction system with the largest abundance of electrons, i.e. water or organic diluents and leads to the formation of electron–radical cation pairs and excited states. It is well known that the dielectric constant ( $\epsilon$ ) of the solvent is a key factor affecting the recombination probability between the radical cation and the ejected electron and, as a consequence, an efficiency of the production of excited solvent molecules. This phenomenon can be described by the Onsager radius ( $R_s$ ), which is defined as the longest distance at which the attractive potential between the ejected electron and its parental radical cation overcomes their thermal energies, i.e.  $e^2/4\pi\epsilon\epsilon_0R_s = kT$  ( $k$ —Boltzmann's constant,  $T$ —temperature in K,  $e$ —electron charge,  $\epsilon_0$ —dielectric permittivity of vacuum) and thus leads to their recombination. In organic diluents used in nuclear applications (e.g. hydrocarbons, which are characterized by low  $\epsilon$ ), a large fraction of the ejected electrons thermalize before they can escape the Coulomb attraction of the positive charges. Therefore, the

majority of these electrons recombines with parental radical cations that results in the formation of the excited states. On the other hand, in diluents characterized by high  $\epsilon$  (alcohols, water) a higher efficiency of electrons or the respective radical ions is expected.

#### 4.1.1 Aqueous Phase

*Neat Water* Water is used as co-diluent in extraction processes during reprocessing of the spent nuclear fuel. In this case, water is mostly exposed to the irradiation of  $\alpha$ -emitters which is characterized by a high LET. The specific features of radiolysis of water with high LET irradiation are given in subchapter 2.4 (vide supra).

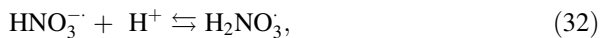
*Diluted Nitric Acid Solutions* In spent nuclear fuel reprocessing, aqueous phase acidified by nitric acid ( $\text{HNO}_3$ ) is generally used. Since the dissociation constant of  $\text{HNO}_3$  in water is relatively high  $pK_a = -1.4$  at  $25^\circ\text{C}$  [132], one can assume that  $\text{HNO}_3$  exists in diluted solutions in the form of ions ( $\text{H}^+$  and  $\text{NO}_3^-$ ). As a consequence, pH of the aqueous phase decreases, and  $e_{\text{aq}}^-$  are efficiently scavenged by  $\text{H}^+$  (vide Eq. 8) with  $k_8 = 2.3 \times 10^{10} \text{ day m}^3 \text{ mol}^{-1} \text{ s}^{-1}$  [133], and to some extent by  $\text{NO}_3^-$  (Eq. 29) with  $k_{29} = 9.7 \times 10^9 \text{ day m}^3 \text{ mol}^{-1} \text{ s}^{-1}$ : [133].



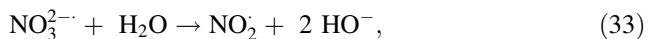
It is worth noting that  $\text{NO}_3^-$  anions react also with the prehydrated electrons;  $C_{37}$  value (defined as the concentration of scavenger that reduces the initial amount of  $e_{\text{aq}}^-$  by  $1/e = 37\%$ ) was reported as  $0.55 \text{ M}$  [134, 135]. Hydrogen atoms ( $\text{H}^\cdot$ ) resulted from the spur reaction depicted in Eq. (8) react also with  $\text{NO}_3^-$  with  $k_{30} = 1.0 \times 10^7 \text{ day m}^3 \text{ mol}^{-1} \text{ s}^{-1}$  (Eq. 30): [133].



Products of reactions (29) and (30) are in the following equilibria (Eqs. 31, 32):



with the respective  $pK_a$  values  $4.4$  and  $7.5$  [136]. These radicals undergo in subsequent reactions transformation to  $\text{NO}_2^\cdot$ , which is the main product of radiolysis in diluted solutions (Eqs. 33–35):



with the rate constants:  $k_{33} = 1.0 \times 10^3 \text{ s}^{-1} \text{ M}^{-1} \text{ s}^{-1}$ ,  $k_{34} = 2.0 \times 10^5 \text{ s}^{-1}$  and  $k_{35} = 7.0 \times 10^5 \text{ s}^{-1}$  [136, 137]. The  $\text{NO}_2^\cdot$  radicals were found to be rather mild oxidants with the reduction potential ( $\text{NO}_2^\cdot/\text{NO}_2^-$ ) within  $0.87\text{--}1.04 \text{ V}$  (vs. NHE)

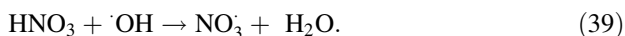
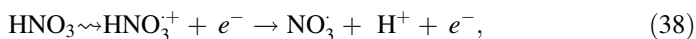
range [138]. They undergo recombination giving  $N_2O_4$ , a product that further slowly hydrolyses ( $k_{36} = 18 \text{ day m}^3 \text{ mol}^{-1} \text{ cm}^{-1}$ ) leading to nitric ( $HNO_3$ ) and nitrous ( $HNO_2$ ) acids (Eq. 36) [139, 140].



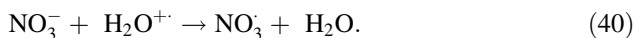
Formation of  $HNO_2$  has important consequences since this acid can affect oxidation states of actinides (vide infra) during extraction processes.

Interestingly, there is no evidence for the direct oxidation of  $NO_3^-$  anions by  $\cdot OH$  radicals [141].

*Concentrated Nitric Acid Solutions* In the nuclear waste reprocessing processes (e.g. PUREX or its various modifications), concentrated aqueous solutions of  $HNO_3$  are usually used. In these conditions one can expect direct ionization of  $HNO_3$  and  $NO_3^-$  as well as their secondary reactions with the primary products of water radiolysis. In contrast to dilute solutions, the most important intermediate formed in concentrated solutions of  $HNO_3$  is  $NO_3\cdot$  radical. This radical is a strong one-electron oxidant with the reduction potential ( $NO_3/NO_3^-$ ) of 2.45 V (vs. NHE) [138, 141]. Several mechanisms of  $NO_3\cdot$  radical formation have been proposed [142–144], including the following reactions (Eqs. 37–39):



The reactions depicted in Eqs. (37) and (38) represent direct effect of ionizing radiation on the nitric acid and its anion. On the other hand, reaction depicted in Eqs. (39) represents secondary reaction of  $\cdot OH$  radicals with undissociated  $HNO_3$  molecules, which takes place with the rate constant  $k_{39} = 1.4 \times 10^8 \text{ day m}^3 \text{ mol}^{-1} \text{ s}^{-1}$  [142]. An occurrence of these reactions has been recently confirmed by applying picosecond pulse radiolysis [145]. Moreover, a careful examination of  $NO_3\cdot$  yields led to the conclusion that the trapping of  $H_2O^{+\cdot}$  by  $NO_3^-$  (Eq. 40) contributes also to  $NO_3\cdot$  formation during the electron pulse:



Several reactions responsible for decay of  $NO_3\cdot$  radicals were suggested [146, 147]; however, recombination of  $NO_2\cdot$  and  $NO_3\cdot$  radicals (with  $k_{41} = 1.7 \times 10^9 \text{ day m}^3 \text{ mol}^{-1} \text{ s}^{-1}$ ) is currently recognized as the most important (Eq. 41):

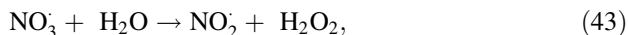


Decomposition of  $N_2O_5$  may lead to the nitronium ion ( $NO_2^+$ ) [148], which was found to be a very strong nitrating agent [149]. Recently reported studies have shown that for concentrated  $HNO_3$  solutions (7 M), radiolytically produced  $NO_3\cdot$  radicals are predominantly consumed by  $NO_2\cdot$  radicals (80 %) (Eq. 41) and  $HNO_2$

(15 %) (Eq. 42) with the respective rate constants  $1.1 \times 10^9 \text{ M}^{-1} \text{ s}^{-1}$  and  $2.0 \times 10^8 \text{ M}^{-1} \text{ s}^{-1}$  [150].



The following reactions are additional sources of the  $\text{NO}_2^\cdot$  radicals (beyond the aforementioned reactions 33–35, 42) (Eqs. 43, 44) in concentrated nitric acid solutions [151, 152]:



In turn, reaction Eq. (45) is an additional source (beyond aforementioned reaction 36) of  $\text{HNO}_2$ :



Evaluation of a total quantity of  $\text{HNO}_2$  generated in the radiolysis of  $\text{HNO}_3$  solutions poses many difficulties because of its low stability [153], and its reactivity towards  $\cdot\text{OH}$  [141],  $\text{NO}_3^\cdot$ , [142], and  $\text{H}_2\text{O}_2$  [154, 155]. Efficiency of some of these reactions depends on LET, dose, and dose rate. Therefore, a change of these parameters may open new reaction paths and create a complicated mix of competing reactions [1, 141]. Moreover, the system becomes even more complex, as far as the number of reactions is concerned, either after accumulation of stable products and/or addition of anti-nitrous agents (e.g. hydrazine). Hydrazine is used in PUREX process in order to inhibit  $\text{HNO}_2$  redox reactions with plutonium and as a consequence to promote efficient extraction in reprocessing solvent systems [156, 157]. It is worth mentioning that  $\text{NO}_3^\cdot$  radicals are able to react with hydrazine, which exists in highly acidic solutions as  $\text{N}_2\text{H}_5^+$  and  $\text{N}_2\text{H}_6^{2+}$ . The respective rate constants were found to be  $(2.9 \pm 0.9) \times 10^7 \text{ M}^{-1} \text{ s}^{-1}$  and  $(1.3 \pm 0.3) \times 10^6 \text{ M}^{-1} \text{ s}^{-1}$  [150].

*Effect on Physical Properties* Information about radiation chemistry impact on physical properties of aqueous phase in nuclear fuel cycle are rather sparse. Recent studies of aqueous phase containing  $\text{HNO}_3$  being in contact with 1-octanol/kerosene mixture (as the model i-SANEX diluents) showed virtually no effect of the radiation neither on viscosity nor density of the system up to the 120 kGy [158, 159].

#### 4.1.2 Organic Phase

*Hydrocarbons and Kerosene* Hydrocarbons and kerosene are usually used as diluents in nuclear solvent extraction. Kerosene is a mixture of hydrocarbons and its chemical composition depends on a source of origin. In principle, kerosene is a mixture of various hydrocarbons containing 10 up to 16 carbon atoms in a molecule. Its main components include linear and branched alkanes (paraffin hydrocarbons) with a molecular formula  $\text{C}_n\text{H}_{2n+2}$  and cyclic hydrocarbons (cycloparaffins/naphthenes) with a molecular formula  $\text{C}_n\text{H}_{2(n+1-g)}$  where n and g denote the number of carbon atoms and number of rings in a molecule, respectively.

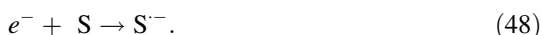
Radiolysis of various hydrocarbons have been studied thoroughly using steady state  $\gamma$ -radiolysis and pulse radiolysis. There are several comprehensive reviews and books, which discuss this topic in a detailed manner [160–164]. Radiolysis of hydrocarbons (RH) produces excited states ( $\text{RH}^*$ ) and electron–hole pairs ( $e^-$ ,  $\text{RH}^+$ ) (Eq. 46):



Because of the low dielectric constant of hydrocarbons (long Onsager radius), a substantial fraction of initially generated electrons undergo geminate recombination yielding excited molecules (Eq. 47):

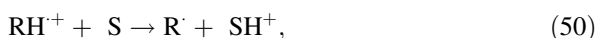
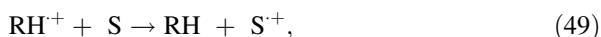


The remaining electrons escape ion recombination and can be either stabilized in a relatively shallow traps (absorption spectrum in near IR region) [165, 166], or in the presence of solute (S), they can react forming solute radical anions Eq. 48):



The reported  $G$  values of trapped electrons ranged between 0.031 and 0.092  $\mu\text{mol J}^{-1}$  and depend on the structure of alkane [165–168].

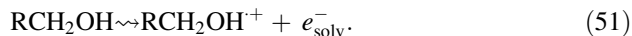
The solvent holes (ionized molecules) are highly mobile and they can undergo several ion–molecule reactions including charge (Eq. 49) and proton (Eq. 50) transfer reactions with solute (S):



The rate constants of charge transfer processes are very high:  $(1\text{--}5) \times 10^{12}$  - day  $\text{m}^3 \text{mol}^{-1} \text{s}^{-1}$  for reactions depicted in Eq. 49 and  $(10^{10}\text{--}10^{11})$  day  $\text{m}^3 \text{mol}^{-1} \text{s}^{-1}$  for reactions depicted in Eq. (50) [163]. The spectral and kinetic properties of cationic transients generated radiolytically in long chain alkanes were addressed in an original paper [169]. Solvent holes can also undergo deprotonation or dissociation yielding  $\text{H}^+$ ,  $\text{H}^{\cdot}$  and C-centered radicals, respectively.

Excited molecules ( $\text{RH}^*$ ) dissociate mostly by a homolytic cleavage of the C–H bonds. A cleavage of C–C bond is also possible, however, with lower probability. Reported  $G(\text{H}^{\cdot})$  and  $G(\text{H}_2)$  values in the  $\gamma$  and  $e^-$ -beam irradiated liquid  $n$ -alkanes are  $\approx 0.070 \mu\text{mol J}^{-1}$  [170], and in the range of 0.43–0.55  $\mu\text{mol J}^{-1}$  [171–173], respectively. The amount of  $\text{H}_2$  generated is lower for branched alkanes (e.g. 0.21  $\mu\text{mol J}^{-1}$  for 2,2-dimethylbutane) [171], and alkenes (e.g. 0.83  $\mu\text{mol J}^{-1}$  for 1-hexene [174]. Aromatic hydrocarbons are significantly more stable towards radiation than aliphatic hydrocarbons [e.g.  $G(\text{H}_2)$  for benzene is equal to  $\approx 0.004 \mu\text{mol J}^{-1}$ ] [175]. The stabilization effect of the aromatic ring can extend to the alkyl groups in the same molecule [176], or even to aliphatic compounds present in a mixture with aromatic compounds [171]. Thus, a variation in the content of commercially available kerosene may alter  $G(\text{H}_2)$  values (radiation stability) of extraction systems.

*Alcohols* Alcohols represent an important class of potential diluents in reprocessing of nuclear wastes. For instance, 1-octanol in a mixture with liquid alkanes is very often used to study separation chemistry of minor actinides. Radiolysis of neat alcohols leads to the formation of the alcohol positive ions and solvated electrons ( $e_{\text{solv}}^-$ ) (Eq. 51):



Generally,  $G(e_{\text{solv}}^-)$  in *n*-alcohols are in the range from 0.073 to 0.21  $\mu\text{mol J}^{-1}$  [177, 178]. The hole undergoes a fast ion–molecule reaction with the intact alcohol molecule, which leads mostly to the C-centered radicals with reducing properties (Eq. 52):



The presence of highly reducing  $e_{\text{solv}}^-$  and C-centered radicals with a simultaneous absence of oxidizing species favors reducing conditions in these media.  $G(\text{H}_2)$  values in  $\gamma$ -irradiation of liquid *n*-alcohols vary between 0.46 and 0.56  $\mu\text{mol J}^{-1}$  [171].

Contrary to hydrocarbons, solubility of water and  $\text{HNO}_3$  is relatively high in alcohols. For instance, concentration of water and  $\text{HNO}_3$  in 1-octanol contacted with 1 M aqueous solution of  $\text{HNO}_3$  is ranged between 4.7 and 5.05 % (by weight) [179, 180], and  $\sim 90$  mM [181], respectively. Therefore, direct ionization of  $\text{HNO}_3$  and  $\text{H}_2\text{O}$  molecules is possible in this system, which leads to  $\text{NO}_2$ ,  $\text{NO}_3$ , and  $\cdot\text{OH}$  radicals. These radicals can react with alcohol molecules. The rate constants of reactions involving  $\cdot\text{OH}$  and  $\text{NO}_3$  radicals with 1-octanol in water were found to be  $5.2 \times 10^9 \text{ day m}^3 \text{ mol}^{-1} \text{ s}^{-1}$  [182], and  $5.8 \times 10^6 \text{ day m}^3 \text{ mol}^{-1} \text{ s}^{-1}$  [183], respectively. These reactions may lead to changes of physical properties of extraction system due to the radical recombination forming products with higher molecular weight [184]. For example, a slight change in viscosity was observed in organic phase of i-SANEX system after delivery of 120 kGy [159].

In a summary, taking into account that extraction processes occur in the biphasic, aerated, and acidic systems, which are exposed to  $\alpha$ ,  $\gamma$ , and neutron irradiation, the following reactive species can be considered as the most important:  $\cdot\text{OH}$ ,  $\text{NO}_3$ ,  $\text{NO}_2$  radicals,  $\text{H}_2\text{O}_2$ ,  $\text{HNO}_2$  molecular products, which are produced in aqueous phase containing  $\text{HNO}_3$ , and C-centered radical and radical cations, which are formed in the organic phase [3].

*Ionic Liquids* Ionic liquids (ILs) are salts consisting entirely of ions with a melting point below 100 °C. They have recently attracted a lot of attention as a new class of environmentally friendly solvents. Among various applications, they can be used in the nuclear fuel cycle [185–197]. A recent review covers main achievements in this field [192]. ILs can be divided into groups depending on the cation structure. In principle, ILs based on aromatic cations (e.g. imidazolium and pyridinium) reveal elevated radiation resistance in comparison to aliphatic ammonium and phosphonium cations [198–201]. For instance, the radiation chemical yields of cation and anion decomposition for 1-butyl-3-methylimidazolium bis(trifluoromethylsulfonyl)imide (MBIm NTf<sub>2</sub>) were found to be 0.28(2) and 0.22(2)  $\mu\text{mol J}^{-1}$ ,



respectively. [200] On the other hand, the respective radiation chemical yields for tributylmethylammonium bis(trifluoro-methylsulfonyl)imide ( $\text{MB}_3\text{N NTf}_2$ ) were found to be equal to 0.38 and  $0.25 \mu\text{mol J}^{-1}$ . [199] Similar tendency was observed for molecular hydrogen generation. The  $G(\text{H}_2)$  values for  $\text{MB}_3\text{N NTf}_2$  and  $\text{MBIm NTf}_2$  are equal to 0.032(4) [202] and  $0.018 \mu\text{mol J}^{-1}$  [200], respectively. The main difference between these two cations lies in the scavenging capability of excess electrons. In ILs containing imidazolium moiety, the lifetime of electrons was found to be less than 1 ps [203].

Radiation stability of ILs depends also to a certain extent on their anions. Radiolytic yields of cation and anion decomposition for imidazolium salts with various anions were in range  $-0.28(2)$  to  $-0.37(3) \mu\text{mol J}^{-1}$  and from  $-0.10(1)$  to  $-0.22 \mu\text{mol J}^{-1}$ , respectively [200].

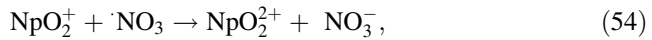
Some attempts have been made to improve radiation stability of ILs by modification of their cation structures. Substantial reduction of  $G(\text{H}_2)$  values has been obtained by replacing of alkyl substituent by benzyl one in ammonium, pyrrolidinium, and imidazolium ILs [202]. On the other hand, benzyl substituted cations undergo reaction with electrons, which leads to an irreversible damage of cations and as a consequence significantly lowers radiation stability of ILs. This unwanted reaction was not observed for 1-benzylpyridinium cation [204].

## 4.2 Radiation Chemical Reactions Affecting Oxidation States of Actinide Metal Ions

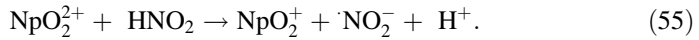
The possibility to alter the oxidation state of extracting metal ions by radiolytic products of concentrated aqueous solutions of  $\text{HNO}_3$  is a crucial issue for reprocessing of spent nuclear fuel. Highly extractable ions can become virtually not extractable by changing their oxidation states. In spite of the fact that  $e_{\text{aq}}^-$  are relatively reactive with actinide ions [1, 205], their reactions in extraction systems are either unlikely or limited. The reactions of  $e_{\text{aq}}^-$  with metal ions in aerated and very strong acid environment will be suppressed due to fast reactions depicted in Eqs. (8) and (11) (vide supra). On the other hand, the reactions of  $\cdot\text{OH}$  radicals depend on the extent to which they are scavenged by solvent extraction diluents like alkanes or alcohols, which typically react at rates of  $10^9 \text{ day m}^3 \text{ mol}^{-1} \text{ s}^{-1}$ .

The most spectacular and carefully investigated system was redox chemistry of neptunium (Np) ions [206], which was also reviewed recently [1, 3]. Interaction of tetra- $(\text{Np}^{4+})$  and particularly hexavalent  $(\text{NpO}_2^{2+})$  ions with products of radiation induced reactions may result in non-extractable pentavalent  $(\text{NpO}_2^+)$  state [130]. Np redox chemistry was successfully modeled using standard reactions occurring in irradiated aqueous systems and confronting results with experimental data obtained in water solutions containing 4 M  $\text{HNO}_3$  [206]. The following most important conclusions can be drawn: (1) in the early stages of irradiation, oxidation of  $\text{NpO}_2^+$  by  $\cdot\text{OH}$  and  $\cdot\text{NO}_3$  radicals (Eqs. 53, 54) is predominant:





(2) at longer irradiation time when  $\text{HNO}_2$  was accumulated, reduction of  $\text{NpO}_2^{2+}$  back to  $\text{NpO}_2^+$  (Eq. 55) is dominant:



It has to be stressed, at this point of exposition, that these results accounted only for reactions in aqueous phase. The presence of the organic phase in the form of diluents might affect redox reactions in this system, by scavenging  $\cdot\text{OH}$  radicals.

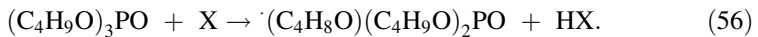
Similar features can be expected in plutonium (Pu) and americium (Am) redox chemistry since these elements have also multivalent oxidation states in aqueous solutions of  $\text{HNO}_3$  [207]. These aspects were recently reviewed [3].

### 4.3 Radiation Chemical Reactions Affecting Stability of Solvent Extraction Ligands

#### 4.3.1 Organophosphorous Compounds

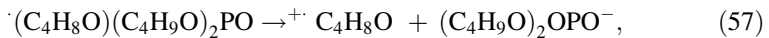
*TBP* Tributylphosphate ( $\text{TBP}$ ,  $\text{C}_4\text{H}_9\text{O}_3\text{PO}$ ) is the most frequently used extracting agent in the nuclear industry. It has been used for many years in the PUREX process or its modifications. In general, the liquid organic phase contains 30 % of *TBP* diluted in alkanes. Gaseous products ( $\text{H}_2$  and  $\text{CH}_4$ ) and dibutylphosphoric acid [*HDBP*,  $(\text{C}_4\text{H}_9\text{O})_2\text{OPOH}$ ] were identified as the main products of its degradation. Formation of the latter product has adverse effects on solvent extraction. For this reason, radiation chemistry of *TBP* was extensively studied.

The rate constants for the reactions of  $\cdot\text{H}$ ,  $\cdot\text{OH}$ ,  $\cdot\text{NO}_3$ , and  $\cdot\text{NO}_2$  radicals with *TBP* (Eq. 56), which involve abstraction of H atoms, and  $\text{X} = \cdot\text{H}$  (Eq. 56);  $\cdot\text{OH}$  (Eq. 56);  $\cdot\text{NO}_3$  (Eq. 56); and  $\cdot\text{NO}_2$  (Eq. 56) were determined [208].

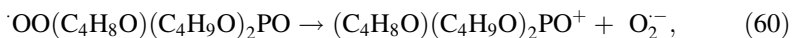


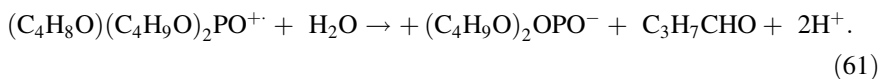
They are equal to:  $1.8 \times 10^8 \text{ day m}^3 \text{ mol}^{-1} \text{ s}^{-1}$ ,  $5 \times 10^9 \text{ day m}^3 \text{ mol}^{-1} \text{ s}^{-1}$ ,  $4.3 \times 10^6 \text{ day m}^3 \text{ mol}^{-1} \text{ s}^{-1}$  and  $<2 \times 10^5 \text{ day m}^3 \text{ mol}^{-1} \text{ s}^{-1}$ , respectively.

*HDBP* is a product of the  $\cdot(\text{C}_4\text{H}_8\text{O})(\text{C}_4\text{H}_9\text{O})_2\text{PO}$  radical decay via fragmentation (Eq. 57) [209], and/or hydrolysis reactions (Eq. 58) [210].



In the presence of  $\text{O}_2$ , the respective peroxy radical is formed (Eq. 59), which in subsequent reactions (Eqs. 60, 61) is transformed to *HDBP* [211].





Since the concentration of TBP is relatively high in the extraction system, its direct ionization resulting in  $\text{TBP}^+$  can be considered. In addition, formation of  $\text{TBP}^+$  can be achieved by a charge transfer from the diluent “holes”. Its degradation mechanism is not clear; however, HDBP was found as a main product of  $\text{TBP}^+$  fragmentation [212]. The possibility of charge transfer involving TBP and diluent “holes” implied that for diluents with low ionization potential degradation of TBP should be reduced. This has been recently confirmed [213, 214].

Integration of HDBP reactions to the overall degradation mechanism of TBP is necessary. This is due to accumulation of HDBP at high absorbed doses. The reported  $G$  values of HDBP in 30 % TBP alkane solution in contact with  $\text{HNO}_3$  ranged from 0.06 to 0.11  $\mu\text{mol J}^{-1}$  [3]. The radiation-induced degradation path of HDBP is very similar to that presented for TBP and involves H-atom abstraction by  $\cdot\text{H}$ ,  $\cdot\text{OH}$ ,  $\cdot\text{NO}_3$ , and  $\cdot\text{NO}_2$  radicals. The respective rate constants are:  $1.1 \times 10^8$  - day  $\text{m}^3 \text{mol}^{-1} \text{s}^{-1}$ ,  $4.4 \times 10^9$  day  $\text{m}^3 \text{mol}^{-1} \text{s}^{-1}$ ,  $2.9 \times 10^6$  day  $\text{m}^3 \text{mol}^{-1} \text{s}^{-1}$ , and  $<2 \times 10^5$  day  $\text{m}^3 \text{mol}^{-1} \text{s}^{-1}$  [208]. The decay of the C-centered radical [ $(\text{C}_4\text{H}_8\text{O})(\text{C}_4\text{H}_9\text{O})\text{OPOH}$ ] formed in these reactions leads to monobutylphosphoric and phosphoric acids, eventually.

In addition,  $\cdot\text{NO}_2$  and  $\cdot\text{NO}_3$  radicals may recombine with radicals generated in reactions (56) and their analogs [215].

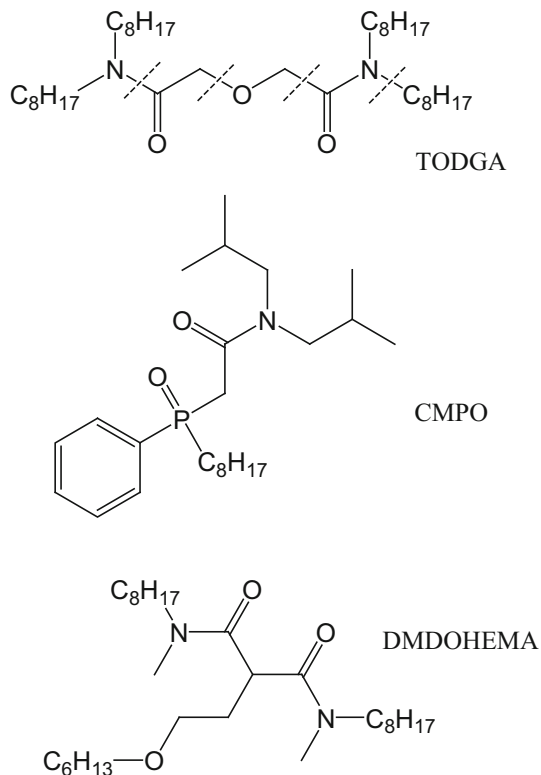
Various phosphoric acids as well nitrophosphates generated in these reactions are highly undesirable products due to their adverse effects on performance of extraction and a third phase formation [184, 216].

*CMPO* Octylphenyl-*N,N*-diisobutylcarbamoylmethyl phosphine oxide (CMPO) is a complexing agent proposed for TRUEX process. Since CMPO contains an amidic functional group (Fig. 4, middle) its radiation chemistry is similar to amidic compounds (vide infra). A cleavage of amidic C–N bond resulting in formation of the respective amines and carboxylic acids has been reported in irradiated alkane solution in contact with an aqueous phase containing  $\text{HNO}_3$  [8, 217–219]. Details concerning radiolysis products, radiation chemical yields, influence of LET can be found in several original papers [3, 220, 221] and reviews [1, 3, 8].

#### 4.3.2 Amidic Compounds

*TODGA* (*N,N,N,N'*-tetraoctyldiglycolamide) (TODGA) is currently considered one of the promising ligands for co-extraction of minor actinides and lanthanides in DIAMEX, GANEX, and SANEX processes [222]. The most important products of its radiation degradation are: n-octan, *N,N,N*-trioctyldiglycolamide ( $\text{C}_{\text{side-chain}}\text{-N}$  scission); *N,N*-dioctylamine, 5-(*N,N*-dioctyl)-amido-3-oxopentanoic acid ( $\text{N-C}_{\text{carbonyl}}$  scission); *N,N*-dioctylglycolamide, *N,N*-dioctylacetamide ( $\text{C-O}_{\text{ether}}$  scission); and to a lesser extent *N,N*-dioctylformamide and *N,N*-dioctyl-2-methoxy-acetamid ( $\text{C-C}_{\text{carbonyl}}$  scission) [223–226]. They are the result of the bond scissions shown in Fig. 4, top.

**Fig. 4** Structures of TODGA, CMPO, and DMDOHEMA



All of these products show low distribution ratio of Am(II) and Eu(III), explaining deterioration of extraction efficiency of the irradiated system [224]. Dose constant ( $d$ ) for degradation of TODGA in *n*-dodecane decreases from  $5.8 \times 10^{-6}$  to  $5.8 \times 10^{-7} \text{ Gy}^{-1}$  with ligand concentration increasing from 0.01 to 1.57 M [227]. The parameter  $d$  can be obtained from the slope of the lines by using the following equation:  $C = C_0 \exp(d \times D)$  where the  $C$  and  $C_0$  are the concentration of TODGA before and after irradiation and  $D$  is a dose delivered to the system. A presence of  $\text{HNO}_3$  in the system has no effect on the dose constant of TODGA; however, it alters product ratio [224, 225]. It is believed that charge transfer reaction between alkene radical cation (diluent holes) and TODGA initiates fragmentation of the ligand [223, 227]. The rate constant of this reaction for *n*-dodecane radical cation was reported to be equal to  $(10 \pm 1) \times 10^9 \text{ day m}^3 \text{ mol}^{-1} \text{ s}^{-1}$  [223]. Surprisingly, a replacement of *n*-dodecane by 1-octanol does not affect the dose constant parameter ( $d$ ), suggesting an existence of another process that initiates fragmentation of TODGA [227].

**DMDOHEMA** Dimethyl-di(2-octyl)hexyl-ethoxymalonamide (DMDOHEMA) (Fig. 4, bottom) is another important ligand proposed for DIAMEX process [1, 3]. Several radiolytic degradation products were identified, among them respective amine (methyloctylamine), amides (dimethyloctyl-2-hexyloxyethyl malonamide, and methyl-di(2-octyl)hexyl-2-hexyloxyethylmalonamide), amidocarboxylic

acids (methoxyoctylcarbonyl 4-hexyl butanoic acid), and monoamide (methylhexyloxybutanamide) [218, 228].

#### 4.3.3 Bis-Triazinylpyridines and Their Derivatives

**BTPs** Bis-Triazinylpyridines (BTPs) ligands (Fig. 5, left) were proposed for selective separation of minor actinides from lanthanides in the SANEX system. This was the first attempt applying intentional structural modifications to develop and improve properties of molecules to adopt into the nuclear fuel cycle [222]. The first generation of BTPs [e.g. 2,6-bis(5,6-dialkyl-1,2,4-triazin-3-yl)pyridine] (Fig. 4, left) was susceptible to oxidative and radiolytic degradation [229]. Since degradation starts from the H-atom abstraction at  $\alpha$ -CH<sub>2</sub> position of the triazin alkyl substituent, efforts have been made to replace them with groups less susceptible to hydrogen abstraction [229]. Especially, substituents without H atoms at vulnerable positions have been tested. A compromise between stability, solubility and extraction capabilities of newly designed molecules was found for cyclohexyl moieties substituted with methyl groups in the benzylic positions (CyMe<sub>4</sub>). Furthermore, in order to eliminate problems with stripping back metal ions, the improved structure based on a bipyridine skeleton was designed as CyMe<sub>4</sub>-BTBP (Fig. 5, right).

**CyMe<sub>4</sub>-BTBP** The 6,6'-bis(5,5,8,8-tetramethyl-5,6,7,8-tetra-hydro-benzo-1,2,4-triazin-3-yl)-2,2'-bi-pyridine (CyMe<sub>4</sub>-BTBP) ligand is currently considered a European standard for development of selective actinide separation [229, 230]. Its relatively significant deterioration of extraction performance was observed in 1-octanol exposed to irradiation [230]. Various radiolytic products have been detected by HPLC–MS indicating decomposition of ligands and saturation of aromatic structure double bonds resulting in an impairment of complexation ability. Surprisingly, deterioration of distribution ratios and separation factors in systems in contact with an aqueous phase containing 1 M HNO<sub>3</sub> (resulting in ~90 mM HNO<sub>3</sub> in organic phase) was negligible up to 300 kGy [181]. Adduct of 1-octanol to CyMe<sub>4</sub>-BTBP molecule was the only detected product with significant abundance. Apparently, this product does not affect extraction efficiency since it is probably formed by an addition of 1-octanol derived carbon-centered radicals at the site of a ligand that is located outside of a tetradentate binding pocket. Similar protection effect on BTP was observed in the presence of nitrobenzene [231]. Since both HNO<sub>3</sub> and nitrobenzene are good electron and H atom scavengers, it is believed that these latter species are involved in degradation of both ligands.

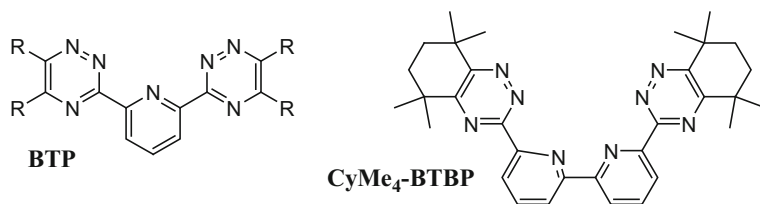


**Fig. 5** Structures of BTP and CyMe<sub>4</sub>-BTBP

The reaction of solvated electrons ( $e_{\text{solv}}^-$ ) with BTP and BTBP derivatives in 1-octanol were measured and found to be very fast. They ranged from  $1.3 \times 10^9$  -  $\text{day m}^3 \text{ mol}^{-1} \text{ s}^{-1}$  to  $2.4 \times 10^9$   $\text{day m}^3 \text{ mol}^{-1} \text{ s}^{-1}$ , depending on a ligand [232].

#### 4.4 Radiation Chemical Reactions Leading to H<sub>2</sub> Generation

Molecular hydrogen generation (H<sub>2</sub>) should not affect capability of the extraction system. However, H<sub>2</sub> formation is of some importance because of safety issues due to its high flammability. For this reason, a lot of attention was paid to evaluate *G* values of gaseous products formed during irradiation of aqueous solutions containing HNO<sub>3</sub> [141]. For instance, an amount of H<sub>2</sub> decreases with HNO<sub>3</sub> concentration due to scavenging reactions of H<sub>2</sub> precursors (vide supra Eqs. 29, 30). On the other hand, an organic phase, which may be partially dissolved in an aqueous phase can increase efficiency of H<sub>2</sub> generation. It was observed during *e*-beam irradiation of an aqueous phase being in contact with 1-octanol/kerosene (organic phase for SANEX system) [179].

### 5 Radiation-Induced Processes During Geological Disposal of Spent Nuclear Fuel

Final disposal of spent nuclear fuel is one of the main challenges for the nuclear industry. The conditions in repositories are not so extreme, as far as high temperatures, pressures, and intense fluxes of radiation are concerned. However, the time frame for safe performance is a key issue. This approach is based on multiple massive barriers, which should prevent a release of radioactive material into the geosphere and ultimately into the biosphere (Fig. 6).

The first barrier is a cladding material of the capsule where the spent nuclear fuel is sealed, and which usually is a zircalloy. The second barrier is a waste package into which the capsules are placed. In some concepts, copper-coated carbon steel canisters are going to be used. The third barrier is a buffer material in which canisters are embedded. Currently, bentonite is the most commonly available material for this purpose. Montmorillonite, which is a smectite mineral, is the main component of bentonite and is characterized by low permeabilities, high sorption capacities and dissipation of heat, properties which are essential for the efficacy of a buffer material as an engineered barrier.

Knowledge related to interfacial radiation chemistry is essential to understand radiation-induced surface processes in geological repositories. Nuclear wastes stored as powders in sealed containers can accumulate water from the humid environment. An understanding of the radiolytic processes in water is important for the safe long-term storage of nuclear waste. These include, for instance, corrosion of cladding material (zircalloy) and copper canisters, production of H<sub>2</sub> and/or potentially explosive mixtures of H<sub>2</sub> and O<sub>2</sub>, as well of HNO<sub>3</sub>, production and decomposition of H<sub>2</sub>O<sub>2</sub> on the fuel and metal oxide surfaces, dissolution of spent nuclear fuel and alterations of bentonite clay in contact with ground water also in case of barrier failures.

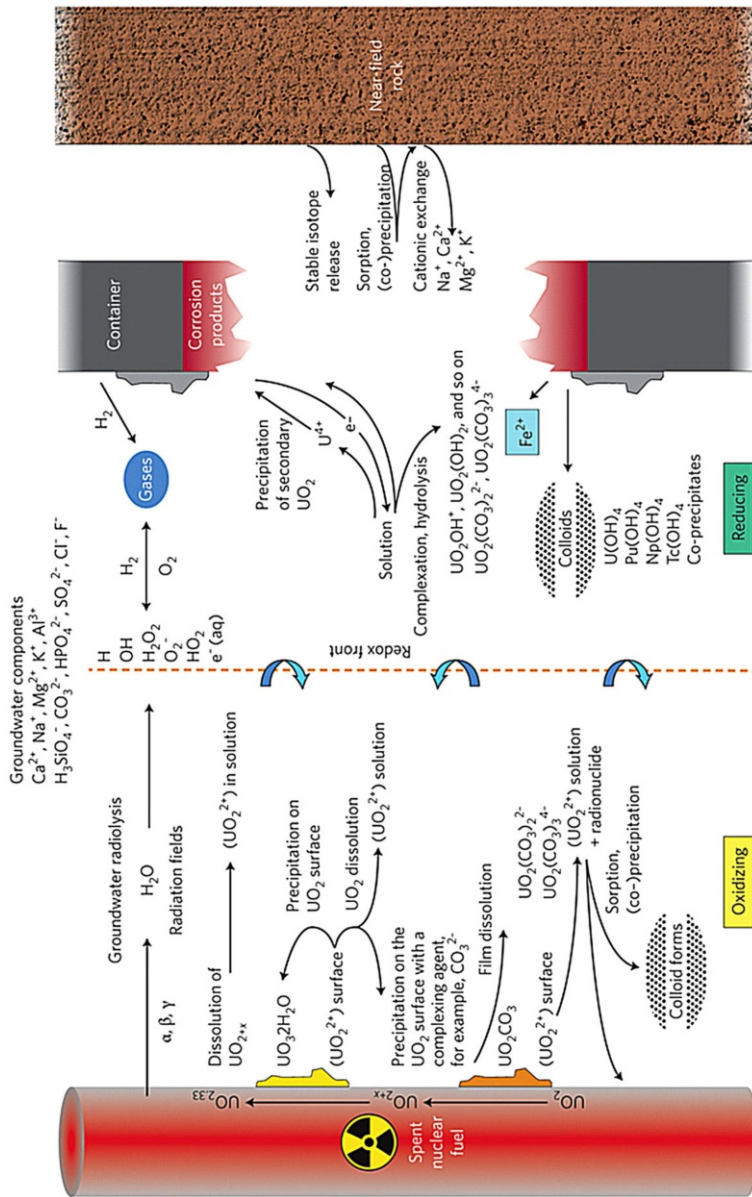


**Fig. 6** Chemical processes that may affect the alteration of spent fuel in contact with groundwater. Schematic representation of spent fuel alteration mechanisms and mechanisms controlling radionuclide concentration in solution in the near-field environment of the fuel, including groundwater, corroded waste package, backfill (if present), and surrounding rock. This figure assumes that the conditions are oxidizing or that radiolysis of the water has resulted in oxidizing conditions near the surface of the fuel. In principle, all of these reactions could be modelled by geochemical reaction path calculations; however, many of the necessary parameters are unknown. Reprinted with permission from [233]



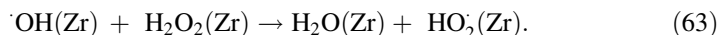
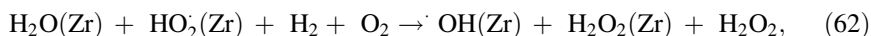
In recent years several comprehensive and critical reviews addressing interfacial radiation chemistry were published [1, 4, 6, 234–236]. The reader is referred to them and references therein for details, which cannot be covered in depth here. The following sections address only the most important findings and highlight the very recently published results.

### 5.1 Radiation-Induced Processes Related to Corrosion of Cladding Materials and Copper-Coated Iron Canisters

Corrosion in repositories influences the lifetime of the cladding material of the capsule and can pose a potential safety hazard. Zircalloy is a cladding material used in the capsules where the spent nuclear fuel is sealed and under normal operation is covered by  $ZrO_2$  layer. Hence, radiation-induced processes at the interface between water and solid oxide are crucial.

The reactivity of  $\cdot OH$  radicals formed on the  $ZrO_2$  surface via catalytic decomposition of  $H_2O_2$  was studied. A site-specific mechanism of  $H_2O_2$  decomposition was proposed and further used for numerical simulations of the dynamics of the reaction system [237].

Recently, the behavior of aqueous  $H_2$  and  $O_2$  in contact with  $ZrO_2$  surface was studied. It was found that all molecular products from water radiolysis are involved in a very peculiar catalytic cycle, which consists of two steps displayed in Eqs. (62) and (63):



This mechanism was supported by the DFT calculations [238].  $ZrO_2$  catalyzes the reaction between  $H_2$  and  $O_2$  dissolved in water. The surface-catalyzed reaction produces  $H_2O_2$ , which is subsequently decomposed to  $\cdot OH$  radicals on the  $ZrO_2$  surface. The mechanism involves a surface-bound  $HO_2$  radical, which catalyzes H atom transfer from  $H_2$  to  $O_2$ .

Radiation-induced corrosion of copper has been studied very occasionally, and results of these studies were not conclusive and, at worst, contradicted each other [4]. For this reason, the studies of radiation-induced corrosion of copper under controlled conditions were undertaken [239, 240]. The experiments performed in anoxic conditions showed that the dissolution of copper as well as formation of the main corrosion product ( $Cu_2O$ ) increased with the absorbed dose. Interestingly, exposure of copper to  $H_2O_2$  did not result in any release of copper into solution. Numerical simulations indicated that radiation-induced corrosion of copper is caused only to a small extent by radiolysis of water [239]. However, two radiolysis products,  $H_2O_2$  and  $\cdot OH$  radicals, should be thermodynamically capable of corroding copper. Recent studies of reactions between  $H_2O_2$  and copper and copper oxides in the form of powders reveal formation of surface bound  $\cdot OH$  radicals [240], originated presumably from catalytic decomposition [241, 242]. In the presence of copper oxides, the kinetics of  $H_2O_2$  consumption is more complex than for the redox-inert oxides.

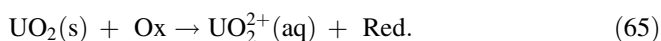


The topic directly related with radiation-induced corrosion in stainless steel containers and oxidation of copper containers and connected to H<sub>2</sub> production was discussed earlier (vide 3.2) [80, 81].

## 5.2 Radiation-Induced Processes Related to Dissolution of Spent Nuclear Fuel

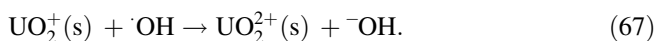
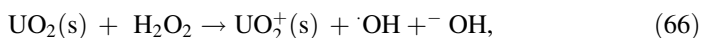
Radiation-induced dissolution of spent nuclear fuel and the consequential release of radionuclides into ground waters are key-processes, which have to be taken into account in the safety analysis of deep geological repositories. In order to understand these processes, many experimental and modelling studies have been performed over recent decades using both spent fuel and various types of materials, which imitate the real spent fuels. In recent years, several critical reviews and articles have been published addressing these issues, mostly parameters that are responsible for radiation-induced dissolution as well those which inhibit this process [4, 234, 235, 243].

The spent nuclear fuel consists mainly of 95 % UO<sub>2</sub>, and the remaining 5 % is fission products and heavier actinides. In principle, UO<sub>2</sub> is poorly dissolved in water; however, upon its oxidation the significantly more soluble U(VI) is formed. Therefore, oxidation is considered the main pathway leading to dissolution of UO<sub>2</sub>. The mechanism of oxidative dissolution of UO<sub>2</sub> can be generally described by the following reactions (Eqs. 64, 65):



In connection with these reactions the following key questions have to be raised: (1) what species and parameters are responsible for fuel matrix dissolution, and (2) what parameters control the fuel dissolution rate?

It has turned out that H<sub>2</sub>O<sub>2</sub> is the most important oxidant in spent fuel dissolution [244, 245]. The mechanism for UO<sub>2</sub> oxidation by H<sub>2</sub>O<sub>2</sub> is described by the following reactions (Eqs. 66, 67):



The  $\cdot\text{OH}$  radicals formed in the reaction depicted in Eq. (62) are very reactive towards the UO<sub>2</sub> surface and presumably react at the site of its formation (Eq. 63) [246]. The calculated rate constants for reactions between UO<sub>2</sub>(s) and oxidizing radiolytic products were given, [244, 246, 247] which allows simulation of radiation-induced dissolution of UO<sub>2</sub> and spent nuclear fuel [248–250].

The influence of HCO<sub>3</sub><sup>-</sup> anions on the kinetics of UO<sub>2</sub> oxidation (consumption of H<sub>2</sub>O<sub>2</sub>) and UO<sub>2</sub> dissolution was studied qualitatively. It was shown that the rates of both processes increased with increasing concentration of carbonate anions. The

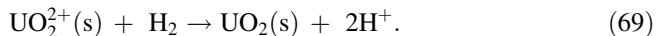
observed trend in the rate of dissolution can be rationalized in terms of formation of soluble complexes between  $\text{HCO}_3^-$  and  $\text{UO}_2^{2+}$  [247].

Interestingly, it was found that in  $\text{UO}_2$  powdered suspensions only 80 % of the consumed  $\text{H}_2\text{O}_2$  leads to the oxidative dissolution of  $\text{UO}_2$ , according to reactions depicted in Eqs. (66) and (67) [251]. The remaining 20 % is supposed to be consumed by surface-catalyzed decomposition (Eq. 68):



Comparison of  $\text{UO}_2$  dissolution in pure  $\text{UO}_2$  pellets with the  $\text{UO}_2$  pellets doped with rare earth oxides ( $\text{Y}_2\text{O}_3$ ) (SIMFUEL) showed almost no  $\text{UO}_2$  dissolution in the latter case [252]. In order to explain this observation a series of papers reporting experiments with  $\text{UO}_2$  pellets doped with  $\text{Y}_2\text{O}_3$  was published [253–255]. Doping seems to alter the ratio between the rate constants  $k_{60}$  and  $k_{62}$ . However, it is not known currently whether the presence of dopants affects one or both of the possible reactions. It should be stressed that the main effect of doping was rather a lower redox reactivity of the solid towards oxidants [254, 255].

Earlier studies showed that radiation-induced dissolution of spent nuclear fuel is inhibited in the presence of  $\text{H}_2$  [243].  $\text{H}_2$  is produced by radiolysis of water and also in considerable amounts by anaerobic corrosion of iron in the canisters for spent nuclear fuel. The insoluble noble metal (Mo, Ru, Tc, Rh, Pd, and Te) clusters, known as  $\epsilon$  particles, are present at the fuel surface and interior of the pellet and were found to catalyze oxidation of  $\text{UO}_2$  (Eqs. 66, 67) as well as reduction of surface bound oxidized  $\text{UO}_2^{2+}$  by  $\text{H}_2$  (Eq. 69) [256]:



This reaction will reduce the dissolution rate and in a consequence the radionuclide release. On the other hand, reduction of  $\text{UO}_2^{2+}$  in aqueous phase does not affect the rate of the radionuclide release, but merely lowers its concentration [257].

The similar inhibiting  $\text{H}_2$  influence on dissolution of  $\text{UO}_2$  was observed in  $\alpha$ -doped  $\text{UO}_2$ . However, the mechanism presented above for spent nuclear fuel cannot be applied since this material does not contain noble metal inclusions. Therefore, this effect can be rationalized in terms of reactions depicted in Eqs. (12) and (15), which lower  $\text{H}_2\text{O}_2$  concentration when concentration of  $\text{H}_2$  is higher than concentration of  $\text{H}_2\text{O}_2$ . Moreover, H atoms which are formed in reaction depicted in Eq. (12) can reduce already dissolved  $\text{UO}_2^{2+}$  to less soluble  $\text{UO}_2$  [258].

The inhibition of radiation-induced dissolution of  $\text{UO}_2$  based spent nuclear fuel was also observed in the presence of  $\text{H}_2\text{S}/\text{HS}^-$  and was rationalized in terms of scavenging of radiolytic oxidants and reduction of  $\text{UO}_2^{2+}$  [259].

### 5.3 Radiation-Induced Processes Related to Changes of Bentonite Clays Properties

The first irradiation studies on bentonite clays showed that their physicochemical properties and the frame structure were little affected by exposure to  $\gamma$ -rays [260].

On the other hand, significant damage leading to amorphization was observed in smectites under electron-beam irradiation [261].

In recent years, the influence of  $\gamma$ -irradiation on the colloidal stability of bentonite suspensions was studied showing that irradiated colloidal suspensions are more stable than those non-irradiated. This phenomenon was assigned to the increase of the surface charge due to irradiation [262].

Effects of  $\gamma$ -irradiation on apparent diffusivity values and sorption coefficients in bentonite for  $\text{Cs}^+$  and  $\text{Co}^{2+}$  was studied showing decreasing sorption abilities for  $\text{Co}^{2+}$ , in contrast to  $\text{Cs}^+$ . This effect implies that irradiation may change surface features that affect  $\text{Co}^{2+}$  affinity [263].

Since the montmorillonite particles may contain iron as, *inter alia*, Fe ions complexed by surface hydroxyl groups on the edge of the layer, the influence of  $\gamma$ -radiation on the structural Fe(II)/Fe(III) ratio in montmorillonite was studied [264]. The observed increase in Fe(II)/Fe(III) ratio resulted in increased reactivity towards  $\text{H}_2\text{O}_2$ . Thus, the structural iron in montmorillonite can play a role of a sink for  $\text{H}_2\text{O}_2$ , which is one of the major oxidants formed upon water radiolysis in the bentonite barrier.

In order to elucidate a presence of bentonite on the oxidative dissolution of spent nuclear fuel (the scenario of possible barriers failure),  $\text{UO}_2$  pellets were exposed to  $\gamma$ -irradiation in the presence of  $\text{H}_2\text{O}_2$  and bentonite. Interestingly, these experiments revealed that the presence of bentonite in water can reduce the rate of dissolution of  $\text{UO}_2$ . This phenomenon was explained in terms of scavenging of radiolytic oxidants by bentonite, but not by adsorption of  $\text{UO}_2$  on bentonite [265].

Very recently, the  $\text{H}_2$  formation was studied in synthetic and natural talcs (taken as a model of clay minerals, which do not have swelling properties, as montmorillonites) [266]. It was found that transition element cationic impurities (present in natural talc) are able to scavenge efficiently the electrons and  $\text{H}^+$  atoms, and thus decrease 30-fold the  $\text{H}_2$  yield in comparison to the synthetic talc.

## 6 Conclusions

Contribution of radiation chemistry to a number of technological applications associated with various areas of nuclear technology is difficult to be overestimated. A substantial and essential knowledge collected over the years (in last two decades, in particular) is invaluable in understanding reaction mechanisms induced by high-energy radiation in various and extreme environmental conditions and heterogeneous systems. With the recent and continuous development of experimental and computational techniques, this branch of chemistry should enable further progress in addressing still unresolved issues related to understanding and controlling radiation processes relevant to nuclear energy production where reactions take place at high temperatures and pressures including supercritical region, high LET, and at interfaces.

**Acknowledgments** This work was supported by the US Department of Energy Office of Science, Office of Basic Energy Science under award number DE-FC02-04ER15533 (KB), the Euratom-Fission Collaborative Project SACSESS, FP7-Fission-2012-323282, co-financed by the Grant No. 2924/7. PR-EURATOM/2013/2 donated by the Ministry of Science and Higher Education (Poland) (TS), and the Strategic Research Project P/J/7/170071/12 financed by the National Research and Development Centre (KS). One of us (KB) would like to thank Professor Ian Carmichael for his hospitality during the stay. This is document number NDRL-5116 from the Notre Dame Radiation Laboratory.

## References

1. Takagi J, Mincher BJ, Yamaguchi M, Katsumura Y (2011) Radiation chemistry in nuclear engineering. In: Hatano Y, Katsumura Y, Mozumder A (eds) Charged Particle and Photon Interactions with Matter. CRC Press, Boca Raton, pp 959–1023
2. Chmielewski AG, Szolucha MM (2016) Radiation chemistry for modern nuclear energy development. *Radiat Phys Chem* 124:235–240
3. Mincher BJ (2015) Radiation chemistry in the reprocessing and recycling of spent nuclear fuels. In: Taylor R (ed) *Reprocessing and Recycling of Spent Nuclear Fuel*. Elsevier, Amsterdam, pp 191–211
4. Jonsson M (2014) An overview of interfacial radiation chemistry in nuclear technology. *Isr J Chem* 54:292–301
5. Lin M, Katsumura Y (2011) Radiation chemistry of high temperature and supercritical water and alcohols. In: Hatano Y, Katsumura Y, Mozumder A (eds) Charged Particle and Photon Interactions with Matter. CRC Press, Boca Raton, pp 401–424
6. LaVerne JA (2011) Radiation chemistry of water with ceramic oxides. In: Hatano Y, Katsumura Y, Mozumder A (eds) Charged Particle and Photon Interactions with Matter, 1st edn. CRC Press, Boca Raton, pp 425–444
7. Mincher BJ, Modolo G, Mezyk SP (2010) Review: the effects of radiation chemistry on solvent extraction 4: separation of the trivalent actinides and considerations for radiation-resistant solvent systems. *Solv Extr Ion Exchange* 28:415–436
8. Mincher BJ, Modolo G, Mezyk SP (2009) Review article: the effects of radiation chemistry on solvent extraction 3: a review of actinide and lanthanide extraction. *Solv Extr Ion Exchange* 27:579–606
9. Mincher BJ (2010) An overview of selected radiation chemical reactions affecting fuel cycle solvent extraction. In: Wai C (ed.) *Nuclear Energy and Environment*. ACS Symposium Series: American Chemical Society, Washington, DC, pp. 181–192
10. Miller W, Russell A, Chapman N, McKinley I, Smellie J (2000) *Geological Disposal of Radioactive Wastes and Natural Analogues*. Pergamon Press, Amsterdam
11. Garrett BC, Dixon DA, Camaioni DM, Chipman DM, Johnson MA, Jonah CD, Kimmel GA, Miller JH, Rescigno TN, Rossky PJ, Xantheas SS, Colson SD, Laufer AH, Ray D, Barbara PF, Bartels DM, Becker KH, Bowen KH Jr, Bradforth SE, Carmichael I, Coe JV, Corrales LR, Cowin JP, Dupuis M, Eisenthal KB, Franz JA, Gutowski MS, Jordan KD, Kay BD, LaVerne JA, Lyman SV, Madey TE, McCurdy CW, Meisel D, Mukamel S, Nilsson AR, Orlando TM, Petrik NG, Pimlott SM, Rustad JR, Schenter GK, Singer SJ, Tokmakoff A, Wang LS, Wettig C, Zwier TS (2005) Role of water in electron-initiated processes and radical chemistry: issues and scientific advances. *Chem Rev* 105:355–390
12. Buxton GV (2008) An overview of the radiation chemistry of liquids. In: Spothem-Maurizot M, Mostafavi M, Douki T, Belloni J (eds) *Radiation Chemistry: From Basics to Applications in Material and Life Sciences*. EDP Sciences, France, pp 3–16
13. Elliot AJ, Bartels D (2009) The reaction set, rate constants and *G* values for the simulation of the radiolysis of light water over the range 20 to 350 °C based on information available in 2008. *AECL EACL* 153-127160-450-00,
14. Bartels DM, Henshaw J, Sims HE (2013) Modeling the critical hydrogen concentration in the AECL test reactor. *Radiat Phys Chem* 82:16–24
15. Kanjana K, Haygarth KS, Wu W, Bartels DM (2013) Laboratory studies in search of the critical hydrogen concentration. *Radiat Phys Chem* 82:25–34

16. Katsumura Y, Kiuchi K, Domae M, Karasawa H, Saito N, Yotsuyanagi T (2005) Research program on water chemistry of supercritical pressure water under radiation field. In: Nakahara M, Matubayasi N, Ueno M, Watanabe K (eds) *Properties of Water and Steam in Kyoto Water, Steam and Aqueous Solutions for Electric Power: Advances in Science and Technology* Kyoto. Maruzen Co. Ltd., Tokyo
17. Katsumura Y, Sunaryo G, Hiroishi D, Ishigure K (1998) Fast neutron radiolysis of water at elevated temperatures relevant to water chemistry. *Prog Nucl Energy* 32:113–121
18. Sunaryo GR, Katsumura Y, Ishigure K (1995) Radiolysis of water at elevated temperatures-III. Simulation of radiolytic products at 25 and 250 °C under the irradiation with  $\gamma$ -rays and fast neutrons. *Radiat Phys Chem* 45:703–714
19. Bartels DM, Takahashi K, Cline JA, Marin TW, Jonah CD (2005) Pulse radiolysis of supercritical water. 3. Spectrum and thermodynamics of the hydrated electron. *J Phys Chem A* 109:1299–1307
20. Wu G, Katsumura Y, Muroya Y, Li X, Terada Y (2000) Hydrated electron in subcritical and supercritical water. A pulse radiolysis study. *Chem Phys Lett* 325:531–536
21. Hare PM, Price EA, Stanisky CM, Janik I, Bartels DM (2010) Solvated electron extinction coefficient and oscillator strength in high temperature water. *J Phys Chem A* 114:1766–1775
22. Hare PM, Price EA, Bartels DM (2008) Hydrated electron extinction coefficient revisited. *J Phys Chem A* 112:6800–6802
23. Wu G, Katsumura Y, Muroya Y, Li X, Terada Y (2001) Pulse radiolysis of high temperature and supercritical water: experimental setup and  $e^{-aq}$  observation. *Radiat Phys Chem* 60:395–398
24. Elliot AJ, Buxton GV (1992) Temperature dependence of the reactions  $OH + O$  and  $OH + HO_2$  in water up to 200 [degree]C. *J Chem Soc, Faraday Trans* 88(17):2465–2470
25. Elliot AJ, McCracken DR, Buxton GV, Wood ND (1990) Estimation of rate constants for near-diffusion-controlled reactions in water at high temperatures. *J Chem Soc, Faraday Trans* 86:1539–1547
26. Janik I, Bartels DM, Jonah CD (2007) Hydroxyl radical self-recombination reaction and absorption spectrum in water up to 350 °C. *J Phys Chem A* 111:1835–1843
27. Wu G, Katsumura Y, Lin M, Morioka T, Muroya Y (2002) Temperature dependence of ketyl radical in aqueous benzophenone solution up to 400 °C. A pulse radiolysis study. *Phys Chem Chem Phys* 4:3980–3988
28. Wu G, Katsumura Y, Lin M, Murota T (2001) Temperature dependence of  $(SCN)_2^-$  in water at 25–400 °C. Absorption spectrum, equilibrium constant, and decay. *J Phys Chem A* 105:4933–4939
29. Katsumura Y, Wu G, Lin M, Muroya Y, Morioka T, Terada Y, Li X (2001) Observation of hydrated electron,  $(SCN)_2^-$  and  $CO_3^-$  radical in high temperature and supercritical water. *Res Chem Intermed* 22:755–763
30. Mostafavi M, Lin M, Wu G, Katsumura Y, Muroya Y (2002) Pulse radiolysis study of absorption spectra of  $Ag^0$  and  $Ag^{2+}$  in water from room temperature up to 380 °C. *J Phys Chem A* 106:3123–3127
31. Lin M, Katsumura Y, Muroya Y, He H, Miyazaki T, Hiroshi D (2008) Pulse radiolysis of sodium formate aqueous solution up to 400 °C: absorption spectra, kinetics and yield of carboxyl radical  $CO_2^-$ . *Radiat Phys Chem* 77:1208–1212
32. Lin M, Katsumura Y, He W, Muroya Y, Wu G, Han Z, Miyazaki T, Kudo H (2005) Pulse radiolysis of 4,4'-bipyridyl aqueous solutions at elevated temperatures: spectral changes and reaction kinetics up to 400 °C. *J Phys Chem A* 109:2847–2854
33. Wu G, Katsumura Y, Muroya Y, Lin M, Murota T (2002) Temperature dependence of carbonate radical in  $NaHCO_3$  and  $Na_2CO_3$  solutions: is the radical a single anion? *J Phys Chem A* 106:2430–2432
34. Lin M, Katsumura Y, Muroya Y, He W, Wu G, Han Z, Miyazaki T, Kudo H (2004) Pulse radiolysis study on the estimation of radiolytic yields of water decomposition products in high-temperature and supercritical water: use of methyl viologen as a scavenger. *J Phys Chem A* 108:8287–8295
35. Sims HE (2006) Yields of radiolysis products from  $\gamma$ -irradiated supercritical water—a re-analysis data by W. G. Burns and W.R. Marsh. *Radiat Phys Chem* 75:1047–1050
36. Burns WG, Marsh WR (1981) Radiation chemistry of high-temperature (300–400 °C) Water. *J Chem Soc Faraday I* 72:197–215
37. Lin M, Muroya Y, Baldacchino G, Katsumura Y (2010) Radiolysis of Supercritical Water. In: Wishart JF, Rao BSM (eds) *Recent Trends in Radiation Chemistry*. World Scientific, New Jersey, pp 255–277

38. Sterniczuk M, Yakabuskie PA, Wren JC, Jacob JA, Bartels D (2015) Low LET radiolysis escape yields for reducing radicals and H<sub>2</sub> in pressurized high temperature water. *Radiat Phys Chem* 121:35–42
39. Shiraishi H, Katsumura Y, Hiroishi D, Ishigure K, Washio M (1988) Pulse-radiolysis study on the yield of hydrated electron at elevated temperatures. *J Phys Chem* 92:3011–3017
40. Shiraishi H, Katsumura Y, Ishigure K (1989) On the yield of hydrated electron at elevated temperatures. *Radiat Phys Chem* 34:705–710
41. Janik D, Janik I, Bartels DM (2007) Neutron and  $\beta/\gamma$  radiolysis of water up to supercritical conditions. 1.  $\beta/\gamma$  Yields for H<sub>2</sub>, H atom, and hydrated electron. *J Phys Chem A* 111:7777–7786
42. Elliot AJ, Chenier MP, Ouellette DC (1993) Temperature dependence of g values for H<sub>2</sub>O and D<sub>2</sub>O irradiated with low linear energy transfer radiation. *J Chem Soc Faraday Trans I* 89:1193–1197
43. Christensen HC, Sehested K (1986) The hydrated electron and its reactions at high temperatures. *J Phys Chem* 90:186–190
44. Marin TW, Takahashi K, Jonah CD, Cheremisinov SD, Bartels DM (2007) Recombination of the hydrated electron at high temperature and pressure in hydrogenated alkaline water. *J Phys Chem A* 111:11540–11551
45. Christensen H, Sehested K, Logager T (1994) Temperature dependence of the rate constant for reactions of hydrated electrons with H, OH and H<sub>2</sub>O<sub>2</sub>. *Radiat Phys Chem* 43:527–531
46. Shiraishi H, Sunaryo GR, Ishigure K (1994) Temperature dependence of equilibrium and rate constants of reactions inducing conversion between hydrated electron and atomic hydrogen. *J Phys Chem* 98:5164–5173
47. Takahashi K, Bartels DM, Cline JA, Jonah CD (2002) Reaction rates of the hydrated electron with NO<sub>2</sub><sup>-</sup> and NO<sub>3</sub><sup>-</sup> and hydronium ions as a function of temperature from 125 to 380 °C. *Chem Phys Lett* 357:358–364
48. Stanisky CM, Bartels DM, Takahashi K (2010) Rate constants for the reaction of hydronium ions with hydrated electrons up to 350 °C. *Radiat Phys Chem* 79:64–65
49. Muroya Y, Lin M, de Waele V, Hatano Y, Katsumura Y, Mostafavi M (2010) First observation of picosecond kinetics of hydrated electrons in supercritical water. *J Phys Chem Lett* 1:331–335
50. Cline J, Takahashi K, Marin TW, Jonah CD, Bartels DM (2002) Pulse radiolysis of supercritical water. 1. Reactions between hydrophobic and anionic species. *J Phys Chem A* 106:12260–12269
51. Marin TW, Cline JA, Takahashi K, Bartels DM, Jonah CD (2002) Pulse radiolysis of supercritical water. 2. Reaction of nitrobenzene with hydrated electrons and hydroxyl radicals. *J Phys Chem A* 106:12270–12279
52. Lin CC (2009) A review of corrosion product transport and radiation field buildup in boiling water reactors. *Prog Nucl Energy* 51:207–224
53. Tsaia T-L, Lina T-Z, Sua T-Y, Weia H-J, Mena L-C, Wenba T-J (2012) Identification of chemical composition of CRUD depositing on fuel surface of a boiling water reactor (BWR-6) plant. *Energy Procedia* 14:867–872
54. Kanjana K, Courtin B, MacConnell A, Bartels DM (2015) Reactions of hexa-aquo transition metal ions with the hydrated electron up to 300 °C. *J Phys Chem A* 119:11094–11104
55. McCracken DR, Tsang KT, Laughton PJ (1998) Aspects of the physics and chemistry of water radiolysis by fast neutrons and fast electrons in nuclear reactors. Report AECL-11895. AECL,
56. Christensen H, Sehested K (1983) Reaction of hydroxyl radicals with hydrogen at elevated temperatures. Determination of the activation energy. *J Phys Chem* 87:118–120
57. Marin TW, Jonah CD, Bartels D (2003) Reaction of OH radicals with H<sub>2</sub> in sub-critical water. *Chem Phys Lett* 371:144–149
58. Janik I, Bartels DM, Marin TW, Jonah CD (2007) Reaction of O<sub>2</sub> with the hydrogen atom in water up to 350 °C. *J Phys Chem A* 111:79–88
59. Christensen H, Sehested K, Corfitzen H (1982) Reactions of hydroxyl radicals with hydrogen peroxide at ambient and elevated temperatures. *J Phys Chem* 86:1588–1590
60. Buxton GV, Elliot AJ (1993) Temperature dependence of the rate constant for the reaction H + OH in liquid water up to 200 °C. *J Chem Soc, Faraday Trans* 89:485–488
61. Lundström T, Christensen H, Sehested K (2002) The reaction of OH with H<sup>+</sup> at elevated temperatures. *Radiat Phys Chem* 64:29–33
62. Lundström T, Christensen H, Sehested K (2004) reactions of HO<sub>2</sub> radical with OH, H, Fe<sup>2+</sup> and Cu<sup>2+</sup> at elevated temperatures. *Radiat Phys Chem* 69:211–216
63. Marin TW, Jonah CD, Bartels DM (2005) Reaction of hydrogen atoms with hydroxide ions in high-temperature and high-pressure water. *J Phys Chem A* 109:1843–1848

64. Swiatla-Wójcik D, Buxton GV (2005) On the possible role of the reaction  $H + H_2O^- > H_2 + OH$  in the radiolysis of water at high temperatures. *Radiat Phys Chem* 74:210–219
65. Hartig KJ, Getoff N (1982) Reactivity of hydrogen atoms with liquid water. *J Photochem* 18:29–38
66. Bartels D (2009) Comment on the possible role of the reaction  $H + H_2O^- > H_2 + OH$  in the radiolysis of water at high temperatures. *Radiat Phys Chem* 78:191–194
67. Swiatla-Wójcik D, Buxton GV (2010) Reply to comment on the possible role of the reaction  $H + H_2O^- > H_2 + OH$  in the radiolysis of water at high temperatures. *Radiat Phys Chem* 79:52–56
68. Lundstrom T, Christensen H, Sehested K (2001) The reaction of hydrogen atoms with hydrogen peroxide as a function of temperature. *Radiat Phys Chem* 61:109–113
69. Mezyk SP, Bartels DM (1995) Direct EPR measurement of Arrhenius parameters for the reaction of H atoms with  $H_2O_2$  and D atoms with  $D_2O_2$  in aqueous solution. *J Chem Soc Faraday Trans* 91:3127–3132
70. Elliot AJ (1989) A pulse radiolysis study of the temperature dependence of reactions involving H, OH and  $e^{-aq}$  in aqueous solutions. *Radiat Phys Chem* 34:753–758
71. Sehested K, Christensen H (1990) The rate constant of the bimolecular reaction of hydrogen atoms at elevated temperatures. *Radiat Phys Chem* 36:499–500
72. Yamashita S, Taguchi M, Baldacchino G, Katsumura Y (2011) Radiation chemistry of liquid water with heavy ions: steady-state and pulse radiolysis studies. In: Hatano Y, Katsumura Y, Mozumder A (eds) *Charged Particle and Photon Interactions with Matter*. CRC Press, Boca Raton, pp 325–354
73. LaVerne JA (2004) Radiation chemical effects of heavy ions. In: Mozumder A, Hatano Y (eds) *Charged Particle and Photon Interactions with Matter*. Marcel Dekker, New York, pp 403–429
74. Meesungnoen J, Jay-Gerrin J-P (2011) Radiation chemistry of liquid water with heavy ions: Monte Carlo simulation studies. In: Hatano Y, Katsumura Y, Mozumder A (eds) *Charged Particle and Photon Interactions with Matter*. CRC Press, Boca Raton, pp 355–400
75. Baldacchino G, Katsumura Y (2010) Chemical processes in heavy ion track. In: Wishart JF, Rao BSM (eds) *Recent Trends in Radiation Chemistry*. World Scientific, New Jersey, pp 231–253
76. Meisel D (2004) Radiation effects in nanoparticle suspensions. In: Lin-Marzan L, Kamat P (eds) *Nanoscale Materials*, 1st edn. Springer, Berlin, pp 119–134
77. Kumbhar AG, Belapurkar AD, Venkateswaran G, Bera S, Naik DB, Kishore K, Sanjukta A, Mythili R (2011) Hydrogen generation by gamma irradiation of aqueous turbid solution of titanium. *Curr Sci* 100:895–900
78. Kumbhar AG, Belapurkar AD, Venkateswaran G, Kishore K (2005) Impact of different metal turbidities on radiolytic hydrogen generation in nuclear power plant. *Power Plant Chem* 7:674–679
79. Schofield J, Reiff SC, Pimblott SM, LaVerne JA (2016) Radiolytic hydrogen generation at silicon carbide-water interfaces. *J Nucl Mater* 469:43–50
80. Reiff SC, LaVerne JA (2015) Radiation-induced chemical changes to iron oxides. *J Nucl Mater* 119:7358–7365
81. Reiff SC, LaVerne JA (2015) Gamma and He ion radiolysis of copper oxides. *J Phys Chem C* 119:8821–8828
82. Kumbhar AG, Bhardwaj YK, Naik DB (2014) Hydrogen generation by gamma radiolysis of aqueous suspension of nano zirconia. *Curr Sci* 107:88–93
83. Merga G, Milosavljevic BH, Meisel D (2006) Radiolytic hydrogen yields in aqueous suspensions of gold particles. *J Phys Chem B* 110:5403–5408
84. Matsumoto Y, Doa T-M-D, Inoue M, Nagaishi R, Ogawa T (2015) Hydrogen generation by water radiolysis with immersion of oxidation products of Zircaloy-4. *J Nucl Sci Technol* 52:1303–1307
85. Chelnokov E, Cuba V, Simeone D, Guigner JM, Schmidhammer U, Mostafavi M, Le Caër S (2014) Electron transfer at oxide/water interfaces induced by ionizing radiation. *J Phys Chem C* 118:7865–7873
86. Petrik NG, Alexandrov AB, Vall AI (2001) Interfacial energy transfer during gamma radiolysis of water on the surface of  $ZrO_2$  and some other oxides. *J Phys Chem B* 105:5935–5944
87. LaVerne JA, Tandon L (2002)  $H_2$  production in the radiolysis of water on  $CeO_2$  and  $ZrO_2$ . *J Phys Chem B* 106:380–386
88. LaVerne JA, Tandon L (2003)  $H_2$  production in the radiolysis of water on  $UO_2$  and other oxides. *J Phys Chem B* 107:13623–13628
89. Sattonnay G (2001) Behavior of a water-uranium dioxide interface subjected to irradiation: effects of water radiolysis on the alteration of uranium dioxide. *J Phys IV* 11(PR1):243–250



90. LaVerne JA (2005) H<sub>2</sub> formation from the radiolysis of liquid water with zirconia. *J Phys Chem B Lett* 109:5395–5397
91. Carrasco-Flores EA, LaVerne JA (2007) Surface species produced in the radiolysis of zirconia nanoparticles. *J Chem Phys* 127:234703–234709
92. Jonsson M (2010) Radiation-induced processes at solid-liquid interfaces. In: Wishart JF, Rao BSM (eds) *Recent Trends in Radiation Chemistry*. World Scientific, New Jersey, pp 301–323
93. Skotnicki K, Bobrowski K (2015) Molecular hydrogen formation during water radiolysis in the presence of zirconium dioxide. *J Radioanal Nucl Chem* 304:473–480
94. Barzykin AV, Tachiya M (2003) Diffusion of probe molecules in polymer gels as observed by fluorescence quenching techniques. *J Phys Chem B* 107(13):2953–2957
95. Steytler DC, Dore JC, Wright CJ (1983) Neutron-diffraction studies of water in meso-pores and micro-pores. *Mol Phys* 48:1031–1051
96. Gallo P, Ricci MA, Rovere M (2002) Layer analysis of the structure of water confined in vycor glass. *J Chem Phys* 116:342–346
97. Musat R, Renault JP, Candelaresi M, Palmer DJ, Le Caer S, Righini R, Righini R, Pommeret S (2008) Finite size effects on hydrogen bonds in confined water. *Angew Chem Int Ed* 47:8033–8035
98. Wang M, Duan F-L (2015) Effect of interfacial hydrogen bonds on the structure and dynamics of confined water. *Acta Phys Sin* 64:201–218
99. Kayal A, Chandra A (2015) Exploring the structure and dynamics of nano-confined water molecules using molecular dynamics simulations. *Mol Simul* 41:463–470
100. Tan HS, Piletic IR, Fayer MD (2005) Orientational dynamics of water confined on a nanometer length scale in reverse micelles. *J Chem Phys* 122:174501
101. Cringus D, Lindner J, Milder MTW, Pshenichnikov MS, Vohringer P, Wiersma DA (2005) Femtosecond water dynamics in reverse-micellar nanodroplets. *Chem Phys Lett* 408:162–168
102. Dokter AM, Woutersen S, Bakker HJ (2007) Ultrafast dynamics of water in cationic micelles. *J Chem Phys* 126:124507
103. Piletic IR, Moilanen DE, Spry DB, Levinger NE, Fayer MD (2006) Testing the core/shell model of nanoconfined water in reverse micelles using linear and nonlinear IR spectroscopy. *J Phys Chem A* 110:4985–4999
104. Cringus D, Bakulin A, Lindner J, Voehringer P, Pshenichnikov MS, Wiersma DA (2007) Ultrafast energy transfer in water—AOT reverse micelles. *J Phys Chem B* 111:14193–14207
105. Akhmatskaya E, Todd BD, Davis PJ, Evans DJ, Gubbins KE, Pozhar LA (1997) A study of viscosity inhomogeneity in porous media. *J Chem Phys* 106:4684–4695
106. Nakazato C, Masuda T (1986) Reactivity of electrons produced in gamma-irradiated zeolite toward several electron scavengers. *Bull Chem Soc Jpn* 59:2237–2239
107. Aoki M, Nakazato C, Masuda T (1988) Hydrogen formation from water adsorbed on zeolite during gamma-irradiation. *Bull Chem Soc Jpn* 61:1899–1902
108. Nakashima M, Aratono Y (1993) Radiolytic hydrogen gas formation from water adsorbed on type A zeolites. *Radiat Phys Chem* 41:461–465
109. Nakashima M, Masaki NM (1996) Radiolytic hydrogen gas formation from water adsorbed on type Y zeolites. *Radiat Phys Chem* 47:241–245
110. Foley S, Rotureau P, Pin S, Baldacchino G, Renault J-P, Mialocq J-C (2005) Radiolysis of confined water: production and reactivity of hydroxyl radicals. *Angew Chem Int Ed* 44:110–112
111. Le Caer S, Rotureau P, Brunet F, Charpentier T, Blain G, Renault J-P, Mialocq J-C (2005) Radiolysis of confined water: hydrogen production at low dose rate. *Chem Phys Chem* 6:2585–2596
112. Le Caer S, Rotureau P, Vigneron G, Blain G, Renault J-P, Mialocq J-C (2005) Irradiation of controlled pore glasses with 10 MeV electrons. *Rev Adv Mat Sci* 10:161–165
113. Le Caer S, Renault J-P, Mialocq J-C (2007) Hydrogen peroxide formation in the radiolysis of hydrated nanoporous glasses: a low and high dose rate study. *Chem Phys Lett* 450:91–95
114. Rotureau P, Renault J-P, Lebeau B, Patarin J, Mialocq J-C (2005) Radiolysis of confined water: molecular hydrogen formation. *Chem Phys Chem* 6:1316–1323
115. Fourdrin C, Aarrachi H, Latrille C, Esnouf S, Bergaya F, Le Caër S (2013) Water radiolysis in exchanged-montmorillonites: the H<sub>2</sub> production mechanisms. *Environ Sci Technol* 47(16):9530–9537
116. Musat R, Moreau S, Poidevin F, Mathon MH, Pommeret S, Renault JP (2010) Radiolysis of water in nanoporous gold. *Phys Chem Chem Phys* 12:12868–12874
117. Moreau S, Fenart M, Renault JP (2014) Radiolysis of water in the vicinity of passive surfaces. *Corrosion Sci* 83:255–260



118. Musat RM, Cook AR, Renault J-P, Crowell RA (2012) Nanosecond pulse radiolysis of nanoconfined water. *J Phys Chem C* 116:13104–13110
119. Avallone E, Baumeister C, Sadegh M (2007) Marks' Standard Handbook for Mechanical Engineers. New York
120. Lowinska-Kluge APP (2008) Effect of gamma irradiation on cement composites observed with XRD and SEM methods in the range of radiation dose 0–1409 MGy. *Acta Phys Pollut A* 114(2):399–411
121. Vagelis G, Papadakis (1991) Physical and chemical characteristics affecting the durability of concrete. *Mater J* 88(2):186–196
122. Bouniol P, Bjergbakke E (2008) A comprehensive model to describe radiolytic processes in cement medium. *J Nucl Mater* 372:1–15
123. Bouniol P (2010) The influence of iron on water radiolysis in cement-based materials. *J Nucl Mater* 403:167–183
124. Foct F, Di Giandomenico MV, Bouniol P (2013) Modelling of hydrogen production from pore water radiolysis in cemented intermediate level waste. Paper presented at the International Workshop Nucperf 2012: Long-Term Performance of Cementitious Barriers and Reinforced Concrete in Nuclear Power Plant and Radioactive Waste Storage and Disposal,
125. Bouniol P, Muzeau B, Dauvois V (2013) Experimental evidence of the influence of iron on pore water radiolysis in cement-based materials. *J Nucl Mater* 437:208–215
126. Poinssot C, Boullis B, Bourg S (2015) Role of recycling in advanced nuclear fuel cycles. In: Taylor R (ed) *Reprocessing and Recycling of Spent Nuclear Fuel*. Woodhead Publishing, Oxford, pp 27–48
127. Bourg S, Geist A, Narbutt J (2015) SACSESS—the EURATOM FP7 project on actinide separation from spent nuclear fuels. *Nukleonika* 60:809–814
128. Herbst RS, Baron P, Nilsson M (2011) Standard and advanced separation: PUREX processes for nuclear fuel reprocessing. In: Nash KL, Nash GJ (eds) *Advanced Separation Techniques for Nuclear Fuel Reprocessing and Radioactive Waste Treatment*. Woodhead Publishing, Oxford, pp 141–175
129. Nash KL, Nilsson M (2015) Introduction to the reprocessing and recycling of spent nuclear fuels. In: Taylor R (ed) *Reprocessing and Recycling of Spent Nuclear Fuel*. Woodhead Publishing, Oxford, pp 3–25
130. Modolo G, Geist A, Miguirditchian M (2015) Minor actinide separations in the reprocessing of spent nuclear fuels: recent advances in Europe. In: Taylor R (ed) *Reprocessing and Recycling of Spent Nuclear Fuel*. Woodhead Publishing, Oxford, pp 245–287
131. Todd TA (2015) Development of closed nuclear fuel cycles in the United States. In: Taylor R (ed) *Reprocessing and Recycling of Spent Nuclear Fuel*. Woodhead Publishing, Oxford, pp 525–530
132. Hood GC, Reilly CA (1960) Ionization of strong electrolytes. 8. Temperature coefficient of dissociation of strong acids by proton magnetic resonance. *J Chem Phys* 32:127–130
133. Buxton GV, Greenstock CL, Helman WP, Ross AB (1988) Critical review of rate constants for reactions of hydrated electrons, hydrogen atoms and hydroxyl radicals ( $\text{OH}/\text{O}^-$ ) in aqueous solution. *J Phys Chem Ref Data* 17:513–886
134. Wolff RK, Bronskill MJ, Hunt JW (1970) Picosecond pulse radiolysis studies. 2. Reactions of electrons with concentrated scavengers. *J Chem Phys* 53:4211–4242
135. Lam KY, Hunt JW (1975) Picosecond pulse-radiolysis. 6. Fast electron reactions in concentrated solutions of scavengers in water and alcohols. *Int J Radiat Phys Chem* 7:317–338
136. Gratzel M, Henglein A, Taniguchi S (1970) Pulse radiolysis of  $\text{NO}_3^-$ —reduction and formation and decomposition of pernitrous acid in aqueous solution ber bunsenges. *Phys Chem* 74:292
137. Logager T, Sehested K (1993) Formation and decay of peroxyxynitrous acid—a pulse-radiolysis study. *J Phys Chem* 97:6664–6669
138. Wardman P (1989) The reduction potentials of one-electron couples involving free radicals in aqueous solution. *J Phys Chem Ref Data* 18:1637–1753
139. Gratzel M, Henglein A, Lilie J, Beck G (1969) Pulse radiolysis of some elementary oxidation-reduction processes of nitrite. *Ber Bunsenges Phys Chem* 73:646
140. Olah GA, Lin HC, Olah JA, Narang SC (1978) Electrophilic and free radical nitration of benzene and toluene with various nitrating agents. *Proc Nat Acad Sci USA* 75:1045–1049
141. Katsumura Y (1998)  $\text{NO}_2$  and  $\text{NO}_3$  radicals in radiolysis of nitric acid solutions. In: Alfassi ZB (ed) *N-Centered Radicals. Vol the Chemistry of Free Radicals*. Wiley, Chichester, pp 393–412
142. Katsumura Y, Jiang P-Y, Nagaishi R, Oishi T, Ishigure K, Yoshida Y (1991) Pulse radiolysis study of aqueous nitric acid solutions. Formation mechanism, yield, and reactivity of  $\text{NO}_3$  radical. *J Phys Chem* 95:4435–4439

143. Nagaishi R, Jiang PY, Katsumura Y, Ishigure K (1994) Primary yields of water radiolysis in concentrated nitric-acid solutions. *J Chem Soc Faraday Trans* 90:591–595
144. Jiang PY, Nagaishi R, Yotsuyanagi T, Katsumura Y, Ishigure K (1994) Gamma-radiolysis study of concentrated nitric-acid solutions. *J Chem Soc Faraday Trans* 90:93–95
145. Balcerzyk A, El Omar AK, Schmidhammer U, Pernot P, Mostafavi M (2012) Picosecond pulse radiolysis study of highly concentrated nitric acid solutions: formation mechanism of  $\text{NO}_3$  radical. *J Phys Chem A* 116:7302–7307
146. Pikaev AK, Sibirskaya GK, Shirshov EM, Glazunov PY, Spitsyn VI (1974) Pulse-radiolysis of concentrated aqueous-solutions of nitric-acid. *Dokl Akad Nauk SSR* 215:645–648
147. Daniels M (1969) Radiation chemistry of aqueous nitrate system. 3. Pulse electron radiolysis of concentrated sodium nitrate solutions. *J Phys Chem* 73:3710
148. Sworski TJ, Matthews RW, Mahlman HA (1968) radiation chemistry of concentrated  $\text{NaNO}_3$  solutions—dependence of  $G(\text{HNO}_2)$  on  $\text{NaNO}_3$  concentrations. *Adv Chem Ser* 82:164–181
149. Mincher BJ, Elias G, Martin LR, Mezyk SP (2009) Radiation chemistry and the nuclear fuel cycle. *J Radioanal Nucl Chem* 282:645–649
150. Garaix G, Horne GP, Venault L, Moisy P, Pimblott SM, Marignier JL, Mostafavi M (2016) Decay mechanism of  $\text{NO}_3$  radical in highly concentrated nitrate and nitric acidic solutions in the absence and presence of hydrazine. *J Phys Chem B* 120(22):5008–5014
151. Vladimirova MV, Milovanova AS (1972)  $\alpha$ -Radiolysis of  $\text{HNO}_3$  solutions and acid  $\text{NaNO}_3$  solutions. *Khimiya Vysokikh Energii* 6:69–72
152. Matthews RW, Mahlman HA, Sworski TJ (1972) Elementary processes in the radiolysis of aqueous nitric acid solutions. Determination of both  $G_{\text{OH}}$  and  $G_{\text{NO}_3}$ . *J Phys Chem* 76:2680–2684
153. Park JY, Lee YN (1988) Solubility and decomposition kinetics of nitrous-acid in aqueous-solution. *J Phys Chem* 92:6294–6302
154. Bhattacharyya PK, Veeraraghavan R (1977) Reaction between nitrous-acid and hydrogen-peroxide in perchloric-acid medium. *Int J Chem Kinet* 9:629–640
155. Vione D, Maurino V, Minero C, Borghesi D, Lucchiari M, Pelizzetti E (2003) New processes in the environmental chemistry of nitrite. 2. The role of hydrogen peroxide. *Environ Sci Technol* 37:4635–4641
156. Belova EV, Egorov GF (1997) Radiochemical behavior of hydrazine nitrate in aqueous nitric acid solutions. *At Energ* 83(2):622–626
157. Dukes EK (1960) Kinetics and mechanisms for the oxidation of trivalent plutonium by nitrous acid. *J Am Chem Soc* 82(1):9–13
158. Mossini E, Macerata E, Giola M, Brambilla L, Castiglioni C, Mariani M (2015) Radiation-induced modifications on physico chemical properties of diluted nitric acid solutions within advanced spent nuclear fuel reprocessing. *J Radioanal Nucl Chem* 304:395–400
159. Mossini E, Macerata E, Giola M, Brambilla L, Castiglioni C, Mariani M (2015) Physico chemical properties of irradiated i-SANEX diluents. *Nukleonika* 60:893–898
160. Foldiák G (1981) Radiation Chemistry of Hydrocarbons. Elsevier, Amsterdam
161. Busi F (1982) Labile species and fast processes in liquid alkanes. In: Baxendale JH, Busi F (eds) *The Study of Fast Processes and Transient Species by Electron Pulse Radiolysis*. D. Reidel Publishing Company, Amsterdam, pp 417–431
162. Warman J (1982) The dynamics of electrons and ions in non-polar liquids. In: Baxendale JH, Busi F (eds) *The Study of Fast Processes and Transient Species by Electron Pulse Radiolysis*. D. Reidel Publishing Company, Dordrecht, p 433
163. Shkrob IA, Sauer MC, Trifunac AD (2001) Radiation chemistry of organic liquids: saturated hydrocarbons. In: Jonah CD, Rao BSM (eds) *Radiation Chemistry: Present Status and Future Trends*. Elsevier, Amsterdam, pp 175–221
164. Belloni J, Delcourt MO, Houee-Levin C, Mostafavi M (2000) Radiation chemistry. *Annu Rep Prog Chem Sect C* 96:225–295
165. Lin J, Tsuji K, Williams F (1968) Radiation-induced trapped electrons in saturated hydrocarbons studied by optical and electron spin resonance spectroscopy. *J Am Chem Soc* 90:2766
166. Klassen NV, Teather GG (1985) Cations and electrons in hydrocarbon glasses and liquids studied by pulse-radiolysis. *J Phys Chem* 89:2048–2053
167. Richards JT, Thomas JK (1970) Trapping of electrons in low-temperature glasses—a pulse radiolysis study. *J Chem Phys* 53:218
168. Lin J, Tsuji K, Williams F (1967) Electrons in organic glasses during photoionization. ESR observations of a photodynamic equilibrium. *J Chem Phys* 46:4982

169. Mehnert R, Brede O, Naumann W (1984) Spectral properties and kinetics of cationic transients generated in electron pulse irradiated C<sub>7</sub>- to C<sub>16</sub>-alkanes. *Ber Bunsenges Phys Chem* 88:71–80
170. Bishop WP, Firestone FR (1970) Radiolysis of liquid normal-pentane. *J Phys Chem* 74:2274
171. Spinks JWT, Woods RJ (1990) *Introduction to Radiation Chemistry*, 3rd edn. Wiley, New York
172. Dewhurst HA (1957) Radiation chemistry of organic compounds. I. *N*-Alkane liquids. *J Phys Chem* 61:1466–1471
173. Swallow AJ (1960) *Radiation Chemistry of Organic Compounds*. Pergamon Press, Oxford
174. Kharasch MS, Chang PC, Wagner CD (1958) Radiolysis of 1-hexene. *J Org Chem* 23:779–780
175. LaVerne JA, Schuler RH (1984) Track effects in radiation chemistry: core processes in heavy-particle tracks as manifest by the hydrogen yield in benzene radiolysis. *J Phys Chem* 88(6):1200–1205
176. Jones KH, Vandusen W, Theard LM (1964) Intermolecular and intramolecular energy transfer in gamma-irradiated alkylbenzenes and related mixtures. *Radiat Res* 22:202
177. Freeman GR (1982) Labile species and fast processes in liquid alcohol radiolysis. In: Baxendale JH, Busi F (eds) *The Study of Fast Processes and Transient Species by Electron Pulse Radiolysis*. D. Reidel Publishing Company, Amsterdam, pp 399–416
178. Jay-Gerin JP, Ferradini C (1994) Compilation of some physicochemical properties of solvated electrons in polar liquids. *J Chim Phys* 91:173–187
179. Szreder T, Kocia R (2015) Electron beam irradiation of *r*-SANEX and *i*-SANEX solvent extraction systems: analysis of gaseous products. *Nukleonika* 60:899–905
180. Backlund S, Hoiland H, Vikholm I (1984) Water-alcohol interactions in the 2-phase system water-alcohol-alkane. *J Solution Chem* 13:749–755
181. Geist A (2010) Extraction of nitric acid into alcohol: kerosene mixtures solvent. *Extr Ion Exch* 28:596–607
182. Scholes G, Willson RL (1967) Gamma-radiolysis of aqueous thymine solutions—determination of relative reaction rates of OH. *Trans Faraday Soc* 63:2983
183. Mezyk SP, Cullen TD, Elias G, Mincher BJ (2010) Aqueous nitric acid radiation effects on solvent extraction process chemistry. In: *Nuclear Energy and the Environment*, vol 1046. ACS Symposium Series, pp. 193–203
184. Tripathi SC, Ramanujam A (2003) Effect of radiation-induced physicochemical transformations on density and viscosity of 30 % TBP-*n*-dodecane-HNO<sub>3</sub> system. *Sep Sci Technol* 38:2307–2326
185. Chaumont A, Wipff G (2004) Solvation of uranyl(II) and europium(III) cations and their chloro complexes in a room-temperature ionic liquid. A theoretical study of the effect of solvent “humidity”. *Inorg Chem* 43:5891–5901
186. Chaumont A, Wipff G (2004) Solvation of uranyl(II), europium(III) and europium(II) cations in basic room-temperature ionic liquids: a theoretical study. *Chem A Eur J* 10:3919–3930
187. Cocalia VA, Jensen MP, Holbrey JD, Spear SK, Stepinski DC, Rogers RD (2005) Identical extraction behavior and coordination of trivalent or hexavalent f-element cations using ionic liquid and molecular solvents. *Dalton Trans* 11:1966–1971
188. Cocalia VA, Gutowski KE, Rogers RD (2006) The coordination chemistry of actinides in ionic liquids: a review of experiment and simulation. *Coord Chem Rev* 250:755–764
189. Dietz ML (2006) Ionic liquids as extraction solvents: where do we stand? *Sep Sci Technol* 41:2047–2063
190. Nikitenko SI, Cannes C, Le Naour C, Moisy P, Trubert D (2005) Spectroscopic and electrochemical studies of U(IV)-hexachloro complexes in hydrophobic room-temperature ionic liquids [BuMeIm][Tf<sub>2</sub>N] and [MeBU<sub>3</sub>N][Tf<sub>2</sub>N]. *Inorg Chem* 44:9497–9505
191. Visser AE, Jensen MP, Laszak I, Nash KL, Choppin GR, Rogers RD (2003) Uranyl coordination environment in hydrophobic ionic liquids: an in situ investigation. *Inorg Chem* 42:2197–2199
192. Mincher BJ, Wishart JF (2014) The radiation chemistry of ionic liquids: a review solvent. *Extr Ion Exch* 32:563–583
193. Venkatesan KA, Srinivasan TG, Rao PRV (2009) A review on the electrochemical applications of room temperature ionic liquids in nuclear fuel cycle. *J Nucl Radiochem Sci* 10:R1–R6
194. Sun X, Luo H, Dai S (2012) Ionic liquids-based extraction: a promising strategy for the advanced nuclear fuel cycle. *Chem Rev* 112:2100–2128
195. Rao PRV, Venkatesan KA, Rout A, Srinivasan TG, Nagarajan K (2012) Potential applications of room temperature ionic liquids for fission products and actinide. *Sep Sci Technol* 47:204–222
196. Takao K, Bell TJ, Ikeda Y (2013) Actinide chemistry in ionic liquids. *Inorg Chem* 52:3459–3472

197. Wishart JF, Shkrob IA (2009) The radiation chemistry of ionic liquids and its implications for their use in nuclear fuel processing. In: *Ionic Liquids: From Knowledge to Application*, vol 1030. ACS Symposium Series, vol 1030. American Chemical Society, pp. 119–134
198. Shkrob IA, Chemerisov SD, Wishart JF (2007) The initial stages of radiation damage in ionic liquids and ionic liquid-based extraction systems. *J Phys Chem B* 2007:11786–11793
199. Bosse E, Berthon L, Zorz N, Monget J, Berthon C, Bisel I, Legand S, Moisy P (2008) Stability of [MeBu<sub>3</sub>N][Tf<sub>2</sub>N] under gamma irradiation. *Dalton Trans* 7:924–931
200. Le Rouzo G, Lamouroux C, Dauvois V, Dannoux A, Legand S, Durand D, Moisy P, Moutiers G (2009) Anion effect on radiochemical stability of room-temperature ionic liquids under gamma irradiation. *Dalton Trans* 31:6175–6184
201. Tarábek P, Liu S, Haygarth K, Bartels DM (2009) Hydrogen gas yields in irradiated room-temperature ionic liquids. *Radiat Phys Chem* 78:168–172
202. Szreder T, Skrzypczak A (2015) Influence of the benzyl substituent on radiation chemistry of selected ionic liquids: gaseous products analysis. *J Radioanal Nucl Chem* 307:195–202
203. Musat RM, Crowell RA, Polyanskiy DE, Thomas MF, Wishart JF, Katsumura Y, Takahashi K (2015) Ultrafast transient absorption spectrum of the room temperature ionic liquid 1-hexyl-3-methylimidazolium bromide: confounding effects of photo-degradation. *Radiat Phys Chem* 117:78–82
204. Shkrob IA, Marin TW, Hatcher JL, Cook AR, Szreder T, Wishart JF (2013) Radiation stability of cations in ionic liquids. 2. Improved radiation resistance through charge de localization in 1-benzylpyridinium. *J Phys Chem B* 117:14385–14399
205. Pikaev AK, Gogolev AV, Shilov VP, Fedoseev AM (1990) Reactivity of ions of actinides towards inorganic free radicals in irradiated aqueous solutions. *Isot Environ Health Stud* 26:465–469
206. Mincher BJ, Precek M, Mezyk SP, Elias G, Martin LR, Paulenova A (2013) The redox chemistry of neptunium in gamma-irradiated aqueous nitric acid. *Radiochim Acta* 101:259–265
207. Paulenova A (2011) Physical and chemical properties of actinides in nuclear fuel reprocessing. In: Nash KL, Lumetta GJ (eds) *Advanced Separation Techniques for Nuclear Fuel Reprocessing and Radioactive Waste Treatment*. Woodhead Publishing, Oxford, pp 23–57
208. Mincher BJ, Mezyk SP, Martin LR (2008) A pulse radiolysis investigation of the reactions of tributyl phosphate with the radical products of aqueous nitric acid irradiation. *J Phys Chem A* 112:6275–6280
209. Burr JG (1958) The radiolysis of tributyl phosphate. *Radiat Res* 8:214–221
210. von Sonntag C, Schulte-Frohlinde D, Sugimori A, Omori T, Koltzenb G, Anson G (1972) Radiation-chemistry of DNA model compounds. 2. Alkyl phosphate cleavage of aliphatic phosphates induced by hydrated electrons and by OH radicals. *Z Naturforsch Pt B* B27:471–475
211. Khaikin GI (1998) Reactions of trialkyl phosphates with hydroxyl radicals and hydrated electrons. *High Energy Chem* 32:287–289
212. Wilkinson RW, Williams TF (1961) The radiolysis of tri-*n*-alkyl phosphates. *J Chem Soc* 1:4098–4107
213. Tahraoui A, Morris JH (1995) decomposition of solvent extraction media during nuclear reprocessing: literature review. *Sep Sci Technol* 30:2603–2630
214. Shkrob IA, Marin TW, Chemerisov SD, Wishart JF (2011) Radiation and radical chemistry of NO<sub>3</sub><sup>-</sup>, HNO<sub>3</sub>, and dialkylphosphoric acids in room-temperature ionic liquids. *J Phys Chem B* 115:10927–10942
215. He H, Lin MZ, Muroya Y, Kudo H, Katsumura Y (2004) Laser photolysis study on the reaction of nitrate radical with tributylphosphate and its analogues-comparison with sulfate radical. *Phys Chem Chem Phys* 6:1264–1268
216. Tripathi SC, Sumathi S, Ramanujam A (1999) Effects of solvent recycling on radiolytic degradation of 30 % tributyl phosphate-*n*-dodecane-HNO<sub>3</sub> system. *Sep Sci Technol* 34:2887–2903
217. Nash KL, Gatrone RC, Clark GA, Rickert PG, Horwitz EP (1988) Hydrolytic and radiolytic degradation of *O*-Phi-D(Ib)Cmpo—continuing studies. *Sep Sci Technol* 23:1355–1372
218. Berthon L, Morel JM, Zorz N, Nicol C, Virelizier H, Madic C (2001) Diamex process for minor actinide partitioning: hydrolytic and radiolytic degradations of malonamide extractants. *Sep Sci Technol* 36:709–728
219. Groenewold GS, Elias G, Mincher BJ, Mezyk SP, LaVerne JA (2012) Characterization of CMPO and its radiolysis products by direct infusion ESI-MS. *Talanta* 99:909–917
220. Mincher BJ, Mezyk SP, Elias G, Groenewold GS, Riddle CL, Olson LG (2013) The radiation chemistry of CMPO: part I. Gamma radiolysis. *Solv Extr Ion Exch* 31:715–730

221. Mincher BJ, Mezyk SP, Elias G, Groenewold GS, LaVerne JA, Nilsson M, Pearson J, Schmitt NC, Tillotson RD, Olson LG (2014) The radiation chemistry of CMPO: part 2. Alpha radiolysis. *Solv Extr Ion Exch* 32:167–168
222. Hudson MJ, Lewis FW, Harwood LM (2013) The circuitous journey from malonamides to BTPhens: ligands for separating actinides from lanthanides. In: Harmata M (ed) *Strategies and Tactics in Organic Synthesis*. Academic Press, London, pp 177–202
223. Zarzana CA, Groenewold GS, Mincher BJ, Mezyk SP, Wilden A, Schmidt H, Modolo G, Wishart JF, Cook AR (2015) A comparison of the gamma-radiolysis of TODGA and T(EH)DGA using UHPLC-ESI-MS analysis. *Solv Extr Ion Exch* 33:431–447
224. Galan H, Nunez A, Espartero AG, Sedano R, Durana A, de Mendoza J (2012) Radiolytic stability of TODGA: characterization of degraded samples under different experimental conditions. *Procedia Chem* 7:195–201
225. Sugo Y, Sasaki Y, Tachimori S (2002) Studies on hydrolysis and radiolysis of *N,N,N',N'*-tetraoctyl-3-oxapentane-1,5-diamide. *Radiochim Acta* 90:161–165
226. Shkrob IA, Marin TW, Bell JR, Luo H, Dai S, Hatcher JL, Rimmer RD, Wishart JF (2012) Radiation-induced fragmentation of diamide extraction agents in ionic liquid diluents. *J Phys Chem B* 116:2234–2243
227. Sugo Y, Izumi Y, Yoshida Y, Nishijima S, Sasaki Y, Kimura T, Sekine T, Kudo H (2007) Influence of diluent on radiolysis of amides in organic solution. *Radiat Phys Chem* 76:794–800
228. Berthon L, Journet S, Lalia V, Morel JM, Zorz N, Berthon C, Amerkraz B (2004) Use of chromatographic techniques to study a degraded solvent for minor actinides partitioning: qualitative and quantitative analysis. Paper presented at the Atalante-2004, Nimes, France,
229. Panak PJ, Geist A (2013) Complexation and extraction of trivalent actinides and lanthanides by triazinylpyridine *N*-donor ligands. *Chem Rev* 113:1199–1236
230. Schmidt H, Wilden A, Modolo G, Švehla J, Grüner B, Ekberg C (2015) Gamma radiolytic stability of CyMe4BTBP and the effect of nitric acid. *Nukleonika* 60:879–884
231. Nilsson M, Andersson S, Ekberg C, Foreman MRS, Hudson MJ, Skarnemark G (2006) Inhibiting radiolysis of BTP molecules by addition of nitrobenzene. *Radiochim Acta* 94:103–106
232. Sulich A, Grodkowski J, Mirkowski J, Kocia R (2014) Reactions of ligands from BT(B)P family with solvated electrons and benzophenone ketyl radicals in 1-octanol solutions. Pulse radiolysis study. *J Radioanal Nucl Chem* 300:415–421
233. Ewing RC (2015) Long-term storage of spent nuclear fuel. *Nat Mater* 14(3):252–257
234. Eriksen TE, Shoesmith DW, Jonsson M (2012) Radiation induced dissolution of UO<sub>2</sub> based nuclear fuel—a critical review of predictive modelling approaches. *J Nucl Mater* 420:409–423
235. Roth O, Jonsson M (2008) Oxidation of UO<sub>2</sub>[s] in aqueous solution. *Cent Eur J Chem* 6:1–14
236. Jonsson M (2010) Radiation-induced processes at solid–liquid interfaces. In: Wishart JF, Rao BSM (eds) *Recent Trends in Radiation Chemistry*. World Scientific, New Jersey, pp 301–323
237. Yang M, Jonsson M (2015) Surface reactivity of hydroxyl radicals formed upon catalytic decomposition of H<sub>2</sub>O<sub>2</sub> on ZrO<sub>2</sub>. *J Mol Catal A Chem* 400:49–55
238. Barreiro Fidalgo A, Dahlgren B, Brinck T, Jonsson M (2016) Surface reactions of H<sub>2</sub>O<sub>2</sub>, H<sub>2</sub>, and O<sub>2</sub> in aqueous systems containing ZrO<sub>2</sub>. *J Phys Chem C* 120:1609–1614
239. Björkbacka Å, Hosseinpour S, Johnson M, Leygraf C, Jonsson M (2013) Radiation induced corrosion of copper for spent nuclear fuel storage. *Radiat Phys Chem* 92:80–86
240. Björkbacka Å, Yang M, Gasparrini C, Leygraf C, Jonsson M (2015) Kinetics and mechanisms of reactions between H<sub>2</sub>O<sub>2</sub> and copper and copper oxides. *Dalton Trans* 44:16045–16051
241. Lousada CM, Johansson AJ, Brinck T, Jonsson M (2012) Mechanism of H<sub>2</sub>O<sub>2</sub> decomposition on transition metal oxide surfaces. *J Phys Chem C* 116:9533–9543
242. Hiroki A, LaVerne JA (2005) Decomposition of hydrogen peroxide at water-ceramic oxide interfaces. *J Phys Chem B* 109:3364–3370
243. Jonsson M, Nielsen F, Roth O, Ekeröth E, Nilsson AR, Hossain MM (2007) Radiation induced spent nuclear fuel dissolution under deep repository conditions. *Environ Chem Lett* 41:7087–7093
244. Ekeröth E, Roth O, Jonsson M (2006) The relative impact of radiolysis products in radiation induced oxidative dissolution of UO<sub>2</sub>. *J Nucl Mater* 355:38–46
245. Jonsson M, Nielsen F, Roth O, Ekeröth E, Nilsson S, Hossain MM (2007) Radiation induced spent nuclear fuel dissolution under deep repository conditions. *Environ Sci Technol* 41:7087–7093
246. Ekeröth E, Jonsson M (2003) Oxidation of UO<sub>2</sub> by radiolytic oxidants. *J Nucl Mater* 322:242–248
247. Hossain MM, Ekeröth E, Jonsson M (2006) Effect of HCO<sub>3</sub><sup>−</sup> on the kinetics of UO<sub>2</sub> oxidation by H<sub>2</sub>O<sub>2</sub>. *J Nucl Mater* 358:202–208

248. Eriksen TE, Jonsson M, Merino J (2008) Modelling of time resolved and long contact time dissolution studies of spent nuclear fuel in 10 mM carbonate solution—a comparison between two different models and experimental data. *J Nucl Mater* 375:331–339
249. Nielsen F, Lundahl K, Jonsson M (2008) Simulations of H<sub>2</sub>O<sub>2</sub> concentration profiles in the water surrounding spent nuclear fuel. *J Nucl Mater* 372:32–35
250. Nielsen F, Ekeröth E, Eriksen TE, Jonsson M (2008) Simulation of radiation induced dissolution of spent nuclear fuel using the steady-state approach. A comparison to experimental data. *J Nucl Mater* 374:286–289
251. Jonsson M, Ekeröth E, Roth O (2004) Oxidation of UO<sub>2</sub> by one- and two-electron oxidants. *Mater Res Soc Symp Proc* 807:77–82
252. Nilsson S, Jonsson M (2011) H<sub>2</sub>O<sub>2</sub> and radiation induced dissolution of UO<sub>2</sub> and SIMFUEL pellets. *J Nucl Mater* 410:89–93
253. Trummer M, Dahlgren B, Jonsson M (2010) The effect of Y<sub>2</sub>O<sub>3</sub> on the dynamics of oxidative dissolution of UO<sub>2</sub>. *J Nucl Mater* 407:195–199
254. Pehrman R, Trummer M, Lousada CM, Jonsson M (2012) On the redox reactivity of doped UO<sub>2</sub> pellets—influence of dopants on the H<sub>2</sub>O<sub>2</sub> decomposition mechanism. *J Nucl Mater* 430:6–11
255. Lousada CM, Trummer M, Jonsson M (2013) Reactivity of H<sub>2</sub>O<sub>2</sub> towards different UO<sub>2</sub>-based materials: the relative impact of radiolysis products revisited. *J Nucl Mater* 434:434–439
256. Trummer M, Nilsson S, Jonsson M (2008) On the effects of fission product noble metal inclusions on the kinetics of radiation induced dissolution of spent nuclear fuel. *J Nucl Mater* 378:55–59
257. Nilsson S, Jonsson M (2008) On the catalytic effect of Pd(s) on the reduction of UO<sub>2</sub><sup>2+</sup> with H<sub>2</sub> in aqueous solution. *J Nucl Mater* 374:290–292
258. Trummer M, Jonsson M (2010) Resolving the H<sub>2</sub> effect on radiation induced dissolution of UO<sub>2</sub>-based spent nuclear fuel. *J Nucl Mater* 396:163–169
259. Yang M, Barreiro Fidalgo A, Sundin S, Jonsson M (2013) Inhibition of radiation induced dissolution of UO<sub>2</sub> by sulfide—a comparison with the hydrogen effect. *J Nucl Mater* 434:38–42
260. Pusch R, Karnland O, Lajudie A, Decarreau A (1992) MX80 Clay Exposed to High Temperatures and Gamma Radiation. Swedish Nuclear Fuel and Waste Management Co., Sockholm
261. Sorieul S, Allard T, Wang LM, Grambin-Lapeyre C, Lian J, Calas G, Ewing RC (2008) Radiation stability of smectite. *Environ Sci Technol* 42:8407–8411
262. Holmboe M, Wold M, Jonsson M, Garcia-Garcia S (2009) Effects of  $\gamma$ -irradiation on the stability of colloidal Na<sup>+</sup>-montmorillonite dispersions. *Appl Clay Sci* 43:86–90
263. Holmboe M, Norrfors KK, Jonsson M, Wold S (2011) Effect of  $\gamma$ -radiation on radionuclide retention in compacted bentonite. *Radiat Phys Chem* 80:1371–1377
264. Holmboe M, Jonsson M, Wold S (2012) Influence of  $\gamma$ -radiation on the reactivity of montmorillonite towards H<sub>2</sub>O<sub>2</sub>. *Radiat Phys Chem* 81:190–194
265. Barreiro Fidalgo A, Sundin S, Jonsson M (2014) Effect of bentonite on radiation induced dissolution of UO<sub>2</sub> in an aqueous system. *J Nucl Mater* 447:73–76
266. Lainé M, Allard T, Balan E, Martin F, Von Bardeleben HJ, Robert J-L, Caër SL (2016) Reaction mechanisms in talc under ionizing radiation: evidence of a high stability of H<sup>+</sup> atoms. *J Phys Chem C* 120(4):2087–2095



# Upgrading and Refining of Crude Oils and Petroleum Products by Ionizing Irradiation

Yuriy A. Zaikin<sup>1</sup> · Raissa F. Zaikina<sup>1</sup>

Received: 22 March 2016 / Accepted: 4 May 2016 / Published online: 24 May 2016  
© Springer International Publishing Switzerland 2016

**Abstract** A general trend in the oil industry is a decrease in the proven reserves of light crude oils so that any increase in future oil exploration is associated with high-viscous sulfuric oils and bitumen. Although the world reserves of heavy oil are much greater than those of sweet light oils, their exploration at present is less than 12 % of the total oil recovery. One of the main constraints is very high expenses for the existing technologies of heavy oil recovery, upgrading, transportation, and refining. Heavy oil processing by conventional methods is difficult and requires high power inputs and capital investments. Effective and economic processing of high viscous oil and oil residues needs not only improvements of the existing methods, such as thermal, catalytic and hydro-cracking, but the development of new technological approaches for upgrading and refining of any type of problem oil feedstock. One of the perspective approaches to this problem is the application of ionizing irradiation for high-viscous oil processing. Radiation methods for upgrading and refining high-viscous crude oils and petroleum products in a wide temperature range, oil desulfurization, radiation technology for refining used oil products, and a perspective method for gasoline radiation isomerization are discussed in this paper. The advantages of radiation technology are simple configuration of radiation facilities, low capital and operational costs, processing at lowered temperatures and nearly atmospheric pressure without the use of any catalysts, high production rates, relatively low energy consumption, and flexibility to the type of oil feedstock.

---

This article is part of the Topical Collection “Applications of Radiation Chemistry”; edited by “Margherita Venturi, Mila D’Angelantonio”.

---

✉ Yuriy A. Zaikin  
[yzaikin@petrobeam.com](mailto:yzaikin@petrobeam.com)

Raissa F. Zaikina  
[rzaikina@petrobeam.com](mailto:rzaikina@petrobeam.com)

<sup>1</sup> PetroBeam, Inc., 606 South Main Street, Sweetwater, TN 37874, USA

**Keywords** High-viscous oils · Radiation-thermal cracking · Low-temperature radiation cracking · Used oil products · Desulfurization · Polymerization · Isomerization

## 1 Introduction

In the beginning of the 1960s, the phenomenon of radiation-thermal cracking (RTC) was discovered and described by L. S. Polak, A. V. Topchiev, R. P. Lavrovskiy and other researchers [1–3]. These studies revealed the basic mechanisms of radiation-induced chemical reactions in hydrocarbons and specific features of chain RTC reactions in particular. These early studies were the first evidence of the high-rate radiation-induced chemical conversion in hydrocarbons under the combined action of radiation and heat. The discovery of RTC was of a great practical importance because only chain reactions could provide sufficiently high rates of oil refining processes at industrial scales.

After this discovery, different aspects of ionizing irradiation applications for oil feedstock processing were the subjects of scientific and technological studies. Before the beginning of the 1990s, these works, with a few exceptions [4–6], were limited with the study of radiation-induced decomposition of model hydrocarbons and light oil fractions. The advantages of radiation technologies became more obvious when they were applied to processing of heavy and highly paraffinic oils, bitumen, wastes of oil extraction, and heavy oil residua. Processing of these types of feedstock by conventional methods is not sufficiently economic and faces considerable technological difficulties. For this reason, chemical and physical aspects of heavy oil radiation processing are of a special technological interest [7, 8].

The systematic experiments on heavy oil radiation processing were started in the early 1990s [9–16]. These studies have shown that radiation-chemical conversion in such complicated hydrocarbon systems had essential distinctions both from that in thermal cracking and RTC of light oils. As distinct from light oils, self-sustaining chemical reactions in heavy hydrocarbon feedstock are characteristic for strong synergetic effects attributed to radiation energy redistribution between the original components of a complex hydrocarbon system and a number of intermediate products. These phenomena promote side reactions of the non-destructive nature and strongly affect the rate of feedstock conversion and final product composition [10, 14].

The most important phenomena observed and studied in the experiments with the problem types of high-paraffin and heavy oils are radiation-enhanced isomerization and radiation-induced polymerization in RTC conditions. Determination of the conditions and evaluation of the intensity of these effects are important for obtaining high yields of light products of oil radiation processing and their quality control. Further investigations [17–20] have shown that the phenomenon of radiation-enhanced isomerization can be effectively used for the increase in gasoline octane numbers using heavy oil residua as stimulators of low-temperature



isomerization. Radiation-enhanced isomerization of hydrocarbons was not widely covered in the literature and this review provides its more detailed description.

New prospects in the development of radiation technologies for oil upgrading and refining were opened with the discovery of low-temperature radiation cracking of hydrocarbons [21–24]. Studies of this phenomenon revealed the mechanisms of radiation cracking in a wide temperature range including the roles of the dose rate of ionizing irradiation, the cage mechanism of correlated radical recombination, and isomerization processes in these reactions.

The studies of low-temperature radiation cracking initiated development of the PetroBeam technology for upgrading and refining of high-viscous petroleum feedstock [25]. This technology combines advantages of RTC with the opportunity of feedstock processing at temperatures lower than 150 °C.

## 2 Methods for Petroleum Processing Based on Radiation-Thermal Cracking

### 2.1 Fundamentals

Radiation-thermal cracking (RTC) is a chain reaction of hydrocarbon molecule decomposition that differs from the classic thermal cracking (TC) mainly by the mechanism of cracking initiation. In the case of radical mechanism of thermal cracking, the initiation stage of the reaction (generation of a sufficient concentration of chain carriers) requires a high activation energy (about 340 kJ/mol). For the purpose of this article, the term “chain carriers” is defined as any radical species, such as hydrogen atoms or light alkyl radicals, capable of chain reaction propagation. Therefore, a noticeable rate of hydrocarbon thermal cracking is possible only at relatively high temperatures, for example, 500–600 °C for heptane. The chain propagation stage (decomposition of hydrocarbon molecules due to their interaction with free radicals and formation of new chain carriers) requires much lower activation energy (about 85 kJ/mol).

Application of RTC minimizes energy consumption for the initiation of the chain cracking reaction. In the case of thermal cracking (TC), both chain initiation and propagation are thermally activated processes. In the case of RTC, the first stage is radiation-initiated: chain carriers are generated by radiation. Radiation initiation of the chain reaction does not depend on temperature; the rate of radical generation depends only on the dose rate of ionizing irradiation. Conventional sources of radiation, such as electron accelerators and isotope gamma sources, provide generation of radicals in concentrations sufficient for the initiation of the chain reaction in hydrocarbons.

It is usually supposed that the stage of RTC propagation still remains thermally activated and heightened temperatures in the range of 350–420 °C are still required for propagation of the chain reaction of hydrocarbon cracking [1–4]. Generally, this statement is valid for relatively low values of the irradiation dose rates when radiation contribution to generation of species responsible for chain propagation is negligibly small. In early works on RTC of hydrocarbons, contribution of radiation

to the chain propagation was not considered because of the very short lifetime of the radiation-excited molecules (about  $10^{-15}$  s). However, the analysis of the dose dependence of the product yields after RTC of hydrocarbons [19, 22] has revealed availability of the radiation component in chain propagation whose relative fraction increases as the dose rate increases. Moreover, the radiation component of chain propagation can be comparable with the thermal one even at moderate dose rates.

Availability of the noticeable radiation contribution to propagation of the RTC chain reaction required clarification of the nature of the long-living unstable molecular states generated by radiation and able to interact with the radical chain carriers. In papers [18, 19], it was shown that such unstable states can be represented by the radical pairs bound in a cage. This conclusion was confirmed by the data of low-temperature hydrocarbon cracking and by demonstration of a special role of correlated radical recombination in the first-order reactions in thermal cracking termination at low temperatures [19].

Generally, the initial rate of the RTC chain reaction by the radical mechanism is determined by equation [19]

$$W^{(\text{RTC})} = \begin{cases} \frac{v-1}{v} R k_p (e^{-E_p/kT} + C_u), & v > 1 \\ 0, & v \leq 1 \end{cases} \quad (1)$$

where  $R$  is dimensionless concentration of radical chain carriers,  $k_p$  is reaction rate constant and  $E_p$  is activation energy for chain propagation,  $v$  is chain length (the ratio of the chain reaction propagation rate to the termination rate), and  $C_u$  is dimensionless concentration of radiation-generated unstable molecular states responsible for chain propagation:

$$C_u = G * P \tau \quad (2)$$

In Eq. (2),  $G^*$  is radiation-chemical yield ( $G$  value),  $\tau$  is lifetime of the radiation-generated unstable states, and  $P$  is dose rate of ionizing irradiation.

In dynamic equilibrium,

$$R = \sqrt{\frac{G_R P + k_i e^{-E_i/kT}}{k_{t2}}} \quad (3)$$

Here,  $G_R$  is radiation-chemical yield of free radicals,  $k_i$  is reaction rate constant and  $E_i$  is activation energy for chain initiation, and  $k_{t2}$  is rate of radical recombination in the second order reactions.

At  $v \gg 1$ , Eq. (1) takes a form

$$W^{(\text{RTC})} = k_p \sqrt{\frac{G_R P + k_i e^{-E_i/kT}}{k_{t2}}} \left( e^{-E_p/kT} + G * P \tau \right) \quad (4)$$

It follows from Eq. (4) that the rate of RTC increases as temperature and irradiation dose rate increase. In the temperature range characteristic for RTC, the rate of cracking initiation by radiation is much higher than the rate of thermal

initiation even at relatively low dose rates. The ratio of the RTC and TC cracking rates can be written as follows:

$$\frac{W^{(\text{RTC})}}{W^{(\text{TC})}} = \left( 1 + \sqrt{\frac{G_R}{k_i}} e^{E_i/2kT} \sqrt{P} \right) \left( 1 + G * P \tau e^{E_p/kT} \right) \quad (5)$$

The ratios of the RTC and TC chain initiation and propagation rates are correspondingly

$$\frac{W_i^{(\text{RTC})}}{W_i^{(\text{TC})}} = \frac{G_R P}{k_i} e^{E_i/kT} \quad (6)$$

$$\frac{W_p^{(\text{RTC})}}{W_p^{(\text{TC})}} = G * P \tau e^{E_p/kT} \quad (7)$$

The analysis of experimental data in studies [18, 19, 22] has shown that the lifetime  $\tau$  may vary in a wide range depending on the type of a hydrocarbon system, its temperature, and structure state.

In particular, using the values of the reaction parameters characteristic for hydrocarbons ( $E_i = 340$  kJ/mol,  $E_p = 85$  kJ/mol,  $G^* = G_R = 5$  radicals/100 eV) and assuming that RTC rate,  $W^{(\text{RTC})}$ , is equal to  $0.4 \text{ s}^{-1}$  at the dose rate of 4 kGy/s, the lifetime of radiation-generated unstable molecular states can be estimated from Eq. (4) as  $\tau \approx 10^{-4}$  s. The dependences of ratios of RTC and TC initiation, propagation rates, and total initial reaction rates on temperature and dose rate of ionizing irradiation calculated using these reaction constants are shown in Fig. 1.

Figure 1 shows that the rate of radiation cracking initiation is much higher than the rate of thermal initiation in the whole temperature range considered here. At the

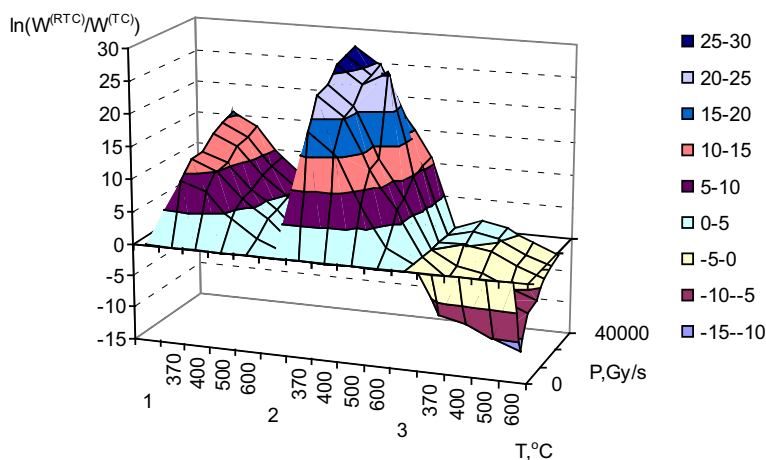


**Fig. 1** Ratios of the RTC and TC total initial reaction rates (1), initiation (2), and propagation rates (3) versus temperature and dose rate

same time, radiation contribution to chain propagation increases as cracking temperature decreases and irradiation dose increases. At sufficiently high irradiation doses, the radiation component of the chain propagation may exceed the thermal one.

The behavior described above can be observed only in the case of a chain length that is long enough ( $\nu \gg 1$ ). As temperature decreases, and approaches the critical temperature of the cracking start, the chain length tends to the unit and the cracking rate falls to zero.

In the general case, the expression for the RTC chain length can be written in the form [19]

$$\nu = \frac{\frac{2k_p}{k_{t1}} (e^{-E_p/kT} + G * P\tau)}{1 + \sqrt{1 + \frac{4k_{t2}}{k_{t1}^2} (k_i e^{-E_i/kT} + GP)}} \quad (8)$$

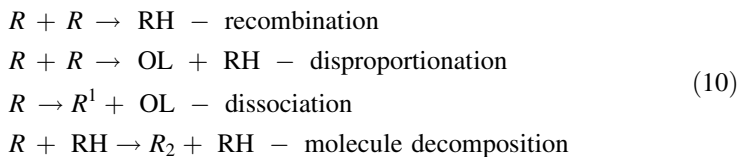
where  $k_{t1}$  is rate of radical recombination in cages in the first-order reactions.

In the case of thermal cracking, dose rate  $P$  in Eq. (8) is equal to zero. Below the critical temperature  $T_c^{(TC)}$  determined by equation [19]

$$T_c^{(TC)} = \frac{E_p}{k \ln \frac{k_p}{k_{t1}}} \quad (9)$$

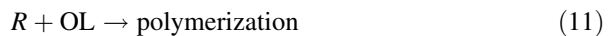
thermal cracking is impossible. Nevertheless, availability of a member in Eq. (8) responsible for radiation contribution chain propagation at temperatures  $T \leq T_c^{(TC)}$  indicates the possibility of chain cracking reactions at  $T \leq T_c^{(TC)}$  (low-temperature radiation cracking, or PetroBeam process [18, 19, 22–24]). Chain reactions of hydrocarbon cracking under ionizing irradiation at temperatures above  $T_c^{(TC)}$  should be related to radiation-thermal cracking. The RTC reactions are characteristic for considerable, often determinative, contribution of the thermal component to the chain propagation.

Radical reactions making considerable contribution to RTC of liquid hydrocarbons are mainly of the same type as TC reactions [26]:



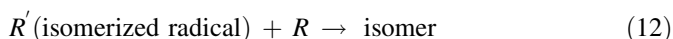
where  $R$  is radical,  $H$  is hydrogen atom, and  $RH$  is the hydrocarbon molecule.

The cracking rate and the maximal yield and stability of radiation cracking products strongly depend on the competing reactions of radiation-induced polymerization [14, 19, 27]:



where  $OL$  is olefin molecule.

This set of reactions should be supplemented with the reaction of isomerization that plays an especially important role in the radiation cracking of heavy oils with the high contents of aromatic compounds [11, 18, 19]:



Despite a formal similarity of the basic RTC and TC reactions, there are substantial differences between them. The same reactions can be caused by the action of radiation or heating but the probabilities of such reactions and their rates are different in radiation and thermal conditions. The specific conditions of the basic RTC reactions give rise to the side effects and reactions characteristic for RTC.

Different mechanisms of cracking initiation and propagation in TC and RTC result not only in different reaction rates but also in different hydrocarbon and hydrocarbon group contents of the cracking products. For example, higher concentrations of isoparaffins and higher octane numbers of the RTC gasoline compared with the gasoline of thermal and thermocatalytic cracking are the result of radiation-induced isomerization of alkanes. This difference becomes especially pronounced in the case of high-viscous (heavy and high-paraffinic) oils. Fractional contents of the overall products obtained by RTC of heavy fuel oil are compared in Fig. 2. In the case of RTC, the contents of commodity products are considerably higher.

Thus, RTC cannot be reduced to intensification of thermal reactions. Moreover, there are radiation-induced reactions that accompany RTC but cannot proceed in TC conditions. In particular, it relates to the reactions of radiation-enhanced isomerization.

## 2.2 Heavy Oil Upgrading and Refining

The technology for heavy oil and oil residua radiation processing based on RTC [29] allowed expanding the raw material base for production of motor fuels by involvement of oil fractions with  $T_b > 450^\circ\text{C}$  into radiation processing with the

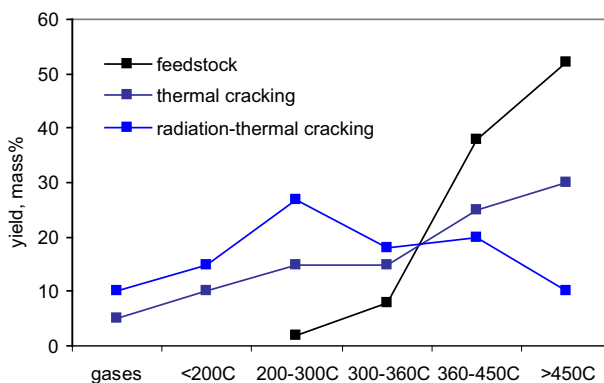


**Fig. 2** Fractional contents of products obtained by TC and RTC of fuel oil (according to data [28])

increased yield and improved quality together with the reduction of energy consumption compared with the conventional thermal cracking.

Radiation-thermal processing of heavy oils and petroleum products is performed at nearly atmospheric pressure in the temperature range of 370–410 °C. In the optimal process conditions, the yields of motor fuels make up to 80 mass%, including up to 20 mass% gasoline and 60 mass% diesel fuel. The byproducts are heavy coking residue (up to 10 mass%) and gases (up to 10 mass%) containing hydrogen, methane, ethylene, and other light hydrocarbon gases.

Potential application of RTC facilities for upgrading and refining crude oils and bitumen provides such advantages as simple configurations of the plants, their flexibility to the type of feedstock processed, much smaller land sizes compared with those in conventional technologies, absence of catalysts and low capital and operational expenses [8, 9]. Application of RTC to heavy fuel oil and bitumen [23, 30] is illustrated in Figs. 3 and 4.

RTC-based radiation methods developed up to date can be used in different fields of oil industry for upgrading and refining crude oils and oil products.

### 2.3 Cleaning and Refining of Used Oil Products

Application of radiation methods is a promising approach to solution of an acute problem of environment pollution by used oil products [13, 19, 33, 34]. Unlike the methods for oil radiation cracking, cleaning and refining of used oil products do not need a high degree of oil conversion. The most effective are the process conditions that provide the combination of a rather low degree of oil decomposition with an intense olefin polymerization.

In a series of experiments, it was observed that a reactive heavy residue formed as a result of oil radiation-induced polymerization that was remarkable for high absorption ability [14]. In the technology for used oil radiation treatment, a small amount of the polymerizing deposit effectively absorbs mechanical and other

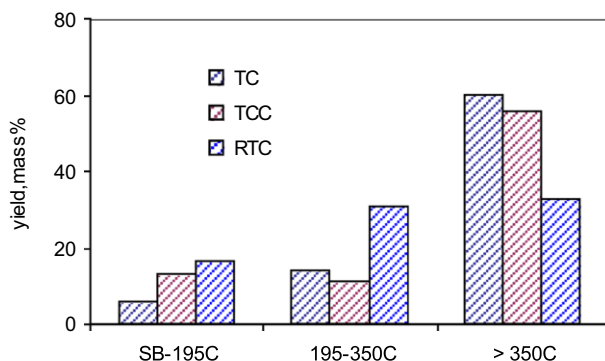


**Fig. 3** Fractional contents of the liquid product obtained from fuel oil (10° API) using different processes. *RTC* radiation-thermal cracking at 390 °C [23]. *TC* thermal cracking in lab conditions at 480 °C [31]. *TCC* thermocatalytic cracking in lab conditions at 450 °C (catalyst based on iron oxides) [31]

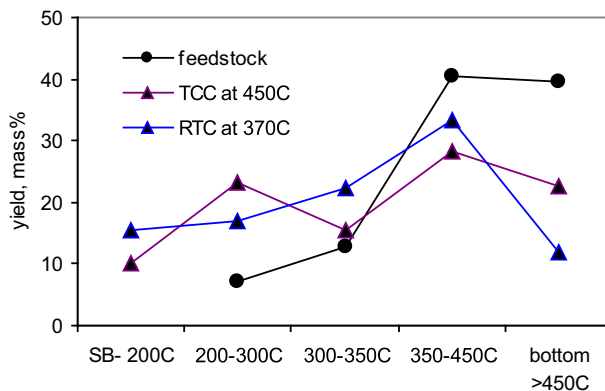


**Fig. 4** Fractional contents of the liquid product obtained from bitumen by radiation processing (RTC) and thermocatalytic cracking. *RTC* radiation-thermal cracking [23]. *TCC* thermocatalytic cracking [32]

contaminants. It can be compared to an approach used in the well-known technology for sewage water purification in polymer industry. In this method, the monomer residues are polymerized in the water phase by radiation initiation. The insoluble polymer deposit is used as a contaminant absorbent. In the case of sewage water that does not contain polymerizing monomers, small amounts of monomers easily polymerizing under ionizing irradiation are specially added. The polymer deposit formed as a result of radiation processing absorbs water contaminants [35].

Used oil products, such as used lubricants and contaminated diesel fuel, are processed with moderate irradiation doses and dose rates at temperatures in the range of 340–380 °C, which is somewhat lower than the temperatures necessary for the start of an intense RTC reaction. The main products of the process are purified basic lubricants and diesel fuel. The total yield of the target products makes 94–96 mass% including the lubricant yield up to 50 %, depending on the original oil composition.

An important application of radiation technology for the environment protection, already implemented in the industrial scale, is the electron beam gas treatment [36, 37] that provides flue gas purification after heavy oil combustion.

## 2.4 Radiation Methods for Oil Demercaptanization and Desulfurization

Application of radiation methods allows obtaining a high degree of sulfur conversion in the petroleum feedstock. The methods developed by now are mainly based on the reactions of radiation-induced oxidation. In particular, contacting the product of oil radiation processing with the reactive ozone-containing air allows combination of radiation-thermal cracking with the intense sulfur oxidation (Fig. 5). It leads to formation of the high-molecular sulfur compounds, such as sulfoxides, sulfones and sulfonic acids accumulated in the heavy residue. Strong oxidation of the sulfur species does away with their chemical aggressiveness and causes sulfur redistribution in the overall product leading to partial desulfurization of light

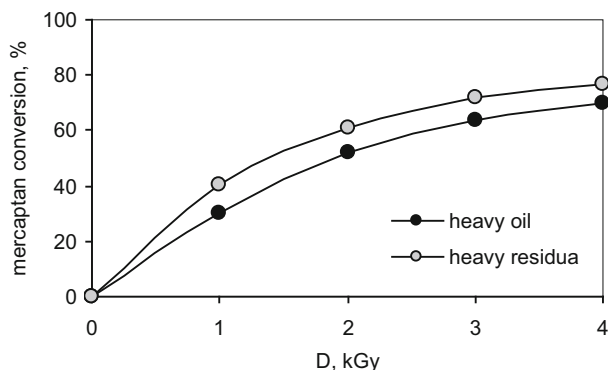


**Fig. 5** Dependence of mercaptan conversion on the dose of electron irradiation for high-viscous crude oil and heavy oil residue (according to data [12])

fractions. The oxidized high-molecular species can be much easier removed from the heavy residue by conventional methods using such extracting agents as water solutions of sulfuric acid or acetone, ethylene glycol, or monoethyl alcohol.

A method for oil desulfurization proposed in the studies [12, 15, 19, 38] includes two stages. At the first stage, oil is subjected to radiation processing. At this stage, radiation-induced oxidation of sulfur compounds and sulfur redistribution in the overall product lead to considerable desulfurization of the light fractions. The next stage is a standard procedure for the extraction of the deeply oxidized sulfur compounds. A high degree of sulfur oxidation results from the double stimulation of the oxidation processes by oil radiation activation and radiolysis of the atmospheric air.

A high degree of gasoline desulfurization was demonstrated in the experiments on electron irradiation of heavy crude oil and fuel oil with the total sulfur content of 2 mass% [12, 15]. After RTC, the sulfur content in the gasoline fraction was 40 times lower than that in the original feedstock. In the cases when considerable conversion of an oil product is undesirable and the only purpose of its processing is desulfurization, oil irradiation can be performed in “mild” conditions providing minimal losses of the original product.

Radiation processing of high sulfuric oil with sulfur contents of 3 mass% and higher becomes more difficult, especially in the cases when feedstock contains high concentrations of dissolved hydrogen sulfide together with mercaptans. To provide considerable sulfur conversion in these cases, the feedstock was subjected to bubbling with ionized ozone-containing air in the field of X-ray irradiation with the subsequent irradiation by high-energy electrons [15]. The efficiency of ionized air application in oil radiation processing was demonstrated in a series of studies [12, 15, 39]. Together with ozone, the radiation-excited air comprises monoatomic oxygen, excited oxygen molecules, and various oxygen-containing complexes. Many components of this mixture are strong oxidizers themselves and some of them are stronger than ozone. In the tests [12, 15], no special devices for conversion electron to bremsstrahlung X-ray radiation were used. Both bremsstrahlung



irradiation and formation of ionized air were the side effects of the electron accelerator operation and their applications did not require any additional expenses.

As a result of such radiation processing of high-sulfuric oils, sulfur partially concentrated in the heavy residue in the form of the oxidized high-molecular species while another part of sulfur passed to the gaseous phase in the form of hydrogen sulfide. The experiments have shown a high efficiency of radiation processing for conversion of both disulfide and thiophene sulfur, which can be hardly removed by conventional methods [19].

Generally, the treatment of high-sulfuric oil and oil products with ionized ozone-containing air provides deep oxidation of sulfur compounds and improves the product fractional contents. The low cost of the ionized air as a by-product of the accelerator operation makes this type of processing highly economic.

Different approaches to oil desulfurization using electron and gamma irradiation were developed in studies [40–45].

### 3 Low-Temperature Radiation Cracking

In the extreme case of low temperatures, Eq. (8) for the cracking chain length, takes a form [19]:

$$v = \frac{\frac{2k_p}{k_{t1}} G * P \tau}{1 + \sqrt{1 + \frac{4k_{t2}}{k_{t1}^2} GP}} \quad (13)$$

where  $\tau \approx \frac{1}{k_{t1}}$ .

The temperature of the cracking start is determined by equation:

$$T_c = \frac{E_p}{k \ln \frac{2k_p/k_{t1}}{1 - 2\frac{k_p}{k_{t1}}G*P + \sqrt{1 + \frac{4k_{t2}}{k_{t1}^2}GP}}} \quad (14)$$

It can be seen from Eq. (14) that  $T_c \rightarrow 0$  as  $P \rightarrow P_c$ , where the critical dose rate  $P_c$  can be found from equation

$$1 - 2\frac{k_p}{k_{t1}^2(T_c)}G*P_c + \sqrt{1 + \frac{4k_{t2}}{k_{t1}^2(T_c)}GP_c} = 0$$

At the dose rates  $P \geq P_c$ , chain cracking reaction can proceed at any temperature  $T \geq T_c$ . This condition (the rate of chain continuation is greater than the rate of its termination) can be written in the form of inequality [19]:

$$P > P_c \approx \frac{k_{t1}^2(T_c)}{k_p G*} \quad (15)$$

According to Eq. (15), dependence of  $P_c$  on temperature is determined by the temperature dependence of radical recombination rate in cages,  $k_{t1}$ .

Evaluation of the recombination constant  $k_{t1}$  is equivalent to determination of the radical lifetime in a cage formed by other hydrocarbon molecules. To get out of the cage, a radical should surmount a potential barrier. The radicals that surmounted the barrier and went out of the cage enter recombination with other free radicals in the second-order reactions. In the dynamic equilibrium, the frequency of radical exits from the cages should be equal to the frequency of their recombination in the second-order reactions:

$$\frac{D}{x^2} c * R = k_{t2} P_{\text{exit}} c * R,$$

or

$$x^2 = \frac{D}{k_{t2} P_{\text{exit}}} \quad (16)$$

In Eq. (16),  $c^*$  is concentration of radicals recombining in cages in the first-order reactions;  $R$  is bulk concentration of free radicals,  $D$  is diffusion coefficient,  $x$  is the cage size, and  $P_{\text{exit}}$  is probability of radical exit from a cage.

Using the Frenkel equation,

$$D = \alpha \frac{2kT}{\delta \eta} \quad (17)$$

expression (16) can be reduced to the form:

$$x^2 = \alpha \frac{2kT}{\delta \eta k_{t2} P_{\text{exit}}}. \quad (18)$$

In Eqs. (17) and (18),  $\eta$  is dynamic viscosity and  $\delta$  is length of a diffusion jump. Coefficient  $\alpha > 1$  is introduced into expression (17) to take into account that the diffusing specie is usually a hydrogen atom or a light radical that has a higher diffusion coefficient than a heavier hydrocarbon radical.

The probability of a radical exit from the cage can be determined as a ratio of the rate of the radical exit from a cage to the total rate of radical intracellular recombination and their exit from the cage:

$$P_{\text{exit}} = \frac{\frac{D}{x^2}}{\frac{D}{x^2} + k_{t2} \frac{\delta}{x}} = \frac{D}{D + k_{t2} \delta x} \quad (19)$$

The cage size can be found by substitution of Eq. (19) into formula (16):

$$x = \frac{\delta}{2} \left( 1 + \sqrt{1 + \frac{4D}{k_{t2} \delta^2}} \right) \quad (20)$$

At very low temperatures when  $\delta^2 k_{t2} \gg 4D$ , the cage size tends to the length of a diffusion jump ( $x \rightarrow \delta$ ). At relatively high temperatures ( $T > 70 \text{ }^\circ\text{C}$ ),  $\delta^2 k_{t2} \gg 4D$  and the expression for the cage size can be written in the form:

$$x \approx \sqrt{\frac{D}{k_{t2}}} = \sqrt{\frac{2\alpha kT}{\eta \delta k_{t2}}} \quad (21)$$

Recombination of a radical pair is a first-order reaction at the macroscopic scale. At the same time, it can be considered a second-order reaction in the single cage scale:

$$k_{t1} \beta c_R = k_{t2} n c_R^2, \quad (22)$$

where  $n$  is number of radical diffusion jumps before its exit from the cage;  $c_R$  is concentration of mobile radicals in the cage:

$$c_R \approx \frac{\delta^3}{x^3}. \quad (23)$$

Coefficient  $\beta > 1$  takes into account that the volume of a radical pair can be much larger than that of a mobile species.

Number  $n$  can be evaluated considering the light radical motion as diffusion with an equal jump probability in each direction. From the random motion theory [46], it is known that the probability for a particle to pass to the distance  $x$  after  $n$  jumps is determined by equation

$$w = \left( \frac{3x^2}{2\pi n \delta^2} \right)^{3/2} \exp\left( -\frac{3x^2}{2n\delta^2} \right). \quad (24)$$

where  $\delta$  is average path of a single jump.

The probability that the particle will remain within a zone of radius  $x_0$  is shown in Fig. 6, where  $X = \frac{x_0}{\delta\sqrt{n}}$ .

The cage size can be defined as a distance  $x_0$  where radical residence within a zone of radius  $x_0$  and its exit out of the zone are equally probable, i.e.,  $W_x = 0.5$ .

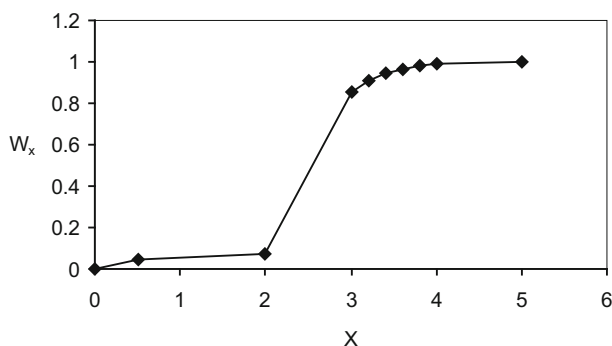


**Fig. 6** Probability of molecular fragment residence,  $W_x$ , in a sphere of dimensionless radius  $X$  after  $n$  diffusion jumps

Figure 5 shows that this condition is satisfied at  $X \approx 2.5$ . It corresponds to the number of diffusion jumps

$$n \approx 0.16 \frac{x^2}{\delta^2} \quad (25)$$

Substitution of expressions (23) and (25) into Eq. (22) yields

$$k_{t1} = \frac{0.16 \delta}{\beta x} k_{t2} \quad (26)$$

Using Eq. (21) for the cage size, the following expressions can be obtained:

$$k_{t1} = B k_{t2}^{3/2} D^{=1/2}, \quad B = \frac{0.16}{\beta} < 1 \quad (27)$$

$$k_{t1} = A (\delta k_{t2})^{3/2} \left( \frac{\eta}{2kT} \right)^{1/2}, \quad A = \frac{0.16}{\beta \sqrt{\alpha}} < 1 \quad (28)$$

Evaluation of the recombination rate constant  $k_{t1}$  and the cage size  $x$  in bitumen is given below.

Figure 7 shows temperature dependence of the cage size calculated using formula (21). For the selected set of parameters, the cage size makes  $5 \times 10^{-8}$  at the temperature of cracking start,  $T_c = 550$  K. This is close to the cage size estimate by Brodskiy et al. [3].

Recombination rate constant  $k_{t1}$  was determined from Eq. (28) using the data on bitumen viscosity [19]. The results are compared with  $k_{t1}$  values determined from Eq. (15) and experimental temperature dependence of the minimal dose rate,  $P_c$ , required for the start of low-temperature cracking reaction [19]. This dependence based on the experimental data on radiation cracking of heavy oil feedstock at low temperatures is plotted in Fig. 8.

Temperature dependence of the calculated recombination rate constant  $k_{t1}$  shown in Fig. 9 is in a good agreement with experimental data on the critical dose rate of

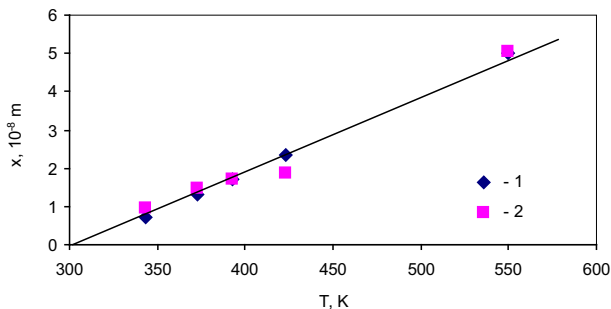
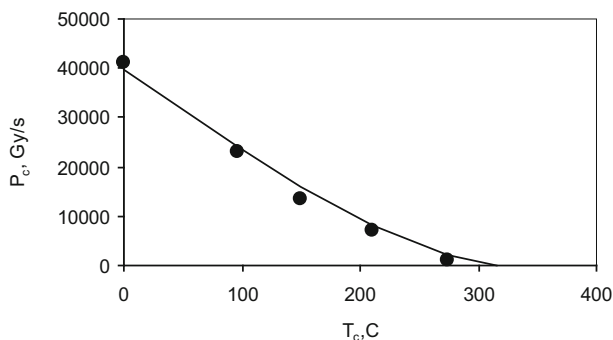
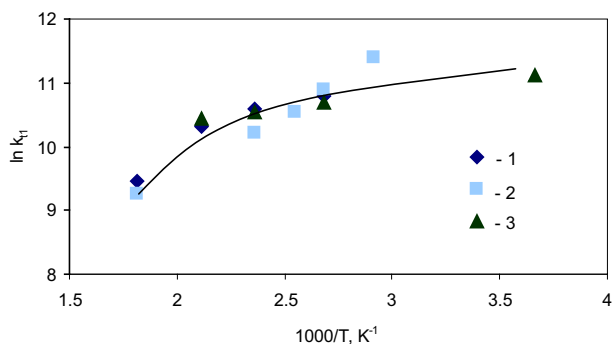


Fig. 7 Temperature dependence of the cage size. 1 Calculated using Eq. (20) ( $\delta = 10^{-9}$  m,  $\sqrt{\alpha} = 32$ ), 2 calculated using Eq. (21) ( $E = 33.6$  kJ/mol,  $D_0 = 2.6 \times 10^{-10}$  m<sup>2</sup>/s,  $\beta = 25$ )



**Fig. 8** Temperature dependence of critical dose rate of ionizing irradiation needed for cracking start (at the dose rate equal to  $P_c$ , radiation cracking can proceed at any temperatures higher than  $T_c$ )



**Fig. 9** Temperature dependence of radical recombination rate in cages. 1 calculated using Eq. (28) ( $E = 33.6$  kJ/mol,  $D_0 = 2.6 \times 10^{-10}$  m<sup>2</sup>/s,  $\beta = 250$ ), 2 calculated using Eq. (27) ( $A = 2 \times 10^{-5}$ ), 3 recombination rate constant determined from Eq. (15) using the data on critical dose rate of low-temperature radiation cracking

the radiation cracking start. These data are also in a satisfactory agreement with the calculations using Eq. (29) at the appropriate values of the diffusion activation energy and pre-exponential factor:

$$D = D_0 e^{-E/kT} \quad (29)$$

The alternate calculations shown in Fig. 9 show the same tendency of a considerable increase in the minimal irradiation dose rate needed for the start of the chain cracking reaction in heavy oils and bitumen as reaction temperature decreases.

This simple analytical model can be used for estimation of the conditions of low-temperature radiation cracking in heavy oil feedstock. It should be noted that temperature dependence and absolute values of the recombination rate constant  $k_{t1}$ , as well as critical dose rate of the cracking start  $P_c$ , strongly depend on the feedstock type, its fractional, hydrocarbon contents and structure state. In super-heavy

petroleum oils and bitumen,  $P_c$  may exceed 20 kGy/s even at temperatures of 120–150 °C [19].

At lowered temperatures, expression (5) for the cracking rate can be reduced to the form

$$W^{(\text{RTC})} = k_p \sqrt{\frac{G_R P}{k_{t2}}} G * P \tau \quad (30)$$

where the lifetime of radiation-generated radical pairs,  $\tau$ , is a function of temperature.

Dependence of the initial cracking rate on temperature and dose rate of ionizing irradiation is plotted in Fig. 10. It should be noted that the maximal yields of light products of both RTC and low-temperature radiation cracking depend not only on the initial cracking rate but also on the cracking kinetics complicated by radiation-enhanced polymerization and absorption of the light products by the reactive heavy residue [19, 27]. As a result of these competing reactions, the cracking rate decreases as the irradiation dose increases. In the case of extra-viscous oils, a maximum may appear in the dose-rate dependences of light product yields at practically reasonable irradiation doses [27]. A dose dependence of the light fraction yields [27] typical for low-temperature cracking of high-viscous oils is shown in Fig. 11.

The technology of low-temperature radiation cracking (PetroBeam process) applicable to any type of high-viscous petroleum feedstock was developed in the studies [21–25]. The tests have shown its high efficiency for processing heavy and high paraffinic oils and natural bitumen. Figure 12 shows the fractional contents of the product obtained in flow conditions of PetroBeam process at a temperature of 35 °C and electron irradiation dose rate of 10 kGy/s. Conversion of the heavy oil

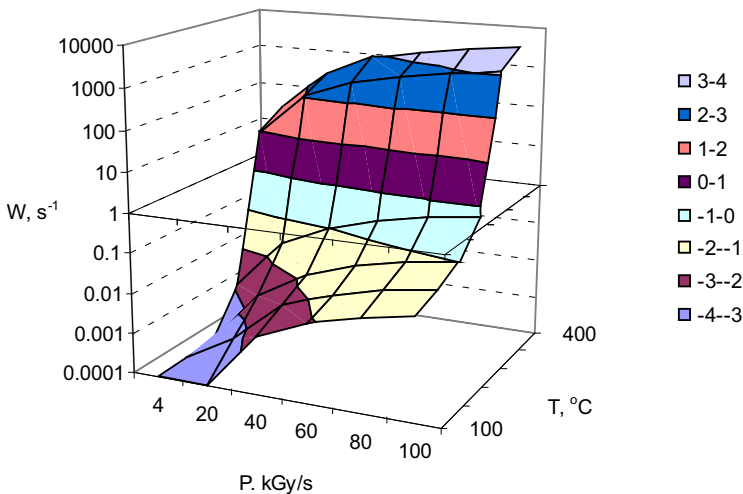


**Fig. 10** Dependence of the initial rate of low-temperature radiation cracking on temperature and dose rate of ionizing irradiation

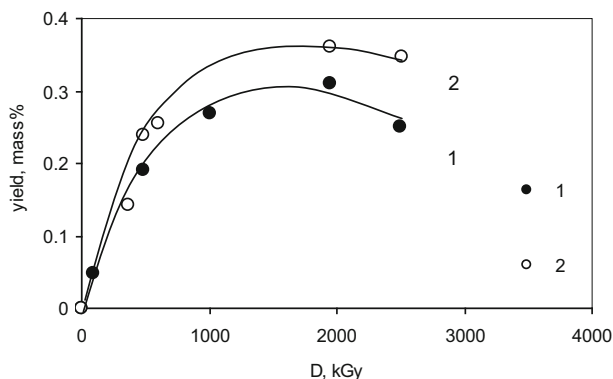


**Fig. 11** Yields of light fractions boiling out below 450 °C after low-temperature radiation cracking of heavy crude oil versus the dose of electron irradiation (according to data [27]): 1  $P = 40$  kGy/s,  $T = 120$  °C; 2  $P = 80$  kGy/s,  $T = 120$  °C

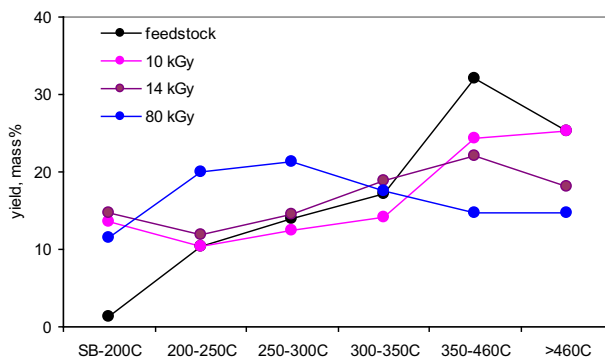


**Fig. 12** Fractional contents of heavy crude oil after PetroBeam processing (according to data [24])

residue and yields of light fractions in PetroBeam process at such low temperature are close to those characteristic for radiation-thermal cracking at 400 °C. As a result of radiation processing, the product viscosity decreased by 87 % compared with the feedstock viscosity.

Figure 13 illustrates the results of PetroBeam processing of high-paraffin oil having a pour point of 60 °C. Due to very strong radiation-induced polymerization at heightened temperatures, conversion of this sort of oil by means of RTC is very difficult. Application of the PetroBeam process provides an effective solution of this problem. As a result of electron-beam processing of oil in flow conditions at a temperature of 60 °C, its fractional content was considerably improved and the pour point dropped to −20 °C.

There are many good reviews of the preferable applications of electron accelerators and isotope gamma sources in the different fields of industry [47, 48] but they usually do not cover technologies, such as low-temperature cracking of

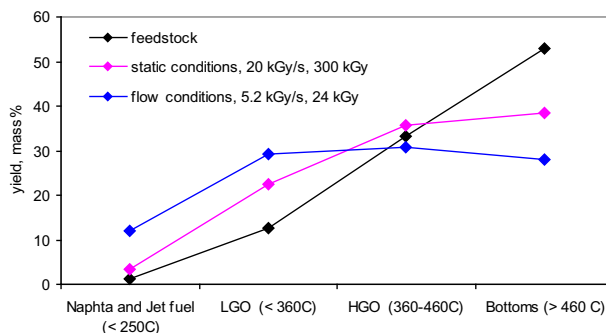


**Fig. 13** Fractional contents of high-paraffin crude oil and product of its PetroBeam processing at 60 °C (according to data [24]). *LGO* light gas oil, *HGO* heavy gas oil

hydrocarbon cracking, where the dose rate of ionizing irradiation is an essential operational parameter and the process rate directly depends on the dose rate. Realization of cold hydrocarbon cracking requires application of high dose rates that cannot be reached when using gamma-irradiation sources. For this reason, electron irradiation is more appropriate for this type of oil processing. Modern electron accelerators provide dose rates of tens and hundreds of kGy per second, which is sufficient for intense reactions of cold cracking of hydrocarbons.

PetroBeam process is characteristic for low capital and operational costs together with the highest energy saving compared with any thermal or thermocatalytic cracking processes. The technology can be applied both to heavy residue processing in refinery operations and upgrading of high-viscous oils near the sites of their extraction.

#### 4 Radiation-Enhanced Isomerization of Hydrocarbon Systems

Isomerization technologies pertain to the most economical methods for production of high-octane gasoline components with improved environmental properties. The demand for isomerization plants considerably increased with the very rigorous requirements to ecological properties of motor fuels including their fractional contents and restrictions on concentrations of aromatics and benzene, in particular.

Radiation-enhanced isomerization of light petroleum fractions has substantial advantages over the methods of catalytic isomerization widely spread today. These advantages include the absence of thermodynamic limitations on the reaction rate at lowered temperatures, high production rate, and realization of the process at atmospheric pressure and room temperature using only natural process stimulators, such as heavy residua of oil processing.

On the other hand, a special choice of the process modes allows combination of radiation cracking of heavy oils with the intense alkane isomerization without using any catalysts. Thus, application of radiation processing provides not only higher yields of gasoline fractions but also a considerable increase in their octane numbers due to radiation-enhanced isomerization of hydrocarbons.



#### 4.1 Radiation-Enhanced Isomerization in the Process of Radiation-Thermal Cracking

The phenomenon of strong radiation-enhanced isomerization was first observed in the studies of RTC of heavy crude oil from Karazhanbas field (Kazakhstan) [11]. In these experiments, oil was irradiated by 2-Mev electrons from a linear electron accelerator ELU-4. The time-averaged dose rate of electron irradiation was varied in the range of 0.5–1.5 kGy/s. The effect of radiation-enhanced isomerization was especially pronounced owing to the availability of heavy aromatic compounds in this type of oil. In the case of RTC of heavy Karazhanbas oil, the isomer yields were an order of magnitude higher than those earlier observed in the processes of low-temperature radiolysis and RTC of light hydrocarbons [1–6]. At a temperature of 375 °C, the yields of isoalkanes were comparable with those observed in the thermocatalytic process at temperatures above 600 °C.

Unusually high iso-paraffin yields in the RTC modes characteristic for relatively low temperatures and dose rates were explained by the effects of radiation energy transfer from paraffin to aromatic components of the hydrocarbon system. Transfer of the excess radiation energy to an alkyl radical in the excited paraffin composition assists its disintegration and impedes intramolecular isomerization. On the contrary, the addition of heavy aromatics allows combination of rather high dose rates and temperatures with favorable conditions for isomerization. Aromatic compounds, known for their high radiation resistance, can absorb the excess energy of a considerable part of radiation-generated radicals. As a result, many alkyl radicals may have enough time to stabilize their electron structure and to form isomers before their disintegration or recombination.

The phenomenon of radiation-enhanced isomerization of hydrocarbons in the RTC process and interpretation of this effect were confirmed in the experiments on radiation processing of bitumen characteristic for still higher concentrations of heavy aromatics and, therefore, still more pronounced isomerization effects [16, 19, 20, 24].

The hydrocarbon group content of the gasoline fraction distilled from the liquid product obtained by RTC of bitumen from Mortuk field (Kazakhstan) [16] is shown in Fig. 14. It shows that the contents of RTC gasoline considerably differ from those obtained by the thermocatalytic method.

Concentration of iso-paraffins after RTC is almost twice lower than n-paraffin concentration while in the case of RTC it is almost twice higher than both n-paraffin concentration in the RTC gasoline and iso-paraffin concentration in the TCC product. Gasoline octane numbers are correspondingly higher in the RTC gasoline.

The experimental data on iso-paraffin concentrations in the gasoline fraction of the liquid product obtained by radiation processing of bitumen and high viscous oil were summarized in study [49]. The most part of iso-alkanes was found in the gasoline fraction of the liquid RTC product. The maximal iso-alkane yields were observed at the minimal dose rate and temperature sufficient for noticeable cracking reactions. At the given dose rate and temperature, the isomer yields increased as the feedstock density increased [19, 24, 30] (Fig. 15). A high concentration of isomers

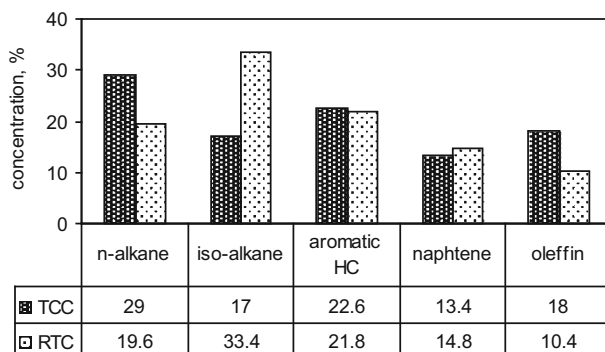


**Fig. 14** Hydrocarbon group contents of gasoline fractions from the liquid products obtained by RTC of bitumen: *TCC* thermocatalytic cracking [32]; *RTC* radiation-thermal cracking [16]

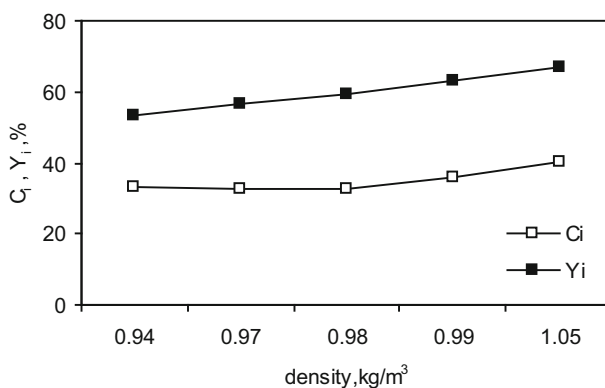


**Fig. 15** Isoalkane concentration in the gasoline fraction of the RTC products versus bitumen density.  $C_i$  isoalkane concentration in the gasoline fraction.  $Y_i$  isoalkane concentration in the paraffin part of the gasoline fraction

is direct evidence of the intense isomerization concomitant to radiation-thermal cracking.

As RTC temperature decreases, a greater part of radiation-generated radicals enter recombination in the first-order reactions [18, 19]. As a result, isomerization of the radicals bound in cages formed by the adjacent molecules becomes the determining isomerization mechanism. The cage effect plays the key role in formation long-living radical pairs and therefore in the kinetics of low-temperature cracking and low-temperature radiation isomerization. The radiation-generated unstable complexes, such as radical pairs, responsible for propagation of the chain cracking reaction, may break apart under a thermal action, interact with free radicals and contribute to propagation of the chain reaction, or realign their electron structures and enter isomerization reactions. The relation between the rates of cracking and isomerization depends on the process temperature and the dose rate of ionizing irradiation.

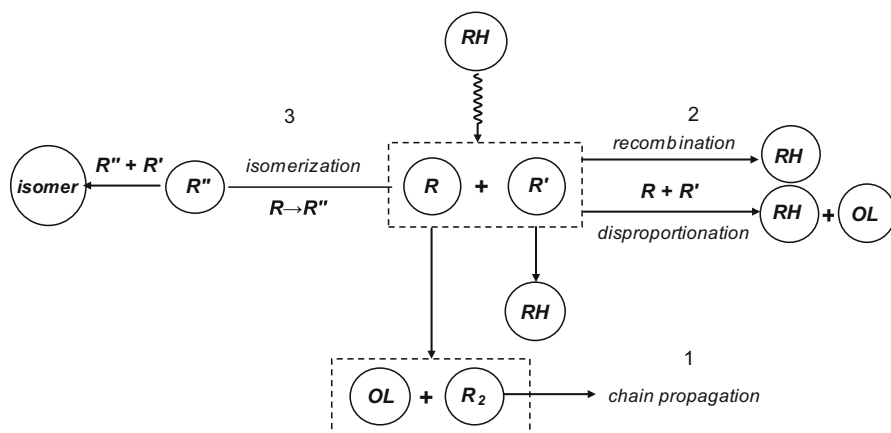


**Fig. 16** Schematic primary reactions of hydrocarbon cracking.  $R$  radicals,  $RH$  saturated hydrocarbon molecule;  $OL$  olefin molecule

In the case of the radical mechanism, an alkane molecule can absorb energy of about 3.5 eV as a result of thermal or radiation activation and break into two radicals: a reactive radical (a hydrogen atom or a light alkyl radical) and a larger unstable residual radical. The fate of the latter can be different. The most probable ways for transformation of such an unstable radical formed as a result of hydrocarbon molecule decomposition [19] are shown in Fig. 16.

The relationship between reactions 1, 2, and 3 (Fig. 16) depends on temperature and, in the case of low-temperature radiation cracking, on the dose rate of ionizing irradiation. Increase in temperature and/or absorbed dose rate increases probability of reaction 1 that leads to decomposition of the large alkyl radicals and contributes to propagation of the chain reaction. As temperature and dose rate increase, the probability of radical stabilization by isomerization or recombination increases. The concentration of thermally activated chain carriers considerably decreases as temperature tends to the lower threshold for the start of the chain cracking reaction. As a result, radical recombination in the first-order reactions becomes predominant.

## 4.2 Kinetics of High-Temperature Radiation Isomerization

Alkane isomerization is considered below in the conditions of radiation-thermal cracking. In this case, normal alkanes are one of the RTC products. It will be assumed that the rate of alkane accumulation in the gasoline fraction is equal to the cracking rate and their maximal yield is limited by quantity  $C^*$ . Then, kinetics of paraffin accumulation in the RTC process can be approximately described by equation

$$\frac{d(C^* - C_{\text{par}})}{dt} = -K(C^* - C_{\text{par}}) \quad (31)$$

with the initial condition

$$C_{\text{par}}|_{t=0} = C_{\text{par}}^{(0)} \quad (32)$$

In Eq. (31),  $C_{\text{par}}$  is total paraffin concentration in the gasoline fraction,

$$K = K_p R, \quad (33)$$

where  $R$  is radical concentration,  $K_p$  is the rate of RTC propagation:

$$K_p = k_p e^{-E_p/kT}, \quad (34)$$

For the numerical estimate, it will be assumed that  $k_p \approx 5 \times 10^{12} \text{ s}^{-1}$ ,  $E_p \approx 84 \text{ kJ/mol}$ .

Solution of Eq. (31) with the initial condition (32) has a form

$$C_{\text{par}} = C^* - \left( C^* - C_{\text{par}}^{(0)} \right) e^{-Kt} = C^* - \left( C^* - C_{\text{par}}^{(0)} \right) e^{-\frac{k_p}{P} D} \quad (35)$$

Obviously, the isomer concentration tends to the same limit  $C^*$  as the total paraffin concentration in the RTC process. Kinetics of iso-alkane accumulation can be described by equation:

$$\frac{d(C^* - C_{\text{iso}})}{dt} = -\alpha (C^* - C_{\text{iso}}) \quad (36)$$

with the initial condition

$$C_{\text{iso}}|_{t=0} = C_{\text{iso}}^{(0)} \quad (37)$$

where  $C_{\text{iso}}$  is iso-alkane concentration in the gasoline fraction.

The rate of radiation-induced isomerization,  $\alpha$ , can written in the form

$$\alpha = k_{\text{iso}}^{(0)} R P_d C_{\text{ar}}^n \left( \frac{\rho - \rho_0}{\rho_0} \right)^{3/2} \quad (38)$$

In Eq. (38),  $k_{\text{iso}}$  is isomerization rate constant (according to the data of low-temperature radiation isomerization [50],  $k_{\text{iso}}^{(0)} \approx 1.5 \times 10^9 \text{ s}^{-1}$ );  $C_{\text{ar}}$  is concentration of heavy aromatic additive;  $\rho$  and  $\rho_0$  are densities of the aromatic additive and paraffin environment, respectively. Probability of the excess energy transfer to the heavier components of the system is proportional to the relative difference in densities of the heavy aromatic additive,  $\rho$ , and paraffin environment,  $\rho_0$ . Basing on the analysis of experimental data on hydrocarbon radiolysis inhibition by different chemical additions, it was stated [1, 2] that inhibitor capacity for energy absorption is proportional to  $\rho^{3/2}$ . As a result, a factor  $\left( \frac{\rho - \rho_0}{\rho_0} \right)^{3/2}$  appears in Eq. (38).

Quantity  $P_d$  is probability that a radiation-generated radical will not undergo additional thermal activation sufficient for its decomposition during its lifetime. At heightened temperatures, radicals recombine in the second-order reactions and their lifetime,  $\tau$ , can be written as

$$\tau = \frac{R}{GP} = \frac{1}{\sqrt{GPk_{t2}}} \quad (39)$$

where  $G$  is radiation-chemical yield of radicals,  $k_{t2}$  is rate constant of the second-order recombination ( $k_{t2} \approx 10^9 \text{ s}^{-1}$ ),  $P$  is irradiation dose rate.

Therefore, probability of that a radical will not disintegrate due to an additional thermal activation can be written in a form

$$P_d = \frac{\sqrt{GPk_{t2}}}{\sqrt{GPk_{t2}} + k_{d0} e^{-E_d/kT}} \quad (40)$$

Solution of Eq. (36) with the initial condition (37) has a form

$$C_{\text{iso}} = C^* - (C^* - C_{\text{iso}}^{(0)}) e^{-\alpha t} = C^* - (C^* - C_{\text{iso}}^{(0)}) e^{-\frac{\alpha}{P} D} \quad (41)$$

It will be assumed that only normal alkanes are formed in the RTC process but a part of them forms isomers due to the effect of the radiation-enhanced isomerization. Then, the degree of isomerization in the RTC process can be determined by equation

$$\frac{C_{\text{iso}}}{C_{\text{par}}} = \frac{C^* - (C^* - C_{\text{iso}}^{(0)}) e^{-\alpha t}}{C^* - (C^* - C_{\text{par}}^{(0)}) e^{-K t}} \quad (42)$$

Conditionally assuming that  $C^* = 1$ , and  $C_{\text{par}}^{(0)} = C_{\text{iso}}^{(0)} = 0$ , we will obtain

$$C_{\text{iso}} = 1 - e^{-\alpha t} \quad (43)$$

$$C_{\text{par}} = 1 - e^{-K t} \quad (44)$$

Equations (38)–(40) show that coefficient  $\frac{\alpha}{P}$  that determines the dose dependence of isomer concentration in Eq. (41) weakly depends on dose rate. On the other hand, coefficient  $\frac{K}{P}$  in Eq. (35) determines the concentration dependence on dose rate for

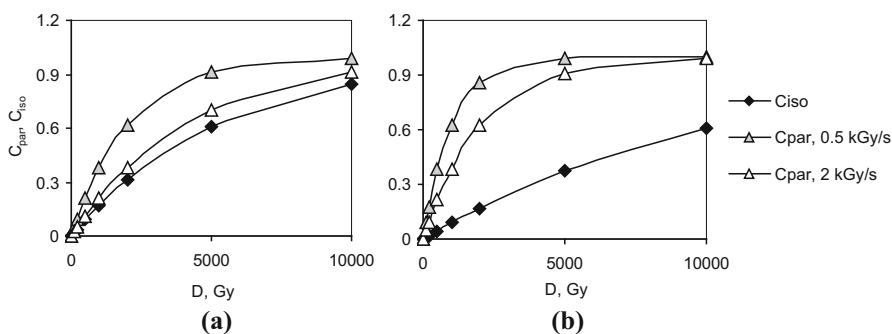


**Fig. 17** Changes in total paraffin,  $C_{\text{par}}$ , and isoalkane,  $C_{\text{iso}}$ , concentrations in the gasoline fractions of the RTC products ( $k_{d0} = 10^{12} \text{ s}^{-1}$ ,  $E_d = 84 \text{ kJ/mol}$ ,  $G = 1.6 \cdot 10^{-7} \text{ kg/J}$ ). **a**  $T = 370 \text{ }^\circ\text{C}$ ; **b**  $T = 400 \text{ }^\circ\text{C}$

the paraffins formed in the RTC process and varies inversely as the square root of the dose rate. Therefore, at the given irradiation dose, the cracking rate increases as dose rate decreases but the isomerization rate practically does not change.

This behavior can be seen in the dose dependences of the total concentration of the paraffins formed in the RTC process and isoparaffin concentrations in conventional units calculated using Eqs. (42) and (43). In Fig. 17, these dependences are represented for different temperatures and dose rates of ionizing irradiation. The cracking rate increases as temperature increases at the given dose rate while the isomerization rate decreases because of the increase in the probability of radical thermal decomposition.

At the given irradiation time, the degree of isomerization strongly depends on the correlation of the constants  $\alpha$  and  $K$ . If  $\alpha < K$ , then  $\frac{C_{\text{iso}}}{C_{\text{par}}} < 1$ ; at  $\alpha \geq K$ , the full isomerization of alkanes formed in the cracking process should be formally observed. However, this qualitative analysis takes into account only an approximate estimate of favorable isomerization conditions using approximate constants of cracking and isomerization rates.

### 4.3 Radiation-Induced Isomerization of Gasoline

Favorable conditions for radiation-induced isomerization are lowered values of temperature and irradiation dose rate. Therefore, a considerable isomerization effect should be observed under gamma or X-ray irradiation of aromatic-rich hydrocarbon mixtures at lowered temperatures and dose rates. It was demonstrated in the experiments on radiation processing of low-octane gas-condensate gasoline at room temperature [17]. Gasoline was irradiated with bremsstrahlung X-rays from the 2-MeV electron beam. The experiments have shown that radiation-induced isomerization was much more considerable after addition of heavy aromatic compounds and irradiation of such mixture with moderate X-ray doses. In these experiments, heavy residua of bitumen radiation processing were used as additional agents for isomerization initiation.

The changes in fractional and hydrocarbon contents of gasoline separated from the irradiated mixture demonstrated the effect of heavy aromatics on radiation-induced isomerization. Experimental data (Figs. 18, 19, 20) show that considerable effect of paraffin isomerization could be observed only in the presence of heavy aromatic compounds and only as a result of radiation processing of such mixture. An addition of 15 mass% residue of bitumen radiation processing to the gas-condensate gasoline and subsequent X-ray irradiation of the mixture at room temperature caused an increase in the iso-alkane concentration by 33.8 % in respect to their initial concentration in gasoline. It was accompanied by increase in the gasoline octane number from 54 to 68 without using any other chemical additives.

In this series of experiments, heavy residua of bitumen processing played a role of isomerization stimulators and did not directly contributed to the changes in the gasoline hydrocarbon contents. Radiation processing caused a considerable increase in the iso-alkane concentrations while the arene concentration remained practically

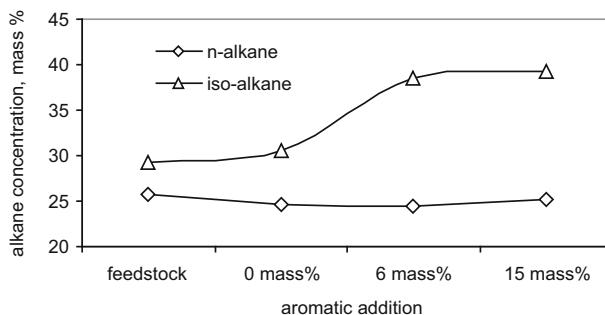


**Fig. 18** Effect of the addition of heavy aromatic compounds on concentrations of n- and iso-alkanes in gasoline fraction [17–20]

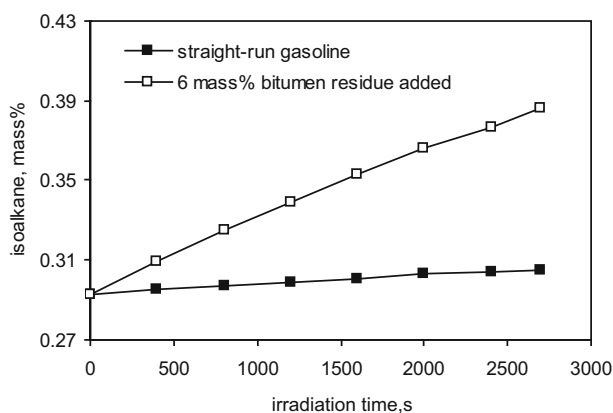


**Fig. 19** Kinetics of alkane isomerization under irradiation of straight-run gasoline with bremsstrahlung X-rays (according to data [17, 20])

the same (about 12 mass%). Thus, the observed increase in the gasoline octane numbers should be completely attributed to radiation-induced isomerization.

The presence of heavy aromatic compounds that effectively absorb the excess energy of radiation-generated radicals increases a probability of isomerization and makes lower a probability of their decomposition at any temperatures. Therefore, an addition of heavy aromatics leads to a decrease in olefin concentrations and increase in the iso-alkane contents in gasoline after radiation processing. This effect is distinctly seen in Fig. 21, which illustrates the effect of X-ray irradiation on the hydrocarbon contents of the low-octane gas-condensate gasoline. Figure 21 shows that the addition of heavy residue of bitumen processing led to an increase in the iso-alkane concentration in gasoline irradiated at room temperature by 34 %. At the same time, olefin concentration decreased more than twice.

Generally, there is no need to convert electron to bremsstrahlung X-ray radiation for gasoline isomerization and increase in its octane numbers. The same results can

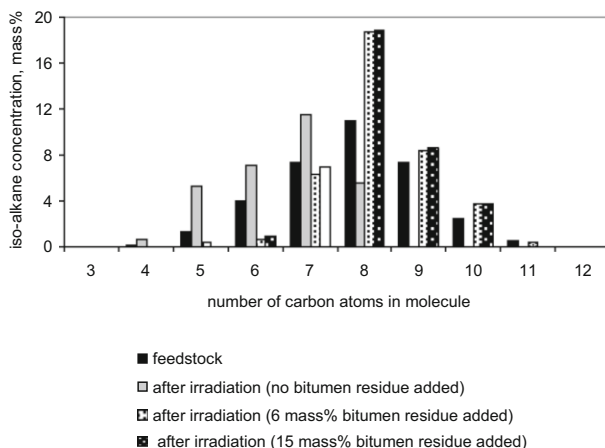


**Fig. 20** Molecular mass distribution of iso-paraffins in the mixtures of straight-run gasoline and heavy aromatics before and after irradiation with bremsstrahlung X-rays (according to data [17, 20]).  $D = 6\text{--}8$  kGy

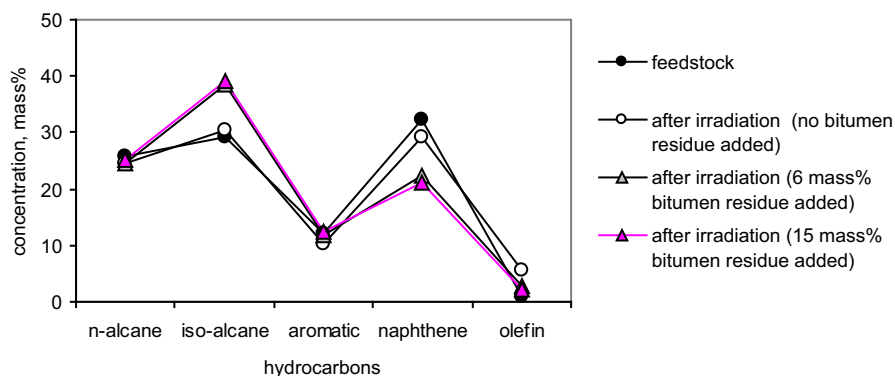


**Fig. 21** Hydrocarbon group contents of gas-condensate gasoline after gamma-irradiation (according to data [17])

be obtained using electron irradiation at relatively low dose rates or gamma irradiation from isotope sources [20].

#### 4.4 Kinetics of Low-Temperature Radiation-Enhanced Isomerization

A kinetic study of gasoline radiation-enhanced isomerization [18] was based on taking into account the evolution of the radiation-generated unstable molecular states responsible for cracking and isomerization of hydrocarbon molecules.

At lowered isomerization temperatures, for example, at room temperature, thermal isomerization and a probability of radiation-induced alkane isomerization in the absence of heavy aromatics can be neglected. In supposition that large radiation-



generated radicals do not break apart under thermal action at low temperatures during their lifetime, the kinetics of iso-alkane accumulation in gasoline can be described by equation

$$\frac{dC_{\text{iso}}}{dt} = (C_{\text{par}}^{(0)} - C_{\text{iso}}) C_{\text{ar}}^n k_{\text{iso}}^{(0)} R \left( \frac{\rho - \rho_0}{\rho_0} \right)^{3/2} \quad (45)$$

where  $C_{\text{ar}}$  is concentration of the heavy aromatic additive;  $(C_{\text{par}}^{(0)} - C_{\text{iso}})$  is concentration of normal alkanes:

$$C_{\text{par}}^{(0)} = 1 - C_{\text{np}} - C_{\text{ar}}, \quad (46)$$

$C_{\text{np}}$  is concentration of non-paraffin components that do not enter isomerization reactions.

Quantity  $C_{\text{par}}^{(0)}$  represents the paraffin concentration in the hydrocarbon system; it will be assumed to be constant since all the reactions except isomerization are neglected. The values of isomerization rate  $k_{\text{iso}}^0$  can be different for different isomers but for the sake of simplicity it will be supposed that a single type of isomer is formed in the reaction.

Concentration of radiation-generated radicals,  $R$ , that recombine in the first- and second-order reactions with the rates  $k_{t1}$  and  $k_{t2}$ , respectively, is determined by equation [19, 51]:

$$R \approx \frac{k_{t1}}{2k_{t2}} \left[ \sqrt{1 + \frac{4k_{t2}}{k_{t1}^2} GP} - 1 \right] \quad (47)$$

At the given difference in densities, the efficiency of excess radiation energy transfer from radicals to heavy aromatic molecules and, therefore, efficiency of radiation-induced isomerization, depends on the number of heavy aromatic molecules,  $n$ , per molecule of normal alkanes. For this reason, Eq. (44) includes concentration of heavy aromatic compounds raised to the power of  $n$ .

With the initial condition  $C_{\text{iso}}|_{t=0} = 0$ , Eq. (45) has solution

$$\ln \frac{C_{\text{par}}^{(0)} - C_{\text{iso}}}{C_{\text{par}}^{(0)} - C_{\text{iso}}^{(0)}} = -k_{\text{iso}}^{(0)} R C_{\text{ar}}^n \left( \frac{\rho - \rho_0}{\rho_0} \right)^{3/2} t, \quad (48)$$

where  $C_{\text{par}}^{(0)}$  is determined by formula (46).

Expression (37) shows that at the given iso-alkane concentration,  $C_{\text{iso}} = C_{\text{iso}}^*$ , the isomerization rate has maximum at

$$C_{\text{ar}}^* = \frac{n(1 - C^* - C_{\text{iso}}^*)}{n + 1}, \quad (49)$$

where from

$$n = \frac{C_{ar}^*}{1 - C_{ar}^* - C_{iso}^*} \quad (50)$$

Formulas (49) and (50) give a relationship between concentrations of normal alkanes and heavy aromatics that corresponds to the maximal isomerization rate. Parameter  $n$  determines the number of heavy aromatic molecules per molecule of normal alkanes in the optimal conditions of radiation-induced isomerization.

Calculations using the cited above experimental data [17] on the changes in isoalkane concentration in irradiated gasoline with heavy aromatic addition provide a value of  $n \approx 0.1$ . Therefore, in optimal isomerization conditions, one heavy aromatic molecule should be surrounded by about ten molecules of normal alkanes.

Equation (50) determines the conditions of the excess energy transfer from a radical formed as a result of radiation-induced decomposition of an alkane molecule to heavier aromatic molecules. If the ratio of heavy aromatic and normal alkane concentrations decreases below the value of  $\frac{n}{n+1}$ , it leads to less intense absorption of the excess energy of large alkyl radicals, a higher probability of their decomposition and, therefore, decrease in the isomerization rate. If the ratio of heavy aromatic and normal alkane concentrations exceeds the value of  $\frac{n}{n+1}$ , then alkyl radicals lose the most part of their energy and become incapable of isomerization.

The dose dependence of isomer accumulation in irradiated gasoline mixed with the heavy residue of bitumen processing is shown in Fig. 22 for different concentrations of the aromatic additive. The isomer concentrations shown in Fig. 22 relate to gasoline obtained after heavy aromatics removal from the irradiated mixture.

Figure 23 shows dependence of the degree of normal alkane isomerization in gasoline irradiated with a dose of 743 Gy on concentration of the aromatic additive

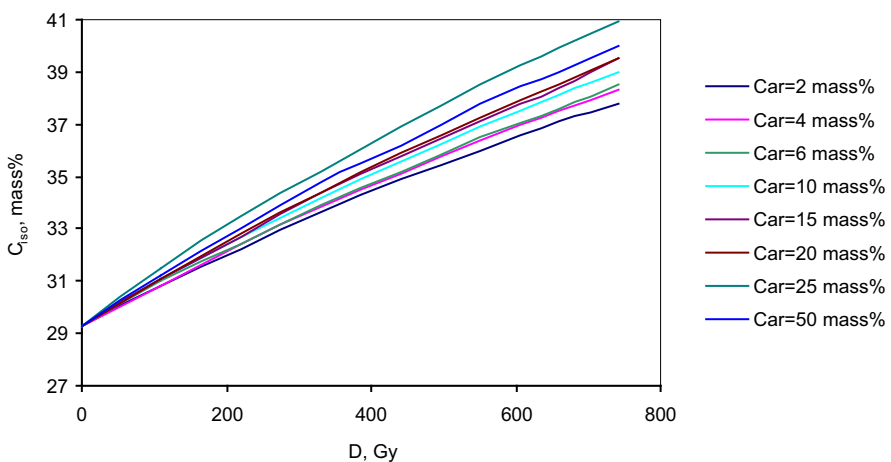


**Fig. 22** Dependence of isoalkane concentration in gasoline,  $C_{iso}$ , on dose of bremsstrahlung X-rays for different concentrations,  $C_{ar}$ , of the aromatic stimulator of isomerization;  $P = 0.275$  Gy/s

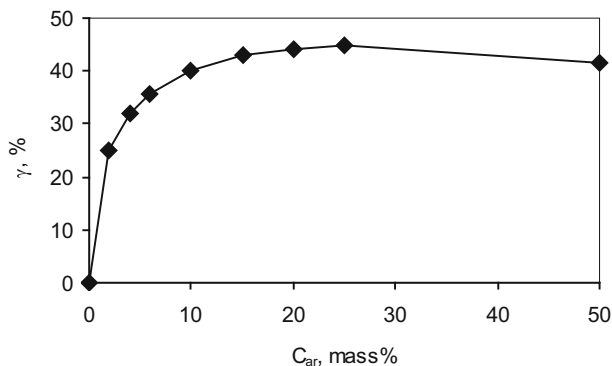


**Fig. 23** Degree of normal alkane isomerization,  $\alpha$ , in irradiated gasoline versus concentration of the aromatic additive,  $C_{ar}$  ( $P = 0.275$  Gy/s,  $D = 743$  Gy)

(heavy aromatics was removed from gasoline after radiation processing). The isomerization degree,  $\gamma$ , is defined here as

$$\gamma = \frac{C_{iso} - C_{iso}^{(0)}}{C_{par}^{(0)} - C_{iso}^{(0)}} \quad (51)$$

where  $C_{iso}$  is isoalkane concentration,  $C_{iso}^{(0)}$  is isoalkane concentration in unirradiated material, and  $C_{par}^{(0)}$  is alkane concentration in unirradiated material.

In the described above irradiation conditions, the maximal degree of isomerization (41 %) was reached with the addition of 25 mass% heavy aromatics. A further increase in the concentration of the aromatic additive resulted in a slow decrease in the isomerization degree under the same conditions of gasoline radiation processing. At the given irradiation time, isomerization efficiency continuously increased as dose rate increased, reaching 75.4 % at the dose rate of 20 kGy/s and the dose of 20 kGy (Fig. 24).

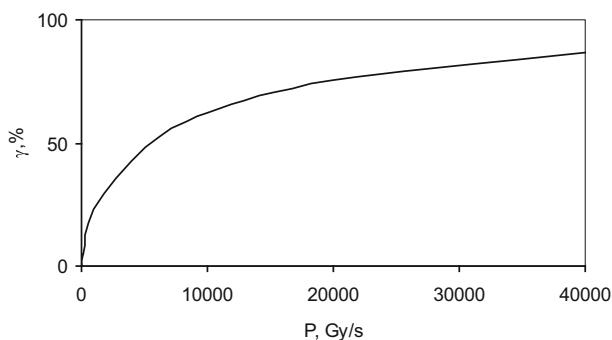


**Fig. 24** Dependence of the degree of normal alkane isomerization,  $\gamma$ , on dose rate,  $P$ , of ionizing irradiation. Concentration of heavy aromatic additive—6 mass%, irradiation time—1 s

## 5 Conclusions

Radiation methods for radiation processing of petroleum oils and oil products developed by now appear to offer economic and technologically efficient solutions of many acute problems of the oil industry, such as upgrading and refining of heavy crude oils, bitumen and oil residua, cleaning and refining of used oil products, oil desulfurization and increase in gasoline octane numbers.

Radiation methods have such advantages over conventional technologies as simpler configurations of the radiation plants and lower capital and operational costs. They are universal in respect to the type of feedstock, do not require special catalysts, and are characteristic of a higher production rate. New technologies, based on the phenomena of low-temperature radiation cracking and radiation-enhanced isomerization of hydrocarbons, allow oil processing at lowered temperatures (down to room temperature) and atmospheric pressure.

New technological approaches combine high production rates and economic efficiency with the ability of easy re-orientation to processing of different types of oil feedstock and production of different types of oil products corresponding to market demands and make a base for a number of perspective applications in the oil industry.

## References

1. Topchiev AV, Polak LS (1962) Radiolysis of hydrocarbons. Acad Sci USSR, Moscow
2. Topchiev AV (1964) Radiolysis of hydrocarbons. El Publ Co., Amsterdam, London
3. Brodskiy AM, Lavrovskiy KP, Zvonov NV, Titov VB (1961) Radiation-thermal conversion of oil fractions. *Neftekhimiya (Oil Chemistry)* 3:370–383
4. Lavrovskiy KP (1976) Catalytic, thermal, and radiation-chemical conversion in hydrocarbons. *Nauka Publ., Moscow*, pp 312–373, 255–263
5. Gabsatararova SA, Kabakchi AM (1969) Effect of gamma-irradiation dose rate on formation of unsaturated compounds during radiation-thermal cracking of *n*-heptane. *Khimiya Vysokikh Energiy (High Energy Chem)* 3:126–128
6. Panchenkov GM, Putilov AV, Zhuravlev GI (1981) Study of basic regularities of *n*-decane radiation-thermal cracking. *Khimiya Vysokikh Energiy (High Energy Chem)* 15:426–430
7. Zaikina RF, Zaikin YA, Mirkin G, Nadirov NK (2002) Prospects of radiation technology application in oil industry. *Radiat Phys Chem* 63:621–624
8. Mirkin G, Zaikin YA, Zaikina RF (2003) Radiation methods for upgrading and refining of feedstock for oil chemistry. *Radiat Phys Chem* 67:311–314
9. Nadirov NK, Zaikina RF, Zaikin YuA (1994) Progress in high viscosity oil and natural bitumen refining by ionizing irradiation. *Oil Bitumen Kazan* 4:1638–1642
10. Nadirov NK, Zaikina RF, Zaikin YA (1995) New high-efficient technologies for heavy oil and oil residue refining. *Energy Fuel Resour Kazakhstan* 1:65–69
11. Zaikin YA, Zaykina RF, Mamonova TB, Nadirov NK (2001) Radiation-thermal processing of high-viscous oil from Karazhanbas field. *Radiat Phys Chem* 60:211–221
12. Zaikina RF, Zaikin YA, Mamonova TB (2002) Radiation methods for demercaptanization and desulfurization of oil products. *Radiat Phys Chem* 63:617–619
13. Zaikina RF, Zaikin YA (2003) Radiation technologies for production and regeneration of motor fuels and lubricants. *Radiat Phys Chem* 65:169–172
14. Zaikin YA, Zaikina RF, Silverman J (2004) Radiation-thermal conversion of paraffinic oil. *Radiat Phys Chem* 69:229–238

15. Zaikina RF, Zaikin YA, Yagudin ShG, Fahrudinov IM (2004) Specific approaches to radiation processing of high-sulfuric oil. *Radiat Phys Chem* 71:467–470
16. Zaikin YA, Zaikina RF (2004) Bitumen radiation processing. *Radiat Phys Chem* 71:471–474
17. Zaikin YA, Zaikina RF (2007) Effect of radiation-induced isomerization on gasoline upgrading. In: Proceedings of the 8th topical meeting on nuclear applications and utilization of accelerators AccApp'07, Pocatello, Idaho, July 29–August 2, 2007. American Nuclear Society, pp 993–998
18. Zaikin YA (2013) On the nature of radiation-excited unstable states of hydrocarbon molecules in heavy oil and bitumen. *Radiat Phys Chem* 84:6–9
19. Zaikin Y, Zaikina R (2013) *Petroleum radiation processing*. Taylor & Francis, CRC, New York, Boca Raton
20. Zaikin YA, Zaikina RF, Nadirov NK (2014) The phenomenon of the radiation-enhanced isomerization of hydrocarbon systems. In: International academy of the authors of scientific discoveries and inventions. Certificate of discovery A-589 of Nov 4, 2013; Diploma #463. The year of priority: 2001
21. Zaikin Y, Zaikina R (2008) PetroBeam process for heavy oil upgrading. World Heavy Oil Conference, Edmonton 10–12 March, 2008, WHOC, paper 2008-461
22. Zaikin YA (2008) Low-temperature radiation-induced cracking of liquid hydrocarbons. *Radiat Phys Chem* 77:1069–1073
23. Zaikin Y A (2013) Radiation-induced cracking of hydrocarbons. In: Kharissov BI, Kharissova OV, Mendez UO (eds) *Radiation synthesis of materials and compounds*. Taylor & Francis, CRC, New York, Boca Raton, pp 355–379
24. Zaikin YA, Zaikina RF (2008) New trends in the radiation processing of petroleum. In: Camillery AN (ed) *Radiation physics research progress*. Nova Science, New York, pp 17–103
25. Zaikin YA, Zaikina RF (2012) Self-sustaining cold cracking of hydrocarbons. US patents 8,192, 591 and 8,911,617; Eurasian patent 016698, Patent of Canada 2633885, Patent of China 200680051814.1, Patent of Mexico 309717, Patent of India 259292
26. Bugaenko LP, Kuzmin MG, Polak LS (1988) *Chemistry of high energy*. Khimiya, Moscow
27. Zaikin YA (2013) Polymerization as a limiting factor for light product yields in radiation cracking of heavy oil and bitumen. *Radiat Phys Chem* 84:2–5
28. Zaikin YA, Zaikina RF, Mirkin G (2003) On energetics of hydrocarbon chemical reactions by ionizing irradiation. *Radiat Phys Chem* 67(3–4):305–309
29. Nadirov NK, Zaikin YA, Zaikina RF, Makulbekov EA, Petukhov VK, Panin YA (1994) Method for processing heavy oil and oil residua. Patent of Kazakhstan 4676
30. Zaikin YA et al (2006) Experimental facility for processing hydrocarbon components of natural bitumen. Almaty, Technical report on ISTC project K-930
31. Akpabio EJ (1992) *Cand. Diss. Thesis*. Baku
32. Musaev GF, Mamonova TB, Malibov MS, Musaeva ZG (1994) Study of Kazakhstani bitumen rocks by the thermocatalytic method. *Energy Fuel Resour Kazakhstan* 4:51–56
33. Zaikin YA, Zaikina RF, Nadirov NK, Sarsembinov ShSh (1999) Method and apparatus for reprocessing of used and residual mixtures of oil products. Patent of Kazakhstan 8142
34. Zaikin YA (2005) New technological approaches to cleaning, upgrading and desulfurization of oil wastes and low-grade oil products. In: Proceedings of the 4th international conference “Oils and Environment”. Gdansk University of Technology, pp 275–282
35. Ivanov VS (1988) *Radiation chemistry of polymers*. Khimiya, Leningrad, pp 299–300
36. Chmielewski AG (2011) Electron accelerators for environmental protection. *Rev Accel Sci Technol* 4:149–161
37. Pawelec A et al (2016) *Fuel Process Technol* 145:123–129
38. Zaikina RF, Zaikin YA, Mamonova TB, Nadirov NK (1999) A method for hydrocarbon feedstock cleaning with the removal of sulfur compounds. Patent of Kazakhstan 11995
39. Likhterova NM, Lunin VV, Kukulin VI, Knipovich OM, Torkhovskiy VN (1998) A method for petroleum feedstock processing. Patent of Russia RU 212040
40. Lunin VV, Frantsuzov VK, Likhterova NM (2012) Desulfurization and demetallization of heavy oil fractions by ozonolysis and radiolysis. *Neftekhimiya (Petrol Chem)* 42(36):195–202
41. Ayukawa Y, Ono M (2004) High-energy beam irradiating desulfurization device. US Patent 6,284,746B2
42. Basfar AA, Khaled A-AM (2012) Method of removing sulfur from crude oil by ionizing irradiation. Pub/No. US 2012/0138449 A1
43. Qu Z, Yan N, Jia J, Wu D (2006) Removal of thiophene-type sulfide by gamma radiation assisted with hydrogen peroxide. *Energy Fuels* 20:142–147

44. Tian Y, Yan N, Li D, Yao S, Wang W (2003) Removal of dibenzothiophene from simulated petroleum by integrated  $\gamma$ -irradiation and Zr/alumina catalyst. *J Chem Ind Eng (China)* 54:1279–1283
45. Zhao YF, Yan NG, Wu D, Jia JP, Qu Z (2004) Investigation on removal of thiophene-type sulfide by gamma rays radiation assisted with hydrogen peroxide. *J Shanghai Jiatong Univ* 38:1719–1723
46. Chandrasekhar S (1947) Stochastic problems in physics and astronomy. Inostrannaya Literatura, Moscow
47. Chmielewski AG, Haji-Saeid M (2004) Radiation technologies: past, present and future. *Radiat Phys Chem* 71:17–21
48. Haji-Saeid M et al (2007) Nuclear instruments and methods in physics research. Sect B Beam Interact Mater Atoms 265:51–57
49. Zaikin YA, Zaikina RF (2004) Criteria of synergetic effects in radiation-induced conversion of complex hydrocarbon mixtures. *Oil Gas (Kazakhstan)* 22(2):64–73
50. Allara DL (1980) A compilation of kinetic parameters for the thermal degradation of *n*-alkane molecules. *J Phys Chem Ref Data* 9(3):523–525
51. Talrose VL (1974) To the theory of radiation-chemical initiation of chain reactions. *Khimiya Vysokikh Energiy (High-Energy Chem)* 8:519–527

# The Use of Gamma Radiation for the Treatment of Cultural Heritage in the Argentine National Atomic Energy Commission: Past, Present, and Future

Ana Maria del Carmen Calvo<sup>1</sup> · Andrea Docters<sup>1</sup> ·  
María Virginia Miranda<sup>1</sup> · Mario Carlos Nazareno Saparrat<sup>2</sup>

Received: 21 April 2016 / Accepted: 18 November 2016  
© Springer International Publishing Switzerland 2016

**Abstract** The use of gamma radiation for treating biodeteriorated cultural heritage on paper has been studied at the Comisión Nacional de Energía Atómica-CNEA (Argentina) since 2001. In order to preserve books, publications, and documents that have been attacked by insects or fungi, gamma radiation techniques have been used at CNEA. The activities include basic research as well as their applications in infected documents and papers currently used in libraries and archives. New papers were subjected to accelerated ageing in order to evaluate the effects of gamma radiation on their physical and mechanical properties. Current studies include resistance to radiation in two batches of highly cellulolytic fungi, associated with indoor environment. They are present in papers and adhesives used for conservation purposes at the Laboratory of Preventive Conservation and Restoration of Documents. A joint study has been started in CNEA with the National University of La Plata.

**Keywords** Cultural objects preservation · Disinfestation preservation · Fungi in paper · Gamma radiation in paper · Gamma radiation preservation · *Cladosporium cladosporioides* · *Chaetomium globosum*

---

This article is part of the Topical Collection “Applications of Radiation Chemistry”; edited by Margherita Venturi, Mila D’Angelantonio.

✉ Ana Maria del Carmen Calvo  
[calvo@cae.cnea.gov.ar](mailto:calvo@cae.cnea.gov.ar)

<sup>1</sup> Comisión Nacional de Energía Atómica, Buenos Aires, Argentina

<sup>2</sup> Instituto de Fisiología Vegetal (INFIVE), Universidad Nacional de La Plata (UNLP)-CCT-La Plata-Consejo Nacional de Investigaciones Científicas y Técnicas (CONICET), Diag. 113 y 61, CC 327, 1900 La Plata, Argentina

## 1 Introduction

Preservation of books and documents in libraries and archives are hampered mainly by inadequate environmental and infrastructural conditions, as well as by occasional floods, explosions, fire, or extinction methods.

For large amounts of wet and dirty materials, there is a high risk of biodeterioration due to inabilities of immediate drying and cleaning actions. Development of fungi can cause losses of valuable cultural objects [65]. Thus, the necessity of a treatment to eliminate the subsequent infection.

There are different physical and chemical methods in order to avoid biodeterioration. Then it is essential to know their advantages and disadvantages, in order to choose the most effective one. Chemical methods as fungistatic products, ETO, formaldehyde and thymol, among others, leave undesirable residues for documentary material and human health. Gamma radiation is a physical method that leaves no residue on paper. Due to its high penetration capacity, large volumes of packaged documentary material can be treated in a short time.

For decades, radiation processing has been used worldwide in order to preserve, modify, or improve the characteristics [33] of a wide variety of products and materials: sterilization of health care products; food irradiation; polymer cross-linking, tire component curing and conservation of art objects [28]. This technology has been successfully used to reduce biodeteriogene level in infected documents and books to a normal level, contributing to their preservation [8, 27].

In Argentina, libraries and archives have in general conservation problems because of inadequate storage conditions or chemical treatments. In 2001, a multidisciplinary team including a chemist, a conservation expert, and a microbiologist, was integrated in CNEA in order to investigate the benefits and disadvantages of gamma radiation to control fungus on paper documentation. A thesis work on the subject was presented and the CNEA started to assist in the treatment of institutional infected documents, books and magazines, as well as other institution needs [11].

In 2001, the collection of BAP's (Public Administrative Bulletins) documents, which contain institutional administrative historical records since 1951 up to the present, suffered a fungal infection. This was one of the first cases in which gamma radiation was used in CNEA to treat infected paper.

Whenever possible, the effects of the different doses were evaluated by different tests on irradiated and un-irradiated paper. Mechanical physical tests were used to determine:

- mechanical resistance
- optical and electron microscopy for evaluation of fibers of photographic documentation
- pH analysis and accelerated ageing with different methods based on international standards
- UV, moist heat
- dry heat.



Gamma radiation treatments proved to be an effective and safe method, which allowed to deal with large volumes of documents in a short time, leaving no residues on paper. This is the reason why this method was adopted in our Laboratory of Preventive Conservation and Restoration of Documentation (LCRD) for restoration of infected material.

## 2 Fungi and Their Role in Paper Deterioration

In museums, collections, and libraries, where paper and its derivatives are the main organic material, fungi play the most important role in biodeterioration [55]. Although bacteria can also deteriorate paper, the environmental conditions of these buildings are usually more prone to the growth of fungi rather than bacteria, since fungi require less moisture to develop [55].

Fungi that deteriorate paper are mostly air borne, or due to dust accumulation in paper and associated supports. These fungi most frequently belong to the phylum Ascomycota with slow-growing species such as xerophilic ones of the genera *Aspergillus*, *Paecilomyces*, *Chrysosporium*, *Penicillium*, and *Cladosporium*. However, there are other fungi, such as some fast-growing species of subphylum Mucoromycotina, as well as ones from the phylum Basidiomycota (Table 1). They can modify the paper substrate or become it in a vector/support for the dispersal of fungal propagules. These fungi colonize paper either by penetrating into the microfibril matrix or growing superficially [57]. Although some data about fungal interaction with substrates and their surface topography exist [57], they are only descriptive and derived from particular cases. Therefore, there is a need to identify the factors that trigger these behaviors, such as those related to limitations or environmental preferences (availability of oxygen, other gases and/or water, among others).

Fungi that colonize documents or art works made of paper can cause structural damage mainly by cellulose decomposition (see Sect. 2.1) and/or by aesthetic detriment (see Sect. 2.2). In addition, handling mould or contaminated paper objects can constitute a serious health risk, because many of them can be pathogenic/toxinogenic, even if they are already dead [47]. Fungi, either airborne and/or deteriorating paper, can cause allergies in people and serious respiratory diseases. In this sense, many fungi available as spores in air, such as those belonging to genus *Cladosporium*, are present at high concentrations in several institutions that conserve heritage documents and are therefore a potential cause of allergic respiratory diseases when inhaled [36].

### 2.1 Fungal Ability to Cause Structural Damage in Paper

Most fungi that infect paper have saprotrophic properties, using the cellulose matrix as a source of carbon and energy. These fungi can involve both enzymatic and non-enzymatic mechanisms to degrade cellulose. The enzyme systems that fungi synthesize in order to depolymerize cellulose include three main types of extracellular hydrolases:

**Table 1** Some fungi reported as biodeteriorating agents associated with several paper documents

Substrate/source of isolation	Taxa	References
Laid-paper	<i>Cladosporium cladosporioides</i> <sup>a</sup> <i>Cladosporium</i> <sup>a</sup> and <i>Penicillium</i> <sup>a</sup>	[38]
Laid-paper	<i>Toxicocladosporium irritans</i> <sup>a</sup> and <i>Chromelosporium carneum</i> <sup>a</sup>	[38]
Wood-pulp paper	<i>C. carneum</i> <sup>a</sup> , <i>Aspergillus versicolor</i> <sup>a</sup> , and <i>P. chrysogenum</i> <sup>a</sup>	[38]
Wood-pulp paper	<i>Chaetomium globosum</i> <sup>a</sup>	[38]
Wood-pulp paper	<i>Phlebiopsis gigantea</i> <sup>b</sup>	[38]
Laid-paper	<i>Alternaria alternata</i> <sup>a</sup> and <i>Toxicocladosporium</i> <sup>a</sup>	[38]
1920 etching	<i>Taeniolella (Torula) sp.</i> <sup>a</sup>	[57]
1958 etching	<i>Chaetomium sp.</i> <sup>a</sup>	[57]
17th-century paper	<i>Cladosporium sp.</i> <sup>a</sup> and <i>Torula sp.</i> <sup>a</sup>	[57]
A mold patch in a book	<i>Aspergillus sclerotiorum</i> <sup>a</sup>	[18]
Maps	<i>Aspergillus sp.</i> <sup>a</sup> and <i>Penicillium sp.</i> <sup>a</sup>	[43]
Indoor air in an archive and one wood-pulp sample	<i>Aspergillus fumigatus</i> <sup>a</sup>	[38]
Registry book of councils from the Santa Cruz Monastery (Coimbra)	<i>Epicoccum nigrum</i> <sup>a</sup>	[38]
In foxing spots in Leonardo da Vinci's self-portrait	<i>Eurotium halophilicum</i> <sup>a</sup>	[49]
Leonardo da Vinci's self-portrait	Lichenized Ascomycota or <i>Acremonium sp.</i> <sup>a</sup> as the most dominant taxa	[49]
A degraded paper of a 16th-century book	<i>Penicillium pinophilum</i> <sup>a</sup> , <i>Aspergillus versicolor</i> <sup>a</sup> , <i>Aspergillus nidulans</i> <sup>a</sup> , <i>Cladosporium cladosporioides</i> <sup>a</sup> , <i>Epicoccum nigrum</i> <sup>a</sup> , <i>Debaryomyces hansenii</i> <sup>a</sup> , <i>Botryotinia fuckeliana</i> <sup>a</sup> , <i>Rhizopus arrhizus</i> <sup>c</sup>	[41]

<sup>a</sup> Phylum Ascomycota<sup>b</sup> Phylum Basidiomycota<sup>c</sup> Subphylum Mucoromycotina

1. endoglucanases (EC 3.2.1.4);
2. exoglucanases, including cellodextrinases (EC 3.2.1.74) and cellobiohydrolases (EC 3.2.1.91 for the enzymes acting on the non-reducing end and EC 3.2.1.176 for ones on the reducing end); and
3.  $\beta$ -glucosidases (EC 3.2.1.21).

Endoglucanases are the key components in the process since they increase notoriously the number of reducing and non-reducing extremes (including chain ends and oligosaccharides). However, a previous step called amorphogenesis is necessary to open up the fibrillary matrix and increase the access of the enzymes to the glycosidic linkages within the sugar polymers.

Additionally, there is recent evidence that different fungi can also degrade cellulose involving oxidative enzymes such as the polysaccharide monooxygenases

(PMOs or LPMOs; they stand for lytic PMOs), cellobiose dehydrogenases (CDHs), and members of the carbohydrate-binding module family (CBM33), which act complementarily to the hydrolytic cellulase system.

Non-enzymatic mechanisms can also participate in the fungal degradation of cellulose. Such processes are associated with the activity of some Basidiomycota fungi such as the brown-rot ones. Through quinone redox cycling and glycopeptide-based Fenton reactions, they generate small molecular weight oxidants such as the hydroxyl free radical that randomly attack the substrate [20].

Although fungi that deteriorate paper are mostly cellulolytic organisms, the microbiota associated with this substrate can also include fungi with different saprotrophic behaviors, such as non-cellulolytic ones. An example is the fungi from the order Mucorales, which belong to the group called “sugar fungi”, which are unable to utilize complex carbohydrates because they lack the extracellular enzyme batteries. However, they can play a role as opportunists on deteriorated paper. If conditions are adequate for spore germination, they develop typical colonies using soluble carbon compounds. They are easily assimilable and derived from the depolymerization of cellulose caused by the activity of extracellular enzymatic systems that have been secreted by cellulolytic fungi.

In addition, fungi developed on paper can nurse themselves from several carbon substrates present on paper other than cellulose or their monomers. They could be either fillers, sizings, or dust, which can be rich in proteins and sugars, or by scavenging CO<sub>2</sub>, combined nitrogen, and carbon-rich gases from the atmosphere under stressful conditions [60]. Also, the survival strategy of fungi deteriorating paper under these conditions might also include alternative endogenous carbon sources such as lipids. All of these limitations can lead to the inconspicuous mycelial development on paper, which is associated with the production of fungal secondary metabolites rather than biomass accumulation.

## 2.2 Fungal Ability to Cause Aesthetical Damage in Paper

Fungal growth on paper can generate colorimetric alterations, whether the substrate degrades or not. However, some changes in the coloration of paper can also result from the physical–chemical transformations of their components such as type-lignin aromatic compounds and the interaction of the cellulose with metal traces that causes deleterious effects on papers. The latter correspond to foxing phenomena by the action of abiotic processes [6].

Paper staining following the activity of the fungi can be due to the *de novo* synthesis of fungal pigments and to the Maillard reaction of by-products of the fungal metabolism. This is the case of organic acids, oligo-saccharides, and other products derived from cellulose degradation that chemically react together with nitrogen-containing compounds and other additional materials from paper under specific conditions. This latter process forms brown products with the consequent formation of foxing type spots [49]. Although the formation mechanisms of foxing have been studied since 1930, there are still no conclusive results and they are controversial [6]. Therefore, additional studies are required in order to identify the

processes and conditions that contribute to development of foxing due to fungi in paper.

### 2.3 Chemical Nature of Fungal Pigmentation in Deteriorated Paper

Many fungi that deteriorate paper synthesize different pigments, such as lipophilic ones (e.g., carotenoids), hydrophilic ones (e.g., anthraquinones) and others, which are only soluble in alkaline solutions (melanins). These secondary metabolites may cause extensive color changes in the paper, even if the growth of fungi is limited. These pigments can play different functional roles, such as a protecting agent against environmental stress (including photo-oxidations), or against other organisms (involving an antimicrobial action) or as an intermediary enzyme-related cofactor. In this sense, there are several fungi growing on paper that increase their pigmentation by the establishment of stressful conditions. Llorente et al. [37] reported data about the nature of a dark pigment (1,8-dihydroxynaphthalene (DHN)-melanin) in agar cultures of *Cladosporium cladosporioides* and found that the pigmentation of their colonies was increased under chemical stress imposed by certain fungicides. This fungus is a frequent inhabitant of indoor air of libraries and museums and is an etiological agent that causes paper deterioration. Therefore it is necessary to study the melanization process in this fungus and its relationship with environmental conditions.

Several pigments found in deteriorated paper are produced and accumulated in different structures that fungi can differentiate, which are dependent on the taxonomic group to which they belong and to their ecophysiology. In this sense, the pigments can locate in spores, fruiting structures, and mycelium as well as resistance somatic structures such as the sclerotia. This can be variable, being the physiological state of the fungus a key in the differential effects that might generate on the substrate [48]. Although Szczepanowska and Cavaliere [57] suggested that the staining of several papers deteriorated by *Cladosporium* sp. and *Chaetomium* sp. was confined to the fungal elements, there are several findings that showed fungal pigments can be secreted into the substrate and so spread far away from the origin source. Choi et al. [19] reported the production of 2-methylresorcinol, a diffusible pigment with antimicrobial activity, by the fungus *Helicosporium* sp. (Ascomycota). Also, the pyomelanin, which is a water-soluble brown pigment, has been reported to be synthesized by different fungi under certain culture conditions. This pigment was shown to protect fungi against different stresses such as those generated by reactive oxygen intermediates [5]. Among the pyomelanin producing fungi, there are species from the genus *Aspergillus*, including *A. fumigatus*, which is a typical fungus that deteriorates paper [38]. However, *A. fumigatus* is also able to produce another melanin type, such as one DHN-type, which is insoluble in water and is predominantly present in the conidia and secondarily accumulated in the hyphae and excreted into the medium [52]. On the other hand, Michaelsen et al. [41] postulated that the pinkish to purple-colored spots in the 16th-century book's leaves have their origin in purple exudates from the cellulolytic fungi, *Aspergillus nidulans* and *A. versicolor*. Therefore, fungal staining is a highly relevant process that deteriorates paper and so a problem that conditions the choice of adequate strategies

of restoration. This is compatible with limited results reported in experiments with bleaching agents to eliminate front spots associated with fungal deterioration. Since the mechanical removal of dark fungal elements on paper where the pigments are attached, such as reported by Szczepanowska and Cavaliere [57], is not a minimally invasive restoration procedure, new sustainable strategies must still be developed.

### **3 Cultural Heritage in Paper: Causes of Biodeterioration and methods for Their Treatment. Benefits and Problems of Various Treatments. Use of Gamma Radiation**

A book or document undergoes biodeterioration when it suffers alteration of its physical, chemical, mechanical, and aesthetic properties due to the action of biological organisms. Inadequate infrastructure and environmental conditions, as well as microorganisms on material, are the main causes of deterioration of cultural heritage on paper and a door open to fungal contamination and attack of insects or rodents [14, 17, 44, 56]. Pollution caused by microorganisms is one of the main problems that affect cultural heritage objects because it not only degrades the material but also affects the quality of the air of archives and libraries where they are stored [65–67]. Pollution can cause severe diseases, mainly by inhalation of spores and/or contact with them, so it is essential to proceed to decontaminate prior to restoration [68]. The growth of microorganisms and insect pests that generate biodeterioration are favored by factors such as temperature, high humidity, crowded deposits, dust, and poor air circulation. Thus, it is necessary to control these factors to avoid attack [9].

When we talk about the conservation of cultural heritage on paper, we refer to a wide range of procedures and techniques, which serve both to prevent, correct, and repair the originated damage. Modern scientific and technological advances have supplied fundamental tools to combat biological factors of deterioration and helped to understand if they were caused by physical and chemical elements. There are several effective treatments, to a greater or lesser extent, that have been used worldwide. These pest-control methods can be physical and chemical.

One method of control is based on the use of chemicals to prevent pests or eradicate insects and fungi. Many institutions make periodic fumigations unaware that these products leave residual vapors which, when daily breathed by employees and/or users, may cause severe health problems [25]. Although a wide diversity of chemicals are used—such as fungistatic compounds, for instance thymol or orthophenylphenol—which inactivate some fungi—the two most commonly used methods are ethylene oxide (ETO) and gamma radiation since they are industrially standardized for use.

Despite ETO's high toxicity at doses necessary to eradicate fungi, it was used worldwide in the 1980s to treat fungal infections in archives and libraries and it is still used regularly in archives. After this type of treatment, adequate ventilation should be made in order to remove residual gas [4].

In 1984, the U.S. Occupational Safety and Health Agency (OSHA) specified a standard for occupational exposure to ethylene oxide which, among other provisions, lowered the permissible exposure level (PEL) from 50 to 1 ppm [64].

However, the need of appropriateness of a short-term exposure limit has not been evaluated [4]. The World Health Organization (WHO) has given clear guidelines for allowable limits for humans, animals, and the environment. They explained the severe health problems caused by ethylene oxide, such as cancer, abortions, and kidney failure, because of their residual vapors or dermal absorption [68].

Ionizing radiation, in particular, has been and is used worldwide for the elimination of biodeteriorating agents in libraries and archives for the recuperation of large volumes of bibliographic material after disasters, especially those caused by water contact [11, 12, 42, 53].

There are several investigations aimed at the evaluation of the use of gamma radiation as a biocide agent in books or documents affected by fungi and/or insects. Due to its physical character, gamma radiation does not leave any residues and books or documents can be used immediately after treatment [1, 2, 3, 10, 24, 35, 54].

Its high penetration capacity makes it possible to treat large volumes of material in a short time and at room temperature, without vacuum or any other type of additional treatments [1]. Materials are irradiated in their packaging and it is not necessary to air them out after the treatment. Another advantage is that only one parameter has to be evaluated: the delivered radiation dose, which depends only on the time of exposition to radiation.

Chemical reactions induced by gamma radiation on the cellulose molecules include breaking of molecular links and oxidation. The generation of free radicals causes secondary reaction in paper constituent elements [1]. Although the cellulose molecule is broken, reducing its size, the length of the polymeric chain is not affected.

No significant deterioration of mechanical resistance has been reported, even after a 70% reduction in its degree of polymerization. It is highly important to consider that the loss of molecular weight does not concur with observations during practical applications [1, 22, 23, 42, 46].

In case of catastrophic events affecting archives, museums, and libraries, and when the contamination degree is important, the use of gamma radiation is the only way to conserve the material. This technique, followed by appropriate storage, will preserve the material from a definitive loss in a short time [21, 42, 50, 51, 61].

A general acceptability criterion is that materials' properties should not be affected in more than 50% of their original value as a consequence of the treatment. Regarding bibliographical materials, acceptability criteria is the ability to continue its use without significant loss of its functionality. In those cases in which materials could not be recovered for normal use, the procedure consists of treating, cleaning, restoring, and digitalizing them, followed by the appropriate storage of the original [11, 22].

In certain areas, the use of gamma radiation for treatment of books or documents is resisted, without a true knowledge of the advantages of the method. Without a suitable treatment, a book could suffer greater deterioration due to oxidation and/or

acidification from undesirable residues in the paper, with the possibility of total loss in case of lack of adequate measures to revert the situation.

In the USA, during 1980, Nancy McCall, archivist in charge of John Hopkins University Alan M. Chesney, Medical Archives at John Hopkins Hospital, received a donation of 295 boxes with a document collection belonging to Dr. William Horsley Gantt, a psychiatrist disciple of Russian physiologist Iván Pavlov. The material of high heritage value was totally contaminated by microorganisms and had suffered an attack of insects and rodents. After the evaluation of the possible treatment methods, and although there was not enough experience on the use of ionizing radiations, Ms. McCall together with nuclear engineer Walter Chappas of the University of Maryland, decided to irradiate all of the boxes using a cobalt-60 linear accelerator for 45 min at a 4.5-kGy dose [39].

Years later, Ms. McCall explained that after 20 years, no problems have arisen with their irradiated documents, that continue available for normal use, cleaned and restored [40]. This experience and its favorable results after many years was in a certain way the starting point for the research and studies, performed at CNEA, in the use of gamma radiation for cultural heritage on paper support treatment.

#### **4 Creation of the Laboratory for Preventive Conservations and Restoration of Documentation (LCRD)**

The Laboratory of Preventive Conservation and Restoration of Documentation (LCRD) was created in August 2005, with the main objective of preserving institutional documental heritage on paper support. Gamma radiation was adopted for the treatment and recuperation of documents with a fungal infection because of its strengths (non-contaminating process, highly penetrating).

Desinsection of cultural heritage objects had already been done at PISI but it was not until 2001 that the evaluation of the effects of gamma radiation on physical and mechanical properties of papers commonly used in libraries and archives was started. Attention was paid to fungi due to the difficulties in their eradication and the highly toxic and contaminating chemical treatments of regular use in the Argentine market.

Thus, it was necessary to face up the great lack of confidence of professionals on cultural heritage conservation especially of paper support to accept the usefulness of this peaceful use of nuclear energy. Although this situation is still present, dissemination and the offer of services to other institutions are very good tools contributing to solve the problem.

#### **5 Radiation Processing-CNEA's Semi-industrial Irradiation Facility (PISI)**

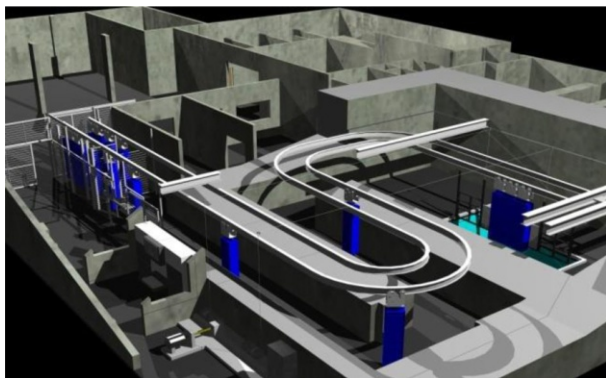
The basic components of irradiation facilities include a



- radiation source (radionuclide gamma or machine source) and the associated systems,
- a product transportation system (in most cases),
- an irradiation chamber with biological shield for protection of personnel and public against radiation,
- storage zones for irradiated and non-irradiated products,
- a dosimetry laboratory,
- a product-handling system and
- the infrastructure for personnel [26].

Argentina's National Atomic Energy Commission has broad experience in radiation processing since the 1960s, mainly in applied research on irradiation of health care products, food polymers, among others. Accompanying this development, Argentina's first irradiation facility—PISI—started operations in 1970, at the Ezeiza Atomic Center. The PISI is a multipurpose facility that uses cobalt-60 sources, with a nominal activity of 1MCi [45].

The process takes place in an irradiation chamber. Products are moved by a conveyor system and exposed to gamma radiation during the time necessary to absorb the proper energy to achieve the objective.



Absorbed dose (sometimes referred to as 'dose')  $D$ , is defined as the quotient of the  $d\varepsilon$  by  $dm$ ,  $d\varepsilon/dm$ . Where  $d\varepsilon$  is the mean energy imparted by ionization radiation to matter of mass  $dm$ . The unit of absorbed dose is Gray (Gy), where 1 Gray is equivalent to the absorption of 1 Joule per kilogram of specified material ( $1 \text{ Gy} = 1 \text{ J/kg}$ ) (ISO 12749-4 2015).

Absorbed dose is the quantity that relates directly to the intended effect. Prior to the actual irradiation treatment, both the minimum dose required to reduce biodeteriogene level to normal (or treatment dose) and the maximum acceptable dose must be determined. The first one depends on the type of biodeteriogens present on the paper, and the second is related to compatibility of the paper, ink, and to the materials with the radiation process. It is the highest dose the object can absorb without having unacceptable modifications of its properties. This dose range is usually determined by a combination of bibliographical recommendations and



adequate testing. Since absorbed dose is the magnitude of interest, suitable dose measurement techniques are required in order to prevent under- or over-exposure of the product.

The dose measurements required in radiation processing concern characterization of irradiation facilities in installation qualification (IQ), operational qualification (OQ), measurement of dose distribution in irradiated products in performance qualification (PQ), and routine monitoring of the irradiation process [30].

At PISI, routine dosimetry is performed with PMMA dosimetry systems, calibrated with alanine dosimetry systems traceable to NPL.

Although at present there is no specific standard for irradiation of cultural heritage objects, since dosimetry and process validation and control practices are—in general terms—quite similar between different processing applications (except for differences in dose level and package characteristics), dosimetry for biodeteriorated cultural heritage on paper treatment is performed following guidelines of good irradiation practices [26, 31, 32, 34].

## 6 Studies Performed at the LCRD

### 6.1 Studies on the Use of Gamma Radiation for Insect and Fungi Control on Paper Support for Conservation Purposes (Magister Thesis, [11])

The ability of this technique was shown to effectively contribute to the conservation of bibliographical material, removing fungi and insects without a significant deterioration of its properties. The study was conducted in three stages. The first two evaluated the seven existing types of paper and cardboard. The third step includes the analysis of paper leafs with advertising from the magazines irradiated at 50 kGy.

The following papers were also analyzed:

- 90 g Permalife paper and 175 g Permalife cardboard, Ecobotanical paper (all of them used in conservation), Epson photographic paper
- Executive Ledesma pulp paper and Fotocopy office paper (acid with pulp fiber),
- leafs from a book and
- a magazine with fungus infection donated for the essay.

These papers were selected due to their regular use in archives and libraries or for having similar characteristics to those used in these places. Samples of irradiated and non-irradiated, aged, and non-aged papers were tested.

*First Stage:* the papers were irradiated using a single dose of 13.4 kGy, trying to cover the necessary dose range for the treatment applied in case of fungi contamination.

*Second Stage:* after successful results in the first stage, this was followed by a second one consisting of the irradiation of samples at doses of 3, 5, 10, 15, 20, and 50 kGy, with the aim of getting the different papers' behavior profile under irradiation and the determination of the minimum dose value to reduce microorganisms to their environmental value. The maximum dose each paper could receive

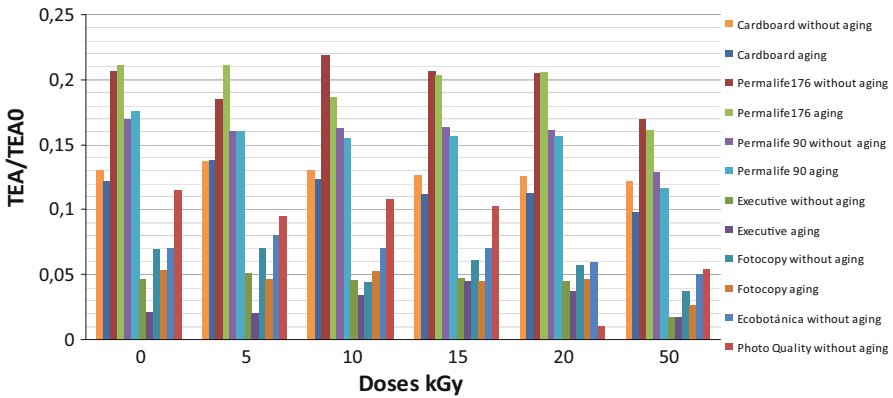


**Fig. 1** Behavior of papers irradiating at different doses (5, 10, 15, 20, 50 kGy), aged and without aging

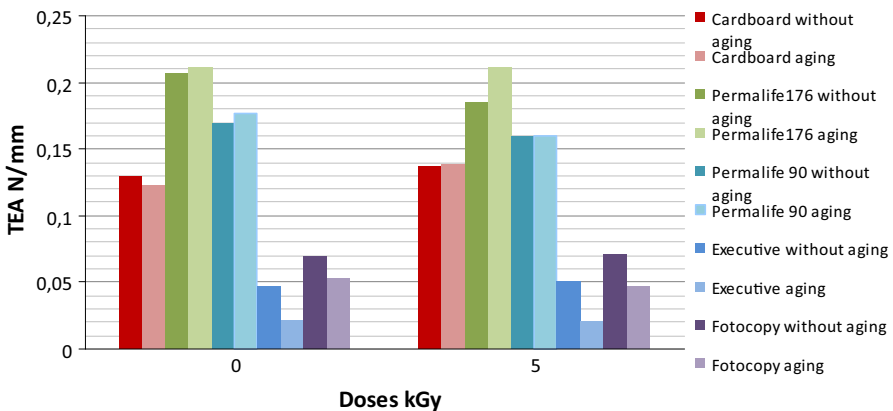


**Fig. 2** Behavior of papers irradiating at low doses to reduce microorganisms to their environmental value, aged and without aging

without noticeable deterioration of its mechanical capacity was also determined (Figs. 1, 2).

*Third Stage:* After the terrorist attack of September 11, 2001, in the USA, all the mail arriving to CNEA was irradiated at the PISI in order to discard any possible attach with filterable virus or other type of etiological agent. Seven boxes of publications containing 125 magazines, coming by post from the USA and Europe, were irradiated at 50 kGy. Three years after their radiation, leafs with publicity were extracted and evaluated under Tappi T494 om96 [59] standard, performing tensile strength tests and pH essays. Although a very high dose was used, five times the necessary to control fungi infections, the material is currently in use without any type of visible deterioration. Physical and mechanical tests of all the material used in the three stages mentioned above were performed in the Laboratory of Polymers, at the Ezeiza Atomic Center. A dynamometer INSTRON model 1122 multipurpose, with a load cell of 500 kg and head speed of 20 mm/

min, was used. Screw grips were used to hold the strips. Tensile strength and percentual stretch were determined according Tappi T494 om 96 standard. Before the tests, all the material was stabilized at 22 °C and 50% RH, for 72 h. Fibers from all the irradiated papers prepared under Tappi T401 om 93 [58] standard were photographically registered and compared against fibers from the unirradiated controls, and the differences were evaluated. Electron micrographs were taken with an optical microscope at 40× and a scanning electron microscope at 800× and 1600×. In this way, it was possible to evaluate the absence of morphological changes in the fibers. The analysis of the fibers by SEM was done with the assistance of the Cellulose and Paper Laboratory of the National Institute of Industrial Technology (INTI), for the determination of the deterioration in fibers and other paper components with a better precision.

Regarding the irradiations of the second stage at different doses, it was possible to confirm that only the biological tests of papers irradiated at 3 kGy presented fungal development. No visible pH changes were observed.

After 3 years of irradiation of magazines at 50 kGy (third stage), samples from these magazines were compared to others taken from unirradiated publications of the same period. It was possible to determine that at this dose there is a 49% loss in the mechanical characteristics of TEA and a 34% loss in the deformation percentage, being both compatible with their normal use.

As a conclusion, it was determined that deterioration of treated materials is not significant, being possible to verify the working hypothesis and the possibility to use gamma radiation or microorganisms and insect control in books and documents [11].

## 6.2 Treatment of CNEA Public Administrative Bulletins

In 2001, it was found that all leather bindings of the Public Administrative Bulletins (BAPs) collection at the Administrative Archive of CNEA were covered by greenish stains. These Bulletins with the institutional administrative memory suffered a fungal infection due to their storage in a deposit without ventilation (airing) and very high temperature and humidity after cleaning with wet towels during summer [13].

The material was analyzed in the Microbiology Laboratory at the Ezeiza Atomic Center for the determination of the irradiation dose. Three hundred books were put into 50 boxes and irradiated at the PISI at 14.4 kGy and a dose rate of 0.15 kGy/min [23]. In this case, the Microbiology Laboratory only performed the dose analysis as it was irreversible risk destroy the material. After the irradiation, the books were cleaned and stored in a deposit built under conservation standards established by the International Center for the Study of the Preservation and Restoration of Cultural Property (ICCROM): floor, ceiling, and walls made of fireproof materials, lightning with UV filters, temperature and relative humidity mechanically controlled at 20 °C and 50%, respectively (smoke and temperature change detectors, anti-panic doors).

### 6.3 Publications Belonging to the Constituyentes Atomic Center Biodeteriorated Due to a Flood Event

In 2001, several boxes with periodical publications at the Information Center of the Constituyentes Atomic Center got wet due to a flood in the area. Drying activities began immediately after the problem had been detected. However, due to high temperature and humidity, a great part of the material was severely infected. After evaluating the degree of the damage, the most adequate solution was selected.

The material was analyzed at the Microbiology Laboratory for the determination of their radiation dose and was irradiated at the PISI at 15 kGy. After irradiation, the material was returned to the Information Center including a report indicating the procedure for its conservation, cleaning, and storage.

### 6.4 Documentary Fund Declared by UNESCO Memory of Humanity

In 2006, the LCRD received an offer to work with a documentary Collection included in the UNESCO Memory of the World Register. The collection consisted of 36 boxes with 100–120 records of 1–20 pages each, in plastic envelopes. Due to a flood, the documents were kept wet in these envelopes for over 2 months. The archivist of the institution where the collection was kept asked the LCRD for an evaluation of the material and of its recuperation. Samples were collected for the determination of the irradiation dose (9 kGy) at the Microbiology Laboratory. An important amount of the material was recuperated by hand. In this case, due to the paper acidity degree (acid papers with ferrogallic inks), calcium carbonate was used to increase alkalinity in the document restoration. The method consisted of the addition of 5 mg of calcium carbonate per liter of 2% methylcellulose solution to stick Japanese paper to the documents after their cleaning. Tests were done for the determination of pH of the irradiated and un-irradiated documents as well as on the aged ones.

In order to verify the degree of improvement, essays were done for accelerated aging using dry heat [62] and wet heat [63] and IRAM ATIPCA P3118 [29] standard for UV aging. Papers treated with methylcellulose and with methylcellulose plus calcium carbonate were compared.

Tensile tests were done and the results compared to those obtained from wet heat aged probes treated with Japanese paper and methylcellulose (A) and with Japanese paper plus methylcellulose plus calcium carbonate (B). Preliminary results showed an increase of about 40% in mechanical resistance to tensile strength for B papers as compared to A papers. It was found that accelerated aging at 80 °C and 65% RH for 24 h did not cause noticeable changes in the tested samples. Mechanical properties of the restored samples were examined in order to evaluate their tolerance to handling for their digitalization or direct reading. As no identical material was available for control purposes, a common office paper of known tolerance to handling and accelerated and natural aging was used. In relation to this control sample, resistance of the paper fibers was about 37% for samples restored using methylcellulose and about 51% for those treated with calcium carbonate. In the direction perpendicular to the fibers, samples treated without calcium carbonate

showed the same resistance as the control samples, and the ones treated with calcium carbonate 45% less. Elongation capacity was slightly higher than that of the control sample for samples restored without calcium carbonate and about 50% for the ones with calcium carbonate—in the direction perpendicular to the fibers and in the sense of the paper fibers, values were 60–68% of the control values. It is interesting to notice that dispersions, expected when working with restored material coming from highly deteriorated originals, were well above the results from samples treated with calcium carbonate, probably due to problems in the carbonate dispersion in the methylcellulose solution. Thermal aging did not cause any important fall of tensile strength and elongation capacity. Irradiated paper, restored with and without carbonate, resulted with enough mechanical resistance for handling in the different studies performed [22].

### **6.5 Influence of the Irradiation Dose and Dose Rate on the Physical Properties of Commercial Papers Commonly Used in Libraries and Archives**

The objective of this study was the evaluation of the dose and dose rate in papers commonly used in libraries and archives for their optimization. Doses between 2 and 11 kGy and dose rates between 1 kGy/h and 11 kG/h were used. Physical and mechanical properties, intrinsic viscosity, tear resistance, and brightness were analyzed.

The three different brands of paper with different pulp compositions were:

- soda-anthraquinone pulp from sugar cane bagasse (author),
- bleached eucalyptus kraft pulp with an elemental chlorine free bleaching sequence (Boreal), and
- a specialty paper with a 25% of cotton fiber in use for paper conservation (Capitol Bond).

Gamma radiation is a valid option for removing mold from books and documents because it has no residual toxicity, is highly penetrating, does not pollute the environment, and large volumes of material can be processed in a short time. Although a lot of research has been conducted about adequate doses, no recent works have been found on the effect of dose rate or on its combination with dose. The aim of this study was to evaluate the effects of dose and dose rate of gamma radiation on the physical properties of commercial papers commonly used in libraries and archives in order to optimize the irradiation conditions for each one.

Three different brands of paper with different fiber composition were used, and a 3<sup>2</sup> factorial design with four replicates of the center point with doses ranging from 2 to 11 kGy and dose rates between 1 and 11 kGy/h were applied. Chemical, mechanical, and optical properties were determined on the samples. With some difference between kinds of paper, tensile strength, elongation, TEA, and air resistance were in general unaffected by the treatment. The lowest loss of intrinsic viscosity, tear resistance, and brightness were obtained with doses in the range of 2–3 kGy for all the papers, where dose rate was different for each paper: 11, 10, and

3 kGy/h for papers A, B, and C, respectively. These conditions are ideal for removing insects. If the irradiation is performed at 10 kGy to remove a mass fungal attack, the additional loss of viscosity would be of about 40% and the loss of tear strength would be about a 10% approximately for all the papers [7, 15].

## 6.6 In-vitro Attack of Paper by Selected Fungi and its Control by Gamma Radiation

At the beginning of 2015, an agreement was signed with the National University of La Plata, in order to work on the following subjects:

- (a) Resistance of abaca paper to attack by *Chaetomium globosum* LPSC 259 and gamma radiation.
- (b) Resistance of Capitol Bond paper to attack by *Cladosporium cladosporioides* LPSC 1088 and gamma radiation.
- (c) Resistance of an adhesive, methylcellulose, to attack by both *Chaetomium globosum* LPSC 259 and *Cladosporium cladosporioides* LPSC 1088 and gamma radiation.

The papers were exposed to the inoculation with biodeterioration causing fungi as *Chaetomium globosum* LPSC 259 y *Cladosporium cladosporioides* LPSC 1088.

In this sense, two experiments were done:

- (a) Inoculation of sexual spores of *Chaetomium globosum* LPSC 259 on circle probes of abaca paper (8 cm in diameter) that were incubated axenically under two humidity levels (65 and 95%) at 28 °C. Paper probes free of spores were incubated under the same conditions.
- (b) A suspension of conidia from *Cladosporium cladosporioides* LPSC 1088 was applied to probes (20 mm × 250 mm) of Capitol Bond paper according to Tappi T494 om96 test, which were then incubated at 75% humidity and 28 °C during 5 months. No signs of fungal deterioration were found in the Capitol Bond probes. This is possibly due to the presence of antifungal compounds in the composition of paper, which might have limited the fungal growth and its effect on the paper quality. However, the spores of *Chaetomium globosum*, when inoculated in abaca paper, germinated both under 65 and 95% of humidity. They showed pigmented sexual structures after 1 month of incubation (Fig. 3). These last probes were exposed to gamma radiation at 3 and 8 kGy. They were then characterized by Fourier transform infrared (FTIR) spectroscopy. Although the results obtained are still preliminary, the FTIR analysis upon the irradiated abaca paper, as compared to non-irradiated sample, suggests that the chemical structure of paper was not affected. However, additional analyses are still necessary in order to evaluate whether their behavior is affected by the absorbed dose. At present, the effects on methylcellulose of fungal alteration and gamma radiation are being analyzed.

**Fig. 3** Probes of abaca paper colonized by *Chaetomium globosum* LPSC 259, showing several pigmented perithecia



### 6.7 IAEA Technical Co-operation Project RLA/0/058

The laboratory is currently taking part in the International Atomic Energy Agency (IAEA) Technical Co-operation Project RLA/0058 on the ‘Use of nuclear techniques for conservation and preservation of cultural heritage objects’. Twelve Latin American countries: Argentina, Bolivia, Brazil, Chile, Costa Rica, Cuba, Ecuador, Mexico, Panama, Peru, Dominican Republic, and Uruguay are participating in the project, Argentina being the project leader. Its objective is to promote and harmonize the use of nuclear techniques in support of cultural heritage preservation and characterization.

The LCRD experience on the benefits of the technique was presented at the IV International Conference on Intervening and Preventing Conservation of Cultural Heritage, Buenos Aires, Argentina, April 4–7, 2016. Particular cases as well as loads of infected material were analyzed.

### 6.8 Dissemination of the Use of Gamma Radiation for the Treatment Of Fungal Infections

Given the low acceptance of the technique, principally due to limited knowledge, the LCRD has faced up to its dissemination. Regarding the general public, the laboratory has been present at scientific fairs for 3 years and spread general information by means of leaflets, institution Web sites, Facebook, etc. The laboratory has participated in a Conference of Preservation of Cultural Heritage objects at Roffo Hospital, especially aimed at museum curators, librarians, archivists, and other potential users of the technique.

Recuperation of wet bibliographical material on paper support [16] was also presented in national and international seminars and conferences. In addition, some workshops were organized for other institutions.

## 7 The Future

For the near future, it is expected to continue with the dissemination of the results obtained in our laboratory. As a complement of the activities done so far, we will deepen our study of the effects of gamma radiation on photographs and different inks.

## 8 Conclusions

Gamma radiation treatments were systematically applied to several heritage documents in CNEA for more than 10 years. They have contributed to solve biodeterioration problems caused by inadequate handling or storing conditions or by natural factors.

Similarly to what happens with alternative methods of preservation or conservation, radiation technology has both strengths and weaknesses, which always have to be taken into account. It is considered that the main difficulty for a generalized use of these techniques is certainly the resistance that conservation professionals have towards radiation technology. This is attributed mainly to misconcepts or preconception emerging from insufficient knowledge in the matter. Designing a communication strategy is mandatory in order to reverse this situation.

**Acknowledgements** Our special thanks to Dr. Mila D'Angelantonio and to Prof. Margherita Venturi for their interest in our work and its dissemination. We would also like to thank scientists and technicians from different laboratories of CNEA and the Irradiation Facility who contributed, especially to Lic. Rita Plá, Dr. Miguel Ipoehorski, and Dr. Diego González, for their support and collaboration.

## References

1. Adamo M et al (2001) Gamma radiation treatment of paper in different environmental conditions. *Restaurator* 22:107–131
2. Adamo M, Maggauda G, Tata A (2004) Radiation technology for cultural heritage restoration. *Restaurator* 25(3):159–170
3. Adamo M, Maggauda G, Rochetti F (2007) The effect of  $\gamma$ -radiation on acidified and artificially aged paper. *Restaurator* 28:227–238
4. Albiano N (2010) Labor toxicology Criteria for monitoring the health of workers exposed to hazardous chemicals". Cap. 25. Ed: Superintendency of Occupational Risks. Bs. As., Argentina
5. Almeida- Paes R, Frases S, deSousaAraújo G, Evangelista Marques, de Oliveira M, Gerfen GJ, Nosanchuk JD, Zancopé-Oliveira RM (2012) Biosynthesis and functions of a melanoid pigment produced by species of the *Sporothrix* complex in the presence of L-tyrosine. *Appl Environ Microbiol* 78:8623–8630
6. Ardelean E, Melniciuc-Puică N (2013) Conservation of paper documents damaged by foxing. *Eur J Sci Technol* 9(2):117–124
7. Area MC, Calvo AM, Felissia FE, Docters A, Miranda MV (2014) Influence of dose and dose rate on the physical properties of commercial papers commonly used in libraries and archives. *Radiat Phys Chem* 96:217–222
8. Rizzo M, Machado, LDB, Rela PR, Yasko K (eds) Associação Brasileira de Energia Nuclear-ABEN. International Nuclear Atlantic Conference-INAC2009. Gamma Rays irradiation process on a restored painting from the XVIIIth. Century Rio de Janeiro, September 27 to October 2, 2009. ISBN: 978-85-99141-03-8



9. Boletín INTI (2013) Evaluación de las condiciones ambientales del depósito de las revistas de la Biblioteca del INTI. Octubre 2013, Celulosa y Papel, Boletín 19. ISSN1851-846x. <http://www.inti.gob.ar/celulosaypapel/boletin/inti2.php>
10. Butterfield, F. 1987. "The potential long term effects of gamma radiation of paper" *Studies in Conservation*. V.32:181-191
11. Calvo AM (2004) Tesis: "El Uso de radiación gamma para el control de microorganismos e insectos en papel como un método de conservación de los materiales bibliográficos en peligro de inutilización". Directora de Tesis: Dra. María Elisa González. Universidad del Museo Social Argentino, Buenos Aires, set. 2004, p 180
12. Calvo AM, Miranda MV (2013) Coloquio "Conservación- Restauración-Salud/Seguridad laboral de las personas y del medioambiente" (Draguignan-Figanières (France): 17–21 jun 2013)
13. Calvo AM, González ME (2001) Irradiación de papel para control de microorganismos. *Revista CNEA*, 2001(abril–junio) 2:25–27
14. Calvo AM, González ME, Alfaro L, Miranda MV (2009) Laboratorio de Conservación y Restauración de Colecciones en Papel de la CNEA: tratamiento de libros y documentos atacados por microorganismos usando rayos gamma. *Revista CNEA* 2009(35–36):31–35
15. Calvo AM, Alfaro LS, Miranda MV, Area MC, Felissia F (2010a) Comportamiento del papel decelulosa frente a la irradiación a distintas dosis y el envejecimiento acelerado. *Asociación Argentina de Tecnología Nuclear*, 22–25 de noviembre de 2010, Hotel Claridge, Buenos Aires
16. Calvo AM, Alfaro LS, Miranda MV, Chinen S (2010b) "Simulacros de desastre climático recuperación de material bibliográfico en el marco de la conservación preventiva" en *Patrimonio Cultural: la gestión el arte, la arqueología y las ciencias exactas aplicadas*, Buenos Aires, CNEA, pp 197–201
17. Calvo Torras MA, Adelantado C, Corcuera Marín E (2005) Criterios: Principales características de los hongos causantes de alteraciones en materiales celulósicos", *PH Boletín Andaluz del Patrimonio Histórico*, No 53, pp 18–23
18. Carrazana-García DI, González-Álvarez D, Díaz-Álvarez E, Mesa-Garriga L, Banguela-Castillo A, Chea-González A, Cupull-Santana R (2014) *Aspergillus sclerotiorum*: riesgo para la herencia cultural y la salud. *Universitas Scientiarum* 19(3):323–332. doi:10.11144/Javeriana.SC19-3.asrh
19. Choi Hye Jung, Sang Myeong Lee, Sun-Hee Kim Dong Wan, Kim Young, Choi Whan, Hong Joo Woo (2012) A novel *Helicospodium* isolate and its antimicrobial and cytotoxic pigment. *J Microbiol Biotechnol* 22(9):1214–1217
20. Cragg SM et al (2015) Lignocellulose degradation mechanisms across the tree of life. *Curr Opin Chem Biol* 29:108–119
21. Cutrubinis M, Tran K, Bratu E, Caillat L, Negut D, Niculescu G (2008) International Conference on Wood Science for Preservation of Cultural Heritage. In: *Disinfection and consolidation by irradiation of wooden samples from three Romanian churches: Mechanical and biological factors*. Museu Diego de Sousa, 5-november de 2008, Braga
22. González ME, Calvo AM, Horak C, Alfaro L, Miranda V (2009) Propiedades del papel de oficina restaurado luego de radiotratamiento para descontaminación de hongos y levaduras" 1er. Congreso Iberoamericano y VIII Jornada "Técnicas de Restauración y Conservación del Patrimonio", 10y 11 de Septiembre de 2009, La Plata, Buenos Aires
23. González ME, Calvo AM, Kairiyama E (2002) "Gamma Radiation for Preservation of Biologically Damaged Paper". XII International Meeting on Radiation Processing, 26–30 March 2001, Avignon, France. *Radiat Phys Chem* 63:263–265
24. Guiomar Carneiro Tomazello M, Wiendl FM (1995) The applicability of gamma radiation to the control of fungi in naturally contaminated paper. *Restaurator* 16:93–99
25. Hengemihle FH, Weberg N, Shahani C (1995) Preservation Research and Testing Series No. 9502. Desorption of Residual Ethylene Oxide from Fumigated Library Materials Preservation Research and Testing". Office Preservation Directorate Library of Congress Washington, D.C. <http://www.loc.gov/preservation/>
26. IAEA Food Dosimetry Handbook (2002) Dosimetry for food irradiation. International Atomic Energy Agency, Vienna, Technical report series, ISSN0074–1914; no. 409.STI/DOC/010/409. ISBN 92–0–115502, p 168
27. IAEA Regional Project RER 8015 (2009–2011) Nuclear Techniques for Characterization and Preservation of Cultural Heritage Artefacts in the European Region. International Atomic Energy Commission. Vienna, p 44
28. IAEA-TECDOC-1386 (2004) Emerging applications of radiation processing. In: *Proceedings of a technical meeting held in Vienna, 28–30 April 2003*, IAEA, Vienna, p 171

29. IRAM ATIPCA 3118 P. Envejecimiento por radiación UV.de papeles y cartones, p 4
30. ISO/ASTM 52628 (2013). Standard Practice for Dosimetry Radiation Processing. American National Standard, p 13
31. ISO11137-1 (2006) Sterilization of health care products—radiation—part 1: requirements for development, validation and routine control of a sterilization process for medical devices, p 37
32. ISO11137-2 (2013) Sterilization of health care products—radiation—part 2: establishing the sterilization dose, p 68
33. ISO12749-4 (2015) Nuclear energy, nuclear technologies, and radiological protection—vocabulary—part 4: dosimetry for radiation processing, p 29
34. ISO14470 (2011) Food irradiation—requirements for the development, validation and routine control of the process of irradiation using ionizing radiation for the treatment of food, p 20
35. Kатуšin-Ražem B, Ražem D, Braun M (2009) Irradiation treatment for the protection and conservation of cultural heritage artefacts in Croatia. *Radiat Phys Chem* 78:729–731. doi:10.1016/j.radphyschem.2009.03.048
36. Lacey J (1996) Spore dispersal-its role in ecology and disease: the British contribution to fungal aerobiology. *Mycol Res* 100:641–660
37. Llorente C, Bárcena A, Vera Bahima J, Saparrat MCN, Arambarri AM, Rozas MF, Mirífico MV, Balatti PA (2012) *Cladosporium cladosporioides* LPSC 1088 produces the 1,8-dihydroxynaphthalene-melanin-like compound and carries a putative pks gene. *Mycopathologia* 174:397–408
38. Mesquita N, Portugal A, Videira S, Rodriguez-Echeverri S, Bandeira AML, Santos MJA, Freitas H (2009) Fungal diversity in ancient documents. A case study on the Archive of the University of Coimbra. *Int Biodeterior Biodegrad.* 63:626–629
39. McCall N (1985) Ionizing radiation as an exterminant: a case study. *Conservation Administration News*, No 23
40. McCall N (2001) Personal communication
41. Michaelsen A, Piñar G, Montanari M, Pinzari F (2009) Biodeterioration and restoration of a 16th-century book using a combination of conventional and molecular techniques: a case study. *Int Biodeterior Biodegrad.* 63:161–168
42. Moise IV et al (2012) Establishing the irradiation dose for paper decontamination. *Radiat Phys Chem* 81(8):1045–1050. doi:10.1016/j.radphyschem.2011.11.063
43. Molina Veloso A, Borrego Alonso SF (2015) El planero como barrera contra agentes biodeteriorantes de mapas y planos. *PH Investigación* 4:45–61
44. Olcott Price L (1999) Traducción: Alan Haley y voluntarios de APOYO (Association for the Conservation of Cultural Heritage of the Americas). Controlling an invasion of mold. Guidelines for intervention in case of disaster. Support 9:6. [http://imaginario.org.ar/apoyo/vol9-1\\_3-htm](http://imaginario.org.ar/apoyo/vol9-1_3-htm)
45. Papadópulos CC (1970) Planta Semi Industrial de Ezeiza. CNEA 272, CNEA, Buenos Aires, p 25
46. Phillips GO, Arthur JC (1985) Photochemistry and radiation chemistry of cellulose. In: Nevell TP, Zeronian SH (eds) *Cellulose chemistry and its applications*, vol 552, pp 290–311. Ellis Horwood Ltd, Chichester
47. Pinheiro AC, Macedo MF, Jurado V, Saiz-Jimenez C, Viegas C, Brandao J, Rosado L (2011) Mould and yeast identification in archival settings: preliminary results on the use of traditional methods and molecular biology options in Portuguese archives. *Int Biodeterior Biodegrad* 65:619–627
48. Pinzari F, Troiano F, Piñar G, Sterflinger K, Montanari M (2011) The contribution of microbiological research in the field of book, paper and parchment conservation. In: Engel P, Schirò J, Larsen R, Moussakova E, Kecskeméti I (eds) *New approaches to book and paper conservation-restoration*, pp 575e–594. Verlag Berger, Horn/Wien
49. Piñar G, Tafer H, Sterflinger K, Pinzari F (2015) A mid the possible causes of a very famous foxing: molecular and microscopic insight into Leonardo da Vinci's self-portrait. *Environ Microbiol Rep* 7(6):849–859
50. Ponta CC (2008) Irradiation conservation of cultural heritage. *Nucl Phys News* 18(1)
51. Ray E (2006) The Prague Library Floods of 2002. *Libraries & Culture. Crisis Exp* 41(3):381–391
52. Schmalder-Ripcke J, Sugareva V, Gebhardt P, Winkler R, Knemeyer O, Heinekamp T, Brakhage A (2009) Production of pyomelanin, a second type of melanin, via the tyrosine degradation pathway in *Aspergillus fumigatus*. *Appl Environ Microbiol* 75(2):493–503
53. Sinco P (2000) The use of gamma rays in book conservation. *Nucl News*, pp 38–40
54. Smith PA, Sheely MV, Hakspiel SJ, Miller S (2003) Volatile organic compounds produced during irradiation of Mai. *AIHA J* 64(2):89–195

55. Sequeira S, Cabrita EJ, Macedo MF (2012) Antifungals on paper conservation: an overview. *Int Biodeterior Biodegrad* 74:67–86
56. Sterflinger K, Pinzari F (2012) The revenge of time: fungal deterioration of cultural heritage with particular reference to books, paper and parchment. *Environ Microbiol* 14(3):559–566. doi:10.1111/j.1462-2920.2011.02584.x
57. Szczepanowska H, Cavaliere AR (2012) Conserving our cultural heritage: the role of fungi in biodeterioration. In: Johanning E, Morey P, Auger P (eds) *Bioaerosols—fungi, bacteria, mycotoxins in indoor and outdoor environments and human health*, pp 293–309. Fungal Research Group, Albany
58. TAPPI T401-93 (1993) Fiber analysis of paper and paperboard, p 12
59. TAPPI T494om96 (1996) Tensile breaking properties of paper and paperboard. Using constant rate of elongation apparatus, p 4
60. Troncozo MI, Gómez RP, Arambarri AM, Balatti PA, Bucsinszky AMM, Saparrat MCN (2015) Growth and oxidative enzymatic activity of in vitro cultures of *Ciliochorella buxifolia*. *Mycoscience* 56:58–65
61. Urban J, Justa P (1986) Conservation by gamma radiation: the Museum of Central Bohemia in Roztoky. *Mus Int* 151:165–167
62. UNE 57092-4 (2002) Papel y Cartón. Envejecimiento acelerado. Pte.4: Tratamiento con calor húmedo a 80 °C y 65% de HR. Asociación Española de Normalización y Certificación (AENOR), p 8
63. UNE 57092-1 (2002) “Papel y Cartón. Envejecimiento acelerado con calor seco a 105 °C. Asociación Española de Normalización y Certificación (AENOR), p 6
64. US Department of Health and Human Services (1987) Toxicology and carcinogenesis studies of ethyleneoxide. CASN<sup>o</sup> 75-21-8 Technical Reports Series No 326, p 117
65. Valentín N (2010) Biodeterioro de libros y documentos en Conservación Preventiva en Archivos y Bibliotecas. IPCE. Ministerio de Cultura, pp 36–45
66. Valentín N (2008) El Biodeterioro de los Bienes Culturales. *Materiales Orgánicos. La Ciencia y el Arte*. Instituto del Patrimonio Histórico Español. Ed. Secretaría General Técnica Ministerio de Cultura, pp 190–197
67. Valentín N (2005) Prevención del Biodeterioro en Archivos y Bibliotecas. *Bienes Culturales*. No 2. IPHE, pp 190–193
68. WHO (World Health Organization. Pan American Health Organization) (1996) Pan American Center for Human Ecology and Health. Health and Environment Division. Ethylene Oxide. “Guide to health and safety”. Mepetec, State of Mexico, No 16, p 13

# Electron Beam Technology and Other Irradiation Technology Applications in the Food Industry

Suresh D. Pillai<sup>1</sup> · Shima Shayanfar<sup>1</sup>

Received: 26 May 2016 / Accepted: 28 November 2016  
© Springer International Publishing Switzerland 2016

**Abstract** Food irradiation is over 100 years old, with the original patent for X-ray treatment of foods being issued in early 1905, 20 years after their discovery by W. C. Roentgen in 1885. Since then, food irradiation technology has become one of the most extensively studied food processing technologies in the history of mankind. Unfortunately, it is the one of the most misunderstood technologies with the result that there are rampant misunderstandings of the core technology, the ideal applications, and how to use it effectively to derive the maximum benefits. There are a number of books, book chapters, and review articles that provide overviews of this technology [25, 32, 36, 39]. Over the last decade or so, the technology has come into greater focus because many of the other pathogen intervention technologies have been unable to provide sustainable solutions on how to address pathogen contamination in foods. The uniqueness of food irradiation is that this technology is a non-thermal food processing technology, which unto itself is a clear high-value differentiator from other competing technologies.

**Keywords** Electron beam · Food irradiation · Phytosanitary · Pathogen · Pasteurization

---

Submitted as a book chapter in *Applications of Radiation Chemistry in the Fields of Industry, Biotechnology and Environment*. By Springer Verlag.  
This article is part of the Topical Collection “Applications of Radiation Chemistry”; edited by Margherita Venturi, Mila D’Angelantonio.

---

✉ Suresh D. Pillai  
[s-pillai@tamu.edu](mailto:s-pillai@tamu.edu)

<sup>1</sup> National Center for Electron Beam Research, An IAEA Collaborating Centre for Electron Beam Technology, Graduate Program in Food Science & Technology, Texas A&M University, College Station, USA

## 1 Introduction

Today, the food industry has to deal with issues that span food safety, food quality, food security, and food defense [36]. In addition to these critical issues, the issue of waste minimization, valorization of food wastes, and environmental sustainability are all critically important. The global population is estimated to grow to around 11 billion by 2050 [23]. Along with this sharp increase in population is the growing economic “middle class” all around the world. This growing segment of the population opens up new opportunities for food companies to become global and cater to this consumer base worldwide. Today’s consumers want all types of foods year-round in conveniently sized packages. Many of today’s food processing technologies may become obsolete in the years to come, and there are probably many more technologies that are yet to be conceived of and tested. Nevertheless, the future is bright for food processing technologies to offer consumers “fresh”, “chemical-free” foods, year-round. This chapter is designed to provide an overview of the applications of food irradiation in the food industry.

The chapter is divided into multiple sections to facilitate enhanced appreciation of the value of this technology and the varied applications of this technology in the food industry. There is a discussion of the core underlying technology, mechanisms of microbial inactivation, international regulations related to food irradiation, phytosanitary treatment applications, poultry and meat pasteurization, and spice decontamination. The value of electron-beam (e-beam) technology as a stand-alone technology or used in combination with other complementary technologies is also discussed. The chapter concludes with a discussion of how the value proposition of this technology should be effectively communicated using quantitative microbial risk assessment (QMRA) and the issue of “consumer acceptance”.

## 2 Underlying Technology

Food irradiation technology is part of the same electromagnetic spectrum which includes radiowaves, incandescent lights, TV broadcasts, microwaves, UV radiation, and cosmic radiation [5]. The electromagnetic spectrum is made up of both ionizing and non-ionizing radiation frequencies. Food irradiation employs the ionizing radiation frequencies and therefore they have significant energy [25]. The primary difference between ionizing and non-ionizing radiation is based on their respective energies as to whether they can ionize the atoms they come into contact with [5]. Gamma irradiation, X-ray irradiation, and e-beam irradiation, the three main types of food irradiation technologies used around the world are all able to “kick” electrons out of their orbital shells on atoms, thereby “ionizing” the atoms. Hence the term, “ionizing radiation”.

Food irradiation relies on either gamma irradiation (from radioactive isotopes such as cesium-137 or cobalt-60), X-rays [from X-ray tubes or linear accelerators (LINAC)], and electron beam irradiation (from linear accelerators or other accelerating structures). Worldwide, food irradiation can use any of the above

mentioned three irradiation technologies [31]. There are fundamental differences between the three irradiation types in terms of their energy profiles, how they are produced, their respective shielding requirements, as well as the regulatory environment around each of these technologies. Radioactive source materials such as cobalt-60 and cesium-137 (produced in nuclear reactors) are the main source for gamma irradiation. Gamma irradiation is primarily photons and they do not have any mass. Therefore, they have high penetrating power in terms of their ability to penetrate through materials of varying bulk density. Generally speaking, the penetrating power of ionizing radiation is a function of their energy (measured in electron volts or million electron volts). Gamma irradiation from cobalt-60 have energy profiles between 1.17 and 1.33 MeV. Gamma irradiation from cesium 137 is in the 0.662 MeV range. In addition to the ionizing radiation energy, another parameter associated with food irradiation technology is the dose rate, i.e., the rate at which the energy is deposited in the target material. Dose rate, therefore, will translate into the processing line speeds when these technologies are employed. The dose rate of gamma irradiation is significantly lower than commercial scale X-ray or e-beam irradiation processes [25]. Thus, an understanding of the dose rate is critical when evaluating processing line speeds and economics.

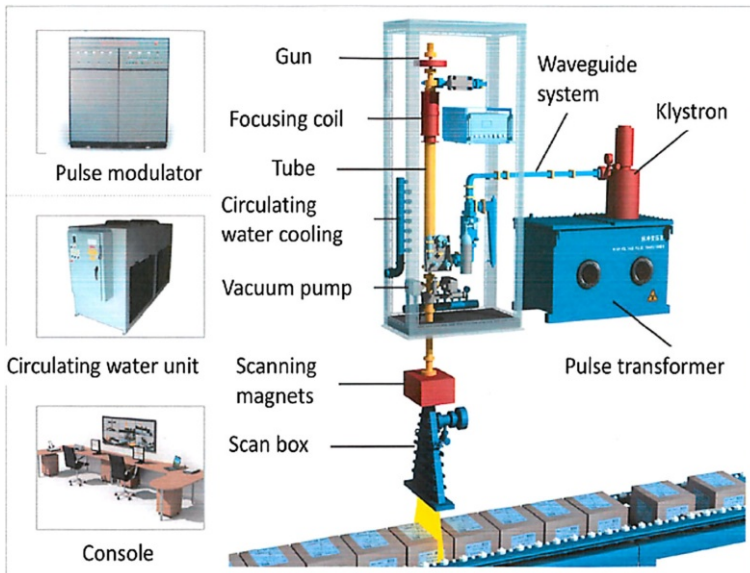
Gamma irradiation relies on radioactive sources such as cobalt-60 and cesium-137, which are potential terrorist targets, international agencies such as the International Atomic Energy Agency (IAEA) and the US Defense Threat Reduction Agency (DTRA) are attempting to replace isotope-based technology with linear accelerator-based e-beam and X-ray technologies. The US National Academy of Science published a report in the early 2000s about the challenges and the need to replace radioactive materials from commercial applications [27]. Today, the limited availability of cobalt-60, the cost of purchasing cobalt-60, the challenges of transporting the material to the commercial facility, the cost of safeguarding cobalt-60 and the cost of replenishing and disposing cobalt-60 all preclude gamma irradiation technologies having any economic value in the future.

Electron beam and X-ray technologies are also examples of ionizing radiation technology. However, the primary difference as compared to gamma irradiation is that e-beam and X-ray are not based on radioactive source materials. e-beam and X-ray technology are generated from commercial electricity and therefore are truly on-off technologies. The equipment that generates e-beams and X-rays are generally called “linear accelerators”. There are different types of accelerators depending on the energy, the possible processing line speeds, the electrical efficiency, etc. [2]. In terms of commercial e-beam accelerators there are three types, namely DC (direct current) accelerators, CW accelerators, and pulsed accelerators (Table 1).

Since high penetrating power of electrons is always desirable, the 10 MeV (Rhodotron and LINAC-style) accelerators are finding increased applications in food irradiation. Figure 1 shows a LINAC-style accelerator with the accelerating structure, the sub-components, and the e-beam horn atop the conveyor belt that brings the product under the e-beam. In the US, food irradiation is regulated (depending on the application) by the FDA (Food and Drug Administration), the USDA–FSIS (United States Department of Agriculture–Food Safety Inspection

**Table 1** Comparative differences between DC, CW, and pulsed accelerators Adapted from Brown [2]

Parameter	DC accelerator	CW accelerator	Pulsed accelerator
Genre	Dynamitron-style	Rhodotron-style	LINAC style
Maximum energy used commercially	5 MeV	7.5–10 MeV	10 MeV
Power (commercial line speeds possible)	High power: as high as 100 kW	High power: as high as 800 kW	Limited: maximum around 20 kW
Electrical use efficiency	High	Medium	Low
Physical size	Large	Medium	Small

**Fig. 1** Schematic representation of a LINAC-style accelerator for food processing. Figure courtesy of Yang Bin, Tianjin, China

Service), and the USDA-APHIS (United States Department of Agriculture-Animal and Plant Health Inspection Service).

X-rays are produced from LINAC or Rhodotron-style accelerators. X-ray generation from an e-beam in a LINAC is based on the placement of a very high atomic mass material, such as tantalum or gold, directly in the path of a stream of a high-energy (5 or 7.5 MeV) e-beam. The collision of high-energy electrons results in the formation of X-ray photons. X-ray photons are similar to gamma irradiation in that they have penetration capabilities (compared to e-beams). However, the energy of X-rays (either 5 or 7.5 MeV) is significantly greater than the energy of cobalt-60 based gamma irradiation. Another major advantage of X-ray photons compared to gamma photons is that the X-ray dose rate ( $\sim 100$  Gy/s) is significantly greater than that of gamma photons ( $\sim 100$  Gy/min) [14]. **Figure 2** is a schematic of e-beams and X-rays from a LINAC-type accelerator.



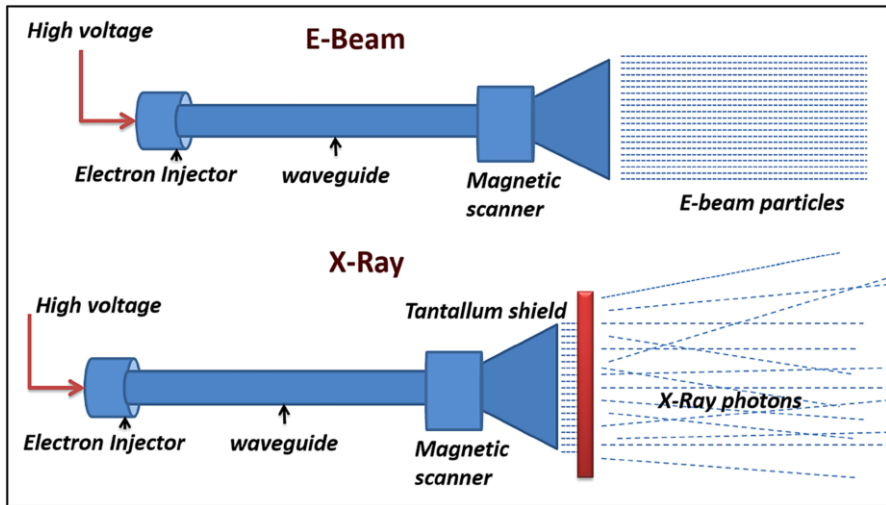


**Fig. 2** Schematic representation of e-beam irradiation and X-ray irradiation using the LINAC-style accelerator

Worldwide, the maximum energy for e-beam technology that can be used for food irradiation is 10 MeV. The reason for this upper limit on energy is that higher energies could potentially induce transient radioactivity in highly dense materials such as bones. The international harmonization entity, Codex Alimentarius, regulates the use of irradiation technology for transboundary shipment of foods. This multinational body has also established 10 MeV energy (similar to the US) as maximum e-beam energy for food irradiation. In the US, e-beam energies as high as 7.5 MeV can be used to generate X-rays for food irradiation. However, worldwide the maximum energy for X-ray is still set at 5 MeV.

### 3 Mechanisms of Microbial Inactivation During Ionizing Radiation

Assume a case-ready package of ground beef is being irradiated either by gamma, X-ray, or e-beam processing. The photons or the electrons will first pass through the packaging before it encounters the food material. When ionizing radiation encounters the packaging material, ionization events take place in the cardboard and associated packaging materials. The electrons that are ejected from their orbital shell then in turn hit electrons in adjoining atoms creating a series of such ionization events. Many of these electrons and secondary electrons enter the food. Once these energized electrons or the primary photons or the primary electrons enter the food, similar ionization events take place. The photons or electrons encounter both the liquid components of the food, as well as the solid components of the food. When ionizing radiation encounters water molecules, the water molecule is ionized with the result that hydrolysis occurs and highly reactive (but extremely short-lived free radicals) are formed. These free radicals cause further radiolysis in addition to



causing double- and single-strand breaks in the DNA of the biological entities on the food. This type of DNA damage is termed “indirect DNA damage”. In contrast to the indirect DNA damage, “direct DNA damage” occurs when the photons or electrons directly encounter the DNA molecule and cause single and double strand breaks (because ionization occurs directly on the DNA molecule when electrons are stripped off).

The free radicals formed during the radiolysis of water (e.g., hydroxyl radicals,  $H^+$  ions, hydrated protons, hydrogen peroxide) do not discriminate between pathogenic microorganisms and normal food associated microbes. The effects of hydrolysis depend on the amount of energy absorbed per unit mass of material (i.e., absorbed dose). The DNA is the largest biomolecule in the cell, and therefore, it is the most ionizing radiation sensitive molecule in cells. The microbial cell is capable of repairing single and double stranded breaks in its DNA. However, if the double-strand breaks are juxtaposed across each other in different strands of the DNA, the microbial cells are incapable of repairing this type of damage. It is estimated that with each 1 kGy of ionizing radiation exposure as many as between 10 and 100 double-strand breaks occur. It is precisely for this reason that when food is treated with ionizing radiation, the decline in the bacterial bioburden results in extended shelf-life. Double strand breaks are the most lethal form of DNA damage because they halt DNA replication. With increasing dose, ionizing radiation can also affect plasmid DNA, RNA molecules, cellular membranes, and even structural and functional proteins (e.g., enzymes). It should be mentioned that the bacterial cells do try to repair the damage that has occurred during ionizing radiation. The cells attempt to repair their DNA damage using a variety of specific and non-specific repair mechanisms such as methyl-directed mismatch repair, guanine oxidations, nucleotide excisions, base excisions, recombination repairs, as well as the generic SOS repair systems.

Structural proteins, catalytic proteins (enzymes), and most vitamins are not damaged at doses regularly used in food irradiation [38]. Exposure to very high doses can, however, cause damage to macro molecules such as proteins. The reason that maturation is retarded or inhibited is because the genes of many of these enzymes may have been structurally damaged during the double-strand and single-strand breaks. Previous studies have shown that for a dose of 100 Gy (0.1 kGy), 2.8% of the DNA, 0.14% of enzymes, and 0.004% of amino acids will be damaged. Taken together, the indirect DNA damage occurs as the net result of radiolysis of water, formation of free radicals, toxic oxygen derivatives, and cellular damage from free radicals and toxic oxygen derivatives. Foods and packaging materials contain a variety of free radical scavengers making these free radicals short lived. It is virtually impossible to measure free radicals in irradiated foods.

The comparative resistance or sensitivity of microorganisms towards ionizing radiation can be understood by their respective D-10 values. The D-10 value is the dose required to achieve a 90% reduction (i.e. 1-log unit decline) in microbial populations. Commercial food irradiation processing dose limits are set based on the approximate log reductions that are desired. The factors controlling radiation resistance include the general physiological differences between the microbial cells (for example the D-10 value of *E. coli* is 0.1 kGy while the D-10 value of

*Salmonella* spp is 0.2 kGy), the physical state of the food (fresh/refrigerated as compared to frozen), the type of food (fresh produce vs ground beef vs. poultry), presence/absence of oxygen, and the atmosphere within the food package, as well as the physiological state of the pathogen (for example, if the cells have been exposed to acid stress or nutritional stress) [6]. Table 2 is an illustrative example of how the D-10 values of organisms could vary depending on the product temperature, organism type, and packaging conditions.

## 4 Regulations Governing Food Irradiation Around the World

### 4.1 United States

The FDA, USDA–FSIS, and USDA-APHIS are the federal agencies that regulate the use and doses that are permitted for foods for human consumption. In the US, there are separate food irradiation regulations for human foods and pet foods. The maximum doses that can be used, the types of food on which this technology can be used, and the specified labeling requirements are hallmarks of US-based food irradiation regulations. In the US, food irradiation is governed by the 1958 Food Additives Amendment of the Food Drug and Cosmetic (FD & C) Act as a “food additive”. This designation has resulted in regulatory burdens on the industry in adopting food irradiation. Per this act, food additives have to be specifically labeled with the radura symbol and must state the phrase “treated with radiation” or “treated by irradiation”. Thus, all irradiated foods that are sold at retail have to have this labeling at the point of sale. The FDA also has specific stipulations as to the type of packaging materials that can be used, the maximum dose that these materials can receive, etc. Presently, in the US, the following foods are permitted to be treated with ionizing radiation (either gamma, e-beam, or X-ray). The foods include fresh

**Table 2** Varying D-10 values as a function of pathogen type, product type, product temperature, atmospheric conditions within package Information compiled from various published research

Product type	Product temperature (°C)	Pathogen	D-10 value (Gy)
Ground beef patties	5	<i>E. coli</i> 0157:H7	0.27–0.38
Ground beef patties	−15	<i>E. coli</i> 0157:H7	0.32–0.63
Ground beef	3	<i>Salmonella enteritidis</i>	0.55–0.78
Beef	5	<i>E. coli</i> 0157:H7	0.30
Beef	3	<i>Yersinia enterocolitica</i>	0.10–0.21
Beef	5	<i>Staphylococcus aureus</i>	0.46
Ground beef	5	<i>Campylobacter jejuni</i>	0.16
Deboned meat	5	<i>B. cereus</i> spores	2.56
Beef	5	<i>L. monocytogenes</i>	0.45
Poultry (air packed)	0	<i>Salmonella heidelberg</i>	0.24
Poultry (vacuum packed)	0	<i>Salmonella heidelberg</i>	0.39

fruits and vegetables, meat (from cattle, sheep, swine, and goat), poultry, shell eggs, iceberg lettuce and fresh spinach, spices, seeds for sprouting, molluscan shellfish. [Table 3](#) lists the dose limits and the foods that can be treated with ionizing radiation in the US.

As can be seen from the above table, there are specific maximum dose limits. Also important to note is that for items such as fresh produce, one cannot use ionizing radiation and claim that pathogens are eliminated (because the regulation is specifically approved for only the use of this technology for growth/maturation inhibition. Only iceberg lettuce and spinach are currently permitted for use for “pathogen elimination” by this technology.

In the US, ionizing radiation is permitted for treating animal diets (bagged complete diets, packaged feeds, feed ingredients, bulk feeds, animal treats, and chews). However, the dose cannot exceed 50 kGy. For complete poultry diets and poultry feed ingredients, the dose cannot be below 2 kGy and cannot exceed 25 kGy. The upper dose limit is based on the assumption that the irradiation treatment is being used to control *Salmonella* spp. Importantly, if an irradiated feed ingredient is less than 5% of the final product, the final product can also be irradiated without being considered re-irradiated.

The FDA also has specific regulations regarding the packaging that can be used for commercial food irradiation ([Table 4](#)).

**Table 3** List of foods and food items permitted for ionizing radiation treatment in the United States [FDA, CFR 179.26(b)]

Food/Food-related item	Specific application	Maximum allowable dose (kGy)
Fresh, non-heated processed pork	Pathogen control	0.3–1.0
Fresh/frozen uncooked poultry products	Pathogen control	3
Refrigerated, uncooked meat products (sheep, cattle, swine, and goat)	Pathogen control	4.5
Frozen uncooked meat products (sheep, cattle, swine, and goat)	Pathogen control	7
Fresh/frozen molluscan shellfish	Pathogen control	5.5
Fresh shell eggs	Pathogen control	3.0
Dry or dehydrated spices and food seasonings	Microbial disinfection	30
Fresh produce	Growth and maturation inhibition	1
Fresh produce	Insect disinfestation	1
Fresh iceberg lettuce and fresh spinach	Pathogen control	4.0
Seeds for sprouting	Pathogen control	8.0
Dry/dehydrated spices and food seasonings	Microbial disinfestation	30
Dry/dehydrated enzyme preparations	Microbial disinfestation	10
Wheat flour	Mold control	0.5
White potatoes	Inhibit sprouting	0.15

**Table 4** Selected packaging materials for use during irradiation of prepackaged foods per FDA, 21 CFR 179.459(b)

Packaging material	Maximum approved ionizing irradiation dose (kGy)
Nitrocellulose coated cellophane	10
Glassine paper	10
Wax-coated paperboard	10
Polyolefin film	10
Kraft paper	0.5
Polyethylene terephthalate	10
Polystyrene film	10
Vinylidene chloride-vinyl chloride co-polymer	10
Ethylene vinyl acetate co-polymer	30
Polyethylene (basic polymer)	60
Polyethylene terephthalate film	60
Nylon 6 (polyamide-6)	60
Vinyl chloride-vinyl acetate co-polymer film	60

## 4.2 European Union

Contrary to what is generally believed, food irradiation is legal in the European Union per Articles 7(3) and 3(2) of Directives 1999/2/EC of the European Parliament. The irradiation of dried aromatic herbs, spices, and vegetable seasonings is authorized within the EU by Directive 1999/3/EC. There is a community list of food and food ingredients that can be treated with ionizing irradiation. In addition to this community list of foods and food ingredients, seven member states have their own list of foods and food ingredients that are above and beyond the community list. Unlike the US, the EU's labeling of irradiated foods is tighter. In the EU any irradiated foodstuff containing one or more irradiated food ingredients must be labeled with the words "irradiated" or "treated with ionizing radiation". Therefore, if an irradiated product is used as an ingredient (e.g., spices on a pizza) the same words shall accompany its designation in the list of ingredients. In the case of products sold in bulk, these words should appear together with the name of the product on a display or notice above or beside the container in which the products are placed. Currently, Belgium, Bulgaria, Czech Republic, Germany, Estonia, France, Spain, Hungary, the Netherlands, Poland, and Romania treat one of more foods or food ingredients by ionizing radiation. [Table 5](#) is a listing of the countries and the food items that are being commercially irradiated in the European Union.

Within the EU, the member states have established data on the administered doses for specific food items such as spices ([Table 6](#)).

The European Food Safety Authority (EFSA) in 2011 recommended that irradiation should be considered as one of several approaches to reducing pathogens in food, and this technology should be integrated into a multi-hurdle strategy, thereby assuring public health protection [9]. The EFSA panel also confirmed the

**Table 5** Listing of EU countries and food items that are commercially irradiated (data from 2011)

EU country	Food and food ingredients irradiated
Belgium	Dehydrated blood, egg white, fish, shellfish, shrimp, frog legs, gum Arabic, herbs and spices, poultry, rice meal, vegetables
Czech Republic	Herbs and spices
Germany	Herbs and spices
Estonia	Herbs and spices
Spain	Herbs and spices
France	Frog legs, gum Arabic, herbs and spices, poultry
Hungary	Herbs and spices
The Netherlands	Egg whites, fish, shellfish, shrimp, frog legs, herbs and spices, poultry, dehydrated products
Poland	Herbs and spices

**Table 6** The administered doses of irradiation on aromatic herbs, spices, and dried vegetable seasoning in some of the EU members (European Commission 2015)

Country	Administered dose (kGy)
Belgium	4–7.9
Czech Republic	5.66–9.92
Germany	5–10
Estonia	10
Spain	9.31
France	5–10
Hungary	2–10
The Netherlands	4–8
Poland	5–10

toxicology and chemical safety of irradiated foods [10]. Importantly, they also recommended that food irradiation should be based on risk assessment and on the desired risk reduction rather than on predetermined food classes, commodities, and doses. They also recommended that upper dose limits should not be specified but rather based on undesirable sensory chemical changes that may happen at increasing doses.

### 4.3 China

Among all countries, China irradiates the largest volume of food. A total of approximately 150,000 tons of food was commercially irradiated in China in 2005 [24]. By volume, the irradiated chicken feet sold as a snack in convenience stores in China is amongst the largest commodity that is treated by ionizing radiation anywhere in the world. Today, the volumes are thought to be in excess of 250,000 tons. In China, the Ministry of Public Health approved food irradiation by different

classes (EU 2009—EU Report on China). There are six mandatory national standards in terms of the foods that can be irradiated, the maximum dose, the packaging, and labeling requirements. The different food classes are (1) fruits and vegetables, (2) beans and grains, (3) poultry (fresh, chilled/frozen) and meats, (4) cooked meats, (5) spices and dehydrated vegetables, and (6) dried fruits and nuts. China's approved list of packaging materials closely resemble that of US and Britain. The maximum dose for cardboard is set at 10 kGy, while polyethylene-polyvinyl acetate co-extruded film the maximum is 30 kGy. Nylon 11 has a maximum dose limit of 10 kGy, while nylon 6 has a maximum dose limit of 60 kGy (USDA, Grain report 2014).

#### 4.4 India

In India, the regulations governing commercial food irradiation are covered by.

Sections 1.2 and 2.13 of the 2011 Food Safety and Standards (Food Products Standards and Food Additives) regulations. In November 2015, the Indian food regulatory agency, Food Safety and Standards Authority of India (FSSAI), proposed a revised set of standards for foods and allied materials (Tables 7, 8). In January 2016, India notified the World Trade Organization (WTO) about the revised food irradiation standards. The Indian food irradiation regulations classify foods and associated materials in different classes.

In India, like the US, all irradiated foods have to be labeled with the radura logo in green with information about the product identity, purpose of radiation processing, radiation processing facility, and date of processing.

### 5 Phytosanitary Applications of Ionizing Radiation

Ionizing radiation technology is gaining widespread applications around the world for treating agricultural produce to eliminate insects and pests. There are strict global standards that govern the use of different technologies (e.g., methyl bromide, hot water treatment, ionizing radiation) for treating agricultural commodities in transboundary shipments. The International Plant Protection Convention (IPPC) is an international agreement focused on preserving standardization of plant health practices around the world to prevent the accidental introduction of regulated pests and pathogens. Consumers around the world desire fresh fruits and vegetables year-round. To meet this growing need, countries around the world are looking at their fresh fruit and vegetable exports as of high economic value. The intrinsic value of fresh produce has spurred the creation of a number of bilateral agreements for the imports/export of fresh produce. The United States has signed such bilateral agreements with many countries around the world. This has allowed the US consumer to access exotic fruits and vegetables which hitherto were unavailable. The USDA-APHIS (Animal and Plant Health Inspection Service) has established protocols for the use of ionizing radiation (either gamma or X-ray or e-beam technology) for treating specific agricultural commodities from specific countries. There is a growing trend in employing ionizing radiation as a phytosanitary

**Table 7** Indian regulations governing ionization irradiation dose limits and applications for different classes of foods

Class	Food type	Application	Dose limits (kGy)	
			Minimum	Maximum
1	Bulbs, stem, and root tubers and rhizomes	Inhibit sprouting	0.02	0.2
2	Fresh fruits and vegetables (other than class 1)	Delay ripening	0.2	1.0
		Insect disinfestation	0.2	1.0
		Shelf-life extension	1.0	2.5
3	Cereals and their milled products, pulses and their milled products, nuts, oil seeds, dried fruits, and their products	quarantine	0.25	1.0
		Insect disinfestation	0.25	1.0
		Bioburden reduction	1.5	5.0
4	Fish, aquaculture, seafood and their products (fresh or frozen), and crustaceans	Pathogen elimination	1.0	7.0
		Shelf-life extension	1.0	3.0
		Control of protozoan parasites	0.3	2.0
5	Meat and meat products including poultry (fresh and frozen) and eggs	Pathogen elimination	1.0	7.0
		Shelf-life extension	1.0	3.0
		Control of protozoan pathogens	0.3	2.0
6	Dry vegetables, seasonings, spices, condiments, dry herbs and their products, tea, coffee, cocoa, and plant products	Bioburden reduction	6.0	14.0
		Insect disinfestation	0.3	1.0
7	Dried foods of animal origin and their products	Pathogen elimination	2.0	7.0
		Control of molds	1.0	3.0
		Insect disinfestation	0.3	1.0
8	Ethnic foods, military rations, space foods, ready-to-eat, ready-to-cook, and minimally processed foods	Bioburden reduction	2.0	10.0
		Quarantine application	0.25	1.0
		Sterilization	5.0	25.0

**Table 8** Indian regulations governing dose limits for ionizing radiation processing of food-related allied products

Allied product	Application	Dose limits (kGy)	
		Minimum	Maximum
Packaging materials for food and allied products	Bioburden reduction	5.0	10.0
	Sterilization	10.0	25.0
Food additives	Bioburden reduction	5.0	10.0
	Insect disinfestation	0.25	1.0
	Sterilization	10.0	25.0
Health foods, dietary supplements, and nutraceuticals	Bioburden reduction	5.0	10.0
	Insect disinfestation	5.0	1.0
	Sterilization	10.0	25.0

**Table 9** Volumes (kg) of irradiated products entering the US from overseas. (Data only reflects only those commodities that are treated off-shore and not at port of entry) [20]

	India	Mexico	South Africa	Thailand	Vietnam	Total
2007	0	0	0	195,000	0	195,000
2008	276,000	262,000	0	2,440,000	121,000	3,099,000
2009	132,000	3,559,000	0	2,247,000	117,000	6,055,000
2010	94,000	5,672,000	0	1,540,000	754,000	8,060,000
2011	80,000	5,539,000	0	743,000	1,445,000	7,807,000
2012	217,500	8,349,500	16,500	937,500	1,764,500	11,286,500
2013	283,000	9,526,000	16,500	1,060,500	1,967,500	12,853,500
2014	265,500	10,119,500	0	843,000	2,293,000	13,617,500

treatment technology. The technology has minimal impact on commodity quality, is environmentally friendly, is a sustainable alternative to methyl bromide, and may be the only practical treatment option for certain commodities in some circumstances. This technology has been adopted on a large scale in shipments between Vietnam and China, between Pakistan and the US, between Mexico and the US, between Australia and the US, and between India and the US. [Table 9](#) shows the steep increase in volumes of irradiated produce entering the US from different trading partners that have signed bilateral agreements with the US for shipment of irradiated produce (for phytosanitary applications). Recent trends suggest that this increase will continue unabated for at least another 5–10 years.



## 6 Ground Beef Irradiation

By all estimates approximately 18 million pounds of ground beef is commercially irradiated in the US for retail and commercial sales. Though the exact figures are hard to ascertain, it is assumed that 50% of this volume is treated with e-beam processing. Irradiation by e-beam processing is recognized as the final critical control point in a validated HACCP (Hazard Analysis and Critical Control Point) system. e-beam technology if used on the post-packaged ground beef will allow the ground beef industry to bring foodborne pathogens, such as toxigenic *E. coli* and *Salmonella* spp., to below detection levels [6]. This technology is well suited for adoption as one of the critical control points (CCP) for the reduction or elimination of the pathogens of concern to the ground beef industry. It must be highlighted that conventional sanitation or pathogen intervention techniques such as lactic acid sprays are ineffective on pathogens internalized inside the product. The ability to inactivate internalized pathogens without affecting the physical, nutritional or sensory attribute of the food item is a clear stand out compared to any pathogen intervention technologies available to the food industry.

The ground beef manufacturer should know the level(s) of the different pathogens as it is being packaged. This will enable setting the irradiation dose required for pasteurization of the product. The ground beef manufacturer in collaboration with the beef processor and the irradiation service provide will establish the required minimum dose for the different products. The aim is to keep the bioburden and the pathogen levels if any at extremely low levels. This will allow the processing of the ground beef at the lowest possible dose. Targeting the lowest possible dose has a number of upsides. For example, the e-beam processing costs can be reduced, the safety assurance margin can be kept very large, the e-beam processing throughput is improved. Most importantly, focusing on lowering the dose completely negates the anti-irradiation lobby's claim that the food industry uses the technology as a "clean-up" technology.

Clemmons et al. [6] has presented an excellent in-depth discussion of how the ground beef industry could and should partner with e-beam processing facilities to develop a validated e-beam processing plan. Based on their extensive experience in managing and operating a commercial e-beam processing facility they suggest that the shelf-life of ground beef and poultry products can be extended significantly by employing e-beam technology (Table 10).

## 7 Microbial Decontamination of Spices

Spice processing has been an important industry for centuries. Spices are both economically and functionally high value commodities that have introduced a world of flavors, aromas, and colors to our lives. The definition of a spice differs according to the country and the region, which is of course not accurate. The term "spice" refers to the dry parts of plants including roots, leaves, and seeds that can impart certain flavor, color, or pungency [15]. The crop is cleared for dust and dirt after

**Table 10** Shelf-life of selected ground beef and poultry products as a function of packaging conditions and e-beam processing Adapted from Clemmons et al. [6]

Meat product	Packaging atmosphere	Shelf-life (days)		
		Non-MAP	MAP-non irradiated	MAP-irradiated
Fresh ground beef	High oxygen	2–3	7–11	Not applicable
Fresh ground beef	Low oxygen	2–3	14–21	30–31
Fresh ground beef	Non-MAP	2–3	Not applicable	22–28
Beef cuts	Vacuum	25–30	Not applicable	47
Fresh ground beef chubs	Chub film	14–20	Not applicable	≥34
Skinless/boneless poultry	Case ready	3–9	11–13	~ 30

being harvested and then washed in water and dried either in the open air or in larger scale dryers. The dried product is graded, ranked for quality, and packed. However, along the processing steps, spices and herbs get contaminated with different bacteria and molds originating from soil, insects, bird, or rodents.

The biggest concern for the spice industry is the presence of foodborne microbial pathogens such as *Salmonella* spp., *Bacillus cereus*, and *Clostridium perfringens* and the presence of molds and mycotoxins. Even though spices are used in very small amounts, the presence of foodborne pathogens in spices can have devastating effects on public health, the industry as a whole, and the exporting country. The presence of mycotoxins such as aflatoxins from the fungus *Aspergillus* spp. has also become a major industry concern that can be extremely expensive for spice exporters. Intervention technologies such as ethylene oxide (EO) fumigation, steam, and irradiation (gamma and e-beam) processing are used worldwide. By all accounts, EO is the most widely used technology. Though EO fumigation is used extensively in Asia and US, EO technology it is not approved in the European Union. Using ionizing radiation for microbial decontamination of spices also achieves extension of the shelf life in addition to ensuring microbiological safety [40]. Sharma et al. [35] reported that bacterial counts of commercially available spices varies between  $10^2$ – $10^3$  CFU/g and 7.5–10 kGy of irradiation will be adequate to decontaminate pepper, cardamom, and nutmeg. In another study involving saffron, the D-10 value for the molds, bacterium, and yeasts were reported to be 0.82, 0.86, and 2.69 kGy respectively, indicating the extreme resistance of yeasts to ionizing radiation when present on specific spices [12]. Microbial decontamination of spices by ionizing radiation does not adversely affect the antioxidant property of cloves, cinnamon, or parsley, nor did it affect the volatile composition and other organoleptic properties [34]. Overall, the results suggest that the dose has to be optimized for the commodity in question to achieve the most desired results. For example attempting to use doses higher than 10 kGy for saffron can lead to color loss [12].

## 8 Ionizing Radiation Effects on Molds and Mycotoxins

In addition to EO being a toxic chemical, another short-coming of EO is the time required to achieve the same sterilization or pasteurization compared to that of ionizing irradiation. Moreover, EO requires at least a 24 h aeration (de-gassing step) to dissipate the EO residuals. Spice processing by e-beam processing is convenient especially because of the high throughput processing requirements. Moreover, e-beam processing is “less harsh” compared to EO in terms of retaining the flavors, colors, aroma, and antioxidant properties. Some spices or spice blends may be sensitive to ionizing radiation. However, this sensitivity can be resolved by combining enhanced GMP with low dose e-beam processing. Spices are the largest food related commodity that is processed with ionizing radiation around the world.

Spices that are stored and handled under humid conditions have issues related to mold infestation and subsequent mycotoxin formation. Some molds can produce mycotoxins that could remain on the product even after the mold has been removed by heat or by irradiation [3, 4]. Mycotoxins are secondary metabolites of some species of fungal genera such as *Aspergillus* spp., *Penicillium* spp., and *Fusarium* spp. Mycotoxins can be carcinogenic, hepatotoxic, mutagenic, teratogenic, cytotoxic, neurotoxic, immunosuppressive, as well as estrogenic [30]. Therefore, any technology that can eliminate the contaminating fungi, as well as address preformed mycotoxins in spices or grains have significant commercial value. It is well known that ionizing radiation at doses greater than 5 kGy are needed to achieve effective elimination of fungal growth [1, 7, 16–18, 22]. Published research suggests also suggests that ionizing radiation when used for insect disinfection also results in reduced mold growth since insects also harbor fungal spores and insect damage tend to promote mold infestation [21].

The literature is, however, unsettled when it comes to the efficacy of ionizing radiation on preformed mycotoxins [4, 19]. There are different types of mycotoxins depending on the fungi that produces it. Mycotoxin is a broad term for aflatoxins (AFs), ochratoxin A (OTA), patulin, fumonosins, zearlenone (ZEN), and trichothecenes [4]. In attempts to reduce ochratoxin A (OTA) and aflatoxins B<sub>1</sub>, B<sub>2</sub>, G<sub>1</sub>, and G<sub>2</sub> (AFB<sub>1</sub>, AFB<sub>2</sub>, AFG<sub>1</sub>, and AFG<sub>2</sub>) in black pepper, [18] applied a range of 0–60 kGy of Gamma irradiation on mycotoxin concentration ranging from 10 to 100 ng g<sup>-1</sup>. The maximum mycotoxin reduction at 60 kGy was about 52, 43, 24, 40, and 36% for OTA, AFB<sub>1</sub>, AFB<sub>2</sub>, AFG<sub>1</sub>, and AFG<sub>2</sub>, respectively. These results suggest that even 60 kGy is unable to completely eliminate ochratoxin and aflatoxins. At the 30 kGy dose (which is the maximum dose FDA allows for spice decontamination), mycotoxin reduction is less than 30%. Aflatoxins in solutions are more sensitive to ionizing radiation than AFs on drier substrates [11, 41]. Research also suggests that doses in the range of 20 kGy (except for patulin) may be required to obtain a reasonable level of assurance that a majority of the mycotoxins are inactivated [26]. Patel et al. [29] showed that a synergistic effect of hydrogen peroxide combined with ionizing radiation to eliminate AF1 in aqueous solutions. Taken together, the current state of research suggest that the elimination of mycotoxins by ionizing radiation is a function of the mycotoxin in question, the

starting mycotoxin concentration, presence of moisture, and synergistic inactivation effects with other intervention technologies.

## 9 Quantitative Microbial Risk Assessment and Food Irradiation

The over 100 years of research on ionizing radiation technologies demonstrate that this is a powerful non-thermal technology that can be applied at varying doses for various applications in the food industry. There is growing demand for the use of this technology for phytosanitary treatment (insect disinfection) ( $\leq 1$  kGy). Even at the low dose used for phytosanitary treatment, at least 3–4 log inactivation of key bacterial pathogens can occur [37]. Irradiation technology at higher doses are used around the world to ensure food safety by eliminating pathogens. Decision makers in government and the retail food industry have to be empowered with specific actionable information to justify the adoption of this technology. We need to “translate” the value of this technology not only in terms of log reductions of pathogens or general statements of protecting public health, but with specific information in terms of how infections can be avoided by adoption of this technology. Quantitative Microbial Risk Assessment (QMRA) is an excellent tool for this purpose [13]. The four component QMRA framework of hazard identification, exposure assessment, dose–response assessment, and risk characterization, can be used to quantify reductions in microbial infection risks associated with the application of e-beam processing [8, 33, 37]. Translating the value of adopting ionizing radiation technology in terms of reduction of potential infections can be used for both microbial risk management, as well as risk communication. Quantitative Microbial Risk assessment. [Table 11](#) shows how QMRA was used in translating the value of this technology in terms of reducing infection risks associated with potential exposure to Shiga-toxin producing non-O157 *E. coli*.

**Table 11** Reduction in infection risks from non-O157 STEC contaminated strawberries associated with 1 kGy dose of e-beam processing [37]

Hypothetical initial contamination per strawberry serving (serving size 150 g)	Potential Infection Risks associated with non-O157 STEC strains	
	Without e-beam processing	With ( $\leq 1$ kGy) e-beam processing
$10^4$ CFU/150 g	5 out of 100 persons	4 out of 1 million persons
$10^3$ CFU/150 g	6 out of 1000 persons	4 out of 10 million persons
$10^2$ CFU/150 g	6 out of 10,000 persons	4 out of 100 million persons

## 10 Consumer Acceptance of Food Irradiation

Many years ago, there was a lot of “hand wringing” about how consumers will not accept foods that have been processed with ionizing radiation technologies. However, today it is very evident that consumers will purchase irradiated foods if irradiated foods are available for purchase in retail stores. Retail sales of irradiated ground beef, raw oysters, and irradiated fruits and vegetables in the United States for the past decade or so are testimony to the apparently inaccurate assumptions that consumers will not accept irradiated foods. Even in the European Union the irradiation and obvious sales of irradiated foods is testimony to the consumer acceptance of irradiated foods in the European Union. There is an exponentially growing market for irradiated foods in Asia, especially in China and India. A number of studies in the US, Mexico, and elsewhere on the willingness of well-informed consumers to purchase irradiated foods have demonstrated that if consumers are provided with accurate, succinct information, they are willing even to pay a premium for irradiated foods [28]. However, the food industry needs to be aware that this technology should never be used as a “clean-up” technology. Consumers have always been skeptical of the food industry using this technology to cover up poor industry practices during pre-harvest and post-harvest processing. The food industry should use this technology as a final step of a comprehensive pathogen reduction and elimination program so that only very high quality food items are treated with this technology. By doing so, the doses that are employed can be significantly reduced to achieve significant improvements in public health (Table 11). The authors are confident that the radura label on irradiated foods will actually become extremely high value and could be an industry differentiator between companies that use advanced validated pathogen elimination technologies to protect public health and those that do not. Moreover, in the context of transparency, the consumers should be provided with information about the type of processing that their foods have experienced. Food traceability has become the cornerstone of a prudent food policy. Food traceability and authenticity are not only consumer driven but are also driven by concerns of about food adulteration, mislabeling, food counterfeiting, and food defense [36].

**Acknowledgements** This work was supported by Hatch grant H8708 administered by the Texas A&M AgriLife Research of the Texas A&M University System. This work was also completed as part of the activities of the IAEA Collaborating Centre for Electron Beam Technology.

## References

1. Aziz NH, Moussa LAA (2002) Influence of gamma-radiation on mycotoxin-producing moulds and mycotoxins in fruits. *Food Control* 13:281–288
2. Brown D (2015) Integrating electron beam equipment into food processing facilities: strategies and design consideration. In: Pillai SD, Shayanfar S (eds) *Electron beam pasteurization and complementary food processing technologies* Chapter 3. Woodhead publishing, Oxford
3. Bullerman LB, Bianchini A (2007) Stability of mycotoxins during food processing. *Int J Food Microbiol* 119(1–2):140–146
4. Calado T, Venancio A, Abrunhosa L (2014) Irradiation for mold and mycotoxin control: a review. *Comp Rev Food Sci Safety* 13:1049–1061

5. Chmielewski AG, Kang CM, Kang CS, Vujic JL (2006) Radiation technology. Introduction to industrial and environmental applications. Seoul National University Press, Seoul, p 274
6. Clemmons HE, Clemmons EJ, Brown EJ (2015) Electron beam processing of fresh and/or frozen raw ground beef. In: Pillai SD, Shayanfar S (eds) Electron beam pasteurization and complimentary food processing technologies Chapter 14. Woodhead publishing, Oxford
7. de Camargo AC, Vieira TMFD, Regitano-d'Arce MAB, de Alencar SM, Calori-Domingues MA, Spoto MHF, Canniatti-Brazaca SG (2012) Gamma irradiation of in-shell and blanched peanuts protects against mycotoxic fungi and retains their nutraceutical components during long-term storage. *Int J Mol Sci* 13:10935–10958
8. Espinosa AC, Jesudhasan P, Arredondo R, Cepeda M, Mazari-Hiriart M, Mena KD, Pillai SD (2012) Quantifying the reduction in potential health risks by determining the sensitivity of poliovirus type 1 chat strain and rotavirus SA-11 to electron beam irradiation of iceberg lettuce and spinach. *Appl Environ Microbiol* 78:988–993
9. European Food Safety Authority (2011) Scientific opinion on the efficacy and microbiological safety of irradiation of food. *EFSA J* 9:2103–2201
10. European Food Safety Authority (2011) Scientific opinion on the chemical safety of irradiation of food. *EFSA J* 9:1930–1956
11. Frank HK (1970) Radiation resistance of aflatoxins. *Irradiat Aliments*. 11:15–20
12. Ghoddsi HB, Glatz B (2004) Decontamination of Saffron (*Crocus sativus* L.) by electron beam irradiation. *Acta Horti ISHS* 650:339–344
13. Haas CN, Rose JB, Gerba CP (1999) Quantitative microbial risk assessment. Wiley, New York
14. Hieke C (2015). Investigating the inactivation, physiological characteristics and transcriptomic responses of bacteria exposed to ionizing radiation. Ph.D. Dissertation, Texas A&M University, College Station, Texas
15. Hirasa K, Takemasa M (1998) Spices and herbs: basic concepts. In: Hirasa K, Takemasa (eds) Spice science and technology. Marcel Dekker, Inc., New York, pp 1–2
16. Ic E, Kottapalli B, Maxim J, Pillai SD (2007) Electron beam irradiation of dried fruits and nuts to reduce yeast and mold bioburden. *J Food Prot* 70:981–985
17. Ito H, Chen H, Bunnak J (1994) Aflatoxin production by microorganisms of the *Aspergillus flavus* group in spices and the effect of irradiation. *J Food Agric* 65:141–142
18. Jalili M, Jinap S, Noranizan A (2010) Effect of gamma radiation on reduction of mycotoxins in black pepper. *Food Control* 21(10):1388–1393
19. Jalili M, Jinap S, Noranizan MA (2012) Aflatoxins and ochratoxin a reduction in black and white pepper by gamma radiation. *Rad Phys Chem* 81:1786–1788
20. Jeffers L (2016) Hands-on electron beam technology workshop. Texas A&M University, College Station
21. Jouany JP (2007) Methods for preventing, decontaminating and minimizing the toxicity of mycotoxins in feeds. *Anim Feed Sci Technol* 137:342–362
22. Kume T, Ito H, Soedarman H, Ishigaki I (1989) Radiosensitivity of toxigenic *Aspergillus* isolated from spices and destruction of aflatoxins by gamma-irradiation. *Radiat Phys Chem* 34:973–978
23. Lutz W, Sanderson W, Scherbov S (2001) The end of world population growth. *Nature* 412:543–545
24. Kume T, Furuta M, Todoriki S, Uenoyama N, Kobayashi Y (2008) Status of food irradiation in the world. *Rad Phy Chem* 78:222–226
25. Miller RB (2005) Electronic irradiation of foods: an introduction to the technology. Springer, New York, p 350
26. Mutluer B, Erkok FU (1987) Effects of gamma irradiation on aflatoxins. *Z Lebensm Unters Forsch* 185:398–401
27. National Academy of Science (2008) Radiation source use and replacement. National Academy Press, Washington, DC
28. Nayga RM, Woodward RM, Aiew W (2006) Willingness to pay for reduced risk of foodborne illness: a nonhypothetical field experiment. *Can J of Agric Econ* 54:461–475
29. Patel UD, Govindarajan P, Dave PJ (1989) Inactivation of aflatoxin B1 by using the synergistic effect of hydrogen peroxide and gamma radiation. *Appl Environ Microbiol* 55:465–467
30. Paterson R, Lima N (2010) How will climate change affect mycotoxins in food? *Food Res Int* 43:1902–1914. doi:10.1016/j.foodres.2009.07.010
31. Pillai SD (2016) Introduction to electron-beam food irradiation. CEP Magazine. AICHE. November

32. Pillai SD (2004) Food Irradiation. In: Bier RC, Pillai SD, Phillips TD, Ziprin RL (eds) Pre-harvest and post-harvest food safety: contemporary issues and future directions. Institute of Food Technologists/Iowa State Press, Ames, pp 375–387
33. Praveen C, Dancho BA, Kingsley DH, Calci KR, Meade GK, Mena KD, Pillai SD (2013) Susceptibility of murine norovirus and hepatitis A virus to electron beam irradiation in oysters and quantifying the reduction in potential infection risks. *Appl Environ Microbiol* 79:3796–3801
34. Sadecka J (2007) Irradiation of spices—a review. *Czech J Food Sci* 25(5):231–242
35. Sharma A, Ghanekar AS, Padwal-Desai SR (1984) Microbiological status and antifungal properties of irradiated spices. *J Agric food Chem* 32(5):1061–1063
36. Shayanfar S, Pillai SD (2015) Future trends in electron beam technology for food processing. In: Pillai SD, Shayanfar S (eds) Electron beam pasteurization and complimentary food processing technologies Chapter 16. Woodhead publishing, Oxford
37. Shayanfar S, Mena K, Pillai SD (2016) Quantifying the reduction in potential infection risks from non-O157 Shiga toxin producing *E. coli* in strawberries by low dose electron beam processing. *Food Control*. doi:10.1016/j.foodcont.2016.04.057
38. Smith JS, Pillai SD (2004) Irradiation and food safety. Scientific status summary. IFT, Chicago
39. Sommers CH, X Fan (2006) Food irradiation research and technology. (Eds). IFT Press/Blackwell Publishing, p 317
40. Suhaj M, Racova J, Polovka M, Brezova V (2006) Effect of  $\gamma$ -irradiation on antioxidant activity of black pepper (*Piper nigrum* L.). *Food Chem* 97:696–704
41. Van Dyck PJ, Tobbacck P, Feyes M, van de Voorde H (1982) Sensitivity of aflatoxin B1 to ionizing radiation. *Appl Environ Microbiol* 43:1317–1319

# Applications of Accelerators and Radiation Sources in the Field of Space Research and Industry

Luigi Campajola<sup>1</sup> · Francesco Di Capua<sup>1</sup>

Received: 12 May 2016 / Accepted: 16 November 2016 / Published online: 28 November 2016  
© Springer International Publishing Switzerland 2016

**Abstract** Beyond their important economic role in commercial communications, satellites in general are critical infrastructure because of the services they provide. In addition to satellites providing information which facilitates a better understanding of the space environment and improved performance of physics experiments, satellite observations are also used to actively monitor weather, geological processes, agricultural development and the evolution of natural and man-made hazards. Defence agencies depend on satellite services for communication in remote locations, as well as for reconnaissance and intelligence. Both commercial and government users rely on communication satellites to provide communication in the event of a disaster that damages ground-based communication systems, provide news, education and entertainment to remote areas and connect global businesses. The space radiation environment is a hazard to most satellite missions and can lead to extremely difficult operating conditions for all of the equipment travelling in space. Here, we first provide an overview of the main components of space radiation environment, followed by a description of the basic mechanism of the interaction of radiation with matter. This is followed by an introduction to the space radiation hardness assurance problem and the main effects of natural radiation on the microelectronics (total ionizing dose, displacement damage and the single-event effect) and a description of how different effects occurring in space can be tested in on-ground experiments by using particle accelerators and radiation sources. We also discuss standards and the recommended procedures to obtain reliable results.

---

This article is part of the Topical Collection “Applications of Radiation Chemistry”; edited by Margherita Venturi, Mila D’Angelantonio.

---

✉ Francesco Di Capua  
[dicapua@na.infn.it](mailto:dicapua@na.infn.it)

<sup>1</sup> Dipartimento di Fisica “E. Pancini”, Università degli Studi di Napoli Federico II, Naples, Italy



**Keywords** Space radiation environment · Space product assurance · Radiation hardness · Single event effect · Total ionizing dose · Displacement damage

## 1 Introduction

Satellites not only have a economically important impact on commercial communication systems, but they are in general critical infrastructure because of the services they provide. Satellites gather information which not only improves our understanding of the space environment and contributes to physics experiments, but is also used to actively monitor weather, geological processes, agricultural development and the evolution of natural and man-made hazards. Defence agencies depend on satellite services for communication in remote locations, reconnaissance and intelligence-gathering. Both commercial and government users rely on communication satellites to provide communication in the event of a disaster that damages ground-based communication systems, provide news, education and entertainment to remote areas and/or connect global businesses.

The space radiation environment is a hazard to most satellite missions and can lead to extremely difficult operating conditions for all of the equipment travelling in space. The performance of the various space systems, such as electronic units, sensors, power and power subsystem units, batteries, payload equipments, communication units, remote sensing instruments, data handling units, externally located units and propulsion subsystem units, is determined by the proper functioning of various electronic systems. Such systems are highly sensitive to space radiation. Radiation can lead to a degradation of the device performance or to functional failure of electronic systems. Moreover, radiation accelerates aging of the devices and materials.

The space radiation environment is complex as well as dynamic. Electrons and protons are trapped in the Earth's magnetic field. The Earth is surrounded by belts of these particles, called the Van Allen belts [1]. In addition, the magnetosphere and the Solar system are exposed to a flux of solar charged particles. Since the flux is a function of the solar activity, it may increase sharply during solar flares. Galactic cosmic rays that originate from outside of the Solar system consist of highly energetic heavy ions which can be detrimental to the proper operation of electronic systems. The characteristics of the radiation environment are strongly dependent on the date, duration and orbit of the mission.

A rigorous procedure is required to ensure that the environmental forms of radiation do not compromise the functionality and efficiency of the different devices during the expected lifetime of the mission. This procedure consists of the detailed analysis of the mission in order to evaluate the radiation dose absorbed by the various systems and of all the tests necessary to ensure that all pieces of equipment operate according to the design specifications.

## 2 The Space Radiation Environment

Space radiation is a combination of several components, each with quite complex dynamics, and is not distributed homogeneously in the Earth magnetosphere. The concentration and type of particles in the space environment vary significantly with altitude, angle of inclination, recent solar activity and amount of spacecraft shielding. Particles present in the Earth's space radiation environment include:

- Particles trapped by the Earth's magnetic field (mainly protons and electrons)
- Galactic cosmic rays (protons and heavy ions)
- Solar cosmic rays (protons and heavy ions).

### 2.1 Trapped particles

The magnetic field is generated within the Earth's core by the daily rotation of the Earth, electrical forces within the core and thermal movements. The dynamo produced in this way sustains a magnetic field which can be closely approximated to the field of a giant dipole positioned at the Earth's centre and inclined by  $11.3^\circ$  from the spin axis. The magnetic field generated by the Earth is called magnetosphere.

The geomagnetic field lines trap charged particles, such as electrons and protons. These trapped particles gyrate spirally around the magnetic field lines. The motion of the trapped particles forms bands of electrons and protons around the Earth, leading to the formation of at least two radiation belts that are called the Van Allen radiation belts. The inner belt [2] is populated by high-energy protons (in the 10- to 100-MeV range) at a density of about  $15 \text{ protons/m}^3$  [3] and by electrons (energy range 50–1000 keV), and it extends from  $\sim 100 \text{ km}$  up to  $\sim 6000 \text{ km}$  in altitude. For satellites on a low Earth orbit (LEO), such as the many satellites designed to provide telephony and internet services, these trapped particles represent a hazard to the proper operation of electronic systems and to the astronauts themselves. The dependence of the proton dose rate in the inner belt as a function of altitude is shown in Table 1.

The outer belt is populated by electrons extending up to 60,000 km in altitude and with energies of up to 10 MeV. This belt is more dynamic than the inner belt and is influenced by the injection of particles from geomagnetic storms. The outer radiation belt coincides with the geostationary orbit of many communication satellites. Properties of the Earth's radiation belts are summarized in Table 2 and Fig. 1 [4].

**Table 1** Proton dose rate in the inner radiation belt as function of altitude

Orbit altitude (km)	Proton dose rate (Sv/day)		
	$0^\circ$	$45^\circ$	$90^\circ$
300	0.05	0.05	0.05
500	0.16	0.16	0.16
2500–3000	110.00	26.00	18.00
7500	2.60	3.40	2.40

**Table 2** Characteristics of the Earth's radiation belts

Particle	Energy	Extension (Earth radii)
Earth		
$e^-$	1 keV–7 MeV	1–10
$p^+$	1 keV–300 MeV	1–7

e, Electron; p, proton

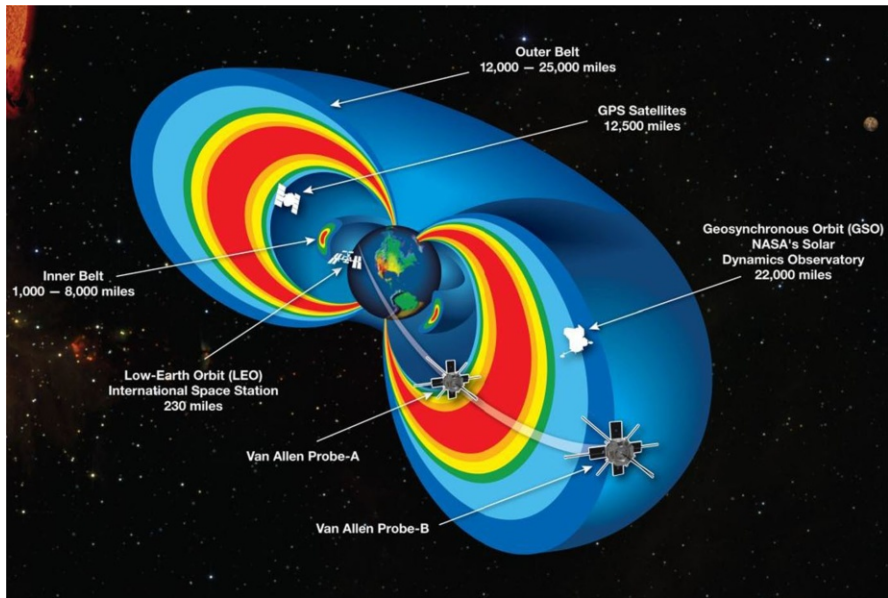


**Fig. 1** Scheme of the Van Allen radiation belt. NASA National Aeronautics and Space Administration, *GPS* global positioning system

The Earth's magnetic field centre does not coincide with its geographical centre because the magnetic poles are not located on its geographic poles. Consequently, the Van Allen belts are slightly closer to the Earth on one side and slightly further away on the other side. They are closest to the South Atlantic area, which is known as the South Atlantic Anomaly (SAA), illustrated in Fig. 2, which has a relatively higher concentration of protons at lower altitudes (<1000 km). This asymmetry results in a spacecraft on an orbital flight being exposed to a much higher flux of protons when it passes through the SAA than when it passes through other locations at the same altitude.

## 2.2 Galactic Cosmic Rays

Cosmic rays were discovered in 1912 by Victor Franz Hess who, with the help of balloons, showed that ionization increases with altitude. Many years of research and the ability to get above the atmosphere, thanks to several space programmes, have provided evidence demonstrating that the Earth is bombarded by a nearly isotropic

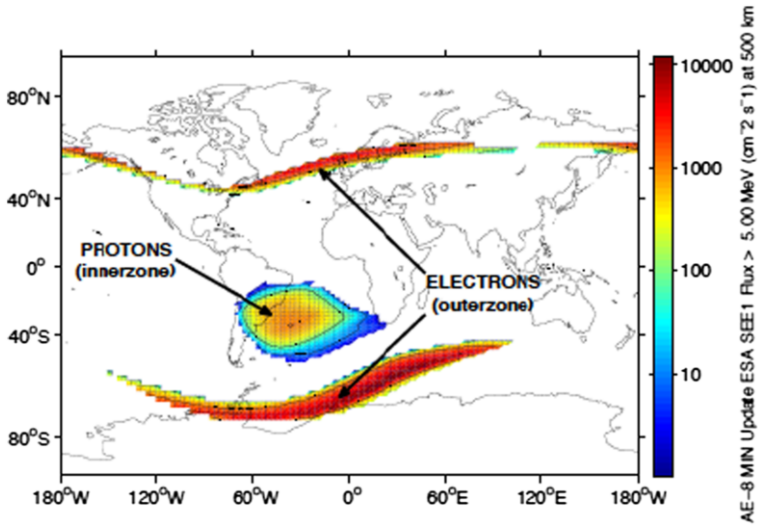


**Fig. 2** Intensity of protons and electrons at an altitude of 500 km, estimated by AP8-MIN and AE8-MIN models, respectively [5, 6]. The South Atlantic Anomaly can be clearly seen in the Atlantic Ocean close to southeast coast of Brazil

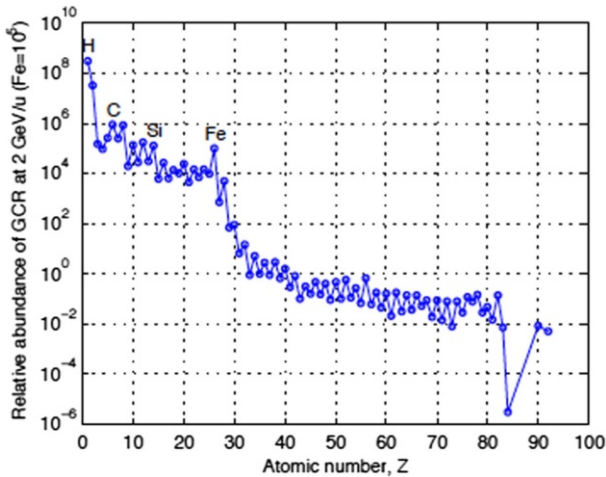


**Fig. 3** Relative abundance of galactic cosmic rays (GCR) for different ion species at energies of about 2 GeV/nucleon as a function of the atomic number [8]

flux of energetic charged particles. Beyond the atmosphere, cosmic rays consist predominantly of protons (about 90%) and helium nuclei (almost 10%), but heavy nuclei are also part of the primary cosmic rays (Fig. 3).

Once these particles arrive in Earth’s atmosphere, they interact with the nuclei of atmospheric molecules to form, in a cascade process, new particles that project forward, called secondary cosmic rays. Galactic cosmic rays (GCRs) travel at close to the speed of light, have huge energies (>GeV) and appear to have been travelling

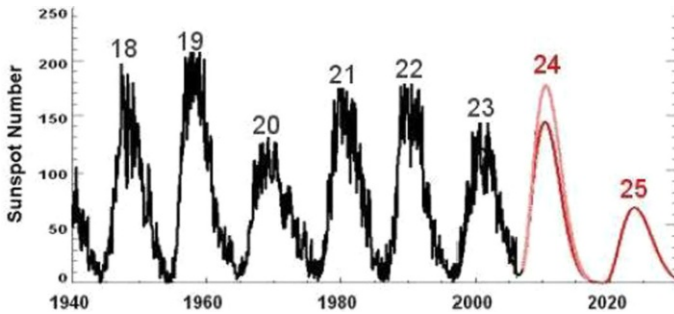


**Fig. 4** Past and expected future sunspot numbers for solar cycles

through the galaxy for some ten million years before intersecting the Earth. They are partly deviated by the Earth's magnetic field and have easier access to the Earth at the poles compared with the equator. The Earth's surface is protected from these particles by geomagnetic shielding as well as by the atmosphere. The primary cosmic rays interacting with air nuclei generate a cascade of secondary particles comprising neutrons, protons, mesons and nuclear fragments. The intensity of radiation builds up to a maximum at an altitude of 18,000 m and then slowly drops off at sea level.

The penetration of these GCRs into the vicinity of the Earth is influenced by solar activity, which emits a continuous wind of ionized gas or plasma that extends beyond the solar system. The strength of the solar wind influences the flux of cosmic rays reaching Earth. This effect is referred as solar modulation and depends on solar activity. There is an 11-year cycle in solar activity, and we are currently experiencing a decreasing phase of solar cycle 24 (Fig. 4), with the last solar maximum having occurred in 2013, at which time the GCR were less intense.

The GCRs are a major radiation concern for long-term missions outside the Earth's magnetosphere. In addition, since they have high energies, most of them pass through the magnetosphere and are observed at LEOs. The flux of GCRs is therefore a possible hazard to spacecraft electronics because GCRs cannot be shielded due to their high energy.

### 2.3 Solar Cosmic Rays/Solar Particle Events

The solar wind mostly consists of high-energy electrons and protons, and the particle plasma of the solar wind travels through space at an average velocity of approximately 400 km/s. The average proton densities, in absence of any major solar events, are in the order of 1–10 protons/cm<sup>3</sup>.

Intense magnetic activities are the origin of *Sunspots*, which are colder areas where the strong magnetic field blocks the transport of heat. The magnetic field also causes strong heating in the corona of the Sun, forming active regions that are the source of intense *Solar Flares* where huge amounts of plasma are ejected. The real massive solar flares are called *corona mass ejections* (CMEs). The CMEs are orders of magnitude larger than regular solar flares. In a CME event, a huge part of the

Sun's corona explodes, and matter of up to  $10^{10}$  tons is ejected at velocities of up to thousands of kilometres per second [9].

Evidence has been found for particle acceleration processes throughout the heliosphere in the years around the solar maximum, in many cases in association with shock waves that are caused by the increasing number of solar flares and CMEs. Near solar maxima the Sun produces three to four CMEs every day, whereas near solar minima there is only about one CME every 5 days [10, 11]. CMEs are very unpredictable phenomena and responsible for the emission of mainly electrons and protons, but there are also heavier ions, such as oxygen and iron, present in the shockwaves. During these events very large amounts of energy can suddenly be released in the solar chromosphere through the ejection of accelerated particles into space. These different processes result in the generation of particles such as solar energetic particles with energies of up to about 10 MeV/nucleon, which accelerate in the solar corona and last a few days [12], and energetic storm particles with energies up to about 500 MeV, which accelerate in the propagating interplanetary shock and last a few hours [13], and anomalous cosmic rays (ACRs) [14]. Although the amount of heavier ions in the CMEs is much lower than that in the constant solar wind protons or electrons, they are more likely to be the cause of problems in the proper functioning of electronics due to their higher ability to ionize matter.

### 3 Interaction of Radiation with Matter

The production and type of radiation damage in matter is related to the energy deposition processes. The interaction of incoming particles with matter results in two major effects: (1) collision energy loss and (2) atomic displacement. Interactions of incoming particles and matter that result in the excitation or emission of atomic electrons are referred to as energy loss by ionization or energy loss by collisions with electrons. Non-ionization energy loss processes are interactions in which the energy imparted by the incoming particle results in atomic displacements or in collisions where the knock-on atom does not move from its lattice location and the energy is dissipated in lattice vibrations.

Defects induced by the interaction of radiation with semiconductors are primary point defects include vacancies and interstitials. Clusters of defects are generated when the incident particle, such as a fast neutron or protons, transfers enough energy to the recoil atoms to allow large cascades of displacements. The change observed in semiconductor conductivity is associated with the formation of defect clusters.

For charged particles, the amount of energy that goes into ionization is determined by the stopping power or linear energy transfer (LET) function, commonly expressed in units of megaelectron-volts square centimetre/gram ( $\text{MeV cm}^2/\text{g}$ ) or more transparently as energy per unit length ( $dE/dx$ ) in kiloelectron-volts per micrometre ( $\text{keV}/\mu\text{m}$ ). The absorbed ionizing dose is the energy deposited per unit mass due to ionization, and the most common unit of measurement is the rad, which corresponds to 100 ergs/g. Because the energy loss per unit mass differs from one material to another, the material in which the dose is

deposited is always specified [e.g., rad(Si) or rad(GaAs)]. The Système International (SI) unit for dose is the gray, which is equivalent to 100 rad.

The LET or the rate of energy loss,  $dE/dx$ , for a charged particle passing through matter can be expressed approximately by  $dE/dx = f(E) \cdot MZ^2/E$ , where  $x$  is the distance travelled in units of mass/area or density  $\times$  distance,  $f(E)$  is a very slowly varying function of the ion energy  $E$ ,  $M$  is the mass of the ionizing particle, and  $Z$  is the charge of the ionizing particle. Thus, for a given energy, the greater the mass and charge of the incident particle, the greater the amount of deposited energy produced over a path length inside the solid state material. For relativistic ions, the mass factor in the above equation becomes almost constant, and the ion charge dominates.

The intensity of heavy cosmic rays as a function of  $Z$  peaks at iron ( $Z = 26$ ), abruptly decreasing thereafter. An energetic iron nucleus of 1 GeV per nucleon produces  $\sim 0.14$  pC in each 10  $\mu\text{m}$  of silicon traversed (the energy release of 22.5 MeV produces 1 pC of charge in silicon).

## 4 Space Product Assurance

### 4.1 Understanding the Problem

The integrated circuits required for applications in the space scenario are quite unique. Since silicon processes are a major corporate prerogative, companies involved in producing such processes serve a very large market. All technological and scientific efforts are focussed on applications that meet the consumer market, including such products as mobile phones, personal and notebook computers, among others. The benefits of a strong research in silicon processes, including size reduction (transistors channel length) and enhanced performance (clock speed), are reflected in more compact and more power final products.

Space electronics is a niche market, but one which has high-level requirements that basically are not satisfied by standard consumer electronics. The first and most important requirement is resistance to radiation, but resistance to both mechanical stresses (during launch) and thermal stresses is also relevant. Due to the low volumes required by the space market, large silicon foundries, do not always meet these requirements, resulting in basic technologies that are not suited for space. Consequently, there is a lack of technologies for the space environment.

Another aspect to be emphasized is linked to the availability of certain dedicated technologies developed for the military industry. Some silicon foundries in the USA (e.g. American Semiconductor Inc., Boise, ID) have developed silicon processes with a given resistance to radiation that are used in device design for military applications. The main problem related to this reality is that these players can only work for the military establishment and cannot provide either their components or their technology to markets outside of the USA. This policy is encoded in a set of rules called the International Traffic in Arms Regulations (ITAR) which controls the export and import of defence-related articles and services. ITAR was established during the Cold War, and its regulations were reinforced after 11 September 2001. It



restricts all base technologies which can be used for weapon building, including fighter planes and personal equipment for soldiers. Resistance to radiation of all forms is obviously considered in these technologies, and silicon processes for integrated circuits realized for the military market fall under ITAR restrictions. The space and the high-energy physics markets unfortunately are disadvantaged by this approach, the consequences of which are, from the point of view of silicon processes, that on the one hand there is a basic shortage of radiation technologies and, on the other hand, when a technology is developed it can fall under ITAR restrictions and therefore also be unavailable.

The ESA and all European large-scale integrators encounter difficulties in acquiring the essential components and technologies for the production of silicon processes, which is why they are pushing for ITAR-free technologies—i.e. a set of base and critical technologies which could be freely used by ESA members and their providers and integrators. A major aim of ESA is to develop a base technology internally (meaning in Europe) that will not fall under ITAR restrictions or any other restrictions.

A key feature of integrated circuits destined to be used for space applications is that of radiation tolerance. Beyond the atmosphere, many particles (electrons, protons and high-energy ions) collide with silicon devices used in the space environment, such as electronic equipment for satellites, probes or, in general, all spacecraft, releasing energy and possibly disrupting their operation.

There are two main effects of radiation on silicon devices:

- Long-term effects [total ionizing dose (TID) and displacement damage (DD)]
- Short-term and random effects [single-event effects (SEE)].

TID and DD result in progressive degradation of the devices, with the chip progressing to a state of general malfunction after months or years. SEE, is strongly dependent on the amount and nature of the energized particles, and in the worst case scenario such effects can be destructive.

Even though these problems have been carefully studied since the 1960s, very few devices have been designed to be rad-hard, primarily due to the fact that the space market represents only a small niche in the overall silicon market. The volumes needed for silicon devices of this nature are very low, while silicon foundries are structured to make a profit on devices designed for mass production. Moreover, the realization of devices of this kind is challenging due to the technology efforts needed to manufacture these products in a process line that is finely tuned to be quick and reactive to a continuously changing consumer market.

Nevertheless, some players do develop and produce rad-tolerant or rad-hard devices. For the most part, these devices are commercial, with a high level of die qualification and redundancy. More than one chip (usually  $\geq 3$ ) is mounted on the same board, and by using a voting method an amount of functioning errors is avoided. Moreover, the space market generally uses “old technologies” in order to take advantage of well-established techniques of both the process and the design arms, but this also leads to delay in the introduction of new technologies, or no introduction at all, which can be profitable as well. [Table 3](#) summarizes the responsible sources of radiation damage, the elementary particles involved and the relative energy range.



**Table 3** Space radiation sources, energies and relative effects on microelectronics

Radiation source	Particle	Energy range	Radiation damage
Radiation belts	Protons	Few keV–500 MeV	SEE → stochastic effect
			DD → cumulative effect
			TID → cumulative effect
Solar flares	Electrons	Few eV–10 MeV	TID → cumulative effect
	Protons	Few keV–500 MeV	SEE → stochastic effect
			DD → cumulative effect
Galactic sources	Protons and HZE ions	Up to 300 MeV/amu	TID → cumulative effect
			SEE → stochastic effect

*HZE* high-energy, high-charge nuclei component of galactic cosmic rays, *SEE* single-event effects, *DD* displacement damage, *TID* total ionizing dose

## 4.2 Total Ionizing Dose

The TID is a long-term degradation of electronics due to the cumulative energy deposited in SiO<sub>2</sub> or other dielectrics. Significant sources of TID exposure in the space environment include trapped electrons, trapped protons and solar protons. Simulations are used to determine the dose received by an electronic component as a function of equivalent aluminium (Al) shielding for a given mission, as the one shown in Fig. 5. In this example, the electrons of the Van Allen Belts dominate the contribution to TID until about 6–7 mm of equivalent Al shielding and then are nearly completely eliminated after 1 cm.

When incident radiation enters a semiconductor solid material, such as silicon, an electron–hole pair may be created if an electron in the valence band is excited across the band gap into the material’s conduction band. Electron–hole pairs generated in the gate oxide of a metal–oxide semiconductor (MOS) device, such as a transistor, are quickly separated by the electric field within the space charge region. The electrons quickly drift away, while the holes of lower mobility drift slowly in the opposite direction. Oxides contain a distribution of sites, such as crystalline flaws, that readily trap the slow holes. Portions of the positively charged holes are trapped at the sites as they slowly flow by. The main degradation mechanism induced by total dose in MOS devices is caused by radiation-induced charge build-up in its gate oxide. Oxide-trapped charge in thicker gate oxide can invert the channel interface, causing leakage current to flow in the OFF state condition ( $V_{GS} = 0$  V) (Fig. 6). For advanced integrated circuits (ICs) with thinner gate oxides, such as complementary metal–oxide semiconductor (CMOS) technology, radiation-induced charge build-up in field oxides normally dominates the radiation-induced degradation of ICs and induces large leakage currents.

The response of MOS devices to TID is complex because of the competing effects of the oxide trap and interface trap-induced threshold voltage shifts, which can change over time. The net result is that the behaviour of the IC is changed because of the induced charge build-up.

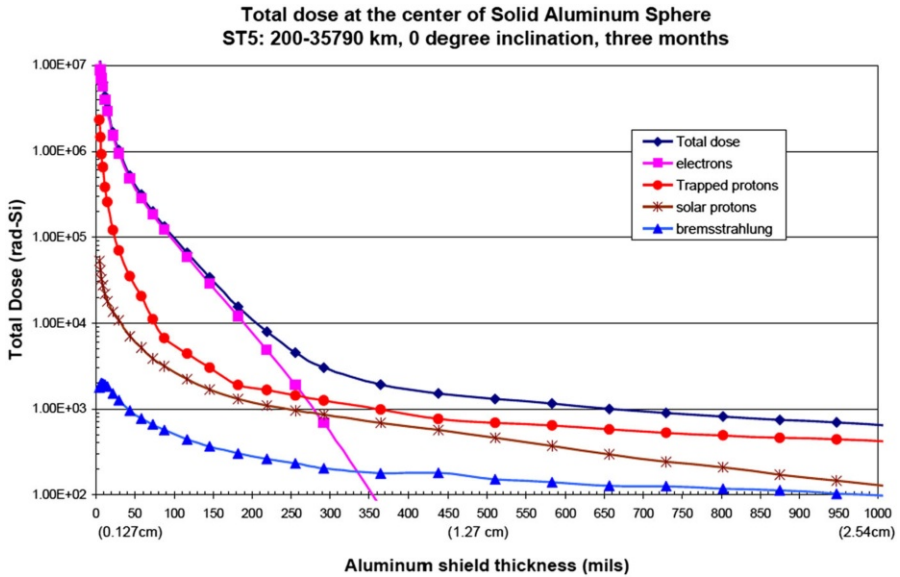
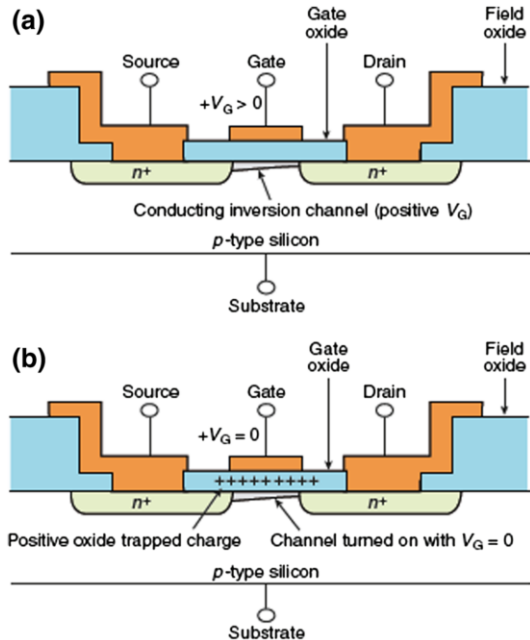


**Fig. 5** Example of a dose as a function of the equivalent aluminium shielding

**Fig. 6** Basic effect of total ionizing dose in a *n*-channel metal oxide–semiconductor field-effect transistor (MOSFET) inducing charge build-up in gate oxide. Normal operation (a) and post-irradiation (b) operation show the residual trapped charge (*holes*) that produces a negative threshold voltage shift



Electrical properties of CMOS, silicon-on-insulator (SOI) and bipolar technologies degrade with the cumulate dose because they are SiO<sub>2</sub>-based devices. Typical effects include parametric failures or variations in device parameters, such as

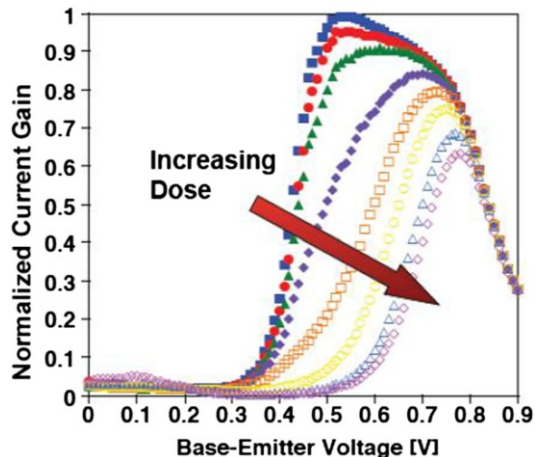
leakage current, threshold voltage, among others, or functional failures. The gain degradation is the primary effect with bipolar technologies and is particularly large at a low bias level (Fig. 7). The gain decrease is due to an increase in the base current resulting from the degradations of the current that are caused by recombination in the emitter–base depletion region and the current due to recombination in the neutral base.

Bias and quiescent currents also commonly increase over the time of a spacecraft mission because of TID. In some cases, the increase in leakage current requires designers to add a significant margin to their power requirements. It is not uncommon for devices to show an order of magnitude increase in the leakage current as a result of TID while otherwise still functioning properly.

Satellite mission duration may extend over years, so a large TID may be accumulated during this time. Changes in the fabrication of ICs over the last decade have led to the development of a number of components with an enhanced sensitivity to radiation when exposed to low dose rates. Bipolar technologies are sensitive to the enhanced low dose rate sensitivity (ELDRS); in other words, the degradation at the end of a low dose rate (LDR) irradiation is greater than the degradation measured after irradiation to the same dose level obtained with a high dose rate (HDR).

The standard TID dose rate for ground testing is generally  $\sim 50$  rad/s. This dose rate allows a qualification test to be run in an 8-h shift. However, typical ELDRS testing is performed at a dose rate of only 10–100 mrad/s; therefore, there is a requirement for test times on the order of weeks to months, which is clearly much closer to the rate at which TID will be accumulated during the mission. This extended but more realistic testing is expensive and can affect a spacecraft programme mission schedule. Fortunately, some vendors producing radiation-hardened devices have determined the underlying cause of ELDRS for their parts and modified their manufacturing process to overcome the problem.

**Fig. 7** Normalized current gain vs. base-emitter voltage for an npn bipolar junction transistor irradiated to various total doses



#### 4.2.1 DD Dose

The long-term degradation characteristics of displacement damage dose (DDD) are often similar to those of TID, but the physical mechanism differs. It should be noted that technologies that are tolerant to TID are not necessarily tolerant to DDD.

DDD is essentially the cumulative degradation resulting from the displacement of nuclei in a material from their lattice position. Over time, sufficient displacement can occur and may change the device or the performance of its material properties. Prime sources of DDD exposure include trapped protons, solar protons and, to a less extent for typically electronic systems, trapped electrons.

Devices that depend on a crystalline bulk structure for operational characteristics, such as solar cells, particle detectors, image sensors, photonic and electro-optic components, have shown sensitivity to high DDD. Radiation particles, such as neutrons, protons and electrons, scatter off lattice atoms, locally deforming the material structure. The band-gap structure may change, affecting fundamental semiconductor properties. For example, the output power of a spacecraft solar array degrades during the mission life of a spacecraft because of the displacement damage. Another example of displacement damage is the increase in recombination centres in silicon particle detectors, ultimately leading to a signal and an energy resolution decrease.

Displacement damage is also important for photonic and electro-optic integrated circuits, such as charge-coupled devices and opto-isolators. Elastic and inelastic nuclear scattering interactions produce vacancy/interstitial pair defects as the regular structure is damaged. The defects produce corrupting states in band gaps, leading to increased dark current and reducing gain and charge transfer efficiency.

The amount of displacement damage is dependent on the incident particle type and energy, as well as on the target material. The characterization of displacement damage is more complex than characterization of TID. The most commonly used method to quantify displacement damage is non-ionizing energy loss (NIEL). NIEL coefficients vary depending on radiation type, energy and the target material.

The NIEL of a particle is usually presented in terms of kiloelectron-volts square centimetre per milligram or megaelectron-volts square centimetre per milligram. For a mono-energetic beam, the product of the NIEL with the particle fluence gives the DDD, which is usually specified in units of kiloelectron-volts per gram or megaelectron-volts per gram. For irradiation by a range of particle energies, the displacement damage dose is obtained by integrating the energy-dependent NIEL over the particle spectrum. Alternatively, a displacement damage equivalent fluence can be defined. This is the fluence of particles at a particular energy that would give an equivalent DDD. Often 10-MeV protons or 1-MeV neutrons are given as the reference. The values for the NIEL of various particles in silicon have been published by Dale et al. [15], Huhtinen et al. [16], Akkerman et al. [17], Summers et al. [18], with an online compilation by Vasilescu and Lindstroem [19]. Values are summarised in Fig. 8. Various calculations tend to agree within a factor of two, which is comparable with the uncertainties involved.

Values for InGaAs have been published by Walters et al. [20] and Fodness et al. have published results for HgCdTe [21]. Jun et al. have published results for protons

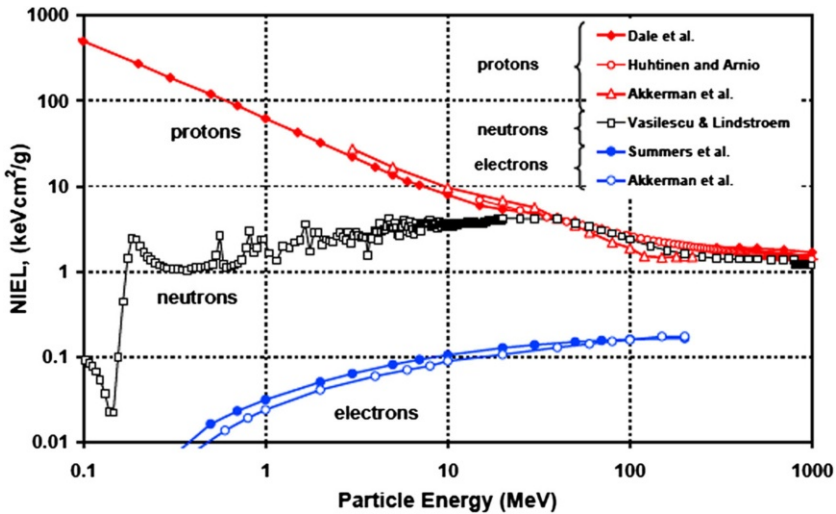


**Fig. 8** Published values of non-ionizing energy loss (*NIEL*) in silicon

in a range of important semiconductor materials [22] and also for electrons [23] (Fig. 8).

#### 4.2.2 Single-Event Effects

Single-event effects occur when a single ion strikes a material, depositing sufficient energy through its primary interaction (e.g. direct ionization of a GCR), or as a result of the secondary ions that occur from the strike induced by neutrons or protons (indirect ionization) to cause an effect in the device.

SEEs are generated by several mechanisms. The charge-collection mechanisms are an interesting and complex set of mechanisms that are continuously being refined in the literature. The charge generated by a single ion strike is collected, producing a spurious voltage signal on a “sensitive” node that causes an effect at the circuit level. The number of electron–hole pairs generated is proportional to the electron stopping power of the incident particle in the target material. The generated charge recombines or is collected at the various nodes. The charge collection threshold for a SEE is called the critical charge ( $Q_{crit}$ ).

SEE tests are performed at particle accelerators. SEE sensitivity is characterized by the cross-section  $\sigma$  as a function of the LET,

$$s = \frac{N}{F},$$

where  $N$  is the number of SEE events and  $\Phi$  is the particle fluence.

The LET can be varied at a particle accelerator by changing the incident particle mass, incident energy and angle of strike. A particle impinging on a device at  $60^\circ$  will deposit twice the energy of a particle entering at normal incidence, thereby effectively doubling the LET:

$$\text{LET}(q) = \frac{\text{LET}(0^\circ)}{\cos(q)}$$

The key measurement for these experiments is the number of single events that occur as a function of the number of incident particles at a given LET. These data are combined with spacecraft trajectory information and are used to predict a specific mission SEE rate.

The many SEE types can be divided into three basic categories [24, 25]:

- Single-event upset (SEU) and multiple bits upset which change the logic state of the internal nodes of a circuit. These errors are called soft error and are recoverable.
- Single-event latch-up (SEL), in CMOS technologies, which may destruct the circuit if SEL is not interrupted within a short time when it occurs.
- Single-event gate rupture/burnout (SEGR/SEB) in power metal oxide–semiconductor field-effect transistor (MOSFET), which causes failure or destruction of the transistor.

**4.2.2.1 Single-Event Upset** A SEU is the change of state of a bistable element, typically a flip-flop, or of another memory cell that is caused by the impact of an energetic heavy ion or proton. The effect is non-destructive and may be corrected by rewriting the affected element. As with other SEEs, a single-particle strike may introduce sufficient charge to exceed the  $Q_{\text{crit}}$  of a sensitive circuit node and change the logic state of the element. The resulting change of state is often known as a bit-flip and can occur in many different semiconductor technologies.

The vulnerability of a device to a SEU is determined by two parameters: the threshold LET, which is the minimum amount necessary to produce upset, and the saturation LET cross-section (in  $\text{cm}^2$ ), which is a function of the surface area of all of the SEU-sensitive nodes.

Static random access memory (SRAM) and dynamic random access memory (DRAM) are two common integrated circuit memories that experience SEU. SRAM structures consist of an array of nearly identical memory cells, and DRAM structures have cells that use the charge storage in a capacitor to represent data. Both types of memory circuits also include supporting circuitry, such as sense amplifiers and control logic, that also may be sensitive to SEEs or single-event transients (SETs). Very dense memory circuits may also have multiple bit upsets when one ion strike causes upsets in multiple bits, which may occur if the ion track is close to both bits or if the angle of incidence is close to parallel to the die.

SETs are short-time voltage excursions at a node in an integrated circuit caused by a transient current generated by the nearby passage of a charged particle. Most SETs are harmless and do not affect device operation. However, there are several types of SETs that can cause harm or corrupt data.

SEUs or SETs are not directly observable at the pins of a device. However, at some time after a SEU or SET occurs, the device may operate in an unpredictable manner. Single-event functional interrupts (SEFIs), a class of SEEs,

have been observed in complex devices, such as microprocessors or flash memories. A SEFI is a SEE that places a device in an unrecoverable mode, often stopping the normal operation of the device. It is usually caused by a particle strike but can be produced by other causes. SEFIs are not usually damaging but can produce data, control or functional-interrupt errors which require a complex recovery action that may include reset of an entire spacecraft subsystem.

**4.2.2.2 Single-Event Latch-up** Transient currents generated by ionizing particles can be amplified by parasitic devices forming a latch-up. A SEL causes the loss of device functionality due to a single event-induced current state [26–28]. SELs can result in permanent damage to the circuit that may not be recoverable [29]. SEL can occur in any semiconductor device that has four layer parasitic PNP paths, which can be triggered by transient currents. Many techniques have been proposed to overcome latch-up by using current sensing circuits, which can be used to temporarily switch off the power supply. The removal of power should be done within milliseconds after development of the latch-up condition to avoid possible damage to the circuit. SELs do not occur in SOI technology due to its nature preventing the presence of the parasitic PNP structure [30].

**4.2.2.3 Single-Event Gate Rupture/Burnout** Power devices may be sensitive to SEB and SEGR. SEB is similar to SEL in that it generates high-current states that ultimately lead to catastrophic device failure. SEB is a high-current condition in a parasitic npn bipolar structure similar to latch-up. It is observed in vertical power MOSFETs and some bipolar transistors. The charged particle strike induces current in the p-structure forward-biased parasitic transistor. If the drain-source voltage is higher than the breakdown voltage of the parasitic npn, an avalanche occurs and high current flows. This effect can be permanently damaging for one or more of the parallel islands in the architecture of the power MOSFET by producing an uncontrolled short.

SEGR is initiated when the incident particle forms a conduction path in a gate oxide, resulting in device damage (Fig. 9). SEGR can occur when charge builds up in dielectric around the gate of a power MOSFET when a large bias is applied to the gate. The localized field builds up enough for the field across the dielectric to exceed the dielectric breakdown voltage, resulting in a low-resistance path across the dielectric. The conduction path in the oxide is an example of classic dielectric breakdown similar to lightning during a thunderstorm.

### 4.3 Radiation Hardness Assurance Testing

The radiation endurance of electronics operating in a harsh radiation environment needs to be assured either by manufacturing them (Rad-Hard) or by testing them. Because of high production costs, the Rad-Hard industry is mainly focussed on parts with high reliability requirements. In addition to lower prices, the performances of commercial electronics [commercial-off-the-shelf (COTS)] is typically much higher than that of Rad-Hard devices. Thus, COTS are often favoured in space projects due



**Fig. 9** A catastrophic single-event gate rupture in a power metal oxide–semiconductor field-effect transistor causing functional failure



to superior performances and low cost. However, the drawback is their lack of being “space-qualified” and unknown radiation performances.

#### 4.3.1 TID Testing

Although the space environment has a low dose rate ( $\sim 10^{-4}$ – $10^{-2}$  rad/s), the duration of missions may be in years, thus resulting in large accumulated doses. Over the life of a spacecraft mission, TID levels on the order of  $10^5$  rad are easily accumulated. Candidate devices need to be characterized and qualified with respect to the requirements of a spacecraft mission.

The total dose test consists of exposing the selected device to ionizing radiation while appropriately biased and then performing a set of electrical measurements either during or after irradiation. One approach, called step-stress, consists of measuring electrical parameters after a dose of ionizing radiation has been reached and determining their changes with respect to the initial measurements. An other approach, called in-flux testing is performed by continually measuring the device response as it is being irradiated. The step stress approach is usually more convenient and much more widely used.

The test is performed with different samples of the same type exposed at same time at a number of accumulated dose levels. Generally the ionizing radiation environment is simulated with 1.25-MeV gamma rays from  $\text{Co}^{60}$  (Fig. 10) sources even though the radiation space environment responsible for TID consists primarily of electrons and protons of various energies. These sources can have a dose rate of up to 600 rad(Si)/s, but it is possible to decrease the dose rates by varying the distance from the source or varying the thickness of absorbing materials.

Since the parts of any device are used under different conditions in a spacecraft, they are generally biased during testing in the condition that gives the worst-case damage.

Standard procedures have been developed in the USA (MIL-STD 1019.5 [31] and ASTM F1892 [32]) and in Europe (ESA/SCC 22900 [33]). These standards define the requirements applicable to the irradiation testing of integrated circuits and



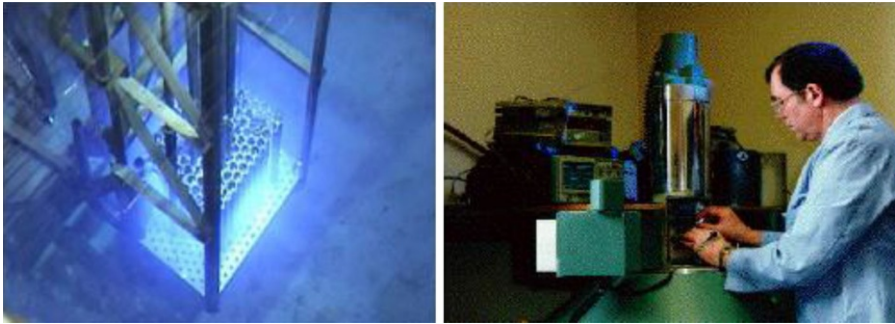


**Fig. 10**  $^{60}\text{Co}$  radiation sources for low and high dose experiments

discrete semiconductors. The MIL-STD 1019.5 procedure was written for military applications and has been adapted for space applications. The European procedure is only applicable to space applications. Both procedures define the test conditions in order to obtain a conservative estimate of the radiation sensitivity of parts of CMOS devices, but in different ways. The dose rate to be used during test is, following ESA/SCC22900, 1–10 rad/s for the standard window and 0.01–0.1 rad/s for the low dose rate window.

The dose to the device under test (DUT) has to be measured alternatively by the appropriate detector (dosimeter or ion chamber) by correcting a previous dosimeter measurement for the decay of  $^{60}\text{Co}$  source intensity in the intervening time.

A proper calibration of the source is crucial before any radiation testing is started. Several organizations use different approaches to calibrate their sources. However, the general recommendation is the guarantee of the uniformity of the radiation field in the volume in which the devices are irradiated within a few percentage points of accuracy.

Many ionization chambers are available for the measurement of the dose. Typically, those of smaller volume are used for HDR calibration (e.g. 0.18 cc) and those of higher volume are used for LDR calibration (e.g. 180 cc).

The dose level at which a part must to be subjected is often dependent on the project requirements. Several missions require testing to the exact dose of the mission plus a margin factor, typically 2 or 3. High-dose missions sometimes require testing to failure in order to obtain maximum leverage of the capabilities of the part before establishing the radiation guideline.

Another common type of laboratory source is the 10-keV X-ray source. Laboratory X-ray sources are available that can achieve dose rates from  $<300 \text{ rad}(\text{Si})/\text{s}$  to  $>3600 \text{ rad}(\text{Si})/\text{s}$ . These sources can be used to irradiate both unleaded packaged devices and devices on a wafer. The HDR of X-ray sources and the capability for testing at the wafer level allows for rapid feedback on radiation hardness during device fabrication [2]. However, these sources are not recommended for radiation qualification.

Two HDR sources can be used to investigate the total dose response of electronic devices at short times: these are electron linear accelerators (LINACs) and proton cyclotrons. Electron LINACs are pulse-type sources with pulse widths ranging from

<20 ns to >10  $\mu$ s with energies from 10 MeV to >40 MeV. Proton cyclotrons are quasi-continuous sources and can have dose rates from a few rad/s up to high-dose rates [1 Mrad(Si)/s] with energies from around 20 MeV to >200 MeV.

#### 4.3.2 DDD Testing

Ideally, for mission evaluation, the devices under test should be irradiated with particles and energies representative of the operating environment to avoid uncertainties in the NIEL approach. An approximation of the proton for low Earth orbits can be simulated using a selection of proton beam degraders and sequential irradiations. The main focus of interest is protons with energies of several tens of megaelectron-volts as the shielded spectrum usually has a peak at around 50–60 MeV, with 10-MeV protons sometimes used for convenience because of beam availability or activation issues.

Also, care must be taken if proton irradiations are being used for a combined test of TID and displacement damage effects. At these low energies intracolumnar recombination of the generated electron hole pairs become significant, leading to a lower degradation due to TID than would be expected if irradiating with  $^{60}\text{Co}$  gamma or higher energy protons.

Neutrons are sometimes used for space simulation to avoid ionization effects that occur when irradiating with charged particles. One possible problem with neutron irradiation is that the energy spectrum is normally not mono-energetic and the dosimetry and application of NIEL can be complex.

Knowledge of the actual energy spectrum of the particles incident on the device is very important for fundamental studies. Using a tuned beam to obtain mono-energetic protons is preferable to using degraders to obtain the required proton energy. The beam energies of degraded beams have significant straggle that can complicate the data analysis. For example, the Proton Irradiation Facility (PIF) at the Paul Scherrer Institute (PSI) provides 13.3-MeV protons with a full width at half maximum of 5.6 MeV by using a 74.3-MeV beam reduced with Copper degraders. It is particularly important for low-energy irradiations that the effects of any material in front of the die be understood, including the device package.

The proton flux is usually selected to ensure that the time required to reach a specified fluence is within acceptable practical limits and to minimize beam time, but not too high so that dosimetry and radioprotection become problematic. In practice, proton irradiations for displacement damage testing are normally performed with fluxes in the range  $10^7$ – $10^8$  p/cm<sup>2</sup>/s.

The initial defect concentrations produced by displacement damage are usually considered to be independent of bias applied during irradiation. Therefore, displacement damage testing is usually undertaken unbiased. Unbiased irradiations tend to lead to a reduction in the effects of TID and, therefore, displacement damage effects can be isolated more easily.

Beam uniformity information should be available from the irradiation facility, and the level of uniformity should be appropriate for the required testing. If the uniformity is marginal, for example if the device under test is particularly large in relation to the specified beam diameter, or if several devices are being irradiated at

the same time, the beam should be characterized prior to irradiation testing being undertaken. There are several ways in which the uniformity can be determined, such as by using a radiochromic film or a scanning photodiode. Once the beam uniformity has been determined the device under test should be carefully aligned to the centre of the beam where the uniformity is likely to be optimum.

**4.3.2.1 Proton Sources** Most proton irradiation facilities supply protons through the use of particle accelerators, such as tandem Van de Graaff generators, cyclotrons or synchrotrons. Linear accelerators are also employed occasionally. Many such particle accelerators are used for medical or industrial purposes and may not always be available for device testing. Most Tandem Van de Graaff-based facilities provide protons having energy of up to  $\sim 10$  MeV. Some facilities do provide protons with higher energies, such as the SIRAD-INFN facility in Italy, which provides protons of up to 30 MeV. Generally the beam sizes tend to be a maximum of a few centimetres in diameter, although the maximum irradiated area can be sometimes increased through the use of scanning techniques. Cyclotrons tend to be employed when protons of higher energies are required. Typically energies of up to a few tens of megaelectron-volts are available from these facilities, but some offer protons with energies as high as 200 MeV. For example, the cyclotron at the Université Catholique de Louvain, Belgium, provides protons with energies of up to 62 MeV and the high-energy beam line at the PSI in Switzerland supplies protons with energies of up to 250 MeV. Beam diameters of 10–20 cm are typically available. If proton energies are required below the maximum energy that is available, energy reduction is possible by either tuning the beam or using degraders. Degraders are material plates, usually aluminium, that are placed between the beam and the device under test, with the material and thickness of the plate being chosen to achieve the required energy. Although convenient, degraders should be considered with care because although the mean energy will be reduced, the straggling causes a broadening of the energy spectrum that may result in a more complex analysis of the test results.

**4.3.2.2 Neutron Sources** Neutrons for device testing can be supplied from radionuclide sources, from nuclear reactors and from nuclear reactions produced with particle accelerators. The most commonly used spontaneous fission source is the radioactive isotope Californium-252, which produces a spectrum of fission neutrons that peak at 1 MeV and extend out to  $\sim 13$  MeV (Fig. 4). Alpha reaction sources are also used, such as the americium–beryllium or americium–lithium reaction. Mono-energetic neutrons can be provided by using the deuterium–tritium (14.1 MeV) or deuterium–deuterium (2.5 MeV) reaction. Such facilities are available at, for example, the Atomic Weapons Establishment in the UK or the Fraunhofer Institute in Germany. High-energy neutrons are available from nuclear spallation facilities where a high-energy proton beam, produced by a cyclotron or synchrotron, for example, impacts target material, such as Tungsten. The neutron energy extends from thermal up to the energy of the incident proton beam. For example, the spallation source at the Svedberg Laboratory at Uppsala University,

Sweden provides neutrons of up to 180 MeV. The quasi-monoenergetic neutron (QMN) facility at the same laboratory produces neutrons from accelerated protons incident onto a  ${}^7\text{Li}$  target. The resultant neutron spectrum is dominated by a high-energy peak at an energy variable between 17 and 180 MeV.

#### 4.3.2.3 Dosimetry

*Faraday cup* A Faraday cup has a shielded, insulated target block thick enough to stop the incident protons. The charge deposited in the block is measured (e.g. with an electrometer) and is proportional to the number of stopped protons. Electrostatic and magnetic fields are often used to suppress the current from external secondary electrons or to prevent secondary electrons generated within the cup from escaping. Faraday cups do not provide absolute real-time monitoring; they are moved in and out of the beam or are placed in a separate area to provide measurements only when needed for calibration of other detectors.

*Scintillators* A scintillator is a material which, when irradiated, converts a fraction of the interacting particle energy into light. The light output is proportional to the ionizing energy lost by the incident particle. The generated photons can be detected by a photomultiplier, avalanche photodiodes or silicon photomultiplier. These detectors can be used for real time monitoring of the flux and various arrangements can be employed.

*Secondary electron monitors* If an irradiating beam passes through thin metal films, such as aluminized Mylar, secondary electrons will be generated. If the films are connected to a picoammeter, the resultant current is proportional to the number of ions passing through the foil. This simple arrangement can be adapted by appropriately biasing and segmenting the foils to enable the determination of the beam uniformity and focus.

*Radiochromic films* Radiochromic films are frequently available for on-demand testing of a beam's uniformity in a purely qualitative manner. The film is exposed to a dose known not to saturate the film. The film is then read by any number of means, but the most popular method is to scan the film with a simple flatbed scanner into a gray scale (0–255) image and process it with a commercially available software package.

#### 4.3.3 SEE Testing

In this case, the environment, due to high-energy GCR and solar event heavy ions, is simulated with low-energy ions available in particle accelerators. Each ion with a given energy is characterized by the amount of energy lost per unit length: the LET. Ground testing is performed with ions with lower energies than GCR or solar events but with similar LET. Commonly used specifications are reported by the Electron Industries Association [34] and ESA [35].

The typically used energy is of an order of several megaelectron-volts per micron, which means a penetration range in silicon from about 30  $\mu\text{m}$  for heavy

ions to few hundreds of microns for the lightest particles. The device package in front of the die is removed for heavy ion SEE testing (Fig. 11).

Different values of LET are obtained by changing the ion species. A typical SEE test uses a minimum of five ion species in order to have a range of LET values from few megavolts per milligram square centimetre to about 60 MeV/mg cm<sup>2</sup>. Typically high LET values are obtained by accelerating Xenon ions with a LET value of ~60 MeV/mg cm<sup>2</sup>. Higher LET values have been obtained or by tilting DUT or accelerating high Z heavy ions, such as gold.

In recent years several accelerators used for nuclear physics have been employed for the radiation hardness assurance test. In Europe, the most used facilities are the Accelerator Laboratory at the University of Jyvaskyla (JYFL), the so-called RADEF facility [36] (Fig. 12), and the cyclotron Cyclone 110 at Université Catholique de Louvain [37].

The single-event test consists of monitoring a certain number of parameters of a device during irradiation, detecting and counting the errors during each irradiation run. The SEE cross-section is measured as the ratio of the number of errors to the ion fluence expressed in particles per square centimeter. For devices that are sensitive to SEE even at low LET values, the test with a proton beam has to be also performed. In this case, since proton energy, as in space, is available at accelerators, the SEE cross-section is measured as function of proton energy. Typical values of ion fluences are 10<sup>6</sup> ions/cm<sup>2</sup> for soft errors and 10<sup>7</sup> ions/cm<sup>2</sup> for hard errors. The required ion fluxes ranged from 100 to 10<sup>5</sup> cm<sup>-2</sup> s<sup>-1</sup>. The number of soft errors are typically counted and stored. At the end of each run, the SEU cross-section per bit can be calculated by using the formula  $\sigma_{SEU} = N_{SEU}/(\text{nbit} \cdot \text{Fluence})$ . The characteristic SEU sensitivity of a device can be obtained by changing the LET using different accelerated ions. Moreover, LET can be varied by DUT tilting, which introduces the concept of effective LET, defined as  $LET_{eff} = LET/\cos\theta$ . In this case, the fluence must be corrected by multiplying by  $\cos\theta$ .

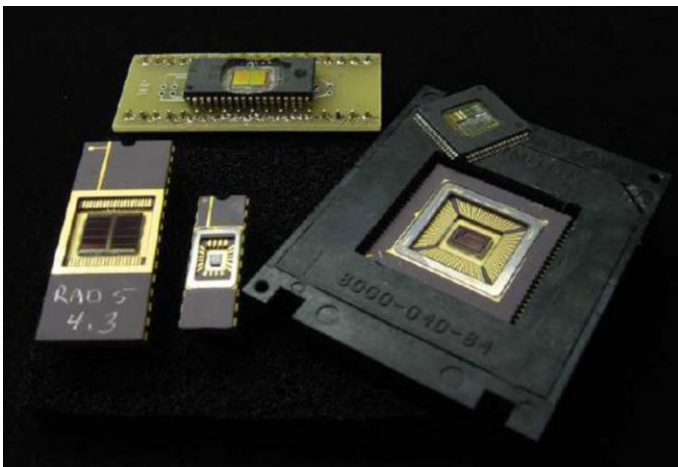


**Fig. 11** Integrated circuits prepared for heavy ion testing by removing package lids or etching the plastic mold compound

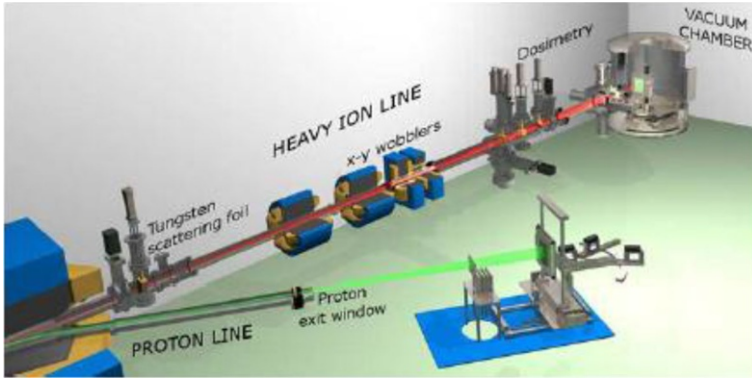


**Fig. 12** Illustration for the overview of the RADEF facility (University of Jyväskylä, Finland)

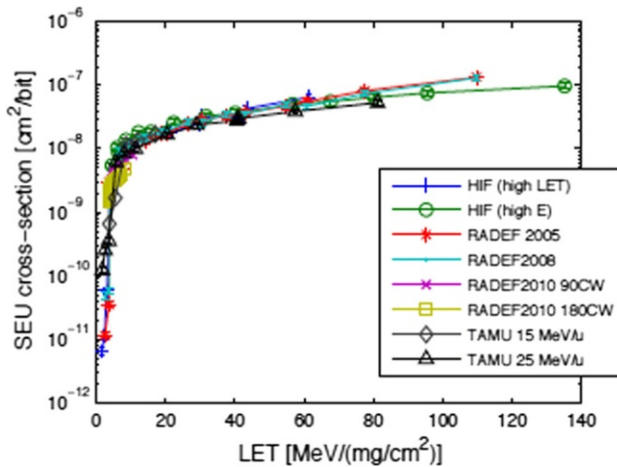


**Fig. 13** Single-event upset cross-section for 4-Mbit Atmel AT60142F SRAM [39]

A typical SEU cross-section versus LET curve is reported for the 4-Mbit Atmel AT60142F SRAM in Fig. 13, which also shows the so-called SEU monitor [38].

This kind of characteristic plot can be used for estimating the SEU rates in the operational environment. The upset cross-section curve can be roughly characterized by a LET threshold and a saturation upset cross-section. To determine the number of circuit errors that will result during a space mission, one must convolve the upset cross-section curve with the heavy ion LET spectrum for the orbit (Fig. 14). This can be done by using dedicated software, e.g. CREME-96 [8], by assigning the environment and entering the parameterized SEU cross-section curve. From these input data the code will give estimation for the SEU rate in orbit.

In the case a device is sensitive to low LET values ( $<15 \text{ MeV}/\text{mg cm}^2$ ) a test with high-energy protons (in the range 50–250 MeV) is required in order to predict the SEE rate induced by protons in the mission environment. Direct ionization by



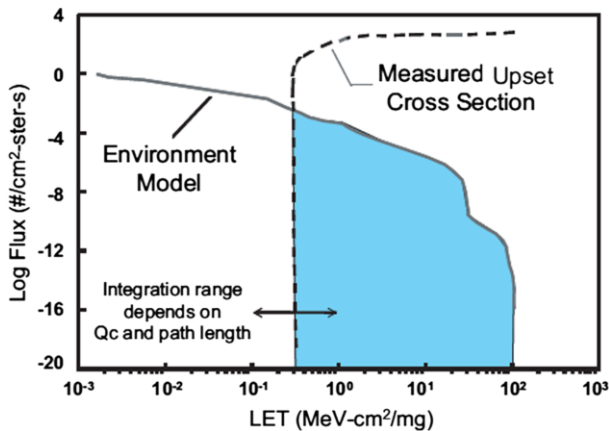


**Fig. 14** Measured cross-section vs. linear energy transfer and particle flux for a hypothetical environment. The error rate is determined by convolving the environment model with the error cross-section

protons does not usually produce sufficient charge to cause SEEs. Protons and neutrons can both produce significant upset rates due to indirect mechanism. A high-energy proton may undergo an inelastic collision with a target nucleus. The reaction products, being much heavier and having high  $Z$ , can deposit a significant amount of charge. The proton SEE test requires large particle fluence ( $10^{10}$ – $10^{11}$  protons/cm<sup>2</sup>) to observe effects with statistical confidence. Because of this high fluence, tens of kilorad in terms of total dose can be accumulated by DUT. The dose level received by devices is monitored during the SEE test. In order to avoid damage to the DUT due to accumulated dose, new devices (not irradiated) are used during SEE test.

A SEL can occur during SEE test. A dedicated SEL test should be made under the condition of maximum power supply voltage. In most cases the See test involves power monitoring and the use of a control circuit during latch-up testing that allow power to be shutdown quickly after the latch-up is detected. Power after a sufficient time is restored. In the case of a high number of SEL, dead time has to be considered for a proper cross-section evaluation.

Successful SEE testing requires that the particle beam, whether composed of protons or heavy ions, can reach the sensitive regions of the device under test with minimal alteration from extraneous materials—e.g. air gaps, device packaging, semiconductor materials (substrate and back-end-of-line), among others. This criterion is generally not an issue for medium- and high-energy proton beams as their range is sufficient to penetrate large volumes of air, packaging and semiconductor materials, but it is critical for heavy ion testing due to the short range of these particles at most test facilities. Because of this, device preparation is an important step in conducting SEE testing and needs to be considered early in the test design phase.

The JEDEC, ESCC, and ASTM standards for the SEE test include provisions for beam uniformity and purity, but these are specific to spatial uniformity and ion

species. SEE testing and analysis techniques typically assume a monoenergetic beam or a beam with energy spread no more than a few percentages of the total kinetic energy. However, a heavy ion beam is often degraded to achieve different stopping powers.

Ion or proton beam dosimetry is one of most important issue in the SEE test. Several detectors positioned on the beam line can be used to monitor beam flux during the irradiation and certify the final fluence achieved. In some cases, photomultiplier tubes (PMTs) equipped with scintillator crystals are positioned at the edge of the beam in order to monitor it during the irradiation. Another possible solution is to use a gaseous detector as a parallel plate avalanche counter. This detector allows very high flux rates (up to  $10^5$  particles/s  $\text{cm}^2$ ) to be counted and has the advantage that it can be placed in front of the beam with a minimal amount of degradation materials and no beam energy spread.

For all types of detectors, a calibration correction factor between the flux measured at the online dosimeter position and the flux at the DUT position has to be evaluated. This is done as a standard facility operation prior to starting the SEE test by measuring the flux with another detector placed at the DUT position and obtaining the correction factor.

Laser light is an easy way to induce SEEs in devices in laboratory. This technique proved to be very useful for SEE mechanism studies and SEE test setup debugging prior to performing the test at the accelerator. Laser light interacts in a very different way with the ions, and this interaction cannot be used to describe the in-orbit behaviour of a device. Laser data always need to be calibrated with heavy ion data.

#### 4.3.4 Solar Cell Degradation

Space solar cells have been used as a power sources by satellites since 1954 [40], and they have played an important role in scientific research and space development applications. The objectives of research and development of space solar cells are to improve conversion efficiency, increase life time (radiation resistance) and reduce the mass and cost of solar cell.

The influence of Earth's radiation belts on satellite solar cells is primarily determined by protons and high-energy electrons (with the energy approximately 1 MeV).

Modern satellites need more electric power than previous ones because they have more challenging missions and require more equipment. Solar cells with high conversion efficiencies are required to keep weight and launch costs low. They are also required for outer space missions (i.e. far away from the Sun) where light intensity is lower. In this context, GaAs solar cells are promising for space applications due to their higher theoretical and practical efficiencies [41, 42] (28.3%) [43] in comparison to silicon cells [44], [45]. An additional benefit is the fact that the GaAs solar cells are more resistant to irradiation by energy electrons [45], [46] which introduces defects into solar cell structures. In semiconductors, radiation usually produces atomic displacements, which in turn result in the generation of lattice defects, such a vacancies, interstitials and complex defects [47].



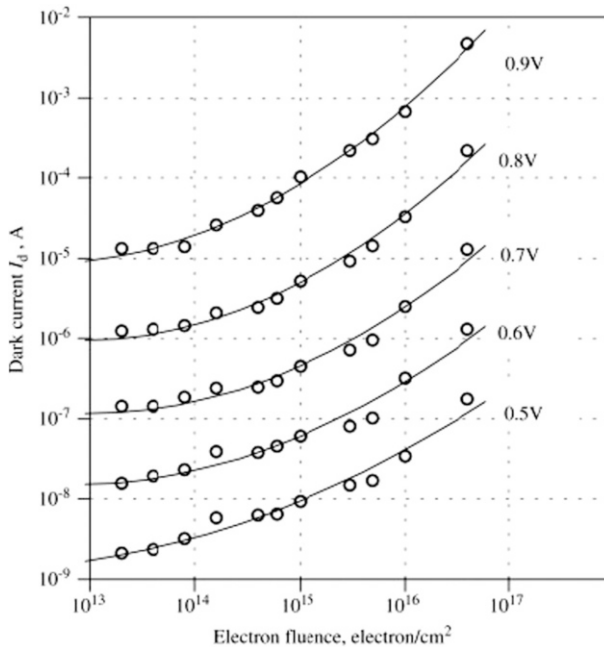


**Fig. 15** The dark current as a function of the irradiation fluence for forward-biased cells

Lattice defects that act as recombination centres or trapping centres cause a decrease in the output power of solar cells.

Solar cells provide power on space vehicles for long-term operations in an environment that includes the electron and protons of the Earth's radiation belts. Satellites are often expected to function for periods as long as 10 years. For some orbits close to maximum flux levels the cells are exposed to an integrated fluence up to  $4 \times 10^{15}$  electrons/cm<sup>2</sup> with an effective energy of 1 MeV and  $4 \times 10^{13}$  protons/cm<sup>2</sup> with energies of between 1 and 80 MeV. All indications are that the changes produced in the cells are cumulative, and therefore it is prudent to assume that the changes in cell characteristics which will result after 10 years are about the same as those which would result from an equivalent integrated flux delivered at a much higher rate.

Electron irradiation typically has effect on dark current and short circuit current as reported in Figs. 15 and 16 [48].

In general, the electrical characteristics of solar cells are evaluated at a measurement facility before the cells are brought to an accelerator facility for irradiation (by protons or electrons) and subsequently returned to the measurement facility for re-measuring. However, this "sequential method" needs relatively high quantities of samples that can be irradiated by different amounts of electrons/protons with different accelerating energies to fully reveal the degradation of solar cells.

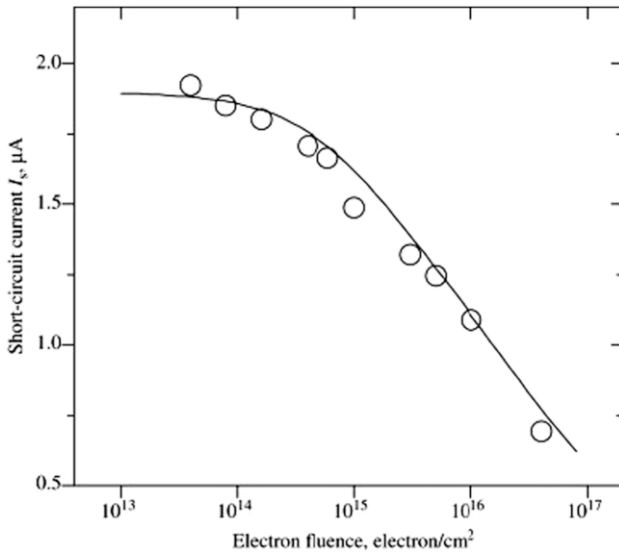


**Fig. 16** The short-circuit current as a function of the irradiation fluence

For solar cells, the primary energy loss mechanism is through non-ionizing effects that lead to the displacement of atoms in the semiconductor lattice. The displacement of atoms results in lattice defects, such as vacancies, interstitials (displaced atoms moving to non-lattice positions), and to the formation of defect energy levels in the semiconductor material [49, 50]. These defects produce carrier-trapping centres (e.g. recombination centres and compensation centres) in the semiconductor bandgap and also generate carriers. Carrier generation leads to an increase in the forward bias dark  $I$ - $V$  curve and degrades  $V_{oc}$ .

Recombination centres reduce minority carrier diffusion length, or minority carrier lifetime, and decrease the photovoltaic output of the cell. For GaAs and Si cells, radiation-induced recombination centres serve as the primary mechanism for the degradation of cell performance. The decrease in the minority carrier diffusion length degrades  $I_{short-circuit}$  and leads to an increased forward biased dark  $I$ - $V$  curve, which also degrades  $V_{oc}$ . In order to generate photocurrent output, charge carriers must diffuse to the junction before recombination occurs [51, 52]. Degradation of the minority carrier diffusion length reduces the cell's efficiency. For GaAs solar cells, the average diffusion length of the photo-generated carrier is large in comparison to the junction distance; for silicon cells, the average diffusion length is comparable to the thickness of the generating region of the photo-carrier. Thus, the decrease in diffusion length of carriers in silicon corresponds to a decrease in efficiency, whereas for GaAs solar cells, carrier diffusion length degradation contributes to a smaller decrease in efficiency.

Detailed treatment of radiation damage of solar cells from electrons and protons is reported on [7].

## References

1. National Aeronautics and Space Administration (NASA) (1999) Space radiation effects on electronic components in low earth orbit. Lesson 824. Johnson Space Center, Houston. <http://lis.nasa.gov/lesson/824>. Accessed 23 Nov 2016
2. Van Allen L, Ludwig G, McIlwain R. Observation of high intensity radiation by satellites 1958 alpha and gamma. In: IGY Satellite Series, vol 3. National Academy of Sciences, Washington DC, p 73
3. Lang KR (2001) The Cambridge encyclopedia of the sun. Cambridge University Press, Cambridge
4. A travel in radiation activities through a Space program—Short course (2011) 12th European Conference on Radiation and its effects on Component and Systems (RADECS), Sevilla
5. Sawyer DM, Vette JI (1976) AP-8 trapped proton environment for solar maximum and solar minimum. NASA STIRcon Technical Report N, vol 77, p 18983. <http://hdl.handle.net/2060/19770012039>. Accessed 23 Nov 2016
6. Vampola AL (1997) Outer zone energetic electron environment update. In: Proceedings of the IEEE conference on high energy radiation background in space, p 128–136
7. SPENVIS Collaboration. The space environment information system, 1997–2009. <http://www.spennis.oma.be>. Accessed 23 Nov 2016
8. The CREME Collaboration. CREME-MC. <https://creme.isde.vanderbilt.edu>. Accessed 23 Nov 2016
9. Jokipii J, Sonett C, Giampapa M (eds) (1997) Cosmic winds and the heliosphere. Space Science Series. Tucson, University of Arizona Press
10. Andrews MD (2003) A search for CMEs associated with big flares. *Sol Phys* 218:261–279
11. Ramesh KB (2010) Coronal mass ejections and sunspots—solar cycle perspective. *Astrophys J Lett* 712:L77–L80
12. Gabriel SB (1998) Cosmic rays and solar protons in the near earth environment and their entry into the magnetosphere. ESA Workshop on Space Weather, ESTEC, The Netherlands, Noordwijk
13. Lario D, Decker RB, Re-examination of the October 20, 1989 ESP event, Conf. Proc. of the ICRC 2001 07–15 August, Hamburg, p 3485
14. Mewaldt RA, Cummings AC, Cummings JR et al (1993) The return of the anomalous cosmic rays to 1 AU in 1992. *Geophys Res Lett* 20:2263
15. Dale CJ, Chen L, McNulty PJ, Marshall PW, Burke EA (1994) A comparison of Monte Carlo and analytic treatments of displacement damage in Si microvolumes. *IEEE Trans Nucl Sci* 41(6):1974–1983
16. Huhtinen M, Aarnio PA (1993) Pion induced displacement damage in silicon devices. *Nucl Instrum Methods Phys Res Sect A* 335(3):580–582
17. Akkerman A, Barak J, Chadwick MB et al (2001) Updated NIEL calculations for estimating the damage induced by particles and gamma rays in Si and GaAs. *Radiat Phys Chem* 62:301–331
18. Summers GP, Burke EA, Shapiro P, Messenger SR, Walters RJ (1993) Damage correlations in semiconductors exposed to gamma, electron and proton radiations. *IEEE Trans Nucl Sci* 40(6):1372–1379
19. Vasilescu A, Lindstroem G. Displacement Damage in Silicon, Online Compilation. <http://sesam.desy.de/members/gunnar/Si-dfuncs.html>. Accessed 15 July 2005
20. Walters RJ, Shaw GJ, Summers GP, Burke EA, Messenger SR (1992) Radiation effects in Ga<sub>0.47</sub>In<sub>0.53</sub>As devices. *IEEE Trans Nucl Sci* 39(6):2257–2264
21. Fodness BC, Marshall PW, Reed RA, Jordan TM, Pickel JC, Jun I, Xapsos MA, Burke EA, Ladbury R (2003) Monte Carlo treatment of displacement damage in bandgap engineered HgCdTe detectors. *IEEE Conf. Proc., 7th European Conference on Radiation and its Effects on Components and Systems (RADECS)*, pp 479–485
22. Jun I, Xapsos MA, Messenger SR, Burke EA, Walters RJ, Summers GP, Jordan T (2003) Proton nonionizing energy loss (NIEL) for device applications. *IEEE Trans Nucl Sci* 50(6):1924–1928
23. Jun I, Kim W, Evans R (2009) Electron nonionizing energy loss for device applications. *IEEE Trans Nucl Sci* 56(6):3229–3235
24. Electronic Industries Association (EIA) (1996) Test procedures for the measurement of single-event effects in semiconductor devices from heavy ion irradiation. EIA/JEDEC Standard No. 57, Arlington, EIA, VA, p 49
25. JEDEC Solid State Technology Association (2006) Measurement and reporting of alpha particle and terrestrial cosmic ray-induced soft errors in semiconductor devices. JEDEC Standard No. 89A. JEDEC Solid State Technology Association 2001 Arlington, VA, pp 2201–3834

26. Bruguiere G, Palau JM (1996) Single particle-induced latchup. *IEEE Trans Nucl Sci* 43:522
27. Pickel JC (1996) Single-event effects rate prediction. *IEEE Trans Nucl Sci* 43:483
28. Dodd PE (1996) Device simulation of charge collection and single event upset. *IEEE Trans Nucl Sci* 43:561
29. Sexton F (2003) Destructive single-event effects in semiconductor devices and ICs. *IEEE Trans Nucl Sci* 50:603–621
30. Schwank J, Ferlet-Cavrois V, Shaneyfelt M, Paillet P, Dodd P (2003) Radiation effects in SOI technologies. *IEEE Trans Nucl Sci* 50:522–538
31. Pease RL, Seiler J (2005) Evaluation of MIL-STD-883/test method 1019.6 for bipolar linear circuits. *J Radiat Effects Res Eng*. <http://focus.ti.com/pdfs/hirel/space/HEART05-G1paper.pdf>. Accessed 23 Nov 2016
32. American Society for Testing and Materials (ASTM) F1892 Standard guide for ionizing radiation (total dose) effects testing of semiconductor. West Conshohocken, PA : ASTM, 2006, Philadelphia, p 39
33. European Space Agency/Space Components Coordination (ESA/SCC) Basic specification n. 22900. Total dose steady-state irradiation test method. Issue 3, MAR 2007
34. Electronic Industries Association (1996) Test procedures for the measurement of single-event effects in semiconductor devices from heavy ion irradiation. EIA/JEDEC Standard, No. 57, Arlington
35. European Space Agency/Space Components Coordination (ESA/SCC) (1995) Basic specification n. 25100 Single event effects test method and guidelines, 1st edn. ESA
36. Virtanen A, Javanainen A, Kettunen H, Pirojenko A, Riihimäki I, Ranttila K. Radiation effects facility at JYFL. <https://www.jyu.fi/fysiikka/en/research/accelerator/radef>. Accessed 23 Nov 2016
37. Heavy ion irradiation facility (HIF). <http://www.cyc.ucl.ac.be/HIF/HIF.php>. Accessed 23 Nov 2016
38. Harboe-Sorensen R, Guerre FX, Roseng A (2005) Design, testing and calibration of a reference SEU monitor system. *IEEE Conf. Proc. European Conference in radiation and its effects on components and systems. RADECS 2005*, pp B3–1–B3–7
39. Harboe-Sorensen R, Poivey C, Guerre F-X, Roseng A, Lochon F, Berger G, Hajdas W, Virtanen A, Kettunen H, Duzellier S (2008) From the reference SEU monitor to the technology demonstration module on-board PROBA-II. *IEEE Trans Nucl Sci* 55:3082–3087
40. Iles PA (2001) Evolution of space solar cells. *Sol Energy Mater Sol Cells* 68:1–13
41. Bett AW, Dimroth F, Stollwerck G, Sulima OV (1999) III–V compounds for solar cell applications. *Appl Phys A69*:129–199
42. Priyanka Singh N, Ravindra M (2012) Temperature dependence of solar cell performance—an analysis. *Sol Energy Mater Sol Cells* 101:36–45
43. Green MA, Emery K, Hishikawa Y, Warta W, Dunlop ED (2012) Solar cell efficiency tables (version 39). *Prog Photovolt Res Appl* 20:12–20
44. Torchynska TV, Polupan GP (2002) III-V material solar cells for space application. *Semiconduct Phys Quant Electron Optoelectron*. 5(1):63–70
45. Li SS, Loo RY (1991) Deep-level defects and numerical simulation of radiation damage in GaAs solar cells. *Solar Cells* 31:349–377
46. de Angelis N, Bourgoin JC, Takamoto T, Khan A, Yamaguchi M (2001) Solar cell degradation by electron irradiation. Comparison between Si, GaAs and GaInP cells. *Sol Energy Mater Sol Cells* 66:495–500
47. Yamaguchi Masafumi (2001) Radiation-resistant solar cells for space use. *Sol Energy Mater Sol Cells* 68:31–53
48. Danilchenko B, Budnyk A, Shpynar L, Poplavskyy D, Zelensky SE, Barnham KWJ, Ekins-Daukes NJ (2008) 1 MeV electron irradiation influence on GaAs solar cell performance. *Sol Energy Mater Sol Cells* 92:1336–1340
49. Weinberg I (1991) Radiation damage in InP solar cells. *Solar Cells* 31:331–348
50. Sumita T, Imaizumi M, Matsuda S, Ohshima T, Ohi A, Itoh H (2003) Proton radiation analysis of multi-junction space solar cells. *Nucl Instrum Methods Phys Res* 206:448–451
51. Hacke P, Uesugi M, Matsuda S (1994) A study of the relationship between junction depth and GaAs solar cell performance under a 1 MeV electron fluence. *Sol Energy Mater Sol Cells* 35:113–119
52. Yamaguchi M (2001) Radiation-resistant solar cells for space use. *Sol Energy Mater Sol Cells* 31–53

## Erratum to: Radiation Engineering of Multifunctional Nanogels

C. Dispenza<sup>1,2</sup> · G. Spadaro<sup>1</sup> · M. Jonsson<sup>2</sup>

Published online: 28 September 2016  
© Springer International Publishing Switzerland 2016

### Erratum to: Top Curr Chem (Z) (2016) 374:69 DOI 10.1007/s41061-016-0071-x

The original version of this article unfortunately contained a mistake.

The presentation of Fig. 1 was incorrect. The correct version of Fig. 1 is given here.

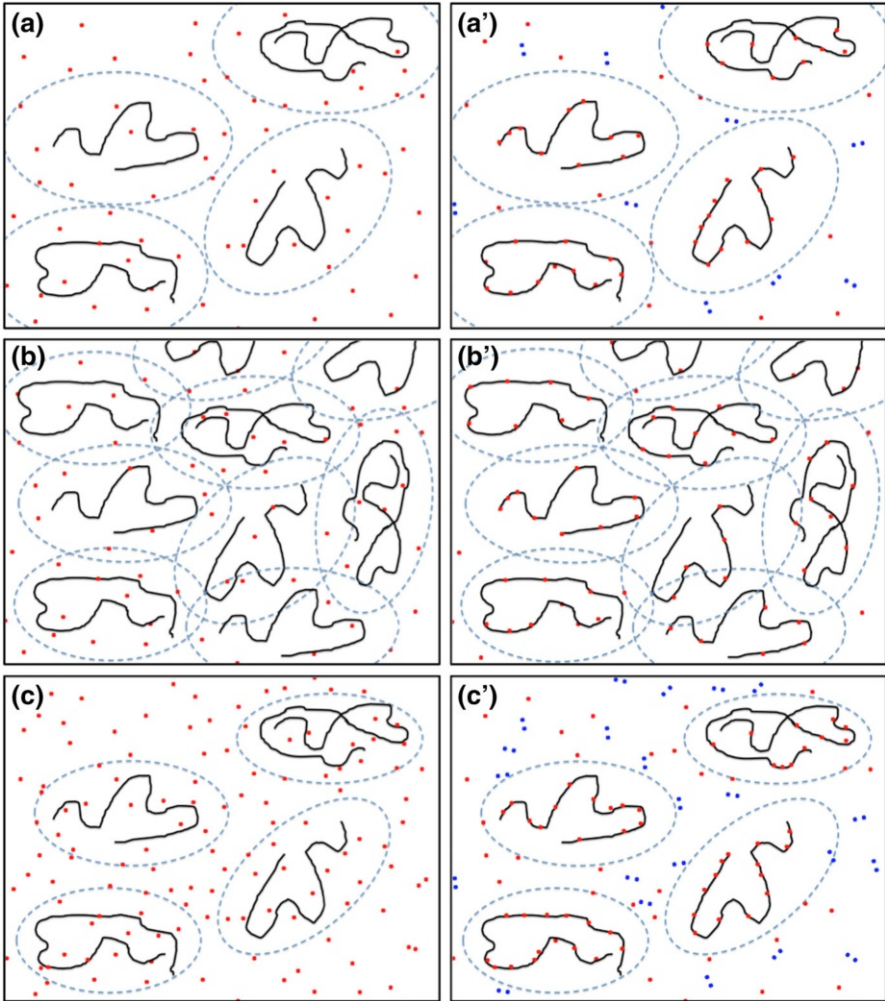
---

The online version of the original article can be found under doi:10.1007/s41061-016-0071-x.

✉ C. Dispenza  
[clelia.dispenza@unipa.it](mailto:clelia.dispenza@unipa.it)


<sup>1</sup> Dipartimento di Ingegneria Chimica, Gestionale, Informatica, Meccanica,  
Università degli Studi di Palermo, Viale delle Scienze, Edificio 6, 90128 Palermo, Italy

<sup>2</sup> School of Chemical Science and Engineering, Royal Institute of Technology (KTH),  
100 44 Stockholm, Sweden



The original article was corrected.

## Erratum to: Application of Radiation Chemistry to Some Selected Technological Issues Related to the Development of Nuclear Energy

Krzysztof Bobrowski<sup>1,2</sup>  · Konrad Skotnicki<sup>1</sup> · Tomasz Szreder<sup>1</sup>

Published online: 18 October 2016  
© Springer International Publishing Switzerland 2016

### Erratum to: Top Curr Chem (Z) (2016) 374:60 DOI 10.1007/s41061-016-0058-7

The original version of this article unfortunately contained mistakes concerning some units of measurement:

Page 4	Line 5 from the bottom	day $\text{m}^3 \text{mol}^{-1} \text{s}^{-1}$ should read $\text{dm}^3 \text{mol}^{-1} \text{cm}^{-1}$
Page 4	Line 4 and 5 from the bottom	day $\text{m}^3 \text{mol}^{-1} \text{s}^{-1}$ should read $\text{dm}^3 \text{mol}^{-1} \text{cm}^{-1}$
Page 5	Line 9 from the bottom	day $\text{m}^{-3}$ should read $\text{dm}^{-3}$
Page 7	Line 11/12 from the top	day $\text{m}^3 \text{mol}^{-1} \text{s}^{-1}$ should read $\text{dm}^3 \text{mol}^{-1} \text{s}^{-1}$
Page 8	Line 1 from the top	day $\text{m}^3 \text{mol}^{-1} \text{s}^{-1}$ should read $\text{dm}^3 \text{mol}^{-1} \text{s}^{-1}$
Page 8	Line 1 from the top	day $\text{m}^3 \text{mol}^{-1} \text{s}^{-1}$ should read $\text{dm}^3 \text{mol}^{-1} \text{s}^{-1}$
Page 9	Line 5 from the top	$\text{M}^{-1} \text{s}^{-1}$ should read $\text{dm}^3 \text{mol}^{-1} \text{s}^{-1}$
Page 9	Line 5 from the top	$\text{M}^{-1} \text{s}^{-1}$ should read $\text{dm}^3 \text{mol}^{-1} \text{s}^{-1}$
Page 9	Line 6 from the top	$\text{M}^{-1} \text{s}^{-1}$ should read $\text{dm}^3 \text{mol}^{-1} \text{s}^{-1}$
Page 9	Line 7 from the top	$\text{M}^{-1} \text{s}^{-1}$ should read $\text{dm}^3 \text{mol}^{-1} \text{s}^{-1}$
Page 10	Line 17/16 from the bottom	day $\text{m}^3 \text{mol}^{-1} \text{s}^{-1}$ should read $\text{dm}^3 \text{mol}^{-1} \text{s}^{-1}$
Page 10	Line 16 from the bottom	day $\text{m}^3 \text{mol}^{-1} \text{s}^{-1}$ should read $\text{dm}^3 \text{mol}^{-1} \text{s}^{-1}$
Page 10	Line 8 from the bottom	day $\text{m}^3 \text{mol}^{-1} \text{s}^{-1}$ should read $\text{dm}^3 \text{mol}^{-1} \text{s}^{-1}$

The online version of the original article can be found under doi:10.1007/s41061-016-0058-7.

✉ Krzysztof Bobrowski  
[k.bobrowski@ichtj.waw.pl](mailto:k.bobrowski@ichtj.waw.pl)

<sup>1</sup> Centre of Radiation Research and Technology, Institute of Nuclear Chemistry and Technology, Dorodna 16, 03-195 Warsaw, Poland

<sup>2</sup> Radiation Laboratory, University of Notre Dame, Notre Dame, IN 46556, USA





Page 29	Line 16 from the top	day $\text{m}^3 \text{mol}^{-1} \text{cm}^{-1}$ should read $\text{dm}^3 \text{mol}^{-1} \text{s}^{-1}$
Page 29	Line 17 from the top	day $\text{m}^3 \text{mol}^{-1} \text{cm}^{-1}$ should read $\text{dm}^3 \text{mol}^{-1} \text{s}^{-1}$
Page 30	Line 9 from the bottom	day $\text{m}^3 \text{mol}^{-1} \text{s}^{-1}$ should read $\text{dm}^3 \text{mol}^{-1} \text{s}^{-1}$
Page 32	Line 3 from the top	day $\text{m}^3 \text{mol}^{-1} \text{cm}^{-1}$ should read $\text{dm}^3 \text{mol}^{-1} \text{s}^{-1}$
Page 32	Line 3 from the top	day $\text{m}^3 \text{mol}^{-1} \text{cm}^{-1}$ should read $\text{dm}^3 \text{mol}^{-1} \text{s}^{-1}$